Introduction to Mechanical Properties of Materials

# Periodic Table of the Elements

_	1 A	II A	III B	1V B	V B	V1 B	VII B		VIII	
2	1 H 13.53 -259 18 <sup>1</sup> 5 L 2 .37 180 3.50½ 18 <sup>2</sup> 25 <sup>1</sup> 11 Na 1.42 10.7 4 .2 <sup>1</sup> / <sub>1</sub>	4 bs 4.35 1.75 2.39 4.55 157 53 12 Mg 61 1.309 5.215		Atonic number Dement lonization potential (eV) Melting point (°C at 1 atm) Lattice parameter (A) Lattice parameter (A)  Body-centered cubic Face-centered cubic Hexagonal close-packed Diamond Diamond Atonic number Dements not solid at room temperature the melting point.						
4	19 K 4.32 63.6 5.344	20 Ca 6.09 850 5.56 48 <sup>2</sup>	21 Sc 6.7 1200 4.541 3D <sup>1</sup> 4S <sup>2</sup>	22.75 6.85 1696 2.956-4.68 3D* 48*	23 V 5.76 (1900 3.039 30 <sup>3</sup> ws <sup>3</sup>	24 Ct 6.74 1550 2.885 3D <sup>5</sup> 45 <sup>4</sup>	25 Mn 7.40 1250	26.Fe 7.S3 1526 1×66 1×66	27 Co 8.5 1490 3.552 3D <sup>7</sup> 4S <sup>2</sup>	28 Ni 7.61 1452 3.524 3D8 4S
5	37 Rb 4 16 19 5 63	38 Sr 5.67 800 6.087 5S <sup>2</sup>	39 ¥ 6.5 1452 40° 58°	40 Zr 6.92 1830 3.61 40 <sup>2</sup> 35 <sup>2</sup>	41 Nb 6.8 2415 3.30 4D <sup>4</sup> 5S <sup>1</sup>	42 Mo 7.06 2600 3.147 4D <sup>5</sup> 5S <sup>1</sup>	45 To 7 S 2700 40° 58°	44 Ru 3.7 2466 2.764-4.283 457.583	45 Rh 7.7 1970 3.803 4D <sup>8</sup> 5S <sup>1</sup>	46 Pd 8.3 1553 3.890 4D <sup>10</sup>
6	55 Cs 3,87 28 6,06	56 Ba 5.19 710 5.025 65 <sup>5</sup>	55-71 RARE EARTHS Fills up	73/14 5/5 2236 3/286-5/08 505/654	73 Ta 6-0 3-027 3-3-02 501-652	74 W 8.1 3390 3.165	75 Re 7.85 3367 2.763-4.458	26-Gs 8.7 1798 2,733-4,375 505-687	77 lr 9.2 2454 3.839 5D° 6S°	78 Pt 8.9 1771 3.924 5D° 6S
7	87 Fr 4.0	88 Ra 5.25	89-103 Actinons						03	03
	7S1	7S <sup>2</sup>	Fills up							

I B	II B	III A	IV A	V A	VI A	VII A	0
							2 No. 24 37 259-5.03 35
		5 B 8.25 2300 2S <sup>2</sup> 2P <sup>1</sup>	6 C 11.20 3.568 2S <sup>2</sup> 2P <sup>2</sup>	7 N 14.47 -210 2S <sup>2</sup> 2P <sup>3</sup>	8 O 13.55 -218 2S <sup>2</sup> 2P <sup>4</sup>	9 F 18.6 -223 2S <sup>2</sup> 2P <sup>5</sup>	10 Ne 21.47 -249 4.52 2S <sup>2</sup> 2P <sup>6</sup>
		13 Al 5.96 660 4.049 3S <sup>2</sup> 3P <sup>1</sup>	14 Si 8.08 1420 5.428 3S <sup>2</sup> 3P <sup>2</sup>	15 P 11.11 44 3S <sup>2</sup> 3P <sup>3</sup>	16 S 10.31 113-119 3S <sup>2</sup> 3P <sup>4</sup>	17 Cl 12.96 -103 3S <sup>2</sup> 3P <sup>5</sup>	18 Ar 15.69 -189 5.43 38 <sup>2</sup> 3P <sup>6</sup>
29 Cu 7.68 1083 3.615 3D <sup>10</sup> 4S <sup>1</sup>	30 Za 9 36 419 2,664+4 945 301 <sup>8</sup> 45 <sup>1</sup>	31 Go 8-97 30 3-62-8.78 68 <sup>3</sup> 49 <sup>5</sup>	32 Ge 8.09 958 5.658 4S <sup>2</sup> 4P <sup>2</sup>	33 As 10.5 817 4S <sup>2</sup> 4P <sup>3</sup>	34 Se 9.70 217 4S <sup>2</sup> 4P <sup>4</sup>	35 Br 11.30 -7 4S <sup>2</sup> 4P <sup>5</sup>	36 Kr 13.94 -157 5.69 4S <sup>2</sup> 4P <sup>6</sup>
47 Ag 7.54 960 4.086 4D <sup>10</sup> 5S <sup>1</sup>	48-54 8-96 925 2-979-5-5-17 40 <sup>58</sup> -55 <sup>2</sup>	49 In 5.76 155 5S <sup>2</sup> 5P <sup>1</sup>	50 Sn 7.30 232 6.46 5S <sup>2</sup> 5P <sup>2</sup>	51 Sb 8.35 630 5S <sup>2</sup> 5P <sup>3</sup>	52 Te 8.96 453 5S <sup>2</sup> 5P <sup>4</sup>	53 I 10.44 113 5S <sup>2</sup> 5P <sup>5</sup>	54 Xe 12.08 -112 6.24 5S <sup>2</sup> 5P <sup>6</sup>
79 Au 9.20 1063 4.078	80 Hg 10.38 -40	81 TI 6.07 303	82 Pb 7.38 327 4.949	83 Bi 8.0 271	84 Po 7.25	85 At 9.4	86 Rn 10.96
5D10 6S1	5D10 6S2	6S2 6P1	6S2 6P2	6S2 6P3	6S2 6P4	6S2 6P5	6S <sup>2</sup> 6P <sup>6</sup>











# Introduction to Mechanical Properties of Materials

Melvin M. Eisenstadt The University of California at Santa Barbara

The Macmillan Company, New York Collier-Macmillan Limited, London Copyright © 1971, Melvin M. Eisenstadt Printed in the United States of America All rights reserved. No part of this book may be reproduced or transmitted in any form or by any means, electronic or mechanical, including photocopying, recording, or any information storage and retrieval system, without permission in writing from the Publisher. The Maemillan Company Se66 Third Avenne, New York, New York 10022 Collier-Maemillan Canada, Ltd., Toronto, Ontario Library of Congress catalog eard number: 77-115297

First printing

# To Pauline and May



# Preface

I HAVE WRITTEN this book for a first course in materials science at the sophomore or junior level. The reader is expected to have some background in calculus. It has been my experience that students do not have a good grasp of thermodynamic concepts until they have had at least one course devoted exclusively to that subject. This book does not assume that the reader has had such a course.

The properties of macroscopic solids depend on what is happening at the microscopic level; that is, the mechanical properties are largely determined by the forces between the atoms and by the geometric arrangement of the atoms in the solid—by chemical bonding and molecular structure. Physical models of solids are postulated throughout the book. These describe atomic structure and bonding and provide a physical picture of the processes that take place. Equations describing the macroscopic behavior of materials are derived from the microscopic models, and the accuracy of these equations is checked by comparing calculated results with experimental data. This approach enables us to use the fundamental principles of engineering, metallurgy, chemistry, and physics in describing the behavior of solids.

The engineer must understand why materials behave as they do, in addition to having information which tells how much. For example, it is essential that an engineer know the strength of a material before he uses it, but it is also necessary that he understands how the strength may vary under different conditions. Such understanding comes from a knowledge of why materials behave as they do. The models used in the book will help to explain both why and how much.

Metals, ceramics, and polymers are treated. Covering these in a single book has the advantage of pointing out both their similarities and their differences. Much of the theory developed in the book is applicable to all three, although the mechanical properties of these materials are quite different.

Questions appear at the end of most of the sections in the book. They are intended to test the reader's comprehension of the principles covered in the section. If the reader cannot answer the questions, he should restudy the section. Answers to these questions are given at the end of each chapter. I should like to express my gratitude to Professor R. Brady Williamson for reading the entire manuscript and offering many fine criticisms and suggestions. I was fortunate in having Miss Barbara Skehan and Miss Jeanne Miller to type the various drafts of the book, and I sincerely thank them. Recognition and thanks also go to my wife, Pauline, who showed a great deal of tolerance and encouragement while the manuscript was gestating.

## **Contents**

#### 1 Introduction 1

- 1-1 Modelina nature 2
- 1-2 Elasticity and Hooke's law 4
- 1-3 Permanent deformation and fracture 7
- 1-4 Engineering and true stress-strain diagrams 10
- 1-5 Toughness 13
- 1-6 Hardness 15
- 1-7 Work hardening and annealing 17
- 1-8 Diffusion 17
- 1-9 Classification of materials 19
- 1-10 Explanation of the observed phenomena 19

#### Atomic structure and bonding 23

- 2-1 Atomic structure 23
  - 2-2 The hydrogen atom 24
  - 2-3 Shielding 28
  - 2-4 Quantum numbers 29
  - 2-5 The Pauli exclusion principle and the periodic table 31
  - 2-6 Ionization energy and electron affinity 35
  - 2-7 The ionic hand 36
  - 2-8 The metallic bond 42
  - 2-9 The covalent bond 44
  - 2-10 Secondary bonds 48
  - 2-11 Addition (or chain) polymerization 50
  - 2-12 Condensation (or step) polymerization 56
  - 2-13 Summary 57

#### 2 Structure of solids 61

- 3-1 Space lattices and crystal structures 62
  - 3-2 Directions in a crystal 66
  - 3-3 Planes in a crystal and Miller indices 68
  - 3-4 Nondirectional bonds with atoms of equal size 71
  - 3-5 Nondirectional bonds with atoms of unequal size 77
  - 3-6 Coordination polyhedra and silicates 80
  - 3-7 Polymer structures 84
    3-8 Stereoisomerism 86
  - 3-9 Elastomers 87
  - 3-10 Thermoplastic and thermosetting polymers 90
  - **3-11** Summary 90

#### ▲ Solidification and crystal imperfections 95

- 4-1 Atomic mechanism of crystal arowth 96
  - 4-2 Homogeneous nucleation 99
  - 4-3 Heterogeneous nucleation 101
  - 4-4 Temperature gradients: dendrites and single crystals 104
  - 4-5 Castings 107
  - 4-6 Amorphous structures; glass transition temperature 110
  - 4-7 Point defects in crystals 114
  - 4-8 Line defects or dislocations 116
  - 4-9 Whiskers 120
  - 4-10 Summary 122

#### 5 Experimental observation of solids 125

- 5-1 The optical microscope 126
- 5-2 The electron microscope 127
- 5-3 The field ion microscope 131
- 5-4 X-ray sources 133
- 5-5 X-ray diffraction 136
- 5-6 Diffraction conditions for cubic unit cells 140
- 5-7 Interpreting experimental data 144
- 5-8 The electron microprobe 147
- 5-9 Verification of models and summary 148

#### Elastic behavior of crystalline solids 153

#### 6-1 Young's modulus, shear modulus, and bulk modulus 153

- 6-1 Toung's modulus, 3
  6-2 Poisson's ratio 157
- 6-3 Interatomic forces in a solid 160
- 6-4 Hooke's law 164
- 6-5 Model of an elastic solid 1706-6 Thermal expansion 171
- 6-7 Theoretical shear strength of a solid 175
- 6-8 Elastic materials in design 180
- 6-9 Summary 182

#### Surface properties and brittle fracture 187

- 7-1 Surface tension and specific surface energy 187
- 7-2 Origin of surface energy 188
- 7-3 Calculation of surface energy from bonding equations 191
- 7-4 Theoretical tensile strength 195
- 7-5 Measurement of surface energy of solids 197
- 7-6 Surface tension and wetting 200
- 7-7 The effect of cracks in a material 2037-8 Griffith theory of brittle fracture 205
- 7-8 Griffith theory of brittle fracture 205
   7-9 Designing with brittle materials 207
- 7-10 Summary 210

#### Plastic behavior of solids 217

- 8-1 Observation of slip 218
- 8-2 The slip mechanism 222
- 8-3 Critical resolved shear stress 227
- 8-4 Slip systems 230
- 8-5 Energy of dislocations 230
- 8-6 Dislocation sources 235
- 8-7 Dislocation annihilation and forces 239
- 8-8 Partial dislocations 242
- 8-9 Dislocation mobility 245
- 8-10 Dislocation interactions 246
  - 8-11 Climb and cross slip 250
  - 8-12 Work hardening of metals 252
  - 8-13 Dislocation motion in ceramics 254
- 8-14 The effect of grain boundaries 257
- 8-15 Effect of impurity particles 259
- 8-16 Twinning 259
- 8-17 Fracture of ductile materials 260
- 8-18 Permanent deformation of polymers 262
- 8-19 Comments on ductile materials 266
- 8-20 Summary 266

#### Effect of temperature on plastic behavior 275

- 9-1 The observed effect of temperature on strength 276
- 9-2 Thermally activated processes 278
- 9-3 Thermally activated processes in solids 282
- 9-4 Effect of strain rate 286 9-5 The ductile to brittle transition 287
- 9-6 Annealing 289
- 9-7 Creep 294
- 9-8 Creep rupture 300
- 9-9 Thermal effects in polymers 301
- 9-10 Summary 333

#### Diffusion 309 10

- 10-1 Diffusion mechanisms 310
- 10-2 Fick's first law 312
- 10-3 Fick's second law-time dependence 316
- 10-4 Quantities affecting the diffusion coefficient 324 10-5 Diffusion in oxides and ionic crystals 326
- 10-6 Grain boundary and surface diffusion 327
  - 10-7 Summary 329

- 11 Solubility, phase diagrams, and phase transformations 333
  - 11-1 Equilibrium phase diagram of a pure substance 334
    - 11-2 Binary diagrams and solubility 336
    - 11-3 Gibbs phase rule 339
    - 11-4 Systems with complete solid solubility 341
    - 11-5 The lever rule 344
    - 11-6 The binary eutectic system 347
    - 11-7 The binary peritectic system 350
    - 11-8 Invariant reactions 351
    - 11-9 Phase diagrams with intermediate phases and
    - intermediate compounds 352
    - 11-10 The iron-carbon system 354
    - 11-11 Nonequilibrium solidification of alloys 360
    - 11-12 Phase diagrams and diffusion 362
    - 11-13 Summary 365

#### 12 Strengthening mechanisms 373

- 12-1 Solution hardening 374
  - 12-2 Dispersion hardening 376
  - 12-3 Precipitation hardening 383
  - 12-4 Guinier-Preston zones 385
  - 12-5 Grain size 388
  - 12-6 Martensite-diffusionless transformations 389
  - 12-7 Heat treatment of steel 391
  - 12-8 The effect of alloying elements on steel transformation hardenability 397
  - 12-9 Strain-induced transformations 401
  - 12-10 Fiber and whisker reinforcement 403
  - 12-11 Designing with strengthened materials 406

#### Appendixes 413

- A Properties of the elements 414
- B Properties of selected ceramics 418
- C Properties of selected polymers at room temperature 420
- D Planes and directions in hexagonal crystals 422
- E Taylor's expansion 424
- F Answers to selected problems 426
- G Physical constants 429
- H Conversion factors 429
- I Systems of units 429
- J Symbols 429





#### CHAPTER 1

### Introduction

THE ENGINEER is faced with a larger variety of problems today than ever before. He must design devices and structures that function over a vast range of environmental conditions. These vary from the low pressures found in outer space to the very high pressures existing in the ocean depths and include temperatures ranging from below that of liquid helium to those encountered in nuclear reactors and rocket engines. It is his responsibility to select materials from which these structures and devices will be fabricated and to take corrective action when materials have failed in their function. There are many engineering problems presently facing us that do not have the exotic image of the environmental extremes but that nevertheless require new materials and new solutions. The technological part of the solutions to problems such as low-cost housing and mass transportation will undoubtedly require new concepts and new materials (the same may be true of the political and economic aspects of these problems). If the engineer is to help solve problems by designing devices or systems, he must have knowledge of the properties and behavior of the materials that he uses

This knowledge can come from two sources. The first is a fundamental understanding, based upon physical laws, of how materials behave and why they behave as they do. The second source is the large amount of experimental information that describes the behavior of solids. Both are often needed to solve materials problems. Solid-state physica, physical chemistry, and metallurgy have provided us with a great deal of information about why solids behave as they do, but the theoretical understanding is not complete. The available theories do, however, provide a great insight into the nature of solids and enable us to intelligently extrapolate existing data and to set up meaningful test programs. The very large number of new materials that have been and are being developed are largely the result of increasing theoretical

knowledge. The lack of complete theoretical understanding means that theory and experiment must complement each other.

The purpose of this book is to teach the how and why of materials behavior and to give some examples of how this knowledge can be applied. This chapter will first explain the general method that will be used and will then define and describe several materials properties that we shall be dealing with.

#### 1-1 Modelina nature

We hear a great deal about first principles in science and engineering. These are laws that cannot be proved mathematically or disproved physically. The "proofs" of Newton's laws of motion and the principles of conservation of mass, energy, and momentum lie in our inability to disprove them. These laws are based upon observation and inductive logic; consequently they cannot be proved by mathematical methods. In this respect, they are like the postulates of plane geometry.

Consider Newton's second law as an example. After observing the motion of many objects under different conditions, Newton concluded that the motion of bodies could be expressed mathematically, and the result was his second law (force is proportional to the rate of change of momentum). In reaching this conclusion, Newton took the results of a large number of observations and generalized them, as shown schematically in Fig. 1-1(a). The mental process of going from a large number of specific cases to the single law which governs all of these cases is called inductive logic. It is not mathematically rigorous because all possible specific cases have not been considered. The inductive logic process is a difficult one and often requires a combination of great intuition and firm logic from the thinker, as in Newton's case. Once the inductive thinking has been done and the general law established, the solution of specific cases becomes much easier. We can then start with the general law and apply it to a specific case with mathematical precision. This is called deductive logic and is illustrated in Fig. 1-1(b),

Consider the logical process that takes place when we solve a dynamics problem. Starting with Newton's second law, we follow one of the paths shown in Fig. 1-1(b) to find a solution. The answer is only as good as the

Fig. 1-1. Inductive and deductive logic. (a) Inductive logic takes the results of many specific cases and finds a general case applicable to all of the specific cases. (b) Deductive logic applies the general case to a specific case. This can be done with mathematical rigor.



General case

general law that we started with, and the validity of this law rests upon inductive logic. As previously stated, inductive logic is not generally as rigorous as deductive logic. For example, Newton's observations did not include all objects moving under all conditions. If they had, he would have found that his second law was not correct when a body traveled at very high velocities. Errors in Newton's law are not usually detectable unless the speed of the object being studied is about 1½ of the speed of light or greater (speed of light = 186,000 miles/sec). Therefore, Newton's laws are usually applicable to engineering problems, but the relativistic mechanics of Einstein must be used for extremely fast-moving objects. For example, electrons can be accelerated in a cyclotron to speeds at which Newton's second law does not annly.

In many physical situations, the inductive logic is accomplished by postulating a "model" and then assuming that nature behaves in a manner which can be predicted deductively from the model. In terms of Fig. 1-1, this would involve substituting the word model wherever general case appears. Once the model is established, it can be applied to specific cases with mathematical rigor, as in Fig. 1-1(b). The solution to a problem is only as accurate as the model. Perhaps one of the best known models of nature is the picture of an atom which has a positive nucleus and electrons orbiting the nucleus. This model was assumed or postulated based upon inductive logic. Once a model is assumed, calculations can be performed using the model, and the results can be compared to experimental data. If the calculations agree with observation, the model is good and may be dignified by calling it a theory or a law. If calculation and observation are not in agreement, the model must be changed. The model of the atom has, in fact, changed as a result of quantum mechanics. The electron is often not considered to be a particle but is visualized in terms of probabilities and waves. The wave model has been able to explain more observations than the particle model.

At this point the reader may be tempted to ask, "What has all this got to do with materials science?" Models of solids will be used throughout this book. In discussing the various phenomena that are of interest, the following method will be used. First, we shall discuss some results that have been obtained experimentally. We shall then construct a model that describes what is happening in the solid, on the atomic scale. These models will be concerned with the way in which the atoms are arranged in the solid, the forces (or bonds) that hold the atoms together, and the conditions under which the atoms rearrange themselves into different configurations. The model will be used as the basis for deriving equations and performing calculations. The calculated quantities will then be compared to the experimental data that we started with, thus providing a check on the validity of the model. The purpose of the procedure is not to prove analytically what we already know experimentally. Once a valid model has been constructed, it can be applied to other materials operating under different conditions. The model becomes part of the theoretical basis of materials science and helps us to predict materials properties and intelligently extrapolate existing data. The models should provide the reader with a "mental picture" of what is happening within a solid under different conditions and of how these happenings affect materials behavior.

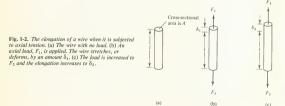
The properties of materials can be changed and manipulated by subjecting the materials to various processes. They can be made stronger, weaker, harder, more ductile, etc., by proper processing. Knowledge of what is happening during these processes enables us to manipulate materials properties to our advantage. Thus, understanding the how and why of materials behavior has important practical consequences. Occasionally a model may be used which appears to be unrealistic or even crude to the reader. This is probably an indication that more knowledge is needed. As the pool of knowledge grows, the models will become more soohisticated and will reflect nature more accurately.

The rest of this chapter will discuss several of the observed properties of materials. The discussion will be based upon experimental data. The remainder of the book will explain why the materials behave in this way, how their behavior can be altered, and how much the properties can be changed.

#### 1-2 Elasticity and Hooke's law

The behavior of a solid material, when it is subjected to forces, is of fundamental interest to engineers since most of the things that we design must withstand applied forces. Many solid materials behave elastically when subjected to a force (or load). By elastically, it is meant that the solid deforms when it is loaded but returns to its original condition when the force is removed. The most familiar elastic material is probably rubber; however, elastic behavior is common to metals, ecramics, and polymers as well. Experience tells us that if a large load is placed upon a solid, it may deform permanently or fracture. This behavior will be covered in Section 1-3.

Robert Hooke (1653–1703) experimented with the elastic properties of metal wires. He was able to generalize his results into a mathematical expression called Hooke's law. The experimental method used by Hooke is shown schematically in Fig. 1-2. A wire specimen having length I and cross-sectional area A is shown in Fig. 1-2(a). When a tensile load  $F_1$  is placed on the wire [Fig. 1-2(b)], the length increases by an amount  $\delta_1$ . The increase in length is called the elongation. As the load increases, the elon-



gation increases. This is shown in Fig. 1-2(c), where the load on the wire has been increased to  $F_3$  and the corresponding elongation is  $\delta_2$ . Hooke's experiments consisted of determining the elongation,  $\delta_2$  as a function of the three parameters  $F_1$ ,  $I_1$  and  $I_2$ . Three separate sets of tests were performed, as described below.

1. A wire of a given initial length and cross-sectional area was subjected to a number of different loads. Elongation was measured as a function of the load, and it was found that  $\delta$  was proportional to F. Thus,

$$\delta \propto F$$
 keeping  $l$  and  $A$  constant (1-1)

The next set of experiments determined the effect of wire length on elongation. A number of wires having different lengths but the same cross section were subjected to identical loads. It was found that elongation was proportional to length:

$$\delta \propto l$$
 keeping F and A constant (1-2)

3. The third variable investigated was the cross-sectional area. For these experiments, a number of wires having the same length but different cross sections were subjected to identical loads. The elongation was found to be inversely proportional to A:

$$\delta \propto \frac{1}{A}$$
 keeping F and l constant (1-3)

Equations 1-1, 1-2, and 1-3 are all satisfied by the single proportionality

$$\delta \propto \frac{Fl}{A}$$
 (1-4)

Equation 1-4 can be written as an equation rather than a proportion by simply introducing a constant. Let the constant be E. Then

$$E\delta = \frac{Fl}{A}$$

and rearranging this equation yields

$$\frac{F}{A} = E \frac{\delta}{l} \tag{1-5}$$

The quantity F/A is called the *stress* and is given the symbol  $\sigma$ . It is the total applied force divided by the cross-sectional area and has units of force per unit area (psi). The quantity  $\delta/l$  is defined as strain and is given the symbol  $\sigma$ . It has units of length per unit length (inches per inch). E is the proportionality constant and is called the modulus  $\sigma/l$  elasticity. Thus,

$$\sigma = E\varepsilon$$
 (1-6)

Equation 1-6 is Hooke's law and expresses the linear relationship between stress and strain. The basis of its derivation rests strictly on the observation and measurement of materials under load. It was originally



Fig. 1-3. A plot of stress vs. strain for the region in which a material shows elastic behavior.

derived for metals and accurately describes the behavior of many, but not all, elastic solids. Rubber does not show the linear relationship between  $\sigma$  and  $\epsilon$ , for example. In Chapter 6, we shall derive Hooke's law from an atomic point of view using a particular model to represent the solid.

Apparatus are available for obtaining data from which curves of stress vs. strain can be plotted. Figure 1-3 shows the elastic part of a stress-strain diagram. The slope of the line is the elastic modulus. This can be seen by differentiating equation 1-6:

$$\frac{d\sigma}{d\varepsilon} = E$$
 (1-7)

The elastic stress-strain curve of a particular material depends only on the modulus of elasticity and not on the dimensions of the specimen. The elastic modulus is a property of the material and is a measure of its stiffness. A high elastic modulus implies a large resistance to deformation, or a stiff material. Values for the elastic moduli of various materials are given in Appendixes A, B, and C.

#### Example 1-1

An aluminum bar is 3 ft long and has a rectangular cross section measuring 2 by 1 in. A tensile force of 5000 lb is applied to the bar.

- (a) Calculate the strain of the bar.
- (b) Calculate the elongation of the bar.
  - (a) The strain can be found from equation 1-6:

$$\varepsilon = \frac{\sigma}{E}$$

σ can be found from the given data:

$$\sigma = \frac{F}{A} = \frac{5000}{(2 \times 1)} = 2500 \text{ lb/in.}^2 \text{ (psi)}.$$

From Appendix A,  $E = 9.9 \times 10^6$  psi for aluminum:

$$\varepsilon = \frac{\sigma}{E} = \frac{2500}{9.9 \times 10^6} = 2.52 \times 10^{-4} = 0.000252 \text{ in./in.}$$

(b) The total elongation can be found from the definition of strain,  $\varepsilon = \delta/l$ :

$$\delta = \varepsilon l = (2.52 \times 10^{-4}) (3) (12) = 9.1 \times 10^{-3} \text{ in.}$$

Note that the strain is simply the elongation of a unit length (1 in.) of the bar.

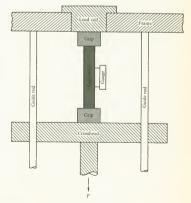
Question

Question 1: Steel has an elastic modulus of 30 × 10<sup>6</sup> psi, while that of copper is 18 × 10<sup>6</sup> psi. A bar of each of these is subjected to a stress of 3000 psi. (a) Calculate the strain for each material. (b) Which is stiffer.

#### 1-3 Permanent deformation and fracture

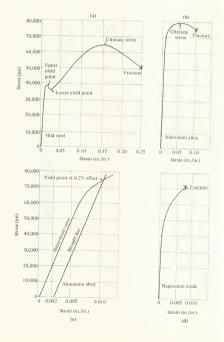
Experience tells us that there are situations in which a stressed material will not return to its original shape when the load is removed. An everyday example of this is bending copper wire to a desired shape. If the wire does not return to its original shape when the load is removed, it is said to be permanently deformed. Permanent deformation is caused by stressing a material beyond its elastic limit. Some materials will fracture before any permanent deformation occurs. If we try to bend a rod of ordinary glass at room temperature, for example, the glass will fracture before it shows permanent deformation. Permanent deformation is desirable when materials are being formed into usable shapes but is undesirable in many other situations, such as when materials are used for structural members.

Fig. 1-4. A schematic drawing of a testing machine. The specimen is held by grips and a load is applied to the monable crasshead. This load is transmitted to the specimen and causes elongation. The specimen is in tension for this arrangement, Reversing the direction of the load subjects the specimen of compressive stress.



Fracture is usually (but not always) undesirable in engineering applications. The behavior of solids stressed beyond the elastic range is an important facet of materials science. This section briefly discusses the

Fig. 1-5. Stress-strain diagrams for three different materials. (a) The diagram for mild steel shows a very well-defined yell point. (b) The yield point in the aluminum alloy is poorly defined. (c) For curves such early, the yield point is defined at 0.2% offset strain. The figure shows the construction of inding this point. (d) The stress diagram of magnetism oxide shows small strain prior to fracture. This diagram is typical of brintle materials.



stress-strain diagrams of materials when they are stressed until they fracture.

Stress-strain diagrams are usually obtained by using a testing machine such as the one shown schematically in Fig. 1-4. The specimen to be tested is shown in the machine. One end of it is fixed to the frame of the machine by means of grips (or clamps), while the other end is similarly fastened to the movable crosshead. A load, F, is placed on the crosshead and the specimen elongates. Power to move the crosshead comes from a mechanical or hydraulic drive system. The magnitude of the load is measured by the load cell. The arrangement shown in Fig. 1-4 places the specimen in tension. Most testing machines have provisions for reversing the direction of the load, in which case the specimen is loaded in compression. Elongation is measured by attaching a gauge to the specimen. The gauge measures the distance between two points on the specimen. A variety of gauges is available; a number of them measure the distance between points that are 2 in. apart when the specimen has no load. As the load increases, the distance between the points increases. The test thus gives elongation as a function of load. Stress and strain can be calculated from load-elongation data, and a plot of stress vs. strain can be made for the material. Some typical stress-strain diagrams for specimens loaded in tension are shown in Fig. 1-5. The first one [Fig. 1-5(a)] was made using a specimen of steel with a low carbon content. The linear part of the curve at the left side represents elastic behavior. The stress which is labeled "upper yield point" marks the end of the elastic region. If the steel is stressed beyond this value, it will deform permanently. This stress value is also called the yield strength. Figure 1-5(a) shows a well-defined upper yield strength. The ultimate strength is shown in the figure as well as the point of fracture. Note that the specimen elongated 24% before fracturing. Figure 1-5(b) is the stress-strain diagram for a high-strength aluminum alloy. It does not show a well-defined yield point. For diagrams such as these, it is customary to define the offset yield strength. The method for determining this quantity is illustrated in Fig. 1-5(c), which shows the elastic region of Fig. 1-5(b) magnified. A line is drawn parallel to the elastic portion of the curve, intersecting the strain ordinate at a predetermined value. The value used in the figure is  $\varepsilon = 0.002$  (or 0.2%). The point at which this line intersects the stress-strain curve is called the yield strength at 0.2% offset strain. It is often used for defining yield strength. Strain is often expressed as percent rather than as inches per inch. The two are equivalent.

Brittle materials show little or no permanent deformation prior to fracture. Many ceramics behave in this way, for example, magnesium oxide, whose stress-strain diagram is shown in Fig. 1-5(d). Brittle behavior is also exhibited by some metals and some plastics. The small elongation prior to fracture means that the material gives no indication of impending fracture, and brittle fracture usually occurs rapidly. It is often accompanied by a loud noise which has been known to send designers back to the drawing board.

#### Question

Question 2: A piece of copper having a cross-sectional area of  $\frac{1}{2}$  in. 2 was placed in a testing machine and stressed in tension until fracture occur-

red. The applied load at fracture was 9000 lb. A gauge was placed on the specimen before the load was applied. The gauge measured the distance between two points that were 2 in. apart when the specimen had no load (this is called a 2-in. gauge length). When the specimen fractured, the distance between the points was 2.88 in. Calculate the stress and strain at fracture, based on the initial (unloaded) area of the specimen and the initial distance between the two points on the specimen.

#### 1\_1 Engineering and true stress-strain diagrams

Stress-strain diagrams are derived from the load vs. elongation data found by testing. There are two different ways of handling these data, and the shape of the stress-strain curve depends on which method is used. The difference between the two methods can be explained by first considering the sequence of events that occurs during a tensile test. In the early stages of the test, the specimen is in the elastic region. For most metals and ceramics, elastic behavior is limited to strains of less than about 0.5%. The specimen elongates elastically and the cross-sectional area diminishes slightly. The reduction in the area during elastic behavior is negligible for most materials. This is not true when permanent deformation occurs. The total volume of the specimen is constant during permanent deformation; therefore

$$A_0l_0 = A_il_i$$
 (1-8)

where the subscript 0 denotes the dimensions at the start of the test, while i denotes an instantaneous value, measured during the test. As I increases, A decreases. The specimen deforms homogeneously during the first portion of the plastic deformation (the terms permanent and plastic will be used interchangeably). As the test progresses, one region of the specimen begins to deform much quicker than the rest. This localized strain results in the formation of a necked region, as shown in Fig. 1-6. The specimen in the figure is made of mild steel, and it was stressed in tension until fracture. The fracture can be seen in the necked region. The cross-sectional area in

Fig. 1-6. A mild steel specimen that has been loaded in tension until it fractured. The specimen was originally cylindrical. The specimen has necked in the neighborhood of the fracture.



the necked region is considerably smaller than that in the remainder of the specimen.

The reduction in area as the test progresses raises a question about what area should be used for calculating stress when the load is known. There are two possibilities; either the original area or the actual area of the specimen can be used. In Question 2, stress was calculated based upon original area. This is called engineering stress. The stress can also be based upon the actual area, and it is then called true stress. Thus,

$$\sigma_{\text{true}} = \frac{F}{A_i} \tag{1-9}$$

A similar situation arises with strain. The diagram of Fig. 1-5(a) provides us with an example. Suppose we want to consider the strain of the specimen when the stress is increased from 58,000 to 60,000 psi. At 58,000 psi the strain is shown as 0.10, or 10%, where can increase the stress to 60,000 psi and measure the elongation,  $\Delta I$ , due to the stress increase. Our definition of strain is  $\varepsilon = \Delta I/I$ . For the example being considered, what is I? Let us assume that a 2-in. gauge length was used when the test began. The actual distance between the two points, when the stress is 58,000 psi, is 2.2 in. If we use the original length to calculate strain, we are calculating engineering strain. If the instantaneous length is used, we are calculating true strain. An expression for true strain can be found by considering the definition

$$\varepsilon = \frac{\delta}{l}$$

In differential form this becomes

$$d\varepsilon = \frac{dl}{l}$$
 (1-10)

where *dl* is an infinitesimal elongation. Equation 1-10 can be integrated to find the true strain;

$$\varepsilon_{\text{true}} = \int_{l_0}^{l_t} \frac{dl}{l} = \ln \frac{l_t}{l_0}$$
 (1-11)

Both the engineering and true stress-strain diagrams are shown for copper in Fig. 1-7. The ultimate strength for the engineering curve corresponds to the beginning of necking. The rapid area reduction that accompanies necking causes the curve to fall. This does not happen with the true stress-strain curve. Recall that strain is not homogeneous after necking begins. Because one part of the specimen is elongating more than the rest, it is not meaningful to use the entire specimen length for finding strain, as is done in equation 1-11. True strain can be expressed in terms of area by substituting equation 1-8 into 1-11.

$$\varepsilon_{\text{true}} = \ln \frac{A_0}{A_c}$$
(1-12)

This expression is used for the nonhomogeneous part of the deformation.

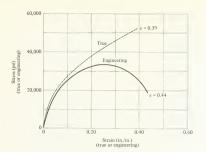


Fig. 1-7. The true stress-strain diagram and the engineering stress-strain diagram for polycrystalline copper. The true stress-strain curve continues to rise until fracture, whereas the engineering curve shows a maximum prior to fracture.

Most of the diagrams used in this book will be engineering stress vs. engineering strain, with true stress-true strain diagrams being required occasionally.

Ductility is a measure of the amount of permanent deformation that has occurred when a material reaches its breaking point. It can be expressed as the percent reduction in the area of the specimen at fracture:

% reduction in area = 
$$\frac{\text{initial area} - \text{final area}}{\text{initial area}} \times 100$$
 (1-13)

It is sometimes expressed in terms of the percentage elongation of a specimen at fracture.

Stress-strain diagrams can also be made for specimens stressed in compression instead of tension. The procedures are practically the same and the stress-strain diagrams generally show a region of elastic behavior followed by plastic deformation.

#### Questions

Question 3: Figure 1-7 shows that a copper test specimen failed at a true strain of 0.39. What is the percentage reduction in area at fracture?

Question 4: Figure 1-7 shows that a piece of polycrystalline copper fractured at an engineering strain of 0.44, which corresponded to a true strain of 0.39. (a) Using the observed value of true strain and equation 1-11, calculate the engineering strain at fracture. (b) Why is the calculated value different from the measured value?

#### 1-5 Toughness

Toughness is a measure of the amount of energy which a material can absorb before fracturing. It becomes an important engineering consideration when we are concerned with the ability of a material to sustain an impact load without fracturing. The energy absorbed by a specimen prior to fracture can be found from its load-deformation curve. Consider the bar in Fig. 1-8. One end is securely fastened while a load, F, is applied to the other end. The elongation,  $\delta$ , due to the load is shown. As Fincreases,  $\delta$  increases. Let  $\delta$ ' be the deformation of the bar when it fractures. The work done on the bar by the force be expressed as

$$W = \int_{-\delta}^{\delta'} F d\delta$$

This integral is just the area under the load-deformation curve. Figure 1-9 shows load-deformation curves for two specimens which have the same dimensions. Curve A represents a brittle material, and the area under the curve is cross-hatched. Curve B was made for a ductile material and shows a much larger area (shaded region). Ductile materials generally have a

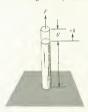
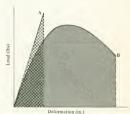


Fig. 1-8 (left). A bar of material with an applied tensile load. The elongation is given as δ, and δ' is the elongation at fracture.

Fig. 1-9 (below). Load-deformation curves for a brittle material (curve A) and a ductile one (curve B). The areas under the curves represent the energies absorbed by the specimens prior to fracture.



13

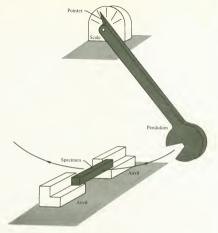


Fig. 1-10. A schematic diagram of an impact-testing machine. The pendulum strikes the specimen at the bottom of its swing and causes the specimen to fracture.

better energy-absorbing capability than brittle ones, which is in accord with our experience.

Toughness is often measured by impact testing rather than by load-deformation curves. The setup for an impact test is shown schematically in Fig. 1-10. A specimen with a notch cut in it is held in the anvil. The anvil is anchored to the base of the impact-testing machine. The machine has a pendulum, as shown. The test is performed by raising the pendulum to a predetermined height and releasing it. The pendulum strikes the specimen, fractures it, and moves upward. By measuring the initial pendulum height and the height which the pendulum reaches after the impact, the energy absorbed by the specimen can be found. The heights can be determined from the pointer and scale. The sizes and shapes of specimens used for impact testing have been standardized, and so have the mass and length of the pendulum. As a consequence of the standardization, impact test results for various materials taken with different testing machines can be compared directly.

#### Question

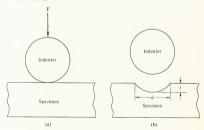
Question 5: A space vehicle is designed to make a single landing on a planet and then return to earth. The ship lands on four pads. The pads are attached to the body of the ship by long rods. Should a tough material be used for the rods? Why?

#### 1-6 Hardness

Hardness is a measure of the resistance of a material to permanent deformation. It is commonly measured by placing an indenter in contact with the material being tested. A known load is placed upon the indenter, as shown schematically in Fig. 1-11(a). The indenter material is much harder than the specimen, with hardened steel, tungsten carbide, or diamond being commonly used. After the indentation has been made, the indenter is removed [Fig. 1-11(b)]. The hardness number depends on the geometry of the indentation and the type of test used. The type of test often leads to some confusion. The four different types of hardness tests are summarized in Table 1-1, and it is seen that different types of indenters are used for different tests. The hardness number depends on the applied load and the shape of the indentation, for the first three tests shown (Brinell, Vickers, and Knoop). For the Rockwell hardness test, both the shape of the indenter and the load are specified. The hardness number depends only on the depth to which the indenter penetrates the specimen. The hardness tests given in Table 1-1 have been found to be convenient and have evolved as standard tests.

From the procedure used for hardness tests, it is apparent that hardness depends on the ease with which materials undergo plastic deformation. Ease of deformation, in turn, is related to the yield stress and the ultimate stress. The relationship between hardness and strength can be found

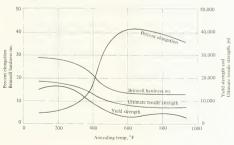
Fig. 1-11. The hardness test. (a) A loaded indenter is placed in contact with the specimen. The indenter is shown as a sphere; however, other shapes are also used (Table 1-1). Of The hardness unmber depends on the indentation that remains when the indenter is removed. The dimension d is used in the Brinnell test, whereas t is used in the Rockwell test.



Test	Indenter	Shape of inc Side view	Load	Formula for hardness number		
Brinell	10-mm sphere of steel or tungsten carbide	→ D → d ←		P	BHN = ${\pi D(}$	$\frac{2P}{D - \sqrt{D^2 - d^2}}$
Vickers	Diamond pyramid		- Antick	P	VHN = 1.72	P/d <sub>1</sub> <sup>2</sup>
Knoop microhardness	Diamond pyramid	t/b = 7.11 b/t = 4.00	T .	P	KHN = 14.2	P/13
Rockwell A C D B F G E	Diamond cone  lacin. diameter steel sphere lacin. diameter steel sphere	120°		60 kg 150 kg 100 kg 100 kg 60 kg 150 kg 100 kg	$egin{aligned} R_A = \ R_C = \ R_D = \ R_B = \ R_F = \ R_G = \ R_E = \ \ \ \ \ \ \ \ \ \ \ \ \ \ \ \ \ \ $	100–500 <i>t</i>

\* H. W. Hayden, W. G. Moffatt, and J. Wulff, The Structure and Properties of Materials, Vol. III, Wiley, New York, 1965.

Fig. 1-12. The effect of amonaling temperature on the properties of cold-rolled, high-purity, sheet adminum (0.04 th. nihek). The alminum was subjected to an area reduction of 87% after which specimens of the sheet were amonded at various temperatures for 1 hr. The properties of the specimens were then determined, (U.S. Department of Commerce Circular C447, Mechanical Properties of Metals and Alloys, 1943.)



empirically for a particular material and a particular hardness test. Such relationships are very useful in the quality control of mass-produced items. Hardness testing is much simpler than testing to obtain stress-strain diagrams; it is also nondestructive. Hardness is sometimes a confusing concept because of the arbitrariness of the standard tests. The tests are admittedly arbitrary and have evolved to their present form because of convenience. The hardness is related to fundamental materials properties such as strength, although the relationship must be found experimentally.

#### Ouestion

Question 6: A material is found to have a hardness number of 50 as measured on the Rockwell C scale. This is represented as 50 Rockwell C. What was the shape of the indenter and what load was used for this test?

## 1-7 Work hardening and annealing

Man has known since prehistoric times that the properties of solids depend, to some extent, on the processes which they have been subjected to. For example, when a material has been permanently deformed, it is found that its yield stress and hardness have increased while its ductility has diminished. This phenomenon is known as work hardening. When a workhardened material has been heated to a sufficiently high temperature (below the melting point), held there for a period of time, and then properly cooled, it is found that the material becomes softer and has a lower yield stress but is more ductile. This process is called amealing and has been used for many years. Prehistoric man formed usable implements from metals by alternately deforming and heating them. This is sometimes referred to as a "heat it and beat it" process.

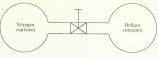
Figure 1-12 shows the effect of annealing on a piece of high-purity aluminum sheet. The sheet was first subjected to an area reduction of 87%; that is, it was deformed until its cross-sectional area was reduced by 87%, after which pieces of it were annealed at different temperatures for 1 hr. Various properties were then measured and plotted as a function of annealing temperature. The results in the figure show that heat treatment has a very significant effect on the properties. Cold working and annealing are two of the simpler processes that can be used to alter the properties of many materials. They will be described more completely in Chapters 8 and 9.

## 1-8 Diffusion

Two containers of gases at equal pressures, separated by a valve, are shown in Fig. 1-13. A short time after the valve is opened, it is found that a mixture of N<sub>2</sub> and He exists in both chambers. Apparently, nitrogen atoms have diffused into the helium container and vice versa. Diffusion would also be observed if the containers were filled with two mutually soluble liquids, such as alcohol and water. Many solids are soluble in other solids and show the effects of diffusion. Solid solubility and diffusion will be discussed in Chapters 10 and 11.

As an example of solid-state diffusion, consider the blocks of copper

Fig. 1-13, Two containers of aas at the same pressure and separated by a valve. The gases diffuse into both containers when the valve is opened.



and nickel shown in Fig. 1-14(a). When the blocks are initially placed in contact, a curve of copper concentration as a function of position can be drawn [Fig. 1-14(b)]. All of the copper is on the left side. The blocks can then be heated to a temperature below the melting point of either the copper or nickel and maintained there for a period of time. If a curve of copper concentration as a function of position is again drawn [Fig. 1-14(c)], it is found that nickel has migrated into the copper and vice versa. Solid-state diffusion is slower than diffusion in the liquid or gaseous state but is nevertheless an important and often used phenomenon. Transistors and diodes are often fabricated by diffusing an appropriate material into a semiconductor: the process is called doning

Diffusion can also be used to bond metals together, although it is more expensive than conventional methods such as welding. A diffusionbonded titanium specimen is shown in Fig. 1-15. Two pieces of titanium were placed in contact and heated to a temperature of 450°C, under vacuum. Atoms diffused between the two pieces and bonded them together. After bonding, the specimen was stressed to failure. The figure shows that failure did not occur at the diffusion weld (or bond). The position of the bond is indicated by the arrow. This process can be very useful for joining dissimilar metals which are not amenable to conventional welding techniques.

Fig. 1-14. (a) A block of copper and a block of nickel in contact. This arrangement forms a diffusion couple. (b) The concentration of copper as a function of position. All of the copper is on the left side of the diffusion couple, (c) The copper concentration after the diffusion couple has been held at a high temperature for a period of time. The copper has diffused into the nickel and vice versa,

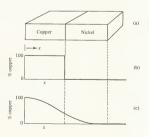




Fig. 1-15. Photograph of a diffusion-welded titanium specimen that has been stressed to failture. The arrow shows the location of the weld joint. [T. H. Batzer and R. Bunshah, J. Vacuum Sci. Tech. 14: 27 (1969).]

# 1-9 Classification of materials

The materials discussed in this book can be grouped into three general categories. These are metals, ceramics, and polymers. The differences between them are based upon the manner in which the atoms bond together and the geometric arrangement of the atoms in the solid. We shall deal with both pure metallic elements and alloys. Alloys are solids that are composed of more than one metallic element. Ceramics are solids that are made up of both metals and nonmetals. This class of materials includes the glasses and a number of useful high-temperature solids. The most familiar examples of polymers are plastics and rubber. Polymers are made up of very large molecules. Those of engineering interest are generally compounds of carbon or silicon.

# 1-10 Explanation of the observed phenomena

A number of observed physical phenomena have been discussed briefly in this chapter. The objective of the remainder of the book is to teach why these phenomena occur as they do and what can be done to modify the properties of materials. It is usually necessary to understand why something functions as it does before we can effectively attempt to change its behavior. This section will discuss what the rest of the book is about. The reader may want to review it from time to time because of a problem that is associated with introductory materials science courses. The student often loses sight of the objectives as he is acquiring the necessary background for understanding materials. This is particularly true in the early part of the course.

The properties of materials have their origin in the chemical bonds that hold the atoms of the solid together. This is the starting point for the

explanation of the mechanical properties of materials, and bonding in solids forms the basis of Chapter 2. In many solids it is found that the atoms arrange themselves in an ordered manner. These geometrically ordered arrangements are called crystal structures. Both crystal and amorphous structures are discussed in Chapter 3. The structure as well as the bonding influences physical properties. The crystal structures of Chapter 3 are ideal crystals and are seldom found in nature. Imperfections are formed while the solid is freezing from the liquid state. Solidification and imperfections form the subject matter of Chapter 4. These chapters provide a necessary background. It was mentioned earlier that analysis and experiment must necessarily complement each other in materials science. Chapter 5 discusses several powerful experimental techniques used in the field. The experimental results verify the models used in Chapters 2, 3, and 4.

Explanation of the observed phenomena which were discussed in this chapter begins with Chapter 6. Hooke's law is derived by considering the bonding and structure of a real solid, and thermal expansion is explained in the same terms. Chapter 7 explains why brittle fracture occurs, while Chapter 8 treats plastic behavior and work hardening. The effect of temperature on mechanical properties and the associated phenomenon of annealing are covered in Chapter 9.

The topics covered up to this point are largely concerned with pure materials. Chapters 10 and 11 deal with diffusion and the solubility of materials. Several methods of varying the mechanical properties of materials will have been discussed up to this point, but the supply of methods has by no means been exhausted. Chapter 12 emphasizes several means for strengthening materials. The methods discussed in this chapter rely upon material presented in the earlier chapters and hopefully give the reader an understanding of both how and why the properties of materials can be manipulated.

#### Problems

- 1 A bar of stainless steel (18% Cr. 8% Ni, 74% Fe) having a diameter of 1 in. and a length of 2 ft supports a 20,000-lb load. The elastic modulus has a value of 30 million psi. (a) What is the stress on the bar? (b) What is the strain? (c) What is the total elongation of the bar due to the load? (d) The yield strength of the bar is 100,000 psi. How large a load can it support without deforming permanently?
- 2 (a) The diameter of the bar in Problem 1 is increased to 1.414 in. Calculate each of the quantities asked for in that problem. (b) If the length of the bar is doubled but the diameter is kept at 1 in., calculate each of the quantities asked for in Problem 1.
- 3 A specimen of an aluminum alloy has a cross-sectional area of ½ in2. It was tested to fracture in a testing machine. A gauge was placed over a 2-in. length of the specimen before the test started, and this length was measured during the test. The data obtained are shown in the accompanying table.
  - (a) Draw the engineering stress-strain diagram, (b) Find Young's modulus. (c) Find the yield point at 0.2% offset strain. (d) The area at the

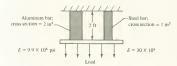
plane of fracture was 50% of the original cross section. What is the true fracture stress of the specimen?

Load (lb)	Length (in.)
1,000	2.0004
2,000	2.0008
5,000	2.0020
10,000	2.0040
15,000	2.0062
20,000	2.022
25,000	2.80
20,000	3.32
15,000	3,46 fract

4 Strength is related to hardness, and the hardness of a material can be used to estimate strength. For steel, there is a "rule of thumb" that the ultimate tensile strength is 500 times the Brinell hardness number. Measured hardness and tensile strengths are given for nine steels. Plot hardness vs. tensile strength and check the validity of the "rule."

Ultimate tensile strengt)
49,500
59,000
71,000
86,300
92,000
98,600
115,000
139,000
152,000

5 A load is supported by a steel bar and an aluminum bar, as shown in the accompanying figure. The aluminum has a yield point of 23,000 psi and the steel yields at 75,000 psi. How large a load can this arrangement support before either bar shows permanent deformation?



Answers

Question 1: (a) Steel: 
$$\varepsilon = \frac{\sigma}{E} = \frac{3000}{3 \times 10^7} = 10^{-4} \text{ in./in.}$$
 Copper: 
$$\varepsilon = \frac{\sigma}{E} = \frac{3000}{18 \times 10^9} = 1.67 \times 10^{-4} \text{ in./in.}$$

(b) Steel has a higher modulus of elasticity than copper and is therefore stiffer. Note that when two materials are subjected to the same stress, the stiffer one shows smaller strain.

Question 2: 
$$\sigma = \frac{F}{A} = \frac{9000}{1/2} = 18,000 \text{ psi}$$
 
$$\varepsilon = \frac{\Delta l}{l} = \frac{2.88 - 2.00}{2.00} = 0.44 = 44\%$$

Question 3: 
$$\ln \frac{A_0}{A_i} = 0.39$$
  $\frac{A_0}{A_i} = 1.478$   $A_0 = 1.478A_i$ 

Substituting into equation 1-13,

% reduction = 
$$\frac{1.478A_i - A_i}{1.478A_i} = \frac{0.478}{1.478} = 0.324 = 32.4\%$$

$$\begin{split} \textit{Question 4:} \text{ (a) } & \epsilon_{\text{true}} = \ln \frac{l_i}{l_0} = 0.39 \qquad \frac{l_i}{l_0} = 1.478 \qquad l_i = 1.478 l_0 \\ & \epsilon_{\text{engineering}} = \frac{\Delta l}{l} = \frac{l_i - l_0}{l_0} = \frac{1.478 l_0 - l_0}{l_0} = 0.478 = 47.8\% \end{split}$$

- (b) The measured engineering strain is lower. This is due to the fact that equation 1-11 assumes homogeneous deformation. Plastic deformation after necking begins is nonhomogeneous and occurs mainly in the necked region. The high-stress portion of the true stress-strain curve uses equation 1-12, not 1-11.
- Question 5: Yes. The space ship will land on the planet with an impact. The rods must be capable of absorbing the impact energy without fracturing. Some permanent deformation of the rods might be allowed because the ship will not use the rods for another landing (assuming that a soft-earth landing is not required).
- Question 6: From Table 1-1, the indenter was a cone-shaped diamond. The included angle at the cone tip is 120°. The load on the indenter was 150 kg. Note: The Rockwell C scale is used for measuring the hardness of many types of steel.

## CHAPTER 2

# Atomic Structure and Bonding

THE PROPERTIES OF MATERIALS depend on both the chemical bonds between the atoms composing the solid and the manner in which these atoms are stacked together to form the solid (the structure). The structure which the atoms form depends on the types of bonds which hold the atoms together. The logical starting point for the study of materials science is the basic building block, the atom. The first part of this chapter is therefore concerned with atomic structure. This leads to a discussion of the periodic table of the elements. The atoms must bond together to form solids; therefore a knowledge of chemical bonding is necessary for understanding the properties of solids. Chemical bonding is treated in the second part of the chapter. The three primary types of bonds (ionic, covalent, and metallic) as well as weaker secondary bonds are treated. The directional nature of the bonds is a primary consideration in determining the structure of a solid; consequently this will be stressed somewhat. The structure of solids will be covered in Chapter 3. The objective of this chapter is to present several concepts of atomic structure and chemical bonding that are necessary for a basic understanding of the properties of engineering materials.

## 2-1 Atomic structure

At the turn of the twentieth century, the atom was visualized as being composed of a positive nucleus with robiting electrons. The motion of the electrons was assumed to be governed by the classical laws of physics. This model predicted some phenomena which were not observed and could not explain several observable phenomena. For example, consider an electron orbiting a proton (a hydrogen atom) as shown in Fig. 2-1(a). The classical physical laws require that the moving electron continuously emit radiation. If this occurred, conservation of energy would require that the distance between the electron and proton diminish. Thus, the model predicted that the electron followed a spiral course such as that shown in Fig. 2-1(b) and eventually united with the proton. This is not observed. Because the results obtained from calculations based upon the model did not agree with observation, the model had to be altered.

In 1900 Max Planck found that radiation was emitted in small bundles,





Fig. 2-1. An electron orbiting a proton.
(a) A circular orbit. (b) the spiral that would be followed if the electron constantly emitted radiation.

or "quanta." This observation formed the basis of quantum theory and resulted in a somewhat different model of the atom. Neils Bohr applied this concept to the hydrogen atom in 1913. Bohr assumed that only certain electron orbits were permitted and that an electron traveling in one of the allowed orbits did not emit radiation. If, however, an electron switched from one allowed orbit to another, specific amounts of energy would be emitted or absorbed. Bohr's theory was verified by experiment and worked well for hydrogen.

Quantum theory was mathematically formalized by Schroedinger in 1926 when he postulated the wave equation. Schroedinger did not consider the electron as being in a particular position in space, but dealt with the probability of finding the electron at various positions in space. This probability is defined in terms of wave functions. This atomic model is considerably different from that of electrons moving around a nucleus. The wave mechanics of Schroedinger will not be used in this book because the mathematics required should be beyond the present ability of the reader. We shall, however, use some quantum mechanics results to show that chemical bonds between atoms can have particular spatial orientations. It is interesting to note that the model of something as basic as the atom has changed very significantly since the turn of this century.

## 2-2 The hydrogen atom

The simplest element which we know is hydrogen, composed of one protion and one electron. This section will discuss the forces which hold the electron and proton together and the energies associated with these forces. The energy equation then will be modified in accordance with Bohr's treatment of the hydrogen atom.

Consider the hydrogen atom of Fig. 2-1(a). We want to write an expression for the total energy of the atom, assuming that the proton is not moving. The electron is in a circular orbit, and an attractive force exists between the proton and the electron because they have opposite electric charges. This force is given by Coulomb's law. The energy of the atom is the sum of two terms, the kinetic energy of the electron and the potential energy due to the Coulomb force. Thus.

$$\mathscr{E}$$
 = energy of atom = potential energy + kinetic energy (2-1)

The potential energy term will be derived first. To quantitatively discuss potential energy, we must first select a potential energy reference level. The potential energy of the two charged particles is taken as zero when they are separated by an infinite distance. Taking this as the starting point, the

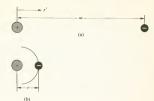


Fig. 2-2. (a) A proton and an electron at rest, infinitely separated from each other. This is selected as the zero-energy configuration. (b) An electron orbiting a proton. The circular orbit radius is r and the proton is at rest.

electron is then brought closer to the proton to form the hydrogen atom. The change in potential energy between the configuration shown in Fig. 2-2(a) and that in Fig. 2-2(b) is just the work done by the Coulomb force during the transition. Thus,

$$V = \text{potential energy} = \int_{r_0}^{r} F \, dr'$$
 (2-2)

where r' is the distance between the proton and the electron as they are being brought together and r is the final distance of separation (or the orbit radius). The force between two charged particles is given by Coulomb's law as

$$F = \frac{-q_1q_2}{r'^2}$$
(2-3)

where

F =force (dynes)

 $q_1$  = charge of the first particle in electrostatic units (esu)

 $q_2$  = charge of the second particle in electrostatic units (esu)

r' = separation between particles (centimeters)

A positive value of F means that the particles attract each other; a negative value means that they repel. We shall use the symbol e to represent the magnitude of the electron charge. Using this notation,  $q_1q_2=-e^2$  for this case. Substituting equation 2-3 into equation 2-2 and integrating,

$$V = \text{potential energy} = \int_{-\infty}^{r} \frac{e^2}{r'^2} dr' = -\frac{e^2}{r}$$
 (2-4)

The kinetic energy of the electron can be found by applying Newton's second law to the circular electron orbit in Fig. 2-2(b):

$$F = ma$$
 (2-5)

The force acting on the electron is the Coulomb force, and the acceleration required for circular motion is given as

$$a = \frac{v^2}{r} \tag{2-6}$$

where v is the electron velocity. Substituting equations 2-3 and 2-6 into 2-5,

$$\frac{e^2}{r^2} = \frac{mv^2}{r}$$

from which

$$\frac{1}{2}mv^2 = \frac{e^2}{2r}$$
(2-7)

providing the kinetic energy term. The total energy of the hydrogen atom is found by substituting equations 2-4 and 2-7 into 2-1. The result is

$$\mathscr{E} = \frac{-e^2}{r} + \frac{e^2}{2r} = -\frac{e^2}{2r} \tag{2-8}$$

This equation gives the energy of a hydrogen atom at rest and was derived using only Coulomb's law and Newton's second law. It shows that as the orbit radius decreases, the energy of the atom decreases. This fact will be quite useful to us. No restrictions are placed upon the orbit radii in this derivation.

Bohr's treatment of the hydrogen atom utilizes equation 2-8; however, he introduced a limitation. The radius of the electron orbit was limited to certain values. The smallest radius which the electron could have was 0.528 Angstrom units (A), where 1Å = 10<sup>-8</sup> cm. The other allowed radii were expressed in terms of the smallest:

$$r_n = n^2 r_1$$
 (2-9)

where

$$n = 1, 2, 3, 4, \dots$$
  
 $r_1 = 0.528 \,\text{Å}$ 

 $r_n$  = allowed radius corresponding to the integer n

The energies which correspond to the allowed orbit radii can be found by substituting equation 2-9 into 2-8:

$$\mathscr{E}_n = \frac{-e^2}{2n^2r_1} \tag{2-10}$$

The subscript n has been added to the energy  $\mathscr E$  to emphasize that the energy depends on the value of n. This form of the energy equation shows that only certain values of  $\mathscr E_n$  are allowed because n is an integer. The energy of the atom is said to be quantized.

## Example 2-1

A hydrogen atom exists with its electron in the state which corresponds to n = 2. The atom undergoes a transition and reverts to the ground state (n = 1). How much energy is emitted by the atom in this transition?

The energy of the atom in each state can be found from equation 2-10. The energy emitted because of the transition is the difference in energy between the two states. Letting  $\Delta \mathcal{E}$  be the energy emitted by the atom.

$$\Delta \mathscr{E} = \mathscr{E}_2 - \mathscr{E}_1 = -\frac{e^2}{8r_1} + \frac{e^2}{2r_1} = \frac{3e^2}{8r_1} = \frac{(3) \ (4.8 \times 10^{-10})^2}{(8) \ (0.528 \times 10^{-8})}$$

 $= 1.635 \times 10^{-11} \text{ ergs} = 10.185 \text{ electron volts}$ 

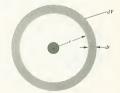
where an electron volt is the energy gained by an electron when it is moved through a potential difference of 1 volt. This unit of energy is often used in atomic calculations:

1 electron volt (eV) = 
$$1.60209 \times 10^{-12}$$
 ergs

Bohr's theory was verified experimentally. Calculations similar to those in the sample problem above can be made, and the energy involved in the various transitions can be calculated. These transitions can be observed in the laboratory, and the energy absorbed or emitted during the transitions can be measured with spectroscopic equipment. Excellent correlation was found between calculated and measured transition energies for the hydrogen atom.

The model was further refined when Schroedinger placed quantum mechanics on a firm mathematical basis. In Schroedinger's formulation we are interested in the probability of finding the electron within a given volume in space. This can be clarified by Fig. 2-3. The hydrogen nucleus is shown. The pertinent question is, "What is the probability of finding the electron within a spherical shell of volume dV?" As shown in the figure, the shell has an inner radius r and an outer radius r r dr. The solution of Schroedinger's equation answers this question, and the probability of finding the electron in the spherical shell of volume dV is plotted as a function of r for a hydrogen atom in its ground state (Fig. 2-4). The maximum in the probability curve occurs at the first Bohr orbit; however, the electron is not required to remain at 0.528 Å. It can be found at other locations.

Fig. 2-3. A hydrogen atom showing the volume dV used for probability calculations.





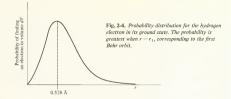


Fig. 2-5. The electron cloud surrounding the nucleus in a hydrogen atom. The darkest region occurs at the first Bohr orbit for a around-state atom.



The probability interpretation enables us to sketch a hydrogen atom in a manner which is somewhat different from that in Fig. 2-1(a). The probability of finding the electron in the shell of volume dV is proportional to the density of dots in Fig. 2-5. The region surrounding the nucleus is sometimes referred to as an electron cloud. The electron cloud in the figure has spherical symmetry and the probability of finding the electron in volume dV depends only on r for the case shown. In some situations this spherical symmetry does not exist, as will be seen in Section 2-9.

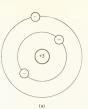
#### Ouestion

Ouestion 1: The negative potential energy in equation 2-4 is sometimes confusing, Consider the following: (a) A 1-lb mass is held 4 ft above the earth. Its potential energy is defined as zero in this state. The mass is dropped and comes to rest on the earth. What is its potential energy after it comes to rest? (b) The same mass is in an airplane at an altitude of 30,000 ft. Its potential energy in this state is defined as zero. What is its potential energy at sea level? (c) Why is the potential energy in equation 2-4 negative?

## 2-3 Shielding

Determining the forces on an electron in a hydrogen atom is straightforward since the Coulomb force is just the attraction between two point charges; the forces are central forces. The situation becomes more complicated when we consider the other atoms. The electron structure of Li is shown in Fig. 2-6(a). The valence electron is attracted to the nucleus but is also repelled by the two inner electrons. The situation can be simplified by considering the nucleus and the inner shell electrons as a "core" which the valence electron orbits [Fig. 2-6(b)]. The electric charge of the core is

Fig. 2-6. The lithium atom.
(a) Diagram of the electrons orbiting the nucleus.
(b) A model in which the core is composed of the nucleus and the filled-shell electrons.





(b)

the sum of the charges that constitute it; consequently the core charge is + le for Li. The model shown in Fig. 2-6(b) is often called a hydrogen-like atom and is fairly good as long as the valence electron does not have a highly elliptic orbit. If it does, it is possible for the valence electron to penetrate the core while orbiting. This would complicate the force calculations. The hydrogen-like model can be used as a first approximation for all of the alkali metals. Generally, this model says that the filled-shell electrons partially shield the valence electron from the nuclear charge.

Figure 2-7 shows a shielding model of beryllium. There are now two electrons outside of the core; consequently the Coulomb force calculations must take account of these. The calculations are more complex for this case.

#### Question

Question 2: The atomic radii of the elements are tabulated in Appendix A.
Lithium has an atomic radius of 1.51 Å, while that of beryllium is
1.11 Å. This means that the valence electrons of Be are closer to the
nucleus than the valence electron of Li. Explain why.

# 2-4 Quantum numbers

The state of an electron in an atom is completely determined by four quantum numbers. If these numbers are known, the electron energy can be found. This section discusses what the quantum numbers represent. The representation will be given in terms of an electron orbiting a nucleus rather than in terms of wave functions, although the wave function can be found

Fig. 2-7. Electron shielding of the nucleus in beryllium.



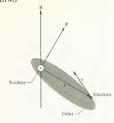


Fig. 2-8. Elliptic electron orbit in a hydrogen atom. P is the orbital angular momentum vector and B is the direction of a magnetic field.

from the quantum numbers. In Section 2-5, we shall use the quantum numbers to "derive" the periodic table of the elements.

The Bohr theory has already provided us with one quantum number; the quantity n in equation 2-9 is called the principal quantum number. For hydrogen, this number alone determines the energy of the atom. The circular orbits postulated in both Fig. 2-2 and the Bohr theory are not the only allowed orbits. Elliptic orbits can also occur as shown in Fig. 2-8. The orbiting electron in the figure has an angular momentum P, where  $P = r \times mv$ . This vector is perpendicular to the plane of the orbit and is a constant for any given orbit. Only certain values of the magnitude of P are allowed; that is, the magnitude of P is quantized. The quantizing of the orbital angular momentum is expressed by the quantum number l, which is related to n.

Allowed values of 
$$l = 1, 2, 3, ..., (n-2), (n-1)$$

This is our second quantum number. Generally, the energy of an electron in an atom depends on l as well as on n. Higher values of l correspond to a more eccentric orbit (or a "flatter" ellipse).

The third quantum numbered is concerned with the spatial orientation of P. Let B in Fig. 2-8 be the direction of a magnetic field. Classical mechanics does not restrict the direction of P (or the orientation of the orbit plane). Quantum mechanics, however, tells us that the component of P in the direction of B can take on only certain discrete values; that is, the component of P in the B direction is quantized. This is accounted for by the quantum number m:

Allowed values of 
$$m_l = -l, (-l+1), ..., -2, -1, 0, 1, 2, ..., l$$

The fourth and final quantum number arises because the electron spins on its own axis as it orbits the nucleus, similar to the way in which the earth rotates on its axis as it orbits the sun. As a result, there is an angular momentum associated with the electron spin. The spin angular momentum vector has two allowed orientations in space, and this is taken into consideration by the quantum number m.:

Allowed values of 
$$m_s = +\frac{1}{2}, -\frac{1}{2}$$

Table 2-1

Quantum number	Description	Allowed values	Number of allowed values
n	Principle quantum number	n = 1, 2, 3, 4,	All positive integers
I	Quantizes the magnitude of the orbital angular momentum	$l = 0, 1, 2, 3, \dots, (n-1)$	n allowed values of I
$m_l$	Quantizes the component of P in the B direction	$m_l = l, l-1,,$ 1, 0, -1,, -l	$2l + 1$ allowed values of $m_l$
$m_{\varepsilon}$	Quantizes the spin angular momentum of an electron	±±	2

The quantum numbers of the electron are seen to be associated with the orbit geometry. The rules for the allowed values of these quantities come about naturally from the mathematics of quantum mechanics, which will not be done here. The four quantum numbers and the rules governing their allowed values are summarized in Table 2-1.

#### Ouestion

Question 3: A circular orbit corresponds to l = 0. Consider a hydrogen atom in its ground state (n = 1). Must the electron orbit be circular or can it be elliptic?

## 2.5 The Pauli exclusion principle and the periodic table

The periodic table of the elements is shown in the inside of the front cover. It gives a great deal of information about the chemical nature of the elements. Mendeleev was able to derive the table by considering the chemical characteristics of many substances. He applied brilliant inductive logic to a large body of experimental data and was able to arrange the elements according to their chemical properties. These properties were later attributed to the manner in which the electrons arranged themselves around the nuclei of the atoms. The idea of electron arrangement stimulated the concept of valence, which tells us that atoms attempt to gain or lose electrons until their electron configurations conform to those of inert gas atoms. The atoms attempt to acquire the inert gas electron configurations because they are very stable.

Quantum theory tells us a great deal about the states of electrons in atoms; it gives enough information to enable us to deductively derive the periodic table. The fact that it can be done deductively has enabled scientists to predict the existence of unobserved elements and then seek them in the laboratory. To derive the periodic table it is necessary only to use the four quantum numbers discussed in the previous section and the Pauli exclusion principle. For our purposes, the exclusion principle states that no two electrons in an atom can have the same set of quantum numbers.

The electrons in an atom try to arrange themselves in their lowest energy configuration because this is the most stable one. Equation 2-8 shows that a low electron energy corresponds to a small orbit radius;

Fig. 2-9. Allowed states for electrons in an atom. (a) Energy levels corresponding to the principal quantum number n. (b) The levels multiply when I is considered. (c) The effect of including m., (d) Construction of the periodic table includes consideration of all four quantum numbers. The energy level of the Ss and Sp states is shown.

however, only certain radii are allowed. The allowed radii are determined by the principle quantum number n, and the energy depends on n. These results were derived for the hydrogen atom; however, it is generally true that a small orbit radius corresponds to a low-energy electron. Figure 2-9(a) schematically shows the energy levels corresponding to the first four values of n. The procedure for deriving the periodic table consists of finding all of the allowed energy states for electrons in atoms and then filling these states with electrons. The lower energy states fill first. This procedure will become clear as we progress.

The second quantum number is I. According to Table 2-1, there are n possible values of I. For the lowest energy level (n = 1) there is one possibility, that being fequal to zero, as shown in Fig. 2-9(b). If we consider n equal to 4, for example, then there are four possible values of I, these being 0, 1, 2, 3, as seen in the figure. Note that the energy depends on I as well as on n. A particular notation is used to describe these energy levels. It consists of one number and one letter. The number is simply the appropriate value of I. The letter designates the value of I corresponding to the energy level, according to the following scheme:

Value of l 0 1 2 3 4 Letter designation s p d f q

Using this notation, the energy level corresponding to n = 1 and l = 0 is called the 1s level, that corresponding to n = 3 and l = 2 is called the 3d level, etc. This notation is used in Fig. 2-9(b).

The third quantum number is  $m_i$ , and Table 2-1 shows that there are 2l + 1 possible values. The 3d energy level, for example, has l = 2, and therefore the allowable values of  $m_l$  are -2, -1, 0, 1, 2. Figure 2-9(c) shows the allowed electron energy levels and includes the third quantum number. Note that the 4s level is shown below the 3d level in the diagram. This will have an interesting effect on the periodic table. Each of the short horizontal lines in Fig. 2-9(c) has a unique set of three quantum numbers. For example, the heavy line in the figure is readily identified as having n = 4, l = 1, and  $m_l = -1$ . It is the only line having these numbers. The fourth quantum number,  $m_s$ , has only two possible values,  $\pm \frac{1}{2}$ . Figure 2-9 (d) shows all of the allowed electron states from the 1s to the 4p energy levels. In our scheme, an arrow pointing upward corresponds to  $m_s = +\frac{1}{2}$ , and one pointing downward means  $m_s = -\frac{1}{2}$ . Each arrow denotes an allowed state and has a unique set of four quantum numbers. For example, the heavy arrow in the figure corresponds to the state having the following quantum numbers:

n = 2 l = 1  $m_l = -1$   $m_s = \frac{1}{2}$ 

The Pauli exclusion principle tells us that only one electron can occupy each of these states. The periodic table is derived by filling the allowed states with electrons, beginning with the lowest energy level. If we place a single electron in the 1s level, we have an atom containing one electron (hydrogen). The notation for this electron configuration is 1s<sup>1</sup>. The 1s denotes the energy level, while the superscript 1 indicates that there is one electron in this level. The 1s level can accept a second electron with

opposite spin. Adding a second electron gives us an atom with atomic number 2 (helium). This electron configuration is written 1s2 (two electrons in the 1s level). The energy level corresponding to a principle quanturn number (n = 1) has been filled, and we have reached the first inert gas of the periodic table (He). It will be convenient to refer to the periodic table on the inside cover for the remainder of this discussion. The next electron goes into the 2s level and corresponds to lithium (1s22s1). The single valence electron of lithium is the 2s electron. There are eight states available in the levels having n equal to 2. Filling these eight states gives us the atoms of the second period, going from Li to Ne, with neon having the 1s22s22n6 electron configuration. The next levels to be filled are the 3s and 3p, which have eight states available between them. These cover the elements in the third period, from sodium (atomic number 11) to the inert gas argon (atomic number 18). An inert gas appears when the 3p states have been filled. Recall that filling the 2n states also resulted in an inert gas (neon).

At this point things become a bit complicated, The 4s and 3d energy levels are very close to each other. The 4s fills first, giving potassium and calcium (numbers 19 and 20). Following calcium, the 3d states begin to fill. The filling of the 3d states gives us the elements from scandium to nickel (atomic numbers 21–28). These elements are called the transition metals of the first long period. The electron configuration of copper (atomic number 29) is  $12^{32}$ -2p $^{3}$ -33 $^{3}$ -3d $^{3}$ -diff-4s', indicating that the 3d level has its full complement of 10 electrons. The 4s and 4p levels then fill, resulting in the elements from copper to krypton (atomic number 36). The inert gas (krypton) appears when the 4p states have been filled. It is seen that the transition metals of the first long period arise as the result of filling the 3d states.

The above procedure can be followed to form the rest of the periodic table. The transition metals of the second long period (yttrium to palladium) fill the 4d states, while those from hafnium to platinum (atomic numbers 72–78) fill the 5d states. The electron configurations of the elements are given in the periodic table.

The arrangement of the elements in their periodic order is seen to be the result of the electron configurations of the atoms. The most stable atoms are the inert gases, and these have their p states full with no electrons having energies higher than the filled p levels. Other atoms try to attain this stable configuration by gaining or losing electrons, in accord with valence theory. The quantum concept of the periodic table is also useful in explaining some properties of elements which will not be discussed in this book. For example, the magnetic properties of the transition elements can be

Table 2-2. Electron shell structure of atoms

Main shell notation	Value of n	Subshell s p d f				Number of electrons in the shell
K	1	2				2
L	2	2	6			8
M	3	2	6	10		18
N	4	2	6	10	14	32

attributed to the incomplete filling of the d states. This also explains why the transition metals are good chemical catalysts.

The electron configuration is often described in terms of shells and subshells. A shell corresponds to a principle quantum number (n), while a subshell corresponds to the quantum number l. This notation is illustrated in Table 2-2 for the first four shells

#### Questions

Question 4: The periodic table shows that the rare-earth elements (atomic numbers 57–71) fill after the 6s states. Why are there 14 of them?

Question 5: What is the electron configuration of indium (In)?

## 2.-6 Ionization energy and electron affinity

The ionization energy and electron affinity are the energies involved in forming positive and negative ions from neutral atoms. They provide a measure of the energy of valence electrons and will be used in the discussion of both ionic and metallic bonding. The ionization energy is defined as the energy required to remove the least tightly bound electron from an atom. It can be determined experimentally or can be calculated in some cases. The calculating procedure can be best illustrated by an example.

## Example 2-2

Calculate the ionization energy of a hydrogen atom with the electron initially in its 1s state (r = 0.528 Å):

$$\mathcal{E}_{\text{ionization}} = \mathcal{E}_{\text{final}} - \mathcal{E}_{\text{initial}}$$
 (2-11)

The final state of the hydrogen atom is a proton and an electron at an infinite distance from each other  $(r=\infty)$ . In the initial state they are separated by 0.528 Å.

Using equation 2-8.

$$\mathcal{E} = -\frac{e^2}{2r}$$

Substituting equation 2-8 into 2-11,

$$\begin{split} \mathscr{E}_{\text{Ionization}} &= \frac{-e^2}{2r_{\text{final}}} + \frac{e^2}{2r_{\text{initial}}} = -\frac{e^2}{\infty} + \frac{(4.8 \times 10^{10})^2}{(2)(0.528 \times 10^{-8})} \\ &= 2.181 \times 10^{-11} \text{ ergs} = 13.58 \text{ eV} \end{split}$$

The ionization energy is a positive quantity, which means that energy must be added to the atom in order to form an ion. The calculation shows that, for a hydrogen atom, the ionization energy depends on the initial distance between the electron and the nucleus. This statement implies that large atoms should generally have lower ionization energies than small atoms because the valence electrons in the large atoms are farther from the nucleus. The ionization energies of the elements in four columns of the periodic table are shown in Table 2-3.

Table 2-3 shows that the ionization energy decreases as we come down the columns. The elements near the bottom of the table are heavier and

L	A	11	A	1	/IA	V	ΊΙΑ
Li	5.37	Ве	9.28	0	13.55	F	17.34
Na	5.14	Mg	7.61	S	10.31	C1	12.96
K	4.32	Ca	6.09	Se	9.70	Br	11.30
RЬ	4.16	Sr	5.67	Te	8.96	I	10.44
Cs	3.87	Ba	5.19	Po	7.25	At	9,4

Table 2-4. Electron
affinity of several atoms

Electron affinity (eV)	
3.6	
3.9	
3.5	
3.2	
2.2	
2.4	
0.7	

larger and therefore have a greater distance between the valence electrons and the nucleus. The elements selected are from groups near the edges of the periodic table. The elements near the center of the table are not as well behaved. The ionization energy of the metals in columns IA and IIA is significantly lower than that of the nonmetals in columns VIA and VIIA. The low ionization energy is characteristic of metals and will be used in discussing the metallic bond.

The electron affinity of an atom is defined as the energy released when an electron is captured by an atom. This process is exothermic and results in the formation of a negative ion. The electron affinities of several atoms are given in Table 2-4.

#### Question

Question 6: The ionization energy of beryllium is 9.28 eV. One valence electron is removed when this energy is added to the atom. The energy required to remove the second valence electron, thus forming Be<sup>2+</sup>, is 18.12 eV. Why is more energy required to remove the second valence electron than the first one?

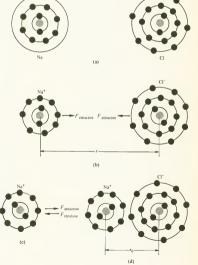
## 2-7 The ionic bond

The bonding forces between the atoms of a solid are one of the primary factors which determine mechanical properties. Large bonding forces are generally associated with materials that are stiff and hard, and vice versa. The ionic bond is the easiest of the primary bonds to discuss. This bond involves attractive and repulsive forces between charged particles, which can be described without resorting to quantum theory. Ionic bonding is associated with the alkali halide molecules, such as NaCl. It is not limited to these, however, and is the predominant bond in a large number of ceramic materials that are of engineering importance.

The model of the ionic bond is well illustrated by NaCl. Figure 2-10(a)

shows a sodium and a chlorine atom. Sodium has a low ionization energy; therefore its single valence electron can easily be removed, forming a positive ion. Chlorine has a high electron affinity and readily acquires the electron removed from the sodium, forming a negative ion. The two ions interact through Coulomb forces. When the distance between ions (r) is large, they appear, practically, as point charges to each other, and the Coulomb force is attractive, as shown in Fig. 2-10(b). When the ions come close to each other, they no longer behave as point charges. The electrons in one ion begin to repel those in the other, as do the nuclei. Thus, both attractive and repulsive forces exist when the ions come close together. The main source of the repelling force is the interaction of the orbiting electrons. If we considered the two nuclei in Fig. 2-10(b) to be surrounded by electron clouds instead of particle electrons, the repulsive force would be due to the electron clouds overlapping each other. Significant overlap

Fig. 2-10. Formation of an NaCl molecule, (a) Transfer of an electron from Na to Cl creates two lons, (b) The net force between ions is attractive at large ion separations, (c) At small separation, (b) repulsive force becomes significant. (d) Attractive and regulsive forces are equal when the separation is to separation is the separation is to separation is the se



occurs only when the ions are close to each other: therefore the repulsive force is a short-range force. At some value of the interionic spacing the attractive and repulsive forces are equal in magnitude, as shown in Fig. 2-10(c). The separation at this point is called ro [Fig. 2-10(d)] or the bond length. If the distance between ions is less than  $r_0$ , the net force is repulsive; a separation greater than  $r_0$  results in an attractive force. The model of the ionic bond is straightforward, and because it yields results which are in agreement with experimental observation, it is considered valid.

An equation can be written which describes the forces between ions:

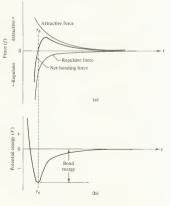
$$f = f_{\text{attractive}} + f_{\text{repulsive}}$$
 (2-12)

The attractive force is the Coulomb force, which results when the two ions are treated as point charges:

$$f_{\text{attractive}} = \frac{-(Z_1 e)(Z_2 e)}{r^2}$$
 (2-13)

where  $Z_1$  and  $Z_2$  are the number of electrons which have been added to the atoms in order to form the ions. If electrons have been removed to form the ion, then Z is negative. Thus, the quantity Ze is the net electric charge of the ion and can be positive or negative, r is the distance between ions.

Fig. 2-11. Force and potential energy curves according to equations 2-15 and 2-16. (a) Schematic diagram of the bonding forces, Attractive and repulsive forces are equal when the distance between ions is ro. (b) The potential energy resulting from the bonding forces. The minimum occurs at r. .



Born suggested that the repulsive force was inversely proportional to a power of r. Thus,

$$f_{\text{repulsive}} = \frac{nb}{r^{n+1}}$$
 (2-14)

where *n* and *b* are constants which can be determined. Typical values of *n* range from 7 to 12, and the value for NaCl will be calculated later. Substituting equations 2-13 and 2-14 into 2-12.

$$f = \frac{-Z_1 Z_2 e^2}{r^2} - \frac{nb}{r^{n+1}}$$
 (2-15)

The attractive and repulsive forces can be plotted as a function of r if the constants are known. This will be an exercise for the student (Problem 2-11). They are plotted schematically in Fig. 2-11(a). The figure shows that the repulsive forces predominate at small values of r; this is due to the large value of r in equation 2-15. At the equilibrium spacing,  $r_0$ , the attractive and repulsive forces balance, and the net force is zero. The net bonding force curve is quite informative. For example, the elastic modulus of a material is related to the slope of the curve at  $r_0$ , and the theoretical strength of a material depends on the maximum value of the net bonding force curve. This will be seen in Chapter 6.

The potential energy, V, of the bond can be determined as a function of the distance between ions from equation 2-15. The zero reference for potential energy is taken as two ions infinitely separated from each other. Because the potential energy is simply the force times the distance,

$$V = \int_{-\infty}^{r} (f_{\text{autractive}} + f_{\text{repulsive}}) dr = \int_{-\infty}^{r} \left[ -\frac{Z_1 Z_2 e^2}{r^2} - \frac{nb}{r^{s+1}} \right] dr$$

$$V = \frac{Z_1 Z_2 e^2}{r} + \frac{b}{r^s}$$
(2-16)

The first term is the energy due to the Coulomb attractive force and is negative because  $Z_1$  and  $Z_2$  have opposite signs. The potential energy is plotted schematically in Fig. 2-11(b). The minimum in the potential energy curve occurs at  $r_0$ . The reason for this can be seen by considering the relationship between force and potential energy:

$$f = \frac{-dV}{dr}$$
 (2-17)

From our definition of  $r_0$ , f=0 when  $r=r_0$ , therefore dV/dr=0 when  $r=r_0$  by virtue of equation 2-17. Thus, an extremum occurs in the energy curve at  $r_0$ . Inspection of the second derivative would show that it is a minimum. The appearance of a minimum in the potential energy at  $r_0$  energy is a minimum. The bond energy at  $r_0$  energy is a minimum. The bond energy shown in Fig. 2-11(b) is related to some physical properties of solids such as the melting point.

The constant b in equations 2-15 and 2-16 can be readily evaluated from the condition that f = 0 when  $r = r_0$ . Substituting these values into equation 2-15,

$$0 = -\frac{Z_1 Z_2 e^2}{r_0^2} - \frac{nb}{r_0^{n+1}}$$

$$b = -\frac{Z_1 Z_2 e^2 r_0^{n-1}}{r_0^{n+1}}$$
(2-18)

This enables us to write a less complicated expression for the bond energy. The bond energy can be found by letting  $r=r_0$  in equation 2-16. Doing this, and using equation 2-18 for b,

Bond energy = 
$$V|_{r=r_0} = \frac{Z_1 Z_2 e^2}{r_0} - \frac{Z_1 Z_2 e^2 r_0^{n-1}}{n r_0^n} = \frac{Z_1 Z_2 e^2}{r_0} \left(1 - \frac{1}{n}\right)$$

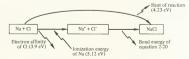
where  $V_{l\rightarrow r_i}$  means "the value of V when  $r = r_n$ ." We have managed to go through a somewhat confusing number of formulas. From here on, only equations 2-15, 2-16, and 2-19 will be used. The value of n in these equations can be found provided that certain experimental data are available. This is best illustrated by an example.

## Example 2-3

Determine the value of the constant n for NaCl. The following experimental data are given:

- (a)  $r_0 = 2.361 \,\text{Å}$ .
- (b) The energy released when a sodium atom unites with a chlorine atom to form an NaCl molecule is 97.5 kcal/g-mole (or 4.23 eV/molecule). That is.

The value of n can be found from equation 2-19 if we know the value of the bond energy. The bond energy in the equation represents the energy released when two ions form a molecule, while the experimental data were taken for two atoms forming a molecule. The relationship between these quantities is in the accompanying figure. The net energy released by the reaction must be the same regardless of which of the two paths shown we consider. Equating the energies involved in following each path.



Bond energy + electron affinity + ionization energy = heat of reaction

(2-20)

Bond energy = heat of reaction - electron affinity - ionization energy

Energy shown as leaving the system in the accompanying sketch will be considered as negative and energy entering the system will be positive. Substituting appropriate values into equation 2-20,

Bond energy = 
$$(-4.23 \text{ eV}) - (-3.9 \text{ eV}) - (5.12 \text{ eV}) = -5.45 \text{ eV}$$

The bond energy can now be substituted into equation 2-19, and we can solve for n. The calculation will be done in egs units; therefore the bond energy must be expressed in ergs rather than in electron volts. Substituting values into equation 2-19 and letting  $Z_1Z_2 = -1$  for this case,

$$\frac{-5.45}{6.2419 \times 10^{11}} = \frac{-(4.8 \times 10^{-10})^2}{2.361 \times 10^{-8}} \left(n - \frac{1}{n}\right)$$

from which

$$n = 9.2$$

This method of determining n is very sensitive to small changes in the measured quantities. Methods which use other measurable physical properties can also be used. Pauling\* suggests a method for evaluating n that is somewhat simpler. This method depends on the data given in Table 2-5.

The first column shows the outer shell structure of the ion being considered. Na $^+$ , for example, has the neon outer shell structure and a value of n equal to 7. Cl $^-$  shows the argon outer shell configuration and an n value of 9. The value of n for NaCl, using this method, is the average of these, or 8. Values obtained from this method correlate well with calculated values. For example, the discrepancy between the value of n as determined in Example 2-3 and that determined from Table 2-5 is 13%, which is not unreasonable. Values of n from Table 2-5 will be used throughout the remainder of the book.

So far we have dealt with ionic *molecules*. The sodium ion in Fig. 2-10(d) is capable of attracting other chlorine ions to it. The force exerted

\* L. Pauling, The Nature of the Chemical Bond, Cornell University Press, Ithaca, N. Y. 1966.

Table 2-5. Values of the exponent n

Outer shell structure	Typical ions having this structure	n
He	Li+, Be2+	5
Ne	F-, Na+, Mg2+, O2-	7
A	Cl-, K+, Ca2+	9
Kr	Br-, Rb+	10
Xe	I-, Cs+	12

Table 2-6. Melting points of some ionic solids

Compound	Melting point (°C)
NaF	988
NaCl	801
NaBr	740
NaI	660
MgO	2640
CaO	2570
SrO	2430
BaO	1933
$Al_2O_3$	2020

on a chlorine ion by the sodium ion depends only on the interionic distance and not on the direction; that is, the ionic bonding force is nondirectional. When forming a solid, the Na ion surrounds itself with as many Cl ions as it can, the number being determined by the relative sizes of the ions. The ion diameters thus determine the structure of ionic solids, as discussed in Chapter 3.

The melting point of a solid strongly depends on the energy of the bonds which hold the atoms together. Increasing the temperature of a solid (or a molecule) causes the atoms to move with respect to each other; that is, they vibrate. The higher the temperature, the greater the vibration. If the vibrational energy exceeds the bond energy, the bond will break and the atom will be free. In a solid, this would appear as sublimation. In most cases melting will occur first, and the melting or sublimation temperature is indicative of the bond energy. Equation 2-19 shows that bond energy depends on Z among other things. The Z dependence leads us to believe that multivalent elements should form stronger ionic bonds than monovalent ones. This is reflected in the high melting temperatures shown by a number of divalent metal oxide solids whose bonding is primarily ionic. A comparison of the melting points of several monovalent and multivalent compounds is shown in Table 2-6. The metal oxides are ceramics and show the high melting temperatures which are characteristic of this type of material.

#### Ouestion

Question 7: The distance between the  $(S^+)$  on and the  $(\Box^+)$  ion in a CsCl molecule has been measured as 2.904 A, (a) Using the data in Table 2.5 to find n, calculate the energy released when a  $CS^+$  ion and a  $CI^-$  ion come together to form CsCl. (b) The heat liberated in the reaction  $CS^+ + CI^- + CsCl$  has been measured as 101.3 kcallg-mole. Calculate this quantity from the answer to part (a) and the data in Tables 2.3 and 2.4. Compare the calculated and measured quantities.

## 2-8 The metallic bond

The model of the metallic bond was proposed by Drude in 1900. He postulated that when metal atoms bonded together to form a solid, each atom contributes it valence electrons to the solid, thereby forming metal ions and "free" electrons. The electrons are called *free electrons* because they

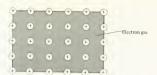


Fig. 2-12. Model of the metallic bond.

are considered free to move throughout the solid similar to the way in which gas atoms are free to move within the container that holds them. Thus, the term electron gas is often used to describe the free electrons. The metallic ions are visualized as arranging themselves in an ordered manner within the electron gas, as shown in Fig. 2-12. Bonding is attributed to the attraction between the ions and the electron gas. This model might tend to provoke the cynical reader, however it has proved to be fairly accurate. Using Drudé's model as the starting point, the mathematical methods of statistical and quantum mechanics have been applied to metals. The resulting calculations quantitatively predicted certain phenomena, which were them measured. Reasonable correlation between theoretical predictions and experimental data existed in many cases, and the model was accepted as reasonable. It is often called the free-electron theory of metals.

We can give qualitative justifications for the model. Metallic elements have low ionization energies; therefore the valence electrons can be removed from these atoms relatively easily, Metals would be more amenable to contributing electrons to the electron gas than nonmetals. From the electron cloud point of view, the low ionization energy means that the valence electron is weakly bound and therefore can roam in a large volume around the nucleus; the electron cloud covers a large extent in space. These large electron clouds are shown schematically in Fig. 2-13 with the atoms close together as in a solid metal. It becomes difficult to say which electron cloud belongs to which atom. Perhaps this is analogous to group living.

The free-electron theory can be used to explain such phenomena as electrical conductivity, optical opaqueness, ductility, and thermionic emission. Thermionic emission depends very strongly on the electron gas concept and will be discussed briefly. When a metal is heated to a high temperature, it emits electrons; this is called thermionic emission. It is of

Fig. 2-13. A schematic electron cloud description of the metallic bond. It is difficult to say which electron belongs to which nucleus.

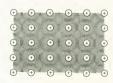




Fig. 2-14. The electron gas in a metal. The motion of the electrons is random. The lengths of the arrows represent the velocities.

great practical consequence because the thermionic emission of electrons from a hot metal can be used as an electron source. The metal is usually in the form of a filament, and such electron sources are used in a great variety of devices including vacuum electronic tubes and cathode-ray tubes (television picture tubes). Figure 2-14 shows an electron gas within a metal. The electrons are in random motion and move with different velocities: therefore they have different kinetic energies. As the metal is heated, some of the thermal energy added to the metal is acquired by the free electrons and appears as an increase in their kinetic energies. When an electron has sufficient kinetic energy, it can escape from the metal; that is, it is thermionically emitted. It is convenient to think of the metal surface as a barrier to the electrons. If the electrons have sufficient energy, they can surmount the barrier and escape from the metal. The free-electron theory provides the model for deriving equations which describe the electron velocities as a function of temperature. From this, the number of electrons which have sufficient kinetic energy to escape can be calculated, and the rate at which electrons leave the metal can then be determined. This has been done, and excellent correlation exists between predicted and measured values of thermionic emission currents. The model for the calculation is the free-electron theory.

The metal atoms which bond together to form a solid want to achieve a stable for low-energy) state. One method of doing this is to form a large number of bonds with other atoms because bond energy is negative. As a conseqence, the atoms tend to surround themselves with as many neighbors as possible. In this respect the metallic and ionic bonds are the same; they are nondirectional. No valence restrictions exist in metallically bonded solids; therefore metals can be mixed with each other to form alloys. The energies of metallic bonds are of the same order as ionic bonds. They range from about \$50 to 200 kcall/z-mole.

Question

Question 8: The melting points of the alkali metals are given in the periodic table (column IA). The melting temperature decreases as the atoms become larger. Explain why, in terms of the metallic bond.

## 2\_9 The covalent bond

Atoms can sometimes acquire the inert gas electron configuration by sharing electrons with each other. For example, Fig. 2-15 shows a simple model of the fluorine molecule. By sharing electrons, both atoms have achieved the electron configuration of neon. Similar models can be sketched

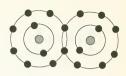
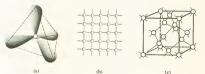


Fig. 2-15. Covalent model of the fluorine molecule, F2.

for many of the diatomic gases such as  $N_2$ ,  $O_2$ , and  $H_2$ . Bonds formed by electron sharing are called covalent bonds. This section will discuss the covalent bond with particular emphasis on carbon. The covalent bond between carbon and other atoms are partially responsible for the physical properties of many polymer materials (which include both plastics and elastomers such as rubber). These constitute a very important group of engineering materials.

Carbon has a valence of 4 and therefore must share four additional electrons with neighboring atoms in order to acquire an inert gas electron configuration. The carbon electrons have a particular spatial orientation; that is, the electron clouds are not spherically symmetrical about the nucleus. The shape of these clouds can be determined from quantum theory, and one possibility is shown in Fig. 2-16(a). The figure shows four electron clouds, each pointing to the corner of a regular tetrahedron. The electron cloud (or wave function) associated with an electron is called an orbital. The four orbitals shown in the figure are equivalent. They are seeking orbitals from other atoms to pair up with, thus providing the carbon atom with shared electrons. When an atom with an appropriate orbital is found, it bonds to the carbon atom in the direction of one of the orbitals shown in Fig. 2-16(a). This causes the covalent bond to be highly directional in carbon. Let us consider what happens when carbon bonds to itself to form a solid, using the equivalent orbitals of Fig. 2-16(a). The orbitals of adjacent atoms will line up with each other in order to participate in electron sharing. The resulting bonds are directional. The structure is shown schematically in Fig. 2-16(b). The lines between atoms represent the bond formed by one pair of shared electrons. The directional nature of

Fig. 2-16. The diamond structure of carbon. (a) A carbon atom with four equivalent orbitals. The orbitals point toward the corners of a terruhedron. (b) A two-dimensional schematic diagram of the diamond structure. Each atom forms four covalent bonds. (c) The three-dimensional diamond structure. The dark lines form a cube.



the bond is well illustrated by the three-dimensional structure [Fig. 2-16(c)]. The spheres represent atoms, while the lines depict bonds. Each atom has four nearest neighbors, and the bond directions correspond to the orbital directions in Fig. 2-16(a). This three-dimensional arrangement is called the diamond structure. A number of bonds are not filled, indicating that the solid can grow. The entire diamond is a single giant molecule. The strength of the covalent bond is aptly illustrated by the strength and hardness of diamonds.

Carbon is usually found as graphite rather than as diamond. The graphite structure results from the orbitals shown in Fig. 2-17(a). Three equivalent orbitals are located 120° from each other in a plane; the fourth is not shown in the figure. This orbital configuration requires that the carbon atoms bond together to form sheets because the covalent bonds are in a single plane. Three such planes are shown in Fig. 2-17(b), The hexagonal geometry reflects the 120° angle of the orbitals. The fourth orbital is metallic and is therefore nondirectional. Sheets of atoms can bond to each other by means of weak secondary bonds, which will be discussed in Section 2-10. These weak bonds have no valence requirements. The structure which results from bonding the sheets together is shown in Fig. 2-17(b) and is the graphite structure. Because the bonds holding the sheets together are weak, the sheets can readily slide past each other. The ease of sliding accounts for the lubricating properties of graphite. The effect of structure on the physical properties of materials is well illustrated by carbon. Both diamond and graphite have the same chemical composition, but the manner in which the atoms are arranged has a vast effect on physical properties. The metallic orbital accounts for the fact that graphite is an electrical conductor while diamond is not.

Next we shall consider compounds of hydrogen and carbon (hydro-carbons). The simplest of these is methane, CH<sub>4</sub>, shown schematically in Fig. 2-18(a). A three-dimensional hard-ball model appears in Fig. 2-18(b).



Fig. 2-17. The graphite structure of carbon. (a) The geometry of three equivalent orbitals. The fourth one is not shown. (b) The sheet structure of graphite. The sheets are held together by weak secondary bonds.

Fig. 2-18. (a) A diagram of methane, a saturated molecule. (b) A hard-ball model of methane.

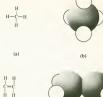


Fig. 2-19. (a) A diagram of ethylene. This molecule is not saturated and contains a double bond, (b) A hard-ball model of ethylene.





(b)

(a)

By hard-ball model it is meant that each atom is represented by a solid sphere. The model is somewhat unrealistic but very instructive. The effect of the tetrahedrally oriented carbon orbitals can be seen in the figure; the bonds are directional. Each carbon orbital participates in a bond with one of the hydrogen atoms. Because each available carbon bond has been filled, no more hydrogen can be brought into the molecule. The molecule is said to be saturated. An example of an unsaturated hydrocarbon is ethylene, C2H4, diagrammed in Fig. 2-19. A double bond (two shared pairs of electrons) exists between the two carbons. If this were reduced to a single bond, one bond would be available to pick up another atom or molecule. For our purposes, the significant thing about unsaturated hydrocarbons is that they can be polymerized. This will be discussed in Section 2-11. Characteristics of several covalent bonds are given in Table 2-7. The bond energies are of the same order as the ionic and metallic bond energies and are typical of bonds involving valence electrons (primary bonds).

#### Question

Question 9: Using the data in Table 2-7, find the heat released when 1 mole of carbon atoms joins with 4 moles of hydrogen atoms to form 1 mole of methane.

Table 2-7. Energy and length of several carbon bonds

Bond	Bond energy (kcal/g-mole)	Bond length (approximate) (Å)
CC	83*	1.54
C—C	146	1.35
C = C	198	1.21
C—H	99	1.08
C—N	70	1.47
C-O	84	1.43
C=0	173	1.22
C—Cl	81	1.76

<sup>\*</sup> This value corresponds to the bond in diamond.

## 2-10 Secondary bonds

The three types of primary bonds discussed in the previous sections relied upon valence electrons. Secondary bonds do not involve the valence electrons and consequently are weak, having energies ranging from less than 1 to about 10 keal/g-mole. Despite their low energy, they become quite significant when they are the only bonds holding atoms or molecules to each other. These bonds have their origin in the interaction of electric dipole moments. A dipole moment arises when two opposite charges are separated, as shown in Fig. 2-20. It is defined as

$$\mu = qs$$
 (2-21)

where  $\mu$  is the dipole moment, q is the magnitude of the electric charge on the particles, and s is the distance between charge centers. Dipoles interact with each other through Coulomb forces.

Molecules are electrically neutral, but they will have permanent dipole moments if their centers of positive and negative charge do not coincide. This can be illustrated by the water molecule [Fig. 2-21(a)]. The shared electrons spend most of their time between the hydrogen and oxygen atoms. As a result, the hydrogen atoms show a net positive charge, and the oxygen atom is negative, as in Fig. 2-21(b). The positively charged end of one water molecule attracts the negative end of another, forming a bond [Fig. 2-21(c)]. Dipole bonds having hydrogen as the positive end of the dipole are called hydrogen bonds and can be moderately strong due to the small size of the hydrogen ion. Many molecules have permanent dipole moments, and the bonds between these molecules are called permanent dipole bonds. They are directional. There is another manner in which dipole bonding can occur. Consider the neon atom shown in Fig. 2-22(a).

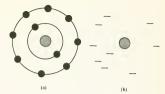
Fig. 2-20. An electric dipole. The dipole moment is qs.



Fig. 2-21. The hydrogen bond. (a) A water molecule. (b) Charge distribution in the molecule showing a permanent dipole. (c) Coulomb interactions between dipoles, in the direction shown, cause alignment. The bond between molecules is a hydrogen bond.



Fig. 2-22. Fluctuating dipole in a neon atom. (a) Electron configuration, (b) The electrons are not usually found in a symmetrical arrangement. This causes a fluctuating dipole moment.



The electrons are shown in a symmetrical distribution about the nucleus. Actually, at any given instant of time it is unlikely that this symmetry exists. It is probable that more electrons are instantaneously on one side of the nucleus than the other, as illustrated schematically in Fig. 2-22(b), In this configuration the atom has a dipole that changes with time; that is, it has a fluctuating dipole. The fluctuating dipole interacts with dipoles of other atoms, the net result being an attractive force called the dispersive attraction. This effect causes weak bonds (called van der Waals' bonds) which are nondirectional.

The inert gases condense and solidify at sufficiently low temperatures by virtue of van der Waals' forces. The weakness of these bonds is reflected in the low melting and boiling points of the inert gases, as tabulated in Table 2-8. The data in the table indicate that the bond strength depends on the nuclear charge. It is seen that the heavier atoms condense and solidify at higher temperatures, implying that they have stronger dipole bonds.

The forces associated with secondary bonds can be described by an equation of the form

$$f = \frac{am}{r^{m+1}} - \frac{bn}{r^{n+1}} \qquad n > m$$
 (2-22)

where a, b, m, and n are constants and r is the distance between atoms. The force equation can be integrated to obtain an energy equation by following the procedure used in Section 2-7. The result is

Table 2-8. Melting and boiling point of inert gases\*

Gas	Melting point (°C)	Boiling point (°C)
He	-272,2	-268.9
Ne	- 248.7	-245.9
A	-189.2	-185.7
Kr	-157.0	-152.9
Xe	-112.0	-107.1
Ra	-71.0	-61.8

<sup>\*</sup> Values are for a pressure of 1 atm.

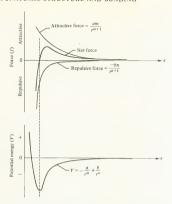


Fig. 2-23. Force and energy curves from equations 2-22 and 2-23. Chemical bonds generally show these types of curves.

$$V = \frac{a}{r^m} + \frac{b}{r^n} \qquad n > m \tag{2-23}$$

These equations are analogous to equations 2-15 and 2-16 for the ionic bond. Again, the first term is due to an attractive force and the second to a repulsive one. The force and energy curves plotted from these equations (Fig. 2-23) have the same shape and characteristics as the curves for the ionic bond (Fig. 2-11), but the constants are different. Equations having the form of 2-22 and 2-23 can generally be used to describe chemical bonding.

#### Question

Question 10: Both water molecules and liquid helium molecules are bonded by secondary bonds. Liquid helium boils at -268.9°C, while water boils at 100°C. Explain the difference in boiling points in terms of bond energies.

# 2-11 Addition (or chain) polymerization

The directional nature of the covalent bond enables covalently bonded atoms to form very large molecules which have a chain-like shape. The element which is synonymous with the directional covalent bond is carbon, and the following discussion will be limited to long-chain molecules con-

taining carbon. These chains form the basis of many polymer materials. The remainder of this chapter will cover the bonding arrangements which permit a large number of small molecules to form a big molecule. The process of forming these large molecules is called polymerization. In Chapter 3, the long-chain (or polymerized) molecules will be joined together to form useful polymers. Most polymers of engineering importance are compounds of either carbon or silicon, both of which have four directional bonds.

Addition polymerization consists of joining a large number of molecules together. This can best be illustrated by an example. Figure 2-24(a) shows both the bonding arrangement and a hard-sphere model of an ethylene molecule. The molecule is unsaturated because a double bond joins the two carbon atoms. If the double bond is reduced to a single bond, two orbitals become available for additional bonding (recall that each bond is due to two shared electrons). The molecule is shown with a single carbon bond in Fig. 2-24(b), and the unshared orbitals are seeking partners. These are provided by other ethylene molecules having a single carbon bond, as illustrated in Fig. 2-24(c) and (d). Figure 2-24(c) shows a large number of ethylene molecules, with three of these having bonded together to form a short chain. The bond directions in the chain correspond to the four equivalent carbon orbitals of Fig. 2-16. The chain-like structure of the bonded molecules is caused by the directional bonds. The unsaturated ethylene molecules have unshared orbitals and will bond to the ends of the chain, causing the chain to grow, as illustrated in Fig. 2-24(d). The long

Fig. 2-24. (a) An ethylene molecule. (b) The double carbon bond has been broken and two carbon orbitals are available for bonding. (c) Some ethylene molecules have bonded to each other; many have not. (d) The addition of ethylene molecules causes the chain to grow or polymerize.

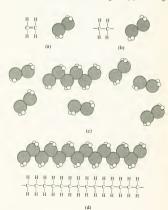


Table 2-9. Polymers that have the same carbon chain as polyethylene

Vinyl polymers						
$\begin{pmatrix} H & H \\ C = C \\ I & R_1 \end{pmatrix}_n \longrightarrow \begin{pmatrix} H & H \\ -C & C \\ I & R_1 \end{pmatrix}_n$						
	Structures	Name	Typical use			
$R_1 \longrightarrow Cl$	н н н н н -С-С-С-С- н сі н сі н	Polyvinyl chloride (PVC)	Plastic pipes, liquid containers			
$\begin{array}{cccccccccccccccccccccccccccccccccccc$	H H H H H H H H H H H H H H H H H H H	Polypropylene	Steering wheels, radiator fans			
$R_1 \longrightarrow \stackrel{\mid}{C} = N$	$\begin{array}{cccccccccccccccccccccccccccccccccccc$	Acrylonitrile (orlon)	Orion fiber			
$\begin{array}{c} R_1 \rightarrow \begin{array}{c} H \\ \downarrow \\ H \end{array} \begin{array}{c} \downarrow \\ \downarrow \\ H \end{array} \begin{array}{c} \downarrow \\ \downarrow \\ H \end{array} \\ \text{(benzene ring)} \end{array}$	H H H H H	Polystyrene	Kitchen appliances, food containers battery cases			
$\begin{array}{c} R_1 & \longrightarrow & \bigcup_{\substack{C=O\\\\ H-C-H\\\\ H\\ (acctate)}} \end{array}$	H H H H H -C-C-C-C-C- H Ac H Ac H	Polyvinyl acetate	Adhesives, paints, flashbulb lining			

chain molecule in the figure is called a polymer and is made up of many repeating units. This particular long-chain molecule is polyethylene and is the basic material of many of the flexible plastic squeeze bottles that the reader is undoubtedly familiar with. The repeating unit is C<sub>2</sub>H<sub>2</sub>.

The polymerization of ethylene can be represented by the notation

$$\begin{pmatrix}
H & H \\
| & | \\
C = C \\
| & | \\
H & H
\end{pmatrix}
\longrightarrow
\begin{pmatrix}
H & H \\
| & | \\
-C - C - \\
| & | \\
H & H
\end{pmatrix}, (2-24)$$

The subscript n defines the number of ethylene molecules which bond together to form a polymer chain. The reaction of equation 2-24 does not occur spontaneously when ethylene molecules are brought together. Polymerization reactions often require heat, pressure, and catalysts before they will occur. The reactants of a polymerization process are called monomers. In the case of ethylene polymerization, only a single monomer  $(C_{3}H_{2})$  is used, and the reactants simply bond to each other.

À number of useful polymers have chain structures which are similar to polyethylene, except that some of the hydrogen atoms are replaced either by other atoms or groups of atoms. This is done in such a way that the tetrahedral bonding which is characteristic of carbon remains. Several of these chains, which form the basis of commercially important plastics, are shown in Table 2-9. The vinyl polymers are shown first. In these, one of the hydrogen atoms of ethylene is replaced by another atom (such as a four clim polyvinyl chloride) or a group of atoms (such as a benzene ring in polystyrene). The atom or group of atoms that replaces a hydrogen atom is significantly larger than hydrogen. This will have a significant effect on the mechanical behavior, as will be covered in Chapter 3.

Table 2-10, Diene polymers

Fig. 2-25. Copolymer of styrene and butadiene. The proportion of each can be varied.



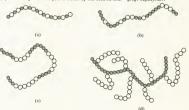
The vinylidene polymers are also shown in Table 2-9. These have two atoms, or groups of atoms, in place of two hydrogens. The carbon "backbone" of these molecules is the same as that shown in Fig. 2-24(d) for polyethylene. The last example in the table is Teflon, in which all of the hydrogen atoms have been replaced by fluorine.

The diene polymers have a somewhat different carbon backbone than the vinyl polymers, as shown in Table 2-10. A double carbon bond remains in each repeat unit even after polymerization has occurred. The diene polymers are elastomers and include natural and synthetic rubbers. They are addition polymers

The polymer chains considered so far have been formed from a single monomer. Many useful materials are formed by the addition polymerization of two or more monomers and are called copolymers. An example of copolymerization is a chain composed of both styrene and butadiene, shown in Fig. 2-25. The properties of this copolymer depend on the proportions of each monomer. The synthetic rubber, Buna-S, has three parts of butadiene to every one part of styrene. It is used in automobile tires. Latex (or rubber-base) house paint has the copolymer of Fig. 2-25 as its base; however, it contains about 60% styrene and 40% butadiene. Polystyrene is a rigid, brittle material, but small additions of butadiene make it more ductile and improve its impact properties. The manner in which the monomers are arranged in a copolymer is of interest, Figure 2-26 shows the possible arrangements and the names associated with them.

The functionality of a monomer is defined as the number of sites at

Fig. 2-26. Copolymer configurations and nomenclature. (a) The two basic units alternate regularly—alternating copolymer. (b) The units are randomly arranged—random copolymer. (c) Blocks of the same type of units are joined—block copolymer. (d) Chains of one unit join a chain of the second unit—araft copolymer.



which the monomer can attach itself to other monomers, by means of primary bonds. The functionality of the monomers has a great effect on the structure and properties of polymers. All of the monomers considered in this section are bifunctional; that is, they have two points at which they can form primary bonds with other monomers. Bifunctional monomers form chain polymers.

#### Condensation (or step) polymerization 2-12

Polymerization reactions are not limited to joining monomers together into chain polymers. Monomers can chemically react with each other to produce a polymer and a second reaction product. The second reaction product is usually a simple molecule such as water or methanol. These reactions are called condensation, or step, polymerizations. A typical condensation polymer is phenol formaldehyde, also called Bakelite. It is formed from phenol and formaldehyde monomers, as shown in Fig. 2-27. The reactants are shown as two phenols and one formaldehyde. In this reaction the two hydrogen atoms and the one oxygen atom, which are shown inside the dashed lines in the figure, unite to form a water molecule. The carbon atoms which the hydrogen and oxygen atoms were bonded to are now unsaturated. The carbon atom in the formaldehyde bonds to the unsaturated carbons in the two phenols and forms a link between them. This link is referred to as a formaldehyde bridge, Figure 2-27 shows a single bridge; however, formaldehyde bridges can be formed at any of the carbon atoms in the phenol except the one which is bonded to an OH molecule. The phenol is polyfunctional.

This polymer is not limited to forming chains but polymerizes as a three-dimensional network. This is shown schematically in Fig. 2-28. All of the bonds in this network are primary bonds. Later on it will be seen that the absence of secondary bonds in a three-dimensional polymer network has a large effect on the mechanical properties at high temperature.

Fig. 2-27. The condensation polymerization of phenol formaldehyde, The formaldehyde loses an oxygen atom and each phenol loses a hydrogen atom. The formaldehyde then serves as a bridge between phenol molecules.

(Bakelite)

Fig. 2-28. Schematic diagram of the network structure of phenol formaldehyde. Only the carbon atoms are shown. The shaded atoms indicate formaldehyde bridges.

Many polymers are formed by condensation polymerization. Among these are melamine-formaldehyde, which is used in Melmac plastic dishes, and ethylene terphthalate, commonly called Dacron or Mylar.

## 2-13 Summary

Atoms bond together in order to attain a more stable state. Chemical bonds which involve either the transfer or sharing of electrons are called primary bonds and are characterized by large bond energies and forces. Primary bonds are categorized as ionic, covalent, and metallic. Many primary bonds do not rigorously fit the models of any of these categorises but can be described as combinations of them. For example, two atoms may share an electron, but the electron may tend to stay closer to one atom than the other. The electron is shared, but one atom shares more. Such a bond is describable as a combination of covalent and ionic bonds. Secondary bonds are weak and arise as the result of dipole interactions.

The physical properties of materials are related to the chemical bonds holding the atoms together. In this chapter, the melting points of ionic solids were qualitatively correlated with bond energies. This is true for the other types of bonds as well. As we progress through the book, it will become apparent that bonding affects all of the mechanical properties. The directional nature of bonding was also covered. It was found that ionic and metallic bonds are nondirectional, while covalent bonds can be highly directional.

Carbon was discussed in some detail, and the effect of bonding on structure was shown for graphite and diamond. The four equivalent orbitals of carbon also account for its ability to form polymers, and several examples were given. These included both chain and network polymers.

#### Problems

1 (a) Calculate the energies of a hydrogen atom in its first three quantum states. (b) How much energy is involved in a transition from the third allowed state (n = 3) to the ground state? (c) If the atom undergoes this transition, is energy absorbed or emitted by the atom? Express your answers in electron volts.

- 2 An electron and a proton come together to form a hydrogen atom. The energy emitted during the formation of the atom has been measured as 13.527 eV, provided that the atom which is formed is in its ground state. How much energy would be emitted if the electron was initially orbiting the proton at a radius of 1 cm and the atom was in the ground state after forming?
- 3 (a) Find the potential energy of a hydrogen atom in its ground state. (b) The answer to part (a) is the change in potential energy due to a proton and an electron moving from an infinite separation to a separation of 0.528 Å. This quantity does not equal the energy emitted due to the transition, as calculated in Problem 2. Explain the difference.
- 4 (a) Find the electric current caused by an electron in the first Bohr orbit of a hydrogen atom. *Note:* 1 Ampere = 6.25 × 10<sup>18</sup> electrons/sec. (b) Would you expect a magnetic field to be associated with the orbiting electron?
- 5 The ionization energy of Li in its ground state is 5.27 eV. If Li is considered a hydrogen-like atom, what is the orbit radius of the valence electron?
- 6 What is the electron configuration of (a) Ca, (b) Fe, (c) Te, and (d) W?
- 7 The sixth period of the periodic table includes the elements from atomic numbers 55 to 86. Why does this period contain so many elements?
- 8 How many 5d electrons do the following ions contain: (a) W<sup>+</sup>, (b) W<sup>2+</sup>, (c) Pt<sup>2+</sup>, and (d) Ir<sup>+</sup>?
- 9 Table 2-3 shows that the ionization energy of atoms in the same period increases as we go from left to right across the periodic table. Explain this.
- 10 Two divalent ions bond together to form a molecule. The equilibrium spacing is found to be 2.6Å and the value of n is 8. (a) Find the distance between ions at which the force is a maximum. (b) Find the change in potential energy due to decreasing the distance between ions from infinity to 2.6Å.
- 11 (a) Plot the curve of force vs. interionic distance for the molecule in Problem 10. To make the plot, find the values at r = 2, 2.6, 3, 4, 5, and 10.Å. (b) Plot the curve of energy vs. interatomic distance for the molecule. (This problem is an easy one for solution on a digital computer. If the reader is reasonably skilled at programming, a computer solution can save time.)
- 12 Figure 2-11 shows that the net bonding force curve has a maximum. For NaCl: (a) Find the value of r at which the maximum occurs. (b) Find the force at this value of r. (c) If this maximum has any significance, explain what it is.
- 13 The melting points of a number of ionic solids are given in Table 2-6. The melting point depends on the bond energy, which, in turn, depends on r<sub>0</sub>. The values of r<sub>0</sub> for the tabulated solids can be found from information in Appendix A. The ionic radii of the elements are listed there. To find the distance between the sodium ion and the fluorine ion in solid NaF, for example, simply add the ionic radii of Na and F. This is the value of r<sub>0</sub>. For NaF, the value is 2.30 Å. (a) Plot melting point vs. r<sub>0</sub> to see if a correlation does exist. Plot the Na compounds on one curve and the oxides on another. (b) Why are two

- different curves necessary? (c) Does  $Al_2O_3$  fall on either curve? If not, why?
- 14 In a two-dimensional sketch, show the manner in which valence electrons are shared by the following substances: (a) solid Si, (b) solid S, (c) I<sub>2</sub>, (d) NH<sup>+</sup><sub>4</sub>, and (e) SiO<sub>4</sub><sup>-4</sup>.
- 15 Briefly explain why metals are good electrical conductors using the free-electron theory as the basis of the explanation.
- 16 Why is graphite a better electrical conductor than diamond?
- 17 The interaction energy between two inert gas atoms is given by an equation of the form

$$\mathscr{E} = -\frac{a}{r^6} + \frac{b}{r^{12}}$$

where the first term is due to attractive forces and the second to repulsive forces. For neon,

$$a = 89 \times 10^{-3} \text{ erg-Å}^6$$
  
 $b = 40.5 \times 10^{-10} \text{ erg-Å}^{12}$ 

- (a) Find the equilibrium spacing between atoms.(b) Calculate the bond energy and compare it to the energies of the primary bond types.(c) Why does neon exist as Ne rather than Ne, at room temperature?
- 18 Ethylene molecules can polymerize to form polyethylene. The polymerization reaction is exothermic. (a) How much heat is given off when 1 g-mole of chylene is polymerized? Table 2-7 will be a help. (b) One g-mole of C<sub>2</sub>H<sub>4</sub> weighs 28 g, or 0.0616 lb. Polyethylene has a specific gravity of about 0.95. Suppose you have a reactor with a volume of 6 ft³ which is used to polymerize ethylene. After polymerization, 10% of the volume is filled with polyethylene. How much heat must be removed during the processing of one batch of polyethylene in this reactor?

Answers

Question 1: (a) 
$$\Delta V = w\Delta x = (1) (-4) = -4 \text{ ft-lb}$$
 where  $w = \text{weight}$ 

$$V = V_{\text{intrial}} + \Delta V = 0 - 4 = -4 \text{ ft-lb}$$

(b) 
$$\Delta V = (1) (-30,000) = -30,000 \text{ ft-lb}$$
  
 $V = V_{\text{initial}} + \Delta V = 0 - 30,000 = -30,000 \text{ ft-lb}$ 

(c) The results of parts (a) and (b) show that the value of potential energy depends on what state is selected as having zero potential energy. We selected the zero-potential energy state as being an electron and a proton with infinite separation. The potential energy of the electron decreases as it approaches the proton; therefore its potential energy must be negative. The negative sign is due to two things: (1) the selection of the zero-potential energy state, and (2) the fact that the potential energy of the electron decreases ar decreases.

- Question 2: The valence electron of Li is attracted by a net nuclear charge (or core charge) of +e, using the shielding model. For Be, the valence electron is attracted by a net nuclear charge (or core charge) of +2e. It is also repelled by the other valence electron. The repulsive force exerted by the extra valence electron is smaller than the attractive force due to the extra nuclear charge ("extra" when compared to Li). The net result is that the valence electron of Be is attracted to the nucleus by a larger Coulomb force than is the Li valence electron; consequently it has a smaller orbit radius.
- Question 3: Circular. Since n = 1, the only allowed value of l is zero; therefore the orbit is circular.
- Question 4: The rare-earth elements fill the 4f states, which are just above the 6s states. There are 14 4f states, as shown in Fig. 2-9(d). This number can also be calculated from Table 2-1.
- Question 5: 1x<sup>2</sup>2x<sup>2</sup>2p<sup>2</sup>3x<sup>3</sup>3y<sup>6</sup>4x<sup>3</sup>3d<sup>10</sup>4p<sup>6</sup>5x<sup>3</sup>4d<sup>10</sup>5p<sup>1</sup> Question 6: The first valence electron is attracted by the "core" and repelled by the second valence electron as it leaves the atom. When the second valence atom leaves, it is also attracted by the core, but no valence electrons are outside the core to repel it. The net attractive force is greater on the second valence electron; consequently more work is required to remove it.
- Question 7: (a) From Table 2-5, n=10.5. Direct substitution into equation 2-19 gives  $V=7.1\times 10^{-12}$  ergs/molecule = 4.43 eV/molecule. (b) Heat of reaction = V- ionization energy + electron affinity = 4.43 3.87 + 3.9 = 4.46 ev/molecule = 103 kcal/mole. The answer agrees within 1.7%.
- Question 8: The attractive forces which hold the metal ions together exist between the nuclei and the electron gas. As the atoms become larger, the distance from the nuclei to the free electrons increases and the bonding becomes weaker.
- Question 9: Table 2-7 shows that energy of the C—H bond is 99 kcal/mole. Each C atom forms four bonds; therefore the heat released = (4) (99) = 396 kcal/mole of CH<sub>4</sub> formed.
- Question 10: The boiling points show that the intermolecular bonds in water are stronger than those in helium. This is attributed to the water molecule having a permanent dipole, while the helium atom does not. Permanent dipole bonds are generally stronger than bonds formed by fluctuating dipoles.

CHAPTER 3

# Structure of Solids

THE PHYSICAL PROPERTIES OF MATERIALS depend on the solid structures which the atoms form as well as the bonding forces between atoms. The effect of structure was illustrated by the diamond and graphite forms of carbon considered in Chapter 2. The properties of these two solids differ dramatically, although both are composed of carbon. Structure is partially determined by the type of bond (or bonds) present. Solids which have nondirectional bonds tend to surround themselves with as many atoms as possible. In the case of directional bonding, the atoms are required to be in a particular orientation with respect to each other. The orientation requirements strongly influence the structure, as in the case of diamond

Two general types of solid structures will be covered in this chapter, crystalline and amorphous. The atoms in crystalline solids are arranged in a very ordered manner; a crystal can be described as an ordered array of atoms in space. Metals and many ceramics form as crystalline solids. Amorphous solids do not show the ideal symmetry of crystals. The amorphous structure is somewhat irregular and is typically found in glasses and many plastics and elastomers. Structure influences many properties among which are density, elastic modulus, coefficient of thermal expansion, ductility, and sublimation energy. There are also a number of materials properties which vary with direction. For example, if a piece of wood was used to support a tensile load, we would design things so that the load was parallel to the grain of the wood. Wood has a higher tensile strength when loaded "along the grain" than when loaded perpendicular to it. Solids whose properties vary with direction are called anisotropic; those having the same properties in all directions are isotropic. The directional dependence of physical properties has its origin in the structure of solids.

This chapter will discuss some of the structures which solids form. The effect of structure on physical properties will be covered in the following chapters, and the material presented in this chapter will then be used extensively. Knowledge of structure is an important part of the background necessary for understanding and using materials science.

#### 3-1 Space lattices and crystal structures

Crystalline solids are characterized by a very orderly arrangement of the atoms which form the solid. The most organized way to discuss crystals is first to describe space lattices. A space lattice is defined as a three-dimensional array of points, infinite in extent, in which every point has identical surroundings. A crystalline structure is formed by placing an atom or group of atoms at each point in the space lattice. Thus, the structure of a crystalline solid is largely determined by its associated space lattice. There are a number of different space lattices which satisfy the above definition; consequently there are also a number of different crystal structures. This section will discuss how the various space lattices are formed, and we shall then describe crystal structure in terms of space lattices.

A two-dimensional space lattice can be constructed by defining a starting point and two nonparallel vectors, a and b, which meet at a point [Fig. 3-1(a)]. The tips and tails of the vectors define the lattice points. To form a two-dimensional lattice, a is translated in the direction of the arrow (positive or negative) by a distance a. By repeating this process, we define an infinite number of equally spaced points on a line, as shown in Fig. 3-1(b). Associated with each point is a vector b. Translation of all the b's creates the two-dimensional (2d) space lattice illustrated in Fig. 3-1(c). The vectors a and b are not unique; that is, there are a large number of pairs of vectors which could be used to form the lattice. Several of these are shown in Fig. 3-2. The vectors a and b are called unit vectors and they determine the geometry of the lattice. The space lattice can also be gener-

Fig. 3-1. Formation of a two-dimensional space lattice. (a) We begin with a starting point and two nonparallel vectors, (b) A line of eauispaced points is created by translating a. (c) The lattice is formed by translating each point in the line

bν b.

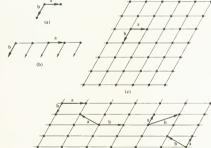
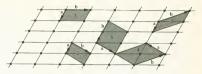


Fig. 3-2. The vectors a and b are not unique. Several pairs of vectors are shown that can create the same two-dimensional lattice.

Fig. 3-3. A lattice can be described by unit cells rather than unit vectors. Five unit cells are shown. Any of these can be translated by its unit vectors to create the lattice.



ated by translating groups of lattice points called unit cells. Several unit cells in a 2d lattice are shown in Fig. 3-3. The vectors a and b in the figure are unit vectors, and the unit cells are simply parallelograms having unit vectors for their sides. The lattice of Fig. 3-3 can be generated by translating any of the unit cells shown by its unit vectors; consequently the unit cell of a lattice is not unique. The choice of which unit cell to use in describing a space lattice is dictated by convenience and convention. It is that unit cell which best describes the lattice symmetry, as will become clear in later sections.

The number of lattice points in a unit cell depends on the particular cell that is being considered. The number of lattice points belonging to a cell will be of interest when we use space lattices to describe crystals. The method for determining this quantity can be explained by considering the unit cell labeld 1 in Fig. 3-3. The cell has a lattice point at each corner. Each of these points is also at the corners of three other unit cells because four unit cells meet at each corner point. These four cells share the point equally; thus one fourth of the lattice point is said to belong to each. Every cell touches four lattice points and "owns" one fourth of each; consequently the cell contains  $4 \times \frac{1}{2}$  or one lattice point. Cell 4 in the figure contains two lattice points. It owns one fourth of each corner point and also has one point completely within the cell. The number of points in a unit cell depends on the particular cell selected. Any cell which contains only one lattice point is called a primitive cell, and its unit vectors are called primitive vectors.

The two-dimensional lattice can readily be extended to three dimensions. We simply define a third unit vector,  $\mathbf{c}$ , which is not in the plane of a and b, and go through another translation process in the third dimension. A 3d space lattice is shown in Fig. 3-4, a, b, and  $\mathbf{c}$  are the unit vectors, and the unit cell is shown by the heavy lines. This particular unit cell touches eight lattice points, one at each corner. Each corner point would be shared by eight unit cells if the figure were extended. This sharing can be seen for the single unshaded lattice point in the figure. Eight cells come together at this point. The unit cell shown touches eight lattice points but owns only one eighth of each; consequently it contains  $\frac{1}{8} \times 8$  or one lattice point. As in the 2d case, a cell containing one lattice point is a primitive cell and its unit vectors are called primitive vectors. It will be seen that it is often convenient to describe crystal structure in terms of unit cells other than primitive cells.

Space lattices have been systematized by the crystallographers. They have shown that there are only 14 possible arrangements of points in space

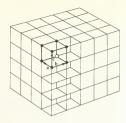
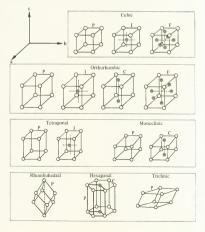


Fig. 3-4. A three-dimensional space lattice. The unit cell is darkly outlined. Eight cells come together at each interior lattice point, a, b, and c are the unit vectors.

which fulfill the symmetry requirements of a space lattice. These are called the Bravais lattices, and the unit cells for these lattices are shown in Fig. 3-5. The unit cells in the figure have been placed in seven groups; each group is called a crystal system. The grouping is based upon the relative lengths of the three unit vectors of the cell and the angles between the unit vectors. For example, the cubic system in the figure contains three unit cells. For all three of these, the unit vectors are perpendicular to each

Fig. 3-5. The seven crystal systems and the unit cells of the 14 Bravais lattices. The letters indicate the type of cell as follows: P, primitive cell: C. cell with a lattice point in the center of two parallel faces; F, cell having a lattice point at the center of each face; I, cell with a lattice point at the center of the cell. There are two accented unit cells for the hexagonal structure. The cell defined by the dark lines can be used (P) ,or the entire cell shown (C) can be used. Unshaded atoms are corner atoms.



#### 3-1: SPACE LATTICES AND CRYSTAL STRUCTURES

other and have the same length. Table 3-1 lists the seven crystal systems and describes the arrangement of the unit vectors for each. Note that one primitive cell is shown for each crystal system.

A crystal is formed by placing one or more atoms at each lattice point. If the solid is a pure element, the crystal structure can usually be represented by placing a single atom at each lattice point. If the solid is a chemical compound, more than one atom may correspond to each point in the lattice. This will be elaborated on later in the chapter. The crystal model presented here can result only in solids having ordered arrays of atoms with a very high degree of symmetry. Experiments have been performed to determine whether or not this model is valid, and it was found that predictions based upon the model were accurate. The experimental validation of the crystal structure model ampears in Chapter 5.

#### Question

Question 1: Figure 3-3 shows five unit cells which can be used to form the space lattice. (a) Find the number of lattice points that each of these unit cells contains. (b) Which of these are primitive cells?

Table 3-1. The fourteen Bravais lattices and the seven crystal systems

Lattice type	Letter in Fig. 3-5	Crystal system	Description of unit vectors	
Simple cubic	P	)		
Body-centered cubic	I	Cubic	Three vectors at right angles, a = b = c	
Face-centered cubic	F	)		
Simple orthorhombic P		)		
Body-centered orthorhombic	I	lanted to	Three vectors at right angles, $\mathbf{a} \neq \mathbf{b} \neq \mathbf{c}$	
Base-centered orthorhombic	C	Orthorhombic		
Face-centered orthorhombic	F	)		
Simple tetragonal	P	1	Three vectors at right angles, $\mathbf{a} = \mathbf{b} \neq \mathbf{c}$	
Body-centered tetragonal	I	Tetragonal		
Simple monoclinic	P	1	Two coplanar vectors not at right angles, third vector 90° to these $\mathbf{a} \neq \mathbf{b} \neq \mathbf{c}$	
Base-centered monoclinic	С	Monoclinic		
Simple rhombohedral	P	Rhombohedral	Three vectors equally inclined but not at right angles, $\mathbf{a} = \mathbf{b} = \mathbf{c}$	
Simple hexagonal	P or C	Hexagonal	Two coplanar vectors at 120°, third vector at 90° to these, $\mathbf{a} = \mathbf{b} \neq \mathbf{c}$	
Simple triclinic	P	Triclinic	Three vectors not at right angles, $\mathbf{a} \neq \mathbf{b} \neq \mathbf{c}$	

## 3\_7 Directions in a crystal

To consider the effect of structure on the properties of materials, we must be able to talk about various directions and planes within the crystal. The distance between neighboring atoms in a crystal, for example, depends on the direction in which the measurement is taken. This is illustrated by the unit cell in Fig. 3-6(a). The two vectors in the figure specify two directions. one along a cell edge and the other along a cell diagonal. It is apparent from the figure that the distance between atoms depends on direction. Figure 3-6(b) shows two planes in the same unit cell. The number of atoms per unit area of these planes differs, with plane B containing a higher number. Both planes touch four atoms, but plane A has a larger area. Physical properties depend on both the strength and the number of interatomic bonds; consequently the properties will vary with direction A crystal is stronger in some directions (or along certain planes) than it is in others; it is anisotropic. To discuss these effects rationally we must have a system for defining planes and directions in a crystal. A simple notation has been devised for doing this.

Direction is defined in terms of the unit cell. Figure 3-7 shows a portion of a space lattice having a simple orthorhombic unit cell. The notation for defining directions is valid for any Bravais lattice; the simple orthorhombic is used here for illustration. Any of the lattice points in the figure can be selected as an origin for a coordinate system; point O has been arbitrarily selected. The axes of the coordinate system are along three edges of the unit cell. Any vector drawn from the origin to a lattice point defines a direction, and any such vector can be defined in terms of the unit vectors by the equation

Direction vector = 
$$u\mathbf{a} + v\mathbf{b} + w\mathbf{c}$$

where u, v, and w are integers. The vector **OM** in Fig. 3-7, for example, can be written as

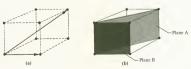
$$OM = 2a + 1b + 1c$$

In our notation, the direction of the vector is specified by the symbol [uvw]. The vector **OM** is thus in the [211] direction. The vector **ON** can be specified similarly:

$$ON = -1a + 1b + 0c$$

The coordinate axes are labeled x, y, and z in the figure, and both positive





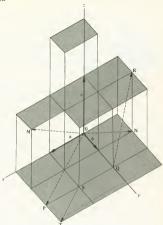


Fig. 3-7. A space lattice having the simple orthorhombic unit cell. The various directions shown are discussed in the text.

and negative values are allowed. In our notation the direction of ON is [T10]. The negative sign appears above the number in the bracket.

The direction of OP would be [220] according to the above scheme. This vector is in exactly the same direction as the [110] vector, the only difference between them being the vector length. Because we are interested only in direction, OP is said to be in the [110] direction. Directions are specified by the smallest possible set of appropriate integers. Recall that the origin of coordinates could have been chosen as any lattice point; point O in Fig. 3-7 was selected arbitrarily. The notation [110] actually defines a whole family of parallel vectors having different origins. Vector ST is in the [110] direction. Every one of the parallel lines has an identical environment and has the same number of lattice points per unit length because of the lattice symmetry; they are said to be crystallographically equivalent. In the case of cubic lattices, the lattice symmetry also causes all directions having the same integers to be crystallographically equivalent. As an example, let the unit cell shown in Fig. 3-6(a) be simple cubic. The cell has four cube diagonals, one of which is shown. The directions of these diagonals can be represented by [111], [111], [111], [111], [111], [111], [111], [111]. Which of these notations we use depends on which diagonal we want to represent and which point we select for the origin, All of these directions are crystallographically equivalent because they have the same number of atoms per unit length and the same environment; they are called *directions of a form*. The notation [[111]] is used to include all of the cube diagonals.

Ouestions

Question 2: Write the direction indices for vector QR in Fig. 3-7. The origin can be taken as any lattice point.

Question 3: What directions in a cubic crystal does the notation [[100]] include?

# 3-3 Planes in a crystal and Miller indices

It is often necessary to talk about the various planes in a crystal, and a system of notation has been devised to facilitate this. The system defines a plane by three numbers which are called Miller indices. To see how this system of notation works, consider the unit cell shown in Fig. 3-8 having unit vectors a, b, and c. The cell edge of length a has been divided into three equal parts, the b edge into two equal parts, and the c edge into two equal parts. A plane is then drawn between the three points at

$$x = \frac{a}{3}$$
  $y = \frac{b}{2}$   $z = \frac{c}{2}$  (3-1)

In Miller index notation, the three points at which the plane intersects the axes are defined as

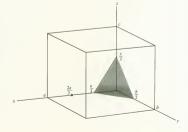
$$x = -\frac{a}{h} \qquad y = -\frac{b}{k} \qquad z = -\frac{c}{l} \tag{3-2}$$

and the plane is described as (hkl). For the example we are considering, comparison of equations 3-1 and 3-2 shows that

$$h = 3$$
  $k = 2$   $l = 2$ 

and the plane is called the (322) plane. Any lattice point can be selected as the origin of coordinates; therefore the notation (322) denotes a large

Fig. 3-8. The shaded plane intersects the three axes at a/3, b/2, and c/2. The Miller indices of the plane are (322).



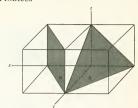


Fig. 3-9. Two adjacent unit cells illustrating the Miller indices of the shaded planes. Plane A is (111); plane B is (110).

number of planes parallel to each other. The planes are equivalent because every (322) plane has an identical environment and possesses the same number of lattice points per unit area. This, of course, is the result of the perfect symmetry of the lattice.

The Miller indices of a plane can be positive or negative integers. This is illustrated in Fig. 3-9, which shows two adjacent unit cells and the coordinate axes. Consider plane A. The points at which this plane intersects the axes are

$$x = \frac{a}{-1} \qquad y = \frac{b}{1} \qquad z = \frac{c}{1}$$

The Miller indices are therefore (T11), where the bar over the first integer indicates a negative sign. Plane B in the figure poses a small problem. The plane obviously intersects two of the axes at x = a/1 and y = b/1, but it is parallel to the z axis. Because a line intersects a parallel plane at infinity, we shall take this as our third intersection. Thus

$$z = \infty = \frac{c}{0}$$

from which l = 0.

The Miller indices of the plane are (110) in accordance with equation 3-2. A number of planes and their Miller indices are shown in Fig. 3-10. The origin of coordinates for Fig. 3-10(a), (b), (c), and (e) are the same. To index the plane of Fig. 3-10(d), however, it is necessary to move the origin up to the position shown.

In the case of cubic crystals, the lattice symmetry requires that planes having the same set of numbers for their indices, but a different arrangement of the numbers, are equivalent. As an example, consider the faces of the unit cell in a cubic crystal [Fig. 3-10(a)]. The faces are the (100), (010), (010), (010), (001), (001) planes. These are all equivalent, having identical lattice point densities and surroundings. They are called planes of a form, and all of these planes are described by the single notation ((100)). This is analogous to the discussion about directions of a form, and both are valid only for cubic crystals. Many useful engineering materials have the cubic crystal structure, as will be seen.

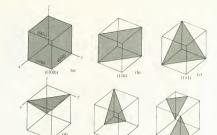
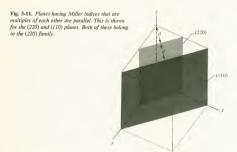


Fig. 3-10. The Miller indices for several planes in a lattice. (d) has a different origin of coordinates than (a), (b), (c), or (e). (f) will be used in a question.

The discussion of direction indices showed that two direction vectors whose indices were multiples of each other indicated the same direction. They were therefore equivalent. This is not true of Miller indices. To illustrate this, the (110) and (220) planes are sketched in Fig. 3-11. They are parallel to each other but are not the same plane. Figure 3-11 is a convenient one for introducing the concept of families of planes. A family of planes is an infinite number of parallel, equispaced planes. Let us consider the (220) family. The (220) plane is shown in the figure, and we imagine another plane parallel to it which passes through the origin. The distance between these two planes defines the distance between adjacent planes in the (220) family. This is shown as d and is measured from the



origin in a direction perpendicular to the (220) plane. The next plane of the family is found by drawing another plane, parallel to the (220) but a distance d in front of it. This plane is the (110). The (110) plane belongs to the (220) family, but the (220) does not belong to the (110) family. Because of the manner in which Miller indices were defined, planes of a family pass through all eight corners of a unit cell. The concept of families of planes will be useful to us in discussing X-ray techniques.

#### Questions

Question 4: (a) Identify the two planes in Fig. 3-10(f). (b) Are these planes equivalent? (Assume a cubic unit cell.)

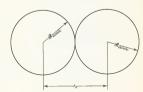
Question 5: What angle does the (010) plane make with the (110) plane in a cubic lattice? Figure 3-10(a) and (b) will be a help.

## 3\_4 Nondirectional bonds with atoms of equal size

Three types of nondirectional bonds were described in Chapter 2. These were the ionic, metallic, and fluctuating dipole bonds. To a great extent, the structures formed by solids having these bonds depend on the relative sizes of the atoms which form the solid. For this reason the crystal structure of solids having nondirectional bonds is divided into two parts. This section discusses structures resulting from atoms of equal size. Materials fitting this category include the pure metals (metallic bond) and solidified noble gases (fluctuating dipole bonds). Nondirectional bonds with atoms of unequal size occur in ionically bonded solids and will be covered in Section 3-5. The remainder of this section will discuss metals, with the understanding that the principles also apply to other solids such as solidified noble gases.

Consider what happens when atoms of a metallic element bond together to form a solid. Each atom will tend to surround itself with as many neighboring atoms as possible. In this way the maximum number of interatomic bonds will be formed per unit volume of solid, and the solid thus formed will be stable. Because we are dealing with elements, all atoms in a structure are the same size. The size of an atom is defined in terms of the "billiard-ball model." In this model, an atom is visualized as a hard sphere. When two such spheres touch each other, the distance between sphere centers is equal to the bond length, as shown in Fig. 3-12. The model does not recognize electron clouds or charge distributions and consequently is unrealistic. The model becomes very useful, however, if we are

Fig. 3-12. The billiard-ball model of atoms. The distance between sphere centers equals the bond length  $(r_0)$  when the spheres touch other.



considering only the geometric arrangement of atoms in crystals. Values of atomic radii, according to this model, have been measured and are tabulated in Appendix A. Using the billiard-ball model, the structure of metals is simply the structure which results when equal-sized spheres are packed in the densest possible manner. There are two different atomic arrangements which yield the closest-packed structure. These are called the face-centered cubic structure (fcc) and the hexagonal close-packed structure (hcp). The reason for these designations should become clear from the following discussion.

Figure 3-13 shows a plane of atoms which are packed as closely as possible. Each atom has six nearest neighbors in the plane. This plane will be called plane A. The figure shows that small empty regions exist between the atoms. These are called voids, and we distinguish between the voids labeled b and those labeled c. We can make a closest-packed structure by simply stacking close-packed planes on top of each other in the densest possible manner. This requires that the atoms of one plane fit into the voids of the plane below it. Consider the close-packed plane in Fig. 3-13. The atoms of the plane which fit over it can align with either the b voids or the c voids. Let us place the second plane over the b voids. The structure of the two planes is shown in Fig. 3-14. The lower plane is plane A. while the upper one will be called B. The third plane (C) fits into the voids of the B plane and has two possible positions. One set of voids in the B plane lies directly above the center of the A plane atoms (Fig. 3-14, cross-hatched voids). If we put the third plane in this position, the third plane is directly above the first plane. If this stacking sequence is continued, the positions

Fig. 3-13. A close-packed plane of atoms having the same size. If a second plane is placed over this one, its atoms will align with either the b voids or the c voids.

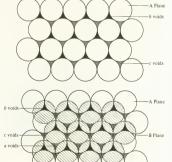


Fig. 3-14. Closest packing of two planes of atoms. The atoms of the upper plane are shaded and are directly above the b voids. The upper plane has two sets of voids, labeled a and c. The next plane of atoms added can fit into either of these.

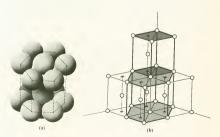
of the planes can be denoted as ABABAB..., where all of the A's are directly above each other, and the same is true of the B's. This defines the hexagonal close-packed structure. The second set of voids on the B plane lies directly above the c voids (lightly shaded) of the A plane. The third plane could be placed over these voids and the densest packing would be maintained. If this is done and the stacking sequence is continued, the configuration of the planes in the resulting solid is ABCABC..., where all of the A planes are directly above each other, etc. This is the face-centered cubic structure.

A hard-ball model of the hexagonal close-packed structure is shown in Fig. 3-15(a). The dashed lines emphasize the hexagonal geometry. The atoms of the top and bottom planes are directly above each other, in accordance with the ABABAB... arrangement of the densely packed planes in the structure. Part of an hep lattice is shown in Fig. 3-15(b). Two different unit cells are in common use for describing this structure. Both are heavily outlined in the figure. The larger unit cell emphasizes the hexagonal geometry, while the smaller one is simpler, containing only two atoms. Planes and directions in the hep lattice are designated in terms of the larger unit cell. The notation used for specifying planes and directions in this structure is different from that discussed in Sections 3-2 and 3-3. The hep notation is explained in Appendix D.

The face-centered cubic structure is illustrated in Fig. 3-16. The hard-sphere model of a unit cell is shown in Fig. 3-16(a). An atom appears in the center of each cube face. The corner atoms touch the face-centered atom but do not touch each other. An fee lattice appears in Fig. 3-16(b), with the unit cell heavily outlined. The length of a cube edge is shown as a in this figure. The cube edge length is called the lattice parameter for all three cubic structures (see Fig. 3-5) and is a quantity which we shall use quite extensively. Values of the lattice parameter for a number of elements are given in the periodic table.

Figure 3-16 clearly shows the cubic geometry of the fcc structure, but the close-packed planes are not apparent. The cube faces, or ((100)) planes, are not densely packed. The close-packed planes can be seen in Fig. 3-17.

Fig. 3-15. The hexagonal close-packed structure. (a) Hard-ball model of a unit-cell. (b) The hcp lattice. This lattice can be formed from either of the unit cells shown. These cells are heavily outlined.



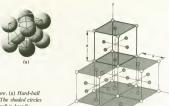
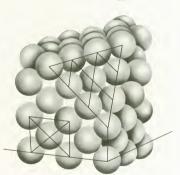


Fig. 3-16. The face-centered cubic structure. (a) Hard-ball model of the unit cell. (b) An fcc lattice. The shaded circles are face-centered lattice points. The unit cell is heavily outlined and the lattice points associated with this cell are cross-hatched.



(b)

Fig. 3-17. Model of an fcc crystal. The horizontal and vertical planes are ((100)); the close-packed plane is ((111)).

The horizontal and vertical planes are ((100)), and the close-packed planes can be seen by cutting away a corner of the crystal and revealing a diagonal plane. The densely packed plane is (111), as can be seen in Fig. 3-18. Thus, the close-packed planes in the fee structure are the ((1111)) families.

## Example 3-1

Determine the number of atoms in the fcc unit cell.

Figure 3-16 shows that there are eight corner atoms and six facecentered atoms per unit cell. According to Fig. 3-16(b), each corner atom is equally shared by eight unit cells, while each face atom is equally shared by two unit cells:

Fig. 3-18. (a) The (111) plane of an fec crystal. The atom locations are shown. (b) The close-packed structure of the (111) plane for an fec structure. The triangle shown in this plane view corresponds to the triangle in the unit cell of (a).





Number of atoms in an fcc unit cell =  $(\frac{1}{8})(8) + (\frac{1}{2})(6) = 4$ 

#### Example 3-2

What fraction of the volume of an fcc unit cell is occupied by atoms? This quantity is called the packing factor:

Packing factor = 
$$\frac{\text{volume of atoms}}{\text{volume of cell}}$$

Because there are four atoms per unit cell and each atom is a sphere,

$$V_{\text{atoms}} = (4)(\frac{4}{3}\pi\mathscr{R}_a^3) = \frac{1.6}{3}\pi\mathscr{R}_a^3$$

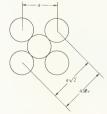
where  $\mathcal{R}_a$  is the atomic radius,

$$V_{\text{cell}} = a^3$$

where a is the lattice parameter. To find the cell volume in terms of  $\mathcal{R}_a$ , consider a cube face. From the accompanying diagram,

$$a\sqrt{2}=4\mathcal{R}_a$$
 
$$a=2\sqrt{2}\mathcal{R}_a$$
 
$$V_{\rm atoms}=\frac{1}{3}a\mathcal{R}_a^3=16\pi$$

Packing factor = 
$$\frac{V_{\text{atoms}}}{V_{\text{cell}}} = \frac{\frac{1.6}{3}\pi \mathcal{R}_a^3}{(2\sqrt{2}\mathcal{R}_a)^3} = \frac{16\pi}{48\sqrt{2}} = \frac{\pi}{3\sqrt{2}} = 0.74$$



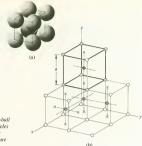
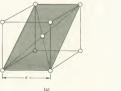


Fig. 3-19. The body-centered cubic structure. (a) Hard-ball model of the unit cell. (b) A bcc lattice. The shaded circles are body-centered lattice points. The unit cell is heavily outlined and the lattice points associated with this cell are cross-hatched.

The periodic table inside the covers shows the crystal structure of most of the elements. Many of the metals have the hep or fee structures; however, a third structure is also quite common. This is the body-centered cubic (bcc), which is illustrated in Fig. 3-19. Each atom has 8 nearest neighbors in this structure compared to 12 nearest neighbors in the fec and hep arrangements. Body-centered cubic crystals do not have the densest possible packing. The bec structure is shown by a number of the transition metals, and the structure is attributed to the bonds in these metals being somewhat directional; that is, they are metallic bonds with some covalent character. This is not surprising if we consider the electron structure of these elements. The alkali metals (group IA of the periodic table) also show the bcc packing; however, these revert to the fee or hep structure at very low temperature.

## Example 3-3

Tungsten has a bcc structure and a lattice parameter of 3.165 Å. Find the number of atoms per square centimeter on the ((110)) planes,



a a √2 (b)

Sketch (a) shows the (101) plane, while sketch (b) is a plan view of the plane. The rectangle in (b) can be considered as a unit cell in a two-dimensional space lattice. It contains two atoms.

$$\frac{\text{Atoms}}{\text{Area}} = \frac{2}{a^2 \sqrt{2}} = \frac{\sqrt{2}}{(3.165 \times 10^{-8})^2} = 1.41 \times 10^{15} \text{ atoms/cm}^2$$

#### Example 3-4

The structure of aluminum is fcc, and it has a lattice parameter of 4.04Å. Find the number of atoms per centimeter in the [[1001] directions.

The [[100]] directions are the cube edges; therefore the problem is that of finding the number of atoms per centimeter when the atoms are 4.04Å apart. From the accompanying sketch.

$$\frac{\text{Number of atoms}}{\text{Length}} = \frac{1}{4.04 \times 10^{-8}} = 2.48 \times 10^7 \text{ atoms/cm}$$

#### Questions

Question 6: How many atoms does the hexagonal unit cell of the hcp structure have? Figure 3-15 should help.

Question 7: Calculate the packing density for the bcc structure.

Question 8: Find the number of atoms per centimeter in the [110] direction in aluminum. Which direction has denser packing, the [100] or [110]? Denser packing in this case means more atoms per centimeter.

## 3-5 Nondirectional bonds with atoms of unequal size

Ionic crystals contain atoms of different sizes, which are held together by nondirectional bonds. Each ion tends to form the maximum number of bonds in order to achieve stability. This tendency does not cause fee and hep structures because the atoms are not the same size. In addition, the entire crystal must maintain electrical neutrality. Solids such as MgO and NaCl must have equal numbers of positive ions (cations) and negative ions (anions) in order for the crystal to be electrically neutral. A solid crystal of MgCl<sub>2</sub>, however, must accommodate twice as many chlorine ions as magnesium ions. These are valence restrictions and they do affect the solid structure.

Before proceeding, two terms need to be introduced. The first is the coordination number, which is the number of nearest neighbors of an atom in a crystal. The second term is the ionic radius. The billiard-ball model will be used for ionic structures, and the ionic radius is simply the radius of the hard sphere that represents the ion. Values of ionic radiu are tabulated in Appendix A and several are listed in Table 3-2. It should be

Table 3-2. Ionic radii

Charge at given ionic radius	Element	Ionic radius (Å)	Atomic radius (Å)
-2	Oxygen	1.32	0.6
-1	Fluorine	1.33	0.6
+1	Sodium	0.98	1.857
-1	Chlorine	1.81	0.905
+2	Magnesium	0.78	1.594
+1	Copper	0.96	1.278
+3	Aluminum	0.51	1.431
+4	Silicon	0.41	1.176

noted that ionic radii can be larger or smaller than atomic radii, depending on whether an atom gains or loses electrons in the ionization process.

The discussion in this section will be limited to those cases in which the number of cations and anions in a crystal are equal. The effect of the relative sizes of the cations and anions on the structure can be understood by considering an example. Figure 3-20(a) shows a cation surrounded by six anions; that is, the cation has a coordination number of 6. The small cation is shaded in the figure and is at the center of the void that is formed when the anions come together. Each anion touches the cation and also touches four neighboring anions. There is only one value of the ratio of cation to anion radius at which this configuration can exist.

#### Example 3-5

Find the value of the ratio  $\mathcal{R}_{\mathbb{C}}/\mathcal{R}_{\mathbb{A}}$  for a coordination number of 6, where

$$\mathcal{R}_{C}$$
 = ionic radius of a cation  $\mathcal{R}_{A}$  = ionic radius of an anion

Figure 3-20(b) is a view of a plane through the figure in 3-20(a). The plane passes through the *centers* of four cations and the anion. Applying the Pythagorean theorem to Fig. 3-20(b),

$$(2\mathcal{R}_{A} + 2\mathcal{R}_{C})^{2} = (2\mathcal{R}_{A})^{2} + (2\mathcal{R}_{A})^{2}$$

$$2\mathcal{R}_{A} + 2\mathcal{R}_{C} = \sqrt{8}\mathcal{R}_{A} = 2\sqrt{2}\mathcal{R}_{A}$$

$$\mathcal{R}_{C} = (\sqrt{2} - 1)\mathcal{R}_{A}$$

$$\frac{\mathcal{R}_{C}}{\mathcal{R}_{A}} = (\sqrt{2} - 1) = 0.414$$

The number 0.414 represents the smallest value of  $\mathcal{B}_c/\mathcal{B}_A$  for which all six anions touch the cation and is called the *critical radius ratio*. If the ratio of  $\mathcal{B}_c/\mathcal{B}_A$  is not exactly 0.414, an anion cannot touch the cation and four neighbors. For values slightly larger, the coordination number may still be 6 and all of the anions will touch the cation, although they will not touch their neighboring anions. At values of  $\mathcal{B}_c/\mathcal{B}_A$  less than 0.414, a coordination number of 6 requires that the anions each touch four neighbors but do not touch the cation. Such bonding does not occur

Fig. 3-20. Packing of unequal sized ions or atoms (a) A cation surrounded by six anions. Each anion touches the cation and four neighbors, (b) A cross section through (a). The plane includes the centers of four cations and one anion.

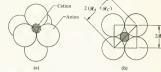
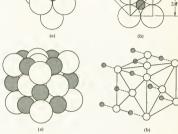


Fig. 3-21. Packing arrangement for a coordination number of 6 (a) A hard-sphere model of the NaCl structure, (b) The structure for a coordination number of 6 is fcc, with one cation and one anion at each lattice site. This structure appears in NaCl, KCl, BaO, MgO, NiO, and others. In these compounds the cations correspond to the shaded ones in the figure.



because the atoms can arrange themselves in structures which have a lower energy. This can be seen qualitatively by considering the energy curve of a cation-anion bond [Fig. 2-11(b)]. If the cation and anion do not touch, the distance between them is greater than  $r_0$  and the bond energy is not a minimum. Recall that  $r_0$  is the equilibrium bond length. The solid would be more stable if the cation surrounded itself with fewer anions but bonded to them with the bond length  $r_0$ . This is observed to happen, and the coordination number in solids having  $\mathcal{R}_C/\mathcal{R}_A$  less than 0.414 is lower than

The hard-sphere packing arrangement for a coordination number of 6 is shown in Fig. 3-21(a). The diagram in Fig. 3-21(b) shows that the structure is formed on an fcc space lattice, with one cation and one anion at each lattice point. The cation-anion pairs are joined by dashed lines in the figure. This is called the NaCl structure and is exhibited by MgO and NaCl as well as by many other compounds. The ionic radius ratios of MgO and NaCl are 0.47 and 0.53, respectively.

The NaCl structure satisfies the symmetry requirements of a perfect crystal and was constructed by placing two ions at each point in a Bravais lattice. For crystals having equal numbers of cations and anions, there are only certain values of the coordination number that satisfy the crystal symmetry requirements. These are 2, 3, 4, 6, 8, and 12. The critical radius ratio can be found for each of these by doing calculations similar to Example 3-5. The results of these calculations are given in Table 3-3 and include the range of values of  $\mathcal{R}_C/\mathcal{R}_A$  for which a particular coordination number appears. A different structure corresponds to each value of the coordination number. As an example, the CsCl structure is shown in Fig. 3-22. The

Table 3-3. Coordination numbers corresponding to various radius ratios

Coordination number	Critical radius ratio	Range of radius ratio showing this coordination	
2	0	0-0.155	
3	0.155	0.155-0.225	
4	0.225	0.225-0.414	
6	0.414	0.414-0.732	
8	0.732	0.732-1.0	
12	1.0	1.0	

coordination number is 8. It should be strongly noted that the structures discussed in this section are certainly not limited to the alkali halides. This impression can sometimes be acquired. For example, the structure of Fig. 3-21 applies to both NaCl and MgO. NaCl has very limited engineering application; however, MgO is a useful high-temperature ceramic.

#### Question

Question 9: Calculate the critical radius ratio for a coordination number of 4. For this structure, the centers of the anions form the apexes of a tetrahedron, and the cation is at the center (see Fig. 3-25).

## 3-6 Coordination polyhedra and silicates

It is often convenient to consider the structure of solids in terms of coordination polyhedra rather than atoms. This is especially true of complex structures. As an example of a coordination polyhedron, consider the structure of MgO again. The hard-ball model of Fig. 3-20(a) is represented in a slightly different fashion in Fig. 3-23. The hard-ball model has been expanded, and lines have been drawn from the center of each of the anions to the centers of its nearest anion neighbors. The resulting figure is a coordination polyhedron. In this case the figure is an octahedron, and this arrangement is called octahedral coordination. Note that an octahedron (eight-sided solid) has only six points, corresponding to the coordination number of 6. The structure of MgO can be represented by properly stacking these octahedra. In the case of ionic bonds, a coordination polyhedron is associated with each range of the radius ratio. These polyhedra are listed in Table 3-4.

Fig. 3-22. The CsCl structure. In this arrangement the cation is surrounded by eight anions.

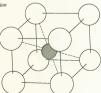


Table 3-4

Coordination number	Range of radius ratio	Coordination polyhedron	Packing
2	0-0.155	Line	Linear
3	0.155-0.225	Triangle	Triangular
4	0.225-0.414	Tetrahedron	Tetrahedra
6	0.414-0.732	Octahedron	Octahedral
8	0.732-1.0	Cube	Cubic
12	1.0		hep or fee

A coordination polyhedron of particular significance is the silicate tetrahedron composed of silicon and oxygen. A hard-ball model of it is shown in Fig. 3-24(a), while the tetrahedral geometry is emphasized in Fig. 3-24(b). It is important because of the large number of silicate compounds that exist. Silicon is the second most abundant element in the earth's crust, while oxygen is first; consequently it is not surprising that many solids exist which include silicate. The bonds in the silicate structure are a mixture of covalent and ionic. The tetrahedral arrangement would result from either one. Pure silicon forms in the diamond structure just as carbon does and therefore shows tetrahedral coordination when bonding covalently (see Fig. 2-16). For ionic bonding, the radius ratio of silicon and oxygen is 0.31, which also corresponds to a tetrahedron.

Silicon has a valence of +4, while oxygen is -2; therefore the silicate

Fig. 3-23. The hard-ball model of Fig. 3-20 represented in a different fashion. The center ion is Mg<sup>2</sup> \*; the others are O<sup>2</sup> -. This figure emphasizes the octahedral coordination of MgO.

Fig. 3-24. The silicate tetrahedron, SiO<sub>4</sub><sup>-8</sup>. (a) A hard-ball model. The ions shown are oxygen. (b) An alternate sketch of (a) showing the silicon ion and emphasizing the tetrahedral coordination. The oxygen ions each have a charge is +4e. the silicon charge is +2e.

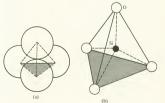


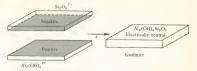
Fig. 3-25. A silicate chain. The cross-hatched oxygen ions have their valence bonds satisfied because each of them bonds to two silicon ions. The remaining oxygen ions have a charge of — le.

Fig. 3-26. The silicate sheet structure. The bonding requirements of some of the oxygen ions are satisfied by forming the sheet structure rather than the chain structure. Each oxygen ion on top of the sheet still has a net charge of —1e.

tetrahedron of Fig. 3-24 is SiO<sub>4</sub>-4. Each oxygen ion has a net charge of -1 e and is seeking to form additional bonds. The valence requirement of some of the oxygen atoms can be satisfied by forming a silicate chain, as shown in Fig. 3-25. In this configuration, the valence requirement of each oxygen ion on the horizontal line (cross-hatched ions) is met because each of these oxygens bonds to two silicon ions. The oxygen ions on the top and sides of the chain seek additional bonds and can form these bonds with other elements or radicals. They can also bond to other silicate chains, thus forming a silicate sheet. The sheet structure is shown in Fig. 3-26. Again, those oxygen atoms whose valence requirements are met have been cross-hatched; the unshaded atoms have unfilled bonds. Note that each cross-hatched oxygen is shared by two tetrahedra. We would therefore expect that the sheet structure has a lower ratio of oxygen to silicon than the chain structure. This is reflected in the chemical formulas of the chain and the sheet; the single chain is SiO32, while the sheet is Si2O52.

The sheet structure enables silicate sheets to form bonds with sheets of other substances. The net charge on the silicate sheet of Fig. 3-26 is negative; consequently it will bond to a positive sheet. An example of sheet bonding is given in Fig. 3-27, which schematically shows the combining of a sheet of  $Si_2O_3^{-2}$  with a sheet of  $Al_2(OH)_4^{+2}$  to form a sheet of kaolinite. Kaolinite is a common and useful clay. All of the primary bonds in the kaolinite sheet are satisfied; consequently bonding between adjacent sheets can occur through secondary bonds only. Tale is another example of this type of structure. To form tale, a sheet of  $Mg_3(OH)_2^{+4}$  is sandwiched between two sheets of  $Si_2O_3^{-2}$ . The result is a sheet of tale,  $Mg_3(OH)_2(Si_2O_3)_2$ , which has all of its primary bonds satisfied and joins

Fig. 3-27. Schematic diagram of the formation of kaolinite from sheets of Al<sub>2</sub>(OH)<sub>4</sub> and Si<sub>2</sub>O<sub>5</sub>. All of the primary bonds of the atom in the kaolinite sheet are satisfied.

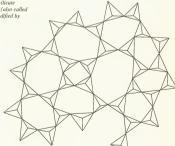


adjacent tale sheets by secondary bonds. This structural arrangement allows the tale sheets to slip past each other easily, and it is similar to graphite in this respect. Mica is another substance which has the silicate sheet structure. The weak bonding between mica sheets makes it very easy to "peel" layers of mica from a solid piece.

Silicate can also form three-dimensional crystal structures. One of these structures can be described by substituting a silicate radical for each carbon atom in the diamond structure [Fig. 2-16(c)]. Both have tetrahedral coordination. In this structure, which is called cristobalite, each oxygen atom is shared by two adjacent silicate tetrahedra. The resulting composition is SiO<sub>2</sub>. Crystalline quartz has the same formula but a different structure.

The silicate radical is very versatile and can form amorphous as well as crystalline structures. The structure of fused quart is schematically shown in Fig. 3-28. The silicate tetrahedra align themselves such that the tetrahedra points touch. The oxygen atom located at the point of contact is shared by two adjacent tetrahedra. Fused quartz is very important in the glass industry, and the amorphous structure of Fig. 3-28 is typical of glasses. The properties of fused quartz are often modified by adding alkali or alkali-earth oxides to the quartz. These are called network

Fig. 3-28. Schematic arrangement of silicate tetrahedra to form amorphous quartz (also called fused quartz). The structure can be modified by introducing certain other elements.



modifiers, and a typical example of network-modified quartz is window glass, which is composed of Na<sub>2</sub>O (soda), CaO (lime), and SiO<sub>2</sub>. It is called soda-lime-silica glass. The glass structure does not have the longrange order shown by crystals. In Section 3-7 we shall encounter other amorphous structures when we again consider polymers.

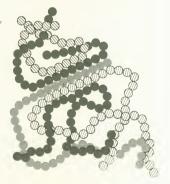
Question

Question 10: The first paragraph of this section states that MgO crystals can be represented by properly stacking MgO octahedra (see Fig. 3-23). The octahedron contains six anions and one cation; consequently it has a net charge of +10. MgO has an equal number of cations and anions. How can the octahedra be stacked such that electrical neutrality is maintained. Note: The answer to this is indicated by the manner in which the silicate tetrahedra bond together.

# 3-7 Polymer structures

Polymer chains join together to form three-dimensional structures. The physical properties of chain polymers depend strongly on the manner in which the bonding between chains occurs. Recall that all of the atoms in a polymer chain have their full complement of primary bonds; therefore the chains can be held together only by secondary bonds. An example of bonding between chains is shown in Fig. 3-29, where five polymer chains are represented schematically. The long-chain molecules are flexible and have a tendency to bend and meander through the solid rather than remaining straight. The chains are held together by secondary bonds will produce a material that is easily deformed, while a larger number will produce a material that is easily deformed, while a larger number will

Fig. 3-29. Schematic drawing of five chains in a polymer. Each circle represents a repeating unit of the polymer. The structure is crystalline in the region where the chains alian.



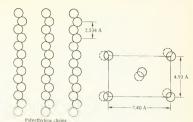


Fig. 3-30. The crystalline structure of polyethylene. The circles are carbon atoms and the hydrogen atoms have been omitted

produce a stronger, stiffer material. The maximum number of secondary bonds would form between straight, parallel chains. A region in which this occurs is shown in Fig. 3-29 and corresponds to a crystalline region. The structure shown in the figure is partially crystalline and partially amorphous.

The side groups that are attached to the carbon backbone of a polymer chain are quite influential in determining whether or not crystalline regions occur. Chains such as polyethylene and Teflon have small atoms symmetrically arranged on the backbone; consequently these chains can align with each other. The crystal structure of polyethylene is shown in Fig. 3-30. Each circle represents a carbon atom; the hydrogens are not shown. The molecules of a chain are held together by primary bonds, while the chains are bonded together by secondary bonds. Polyethylene chains generally form a solid that has both crystalline and amorphous regions.

Chains having large, bulky side groups do not tend to align with each other to form crystalline regions. Polymers such as polystyrene and polyvinyl acetate (see Table 2-9) have large groups on one side of the chain, and these inhibit chain alignment. In the case of polymethyl methacrylate, side groups occur on two sides of the chain and crystallization is very unlikely. While the bulky side groups reduce the number of secondary bonds, they also make it difficult for one chain to slide past another. This has a strengthening effect, as will be discussed in Chapter 9. Copolymers are difficult to crystallize because different regions of the chains have different structures and the chains do not align well.

Many amorphous polymers can be strengthened and stiffened by cross linking, which consists of joining two chains together by either a third chain, an atom, or a group of atoms. This is shown schematically in Fig. 3-31. In this illustration, the chains are linked together by the shaded atoms. These atoms are bonded to the chains by primary bonds and thus enhance the strength of the polymer. Polystrene can be cross-linked by divinylbenzene, for example. Each divinylbenzene molecule is capable of linking two polystryene chains together by bonding to each at one point. Cross linking strengthens polymers but inhibits crystallization.

The length of the chains which form a polymer also affect the properties.





Fig. 3-31. Cross linking in a chain polymer. The dark circles are the cross links and represent atoms, groups of atoms, or chains, The unshaded circles are polymer units,

A long chain will form more secondary bonds with its neighbors than a short one, and a material made from long chains is stronger than one made of short chains. The length of a chain is defined by its degree of polymerization. The degree of polymerization is equal to the number of repeating units in the polymer chain. In the case of polyethylene, for example, the repeating unit is C2H4, and the degree of polymerization is just the number of ethylene molecules that have joined together to form a chain. In terms of molecular weight.

Degree of polymerization =  $\frac{\text{molecular weight of a chain}}{\text{molecular weight of a repeating unit}}$ 

The chains in a polymer material are not all of the same length; therefore it is necessary to use the average molecular weight of the chains when computing the degree of polymerization.

The mechanisms described in this section have been concerned with strengthening or weakening polymer materials. These mechanisms all involve modifications to the manner in which the chains are bound together, that is, structure modifications, and they serve as good illustrations of the effect of structure and bonding on properties.

#### Question

Ouestion 11: Appendix C lists some of the physical properties for a number of polymers. The data for polyethylene show that the strength decreases as the density diminishes. Explain this by considering the secondary bonds between polyethylene chains.

## Stereoisomerism

In many cases, polymers having the same chemical composition are observed to have different chain structures. They are called stereoisomers or geometric isomers. As an example, consider the vinyl polymers of Table 2-9. Their chain structure is similar to polyethylene but one hydrogen is replaced by a side group. The side groups can attach themselves in different ways, resulting in stereoisomers. This is shown in Fig. 3-32. If all

(a)
(b)
Curbon
Side gro

Fig. 3-32. Stereoisomers of vinyl chains. The hydrogen atoms are not shown. Three different structures are shown for three different side groups. (a) Isotactic, same side; (b) syndiotactic, alternating; (c) atactic, random.

of the side groups are attached to the same side of the chain, the chain is called isotactic. Alternating side groups give the syndiotactic structure, while side groups which are placed randomly on opposite sides of the chain yield the atactic structure.

The structure of a polymer chain affects physical properties. For example, isotactic polystyrene has been crystallized, but this is not true of atactic polystyrene. The strength and stiffness of the crystalline form is greater than that of the amorphous form. In addition, the properties of the crystalline polymer are not as temperature sensitive as the properties of the amorphous polymer.

### 3\_9 Elastomers

Elastomers are polymers which can undergo large elongations under load at room temperature and return to their original shape when the load is released. The extensions can range up to several hundred percent. This behavior can be explained by considering rubber (polyisoprene), whose behavior is typical of elastomers. It also provides an excellent example of the effects of stereoisomers and cross links.

Polyisoptene is one of the diene polymers shown in Table 2-10. Two repeating units for this polymer are illustrated in Fig. 3-33(a). The only difference between the two units is the location of the circled hydrogen atoms. This small change in structure causes very different polymer properties. Two structures are shown in Fig. 3-33(b). The structure on the left corresponds to the hydrogen atom being on the side of the chain which is opposite to the CH<sub>3</sub> group, as illustrated by the circled hydrogens. In this configuration, the positions for further bonding (arrows) are on opposite sides of the chain. This is called trans-polyisoprene and is commonly known as gutta percha. The carbon backbone and the CH<sub>3</sub> groups are shown in Fig. 3-33(c). Gutta percha is not an elastomer. It forms a rigid solid.

The structure shown on the right side of Fig. 3-33 has the hydrogen

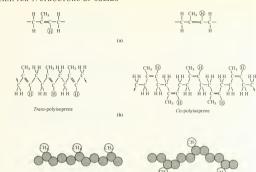
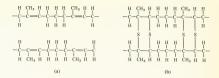


Fig. 3-33. Stereoisomers of polyisoprene. (a) The repeating unit showing two possible positions of a hydrogen atom. (b) Diagrams of the cis and trans somers of polyisoprene. (c) Hard-sphere diagram of the carbon atoms and CH<sub>3</sub> side groups for the two structures. Double bonds appear as overlapping spheres.

atom (circled) and the CH<sub>3</sub> group on the same side of the chain. This causes a geometric problem; they interfere with each other. Interference between atoms or atomic groups that want to occupy the same space is called steric hindrance. As a result of steric hindrance, the structure shown in Fig. 3-33(b) (*siz*-polyisoprene) forms. The bonding positions (arrows) for this configuration are on the same side of the chain, hence the term *cis*. The hard-sphere diagram shows that *cis*-polyisoprene hains are flexible and are not straight when unstressed. In natural rubber, the chains tend to coil as a result of the steric hindrance. When the rubber is placed in tension, the chains uncoil and become straighter as the rubber elongates. It is the uncoiling of the chains that accounts for the large deformation of elastomers. Rubber elasticity can be explained by thermodynamic arguments which depend strongly on the shape of the chain. This explanation, however, is bewond the scope of the book.

Natural rubber is not a very useful material before it is vulcanized. Vulcanization is a process which causes cross linking of rubber chains and depends on the one double-carbon bond in isoprene. Two polyisoprene chains are shown in Fig. 3-34(a). If the double-carbon bonds could be broken, bonding sites would be available on the chains. In the vulcanizing process, these bonds are broken and new bonding sites are thereby created. A substance such as sulfur is introduced, and it bonds to both

Fig. 3-34.
Vulcanization of rubber.
(a) Two polyisoprene
chains. (b) Breaking of
the carbon double bonds
provides further
bonding sites. Sulfur
bonds to these sites
and cross-links the
chains.



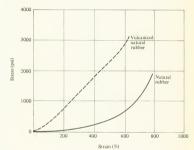


Fig. 3-35. The stress-strain diagram of vulcanized and unvulcanized natural rubber. For unvulcanized natural rubber the slope of the curve increases as the strain increases.

chains at these sites. As shown in Fig. 3-34(b), the sulfur provides a cross link between chains. The physical properties of natural rubber can be significantly changed in this manner and depend on sulfur content (or the number of cross links). For example, automobile tire treads have about 3-5%, sulfur and are elastic. Battery cases are much more rigid and have a higher sulfur content. A stress-strain curve for vulcanized and unvulcanized rubber is shown in Fig. 3-35. Synthetic elastomers (neoprene, polybuta-diene) show the carbon double bond just as natural rubber does and can therefore be vulcanized. The vulcanization process discussed here is a simplification and can be considered as a schematic explanation.

### Ouestion

Question 12: Perform the following experiment. Hold an unstretched rubber band to your lip. While maintaining contact between your lip and the rubber band, stretch the rubber (but do not break it). Your lip should detect a temperature increase. This is due to the heat released as the rubber chains uncoil and the number of secondary bonds between chains increases. Based upon this experiment, explain why the slope of the stress-strain curve for natural rubber (Fig. 3-25) increases with increasing strain.

# 3-10 Thermoplastic and thermosetting polymers

Polymers are often classified as thermoplastic or thermosetting. A thermoplastic polymer is one which, when heated, softens before it decomposes. A thermosetting polymer decomposes first. This behavior can be explained in terms of bonding and structure. Consider a solid composed of linear polymer chains held together by secondary bonds. As the material is heated, the motion of the atoms about their equilibrium positions increases. and bonds can be broken as a result. The first bonds to break are the weakest ones, which hold the chains to each other. When this occurs chains can slide past each other. The material becomes soft and begins to flow. Upon cooling, it resumes its original structure. This behavior is advantageous for processes such as molding but can be disastrous if such polymers are used to support heavy loads at high temperatures. Thermoplastic behavior is often (but not always) exhibited by chain polymers. An exception to this is cellulose, whose chains are bound together with hydrogen bonds. These are strong enough so that the entire material begins to decompose before the hydrogen bonds break.

Two network-forming polymers were discussed in Chapter 2; these were phenol-formaldehyde and melamine-formaldehyde. They form three-dimensional structures and have primary bonds only. Such materials often show an increase in hardness as temperature is increased. This is attributed to reactions within the material. The polymerization process is accelerated by increasing the temperature; consequently any of the monomers which had not previously polymerized would have a tendency to do so as temperature increased. Organic polymers which form network structures are generally thermosetting.

# **3-11** Summary

The nondirectional characteristics of the metallic and ionic bonds cause each atom to surround itself with as many neighbors as possible. In the case of metals, this results in close-packed structures. Ionically bonded substances contain ions of different sizes. This, together with the valence of the ions, influences the structure. Solids formed by these bond types are crystalline. Mixed bonding can also occur. For example, the bcc structure of several transition metals is attributed to the bonding being a mixture of metallic and covalent. Bonding in the silicate radical is a mixture of covalent and ionic. These structures are the direct result of the bond type, and therefore structure and bonding are related parameters.

Solids formed from silicate can be either crystalline or amorphous. The same is true of carbon and its compounds. Pure carbon forms crystals with the diamond structure, utilizing covalent bonds. The same covalent carbon bond, however, will also produce polymers. Chain polymers have an ordered structure within a chain, and the atoms composing the chain are held together by primarily covalent bonds. Bonding between chains is weak unless cross linking is used or a crystal structure is formed. The mechanical properties of polymers depend rather strongly on the forces between chains, and these properties are therefore sensitive to structure

and bonding. Polymers forming three-dimensional networks which utilize only primary bonds are generally stronger and more rigid than non-crosslinked chain polymers, again indicating a structure and bonding dependence.

### Problems

- 1 Sketch a two-dimensional space lattice. (a) Show one of the primitive cells having unit vectors a and b. (b) Show the same primitive cell at another location in the same lattice. Draw a vector which joins the tips of the two a unit vectors. Write the equation for this vector in terms of a and b. (c) Do the same thing for a vector joining the tips of the two b vectors. The equation defines what is often called a translation vector.
- 2 (a) Sketch a unit cell in a two-dimensional lattice, and let each unit vector touch three lattice points (vector b in cell 5, Fig. 3-3, does this). How many lattice points are in the cell? (b) Do part (a) for the threedimensional lattice shown in Fig. 3-4. Let each of the unit vectors touch three lattice points.
- 3 For a cubic unit cell, sketch the eight directions indicated by the notation [[111]]. Any lattice point may be used as the origin of coordinates, but the coordinate systems must be right-handed.
- 4 (a) Sketch the (110) plane in a cubic unit cell. Show all directions of the form [[111]] which lie in this plane. (b) Sketch the (111) plane in a cubic unit cell. Show the [112] direction, which lies in the plane.
- 5 For a cubic crystal, show that the [umv] direction is perpendicular to the (hkl) plane if h = u, k = v, and w = l. Hint: A line is perpendicular to a plane if it is perpendicular to any two lines in the plane. Also, two lines are perpendicular if the dot product of two vectors in the directions of the lines is zero.
- 6 (a) Sketch three planes of the (111) family in an orthorhombic lattice.(b) Do the same for the (221) family.
- 7 Find the number of atoms per square centimeter on the following planes: (a) (110) plane in chromium, (b) (111) plane in chromium, (c) (110) plane in nickel, and (d) (111) plane in nickel.
- 8 (a) Find the number of atoms per centimeter in the [100], [110], and [111] directions of tungsten. (b) Which direction has the densest packing? (c) What is the direction of densest packing in the fcc structure?
- 9 Platinum has a density of 21.45 g/cm³ and an atomic weight of 195.1 and is fcc. (a) How many atoms are in 1 cm³? (b) Calculate the dimensions of the unit cell. (c) Find the atomic radius of Pt.
- 10 Calculate the packing density for the following structures: (a) simple cubic and (b) Hexagonal close-packed. Compare your answer to part (b) with Example 3-2.
- 11 Iron is bec below 910°C but changes its structure to fee above this temperature. (a) If the atomic radius is the same in both structures, find the decrease in volume (expressed as a percentage of the bec volume) due to the structure change. (b) In the real case, it is found that the bec structure has a lattice parameter of 2.89Å at 910°C and

- the fcc has a lattice parameter of 3.66 Å. Calculate the volume change due to the structure change, expressed as a fraction of the bcc volume. (c) Calculate the atomic radius for each structure
- 12 Calculate the critical radius ratio for a coordination number of 8
- 13 The MgO structure is shown in Fig. 3-21, (a) Find the lattice parameter. The ionic radii are given in Appendix A. (b) Calculate the density of MgO in grams per cubic centimeter.
- 14 (a) Make a two-dimensional sketch of the silicate chain structure. The sketch should show the arrangement of the valence electrons in the manner illustrated in Fig. 2-15. (b) Indicate which of the oxygens has a negative charge. (c) What is the chemical formula for the chain structure?
- 15 The degree of polymerization is the number of building units which join together to form a molecule. If the average degree of polymerization in a polyethylene specimen is 500, what is the molecular weight?
- 16 The carbon chain shown in Fig. 3-32 forms the basis of a large number of polymers. The C atoms are not aligned. Using the tetrahedral orbitals of Fig. 2-16(a) and the measured C-C bond distance of 1.54 Å from Table 2-7, calculate the distance between carbon atoms as measured on a straight line joining the centers of every other C atom. The calculation is simplified by the accompanying sketch of the C orbitals,



- 17 Polytetrafluoroethylene (Teflon) has the same structure as polyethylene except that each H atom is replaced by an F atom. The distance between carbon atoms, as defined in Problem 16 is 1,27 Å. The density of Teflon is 2.2 g/cm3. If all of the chains are aligned at this density, what is the distance between the centers of the chains?
- 18 Natural rubber is observed to harden and develop small cracks when exposed to the atmosphere. Analysis shows that oxygen has entered the structure. Explain.

### Answers

Ouestion 1: (a) Cell 1, one point; cell 2, one point; cell 3, one point; cell 4, two points; cell 5, two points, (b) Cells 1, 2, and 3 are primitive.

Ouestion 2: Taking O as the origin, the direction is  $\lceil \overline{11} \rceil \rceil$ .

Ouestion 3:  $\lceil 100 \rceil$ ,  $\lceil \overline{1}00 \rceil$ ,  $\lceil 010 \rceil$ ,  $\lceil 0\overline{1}0 \rceil$ ,  $\lceil 001 \rceil$ ,  $\lceil 00\overline{1} \rceil$ .

Question 4: (a) Taking the origin as the upper rear corner, the rear plane is (221). Taking the origin as the lower front corner, the front plane is (221), (b) Yes,

Ouestion 5: 45°.

Question 6: Six. Corner atoms are shared by six unit cells and face atoms by two cells. The three interior atoms belong completely to the cell.

Question 7:  $\frac{\pi\sqrt{3}}{8}$  or 68%.

Question 8:  $3.50 \times 10^7$  atoms/cm. [110] is denser than [100].

Question 9:  $\Re_{C}/\Re_{A} = 0.255$ .

- Question 10: Each anion shown in the figure is shared by three MgO octahedra. The shape of the octahedron allows this. Only one-third of each anion belongs to the octahedron, for a net charge of -2. The Mg ion is +2, resulting in neutrality.
- Question 11: The chains are held together by primary bonds of fixed bond length. Decreasing the density must therefore indicate that the average distance between chains is increasing. This means that the number of secondary bonds between chains is becoming smaller, and the material becomes weaker.
- Question 12: The increasing slope means that the material is becoming stiffer. The increase in stiffness is due to the increase in the number of secondary bonds; the rubber takes on a more crystalline structure. The heat released during stretching is due to the formation of secondary bonds between chains.



# and Crystal Imperfections

THE IDEAL CRYSTAL STRUCTURES presented in Chapter 3 provide the starting point for discussing the structure of real crystalline solids. The crystalline solids found in nature do not quite have the perfect symmetry of ideal crystals; they contain structural imperfections which have a great effect on some of their mechanical properties. The imperfections discussed in this chapter can be placed in two general categories: those that exist at boundaries between adjacent single crystals and those that exist within single crystals.

Metals and ceramics are usually composed of a large number of randomly oriented crystals. These crystals are not aligned with each other; therefore a boundary is formed when two of them meet. The small single crystals (called grains) and the boundaries between crystals (called grain boundaries) are usually observed with an optical microscope, and the grain structure seen in this way is called the microstructure. Solids composed of grains are called polycrystals, and their properties are affected by the size of the grains. Most solid materials were molten at some point in their processing. The grain structure was formed when the liquid solidified, and the manner in which solidification occurred affected the microstructure. The solidification process can be controlled: therefore microstructure is controllable. The first part of the chapter deals with the principles of solidification. Once these are understood we can find methods of manipulating grain size, thereby controlling mechanical properties to some extent. Solidification principles are then applied to the important process of casting. The solidification behavior of amorphous materials is different from that of crystalline solids, and this topic is also considered.

Individual grains have imperfections at the atomic level; that is, single atoms or small groups of atoms are disarranged. Plastic behavior and diffusion depend strongly on these imperfections. Chapters 8 and 9 will explain how they affect properties and how they can be used to control properties. This chapter presents only

the geometry of these imperfections. The imperfection geometry affects solidification in some cases. One of these cases is the formation of whiskers, which are superstrong solids. The extremely high strength of whiskers is mainly attributed to an almost perfect structure.

# 4-1 Atomic mechanism of crystal growth

A crystal that is in contact with a liquid of the same substance will grow as the liquid freezes. The mechanism by which this occurs can be explained by means of a model. As a starting point, consider a container holding both the liquid and solid phases of a pure substance at its melting point. As heat is removed from the container, the liquid solidifies. The change from the liquid to the solid state reflects the tendency of the substance to maintain itself in its most stable (or equilibrium) state. The liquid and solid can coexist in equilibrium at the melting point; therefore both states are equally stable at this temperature. At lower temperatures the solid state is the stable one, while equilibrium at higher temperatures requires the liquid state.

To describe our model it is necessary to consider the atomic motion in both the solid and the liquid. We shall start with the solid and shall consider what happens as a cool solid is heated. Heating a solid increases its thermal energy. The amount of heat added in order to increase the temperature from an initial value T<sub>1</sub> to a higher value T<sub>2</sub> can be calculated from the well-known formula

$$\Delta Q = \int_{T_{c}}^{T_{2}} c_{\rho} dT \tag{4-1}$$

where

 $\Delta Q$  = heat added to increase the temperature

c = specific heat at constant pressure

 $T_1$ ,  $T_2$  = initial and final temperatures

The use of  $c_p$  implies that the heating takes place at constant pressure. Heating increases the energy of the solid, but in what form does this energy appear? It appears as an increase in the kinetic and potential energies of the atoms in the crystal. The atoms vibrate about their equilibrium positions. As the temperature increases, the amplitude of the vibrations increases. Referring to Fig. 2-23, the atoms can be visualized as moving back and forth on the potential energy curve in the neighborhood of  $r_0$ . The atoms on the surface of the solid have fewer nearest neighbors than those in the interior, and consequently are not as strongly bound to the solid. If a surface atom acquires sufficient vibrational energy to break the bonds with its neighbors, it can enter the liquid. This, of course, is melting.

All of the atoms in the crystal do not have the same vibrational (or thermal) energy. The energy is divided among the atoms in accordance with the Boltzmann distribution, shown in Fig. 4-1. This curve describes

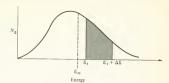


Fig. 4-1. The Boltzmann energy distribution, which describes the distribution of energy among the atoms of a solid. The number of atoms having energies in the range between  $\ell_1$  and  $\ell_1 + \lambda \delta$  is proportional to the gray area shown.

the number of atoms having a particular energy  $(N_{\mathcal{E}})$  as a function of energy (&). As an example of the information contained in the curve, suppose that we wanted to find the fraction of atoms in a crystal having thermal energies between  $\mathcal{E}_1$  and  $\mathcal{E}_1 + \Delta \mathcal{E}$ . This fraction is just the ratio of the shaded area in Fig. 4-1 to the entire area under the curve. The quantity &m in the figure is the mean energy of all of the atoms which make up the solid, and it is related to the temperature of the solid. As temperature increases, the curve shifts to the right, indicating that the atoms have higher thermal energy. The most important feature of the distribution curve, for our present purposes, is that some of the atoms have sufficient energy to break away from the solid and join the liquid. These are the atoms on the high-energy side of the distribution curve, and their number increases as the temperature increases. When a high-energy atom leaves the solid, the energy of the solid is reduced. The temperature will also be reduced if the atom which leaves has an energy higher than  $\mathscr{E}_m$ . Heat is constantly added to the solid during a melting process, however, and the temperature can be kept constant by controlling the rate at which heat is added. Thus, when a high-energy atom leaves the solid, heat is transferred to the solid from a heat source and both the temperature and the energy distribution remain unchanged.

The liquid state is not as well understood as the solid or gaseous states; however, it is generally agreed that the energies of the atoms in a liquid have a distribution function similar to that of Fig. 4-1. The solidification model can be explained in terms of the solid-liquid interface shown in Fig. 4-2. A side view of the interface is illustrated by Fig. 4-2(a), while Fig. 4-2(b) is a top view. The liquid atoms are in motion and some liquid atoms will impinge upon the solid surface. If the energy of the impinging liquid atom is low enough, it will stick to the surface because it is attracted by the surface atoms. The impinging atoms will strike different types of bonding sites on the solid surface. The most probable site is one such as the A site shown in Fig. 4-2(b). The atom has only three nearest neighbors here and consequently is weakly bound. It can migrate along the surface until it either acquires energy from the vibrating lattice atoms and rejoins the liquid or finds a site which will bond it more strongly to the solid. The stronger bonding is supplied by sites such as B and C in the figure, where the atom has six and seven nearest neighbors, respectively. It is also possible for a number of migrating atoms to coalesce by bonding to each other, forming an "island" of atoms. Other atoms can attach to the island, and it will grow into a plane. When a plane has been completed and

∠Atom in a B site

Atom in a C site

(b)

Fig. 4-2. The solid-liquid interface. (a) A side view: The liquid atons are shaded. (b) Top view of the interface: The number of nearest neighbors that an atom on the surface has depends on its location. The atoms occupying A, B, and C sites have 3, 6, and 7 nearest neighbors, respectively.

the next plane is ready to begin growing, only A sites are available. Growth can begin only if a number of mobile atoms at A sites coalesce. This process is considerably slower than just adding atoms to a partially completed plane, and the necessity of forming new islands reduces the solidification rate. Our model is based largely upon the premise that a surface atom can migrate. There is a large amount of experimental data available to back up this assumption.\*

Atom in an A site

We now have two processes occurring simultaneously at the solid-liquid interface. Atoms at the solid surface having sufficiently high energies are leaving the solid to join the liquid (melting), while the lower-energy liquid atoms are being bonded to the solid surface (freezing). At temperatures below the melting point, the freezing rate exceeds the melting parte and the substance solidifies. At temperatures above the melting point and dynamic equilibrium exists. The term dynamic equilibrium implies that two opposite processes are taking place at equal rates. The melting and freezing rates of copper as a function of temperature have been determined by Jackson and Chalmers and are shown in Fig. 4-3. The two curves intersect at the melting point.

### Ouestion

Question 1: Consider an atom in a pure substance. The atom is in a lower-

\* As an example, the surface migration of tungsten atoms has been observed by G. Ehrlich and F. G. Hudda, J. Chem. Phys. 44:1039 (1966).

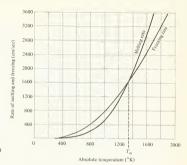


Fig. 4-3. The melting and freezing rates of copper as a function of temperature. Both processes occur simultaneously. At the melting point the two rates are equal. (K. A. Jackson and B. Chalmers, Can. J. Phys. 34:473 (1956).]

energy state when the substance is a crystalline solid than when it is a liquid, i.e., heat is released when the substance freezes. From this and Fig. 4-3, explain why heat must be constantly removed from a material as it freezes if freezing is to continue.

# 4-2 Homogeneous nucleation

Section 4-1 described the mechanism by which a solid existing in a solidliquid mixture grows but said nothing about how the solid got there in the first place. Solidification begins at particular locations called nucleation sites. These sites are small solid particles, and they grow according to the solidification model. Two types of sites can be distinguished, homogeneous and heterogeneous. The first will be discussed in this section, while the second is covered in Section 4-3.

Consider a liquid which has been cooled below its melting point, that is, a supercooled liquid. It is in an unstable state because it would readily freeze if a surface were available to capture liquid atoms. The liquid will remain supercooled until surfaces (or sites) are available for solidification. These are called nucleation sites. If these sites are provided by the liquid itself, the term homogeneous nucleation site is used to describe them.

The formation of homogeneous nucleation sites can be explained in terms of the energy distribution among the liquid atoms. As the temperature of the melt decreases, the number of slow-moving liquid atoms increases. The slow-moving atoms can bond to each other, forming a small solid. This small aggregation of atoms in the supercooled liquid can either grow through the solidification process or go back into the liquid state. Which of these occurs depends on the size of the small solid. This statement may sound odd because we said that a supercooled liquid was unstable, but it has a firm theoretical basis. Energy is released when the

Table 4-1. Maximum supercooling and melting point of some elements\*

Element	Melting point (°C)	Maximum supercooling observed (°C)
Gallium	30	76
Mercury	-40	77
Lead	327	80
Bismuth	271	90
Tin	232	118
Antimony	630	135
Germanium	958	227
Silver	960	227
Gold	1063	230
Copper	1083	236
Iron	1530	295
Manganese	1250	308
Nickel	1452	319
Cobalt	1490	330
Palladium	1553	332
Platinum	1771	370

<sup>\*</sup> Data from D. Turnbull, Prog. Metal Phys. 4:333 (1953).

atoms bond together to form a solid, and a solid with a surface is created It is necessary to provide energy to the aggregation of atoms in order to form the surface. An excess of energy is associated with a surface. This is called the surface energy and will be discussed in detail in Chapter 7. If the stability of small aggregations of atoms is analyzed using the principles of thermodynamics, and the surface energy is included in the analysis, it is found that very small aggregations of atoms are unstable and will revert back to the liquid phase. Larger aggregations are stable and provide sites upon which the liquid atoms can freeze. Rigorous analysis of the problem enables us to define a quantity called the critical radius. The small solid formed by the aggregation of slow-moving liquid atoms can be considered as spherical in shape. If the radius of the sphere is less than the critical radius, the sphere will revert to the liquid phase. This sphere is called an embryo. If the sphere has a radius larger than the critical radius, it is called a nucleus and serves as a nucleation site. We shall not go into the derivation of the critical radius because it probably requires a better thermodynamics background than the reader currently has.†

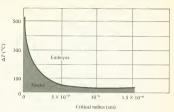
The size of the critical radius depends on the degree of supercooling of the liquid. This relationship is shown in Fig. 4-4 for copper. The shaded area represents the region in which nuclei are formed, while the unshaded region corresponds to embryos. The figure shows that copper can be supercooled by several hundred degrees Centigrade. Large amounts of supercooling have been observed for many materials, and some of these are listed in Table 4-1

### Question

Question 2: Nuclei are formed by the agglomeration of slow-moving liquid particles. They move in a random manner before forming a nucleus. The data in Table 4-1 were obtained from small drops of

<sup>†</sup> The derivation of the critical radius is clearly presented by B. Chalmers, *Principles of Solidification*, Chapter 3, Wiley, New York, 1964.

Fig. 4-4. The critical radius of copper as a function of the degree of supercooling. Dt denotes the number of degrees of supercooling. The shaded area represents nuclei; the unshaded one represents embryos. (After B. Chalmers, Principles of Solidification, Wiley, New York, 1964)



liquid. It is found that increasing the liquid volume causes a decrease in the degree of supercooling that the liquid will tolerate prior to freezing. Thus, the maximum observed supercooling depends on the liquid volume. Explain why. Note that only one nucleus is necessary to initiate freezine.

## 4\_3 Heterogeneous nucleation

It is often observed that when a substance changes its phase, the phase change begins at a particular location. An everyday example of this is water boiling in a pot on the kitchen stove. The steam bubbles usually originate at particular locations on the bottom of the pot. Careful inspection will show that these locations are rough areas. They are called heterogeneous nucleation sites (or simply nuclei). In this case, nucleation of the second phase (steam) takes place at particular sites. A similar effect is found when crystalline substances solidify from the melt. In this case the nuclei are generally solid impurity particles or particular locations at the wall of the container holding the liquid. If such sites are available, solidification generally begins at these sites when the liquid temperature drops slightly below the freezing point. When heterogeneous nuclei are available, they are usually abundant, and solidification will begin at a large number of sites within the melt.

The effect of a liquid solidifying on several nuclei is illustrated in Fig. 4-5. The small, dark spots in Fig. 4-5(a) represent nuclei within the liquid. As the temperature of the melt diminishes, liquid solidifies on the nuclei and crystals grow [Fig. 4-5(b)]. One crystal grows from each nucleus. The

Fig. 4-5. Solidification of a solid containing nuclei, (a) Several nuclei in the melt. (b) Crystals arow around each nucleus at temperatures below the melting point. The lines on the crystals all represent the same crystallographic direction. The crystals are not aligned, (c) The crystals grow together forming grain boundaries, The crystals, or grains, are randomly oriented in the solid.







parallel lines in the figure represent the same direction in each crystal. It is seen that the crystals are not in alignment with each other. Their orientation is random. As solidification progresses, the crystals join each other and form boundaries, as shown in Fig. 4-5(c). Each boundary marks a discontinuity in the crystal structure. The individual crystals are called grains, and the boundaries are called grain boundaries. If solidification begins at a large number of nuclei, the resulting solid will have many grains and is said to be polycrystalline. Most engineering materials are polycrystalline.

The observed grain size varies over a wide range. Materials can solidify with large grains that are visible to the naked eye, but more often it is necessary to use an optical microscope with a magnification up to perhaps 200 or 300. The grain structure (or microstructure) of copper is shown in Fig. 4-6. The grains are randomly oriented and show some variation in size. Grain size can be controlled. One way of doing this would be to supply a controlled number of nuclei to the liquid. These could be in the form of impurities. A large number of nuclei would result in small grains and vice versa. Grain size affects physical properties, with a fine-grained microstructure generally being somewhat stronger than a coarse-grained one. The size of a grain can be defined with the aid of Fig. 4-7. Random lines are drawn on a photomicrograph, and the number of grains which the lines intersect are counted. The grain size is then

$$d = \frac{l}{mN} \tag{4-2}$$

where

d = grain size (millimeters)

l = line length (millimeters)

N = number of grains which the line intersects

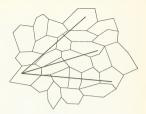
m = magnification of the photomicrograph

The grain size defined by equation 4-2 is simply a characteristic grain dimension. The procedure yields an average value.

Fig. 4-6. The polycrystalline structure of copper as observed through an optical microscope. Magnification, 150 ×.



Fig. 4-7. Schematic diagram of a polycrystalline material illustrating a method for determining grain size,



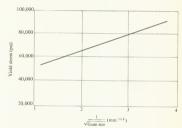


Fig. 4-8. Variation in the compressive yield stress of mild steel as a function of grain size at 77°K. (J. R. Low, Madrid Colloquium on Deformation and Flow of Solids, Springer, New York, 1956).

The effect of grain size on the compressive yield stress of mild steel is shown in Fig. 4-8. The data show that yield stress is inversely proportional to the square root of the grain size. This can be expressed by an equation of the form

$$\sigma_{\text{yield}} = \sigma_{0_{\text{yield}}} + \frac{K}{\sqrt{d}}$$
(4-3)

where K and  $\sigma_{\theta_{\text{plata}}}$  are constants. This equation has been found to have general validity for yield stress calculations. The grain size effect appears in polycrystalline ceramics as well as metals. Figure 49-shows the fracture stress of aluminum oxide as a function of grain size. The effect is quite significant here.

The above discussion shows that the physical properties of materials can be changed to some extent by varying grain size, and grain size is controllable. Grain size control is sometimes used as a strengthening mechanism. In practice, there are other methods for increasing strength which are more effective and easier to implement. The effect of grain size is



Fig. 4-9. Effect of grain size on the strength of aluminum oxide. [R. M. Spriggs and T. Vasilos, Bull. Am. Ceram Soc. 40:187 (1961).]

introduced to convince the reader that materials properties can be manipulated. Bigger and better methods are coming later in the book. No explanation has been given of why grain size influences behavior. This will be done in Chapter 8.

### Question

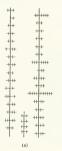
Question 3: What is the physical significance of  $\sigma_{0_{\text{vield}}}$  in equation 4-3?

# 4\_4 Temperature gradients; dendrites and single crystals

Freezing is accompanied by the release of the latent heat of fusion. This heat has to be removed in order for freezing to progress; therefore temperature gradients must exist within the solid, or liquid, or both. The gradients influence the solid structure which is formed. This section will consider solidification under two different types of thermal gradients. The first results in long, thin grains having a preferred orientation, while the second yields large single crystals. The physical properties of the solid are influenced by the microstructure that forms during solidification.

Solidification of metals often results in the appearance of branched, tree-like particles called dendrites. An example of dendritic structure in solid lead is shown in Fig. 4-10. The lead began to solidify in a particular

Fig. 4-10. Dendritic structure. (a) Schematic diagram of dendrite growth. Small dendrites branch from the main ones. (b) The dendritic structure observed in lead. (B. Chalmers, Principles of Solidification, Wiley, New York, 1964.)





direction, as shown by the straight lines in the figure. Other dendrites then branched out from the main one. The mechanism by which this type of solidification proceeds can be explained in terms of the temperature gradient near the solid-liquid interface. We start with a supercooled liquid which begins freezing at a nucleus.

As freezing progresses, the solid-liquid interface moves away from the nucleus. Latent heat is evolved in the freezing process. The heat is first absorbed by the solid and the liquid in the vicinity of the interface, raising the temperature in this region. The temperature gradient after some freezing has occurred is shown in Fig. 4-11(a). The temperature of the supercooled liquid before solidification began was T1. The liquid just in front of the interface has been heated by the latent heat evolved during freezing, while the liquid farther from the interface is still at T1 and is supercooled. The configuration of the interface is not necessarily the smooth plane implied by Fig. 4-11(a). It can deviate from this, and Fig. 4-11(b) shows a small solid region protruding into the liquid. The temperature at the surface of the protrusion will be slightly lower than that at the plane surface because of the temperature gradient. Because growth rate depends on the degree of supercooling of the liquid, the protrusion will grow faster than the plane and will form a dendrite. The problem is complicated by the fact that the dendrite gives off latent heat as it freezes. Branch dendrites can grow from the main one by a similar process. It is emphasized that dendritic growth requires a temperature gradient in the liquid, such as that shown in Fig. 4-11. The dendrites have a preferred crystallographic orientation. In bcc or fcc crystals, they grow in the [[100]] directions. It has been found that the growth rate of a crystal generally depends on the Miller indices (or atomic packing) of the surface planes. Some planes provide conditions which are more conducive to crystal growth than others.

The use of controlled temperature gradients permits the growth of large single crystals having characteristic dimensions of several inches. Before discussing single-crystal production, we shall briefly consider what they are used for, Solid-state electronic components such as transistors, photodiodes, etc., are generally fabricated from single crystals of semiconducting elements and compounds. Single crystals are necessary because grain boundaries would interfere with the electrical characteristics of the components. The mechanical properties of large single crystals are no better

Fig. 4-11. Temperature gradient necessary for dendritic growth. Temperature is shown by the heavy line. T<sub>i</sub> is the melting point; T<sub>i</sub> is the original temperature of the supercooled liquid. (a) Melt temperature decreases beyond the interface. (b) Part of the timetize permutels into the liquid. The temperature at the surface of the protrusion is lower than the temperature at the remainder of the interface.





(and in many cases are worse) than those of polycrystals, and single crystals are not generally used in mechanical devices. They are very useful in research concerned with mechanical properties, however. Use of single crystals climinates the effects of grain boundaries and randomy oriented grains; consequently the number of variables in an experiment is reduced. Single crystals are commercially available from a number of manufacturers.

Single-crystal growth requires that solidification take place around a single nucleus and that no new crystals nucleate while the growth process is going on. This condition can be met if the interface temperature is kept slightly below the melting point and the liquid temperature increases beyond the interface, as illustrated in Fig. 4-12. The required temperature gradient can be achieved if the latent heat is removed by conducting it through the solid. Dendrites will not grow in this arrangement because a protrusion at the interface would be in a region of higher temperature and would therefore grow slower than the remainder of the interface. The growth rate of the crystal is slow because the temperature at the interface is kept close to the melting point.

Figure 4-13 shows the Bridgeman method for single-crystal growth. A small seed crystal acts as the nucleus. The seed can be placed in a desired orientation, and the crystal will grow with that orientation. The furnace is

Fig. 4-12. The temperature gradient required for single crystal growth. The temperature of the liquid rises in front of the interface.

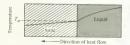
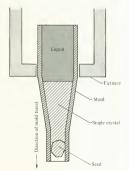


Fig. 4-13. Single crystal growth using the Bridgeman method. Solidification begins at the seed crystal. The mold holding the melt is slowly lowered from the furnace and heat is removed from the solid. This arrangement causes a temperature aradient similar to that shown in Fia. 4-19.



maintained at a temperature slightly above the melting point, and heat is extracted from the bottom of the mold while the mold is slowly withdrawn from the furnace. By properly controlling the rates at which heat is removed and the mold is lowered, the thermal gradient shown in Fig. 4-12 can be maintained. This is one of several methods that are used by crystal growers. The crystals can also be grown by condensing atoms from a vapor onto appropriate nucleation sites. Tungsten crystals grown in this manner are shown in Fig. 4-14. Single crystals of many elements and compounds have been grown by a variety of methods.

Question

Question 4: High-purity materials are generally used when growing single crystals. What might be the effect of impurity particles in the melt when trying to produce single crystals?

# 4-5 Castings

Casting is a process of great practical importance. Many items are fabricated by pouring a molten material into a mold and allowing the material to solidify. Thermal gradients and temperature changes can become complex during the process. These affect the microstructure of the casting. In this section we shall consider the microstructure of cast metal ingots which are formed by pouring the melt into cylindrical molds. Heat is taken out through the walls of the mold during freezil.

Figure 4-15 shows one structure that is observed in cylindrical metal ingots. The two figures are sections taken through the ingot. An equiaxed (equal-sized) grain structure appears in the region next to the mold wall. This region is followed by the columnar zone in which the grains are long and thin and oriented in the radial direction. How much of each zone appears in a particular ingot depends on the temperatures of the liquid and the mold at the time of pouring. Ingots composed of metal alloys sometimes show a second equiaxed zone in the center. This structure is unique to alloys and will not be explained now.

The structure shown in the figure can be explained in terms of the freezing mechanisms (or models). In most casting processes, the mold is considerably cooler than the melt before pouring; the mold is often at room temperature. When the molten metal is poured, the portion of the liquid near the mold wall chills quickly and supercools. Nucleation (usually heterogeneous) occurs at many points in the chill zone. The nuclei grow until the grains join each other, resulting in a large number of randomly oriented grains. This is the structure of the chill zone. The grain size in this region depends on the number of nuclei which were able to grow into grains. This, in turn, depends on the degree of liquid supercooling in the chill zone area. If the liquid is highly supercooled, many nuclei will grow and the structure will be fine-grained. Conversely, a small amount of supercooling results in a coarse-grained structure. For a given mold temperature, the amount of supercooling depends on the melt temperature at the time of pouring. A low melt temperature causes a high degree of supercooling (small grains) and vice versa. As melt temperature increases, so does grain size.

Structure in the columnar zone can be explained in terms of two freezing

Fig. 4-14. Tangsten crystals formed by condensing tangsten vapor on a substrate.
(a) The axis of the crystal is [100]. (b) The growth direction is [111], [K. Moliere and D. Wagner, Z. Elektrochem. 61:65 (1959), Photograph courtesy of S. Brenner.]





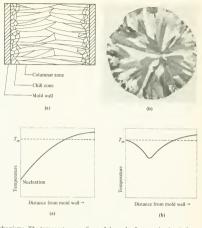
### 4-5: CASTINGS

Fig. 4-15. (a) Schematic drawing of a section through an ingot of a metal showing the two freezina zones (h) Cross section of a brass casting. The chill zone is small in this particular structure: the columnar zone predominates. Magnification, 2× (A. R. Bailey, The Role of Microstructure in Metals. Metallurgical Services, Betchworth. Surrey England 1966)

Fig. 4-16. Temperature profiles in an inperfusion in continuous during freezing.

(a) Temperatures near the mold wall before solidification begins.

Nucleation occurs near the wall, (b) Temperature profile after the chill zone has solidified. The latent heat evolved during freezing has increased the temperature of the solid.



mechanisms. The temperature gradient of the melt after pouring but before nucleation starts is shown in Fig. 4-16(a). The melt has transferred heat to the mold wall, and maximum supercooling occurs there. Grain growth begins at the wall. As the grains grow, latent heat is given off. The latent heat is not removed as quickly as it is generated; therefore the temperature of the solidified metal increases. After some freezing has occurred, the temperature gradient shown in Fig. 4-16(b) prevails. This is precisely the condition for dendritic growth, and dendrites will form. The figure shows that the liquid is supercooled for only a short distance in front of the interface; therefore the dendrites will not grow very far. They will have preferred orientations, and those dendrites whose [[100]] directions corresponds to the radial direction in the mold will grow fastest. Solidification of dendrites releases latent heat; therefore the supercooling shown in Fig. 4-16(b) will disappear as dendrites form. During the remainder of the freezing process, heat is conducted from the solid-liquid interface, through the solidified metal, and through the mold wall. The temperature of the remaining liquid is above the freezing point, and the gradient is similar to that shown in Fig. 4-12. Growth progresses by the advance of the interfaces formed by the dendrites. The columnar structure results.

The microstructure of cast parts can be controlled by means of the melt temperature, as shown schematically in Fig. 4-17. The figure is drawn for a given mold temperature before pouring. A low melt temperature

Fig. 4-17. The effect of the melt temperature at the time of pouring on the structure of an ingot. Higher melt temperatures increase the size of the columna zone. (After B. Chalmers, Principles of Solidification. Wiley. New York. 1964.)

results in a fine-grained structure in the chill zone, together with a small columnar zone. The reverse occurs for high pouring temperatures.

The freezing processes have been described qualitatively. Accurate prediction of cast structures would require detailed knowledge of the density of nucleation sites and growth rates. This information would come from experimental observations, and not much of it is currently available. The nucleation and growth information could then be used in the rigorous solution of the transient heat-transfer problem of cooling a casting. Progress is being made in both the analytical and experimental fields, and the results so far indicate that the freezing models used are valid. If we were given the problem of producing a casting with a particular microstructure we would probably have to set up an experimental program to determine the pouring conditions and mold temperature which yielded the desired results. The freezing models would enable us to decide intelligently which quantities should be varied in the experiments. While we might not be able to calculate the easting conditions, we would be far ahead of resorting to a strictly trial and error determination.

### Ouestions

Question 5: The text states that as the liquid in contact with the mold becomes more supercooled, the grain size which it forms upon freezing becomes smaller. Explain this in terms of Fig. 4-4.

Question 6: The temperature gradients that occur during solidification of a casting can be minimized by stirring the melt as solidification progresses. What structure would result from this procedure?

# 4-6 Amorphous structures; glass transition temperature

In all of the processes discussed so far, the liquid atoms have been fairly free to move about; they have been mobile. Mobility was required so that liquid atoms could move to a solid surface or could aggregate together to form nuclei. The basic building unit used was the atom. If we consider polymers or silicates, the situation changes somewhat. The building block for many polymers is the polymer chain, while silicate structures involve chains or sheets. These molecules are larger than the atoms we have been

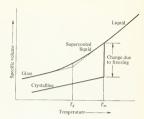


Fig. 4-18. Solidification of crystalline and amorphous (glassy) materials showing changes in specific volume. T<sub>g</sub> is the glass transition temperature.

considering and their mobility is lower. When a melt containing large-chain molecules is cooled, solidification can occur by either (or both) of two mechanisms. These are crystallization and vitrification. A substance which vitrifies forms an amorphous glass when it cools. To illustrate how these processes compete, consider a substance which is capable of either crystallizing or vitrifying. Let us start with the substance in the liquid state and cool it. Figure 4-18 shows the effect of temperature on the specific volume of the material. The specific volume of the liquid decreases slowly with temperature in the liquid region. At the melting point  $(T_m)$ , the substance can follow either of two routes. If nuclei are available for solidification and the liquid molecules are mobile, crystallization will occur. The freezing of crystalline solids occurs at well-defined temperatures and is accompanied by the release of latent heat and usually a reduction in specific volume. The specific volume change due to freezing appears in the figure. An alternate cooling path is also available and leads to a vitreous or glassy solid. Suppose that the mobility of the molecules in the melt was very low when the melt reached  $T_m$  so that crystallization could not occur readily. Decreasing the temperature below  $T_m$  would result in a supercooled liquid. The molecular mobility in the supercooled region is even lower than at Tm because the mobility decreases with decreasing temperature. The molecular mobility can be related to the viscosity of the liquid. Viscous liquids have low mobility, and liquids become more viscous as the temperature is lowered. Further cooling of the supercooled liquid results in the formation of a glassy material. This material has an amorphous structure like the liquid, but its high viscosity causes it to behave very much like a solid. The upper curve in Fig. 4-18 changes its slope in the neighborhood of  $T_g$ .  $T_g$  is called the glass transition temperature. Significant changes occur in physical properties other than specific volume in this temperature region. For example, the elastic modulus of polymethyl methacrylate is shown as a function of temperature in Fig. 4-19. A rapid change takes place in the neighborhood of 100°C. If a plot such as Fig. 4-18 were made for this polymer, Ta would be at approximately 105°C. Large changes in viscosity would also be noted at this temperature. Polymethyl methacrylate does not crystallize because of the bulky side groups on the chain.

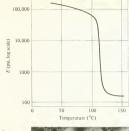


Fig. 4-19. The elastic modulus of polymethyl methacrylate as a function of temperature. A large change in E occurs over a narrow temperature range. After A. V. Toholsky in Rheology, F. R. Eirich, ed., Vol. 2. Academic Press, New York, 1958.)

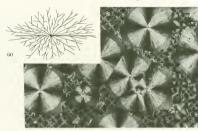


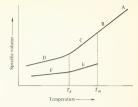
Fig. 4-20. (a) Schematic diagram of spherulite growth, (b) Spherulite structure of a silicon polymer. Crystalline and amorphous regions appear. (Courtesy of F. P. Price.)

T<sub>a</sub> marks the center of a narrow temperature range in which properties are highly temperature sensitive. When many amorphous polymers are cooled through this range, their properties change from those of rubber-like substances to those of brittle, glass-like substances,

(b)

Some polymers are capable of solidifying in crystalline structures, amorphous structures, or both. An example of this is polyethylene, whose structure is shown schematically in Fig. 3-29. Both crystalline and amorphous regions appear. The manner in which these regions occur depends on the conditions under which solidification took place. One commonly observed structure consists of spherulites. The formation of a spherulite is shown schematically in Fig. 4-20(a). The polymer begins to crystallize about the nucleus shown at the center. The crystallized material is in the form of thin ribbons, and the ribbons move outward from the nucleus. These ribbons branch out to form other ribbons, etc. The process is similar to dendrite formation in metals. The ribbons grow until either all of

Fig. 421. Solidification of polymers that form crystalline and amorphous regions. A liquid. § highly viscous liquid: C, supercooled liquid, rubbery behavior, D, glass, hard and brittle: E, crystals surrounded by supercooled liquid, some rubbery behavior; F, crystals surrounded by glass. (After T. Aftey and F. Gurthey Organic Polymers, Prentice-Hall, Englewood Cliffs, NJ. 1967.)



the melt has been consumed or the last remaining portion of the melt can solidify into an amorphous structure. If many nuclei exist in the melt, a large number of spherulites can begin growing, and growth will continue until a spherulite comes into contact with its neighbors. In this respect, spherulite growth is similar to grain growth. Figure 4-2(by) shows the spherulite structure of a polymer. Both crystalline and amorphous regions appear. A number of polymers can show this structure.

The curves of Fig. 4-18 must be modified for polymers which have both crystalline and amorphous regions when they have solidified. For these materials, the curves of specific volume vs. temperature are shown in Fig. 4-21. The upper curve remains the same; however, the crystalline curve is somewhat different. Region E in the figure corresponds to small crystals which are surrounded by a supercooled liquid. The supercooled liquid transforms to a glass below  $T_{\theta}$ , and region F has small crystals surrounded by an amorphous glass. The type of behavior exhibited by polymers in each region is given in the figure caption. Table 4-2 lists the glass transition temperatures of several amorphous polymers and also shows the melting points of the crystalline forms. The word approximate is used in the table because the glass transition temperature varies somewhat with the degree of polymerization, among other things.\* The values listed show that some polymers are rubbery at room temperature while others are glassy.

\* E. V. Thompson, J. Polymer Sci. Part A-2, 4:199 (1966), discusses this dependence for polymethyl methacrylate.

Table 4-2. Melting temperatures and approximate glass transition temperatures for several polymers†

Polymers	$T_{g}$ (°C)	Tm (°C)
Polyethylene	-110	135
Natural rubber	-70	28
Polyvinyl chloride	80	180
Polystyrene	100	230 (isotactic)

<sup>†</sup> Adapted from A. T. Di Benedetto, *The Structure and Properties of Materials*, McGraw-Hill, New York, 1967, p. 251.

Ouestion

Question 7: Polyethylene can form crystalline or amorphous structures.

Which crystallizes easier, polyethylene with a high degree of polymerization or a low degree of polymerization? Why?

Atomic imperfections in crystals

The discussion so far in this chapter has been concerned with the structures that result from freezing liquids under various conditions and the effect of these structures on properties. For crystalline materials, microstructure arose as the result of grain boundary formation. Crystalline defects also exist at the atomic level; that is, the structure of a single grain (or single grain (or single grain to make the considered. They may involve a single atom or small groups of atoms. We shall divide atomic imperfections into two categories, point defects and line defects. Surfaces are also classified as defects because our infinite space lattices had none. They will be discussed separately in Chapter 7.

# 4-7 Point defects in crystals

The simplest crystalline imperfection is the point defect. These defects have a significant effect on mechanical properties and diffusion, as will be seen in Chapters 8, 9, and 10. This section will be limited to describing them.

Two types of point imperfections that can occur in a crystal are shown in Fig. 4-22. A vacancy is caused by an atom simply not appearing at an atom site. Interstitial defects are caused by an atom taking up residence in a space between lattice atoms. These spaces are called interstices. Interstitial defects are more probable in structures which have low packing factors. If impurity atoms are present, they may appear at either interstitual or lattice sites, and they also constitute point defects. The point defect of most interest to us is the vacancy. A crystal in its equilibrium condition possesses some vacancies, and their number can be calculated. This quantity will be of use to us later; therefore the method used to find the equilibrium number of vacancies will be described. The derivation will be more descriptive than analytical but is still better than "it can be shown"

Consider a crystal having a given temperature and volume. Thermodynamics tells us that the crystal will be in its most stable state when its free energy is a minimum. The free energy is defined as

$$H = \mathcal{E} - TS \tag{4-4}$$

where

H =free energy of the crystal (ergs)

& = energy of the crystal (ergs)

T = crystal temperature (°C)

S = entropy of the crystal (ergs/°C)

The effect of vacancies on each term on the right-hand side of equation 4-4

### 4-7: POINT DEFECTS IN CRYSTALS

Fig. 4-22. A plane of atoms in a crystal showing a vacancy and a self-interstitial. These are both point defects.

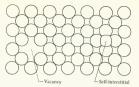
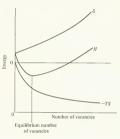


Fig. 4-23. Schematic representation of the terms in equation 4-5. The equilibrium number of vacancies corresponds to the minimum in the free-energy curve.



can be evaluated qualitatively. The problem is to find the number of vacancies corresponding to the minimum value of H. Because the crystal is at a given temperature, T is a constant. The entropy, S, is related to the amount of disorder in the crystal; the more disorder, the higher the entropy. When vacancies are introduced into a perfect lattice, disorder is introduced and entropy increases. Thus, the magnitude of the TS term increases as the number of vacancies increase. Because the TS term is negative in equation 4-4, H tends to decrease as S increases if we consider only the second term. The quantity -TS is schematically shown as a function of the number of vacancies in Fig. 4-23. Now consider & in the equation. This quantity is equal to the bond energy and the thermal (or vibrational) energy of the atoms in the crystal. To create a vacancy, an atom must be removed from a lattice site. This requires the breaking of bonds; therefore energy must be added to the crystal to create a vacancy. Thus, & increases as the number of vacancies increases. This is shown schematically in Fig. 4-23. The free energy is the sum of the two curves in the figure and shows a definite minimum. The number of vacancies in the crystal at equilibrium corresponds to the number at the free-energy minimum.

A rigorous derivation to find the equilibrium number of vacancies would require that  $\mathscr E$  and S in equation 4-4 be expressed in terms of the

number of vacancies. This expression would then be differentiated and the first derivative set equal to zero in order to find the minimum value of H. The number of vacancies corresponding to the minimum H is then the equilibrium number of vacancies. The derivation can be done using the methods of statistical thermodynamics. The result is

$$\frac{N_v}{N} = e^{-q_v/kT} \tag{4-5}$$

where

 $N_n$  = number of vacancies in the crystal

N = number of lattice sites in the crystal

 $q_{\rm p}$  = energy required to form a vacancy

k = Boltzmann's constant

T = absolute temperature

Equation 4-5 will be used later. Its derivation is based upon a crystal at equilibrium.

# 4-8 Line defects or dislocations

The crystal symmetry can be disrupted along a line. Line defects are called dislocations and distort crystal structures more severely than point defects. The theories which explain the plastic behavior of materials are heavily dependent on dislocations and will be considered in Chapter 8. This section will discuss only the geometry of dislocations because they play a role in some types of solidification. Before beginning, a few words to the skeptics might be in order. The first exposure to the geometry of dislocations sometimes convinces people that they are the products of active imaginations and have no relationship to the physical world. Actually, they were predicted before they were observed. The theoreticians assumed their existence in order to explain some observed phenomena. The experimenters did come through, however, and the existence of dislocations has been verified profusely.\* They are real.

An edge dislocation is shown in Fig. 4-24. It is formed by adding an extra partial plane of atoms to the crystal as shown in the figure. The dislocation itself is the interior edge of the extra partial plane. The position of the dislocation line is marked by the symbol 1., with the vertical line pointing in the direction of the partial plane. The crystal is distorted in the neighborhood of the dislocation. The distortion is measured by the Burgers vector b, shown in Fig. 4-25. The Burgers vector is found by traversing a path around the dislocation line. A starting point is selected, and the path consists of an equal number of atomic spacings in the vertical and horizontal directions as shown in the figure. A vector drawn from the

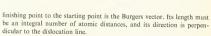
<sup>\*</sup> As an example of the large body of data confirming dislocations, see *Direct Observation of Imperfections in Crystals*, J. B. Newkirk and J. H. Wernick, ed., Wiley-Interscience, New York, 1962.

Extra partial plane of atoms Dislocation line

Fig. 4-24. An edge dislocation. This defect is caused by an extra partial plane of atoms in the crystal. The crystal symmetry is along the dislocation line. (A. G. Guy, Elements of Physical Metallurgy, Addison-Wesley, Reading, Mass., 1959.)

Fig. 4-25. A Burgers circuit around an edge dislocation. The circuit is shown by the heavy lines. The Burgers vector completes the circuit.

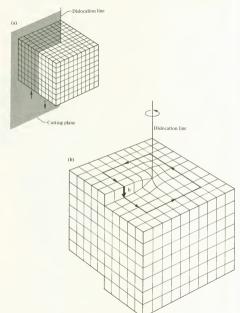




Dislocations are not equilibrium defects as vacancies were. Their formation requires significant energy, which is stored in the portion of the crystal near the dislocation. Figure 4-26 shows that the spacing of the

atoms above the dislocation is less than the equilibrium spacing (or lattice parameter). Similarly, the atoms below the dislocation have a spacing which is greater than that at equilibrium. This means that the region above the dislocation line has a compressive strain, while that below has a tensile strain (see Fig. 4-26). Energy is required to distort the lattice, and this energy is stored as strain energy in the distorted regions.

Fig. 4-27. Formation of a screw dislocation. (a) A perfect crystal and a plane, One part of the crystal is displaced with respect to the other part. The arrows show the displacement direction. (b) A screw dislocation showing the Burgers circuit, Burgers vector, and dislocation line. The crystal region near the dislocation line is strained.



The formation of a serew dislocation is illustrated in Fig. 4-27. A perfect crystal and a plane cutting part way through it are shown in Fig. 4-27(a). Let the crystal be distorted such that one side moves upward and the other downward, with the atoms sliding past each other on the cutting plane. The directions in which the two sides big ner shown by the arrows in the figure. It is emphasized that atoms slip past each other only on the cutting plane. When the two sides have slipped past each other by one atomic distance, the atoms are again in registry with each other and a screw dislocation has been created [Fig. 4-27(b)]. The dislocation line marks the edge of the cutting plane, as shown. The Burgers circuit and Burgers vector are also shown. For a screw dislocation, the Burgers vector is parallel to the dislocation line.

The geometry of the screw dislocation has an interesting effect on the solidification process. The discussion of Fig. 4-2 (Section 4-1) showed that solidifying atoms tended to bond at the B or C sites. When a plane was completely filled, only A sites were available, and it was necessary for mobile surface atoms to aggregate into an island before B or C sites could be created. The screw dislocation provides a continuous source of B and C sites because a crystal can continuously grow in the direction of the dislocation and maintain a step. This is shown schematically in Fig. 4-28 and results in a fast-growing spiral. This growth pattern has been observed in many cases and will be used to explain the growth of whiskers in Section 4-9. Figure 4-29 shows the growth spiral observed in a crystal of parafflin.

Fig. 4-28. Crystal growth along a screw dislocation. The dislocation provides a continuous supply of sites that are favorable for crystal growth.

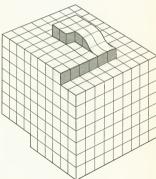






Fig. 4-29. Growth spiral in a crystal of paraffin. The pattern is caused by a screw dislocation. The type of growth is shown schematically in Fig. 4-28. [Dawson and Vand. Nature 167:476] (1951).3

# Whiskers

Most crystalline engineering materials are capable of withstanding stresses in the neighborhood of about 50,000-150,000 psi before fracturing. If these same materials are solidified as whiskers, they are found to withstand stresses of over 1 million psi, They are about 10-30 times as strong as their polycrystalline counterparts. Whiskers have understandably generated a great deal of interest. The term whisker is quite descriptive. These highstrength solids are generally about \( \frac{1}{2} \) in, long and perhaps 10-4 in, in diameter. Their exact dimensions depend on the material that they are made from and the process by which they are solidified, but they are always long and thin.

Whiskers are often grown by condensing gaseous atoms of the material on preferred growth sites, although methods of growing them from the melt have been developed for some materials. In the vapor deposition method, a vapor of the material being used is maintained in a vacuum chamber. The vapor is deposited on a suitable substrate and the whiskers grow. Iron whiskers are shown in Fig. 4-30, while a single silicon carbide whisker appears in Fig. 4-31. Both were grown from vapor, The very regular shape of the SiC whisker indicates that it is a single crystal. The unusually high strength of whiskers is attributed to the perfection of their structure. They are single crystals which are practically free of dislocations. Why this results in their high strength will be discussed in Chapter 8. It is apparent that the crystals in Figs. 4-30 and 4-31 have preferred growth directions. This is usually attributed to one (or perhaps several) screw dislocations in the axial direction. Growth proceeds in the spiral fashion shown in Fig. 4-28. Whiskers are an extreme example of the effect of solidification processes on the properties of materials. Whiskers are far stronger than polycrystals of the same material, and the difference is attributed to structure.

It is difficult to utilize the strength of whiskers because of their uncooperative shape. They are utilized in composite materials, where a large number of whiskers are bound together by a second material called a matrix. This two-component aggregation has properties that lie somewhere between the properties of the components. The price of whisker composite

Fig. 4-30. Iron whiskers grown by condensing from vapor. Magnification, 8 ×. (S. S. Brenner in The Art and Science of Growing Crystals, J. J. Gilman, ed., Wiley, New York, 1963.)



Fig. 4-31. An electron micrograph of a silicon carbide whisker. The whisker shows a high degree of symmetry. Magnification, 70,000 × (P. T. B. Shaffer in Modern Composite Materials, L. J. Broutman and R. H. Krock, eds., Addison-Wesley, Reading, Mass., 1967.)



Whiskers are currently the most defect-free crystalline solids available. Their properties have provided experimental verification of theories concerned with the ultimate strength of perfect solids. We shall have cause to use these properties later on in order to justify some of our models.

Ouestion

Question 8: Let the crystals shown in Figs. 4-25 and 4-27 both have the simple cubic structure with a lattice parameter of 3Å. What is the magnitude of the Burgers vector in each of these figures?

# 4-10 Summary

The perfect crystal structures described in Chapter 3 are idealizations. An accurate description of real materials must take cognizance of imperfections. Grain boundaries were the first imperfections treated. They arise as a result of the freezing process. The microstructure of a crystalline solid depends on how the freezing process took place. A polycrystal composed of randomly oriented, equiaxed grains has isotropic properties. Each individual grain has anisotropic properties; however, their random arrangement causes the solid to be isotropic. If the crystals grow in preferred directions as in the case of dendrites, the isotropy is lost. To some extent, the strength of a solid depends on its grain size, which is controllable. This was the first example we have had illustrating how properties can be controlled.

Many polymers form amorphous structures, and these do not have a well-defined melting point. There is a narrow temperature range in which the material properties experience very large changes, however, and the center of this range is the glass transition temperature. Polymers change from glassy behavior to rubbery behavior when they are heated through this range.

Imperfections are present at the atomic level as well as at the microstructure level. Point defects can be explained in terms of the equilibrium state of a solid. Nature requires that some disorder be present in a crystal, and this is reflected by the presence of vacancies. Dislocations defy an equilibrium explanation, but their existence has been amply verified. The growth characteristics of crystals containing screw dislocations provided one explanation of preferred growth directions and led to a discussion of whiskers. The high strength of whiskers can be explained by their low concentration of dislocations. Structural defects at the atomic level have a great effect on the physical properties of materials, and this will be covered in later characters.

This chapter begins to show the effects of structure and bonding on mechanical properties. The first example we found was concerned with the effect of grain structure on strength. The polymer discussion showed that significant differences existed between crystalline and amorphous solids, and we would expect that the ability or inability of a polymer to crystallize significantly affects physical properties. The short discussion of whiskers attributed their high strength to the absence of atomic-level structural

defects and showed that even small structural defects can have a very large effect on mechanical properties.

### Problems

- 1 Figure 4-3 shows the melting and freezing rates of copper as a function of temperature. (a) Plot the net freezing rate as a function of temperature from 600 to 1356°K (the melting point), (b) The curve of part (a) should have a maximum. In terms of the freezing model, explain why the maximum occurs. The low-energy liquid atoms join the solid when they strike the surface. These atoms also have a low velocity in the liquid state, and the rate at which they impinge upon the surface is therefore low.
  - 2 Find the values of k and σ<sub>0yield</sub> in equation 4-3 for the mild steel shown in Fig. 4-8.
  - 3 Atoms at a grain boundary have fewer nearest neighbors than those within a grain. (a) Which of these atoms has a larger bonding energy? Why? (b) Large bond energies imply large bonding forces and vice versa. Does your answer to part (a) explain the observed dependence of yield stress on grain size, or must there be some other explanation?
  - 4 Ten grams of molten aluminum is held in a cylindrical container. The liquid is cooled slowly until it has been supercooled 5°C. Dendrites begin to solidify at this point. What is the maximum fraction (by mass) of the liquid that can solidify as dendrites? The latent heat of fusion for Al is 71 callg and the specific heat of liquid Al is 0.21 callg 8°C.
  - 5 A molten metal at a temperature well above the melting point is poured into a cylindrical mold. The sides and bottom of the mold are thick and are good heat conductors. The top is open. Heat is removed through the walls as the metal solidifies. Sketch the structure of the solid inpot.
  - 6 A large casting is to be made and must solidify in a structure having equiaxed grains with no significant columnar region. The mold can be heated or cooled prior to casting, and facilities are available to provide molten metal at temperatures ranging from just above the melting point to double the melting temperature. Describe the procedure you would use in order to obtain an equiaxed easting.
  - 7 Under some conditions, and at temperatures below the freezing point, amorphous glasses are observed to take on a more crystalline structure. This process is called devitrification. Is it more fikely to occur at high temperatures (but still below the freezing point) or at low temperatures? Why?
  - 8 A cube of copper has dimensions of 1 cm for each edge at 0°C. The copper is heated to 400°C and it expands. The edge dimension is now 1.00067 cm. Vacancies have been created by interior atoms migrating to the surface; therefore the specimen has the same number of atoms at both temperatures. (a) Using equation 4-5, calculate the number of vacancies that have been created by heating. The energy required to create a vacancy is about 1 eV. (b) What fraction of the volume expansion can be attributed to the creation of vacancies? (c) Can thermal expansion be accounted for by vacancy creation?

- 9 The screw dislocation in Fig. 4-27 was constructed by defining a cutting plane and causing one part of the crystal to slip past another on the plane. (a) Show that an edge dislocation can be formed in this way. Use a simple cubic lattice. (b) What crystallographic plane is parallel to the cutting olane?
- 10 (a) Sketch a (100) plane of Ni containing an edge dislocation, with the dislocation line being in the [100] direction. (b) Show the magnitude and direction of the Burgers vector.
- 11 Select the smallest Burgers vector which can exist in a bcc solid. (a) Sketch an edge dislocation having this Burgers vector. Identify the plane sketched, the direction of the dislocation line, and the direction of the Burgers vector. (b) If the solid is chromium, what is the length of the Burgers vector?

### Answers

- Question 1: Heat is released when a liquid atom joins the solid because the atom goes to a lower energy state. This heat raises the temperature of both liquid and solid, thus reducing the freezing rate. When the temperature reaches the melting point, the melting rate caulast the freezing rate and no net freezing occurs. Heat must be removed and the temperature reduced in order for the freezing process to continue. Solidification occurs below the melting point, not at the melting point.
  - Question 2: One nucleus is required to start the freezing process in a supercooled liquid. The low-energy liquid atoms are randomly distributed through the liquid. The probability of a single nucleus forming increases as the number of low-energy atoms increases, and a large volume contains more low-energy atoms.
- Question 3: As the grain size becomes large, the last term in equation 4-3 becomes small. A very large grain size corresponds to a material having one grain; consequently the material is a single crystal. Thus, \(\sigma\_{0\text{-yteld}}\) is approximately the yield point of a single crystal of the material.
- Question 4: Impurity particles provide nuclei. Solidification can begin on these nuclei when they are just in front of the interface. If this occurred, the resulting solid would no longer be a single crystal.
- Question 5: The melt contains a given number of possible nucleation sites; these are both embryos and nuclei. As the supercooling increases, the critical radius decreases, and the ratio of nuclei to embryos increases. A larger number of nuclei produce a larger number of grains, or a smaller grain size.
- Question 6: The entire structure would have randomly oriented grains.

  The grain size near the wall might be different from that in the interior.
- Question 7: A low degree of polymerization crystallizes easier. Short chains are more mobile than long ones because they are not as entangled with the other chains of the polymers. Mobility is required for crystallization.

Question 8: Both are 3 Å.

CHAPTER 5

# Experimental Observation of Solids

PROGRESS IN MATERIALS SCIENCE has been made largely by the interplay of theoretical and experimental methods. New knowledge has been generated by both. In some cases, phenomena have been observed in experiments, and it was necessary to formulate consistent theories to explain them. In other cases, phenomena were predicted from theory and were subsequently verified by experiment. The previous chapters have used a number of theoretical models which may or may not have appeared reasonable to the reader. Experimental verification of the models adds to their credence and often improves them. To understand the experimental results we must have some knowledge of the methods used to obtain them. A multitude of experimental methods are used in materials science, and they cannot be covered in a book of this scope. This chapter will discuss five typical methods; four of them will be covered briefly and one in some detail.

Visual observation of materials is discussed first and three methods are described. These are optical microscopy, electron microscopy, and field ion microscopy. Each of them operates in a different magnification range. The optical microscope operates over a range from about 20 to  $2000\times$  and is used to observe features such as grains (microstructure). The electron microscope then takes over and provides magnifications up to about  $300,000\times$  at present, although more powerful (and more expensive) ones are being developed. Dislocations can be observed directly with this instrument, and the electron miscroscope has served as the workhorse for verifying and advancing dislocation theory. The field ionization microscope is capable of magnification up to several million and enables us to see individual atoms in solids.

The experimental method selected for coverage in some detail is X-ray diffraction. It is used extensively in determining crystal structure and verifies the billiard-ball model used for describing structures in Chapter 3. Dislocations can be observed using X-ray diffraction techniques,\* providing more experimental evidence for

<sup>\*</sup> W. W. Webb in *Growth and Perfection of Crystals*, R. H. Doremus, B. W. Roberts, and D. Turnbull, eds., Wiley, New York, 1958.

them. In this chapter, X-ray diffraction will be developed far enough for us to determine the unit cells of cubic crystals from experimental data.

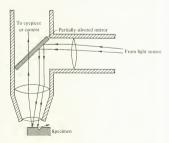
The last method discussed is concerned with the chemical composition of solids. The instrument used is the electron microprobe, and the technique is very useful in the study of alloys and diffusion. The chemical analysis is carried out by means of X-rays, but it is not related to diffraction. This is an example of using a physical phenomenon (X-rays) in different ways for different instruments.

# 5-1 The optical microscope

The optical microscope is a familiar instrument and comes in a variety of designs. They can be classified as either transmission or reflection instruments, depending on whether light is transmitted through or reflected by the specimen. Most of the materials that we are interested in are opaque; therefore the reflection microscope will be discussed. A schematic diagram of this instrument is shown in Fig. 5-1.

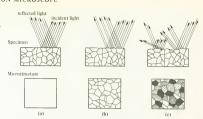
The use of the optical microscope for observing microstructure was mentioned in Chapter 4. The specimen surface must receive some special treatment before the microstructure can be seen, however. The specimen shown in Fig. 5-1 has a smooth surface with a scratch on it. The scratch reflects the light away from the lens system, causing it to appear as a dark area to the viewer or camera. The first step in preparing a specimen for observation in a microscope consists of grinding and polishing the surface until it has a mirror finish. In this condition, all regions of the surface reflect incident light back into the lens system and no microstructure is visible [Fig. 5-2(a)]. Grain boundaries are made visible by erching. This is generally done by placing the specimen surface in contact with chemical stack the surface, beginning at the grain boundaries are the presents. The chemicals attack the surface, beginning at the grain boundaries are the presents. The chemicals attack the surface, beginning at the grain boundaries are the grain surface in contact with chemical

Fig. 5-1. Schematic diagram of a reflection microscope showing the effect of a groove in the specimen surface. Light reflected by the groove does not re-enter the microscope and the groove appears as a dark line.



#### 5-2: THE ELECTRON MICROSCOPE

Fig. 5-2. Etching of a specimen. The upper sketches represent cross sections of the specimens; the lower ones show the correspondina microstructures on top of the specimens (a) Polished specimen showing no microstructure. (b) Grain boundary etchina. The boundaries appear as dark lines. (c) Grain etchina. The arains appear as dark and liaht areas.



aries. The chemical attack causes the grain boundaries to take the shape of grooves, as shown in Fig. 5-2(b). The light reflected by the grooves does not go back to the camera; consequently the grain boundaries appear as dark lines. Further etching results in the grain surfaces being attacked. The rate at which material is etched from the surface depends on the crystallographic orientation of the grain; the rate of chemical reaction is anisotropic. Some grain surfaces etch more rapidly than others. The result of grain etching is shown in Fig. 5-2(c). Those grains which are oriented so that they do not reflect light back into the microscope appear darker. Grain etching appears in the photomicrograph of copper (Fig. 4-6). Etching is effective for ceramics as well as metals. The grain structure of MgO is shown in Fig. 5-3. Different chemical reagents are used for etching different solids, and the etchant recipes can be found in several reference books,\*

The useful limit of any microscope is determined by its resolving power. The resolving power is defined as the minimum separation between two objects for which they will appear separate and distinct when viewed through the microscope. The resolving power of the optical microscope is limited by the wavelength of the light, assuming perfect optical components. Visible light has a wavelength in the neighborhood of 5000 Å, and any features of interest on a specimen surface which are not separated by at least half this distance will not appear separate and distinct. If greater resolution and magnification are required than can be obtained with an optical microscope, we must go to the electron or field ion microscopes.

#### Question

Question 1: Will the resolution of an optical microscope be improved if ultraviolet light is used instead of visible light? Why?

# 5-2 The electron microscope

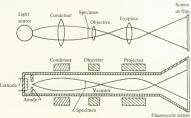
The transmission electron microscope is similar to the transmitted light microscope in some respects, but an electron beam is used instead of a light beam. The similarities are illustrated in Fig. 5-4. The electron beam is

\* G. L. Kehl, The Principles of Metallographic Laboratory Practice, McGraw-Hill, New York, 1949, p. 293–300.

Fig. 5-3. Photomicrograph of MgO showing the grain structure. Magnification, 100 ×. (R. D. Carnahan and W. J. Knapp in Ceramics for Advanced Technologies, J. E. Hove and W. C. Riley, eds., Wiley, New York, 1965.)



Fig. 5-4. Similarities between the transmission optical microscope and the transmission dependent microscope. An electron source (the cathods) replaces the light source. The light beam is replaced by an electron beam and electromagnetic elesses are used instead of optical lenses. The specimen must be thin enough so that electrons can past shrough it.



usually composed of electrons which have been thermionically emitted from a hot metal filament. They are focused by electromagnetic coils which serve the same function as lenses in a light microscope. The electrons pass through the specimen being investigated, which is analogous to light passing through a transparent specimen in the optical microscope. Finally, the electrons impinge upon a fluorescent screen. Light is emitted when the electrons collide with the screen, and the light intensity at any point is determined by the rate at which electrons impinge upon that point. A magnified image of the specimen forms because the rate of electron arrival is higher at some places on the screen than it is at others (just like the picture tube in a television set).

The electron beam is modified when it passes through the specimen. In a transmission optical microscope, different areas of the specimen absorb different quantities of light. Those areas that absorb appear dark in the image, while those that transmit appear light. Image formation in the electron microscope is a little different, as the electrons pass through the specimen, some are absorbed, some are reflected at the surface, a large number go through unperturbed, but many of them are scattered; that is, they pass through the specimen but their direction is changed. Scattering is caused by an electron interacting with the electric field of an atom as it passes close to the atom. A region of the specimen which tends to scatter electrons will appear dark on the screen, thus providing the contrast necessary for producing an image.

The question that now arises is, "Why does the electron microscope give better resolution than the optical one?" The answer lies in the fact that the wavelength of the electrons is shorter than that of the light used in the optical microscope. Electrons can be considered as waves rather than particles according to quantum theory. The electron clouds used in Chapter 2 result from consideration of electron waves. The wavelengths of electrons used in electron microscopes are considerably smaller than the distance between atoms in a crystal. The electron microscope is not now capable of reaching its theoretical resolution, and in a practical sense is therefore not limited by wavelength. The resolution is limited by imperfections in the electromagnetic lenses and by the nature of the scattering process. Resolution of several angstron units can currently be obtained.

The preparation of specimens for electron microscopy requires specialized techniques. Figure 5-4 shows that the electrons pass through the specimen. This requires that the specimen be very thin, of the order of 1000 Å. Techniques have been developed for preparing these specimens and include such methods as electrolytic thinning of the specimen, cutting thin slices with a diamond knife, etc. \*A transmission electron micrograph of a thin stainless steel specimen is shown in Fig. 5-5. The heavy line is a grain boundary, while the short, curved lines are dislocations. Because the electron beam has passed through the specimen, dislocations inside the specimen will appear in the image. Transmission electron microscopy yields details of the bulk structure.

Surfaces of thick specimens can be examined indirectly by means of surface replicas. The specimen surface can be replicated in materials such

<sup>\*</sup> G. Thomas, Transmission Electron Microscopy in Metals, Wiley, New York, 1962.

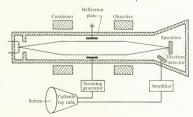


Fig. 5-5. Transmission electron micrograph of a stainless steel specimen. The heavy line is a grain boundary; the short lines are dislocations. Magnification, 14,000 ×. [M. J. Whelan, P. B. Hirsch, R. W. Horne, and W. Bollman, Proc. Roy. Soc., A240:524 (1957).]

as carbon or polystyrene, and the thin replica can then be used as the specimen. This technique yields information about the surface only.

The scanning electron miscroscope is becoming widely used for siudying specimen surfaces, among other things. It operates in a different manner than the transmission instrument. The scanning electron microscope is shown schematically in Fig. 5-6. The electron source is the same as that for the transmission electron microscope; however, the lens arrangement is different. The beam is focused at a point in the plane of the specimen. In present instruments, this "point" has a diameter of about 100 Å. The position of the point can be varied by applying a voltage to the deflection plates. If a positive voltage is applied to the lower plate in Fig. 5-6, the electron beam will be deflected downward, and vice versa for a negative voltage. A second set of deflection plates enables the beam to be deflected perpendicular to the plane of the paper. These are not shown in the figure. Thus, by controlling the voltage to the two sets of deflection plates, the beam can be seanned across the entire surface of the specimen.

Fig. 5-6. Schematic diagram of a scanning electron microscope. The beam is scanned across the specimen surface by controlling the voltage on the deflection plates. A magnified image of the surface is reproduced on the screen of the cathode-ray tube



Consider the beam as being focused at a particular point on the specimen surface. As the electrons strike the surface, some of them will be scattered toward the electron detector (this is often an electron multiplier device). The rate at which electrons strike the detector depends on the intensity of the incoming electron beam and the fraction of the incoming electrons that are scattered toward the detector. The beam intensity is controlled by the electron source, while the scattering depends on the geometry of the surface at the point where the electron beam impinges upon it. The beam can be scanned across the surface. If this is done, the rate at which scattered electrons hit the detector will depend on the surface geometry. The signal from the detector goes to the cathode-ray tube. The cathode-ray-tube display is synchronized with the beam in the microscope, and each point on the screen of the tube corresponds to a point on the specimen. The detector signal modifies (or modulates) the light intensity appearing on the screen. For example, those points on the specimen which cause a large number of electrons to strike the detector will appear as light regions on the screen and vice versa. In this way, contrast is provided and the cathode-ray tube provides a picture of the surface. The resolution of this instrument is determined by the size of the beam when it impinges upon the specimen and is presently limited to about 100 Å. Note that neither thin specimens nor surface replicas are required for this microscope.

## Question

Question 2: What determines the magnification of the scanning electron microscope?

## 5-3 The field ion microscope

The field ion microscope is a fascinating instrument that enables us to see individual atoms in a solid. It also permits the direct observation of the various crystal imperfections discussed in Chapter 4.\* A field ion microscope is shown in Fig. 5-7. It contains no lenses. The specimen must have a very sharp point, and it is the region around the point that is magnified.

To operate the instrument, the glass chamber shown in the figure is evacuated by vacuum pumps. A pure gas, generally hydrogen or helium, is then admitted until the gas pressure in the chamber is about 10<sup>-3</sup> mm Hg. A high positive voltage in the neighborhood of 30,000 V is applied to the specimen. This causes an extremely high voltage gradient in the neighborhood of the tip. The gradient is of the order of 100 million V/cm. Recall that when a voltage is applied to an electrically isolated conductor, the voltage gradient is high near sharp corners. The same effect causes the high gradient at the tip. A gas particle which touches the tip when the electric field is applied will lose an electron and become a positive ion. It will then be repulsed by the positively charged specimen and will follow a straight line path to the chamber wall. Here it will collide with a fluorescent coating on the glass, and light will be given off as a result. The gas pressure in the chamber is low enough so that most of the ions can travel

<sup>\*</sup> A number of these are shown in E. W. Muller in *Direct Observation of Imperfections in Crystals*, J. B. Newkirk and J. H. Wernick, eds., Wiley-Interscience, New York, 1962, pp. 77–99.

To vacuum pumps and gas supply
High voltage source

Vacuum

Conducting coating

Fluorescent coating

Class chamber

Fig. 5-7. Schematic diagram of the field ion microscope. The specimen has a very sharp point. The region near the point is magnified.

from the specimen tip to the glass envelope without colliding with gas particles.

The process by which ionization occurs is called field ionization. It will occur only in the presence of a very high voltage gradient; therefore the specimen must have a sharp tip and be an electrical conductor. Ionization occurs at atom sites on the tip. Because the gas particles travel in straight lines after they are ionized, bright spots on the fluorescent screen correspond to atoms on the tip. The magnification of the instrument is the ratio of the tip radius to the screen radius. Tip radii generally range from about 100 to 3000 Å, with screen radii being several inches. Magnifications of the order of I million are commonly achieved. The tip is usually cooled to very low temperatures by means of liquid hydrogen or liquid helium. Cooling reduces thermal vibration of the solid atoms and random motion of the gas atoms, which results in improved resolution. For this instrument, resolution is in the neighborhood of 1Å and is governed by atomic vibration and electric field uniformity.

A field ion micrograph of a tungsten tip is shown in Fig. 5-8. The pattern is rather complex, but this is expected because the surface of the tip is composed of a large number of different crystallographic planes. Interpretation of field ion micrographs requires some experience; however, even the beginner can detect an imperfection in Fig. 5-8. Each of the light spots represents an atom, and each region of the micrograph is symmetrical. There is a line running from the lower left corner towards the center, and then vertically upward, along which the symmetry is disrupted. The disrupted region is a grain boundary, and it is seen to be several atomic spacings wide. Vacancies, interstitials, impurities, and dislocations have all been observed with this instrument.

Field ion microscopy gives information about the surface only. If we want to investigate the interior of the specimen, it is possible to strip one atomic layer at a time from the specimen and observe the specimen surface each time. The stripping process is called field evaporation and requires that the specimen voltage be increased momentarily. Imperfections can be followed through a specimen by peeling away successive atomic layers.



micrograph of a tungsten tip. Each bright spot represents an atom. The line along which the symmetry is disrupted is a grain boundary. Magnification, approximately 3,500,000 ×. (Courtesy of J. J. Hren.)

Fig. 5-8. Field ion

# 5-4 X-ray sources

X-ray sources

Before discussing X-ray diffraction, methods of generating X-rays will be considered. The atomic mechanism by which they are generated is important not only for diffraction work but also for the electron beam microprobe described in Section 5-8.

A simple X-ray tube is shown in Fig. 5-9. The heated cathode releases electrons by thermionic emission. The metal target is held at a high positive potential, typically in the neighborhood of several thousand volts. The electrons are accelerated through the vacuum by the large voltage difference and gain kinetic energy. This can be expressed as

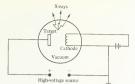


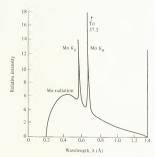
Fig. 5-9. Schematic drawing of an X-ray tube. Electrons emitted by the cathode are accelerated toward the target and collide with it. X-rays are emitted after the collision.

Kinetic energy = V' eV

where V' is the target voltage. Upon striking the target, most of this kinetic energy (about 98%) is converted to heat; however, a small fraction of it is converted into X-rays.

The X-ray spectrum emitted by a molybdenum target bombarded with 35,000-eV electrons is shown in Fig. 5-10. The spectrum has a continuous X-ray output with wavelengths greater than 0.24 as well as spikes labeled  $K_a$  and  $K_\beta$ . The wavelengths at which these spikes occur are characteristic of the target material. To understand the origin of the spikes, we must consider the energy levels of the electrons in molybdenum. Figure 5-11 is a simplified energy diagram. All of the electrons in a particular shell are assumed to be at the same energy level, which neglects the small energy differences of subshells (see Section 2-5). Molybdenum has an atomic number of 42; consequently the electrons in the K shell (n=1) are very strongly bound to the nucleus. It is possible for a highly energetic electron from the incoming electron beam to strike one of the inner shell electrons and transfer energy to it in the collision. The incoming electron escapes, while the electron in the atom can no longer remain in the K shell; its

Fig. 5-10. The X-ray emission spectrum of molybdenum bombarded by 35,000-eV electrons.



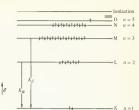


Fig. 5-11. Energy levels of electrons in molybdenum, showing the origin of  $K_z$  and  $K_\beta$  radiation.

energy is too great. This electron finds a place at a higher energy level (note that the L and M shells are filled; consequently it can be accommodated in the N shell or higher). Which level it goes into depends on the amount of energy it acquired in the collision.

The K shell is now missing one electron, and the atom will revert back to a lower energy (more stable) state when one of the L shell electrons drops into the K shell. Because the energy of the electron decreases in this transition, it radiates energy. The wavelength of the energy radiated can be calculated by the formula

$$\mathcal{E} = \frac{hc}{\lambda}$$

where

 $\mathscr{E} = \text{energy change of the electron}$ 

h = Planck's constant

 $\lambda$  = wavelength of the radiation

c = speed of light

The value of  $\lambda$  corresponding to this transition creates the K<sub>a</sub> line. If an electron from the M shell had dropped into the K shell vacancy, the radiation emitted would have the wavelength of the K<sub>g</sub> spike in Fig. 5-10. Figure 5-11 shows that a number of transitions may take place, but we shall not pursue this further. The wavelength of the radiation emitted depends on the electron configuration of the atom and is therefore a characteristic of the atom. It is a fingerprint and can be used to identify elements. The electron microprobe operates on this principle. The continuous part of the spectrum appearing in Fig. 5-10 is due to other interactions between the incoming electrons and the target. It can be removed from the X-ray beam by passing the beam through appropriate filters.

Question

Question 3: The emission of X-radiation from a target can be used to find the energy difference between the various electron shells. Molybdenum K<sub>z</sub> radiation has a wavelength of 0.710Å. What is the energy difference between an electron in the K shell and one in the L shell?

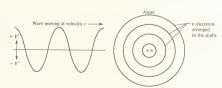
# 5-5 X-ray diffraction

The diffraction of visible light is a well-known phenomenon. It can be demonstrated by shining light through a diffraction grating. A grating has a large number of equally spaced lines that are transparent, with opaque regions in between. If the wavelength of the light is about the same as (or smaller than) the distance between the transparent lines, diffraction is observed. In 1912, Max von Laue suggested that crystalline solids could be used as diffraction gratings. Diffraction would occur if radiation having a wavelength in the neighborhood of I A was used because this length is comparable to the interatomic spacing in crystals. X-rays meet this wavelength requirement. Laue postulated that X-ray diffraction patterns could be obtained from crystals just as visible light diffraction patterns could be obtained from gratings. Interpretation of the patterns would then give detailed information about the crystal structure. In the X-ray diffraction arrangement, each atom in the crystal would act as a site at which Xrays were scattered, and the radiation scattered from a large number of atoms would interfere constructively or destructively to produce diffraction effects.

Figure 5-12 illustrates the scattering phenomenon. The incoming electromagnetic radiation is represented as a sine wave. For the sake of simplicity, consider that the sine wave represents electric potential. If the atom is stationary and the wave moves past it, each charged particle in the atom will be subjected to a periodic electric field having a frequency equal to the frequency of the incoming wave. The varying field will cause the charged particles of the atom to oscillate at the same frequency as the incoming radiation. Because the electrons have a much smaller mass than the nucleus, the amplitude of their oscillations will be much larger than that of the nucleus. An oscillating charged particle radiates energy at the frequency of oscillation (a radio transmitter antenna operates on this principle). Thus, all of the electrons will act as radiation sources, and the energy radiated from them will go out in all directions. Summarizing, the electrons acquire energy from the directional incoming wave and then radiate this energy in all directions. They have, in effect, scattered the incoming radiation. Energy conservation requires that the incident wave be attenuated in this process.

The atom rather than the electrons will be considered as the scattering site. This can be justified by introducing the atomic scattering factor. The

Fig. 5-12. An electromagnetic wave moving past an atom. The n electrons in the atom will oscillate at the wave frequency.



scattering factor is the ratio of the radiation scattered by the charge distribution in the atom to that scattered by a point electron. Its values have been calculated and tabulated; however, the X-ray discussion presented here will not require its use. From the point of view of a Huygen's construction, each atom is considered as a source of spherical secondary wavelets.

The conditions necessary for diffraction can be determined from Fig. 5-13. The points A, B, and C represent atoms on three planes of a family, with d being the distance between planes. The incoming radiation is represented by sine waves of wavelength \(\lambda\) in Fig. 5-13(a). The lines \(a\_i\) b' and \(c'\) have been drawn through the peaks of the sine waves; these lines are wavefronts. The incident wave is at an angle to the planes, and wavefront \(a'\) is at obswin impinging upon atom \(A\). For the geometry selected, the wavefront \(a'\) is at distance \(\lambda\) from atom \(B\) and a distance \(A\) from atom \(B\) and \(A\)

A short time later, wavefront a' has traveled through a distance  $\lambda$  and is in the position illustrated in Fig. 5-13(b). The wavefront has reached C. and portions of it have been scattered by A and B. The circles around A and B represent the peaks of the scattered waves. The incident wave continues to travel and the atoms continue to scatter. At some later time, the peaks of waves radiated by the three atoms will be as shown in Fig. 5-13(c). Each atom can be considered as a generator of spherical waves. The scattered waves have spherical symmetry but are shown only on the right side of the figure for purposes of clarity. The wavefronts of the scattered waves can be found from Fig. 5-13(c). The wavefronts are lines which join the peaks of the waves; therefore a line which is tangent to the peaks of the scattered waves is a wavefront. Four of these are shown. They are labeled by the circles numbered 0, 1, and 2, with 1 appearing twice. The directions of propagation of the wavefronts are shown by the vectors 0', 1', 1", and 2', which are perpendicular to the wavefronts. The scattered waves are in phase in these directions and reinforce each other. Wavefront 0 moves in the same direction as the incident wavefronts and is called a zero-order diffraction wave. First-order diffracted wavefronts are labeled 1, and two of them are shown. Their propagation directions are 1' and 1". The two sets of wavefronts are due to the spherical symmetry of the radiated waves. The angle between 0' and 1' is equal to the angle between 0' and 1", again because of the symmetry. This angle is defined as  $2\theta_1$ . The subscript 1 means that the angle is measured between the incident direction and the direction of propagation of the first-order diffracted wave. Reinforcement of the scattered waves can also occur in other directions. One of these is shown as 2', which is the direction of propagation of wavefront 2. Diffraction in this direction is called second-order diffraction, and the angle between the incident and diffracted directions is  $2\theta_2$ . Higher-order diffraction also occurs but is not shown.

Let us consider what sort of useful relationship we can derive from the figure. In a diffraction experiment, we are after information concerning interatomic distance and crystal structure. In terms of Fig. 5-13(a), we want to find the dimension d. The wavelength of the X-rays is determined

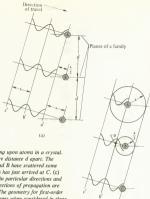
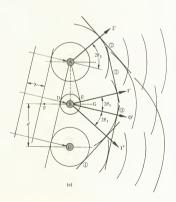


Fig. 5-13. X-ray diffraction. (a) X-rays impinging upon atoms in a crystal. The family of planes that the atoms belong to are distance dayar. The wavelength of the radiation is X, log Atoms A and B have scattered some of the incoming radiation. The incident radiation has just arrived at C. (c) The radiation sustered by the atoms reinforces in particular directions and forms wavefronts. Four wavefronts and their directions of propagation are shown. These are the diffraction directions. (d) The geometry for first-order diffraction. (e) The diffraction directions from cones when considered in three dimensions.



by the X-ray source and is therefore known. The angle  $2\theta$  can be measured. If we can find a relationship between d,  $\lambda$ , and  $\theta$ , we can solve it for d.

The relationships between angle DBF and angle EBG can be found from the two triangles ABD and ABE [Fig. 5.13(e)]. It is readily seen that the triangles are identical. Because AB is perpendicular to FG, angle DBF = EBG. The figure also shows that GBO' = DBF. Thus, line FG bisects angle  $2\theta$ : therefore DBF = EBG =  $6BO' = \theta$ .

A portion of Fig. 5-13(c) is shown in Fig. 5-13(d) and illustrates the angular relationships for first-order diffraction. The angles between line FG and the incident and diffracted directions (0° and 1°) are called the angle of incidence and the angle of diffraction, respectively. They are equal for first-order diffraction only. Figure 5-13(c) shows that this is not true for second-order diffraction. From Fig. 5-13(d), it can be seen that

$$\overline{DB} = d \sin \theta_1$$
 (5-1)

From Fig. 5-13(b),

$$\overline{DB} = \lambda/2$$
 (5-2)

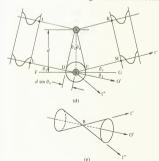
Combining equations 5-1 and 5-2,

$$\lambda = 2d \sin \theta_1$$
 (5-3)

This equation is valid for first-order diffraction only.

The results derived so far can be viewed in another way. Because the length of line  $\overline{DBE}$  in Fig. 5-13(d) is just the wavelength  $\lambda$ , the distance  $\overline{JAK}$  is exactly one wavelength shorter than distance  $\overline{LBM}$ . Waves traveling these two paths must have the same phase relationship at  $\overline{KM}$  as they had at  $\overline{JL}$ . They reinforce each other.

The geometric conditions can be worked out for higher-order diffraction,



$$2\lambda = 2d \sin \theta_{\bullet}$$

for second-order diffraction, and that

$$3\lambda = 2d \sin \theta_3$$

for third-order diffraction. The general form of this equation, which defines the diffraction conditions for *n*th order diffraction, is

$$n\lambda = 2d \sin \theta_n \tag{5-4}$$

This is Bragg's law and relates the distance between planes of a family in a crystal with measurable quantities. It is emphasized that  $\theta_n$  is half the angle between the incident and diffracted directions by definition.

Our two-dimensional sketches show that diffraction takes place in particular directions. If this is extended to three dimensions, diffraction occurs on the surfaces of two cones, as shown in Fig. 5-13(e). The cones for first-order diffraction are formed by rotating lines I' and I', using line 0' as the rotation axis. Recall that these lines extend on both sight of atom B, although we have shown the wave construction only on the right side of B. Diffraction occurs on cones because of the spherical symmetry of the scattered waves.

Question

Question 4: Using Bragg's law, show that the wavelength of the radiation cannot exceed twice the distance between atoms if diffraction is to occur. It is necessary to do this only for first-order diffraction.

# 5-6 Diffraction conditions for cubic unit cells

Bragg's law enables us to find the distance d between planes of a family but does not provide enough information by itself to enable us to determine both the crystal structure and the lattice parameter. Two things remain to be done. First, the quantity d by itself is not very informative because there are many different families of planes in a crystal. We shall, however, express d as a function of the lattice parameter and the Miller indices, which are unique numbers. Second, the crystal structure determines which families of planes diffract and which do not. This information will enable us to find the structure of a specimen from its diffraction pattern, as will become clear (hopefully). From here on we shall limit our discussion to the three cubic structures.

Figure 5-14 will aid in deriving the relation between d, the lattice parameter, and the Miller indices. A cubic unit cell and the plane (hkl) are shown in Fig. 5-14(a). Line  $\overline{OD}$  is perpendicular to (hkl) and passes through the origin. From our definition of families of planes, the distance between planes of the (hkl) family is equal to  $\overline{OD}$ . We want to express this distance, d, in terms of the lattice parameter and Miller indices. Consider the triangle ODH in Fig. 5-14(a). This has been redrawn in Fig. 5-14(b),

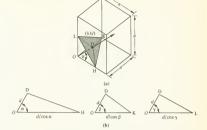


Fig. 5-14. Diagrams for finding the distance between planes as a function of lattice parameter and Miller indices. (a) Plane (hk!) in a call attice. OD is perpendicular to the plane and passes through the origin. It is the distance between planes of the (hk!) family. (b) The direction angles of OD are a, β, and y, angles of OD are a, β, and y,

and it is seen that  $OH = d/\cos \alpha$ .  $\alpha$ ,  $\beta$ , and  $\gamma$  are the angles between  $\overline{OD}$  and the three coordinate axes. From the definition of the Miller indices, we can write

$$\overline{OH} = \frac{a}{h}$$

where h is a plane index. Thus,

$$\frac{d}{\cos \alpha} = \frac{a}{h}$$

Similarly,

$$\frac{d}{\cos \beta} = \frac{a}{k} \qquad \frac{d}{\cos \gamma} = \frac{a}{l}$$

Squaring these three equations and then adding them and rearranging yields

$$\cos^2 \alpha + \cos^2 \beta + \cos^2 \gamma = d^2 \left( \frac{h^2}{a^2} + \frac{k^2}{a^2} + \frac{l^2}{a^2} \right)$$
 (5-5)

The quantities  $\cos \alpha$ ,  $\cos \beta$ , and  $\cos \gamma$  are the direction cosines of  $\overline{OD}$ . From analytical geometry,

$$\cos^2 \alpha + \cos^2 \beta + \cos^2 \gamma = 1$$

Substituting this equation into equation 5-5 and rearranging,

$$d = \frac{a}{\sqrt{h^2 + k^2 + l^2}} \tag{5-6}$$

We can now use equation 5-6 to eliminate d from Bragg's law (equation 5-4). Making the substitution,

$$n\lambda = \frac{2a\sin\theta_n}{\sqrt{h^2 + k^2 + l^2}}$$
 (5-7)

This equation will be used to find both a and the crystal structure from experimental data.

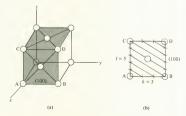
The families of planes which do and do not diffract in the various cubic crystal structures can be determined. The necessity for doing this can be dilustrated with Fig. 5-15, which shows a bec unit cell oriented in an X-ray beam such that equation 5-7 is satisfied for first-order diffraction from the (100) family. Diffraction from planes x and z causes reinforcement as shown; however, the diffracted radiation from plane y is 180° out of phase and will consequently cancel the wave. The net result is no first-order diffraction from the (100) family of a bec crystal. Diffraction account only from families of planes which include all of the atoms in a crystal because all atoms act as scattering sites. In the bec example, the (100) family does not include all of the atoms.

An fcc unit cell is shown in Fig. 5-16(a), and those families of planes which include all of the atoms will be found for this cell. The (100) plane of the unit cell appears in Fig. 5-16(b). Any family of planes which shows diffraction must pass through all of the atoms shown in the figure. Now divide  $\overline{AB}$  into k parts and  $\overline{AC}$  into l parts. For the example shown, k=3 and l=5. Lines corresponding to these values of k and l have been drawn on the (100) plane and represent the intersection of the (100) plane with planes of the family ( $\overline{AS}$ ), where k is undetermined. The procedure

Fig. 5-15. Diffraction does not occur for the (100) family in a bcc crystal. The diffraction condition is met by planes x and z. Radiation from plane y is 180° out of phase.



Fig. 5-16. (a) An fcc unit cell. Any family of planes that causes diffraction must include all of the atoms in the cell. (b) The intersection of planes of the (h25) family with the (100). Line AD must be divided into an even number of parts if a plane is to include the face-centered atom.



#### 5-6: DIFFRACTION CONDITIONS FOR CUBIC UNIT CELLS

Table 5-1. Indices of diffracting planes in simple, face-centered, and body-centered cubic lattices

hkl	$h^2 + k^2 + I^2$			
	Simple	Face-centered	Body-centered	
100	1	_		
110	2	_	2	
111	3	3	_	
200	4	4	4	
210	5	_	_	
211	6	_	6	
220	8	8	8	
300	9	_	_	
221				
310	10	_	10	
311	11	11	_	

used divides the diagonal  $\overline{AD}$  into k+l parts. If the family (h35) is to include the atom at the face-centered position, diagonal  $\overline{AD}$  must be divided into an even number of parts. This requires that

$$k + l = \text{even number}$$
 (5-8)

A similar treatment of the (001) plane shows that

$$h + k = \text{even number}$$
 (5-9)

Equation 5-8 requires that k and l are both odd or both even. Equation 5-9 places the same requirement on h and k. Both of these are met if

$$h$$
,  $k$ , and  $l$  are all odd or all even FCC (5-10)

Only those families of planes satisfying condition 5-10 will cause diffraction in an fcc crystal.

A similar analysis applied to the bcc structure shows that diffraction occurs only if

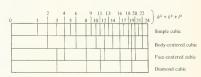
$$h + k + l = \text{even BCC} \tag{5-11}$$

Simple cubic structures will show diffraction from all families of planes (no restrictions on h, k, and l). These results are tabulated in Table 5-1, along with values of  $h^2 + k^2 + l^2$  corresponding to the diffracting planes. Allowed values of  $h^2 + k^2 + l^2$  for various structures are also shown in Fig. 5-17.

Question

Question 5: Derive equation 5-11.

Fig. 5-17. Diffracting families of planes for various cubic structures.



## 5-7 Interpreting experimental data

A large variety of X-ray diffraction cameras are available and in use. Which type one uses depends on the specific application and the form of the specimen (single-crystal, polycrystal, etc). The discussion of this section will be limited to the X-ray powder camera and the interpretation of experimental results derived from it. Further information about X-ray methods can be found in a number of good references.\*

The powder camera is shown schematically in Fig. 5-18(a). It consists of an X-ray source, a powdered specimen of the material to be analyzed, and a circular strip of X-ray film. A very large number of small specimen particles are randomly oriented in the specimen holder. Due to the random orientation and the large number of particles, some of the particles will be oriented in the X-ray beam such that the diffraction conditions are met. These particles will diffract the beam; the others will not. The diffracted rays will form cones, as explained in Section 5-5. The lines along which the cones intersect the film will show up as exposed regions when the film is developed. This is shown in Fig. 5-18(b). The diffraction angles can be found from the positions of the lines on the film. Using a powdered specimen is equivalent to using a single-crystal specimen and rotating it through all possible orientations. The powder merely does away with the necessity for rotation.

## Example 5-1

The interpretation of powder patterns can be illustrated by the following example. Assume that an X-ray diffraction powder pattern has been made of an element which has one of the cubic structures. Diffraction was found at the following values of 20: 40°, 58°, 73°, 86.8°, 100.4°, 114.7°, and 131.1°. The wavelength of the radiation used was 1.544 (copper K, line).

- (a) Determine the crystal structure.
- (b) Find the lattice constant.

(c) Identify the element. The entire analysis will be ba

The entire analysis will be based on first-order diffraction. This will be justified at the end of the problem. The only information which we need is equation 5-7 and Table 5-1.

(a) Find the crystal structure. The crystal structure can be found by considering the planes which cause diffraction in the various cubic structures. We start by solving equation 5-7 for  $\sin^2 \theta$ , considering only first-order diffraction:

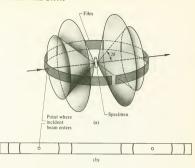
$$\sin^2 \theta = \frac{\lambda^2 (h^2 + k^2 + l^2)}{4a^2}$$
 (5-12)

We have experimental values for  $\theta$ , and we know which values of hkl cause diffraction in the various cubic structures. The lattice parameter is un-

<sup>\*</sup> B. D. Cullity, Elements of X-Ray Diffraction, Addison-Wesley, Reading, Mass., 1956; J. B. Cohen, Diffraction Methods in Materials Science, Macmillan, New York, 1966.

### 5-7: INTERPRETING EXPERIMENTAL DATA

Fig. 5-18. The powder camera, (a) A powdered specimen is placed in the center of the camera. The cones that define the diffraction directions are shown, (b) Lines appear when the film is developed. These lines mark the intersection of the cones and the film (B. D. Cullity. Elements of X-Ray Diffraction, Addison-Wesley, Reading. Mass., 1956).



known but can be eliminated by forming a ratio with equation 5-12:

$$\frac{\sin^2 \theta_{\rm A}}{\sin^2 \theta_{\rm B}} = \frac{h_{\rm A}^2 + k_{\rm A}^2 + l_{\rm A}^2}{h_{\rm B}^2 + k_{\rm B}^2 + l_{\rm B}^2} \tag{5-13}$$

where  $\theta_A$  is the first experimentally measured diffraction angle and  $\theta_B$  is the second. If the structure is fcc, Table 5-1 shows that the first two families of planes which will show diffraction effects are the (111) and (200). Using these values of the Miller indices in equation 5-13,

$$\frac{\sin^2 \theta_A}{\sin^2 \theta_B} = \frac{1^2 + 1^2 + 1^2}{2^2 + 0^2 + 0^2} = \frac{3}{4}$$
 fcc

For the bcc structure, this ratio is

$$\frac{\sin^2 \theta_A}{\sin^2 \theta_B} = \frac{1^2 + 1^2 + 0^2}{2^2 + 0^2 + 0^2} = \frac{1}{2} bcc$$

The experimental data are given in Table 5-2.

Table 5-2

2θ (deg)	θ (deg)	$\sin \theta$	sin ²θ
		0.2420	0.117/
40	20	0.3420	0.1170
58	29	0.4548	0.2350
73	36.5	0.5984	0,3538
86.8	43.4	0.6871	0.4721
100.4	50.2	0.7683	0.5903
114.7	57.35	0.8420	0.709

The ratio can now be formed:

$$\frac{\sin^2 \theta_A}{\sin^2 \theta_B} = \frac{0.1170}{0.2350} = 0.498$$

The structure is seen to be bcc. This could be checked by computing  $\sin^2 \theta_B / \sin^2 \theta_C$ . Using the data in Table 5-1, this value should be  $\frac{2}{7}$ . The calculated value is 0.664.

(b) Find the lattice parameter. From equation 5-12,

$$a^{2} = \left(\frac{\lambda}{2}\right)^{2} \frac{(h^{2} + k^{2} + l^{2})}{\sin^{2} \theta}$$
 (5-14)

The values of  $\theta$  are known. A set of values for hkl corresponds to each value of  $\theta$ . The smallest value of  $(h^2 + k^2 + l^2)$  corresponds to the smallest  $\theta$ . etc. The values of  $\sin^2 \theta$  and the corresponding value of  $(h^2 + k^2 + l^2)$  are shown in Table 5-3. The Miller indices come from Table 5-1. A value of a can now be found for each value of  $\theta$  and the corresponding Miller indices. The results of substituting these values into equation 5-14 are given in Table 5-3. The average value of a is 3.172.

(c) The periodic table on the front cover shows that the bcc structure with a lattice constant of 3.172 corresponds to W (tungsten).

The analysis was done by considering only first-order diffraction. Higher-order diffraction must be accounted for. To do this, we rewrite equation 5-7 to include higher-order diffraction:

$$a^{2} = \left(\frac{\lambda}{2\sin\theta_{n}}\right)^{2} n^{2} (h^{2} + k^{2} + l^{2})$$
 (5-15)

The only difference between equations 5-15 and 5-14 is the quantity  $n^2$ . Let us consider a bcc crystal. Second-order diffraction from the (110) planes gives a value of  $n^2(h^2 + k^2 + l^2)$  equal to 8. Table 5-3 shows that this also corresponds to first-order diffraction from the (220) planes; consequently both of these lines will appear at the same position on the film. Third-order diffraction from (110) planes yields  $n^2(h^2 + k^2 + l^2)$  equal to 18, corresponding to first-order diffraction from the (330) planes. This argument can be continued to show that any higher-order diffraction from a given family of planes corresponds to first-order diffraction from an allowed family having larger values of the Miller indices. This is also true for the fcc and simple cubic structures. Interpretation of X-ray patterns

Table 5-3

$\sin^2 \theta$	Diffracting plane	$h^2 + k^2 + I^2$	$\left(\frac{\lambda}{2}\right)^2$	$a^2$	а
0.1170	110	2	0.5929	10.122	3.180
0.2350	200	4	0.5929	10.092	3.177
0.3538	211	6	0.5929	10.056	3.171
0.4721	220	8	0.5929	10.048	3.170
0.5903	310	10	0.5929	10.044	3,169
0.7090	222	12	0.5929	10.036	3.168

#### 5-8: THE ELECTRON MICROPROBE

for cubic crystals can therefore be done using only first-order diffraction equations.

### Ouestion

Question 6: The diffraction lines which have the smallest value of  $\theta$  for an fee crystal come from first-order diffraction of the ((111)) planes. These planes also show second-order diffraction, third-order diffraction, etc. What family of planes has first-order diffraction that appears at the same position as second-order diffraction from the ((111)) planes? As third-order diffraction from ((111))?

## 5\_8 The electron microprobe

The identification of chemical elements is of great importance for many aspects of materials science. From Chapter 8 on we shall be concerned with impurities, mixtures of elements, and the manner in which one element diffuses into another. These topics require that various elements be identified and their concentrations measured. The electron microprobe provides one method for doing this.

The electron microprobe identifies materials by their characteristic X-ray emission. Section 5-4 showed that materials emitted X-rays when bombarded by high-energy electrons and that the wavelength of the X-radiation depended on the material. The chemical composition of a material can therefore be found by bombarding it with high-energy electrons and analyzing the emitted X-ray spectrum. The optical principles involved in finding X-ray wavelengths are similar to those used for finding the wavelengths of visible light, although the equipment is different. We shall not go into the subject of X-ray ontics and detection but shall assume that an X-ray spectrometer is available. This device enables us to measure both X-ray intensity and wavelength and gives an electrical signal which is proportional to the intensity. If the electron detector in the scanning electron microscope (Fig. 5-6) is replaced by the X-ray spectrometer, the resulting instrument is an electron microprobe. X-rays are generated by the electron beam striking the specimen, and the emitted X-rays are analyzed by the spectrometer. Recall that the electron beam has a diameter in the neighborhood of 100 Å when it impinges upon the specimen, and this is therefore the size of the area being analyzed.

The electron beam can scan the specimen and a map can be made of the location and concentration of various elements. To make such a map, the spectrometer would be set to detect a wavelength that is characteristic of the element we are looking for. The electrical output of the spectrometer depends on the intensity of the X-rays striking it. The intensity, in turn, depends on the concentration of the element of interest. The spectrometer output is used to modulate a cathode-ray tube, just as the output of an electron detector modulated the tube in the scanning electron microscope. Using this arrangement, light spots appear on the cathode-ray tube which correspond to the presence of a particular element in the specimen. Figure 5-19 shows a micrograph of an impurity inclusion in chromium steel. The impurity was checked for Mn, Al, and Si using the procedure described above. A separate scan was required for each element. Magnification can be obtained by this method.

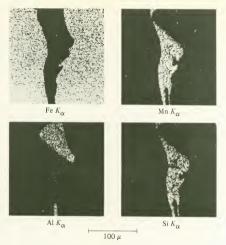


Fig. 5-19. An impurity region was found in a specimen of 1% chromium steel. The specimen was analyzed by an electron microprobe for Mn, Al, and Sl. The cathode-ray nube was photographed during each scan, and the location of these impurities is shown. (L. S. Birks, Electron Probe Microanalysis, Wiley, Interscience, New York, 1962.

## 5\_0 Verification of models and summary

Several experimental methods used in materials science have been discussed. Visual observation was discussed first, and the results obtained with the instruments considered have confirmed a number of models that we have used. The optical microscope enables us to see the grain boundaries, dendrites, and other microstructure features predicted by solidification theory. The electron microscope provides visual verification of the dislocations postulated in Chapter 4, while the field ion microscope enables us to see all of the various crystal imperfections on an atomic scale. These microscopes can also be used to verify many other models. For example, the migrating surface atoms postulated in Section 4:1 have been observed in the field ion microscope. Scanning electron microscopes are available for a large number of applications; electron microscops is not

Table 5-4

Instrument	Maximum magnification (approx.)	Resolution (Å) (approx.)	Method of providing image contrast
Reflecting optical microscope	2000×	3000 Å	Light is not reflected into the microscope by some regions o the specimen
Transmission electron microscope	300,000×	Several Å	Electron scattering causes a vari ation in the rate at which electrons strike a phosphot screen
Scanning electron microscope		100 Å	The light intensity on the screen of a cathode-ray tube is modu- lated by an electron detector in the microscope
Field ion microscope	3,500,000×	1 Å	Ions strike a phosphor screen the rate at which they strike the screen reflects the atomic struc- ture of the specimen

limited to transmission. Table 5-4 compares some of the characteristics of the microscopes. All values given are approximate.

X-ray diffraction was discussed in some detail and the powder camera was considered. The X-ray results verified the crystal structures of Chapter 3. Many types of cameras other than powder cameras are in use. Single crystals and polycrystals can be analyzed by X-ray techniques, and the crystallographic orientation of single crystals can be found by this method. Lattice distortions can also be observed, and screw dislocations have been found in whiskers by X-ray diffraction methods. The diffraction techniques are not limited to X-rays. Crystal structure can also be determined by the diffraction of electrons and neutrons. Electron diffraction is also used for studying surface structure.

The last topic covered was concerned with the chemical analysis of solids. The electron microprobe is just one method of analysis. Many others are available, including the chemical methods of quantitative analysis.

This chapter has presented several widely used experimental methods, but these are certainly not the only ones used. The solutions of new problems in materials science require the development of new experimental techniques, and these are constantly being found.

#### Problems

1 A whisker having a diameter of 10  $\mu$  was found to have a tensile strength of 10 $^6$  ps. If the whisker diameter was measured in an optical microscope, an error would be introduced due to the resolving power of the microscope. Suppose the diameter was measured in an optical microscope using a wavelength of 5000 Å (0.5  $\mu$ ), (a) What would be the maximum and minimum values of the diameter when measured in this way? (b) What would be the maximum and minimum values of the

<sup>\*</sup> W. W. Webb, op. cit.

- tensile strength, based upon the whisker diameters found in part (a)? (c) What is the percent error in the measured tensile strength due to the resolving limit of the microscope?
- 2 The wavelength of a particle is related to its momentum by the de Broglie relation,  $\lambda = h/mv$ , where h is Planck's constant  $(6.626 \times 10^{-27})$ erg-secs) and m and v are the mass and velocity of the particle, while  $\lambda$ is the wavelength, (a) Taking the theoretical resolving power of a microscope as half a wavelength, what is the theoretical resolving power of an electron microscope whose electrons have been accelerated through a 1000-V potential difference before striking the specimen? The mass of an electron is  $9.109 \times 10^{-28}$  g. (b) Why is this resolution not observed? (Note: Electron microscopes usually use accelerating potentials quite a bit higher than 1 kV. This number was selected because the electron follows the laws of Newtonian mechanics fairly well at this energy. If the same problem is considered with a 10-kV accelerating potential, relativistic mechanics must be used because the velocity would be great enough to require consideration of the increase in the mass of the electron.)
- 3 The field emission microscope is an instrument much like the field ion microscope, but with a couple of differences. In the field emission microscope, the sharply pointed specimen is held at a high negative voltage, and the glass chamber (Fig. 5-7) is kept at high vacuum (no gas is introduced after the air has been removed). The high voltage gradient near the tip causes electrons to leave the electron gas in the metal specimen, and these impinge upon the fluorescent screen to provide a magnified image of the tip. The specimen is usually kept at room temperature or high temperatures because this helps the electron emission process. The resolution of this instrument is not as good as that of the field ion microscope. Why? (Hint: The wavelengths of the image-forming ions and electrons are considerably smaller than the resolution in both of these instruments. Consider the temperatures of the specimens and the effect of temperature on the random motion of the He ions and the electrons.)
- 4 When an electron in copper moves from the L shell to the K shell, it emits 1.29 × 10<sup>-8</sup> ergs (or 8490 eV). What is the wavelength of this radiation?
- 5 A beam of X-rays having a wavelength of 1.541 Å (Cu K<sub>e</sub>) impinges on a simple cubic crystal having a lattice parameter of 2.35 Å. (a) Find the angle which the beam must make with the (111) planes in order for diffraction to occur. (b) Make a sketch showing the incoming X-ray beam, the crystal and the (111) planes, and the direction of the diffracted beams for first- and second-order diffraction. Calculate and label the angles between the incoming beam and the diffracted beams (twodimensional sketch)
- 6 Calculate the distance between planes of the (110), (220), (111), and (222) families in chromium.
- 7 A specimen of silver is placed in a powder camera which uses MoK. radiation (0.709 Å). It is found that the smallest observed diffraction angle changes by 0.11° as the silver is heated from room temperature to 800°C. Find the change in a (the lattice parameter) due to heating.

- 8 A specimen of an element which has one of the cubic structures was placed in a powder camera, with  $\lambda=1.541$  Å. The following values of  $2\theta$  were observed:  $44.46^\circ$ ,  $51.64^\circ$ ,  $75.78^\circ$ , and  $93.22^\circ$ . Identify the element.
- 9 The X-ray film from a powder camera is shown here. λ = 1.541 Å. The pattern was made by an element which has one of the cubic structures. The diameter of the powder camera was 6 in. Identify the element.



10 Some experimental error is present when diffraction angles are measured. (a) Derive an expression for the fractional error Δd/d in terms of Δθ for a diffraction experiment using monochromatic radiation. (Hint: Differentiate Bragg's law and then substitute Δθ for dθ and Δd for dd, implying that the error is small.) (b) If the error in a particular experiment is 0.05°, find the fractional error in d at 15° and 75°. (c) If the error in the angle measurement is the same for all angles, would greater accuracy in measuring d come from using large or small diffraction angles?

Answers

- Question 1: Yes. Ultraviolet light has a shorter wavelength than visible light, and resolution of an optical microscope is limited by wavelength. Question 2: The image of a preselected area of the specimen appears on the cathode-ray tube. The magnification is the ratio of the image area, as seen on the tube, to the specimen area which the beam has scanned.
- Question 3:  $2.8 \times 10^{-8}$  ergs or 17,500 eV since  $\mathscr{E} = \frac{hc}{2}$ .
- Question 4: Rewriting equation 5-4 with n = 1,  $\sin \theta = \lambda/2d$ . The maximum value of  $\sin \theta$  is 1; therefore the maximum value of  $\lambda$  is 2d. If  $\lambda > 2d$ , the equation cannot be valid because  $\sin \theta$  cannot be greater than 1.
- Question 5: The families of planes which diffract must include the bodycentered atom; therefore the cube diagonal must be divided into an even number of parts. The cube diagonal is divided into h + k + lparts; therefore h + k + l = even number.
- Question 6:  $n^2(h^2 + k^2 + l^2) = 12$  for second order, which corresponds to first order from ((222)).  $n^2(h^2 + k^2 + l^2) = 27$  for third order, which corresponds to first order from ((333)).



CHAPTER 6

# Elastic Behavior of Crystalline Solids

The elastic properties of materials are of great practical importance to the engineer and are often a major consideration when selecting a material for a particular purpose. The designs of most devices require that the stresses on the materials be below the elastic limit. Elasticity was briefly discussed in Chapter I, and Hooke's law ( $\sigma = Ee$ ) was found from experimental observation of a specimen subjected to an axial load. Elastic behavior is also associated with other types of loading, and constants analogous to the elastic modulus can be defined. The definitions of these moduli are the first topics discussed in this chapter.

Elasticity has its origin in the forces between the atoms of the solid and therefore depends on both the chemical bonding and the structure of the solid. Using the models which we have developed, Hooke's law will be derived by considering interatomic forces. The derivation will be done for an ionic solid because this is the bond type which we have treated rigorously, and it will be applied to a useful ceramic. Similar calculations can be done for other bond types, but they are more difficult. The derivation should give the reader some insight into the origin of elastic behavior. Thermal expansion can also be explained in terms of interatomic bonds and crystal structure. This is discussed in the last portion of the chapter.

The materials properties covered in this chapter are independent of imperfections in the crystal structure and are called *microstructure-insensitive properties*. The term simply means that the elastic properties are independent of crystalline imperfections such as vacancies and dislocations. Later chapters will treat properties which depend on imperfections—the so-called *microstructure-sensitive* properties.

6-1 Young's modulus, shear modulus, and bulk modulus

There are a number of measurable constants that define the elastic behavior of a material. One of these, the modulus of elasticity (also called Young's modulus), was discussed in Chapter 1 for materials in tension. Materials

also show elastic behavior when subjected to compressive loads. The elastic modulus can be found by plotting a stress-strain diagram from experimental data. Figure 6-1 is the stress-strain diagram for a material which was loaded in both tension and compression. The yield stress was not reached in either case. Young's modulus is seen to be the same for both types of loading because the slope of the curve is the same throughout the entire elastic region. This is generally true for crystalline materials but does not necessarily hold for amorphous ones. The behavior of the material beyond the elastic limit will probably not be the same in tension and compression, as will be discussed in Chapters 7 and 8.

#### Shear modulus

An unstressed specimen is shown in Fig. 6-2(a). Several atoms on a vertical plane of the specimen are illustrated schematically. Figure 6-2(b) shows the shape of the specimen when it has been subjected to a shear force. The shear force is actually a couple and tends to move two parallel surfaces of the specimen in opposite directions. On the atomic scale, the shear force is such that one plane of atoms tries to slide past an adjacent plane. Application of the shear force distorts the atoms, as shown schematically in the figure. Each atom retains the same number of nearest neighbors that it had in the unstressed condition, but the shear force has distorted the entire crystal by the angle a. The specimen will return to its

Fig. 6-1. The stress-strain diagram for a specimen loaded in tension and then in compression, or vice versa. The slope of the curve is the same for both types of loading; therefore Young's modulus is the same.

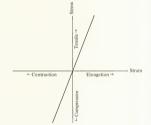


Fig. 6-2. (a) An unstressed specimen, The atoms on one plane are shown. (b) Application of a shear force causes a change in the specimen shape. The angle a is a measure of the deformation resulting from the applied force.

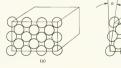
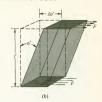


Fig. 6-3. Two specimens of the same material having different lengths but the same cross-sectional area. Both are loaded with the same shear force, F. The deformation of the long specimen is greater than that of the short one (As ~ As); however, x = a' since both have the same applied stress.





original shape when the force is removed, provided that the elastic limit in shear has not been exceeded.

Shear stress, shear strain, and shear modulus are analogous to tensile stress, strain, and modulus. They will be defined with the aid of Fig. 6-3. The two bars shown in the figure are made of the same material and have the same cross section; however, one is longer than the other. Both bars are subjected to the same shear force  $F_F$ . If  $\Lambda$  is taken as the cross-sectional area of the bar, the shear stress ( $\tau$ ) is defined as

$$\tau = \frac{F_s}{A}$$
 (6-1)

The units of  $\tau$  are force per unit area, just as in the case of tensile or compressive stress. The shape of the bars before the load was applied is shown by the dotted lines in Fig. 6-3. The deformation of the two bars, due to the shear stress, is shown as  $\Delta s$  and  $\Delta s'$ . Inspection of the two figures reveals that

$$\frac{\Delta s}{l} = \frac{\Delta s'}{l'} \quad \text{if } \alpha = \alpha'$$

For a given material, experiments show that the angle  $\alpha$  depends only on the shear stress and is independent of the dimensions of the specimen. The *shear strain*  $(\gamma)$  is defined as

$$\gamma = \frac{\Delta s}{l} \tag{6-2}$$

It is dimensionless, just like tensile or compressive strain. Most solids show elastic behavior when subjected to shear stresses, and it is found that  $\tau$  is proportional to  $\gamma$ :

$$\tau = G\gamma$$
 (6-3)

The constant of proportionality G is called the *shear modulus*. An elastic limit exists for shear stress just as it does for tensile and compressive stresses, and if this limit is exceeded, the material will be permanently deformed.

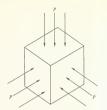


Fig. 6-4. A solid loaded by hydrostatic compression, Compressive stress (pressure) is applied uniformly over the entire surface,

## Question

Question 1: The angle  $\alpha$  is often called the shear angle. Write an equation relating  $\alpha$  and  $\gamma$ .

#### Bulk modulus

The bulk modulus provides a measure of the deformation that a material undergoes when it is subjected to hydrostatic pressure, and is strongly related to the repulsive interatomic forces. Consider a rectangular solid of volume V subjected to a hydrostatic pressure P, as shown in Fig. 6-4. The pressure exerts a compressive stries on all faces of the solid. The stress causes a compressive strain in all directions; consequently the dimensions of the specimen decrease. The magnitude of the dimensional changes depends on the applied pressure. Figure 6-5 shows the shape of a specimen before and after the application of pressure.

The bulk modulus is defined as the ratio of the hydrostatic pressure to the fractional change in volume due to applying the pressure

$$B = -\frac{\sigma_{\text{hydrostatic}}}{\Delta V/V}$$
(6-4)

where

B = bulk modulus

 $\sigma_{\text{hydrostatic}} = \text{hydrostatic stress (or pressure)}$ 

V = volume of the solid before hydrostatic stress was applied

 $\Delta V$  = change in volume due to the hydrostatic stress (a negative quantity)

The volume change,  $\Delta V$ , is a measure of the ease with which a material deforms under hydrostatic pressure and is related to the interatomic bonding forces, particularly the repulsive forces. Equations can be derived which relate the bulk modulus to the repulsive force term in equation 2-22, and the repulsive term exponent (n) can be found from measured values of the bulk modulus. <sup>4</sup> The derivation will not be done here but is mentioned

<sup>\*</sup> The derivation can be found in C. Kittel, Introduction to Solid State Physics, 2nd ed., Wiley, New York, 1956, p. 78.

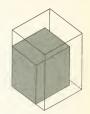


Fig. 6-5. Contraction of a solid resulting from a hydrostatic compressive stress. The unshaded planes represent the shape of the unstressed specimen, while the shaded planes show the specimen under hydrostatic stress.

because it is another link between the macroscopic elastic constants and our atomic model of solids.

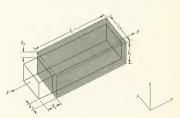
#### Ouestion

Question 2: The bulk modulus of iron is 2.46 × 10<sup>7</sup> psi. A piece of iron has a volume of 1 in 3 at atmospheric pressure and temperature. What is the volume of the specimen if it is 5000 ft under the ocean? Assume that the temperature remains constant and that the density of sea water is 64 bl/ft<sup>3</sup>.

# 6-2 Poisson's ratio

We have found that when a material is subjected to an axial stress, it deforms in the direction of the stress. Measurements show that deformation also occurs in other directions. For example, a specimen subjected to tension will elongate in the direction of the applied force (axial direction) and will simultaneously contract in the directions perpendicular to the axial direction (transverse directions). The ratio of axial strain to transverse strain is called Poisson's ratio and can be better explained with the aid of Fig. 6-6. The shaded planes show the shape of a specimen before the force F was applied in the x direction. From the figure, an elongation  $\delta x$  and  $\delta x$  take has occurred due to the applied force. The contractions  $\delta y$  and  $\delta x$  take

Fig. 6-6. Deformation of a specimen subjected to an axial tensile force, F. The shaded planes represent the specimen shape before the load was applied. Eliopation occurs in the axial direction and contraction in the transverse directions. The deformations resulting from the applied force are 8., 8., and 8.



place simultaneously with the elongation. The three deformations can be expressed as strains:

$$\varepsilon_x = \frac{\delta_x}{l_x}$$
  $\varepsilon_y = \frac{\delta_y}{l_y}$   $\varepsilon_z = \frac{\delta_z}{l_z}$ 

Note that  $\delta_x$  is positive, while  $\delta_y$  and  $\delta_z$  are negative. Experimentally, it is found that the ratios  $\varepsilon_y/\varepsilon_z$  and  $\varepsilon_z/\varepsilon_z$  are equal for isotropic materials. These ratios are also constant within the elastic limit. The constant is called Poisson's ratio and is defined as

$$\mu = -\frac{\varepsilon_y}{\varepsilon_x} \tag{6-5}$$

and is a positive quantity because  $\varepsilon_x$  and  $\varepsilon_y$  have opposite signs.

Poisson's ratio is explainable in terms of interatomic bonds. To do this, a rather rough model will be postulated. Figure 6-7(a) shows a closest-packed plane of a metal which is to be stressed. When the stress is applied [Fig. 6-7(b)], it is assumed that the nearest-neighbor distance in the axial direction (distance ab) will increase because of the stress but that nearest-neighbor bond lengths in other directions will remain the same (distances ac, ad, etc.). No restrictions are imposed on the distance between next nearest neighbors (distance cd). This model essentially says that nearest-neighbor bonds are much stronger than other bonds, which is reasonable. The model could not be called rigorous. The arrangement of the atoms after the stress is applied is shown in Fig. 6-7(b), in accordance with the postulated model. Comparison of the polygons abcd and a'b'c'd' shows that ab < a'b' and cd > c'd', indicating axial elongation and transverse contraction. Poisson's ratio can be calculated from the model. The two figures are shown superimposed upon each other with points b and b' at the same position [Fig. 6-7(c)]. The axial and transverse strains are

$$\varepsilon_x = \frac{\delta x}{ob}$$
 and  $\varepsilon_y = -\frac{\delta y}{oc}$ 

Poisson's ratio is thus

$$\mu = \frac{\delta y}{oc} \frac{ob}{\delta x} = \frac{ob}{oc} \frac{\delta y}{\delta x}$$
(6-6)

Each term on the right side of equation 6-6 can be evaluated by applying plane geometry to Fig. 6-7(c). Triangle obc is a 30-60° right triangle because the plane is close-packed; therefore

$$\frac{ob}{oc} = \tan 30^\circ = \frac{1}{\sqrt{3}} \tag{6-7}$$

Now consider triangle e'ef. Point e' was found by swinging arcs of radius 2r from points a' and b', with their intersection being e'. The model dictates this procedure. Because we are dealing only with deformation within the

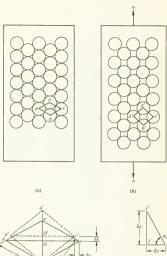


Fig. 6-7. An illustration of Poissons'; ratio, (a) Closest packed planes in a metal. (b) Rearrangement of the atoms caused by the applied stress, according to the postulated model. All nearest-neighbor bond lengths except ab' are the same before and after the stress is applied, (c) The polygons abed and a' b'-c' a' are super-imposed, showing the axial and transverse displacements, (d) A triangle showing the anytaler relationship of 5x and 5y, according to the model.



elastic limit,  $\delta x/ob$  is small. Because of this, cc' is practically perpendicular to bc. cf is perpendicular to ob, and triangles ocb and c'cf are taken as similar. Both are 30– $60^\circ$  right triangles; therefore

$$\frac{\delta y}{\delta x} = \tan 30^\circ = \frac{1}{\sqrt{3}} \tag{6-8}$$

Substituting 6-7 and 6-8 into 6-6,

$$\mu = \tan^2 30^\circ = \frac{1}{3}$$

Most metals have values of  $\mu$  of about  $\frac{1}{3}$ ; therefore the results obtained with our simple model are fairly good and the postulated mechanism is at least a reasonable one.

The shear modulus and Young's modulus are related to each other by Poisson's ratio. The relationship is

$$G = \frac{E}{2(1 + \mu)} \tag{6-9}$$

It is derived in most texts covering strength of materials.\*

# 6-3 Interatomic forces in a solidt

Hooke's law will be derived in Sections 6-3 and 6-4. The derivation will be based upon interatomic forces and crystal structure. The only bonding forces that we have considered in detail have been ionic bonds; therefore the derivation will be limited to ionic solids. It will also be necessary to select a particular structure for the derivation. The NaCl structure (Fig. 3-21) will be used because of its geometric simplicity. It is emphasized that many useful materials show this structure, including several metallic carbides. Although the derivation is limited to a single (but useful) case, the reader should gain some insight into the factors which cause elastic behavior and how effective each factor is. Elastic constants have been computed for several metallic solids as well as ionic ones.\*\* The fact that only a few metals have been treated is indicative of the mathematical difficulties encountered with metallic bond calculations.

Bonding between atoms was discussed in Chapter 2, and the force between two atoms was expressed as

$$f = f_a + f_r = \frac{ma}{r^{(m+1)}} - \frac{nb}{r^{(n+1)}}$$
  $m < n$ 

with the force acting along a line joining the atom centers. Because we are considering only ionic bonds, this equation can be written as

$$f = \frac{Z_1 Z_2 e^2}{r^2} - \frac{nb}{r^{n+1}} \tag{6-10}$$

Recall that r is the distance between ions; it is not the atomic or ionic radius. ro is the equilibrium distance between ions, in accord with the notation of Chapter 2. A plot of f vs. r is shown in Fig. 2-11. Equation 6-10 can be used to find the force exerted on a single ion by all of the other ions in the crystal. Figure 6-8 represents a solid having the NaCl structure. The positions of some of the positive and negative ions are shown. The downward force exerted on the cation C can be determined by summing the forces acting between C and each ion in the crystal. In this section we shall derive an equation relating the downward force on ion C to the inter-

<sup>\*</sup> See, for example, J. N. Cernica, Strength of Materials, Holt, Rinehart and Winston, New York, 1966, p. 101,

<sup>†</sup> The presentation in this section follows that given by D. Rosenthal, Introduction to Properties of Materiols, Van Nostrand, Princeton, N.J., 1964, sec. 6-2.

<sup>\*\*</sup> H. Brooks in The Science of Engineering Materials, J. E. Goldman, ed., Wiley, New York, 1957.

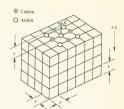


Fig. 6-8. An ionic solid having the NaCl structure. The ((200)) planes are shown. Cation C is a distance r above the top plane of the solid. The spacing between ions is r, not r<sub>0</sub>, indicating that the crystal is stressed.

atomic spacing. The downward (or positive x) direction in the figure corresponds to the [100] direction in the crystal.

The derivation begins by evaluating the x component of the Coulomb force term in equation 6-10. This force can be found with the aid of Fig. 6-9, which shows two planes of the (200) family. In terms of Fig. 6-9, the net downward Coulomb force can be expressed as

$$f_{\text{Coulomb}_x} = f_{(C-1)_x} + 4f_{(C-2)_x} + 4f_{(C-3)_x} + f_{(C-4)_x} + \cdots$$
 (6-11)

where

 $\mathbf{f}_{Coulomb_x}$  = net Coulomb force in the x direction exerted on ion C by all the ions in the crystal

 $f_{(C-1)_x}$  = Coulomb force in the x direction exerted on ion C by ion 1

 $f_{(C-2)_x} =$ Coulomb force in the x direction exerted on ion C by one of the ions labeled 2

The symbol f indicates a force exerted on ion C by all of the other ions in the crystal. f indicates a force exerted on ion C by one other ion. The factor of 4 used with  $f_{(C-2)_g}$  indicates that four atoms are located symmetrically with respect to C. These are shown as shaded ions in Fig. 6-9. Each term in equation 6-11 can be evaluated:

$$f_{(C-1)_x} = \frac{Z_C Z_1 e^2}{r^2}$$

$$f_{(C-2)_x} = \frac{Z_C Z_2 e^2}{2r^2} \frac{r}{\sqrt{2r^2}}$$

$$f_{(C-3)_x} = \frac{Z_C Z_3 e^2}{3r^2} \frac{r}{\sqrt{3r^2}}$$

$$f_{(C-4)_x} = \cdots$$
(6-12)

Consider  $f_{(C-2)_n}$  for a moment. The term  $Z_CZ_2e^2/2r^2$  expresses the Coulomb force exerted on ion C by one of the ions labeled 2, while the term  $r/\sqrt{2r^2}$  takes account of the fact that we only want the x component of the force. This term is the cosine of the angle which line C-2 makes with the x

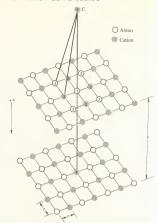


Fig. 6-9. Cation C and the two top planes of Fig. 6-8. The forces between C and the other ions of the crystal can be summed by using this construction. The planes belong to the (200) family. The figure is not to scale.

direction. The sign of each term in equation 6-11 depends on whether the quantity  $Z_{-N}$  (n is an integer) is positive on negative. The series as shown has alternating positive and negative terms. The series is an infinite one and it can be summed. The mathematical manipulations involved are not particularly enlightening, so only the result is given:

$$\mathbf{f}_{\mathsf{Coulomb}_x} = \frac{0.29 Z_{\mathsf{C}} Z_{\mathsf{A}} e^2}{r^2} \tag{6-13}$$

where  $Z_{\rm C}$  and  $Z_{\rm A}$  are the magnitudes of the cation and anion charges, respectively.

Equation 6-13 has several conditions imposed upon it. As previously mentioned, it holds only for ionic crystals with the NaCl structure. In addition, the geometry of Fig. 6-9 shows that it is the force in the [100] direction. If a different crystallographic direction is chosen, each term of equation 6-11 will change and the value 0.29 in equation 6-13 will change. This fact causes anisotropic elastic behavior in single crystals. The last condition on this equation has to do with the distance between ions. The series of equation 6-11 was summed assuming that r was the same in all directions  $(r_r = r_p = r_k)$ . This is true for the unstressed crystal; however, if an axial tensile force is placed upon the crystal, r will increase in the

direction of the force and decrease in the transverse directions by virtue of Poisson's ratio. If equal tensile stresses are applied to all faces of the crystal, however, r will be the same in the x, y, and z directions. Thus, equation 6-13 is valid for hydrostatic stress (tension or compression). This will come un again in Section 6-4

The repulsive force between two ions due to the overlap of their electron clouds is given by the second term of equation 6-10:

$$f_r = -\frac{nb}{n+1} \tag{6-14}$$

To find the net repulsive force exerted on ion C by the rest of the ions, the individual repulsive forces could be summed as we did for the Coulomb forces. If this were done, an additional constant would be introduced into equation 6-14. Rather than doing the summation, the constant  $\boldsymbol{c}$  is introduced:

$$f_{r_x} = -\frac{cnb}{\frac{c}{n^n+1}} \tag{6-15}$$

where  $\mathbf{f}_{r_x}$  is the repulsive force in the x direction (due to electron cloud overlap) which is exerted on ion  $\mathbb{C}$  by all of the ions in the crystal lying below it. The net force on ion  $\mathbb{C}$  in the x direction is the sum of the Coulombic and repulsive forces. The symbol  $\mathbf{f}_x$  will be used for this quantity:

$$f_x = f_{Coulomb_x} + f_{r_x} = \frac{0.29Z_CZ_Ae^2}{r^2} - \frac{cnb}{r^{n+1}}$$
 (6-16)

The quantity cnb is a constant and can be evaluated by letting

$$f_x = 0$$
 when  $r = r_0$  (6-17)

where  $r_0$  is the interionic spacing in the unstressed crystal. Note the distinction between r and  $r_0$ , r is the interionic spacing under any condition, while  $r_0$  is the interionic spacing for the special case of no stress. Substituting 6-17 into 6-16,

$$cnb = 0.29Z_CZ_Ae^2r_0^{n-1}$$
 (6-18)

The equation relating  $f_x$  and r can now be obtained by substituting equation 6.18 into 6-16:

$$f_{x} = \frac{0.29Z_{C}Z_{A}\epsilon^{2}}{r^{2}} - \frac{0.29Z_{C}Z_{A}\epsilon^{2}r_{0}^{n-1}}{r^{n+1}} = \frac{0.29Z_{C}Z_{A}\epsilon^{2}}{r^{2}} \left[1 - \left(\frac{r_{0}}{r}\right)^{n-1}\right]$$
(6-19)

For a given material, the only variables in equation 6-19 are  $f_x$  and r.

#### Ouestion

Question 3: Equation 6-19 is limited by the following restrictions: (a) The solid is ionically bonded. (b) It has the NaCl structure. (c) The force  $f_x$  is in the [100] direction. (d) The equation is valid if the

crystal is either unstressed or hydrostatically stressed. It is not valid for axial stress. Where in the derivation do each of these limitations occur?

# 6-4 Hooke's law

Hooke's law can be derived by applying equation 6-19 to the stressed crystal shown in Fig. 6-10(a). The crystal has equal tensile stresses applied to all of its faces; that is, it is subjected to hydrostatic tension. Figure 6-10(b) shows the crystal in two pieces; it has been split along plane A, which is an interior crystal plane. Figure 6-10(b) is a free-body diagram of the two parts of the crystal. The forces exerted on the atoms of plane A by the atoms on the right side of the crystal have been replaced by  $\sigma_{\nu}$ . Stresses in the y and z directions are not shown. Figure 6-10(c) shows the part of the crystal containing plane A. The structure has been emphasized, and it is seen that the crystal has the NaCl structure. The tensile stresses are in the [[100]] directions. All of the forces acting on plane A in the x direction are shown. The force fx exerted on each atom in the plane by the other atoms in the crystal is given by equation 6-19. The sum of these forces equals the applied stress,  $\sigma_x$ , times the area over which the stress is applied. The situation is the same in the v and z directions. Let the area of plane A be 1 unit. The forces on plane A show that

$$\sigma_{\rm v} = \sum_{\rm f} f_{\rm v} = \mathcal{N} f_{\rm v}$$
 (6-20)

where  $\mathscr{N}$  is the number of atoms per unit area in plane A and  $f_{\mathfrak{g}}$  is given by equation 6-19. In this derivation, stress will be based upon the area of the crystal face before the load was applied (engineering stress). On this basis,

$$\mathcal{N} = \frac{1}{r_0^2} \tag{6-21}$$

because each atom occupies an area of  $r_0^2$ . Substituting equation 6-21 into 6-20,

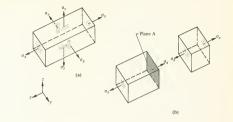
$$\sigma_x = \frac{f_x}{r_x^2}$$
(6-22)

Equation 6-22 can yield the relationship between stress and strain if  $f_x$  can be expressed in terms of either strain or elongation. The strain in the x direction is

$$\varepsilon_x' = \frac{r - r_0}{r_0} \quad \text{or} \quad r - r_0 = \varepsilon_x' r_0 \tag{6-23}$$

where  $v_x'$  denotes the strain in the x direction when the specimen is in hydrostatic tension. The force on an atom can be expressed as a function of  $r - r_0$  instead of r. This is shown graphically in Fig. 6-10(d). The curve of f vs. r has the same shape as the f vs. r curve of Fig. 2-11. The mathematical expression for f as a function of  $r - r_0$  can be found by expanding equation 6-19 in a Taylor's series about  $r_0$ :

<sup>\*</sup> Expansion of a function in a Taylor's series is discussed in appendix D.



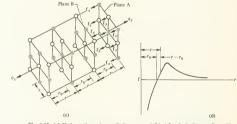


Fig. 6-10. (a) Hydrostatic tension applied to a crystal, (b) A free-body diagram formed by dividing the crystal at plane A. Stress in the y and z directions are omitted, (c) The crystal has the NaCl structure, and the (200) planes are shown. The applied stress has increased the distance between atoms from r<sub>t</sub> to r. All of the forces on plane A, in the x direction, are shown. (d) The force, f. exerted on an atom in plane A by all of the atoms to its left. The magnitude of the quantitude of the quantitude of the quantitude of the quantitude of the property of the property of the third property of the property of the

$$f_x(r) = f_x(r_0) + \left(\frac{df_x}{dr}\right)_{r=r_0} \frac{(r - r_0)}{1!} + \left(\frac{d^2f_x}{dr^2}\right)_{r=r_0} \frac{(r - r_0)^2}{2!} + \dots + \left(\frac{d^2f_x}{dr^2}\right)_{r=r_0} \frac{(r - r_0)^2}{n!} + \dots$$
(6-24)

where  $f_x(r_0)$  means the value of  $f_x$  evaluated at  $r_0$  and the subscript  $(r = r_0)$  means that the derivative is evaluated at r equals  $r_0$ . This series can be simplified by considering the following conditions:

1. The net force on an atom in any direction is zero when  $r = r_0$ ; therefore  $f_x(r_0) = 0$  and the first term is eliminated.

2. We intend to use equation 6-24 only within the elastic limit. As long as we use it only for small elongations, the expression  $r-r_0$  is a small number. Terms such as  $(r-r_0)^2$ ,  $(r-r_0)^3$ , etc., will be small compared to  $r-r_0$  and will be neglected. This is often called the small strain assumption. Using these conditions, equation 6-24 reduces to

$$\mathbf{f}_{\mathbf{x}}(r) = \left(\frac{d\mathbf{f}_{\mathbf{x}}}{dr}\right)_{r=r_0} (r - r_0) \tag{6-25}$$

The derivative can be evaluated from equation 6-19:

$$\left(\frac{dI_s}{dr}\right)_{r=r_0} = 0.29Z_cZ_Ae^2\left[-\frac{2}{r^3} + \frac{(n+1)r_0^{n-1}}{r^{n+2}}\right]_{r=r_0}$$
  
=  $0.29Z_cZ_Ae^2\left[-\frac{2}{r^3} + \frac{n+1}{r^3}\right]$  (6-26)

Substituting 6-26 into 6-25,

$$\mathbf{f}_{x}(r) = \left[0.29Z_{C}Z_{A}e^{2}\left(\frac{n-1}{r_{0}^{3}}\right)\right](\mathbf{r} - r_{0})$$
 (6-27)

The bracketed term in equation 6-27 is a constant; thus,  $f_x$  is a linear function of the elongation between planes,  $r - r_0$ . Substituting equation 6-22 into 6-27 to eliminate  $f_x$  and then using equation 6-23 to eliminate  $r - r_0$ .

$$\sigma_{x}r_{0}^{2} = \left[0.29Z_{\mathrm{C}}Z_{\mathrm{A}}e^{2}\left(\frac{n-1}{r_{0}^{3}}\right)\right]\varepsilon_{x}'r_{0}$$

which can be rearranged to give

$$\frac{\sigma_{x}}{\varepsilon_{x}'} = \frac{0.29Z_{c}Z_{A}e^{2}(n-1)}{r_{0}^{4}}$$
(6-28)

This equation almost defines Young's modulus; however, the restriction of hydrostatic tension must be removed. Recall that Young's modulus was defined as the ratio of stress to strain when the stress was applied in a single direction. Equation 628 can be modified with the aid of Fig. 6-11 (a). The application of hydrostatic tension causes elongation in all directions, as shown in Fig. 6-11(b). The shaded planes define the original shape of the solid. This figure illustrates the condition described by equation 6-28;  $e_\mu$ ,  $e_\nu$ , and  $e_z$  are the strains. Note that  $e_z$  is caused by elongation due to  $\sigma_\mu$  and contaction due to the stresses  $\sigma_y$  and  $\sigma_z$ . We now want to remove  $\sigma_y$  and  $\sigma_z$  so that only a single axial stress remains. Doing this causes the solid to contract in the y and z directions while elongating further in the x direction, as shown in Fig. 6-11(c),  $e_z$ ,  $e_z$  and  $e_z$  are the strains due to the single applied stress,  $\sigma_x$ . Note the similarity of Figs. 6-11(c) and 6-6.

An equation can be found which relates  $e'_x$  and  $e_x$ . The strain  $e'_x$  is due to all three applied stresses and can be expressed as

$$\varepsilon_{x}' = \frac{\sigma_{x}}{E} - \mu \frac{\sigma_{y}}{E} - \mu \frac{\sigma_{z}}{E}$$

where each term expresses the strain in the x direction due to one of the applied stresses. Because  $\sigma_x = \sigma_y = \sigma_z$  for hydrostatic stress,

$$\varepsilon'_{x} = \frac{\sigma_{x}}{F}(1 - 2\mu) = \varepsilon_{x}(1 - 2\mu)$$
 (6-29)

where  $\sigma_x/E = \varepsilon_x$  by definition. Substituting equation 6-29 into 6-28,

$$\frac{\sigma_x}{\varepsilon_x} = E = \left[ 0.29 Z_{\rm C} Z_{\rm A} e^2 \left( \frac{n-1}{r_0^4} \right) \right] (1-2\mu)$$
 (6.30)

The quantity on the right side of equation 6-30 is Young's modulus. It is seen that the modulus is strongly dependent on  $r_0$ , and  $r_0$  depends on the ionic radii of the elements forming the solid. Solids composed of multivalent elements will tend to be stiffer because of the dependence of E on  $Z_cZ_h$ . The effect of structure is reflected by the numerical constant. Different structures will yield different values.

#### Example 6-1

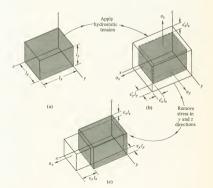
Calculate Young's modulus in the [100] direction for MgO.

The calculation requires the substitution of appropriate values into equation 6-30. The value of  $r_0$  can be found from the ionic radii given in Appendix A:

$$r_0 = \mathcal{R}_{Mg} + \mathcal{R}_{oxygen} = 0.78 + 1.32 = 2.10 \text{ Å}$$

The value of n is 7, as given by Table 2-5.

Fig. 6-11. Elongation of a material resulting from applied stresses. (a) The unstressed specimen. (b) Application of phydrostatic tension causes elongation in all directions. (c) Stresses in the y and z directions are removed. Elongation in increases in the x directions contraction occurs in the y and z directions. Shaded planes represent the unstressed specimen in all three figures.



Poisson's ratio has been found to be 0.30.\* Thus,

$$E = \left[ \frac{(0.29)(2)(2)(4.77 \times 10^{-10})^2(6)}{(2.1 \times 10^{-8})^4} \right] \left[ 1 - (2)(0.30) \right]$$
  
= 3.26 × 10<sup>12</sup> dynes/cm<sup>2</sup>

The experimental value of E in the [100] direction is  $2.6 \times 10^{12}$  dynes/cm², and the calculated value is somewhat higher. The discrepancy can be attributed to the fact that the bond in MgO is not completely ionic†; therefore the  $r_{\alpha}^{*}$  term in equation 6-30 is slightly in error for this case.

The shear moduli of a number of ionic crystals are plotted as a function of  $r_0$  in Fig. 6-12(a). Shear modulus and Young's modulus both depend on  $r_0$  in the same way because they are related through equation 6-9. Equation 6-30 can be written as

$$E = \frac{c'}{r_0^4}$$

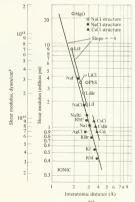
from which

$$G = \frac{c}{r_0^4} = cr_0^{-4} \tag{6-31}$$

\* E. R. Parker, Materials Data Book, McGraw-Hill, New York, 1967, p. 272.

† See J. J. Gilman in *Progress in Ceramic Science*, Vol. I, J. E. Burke, ed., Pergamon Press, New York, 1961.

Fig. 6-12. Shear modulus as a function of interatomic distance for the three types of bonds. The slope of the curve is the table of the exponent in equation 6-31. (Data from J. J. Gilman in Mechanical Behavior of Crystalline Solids, A. V. Austin, ed., NBS Monograph 59. Washinaton, D.C. 1963.



where c and c' depend on n,  $\mu$ , and crystal structure. c and c' are constants for a particular material. Taking the logarithm of equation 6-31.

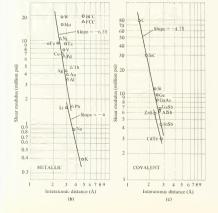
$$\log G = \log c - 4 \log r_0 \tag{6-32}$$

This equation tells us that a plot of  $\log G$  vs.  $\log r_0$  for ionic solids should be a straight line with a slope of -4, as is verified by the data plotted in Fig. 6-12(a). The intercept of the line depends on the value of c; therefore ionic crystals having different structures and different values of the exponent in the repulsive force term will fall on different lines, but all of the lines will have a slope of -4.

The numerical value of the slope depends on the type of bonding between atoms. Figure 6-12(b) and (c) shows plots of  $\log G$  vs.  $\log r_0$  for solids having metallic and covalent bonds. The straight-line relationship appears again, and shear modulus is inversely proportional to  $r_0$  raised to a power. The value of this power depends on the type of bonding and illustrates the dependence of elastic properties on bonding. A small interatomic distance corresponds to a stiff material, indicating the influence of structure on elastic behavior. The slopes of the lines in Fig. 6-12 can be related to the exponents in the bondine counties.

#### Questions

Question 4: In going from equation 6-24 to 6-25, a number of terms were dropped from the Taylor's series. The result (equation 6-25) requires that the curve of f vs. r in Fig. 6-10(d) be linear in a region in the neighborhood of  $r = r_0$ . Can this be justified because a stress–strain curve has a linear region? Explain.



Question 5: Are equations 6-24 and 6-25 limited to ionic solids, or can they be used for other types of bonds. Explain.

## 6\_5 Model of an elastic solid

The elastic behavior of materials was described as being the result of interatomic forces. The results of Section 6-4 can be used to formulate a model for a solid within the elastic limit, and this model is related to the bonding force and energy curves. To illustrate the relationships between elasticity and the force curve, consider equation 6-25 and Fig. 6-13:

$$f_x(r) = \left(\frac{df_x}{dr}\right)_{r=r_0} (r-r_0)$$
 for small strain (6-25)

Recall that this equation includes the small strain assumption. It is not limited to ionically bound solids. The quantity  $(dx_1/dr)_{r=0}$  is simply the slope of the force curve at the point where it crosses the abscissa. This quantity has a single numerical value for a particular material, and equation 6-25 shows that the force on an atom is linearly proportional to the displacement of the atom from its equilibrium position. The proportionality constant is the slope of the force curve at  $r=r_0$ . This is valid only in the elastic region. Equation 6-25 has the same form as the equation for the force exerted on a spring as the spring is elongated (see Fig. 6-14):

$$F = k(r - r_0) \tag{6-33}$$

The quantity k in equation 6-33 is the spring constant. Our analogy says

Fig. 6-13. The curve of  $\mathbf{f}$  vs. r. Elastic behavior requires that the slope of the curve is linear in a small region about r o. In this region,  $\mathbf{f}$  is proportional to  $r - r_0$ . The constant of proportionality is the slope of the curve in the linear region.

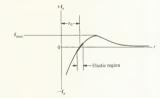
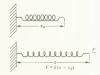


Fig. 6-14. A spring having a free length of  $x_0$ . The equation for the length when loaded is given. This equation has the same form as the linear part of the curve in Fig. 6-13.



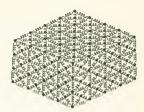


Fig. 6-15. Simplified model for the elastic behavior of a face-centered cubic solid. The atoms are joined by springs.

that  $(df_x/dr)_{r=r_0}$  is analogous to a spring constant in the region where the force curve is linear. This is the elastic region shown in Fig. 6-13.

The similarity of equations 6-25 and 6-33 can be used as the basis of a rather simple (though not rigorous) model of a solid. The atoms can be represented as hard spheres joined by linear springs. Figure 6-15 shows such a model for a solid having the face-centered cubic structure. It represents a rough approximation to the bonding situation within the elastic limit.

The spring-mass model also gives some information about the energy curve. The energy stored in a linear spring can be found as a function of spring displacement by integrating equation 6-33:

Energy stored = 
$$\int_{r_0}^{r} F dr = \int_{r_0}^{r} k(r - r_0) dr = \left(\frac{kr^2}{2} - kr_0r\right)_{r_0}^{r}$$
  
=  $\frac{k}{2}(r - r_0)^2$  (6-34)

Equation 6-34 shows that a plot of energy as a function of displacement is a parabola. Accordingly, the curve of bond energy vs. r should be parabolic in the small region about  $r_0$  in which the solid shows elastic behavior. At this point it is emphasized that the mathematical reason for f being a linear function of  $r - r_0$  lies in the procedure followed in going from equation 6-24 to 6-25. Terms containing  $r - r_0$  to powers higher than 1 were dropped. Experimental data show that this procedure is valid,

# 6-6 Thermal expansion

It is commonly observed that crystalline solids expand as their temperatures increase. Thermal expansion will be explained in terms of the potential energy (or bond energy) curve and the effect of thermal expansion on Young's modulus will be considered in this section. Figure 6-16 shows the same specimen at both room temperature and some higher temperature. The specimen has expanded due to heating. The change in length,  $\Delta l$ , which corresponds to a temperature change,  $\Delta T$ ; can readily be measured. Such a measurement enables us to find the linear coefficient of thermal expan-

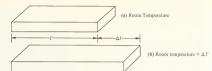


Fig. 6-16. (a) A solid at room temperature. (b) A change in the temperature of the solid,  $\Delta T$ , causes a change in length  $\Delta l$ .

sion, which is defined as the fraction change in length per degree of temperature change:

$$\alpha = \frac{\Delta l/l}{\Delta T} = \frac{1}{l} \frac{\Delta l}{\Delta T}$$
(6-35)

where

 $\alpha$  = thermal expansion coefficient (1/°C)

l = initial specimen length

 $\Delta l = \text{change in length}$ 

 $\Delta T$  = change in temperature

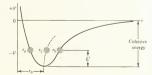
In differential form this becomes

$$\alpha = \frac{1}{l} \frac{dl}{dT}$$
(6-36)

and represents the slope of a plot of l vs. T.

The atoms in a solid oscillate about their equilibrium positions at all temperatures (including absolute zero). As heat is added to a solid, the increase in thermal energy appears as an increase in the energy associated with the oscillatory motion. The higher the temperature, the greater is the amplitude of the atomic oscillations. The potential energy curve is shown in Fig. 6-17. An atom which has an energy of oscillation  $\delta^c$  will oscillate between points  $r_a$  and  $r_b$ . Because the energy curve is not symmetrical  $r_0 - r_a < r_b - r_0$ . The mean position of the atom becomes  $r_c$ . Because  $r_c > r_0$ , the interatomic spacing is increased and the crystal expands. Thermal expansion can therefore be attributed to the asymmetry of the potential energy curve. As the temperature increases,  $\delta^c$  increases. The

Fig. 6-17. Oscillation of atoms in the potential well. The mean spacing between atoms increases as temperature increases.



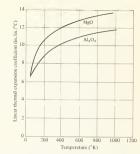


Fig. 6-18. The linear coefficient of thermal expansion as a function of temperature for magnesia and alumina. as increases at 7 increases. This would be expected because of the shape of the potential energy curve in Fig. 6-17. (W. D. Kingery, Introduction to Ceramics, Wiley, New York, 1960.)

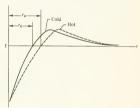


Fig. 6-19. Interatomic force curves for a material at two different temperatures. The slopes of the two curves at f = 0 differ.

mean interatomic spacing for various temperatures is shown by the dashed line. Because the dashed line is not straight, we would expect the thermal expansion coefficient to be temperature dependent. This dependence is illustrated in Fig. 6-18 for two ceramics. The thermal expansion coefficient increases with temperature. This is in accordance with the shape of the potential energy curve.

Young's modulus was found to be strongly dependent on  $r_0$ , and we would therefore expect thermal expansion to affect it. This is shown in the force curves of Fig. 6-19, which represents a material at two different temperatures. The curves are the same as r approaches zero or infinity; however, they cross the r axis at different points and the hotter material has a smaller slope at f=0. The effect does appear experimentally. Figure 6-20 shows the variation of Young's modulus with temperature for one ceramic material and four metals.

The effect of the crystallographic direction of the applied load is shown for MgO in the figure. It is seen that Young's modulus is significantly

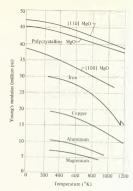


Fig. 6-20. Variation of Young's modulus with temperature for several materials. The effect of crystallographic direction is shown for MgO. [MgO data from D. H. Chung and W. S. Lawrence, J. Am. Ceram. Soc. 47:448 (1964). Metal data from W. Koster, Z. Metallk. 39:145 (1948)

higher in the [110] direction than it is in the [100] direction. Because the value depends on direction, it is anisotropic. Note the kink in the curve for iron. Iron changes from bec to the fec at 1163°K, which is where the kink appears. The kink in the curve at this temperature reflects the fact that Young's modulus depends on the crystallographic structure of the solid as well as the bonding.

Thermal expansion is a quantity that must often be considered in practical designs. For example, bridges are provided with expansion joints to compensate for thermal expansion and contraction.

## Example 6-2

A bridge 1 mile long has a steel superstructure. The temperature of the bridge will vary from -30 to 100°F during the year. How much thermal expansion must the expansion joints accommodate?

$$\alpha = 8 \times 10^{-6}$$
 in./in./°F for this temperature range  $\Delta I = I\alpha \Delta T = (5280) (12) (8 \times 10^{-6}) (130) = 65.8$  in.

#### Questions

Question 6: If expansion joints were not provided and the bridge was erected at a temperature of  $70^{\circ}F$ , what would the stress in the steel be at  $-30^{\circ}F$ ? Young's modulus is  $30 \times 10^6$  psi. Does the stress depend on the length of the bridge?

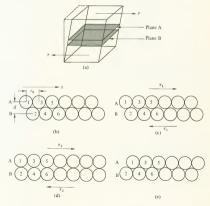
Question 7: What is the spacing between atoms (Fig. 6-17) if they have an energy equal to the cohesive energy? What process occurs when this happens?

## 6-7 Theoretical shear strength of a solid

The stress which a crystalline solid is theoretically capable of withstanding is of practical interest to us because this tells us the maximum strength that we can ever expect from a given material. An equation describing the maximum shear stress which a solid can theoretically withstand without fracturing will be derived in this section, and calculated strengths will be compared with experimentally observed strengths.

The model used for the derivation can be explained with the aid of Fig. 6-1. A solid subjected to a shear stress is shown in Fig. 6-21(a). Planes A and B are two adjacent atomic planes which are parallel and are separated by a distance d. They are shown in Fig. 6-21(b) with no applied shear stress. When a stress  $\tau_1$  is applied [Fig. 6-21(c)], the planes move with respect to each other. In this case, the upper plane has moved to the

Fig. 6-21. Slip between adjacent planes of atoms. (a) A solid subjected to a shear stress. Planes at and B are adjacent. (b) The configuration of planes A and B when the solid is no stressed. (c) Application of a shear stress, r., causes plane A to move with respect to plane B. (a) Increasing the shear stress increases the relative displacement of the two planes. Bris configuration corresponds to the maximum storage of elastic energy. (c) The two planes have been displaced by a distance re, with respect to each other. This configuration will be maintained if the load is removed. If the load remains, the planes will configuration will be maintained if



right (with respect to the lower plane). In going from the configuration shown in Fig. 6-21(b) to that in 6-21(c), the stress has moved through a distance and consequently work has been done. This work appears as elastic energy stored in the crystal. If the stress is released, the interatomic forces will return the planes to the configuration shown in Fig. 6-21(b). If the stress is increased, however, the planes continue to slip past each other until the configuration shown in Fig. 6-21(d) is reached. Here the interatomic forces on plane A, acting to the left, are exactly equal to those acting to the right. If the shear stress is removed, the crystal will remain in the configuration shown. A slight movement of plane A to the right. however, will cause a change in the force picture. Should this occur, the interatomic forces to the right, on plane A, will be greater than those to the left, and the plane will assume the stable (low-energy) configuration shown in Fig. 6-21(e). Had plane A moved slightly to the left, the crystal would have reverted to its original condition [Fig. 6-21(b)]. The maximum elastic energy is stored in the crystal when it has the configuration of Fig. 6-21(d). The situation is somewhat analogous to a ball rolling over a crest between two valleys, as shown in Fig. 6-22. The ball is shown in four different locations, corresponding to Fig. 6-21(b), (c), (d), and (e). It can roll from (d) to either (b) or (e) and reduce its potential energy.

From the description of the two planes sliding past each other, it is apparent that if the applied shear stress is slightly greater than that required to get the planes into the configuration of Fig. 6-21(d), the planes will continue to slide past each other and the material will fail. We want an expression for this stress. It can be found by considering the potential energy of plane A as a function of displacement from its position at zero shear stress. Displacement will be taken as positive to the right and will be denoted by x, as shown in Fig. 6-21(b). We know that potential energy is a periodic function of displacement because plane A has the same potential energy when it is in the configurations shown in Fig. 6-21(b) and (e). The

Fig. 6-22, Simple mechanical analog of the slip situation in Fig. 6-21. The potential energy of the ball depends on its position. Positions b, c, d, and e correspond to the configurations in Fig. 6-21. Potential energy is a maximum at d and a minimum at h and e.

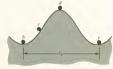
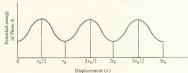


Fig. 6-23. The potential energy of a plane of atoms as a function of displacement. The curve has a wavelength of ro and reaches a maximum once per period, as required by the model in Fig. 6-21.



wavelength of our periodic function must therefore be  $r_0$ . The potential energy reaches a maximum at one point during each period, this being when the planes are directly above each other [Fig. 6-21(d)]. Note that we are discussing the potential energy of the entire plane of atoms in a large crystal. A potential energy vs. displacement curve which satisfies the above requirements is shown in Fig. 6-23. The exact form of the function is not known to us; however, it appears reasonable to approximate the curves how by a cosine curve. This is shown in Fig. 6-24. The quantity  $V_{ret}$  is a reference potential energy which serves as the axis for the cosine curve. C is the amplitude of the curve, and Fig. 6-24 is a graph of the equation

$$V = V_{\text{ref}} - C \cos \frac{2\pi x}{r_0} \tag{6-37}$$

The force equation can be found from

$$F = -\frac{dV}{dx} = -C\frac{2\pi}{r_0}\sin\frac{2\pi x}{r_0}$$
 (6-38)

where F is the force exerted on the atoms of plane A by the other atoms in the crystal. This equation is plotted in Fig. 6-25. A negative sign implies that the force on the plane of atoms is to the left, and the zero force at  $r_0/2$  corresponds to Fig. 6-21(d).

Fig. 6-24. One cycle of the potential energy vs. displacement curve of Fig. 6-23. The requirements of the model are satisfied by a cosine. The curve plotted is  $V = V_{\rm ref} - \cos(2\pi x/r_0)$ .

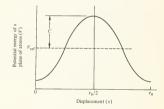
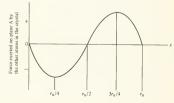


Fig. 6-25. The force exerted on a plane of atoms by the other atoms in the crystal as a function of displacement. The maximum occurs at 3r<sub>0</sub>/4. If the applied shear stress is greater than the maximum, the plane will slip past its neighbors. Slip will continue until the material fails.



These interatomic forces are exactly equal and opposite to the applied shear force. If the applied force is greater than the maximum interatomic force, the crystal planes will slip across each other and the material will fracture. Thus, the maximum applied shear force that the crystal can theoretically withstand corresponds to the force which occur at 3r<sub>0</sub>/4 in Fig. 6-25. We shall calculate this quantity in terms of shear stress rather than force. Dividing both sides of equation 6-38 by A (the area over which the shear stress is applied).

$$\frac{F}{A} = \tau = -\frac{2\pi C}{r_0 A} \sin \frac{2\pi x}{r_0}$$

Each term in the quantity  $-(2\pi C/r_0A)$  is a constant for a given material; therefore let the term equal K, which is an undetermined constant. Then

$$\tau = K \sin \frac{2\pi x}{r_0} \tag{6-39}$$

This equation holds for *all* values of x. We can evaluate K by applying equation 6-39 for very *small* values of x. Recall the well-known approximation

$$\sin \theta = \theta$$
 for small values of  $\theta$ 

Using this approximation in equation 6.39,

$$\tau = K \frac{2\pi x}{r_0} \quad \text{for small } x \tag{6-40}$$

The shear stress can also be expressed in terms of shear strain and shear modulus. By definition,

$$\tau = G\gamma$$
 and  $\gamma = \frac{x}{d}$ 

where d is the interplanar distance (see Fig. 6-21). Combining these two equations,

$$\tau = \frac{Gx}{d}$$
(6-41)

Substituting equation 6-41 into 6-40 and rearranging,

$$K = \frac{Gr_0}{2\pi d} \quad \text{for small } x \tag{6-42}$$

The condition which states "for small x" can be dropped because K is a constant and is not a function of x. We merely used the condition in order to evaluate K. Substitution of equation 6-42 into 6-39 yields the equation of the stress-displacement curve:

$$\tau = \frac{Gr_0}{2\pi d}\sin\frac{2\pi x}{r_0} \tag{6-43}$$

The quantity of interest is the maximum shear stress that the solid can withstand, which will be called  $\tau_{\rm max}$ . This occurs when  $r=3r_0/4$ . Using this value.

$$\tau_{\text{max}} = \frac{Gr_0}{2\pi d} \tag{6-44}$$

The value of  $r_0/d$  will depend on the crystallographic planes being considered. Because d is approximately the same size as  $r_0$ , we can let this ratio be 1 as an approximation. Then

$$\tau_{\text{max}} = \frac{G}{2\pi} = 0.16G$$
 (6-45)

Values of the theoretical shear strength of several materials, as calculated from equation 6-45, are compared with observed values in Table 6-1. The values listed in the table are typical values. The shear strength of two specimens of the same material will be different if the specimens have been subjected to different processes prior to testing. Table 6-1 shows that the calculated values are in gross disagreement with the observed values for polycrystals. The calculated values are from about 40 to 150 times larger. When compared to whiskers, however, the calculated and observed values correlate within a factor ranging from 3.75 (for Cu) to 1.39 (for Fe). Recall that two assumptions were made in deriving equation 6-45. The first was that the periodic curve representing energy (Fig. 6-23) was a cosine and the second was that  $d/r_0$  was equal to 1. The error introduced by these might explain the discrepancy between calculated strengths and observed whisker strengths, but it cannot explain the very large differences between calculated strengths and the observed polycrystalline data. An even larger discrepancy would appear for single crystals. Because our results are only as accurate as our model, it must be concluded that while the model postulated in Fig. 6-21 is reasonably valid for whiskers, it does not describe the behavior of polycrystals (or single crystals) beyond the

Table 6-1. Theoretical and observed shear strength

Material	Shear modulus (psi)	Observed ultimate shear strength (polycrystalline) (psi)	Calculated ultimate shear strength (psi)	Observed ultimate shear strength (whisker) (psi)*
Copper	$7.0 \times 10^{6}$	32,000	1,120,000	302,000
Iron	$11.6 \times 10^{6}$	42,000	1,805,000	1.380.000
Nickel	$11.0 \times 10^{6}$	69,000	1,750,000	395,000
$Al_2O_3$	$24.7 \times 10^{6}$		3,950,000	2,120,000
BeO	$19.7 \times 10^{6}$	40,000 (tension)	3,150,000	1,340,000
SiC	$29.3 \times 10^{6}$	25,000 (tension)	4,690,000	2,120,000

<sup>\*</sup> The shape of whiskers is not conducive to shear testing. The tabulated values were calculated from tensile strength data given by L. J. Broutman and R. H. Krock, Modern Composite Materials, Addison-Wesley, Reading, Mass., 1967.

elastic limit. Deformation does not occur by complete planes sliding past each other.

The main difference between whiskers and single crystals or polycrystals was the perfection of the crystal structure; therefore we would expect that a valid model must include the effects of surfaces and dislocations. Consideration of these imperfections leads to a rational explanation of brittle fracture and ductile behavior and will be discussed in Chapters 7 and 8

#### Ouestion

Question 8: The assumption that the energy curves in Figs. 6-23 and 6-24 are cosines seems to disturb some readers. It might seem reasonable to draw a straight line from an energy minimum to an energy maximum, joined to another straight line from the maximum to the next minimum, etc. This would give a sawtooth curve for Fig. 6-23. Show that a sawtooth energy curve is not permissible. (Hint: The force on a plane of atoms is F = -dV/dr, and force is a single-valued function of displacement).

## 6-8 Elastic materials in design

Many engineering devices are designed such that the materials from which they are fabricated are not stressed beyond the elastic limit. These devices (or machines) can be loaded and will return to their original shapes when the load is removed. This section will briefly present examples of designing with elastic materials. Many books have been written on the subject.

Which material is selected to perform a particular function depends on a number of criteria, and these will differ from one situation to another. Several examples of criteria for different cases might be cost, strength, durability, stiffness, size, weight, appearance, fabrication, and thermal expansion. As an example, consider automobile bodies. They are made from both steel and fiberglass. The designs are such that both can withstand the applied stresses and remain within their elastic limit. The cost of materials for steel bodies is lower than that for fiberglass bodies, but the tooling required for fabricating the steel is far greater than that for fabricating fiberglass. Steel bodies are cheaper if a large number of them are made because large quantities can justify expensive tooling. Small numbers of bodies can be produced more cheaply from fiberglass. In this case, materials selection is based upon cost, but the number of items produced determines which material is used.

The total "cost" of a part is not always limited to the cost of materials and fabrication, as shown in Example 6-3.

## Example 6-3

A cargo aircraft is being designed, and part of the design requires 100 bolts which are 3 in. long and can withstand a load of 1000 lb. The bolts can be loaded to 80% of the elastic limit. Two materials are being considered, an aluminum alloy and a steel. The aluminum alloy bolts cost \$5/lb, while the steel ones cost \$2/lb. The weight of cargo that the plane can carry will be reduced by an amount equal to the weight of the bolts. Cargo capacity is worth \$100/lb. Which bolts are cheaper? The "cost" of the bolts

#### 6-8: ELASTIC MATERIALS IN DESIGN

includes both the cost of buying them and the cost of the reduced cargo capacity of the airplane. The following data are given:

	Elastic limit (psi)	Density (lb/in.3)	Allowable stress (psi)
Al alloy	50,000	2.7	40,000
Steel	100,000	7.8	80,000

(a) Find the weight of each set of bolts:

$$\sigma = \frac{F}{A}$$
 or  $A = \frac{F}{\sigma}$  (6-46)

Weight = (number of bolts) (density) (volume per bolt)

$$= 100 \ \rho lA$$
 (6-47)

where l is the bolt length (3 in.). Substituting equation 6-46 into 6-47,

Weight of 100 3-in. bolts = 
$$\frac{300\rho F}{\sigma}$$
  
Weight (Al) =  $\frac{(300)(2.7)(1000)}{40,000}$  = 20 lb  
Weight (steel) =  $\frac{(300)(7.8)(1000)}{80,000}$  = 28 lb

(b) Determine the cost of each:

Cost of Al alloy bolts = purchase price + cost of reduced cargo capacity

$$=(20)(5) + (20)(100) = $2100$$
  
Cost of steel bolts  $=(28)(2) + (28)(100) = $2856$ 

Use the aluminum and save \$756. The aluminum comes out cheaper in this case because of its low density. For this particular problem, weight is at a premium. Note that the steel bolts will have half the cross-sectional area of the aluminum alloy bolts. If space is a critical factor, steel could be used.

Land surveyors use tapes (or chains) for measuring distances. The tapes have lengths of 100 ft or longer and must be the same length every time they are used. An alloy known as Invar (63%, Fe-36%, N) is used for them because the thermal expansion of this alloy is negligible between 0 and 100°C. In this case, the thermal expansion properties of the material are the primary concern. The material must also be durable enough to with-stand conditions met in the field. In other cases, the ability to withstand an environment is a primary consideration in materials selection. This would apply to structures in an ocean environment. The components of the structure would be made of corrosion-resistant materials, and their size would depend on their elastic properties.

This discussion could go on almost indefinitely by considering different cases. One feature would be common to almost all of them; the strength and elastic properties of materials play a major role when materials are selected for particular functions. Other parameters may enter the problem, but elastic properties are almost always considered.

Question

Question 9: Surveyors measure distances with Invar tapes. One man holds each end of the tape, and they pull against each other until the tape is taut. The length of the tape depends on the applied tension. What simple device could be used to make sure that the tensile load on the tape is the same every time it is used?

6-9 Summarv

The elastic behavior of materials was explained by means of a model. The model represented atoms as hard balls which were held together by bonding forces. An expression was derived for Young's modulus based solely upon structure and bonding. We were limited to the case of ionic bonding because this was the bond which we treated with some mathematical rigor. Flastic behavior was seen to be the result of an almost linear portion on the curve of f vs. r. The linear region occurred in the neighborhood of  $r = r_0$ . Thermal motion of the atoms in a crystal was considered, and the thermal expansion of solids was attributed to the fact that the curve of bond energy vs. r was not symmetrical about  $r = r_0$ .

The model provides a very good explanation of elastic behavior, but problems arise when it is applied to situations beyond the elastic limit. The ultimate shear strength of materials can be calculated from the elastic model. The calculations show reasonable agreement with the observed ultimate shear strength of whiskers but fail to correlate with observed properties of polycrystals and single crystals. The reason for the model failure lies in our neglect of the effect of crystal imperfections. Elastic behavior does not depend on imperfections and is classified as a microstructure-insensitive property. Mechanical behavior of materials beyond the elastic limit must include the effects of crystal imperfections, and our failure to do so in Section 6-7 caused a lack of correlation between calculated and observed quantities. Our model is valid within the elastic region but must be modified to include surfaces, vacancies, and dislocations if we are to explain permanent deformation and brittle fracture.

Surfaces are classified as imperfections because the ideal crystal was defined as having an infinite extent in space. Consideration of surfaces enables us to explain the brittle fracture of materials, and this is done in Chapter 7. Plastic behavior and permanent deformation are the result of dislocations and form the subject matter of Chapter 8. It will be seen that our model of hard-sphere atoms with bonds between them is still valid;

however, it must be modified to account for imperfections.

Problems

1 Polycrystalline aluminum oxide has a shear modulus of 21 × 106 psi. A shear load of 20,000 lb is placed on a specimen having dimensions of

- $2 \times 1 \times 3$  in. The load is perpendicular to the 3 in. dimension, as shown in Fig. 6-3. (a) Find the shear strain of the specimen. (b) Calculate the deformation,  $\Delta s$ . (c) Find the shear angle,  $\alpha$ .
- 2 A round bar of steel, which is 6 in. long and has a diameter of  $\frac{1}{2}$  in., is subjected to a tensile force of 10,000 lb. What are the dimensions of the bar after the stress is applied? Young's modulus is  $30 \times 10^6$  psi and Poisson's ratio is 0.3.
- 3 An axial stress of 15,000 psi is applied to a piece of nickel. The stress is in the [100] direction. Find the dimensions of the unit cell in the stressed specimen. Young's modulus is  $30 \times 10^6$  psi and Poisson's ratio is 0.32.
- 4 A cube of polycrystalline nickel has an edge length of 1 in. when unstressed. A tensile stress of 10,000 psi is applied normal to one pair of parallel faces, and a tensile stress of 15,000 psi is applied normal to the second pair of parallel faces. After the cube is loaded in this manner, what is the distance between the third pair of parallel faces? Values for Ni are given in Problem 3.
- 5 What value must Poisson's ratio have if the volume of a material remains constant when it is elastically deformed?
- 6 (a) Figure 6-9 shows (200) planes of the NaCl structure. The family of (222) planes in this structure is composed of alternate sheets of Na<sup>+</sup> ions and Cl<sup>-</sup> ions. Let a Na<sup>+</sup> ion be in the position of the cation C<sup>+</sup> in Fig. 6-9. Write three terms of the series which express the Coulomb force on this ion in the [111] direction. Let two of the terms be attractive and one be repulsive. (b) Would you expect this force to be greater in the [111] direction or in the [100] direction?
- 7 The elastic modulus of NaCl in the [100] direction has been experimentally determined as being 5.35 × 10<sup>11</sup> dynes/cm<sup>2</sup> in the [100] direction and Poisson's ratio is 0.16. Calculate E for NaCl and compare it to the measured value.
- 8 (a) Write an equation similar to equation 6-32 which is valid for the metals that are on the upper curve in Fig. 6-12(b). (b) The shear modulus of Ni is 11.5 × 10° psi, and the interatomic distance is 2.50Å. Evaluate the constant c for this curve.
- 9 (a) How much elastic energy is stored in a steel rod having a diameter of 1 in., a length of 10 in., and an applied load of 50,000 lb. (b) To what height must the bar be lifted in order to acquire a potential energy equal to the energy calculated in part (a) (density, 480 lb)ft<sup>2</sup>).
- 10 Calculate the ratio of the elastic energy stored in equal volumes of nickel and aluminum when they are loaded so that both have the same strain
- 11 Stress-strain curves for two iron whiskers having different orientations are shown in Fig. 7-4. (a) Find Young's modulus for the whisker stressed in the [100] direction. (b) Each atom in the whisker has a force curve similar to Fig. 6-13. Calculate the slope of this curve, at r = r<sub>0</sub>, for an atom of the whisker, using the value of E from part (a). (c) To what crystallographic direction does this curve apply?
- 12 A structural member in a spaceship will be subjected to a tensile load of 500 lb. The piece is 1 in. long and can deform a maximum of 0.0005 in. Three materials are being considered. These are steel, an

- 13 Copper has an average coefficient of thermal expansion of 17.3 × 10<sup>-6</sup> in./in./°C over a temperature range of 300-800°K and a bulk modulus of 17.9 × 10<sup>6</sup> bsi. A block of copper is placed in a bath of water at 300°K, and the temperature is increased to 800°K. How much hydrostatic pressure must the water exert on the copper at 800°K if the volume of copper is to remain constant?
- 14 A bar of stainless steel and a bar of magnesium, each having an area of 0.5 in.2, are both used to support a compressive load of 5000 lb. In the unloaded condition at room temperature the stainless steel bar is 3 in. long. (a) What should be the length of the unloaded magnesium bar if each bar is to support half the load?  $E = 30 \times 10^6$  for stainless steel. (b) The temperature is raised.  $\alpha = 10 \times 10^{-6}$  in./in./F for stainless steel and  $\alpha = 14 \times 10^{-6}$  in./in./F for Mg. As the temperature rises, which bar will support more than half the weight? (c) If the sar are made to the lengths calculated in part (a) and the load is evenly divided at room temperature (78°F), at what temperature will the magnesium bar carry all of the load? (d) If the temperature is increased above that calculated in part (b), will the load on the Mg bar be greater than 5000 lb? Explain.

Answers

Question 1:  $\tan \alpha = \Delta s/l = \gamma$ .

Question 2: Pressure =  $(64)(5000)/144 = 2220 \text{ psi.} \Delta V = -9.1 \times 10^{-5} \text{ in}^3$ . Therefore, V = 0.999909.

- Question 3: (a) Use of equation 6-10 limits the derivation to ionic bonding, (b), (c). These occur from Figs. 6-8 and 6-9. The NaCl structure was selected, and the force was derived for the [100] direction. (d) In going from equations 6-12 to the summation in equation 6-13, it was assumed that the distance between adjacent atoms was the same in the x, y, and z directions. This is true only for an unstressed or hydrostatically stressed crystal.
- Question 4: Yes. The stress on a solid is resisted by the interatomic forces. The stress is exactly the sum of these forces per unit area, in the stress direction. Thus, f is proportional to  $\sigma$ . From equations 6-23 and 6-29,  $\varepsilon$  is proportional to  $r-r_0$ . Because  $\sigma/\varepsilon$  is a constant in the elastic region,  $f/(r-r_0)$  must also be a constant in this region because of the proportions just given. The two constants are not the same.
- Question 5: They can be used for other types of bonds. Bonding force equations such as equation 2-22 can be expanded in a Taylor's series, and equation 6-24 results. The small strain assumption is valid if the material being considered is elastic; therefore equation 6-25 is valid for

- elastic materials. The exact form of the bonding equation enters when the derivative is evaluated, as in going from equation 6-26 to 6-27.
- Question 6:  $\sigma = E\varepsilon = E(\Delta l/l) = E\alpha \Delta T = (30 \times 10^6) (8 \times 10^{-6}) (100) = 24,000 \text{ psi. } \sigma \text{ is independent of length.}$
- Question 7: Interatomic separation is infinite. The material sublimates.
- Question 8: A sawtooth energy curve has two values for the first derivative at each maximum and minimum. If the force is a single-valued function of r, then the curve of  $\delta'$  vs. r must have continuous first derivatives. Note that the sawtoothed curve never has F = 0, and therefore does not predict an equilibrium confluention.
- Question 9: A small spring scale is usually attached to one end of the tape.

  The tape is stretched by the two men until the spring scale indicates that the required tensile load is applied.



## CHAPTER 7

# Surface Properties and Brittle Fracture

OUR MODEL OF A SOLID has so far consisted of an infinite array of hard spheres bonded together. It was successful in explaining elastic behavior but predicted ultimate strengths for materials that were much too high. In this chapter a very practical modification is made to the model. The solid is given surfaces so that it no longer occupies an infinite volume. The presence of surfaces enables us to explain why brittle fracture occurs.

The atoms at a surface do not have as many neighbors as those in the interior of a solid; consequently they form fewer bonds. As a result, surface atoms are in a higher energy state than interior atoms, and a plane of surface atoms has a higher energy than a plane of interior atoms. On a macroscopic scale, we can say that there is an excess of energy associated with a surface. The excess energy is called the surface energy. The first part of this chapter discusses the origin and magnitude of surface energy and the associated property of surface tension.

The surface energy concept provides the key to explaining the brittle fracture of materials. Brittle fracture occurs when a small crack in a material grows. Growth continues until fracture occurs. The condition for crack growth depends on the surface energy, among other things. The second part of the chapter discusses brittle fracture, and the equations which govern brittle behavior are derived.

Many observed phenomena other than brittle fracture depend on surface properties. These include capillary effects in liquids, corrosion, friction, catalytic chemical reactions, wetting of surfaces by liquids (important in brazing and soldering), and a number of other effects.

## 7\_1 Surface tension and specific surface energy

The quantities which we shall be dealing with are surface tension and surface energy. They can be described with the aid of a soap film stretched on a wire frame, as shown in Fig. 7-1(a). The stretched soap film attempts to contract but is restrained from doing so by the force F. Figure 7-1(b) shows a free-body diagram of the arrangement. The force F necessary to

Fig. 7-1. (a) A soap film stretched over a wire frame. One wire is free to slide. The force F keeps the soap film from contracting. (b) A free-body diagram of part of the soap film. The force F is equal and opposite to the surface forces.





prevent the soap film from contracting is found to be proportional to the dimension l. Let  $2\gamma$  be the proportionality constant. Then

$$F = 2l\gamma$$
 (7-1)

The quantity  $\gamma$  is related to the surface forces.  $2\gamma$  is the force per unit length exerted on the soap film in Fig. 7-1(b) by the remainder of the soap film. The remainder was removed in order to draw the free-body diagram. The soap film has two surfaces, and  $\gamma$  is interpreted as being the force per unit length exerted on one portion of a surface by the remainder of the surface. It is called surface tension and has units of force per unit length (dynes per centimeter or pounds per inch). From a physical point of view, we are saying that the force F is resisted by the interatomic forces between the surface atoms. The film has a finite thickness; however, none of the interior atoms are assumed to set up forces opposed to F. The internal atoms are part of a liquid (soap in this case), and liquids of low viscosity will not support a static tensile load.

The specific surface energy is the work required to form a unit area of surface. The surface area of the film in Fig. 7-1(a) can be increased by moving the force F to the left. Let the force move a small distance  $\Delta x$ . The work done by the force is  $F \Delta x$ , and the new surface area created is  $2l \Delta x$ . The specific surface energy is

$$\omega = \frac{\text{work}}{\text{area change}} = \frac{F \Delta x}{2l \Delta x} = \frac{2l\gamma \Delta x}{2l \Delta x} = \gamma$$
 (7-2)

where  $\omega$  is the specific surface energy and has units of ergs per square centimeter. Apparently  $\omega$  equals  $\gamma$  for our soap film, and for liquids in general. The value of  $\gamma$  depends on the two phases which the surface separates. The surface in Fig. 7-1 separates the soap from the air; consequently it is specified as  $\gamma_{\rm sup-sair}$ .

Question

Question 1: A film of water is placed over a wire frame like that shown in Fig. 7-1. The frame is 10 cm long (x dimension) and 3 cm wide (dimension). The x dimension increases when a force just greater than 438 dynes is applied to the frame. What is the specific surface energy of water? The surface tension?

# 7\_2 Origin of surface energy

From a microscopic point of view, the concept of surface energy occurs because surface atoms are not as tightly bonded as interior atoms. In this

Fig. 7-2. A solid specimen having a close-packed plane on the surface. A surface atom, such as atom A, has 9 nearest neighbors compared to 12 nearest neighbors for an interior atom.



section we shall estimate the surface energy of solid copper by using a rather rough model which considers only the number of nearest neighbors that a surface atom has and the total bonding energy. Consider Fig. 7-2, which shows a solid having close-packed planes on the surface. The surface plane would be either a ((III)) plane of an fice structure or the base plane of an hep structure. A surface atom (such as A in the figure) has nine nearest neighbors, as can readily be seen from the hep cell in Fig. 3-15. Atoms within the solid have 12 nearest neighbors. Because the surface atoms form fewer bonds, they have a higher potential energy than the interior atoms. This excess potential energy is simply the surface energy. If it is expressed as energy per unit area, it is the specific surface energy.

Let the specimen shown in Fig. 7-2 be copper with the ((111)) planes on the surface. The specific surface energy can be estimated if the following two assumptions are made,

- The potential energy of a surface atom depends only on nearestneighbor interactions. This assumption implies that only short-range forces need to be considered.
- 2. A surface atom bonds to each of its nearest neighbors with the same bond energy.

These two assumptions constitute a model.

The specific surface energy can be estimated with the aid of the experimentally determined heat of sublimation,  $H_s$ . Assume that atom A in Fig. 7-2 leaves the solid surface and enters the gaseous phase; it sublimates. The atom must break nine bonds when it leaves the surface, and it does not form any bonds in the gaseous state. The potential energy of atom A is increased by the sublimation process and so is the potential energy of each former nearest neighbor. Consider atom B. Before A sublimated, B had nine nearest neighbors. Sublimation of A leaves B with only eight nearest neighbors; therefore it forms only eight bonds, and its potential energy has increased.

The sublimation energy of copper is

$$H_s = 75,900 \text{ cal/g-mole} = 5.26 \times 10^{-12} \text{ ergs/atom}$$
 (7-3)

This is the energy required to break nine bonds. The excess energy associated with the surface is due to a surface atom forming 9 bonds, while an interior atom forms 12. Thus, the surface energy per atom can be found by estimating the energy which these 3 bonds would have if the atom had been in the interior of the solid. The energy per bond can be found by considering the energy increase of atom A when it sublimates. This is exactly the value of  $H_R$  given in equation 7-3 divided by 2. The division accounts for the fact that the total energy added to the solid in order to

sublimate the atom is shared equally by the atom and its nearest neighbors (recall that the nearest neighbors remain with fewer bonds and consequently are in a higher energy state).

The potential energy change of the sublimated atom due to breaking nine bonds is

$$\frac{5.26 \times 10^{-12}}{2} = 2.63 \times 10^{-12} \text{ ergs}$$
 (7-4)

The surface energy of the atom before it sublimated was attributed to three unfilled bonds, while equation 7-4 gives the energy of nine bonds: thus

Surface energy per atom = 
$$\frac{(2.63 \times 10^{-12})(3)}{9} = 8.74 \times 10^{-13} \text{ ergs}$$
 (7-5)

The quantity that we want is surface energy per square centimeter. consequently equation 7-5 must be multiplied by the number of atoms per square centimeter. This can be calculated from the data in Appendix A and comes out to be 1.77 × 1015 atoms/cm2 for the (111) plane:

$$\omega = (8.74) (10^{-13}) (1.77) (10^{15}) = 1550 \text{ ergs/cm}^2$$
 (7-6)

Table 7-1 gives the measured surface-tension values of a number of metals. We shall use surface tension and specific surface energy interchangeably. This is not strictly correct for solids, but from a practical point of view the difference between  $\gamma$  and  $\omega$  is probably smaller than the experimental error involved in measuring either one. The calculated and measured values of ω for copper agree very well. This is probably fortuitous and cannot be taken to mean that our model is rigorous. Similar calculations for the other metals in Table 7-1 correlate reasonably well with the measured values

Our model shows that surface energy depends on both bonding and structure. The bonding dependence appears through the use of sublimation energy in the calculations. This was necessary because we did not calculate metallic bonding energies from first principles. The effect of the number of nearest neighbors and the packing density of a surface plane show the

Table 7-1. Measured values of surface tension\*

Metal	Experimental condition	γ (dynes/cm)	
Gold	In an air environment at 1130°C (molten)	1100	
Gold	In a helium environment at 1030°C (solid)	1400	
Copper	In a helium environment at 1000°C (solid)	1680	
Iron	In a helium environment at 1495°C (solid)	1950	

<sup>\*</sup> Data are from A. H. Cottrell, The Mechanical Properties of Matter, Wiley, New York, 1964, p. 234,

influence of structure on surface energy. Generally, the more densely packed planes have lower specific surface energies. Although a densely packed plane has a large number of atoms per unit area, an atom in such a plane has more nearest neighbors (and consequently more bonds) than an atom in a plane with less dense packing. Solids attempt to form in their lowest energy (or free energy) state because this state is most stable; therefore solid surfaces will often be made up of planes having dense packing. The planes which appear on the surface are determined by the solidification process (Chapter 4) as well as energy considerations; therefore the entire solid surface will not be completely composed of most densely packed planes, although they are predominant. These comments are confirmed by the surface configurations of metals observed with the field ionization microscopes.

#### Question

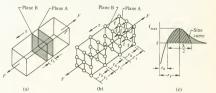
Question 2: (a) Using the above procedure, estimate the surface energy per atom on the (100) plane of copper. (b) Find the specific surface energy of this plane.

# 7-3 Calculation of surface energy from bonding equations

The surface energy, like many materials properties, depends on bonding and structure. In this section an equation will be derived for surface energy by considering these two basic quantities. The derivation should enable the reader to get a better understanding of the manner in which structure and bonding influence surface energy.

The model for the derivation can be described with Fig. 7-3. A block of material having an interplanar spacing  $r_0$  when unstressed is subjected to a tensile load F [Fig. 7-3(a)]. The load causes the distance between planes to increase. Figure 7-3(b) is a free-body diagram of part of the block of material. The spacing between planes is shown as  $r_1$ . The quantity f represents the force exerted in the x direction on one atom in plane  $\lambda$  by the other atoms in the figure. Figure 7-3(c) shows the curve of f  $y_8$ ,  $r_8$ .

Fig. 7-3. (a) A single crystal subjected to a tensile force. Planes A and B are adjacent planes. (b) A free-body diagram showing the forces on the atoms in plane A. The distance between planes is r. I file tensile load were removed, the interplaner spacing would be r<sub>0</sub>. (c) The force in the x direction exerted on an atom in plane A by all of the atoms in (b). The sine approximation for the (a), c rurne is shown.



It is seen that  $r_1$  corresponds to the maximum in the force curve: if the applied force is large enough to cause an interplanar spacing greater than r1, the material will fracture. Let the distance between planes A and B in Fig. 7-3(b) be increased slightly, perhaps by means of a very small crack. This will increase the interplanar spacing to a distance greater than  $r_1$ , and the crystal will fracture under the applied load. Work was done on the crystal when the force was applied. This was stored as elastic energy. The crystal fractured by breaking the bonds between planes A and B. Each element of volume in the solid contained stored elastic energy before fracture, and this could be recovered as potential or kinetic energy after fracture, in principle. The elastic energy stored in the volume between planes A and B cannot be recovered in this way because the distance between these planes does not return to  $r_0$  but instead becomes very large. The elastic energy stored in the volume between planes A and B appears as the surface energy of the two surfaces created by the fracture. The shaded area under the curve in Fig. 7-3(c) represents the energy required to separate one atom of plane A from all of the atoms to its left in Fig. 7-3(b). The energy required to separate planes A and B is then this quantity multiplied by the number of atoms in the plane. If  $cr_0^2$  equals the area of plane A occupied by one atom, then the energy required to separate a unit area of planes A and B is

$$\frac{1}{cr_0^2}$$
 × [area under the curve in Fig. 7-3(c)]

When the separation occurs, the surface area created is two units—one unit on plane A and one unit on plane B. Equating the surface energy of the newly created surfaces to the elastic energy stored in the volume between planes A and B,

$$2\omega = \frac{1}{cr_0^2} \times \text{[area under the curve in Fig. 7-3(c)]}$$
 (7-7)

The constant c accounts for the effect of crystal structure on the area occupied by an atom. For the simple cubic structure in Fig. 7-3(b), c equals 1.

The curve of f vs. r can be reasonably approximated by a sine curve. The area under the sine curve is cross-hatched in Fig. 7-3(e). Note that the selection of a sine curve satisfies the requirement that the slope of the curve be linear in a small region about  $r_0$  (for small angles,  $\sin\theta=\theta$ ). The sine curve in the figure is

$$\mathbf{f} = \mathbf{f}_{\text{max}} \sin \frac{2\pi (r - r_0)}{\lambda} \quad \text{and} \quad \lambda = 4(r_1 - r_0)$$
 (7-8)

where  $\lambda$  is the wavelength. Integrating equation 7-8 to find the cross-hatched area of Fig. 7-3(c),

Area under the curve = 
$$\int_0^{\lambda/2} \mathbf{f}_{\max} \sin \frac{2\pi (r-r_0)}{\lambda} \, d(r-r_0) = \mathbf{f}_{\max} \frac{\lambda}{\pi} \quad (7-9)$$

#### 7-3: CALCULATION OF SURFACE ENERGY FROM BONDING EQUATIONS

Substituting equation 7-9 into 7-7,

$$\omega = \frac{f_{\text{max}} \lambda}{2\pi c r_0^2} \tag{7-10}$$

Equation 7-10 is applicable to any solid whose curve of f vs. r can be reasonably represented by a sine curve. This is the only limitation placed upon it. The equation is usable as it is but can be put into a more convenient form. The quantity  $\mathbf{f}_{n\omega}/\sigma_0^2$  is the maximum force which can be placed on an atom before fracture occurs, divided by the area which the atom occupies; therefore

$$\frac{f_{\text{max}}}{cr_0^2} = \sigma_{\text{max}} \tag{7-11}$$

where  $\sigma_{max}$  is the maximum tensile stress which the crystal can withstand before fracturing. It is a constant which can be expressed in terms of E,  $r_0$ , and  $\lambda$ . To find this expression, we divide both sides of equation 7-8 by  $cr_0^2$ . The result is

$$\sigma = \sigma_{\text{max}} \sin 2\pi \frac{r - r_0}{\lambda} \tag{7-12}$$

This equation is valid for all values of  $r-r_0$ ; therefore it must be valid in the elastic range where  $r-r_0$  is small. In the elastic region, the argument of the sine is small, and we can again use the small-angle assumption (sin  $\theta=\theta$ ). Thus,

$$\sigma = \sigma_{\text{max}} 2\pi \frac{r - r_0}{\lambda} \quad \text{for small } r - r_0$$
 (7-13)

In the elastic range we can also write

$$\sigma = E\varepsilon = E \frac{r - r_0}{r_0} \quad \text{for small } r - r_0$$
 (7-14)

Substituting equation 7-14 into 7-13 and rearranging,

$$\sigma_{\text{max}} = \frac{E\lambda}{2\pi r_0} \tag{7-15}$$

The small strain condition has been dropped in equation 7-15 because  $\sigma_{\rm ave}$  is not a function of  $r-r_0$ . The manipulations involved in going from equation 7-12 to 7-15 actually involve no assumption. We have simply evaluated one constant,  $\sigma_{\rm mx}$ , in terms of others. The evaluation could have been done for  $\sigma_{\rm ave}$  point on the f vs. r curve. The elastic region was selected because we have more information about the curve here (Hooke's law can be used).

Substituting  $\sigma_{\rm max}$  in equation 7-15 for  $f_{\rm max}/cr_0^2$  in 7-10 and rearranging,

$$\omega = \left(\frac{\lambda}{2\pi}\right)^2 \frac{E}{r_0} \tag{7-16}$$

It is emphasized that the only mathematical assumption made in deriving equation 7-16 was that the curve of f vs. r can be approximated by a sine wave. If the postulated model was reasonable, we expect fairly good correlation between measured and calculated values of  $\omega$ . No particular bond type was assumed for the model, although a crystalline solid was used. To evaluate  $\lambda$ , however, we must know either the equation relating f and r or have experimental data which will allow us to evaluate  $\lambda$ . For ionic crystals with the NaCl structure, equation 6-19 is amplicable.

#### Example 7-1

Calculate the specific surface energy of the (100) plane of MgO. From equation 7-16,

$$\omega = \left(\frac{\lambda}{2\pi}\right)^2 \frac{E}{r_0} = \left[\frac{4(r_1 - r_0)}{2\pi}\right]^2 \frac{E}{r_0}$$

because  $\lambda=4(r_1-r_0).$  From Appendix A,  $r_0=0.78\,\rm{\AA}+1.32\,\rm{\AA}=2.10$   $\times\,10^{-8}$  cm.

To find  $r_1$ , the relationship between f and r for an ionic solid must be used. This is given in equation 6-19 for the (100) plane:

$$f = \frac{0.29Z_{C}Z_{A}e^{2}}{r^{2}} - \frac{0.29Z_{C}Z_{A}e^{2}r_{0}^{n-1}}{r^{n+1}}$$
(6-19)

Figure 7-3(c) shows that

$$\frac{d\mathbf{f}}{dr} = 0$$
 when  $r = r_1$ 

Differentiating equation 6-19 and letting  $r = r_1$ ,

$$\frac{d\mathbf{f}}{dr} = 0 = -\frac{0.58Z_{\rm C}Z_{\rm A}e^2}{r_1^3} + \frac{(n+1)0.29Z_{\rm C}Z_{\rm A}e^2r_0^{n-1}}{r_1^{n+2}}$$

Solving for  $r_1$  and rearranging,

$$r_1 = \left(\frac{n+1}{2}\right)^{1/n-1} r_0$$

The value of n can be found from Table 2-5 and is equal to 7:

$$r_1 = (4)^{1/6} (2.10 \times 10^{-8}) = 2.64 \times 10^{-8} \text{ cm}$$

The value of E in the (100) direction is  $36 \times 10^6$  psi from Fig. 6-20:

$$E = 2.47 \times 10^{12} \text{ dynes/cm}^2$$

Substituting values into equation 7-16,

$$\omega = \left[ \frac{4(2.64 \times 10^{-8} - 2.10 \times 10^{-8})}{2\pi} \right]^2 \frac{(2.47 \times 10^{12})}{(2.10 \times 10^{-8})} = 1380 \text{ ergs/cm}^2$$

Gilman\* used a very similar method to calculate the surface energy of

<sup>\*</sup> J. J. Gilman, J. Appl. Phys. 31: 2208 (1960).

Table 7-2.

Experimental and theoretical values of surface energy (eras|cm²)\*

Crystal	Plane	Experimental	Calculated	Crystal	Plane	Experimental	Calculated
NaCl	(100)	270	310	CaF <sub>2</sub>	(111)	450	540
		366		BaF <sub>2</sub>	(111)	280	350
		381		CaCO <sub>3</sub>	(1010)	230	380
		300		Si	(111)	1240	890
LiF	(100)	340	370	Zn	(0001)	105	185
		350		Fe (3% Si)	(100)	1360	1400
MgO	(100)	1200	1300			2500	
		1040					

<sup>\*</sup> J. J. Gilman, J. Appl. Phys. 31: 2208 (1960).

elements having ionic, covalent, and metallic bonds. The results which he obtained are compared to experimental results in Table 7-2. More than one experimental value is given for four of the substances. These represent the surface energy as measured by different investigators.

The small discrepancy between the calculated value of MgO in Table 7-2 and that found in Example 7-1 is due to a minor difference in the procedure used by Gilman and that used in the sample problem. The table shows that a good deal of work remains to be done in both the theoretical and experimental methods of determining surface energy.

#### Question

Question 3: The assumption that the curve in Fig. 7-3(c) can be approximated by a sine wave is sometimes disturbing. The curve of f vs. r extends to  $r = \infty$ , and it is sometimes felt that a large part of the area under the curve is left out when the sine approximation is used. Explain why the area under the curve must be finite and not infinite (consider bond energies). Note: the bonding curve has also been approximated by a combination of a sine curve and an exponential function. The exponential function approaches the r axis asymptotically, as does the bonding force curve. The difference between using this procedure and using the sine curve alone has been found to be small.

# 7-4 Theoretical tensile strength

There is a fringe benefit that can readily be obtained from the equations of Section 7-3; an expression can be derived for the theoretical tensile strength of a solid in terms of measurable quantities. Equations 7-10 and 7-11 can be combined to yield

$$\omega = \sigma_{\text{max}} \frac{\lambda}{2\pi} \tag{7-1}$$

and equation 7-15 can be rearranged to read

$$\frac{\lambda}{2\pi} = \frac{\sigma_{\text{max}} r_0}{E} \tag{7-18}$$

Substituting 7-18 into 7-17 to eliminate  $\lambda/2\pi$  and rearranging,

$$\sigma_{\text{max}} = \sqrt{\frac{\omega E}{r_0}}$$
(7-19)

Thus, the maximum tensile strength is rather simply related to Young's modulus and surface energy. Note that both of these quantities, as well as  $r_0$ , depend on bonding and structure.

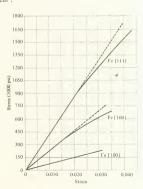
At this point it might be helpful to examine the stress-strain curves of whiskers, because whiskers approach our idealized solid more closely than other observed solid forms. The stress-strain curves for two iron whiskers and one copper whisker stressed in tension are shown in Fig. 7-4. The elastic anisotropy of Fe is well illustrated by these curves;  $\sigma_{max}$  and E both depend on the direction of the applied load. These stress-strain curves follow the general shape of the f vs. r curve in Fig. 7-3(c), as would be expected.

### Example 7-2

Calculate the maximum theoretical tensile stress that can be applied normal to the (111) plane of iron.

From Table 7-1,  $\omega = 1950 \text{ ergs/cm}^2$ . From Fig. 7-4,  $E = 42.8 \times 10^6 \text{ psi} = 2.95 \times 10^{12} \text{ dynes/cm}^2$ .

Fig. 7-4. Stress-strain curves of iron and copper whiskers stressed in tension. The crystallographic direction of the applied load is shown. [S. S. Brenner, J. Appl. Phys. 27:1484 (1956).]



The distance between atoms in the [111] direction of a bcc crystal is half of a cube diagonal. For iron, this is 2.484Å. Substituting values into equation 7-19.

$$\sigma_{max} = \left[ \frac{(1950) (2.95 \times 10^{12})}{2.484 \times 10^{-8}} \right]^{1/2} = 4.83 \times 10^{11} \text{ dynes/cm}^2$$
$$= 7.0 \times 10^6 \text{ psi}$$

Iron whiskers have been found to have about half this strength. Single crystals and polycrystals fail at a significantly lower stress level. The value of surface energy used in the calculation is for polycrystalline iron; therefore some error has been introduced.

Example 7-2 shows that  $\sigma_{max} = E/6.1$  for iron in the [111] direction. An approximation for the theoretical tensile strength of a material is provided by the equation

$$\sigma_{\rm max} \approx \frac{E}{10}$$
 (7-20)

Calculations for various materials have shown that equation 7-20 is reasonable. Materials other than whiskers do not show these strength characteristics. For example, single crystal and polycrystalline steel fracture at stresses of about  $\frac{1}{3}$ 0 $\sigma_{max}$ . The reasons for nonwhisker materials not exhibiting theoretical behavior will be discussed later in this chapter and in Chapter 8.

Question

Question 4: Figure 7-4 shows that an iron whisker has a stress of 600,000 psi (or 4.14 × 10<sup>10</sup> dynes/cm<sup>2</sup>) when the strain is 0.028. Find the value of f [Fig. 7-3(c)] when the strain is 0.028. Note that the strain is just  $(r - r_0)/r_0$ .

# 7-5 Measurement of surface energy of solids

The experimental data given in Table 7-1 were all obtained at high temperatures. The experimental method used to obtain these values of surface energy was described by Udin, Shaler, and Wulff,\* and the apparatus is shown schematically in Fig. 7-5. Their experiments with copper will be discussed; the procedure is similar for other metals. The apparatus consists of a vacuum chamber which is in an oven.

Several copper wires were placed in a vacuum chamber and a different weight was attached to each, as shown in Fig. 7-5. The temperature of the wires was then raised to a predetermined level by raising the oven temperature. The wires were maintained at high temperatures for periods of up to 6 days, after which the strains of the wires were measured. The stress was determined from the weights and the wire cross section. A plot of stress vs. strain for six specimens held at 1000°C for 72 hr is shown in Fig. 7-6. The curve indicates that the specimens can either elongate or

<sup>\*</sup> H. Udin, A. J. Shaler, and J. Wulff, Trans. AIME 185:186 (1959).

Fig. 7-5. Schematic diagram of the apparatus used for determining the surface energy of copper. A number of wires having the same diameter are stressed in a vacuum oven. Each wire has a different stress.

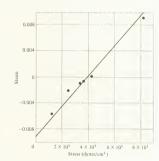


Fig. 7-6. Stress us, strain curve for copper wires having a diameter of 0.0072 cm. These data were obtained at 1000°C. Each point represents a wire with a different load. Surface energy is calculated from the stress at which strain is zero. [From H. Udin, A. J. Shaler, and J. Wulff, Trans, AIME 185:187 (1959).

contract during a test, depending on the applied stress. Contraction reduces the surface area of the specimen and therefore diminishes the surface energy. The stress at which no strain occurs is of particular significance. At this point, the downward force exerted by the weight is balanced by the surface tension:

Weight = 
$$\sigma A = \pi d\gamma$$
 (7-21)

where  $\sigma$  is the applied stress, A is the cross-sectional area of the wire, and d is the wire diameter. This equation holds for single crystal wires. In the case of polycrystalline specimens, a correction must be made to account for the presence of grain boundaries (which are also surfaces).

Equation 7-21 implies that all of the weight is supported by surface forces (see Fig. 7-7) and none by the interior interatomic forces, despite

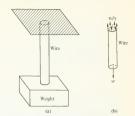


Fig. 7-7. (a) The testing arrangement for one of the wires shown in Fig. 7-5. The cross-hatched plane represents the top of the vacuum chamber. (b) Free-body diagram of the forces acting on the wire. When the surface forces equal the weight, creep does not occur.

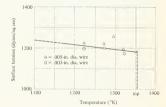


Fig. 7-8. The surface tension depends on temperature and increases as the temperature decreases. The data are for copper. [H. Udin, A. J. Shaler, and J. Wulff, Trans. AIME 185:189 (1959).]

the fact that the copper is below (but near) its melting temperature. At temperatures near the melting point, metals will creep; that is, they will continue to deform as long as a stress is applied. In effect, they behave like very viscous liquids, as will be explained in Chapter 9. This behavior justifies equation 7-21. The long testing times (up to 3 days for the copper tests) permit a significant amount of deformation to occur unless the weight which causes the tensile stress is equal to the surface tension. The method is valid only if creep occurs and is therefore limited to high temperatures.

This experiment can be performed at a number of different high temperatures, and a value of  $\gamma$  can be found for each. Figure 7-8 shows the temperature dependence of the surface tension for copper. No distinction is made here between surface tension and specific surface energy of a solid, although there actually is a small difference.

Surface energy can also be measured by cleaving a specimen of material along a crystal plane and measuring the energy required to fracture the specimen. A cleavage technique was used to obtain some of the data in Table 7-2. This method, too, has its difficulties. To obtain meaningful results, the test material must fracture without sustaining permanent deformation. This often requires that experiments be made at very low temperatures. To compound the difficulties, metals do not cleave well although ionic solids do, and surface energies of metals measured by cleary.

age methods are sometimes questionable. Neither of the methods discussed are easy, particularly for useful engineering materials. This helps to explain the small amount of surface energy data available for engineering solids.

Question

Question 5: If one of the wires in Fig. 7-5 has no weight placed upon it, and the weight of the wire is small, what shape will the metal take when it has been held at high temperature for a long period of time? Why?

# 7-6 Surface tension and wetting

The surface tension of liquids can be measured more readily than that of solids. Liquid surface tension is an important consideration when determining whether or not a liquid will wet a solid surface. Wetting is of great concern in a number of important processes such as soldering and brazing. In this section we shall consider methods of measuring liquid surface tension and shall consider wettability from a surface energy point of view.

One method of measuring liquid surface tension is somewhat analogous to that used for high-temperature metals. The liquid is placed in a thin-walled tube made from a material to which it adheres [Fig. 7-9(a)]. A drop forms at the bottom of the tube and continues to grow until it breaks away and falls. If the liquid strongly adheres to the tube surface, the break will occur below the bottom of the tube. Figure 7-9(b) shows a free-body diagram of a drop just before it falls. The weight is supported by the surface tension and

$$w = \pi d\gamma \tag{7-22}$$

where w is the weight of the drop and d is the tube diameter. Equation 7-22 assumes that the liquid within the drop cannot support a static tensile load, which is valid. The value of p measured is the value for the interface between the liquid and the environment, the liquid-air interface if the measurement is done in the atmosphere. A number of methods can be used to measure the surface tension of liquids in contact with surfaces, including the rise or

Fig. 7-9. Schematic diagram of surface tension measurement by the liquid drop method. (a) The liquid is contained in a tube and a drop forms at the end. (b) Free-body diagram of the drop just before it breaks away.



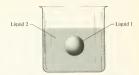


Fig. 7-10. Two immiscible liquids having the same density. Liquid 1 assumes a spherical shape and thus minimizes the surface energy.

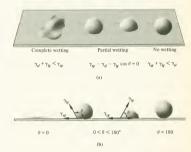


Fig. 7-11. Wetting of a surface by a liquid. (a) Schematic drawing of wetting, partial wetting, and no wetting, partial wetting, and no wetting. (b) Illustration of the surface-tension vectors and the contact angle 0. The angle depends on the surface tensions of the three interfaces.

fall of a liquid in a capillary tube. Techniques used for measuring the surface tension of molten metals are discussed extensively by Semenchenko.\*

The ability of a liquid to wet a surface of another substance depends on the surface energies of both. As a first example, consider a drop of liquid with no external forces acting upon it (such as gravity). Figure 7-10 shows such a drop immersed in a second liquid. The liquids in the figure are immissible and have the same density. Liquid 1 is observed to take a spherical shape. The ratio of surface to volume is smaller for a sphere than for any other geometric shape; therefore liquid 1 has minimized its surface area (and its surface energy). Solids do not show this behavior because the atoms are tightly bound; they do not have the mobility which liquid atoms possess.

The minimum energy principle can be applied to a liquid drop on a solid surface in the presence of a gas [Fig. 7-11(a)]. We are dealing with three surfaces here, the solid-liquid, solid-gas, and liquid-gas interfaces. The liquid drop will assume that shape which minimizes the energy of the system. In this case, the system consists of the solid, liquid, and gas. For each of these, the energy per unit volume does not depend on the surface

<sup>\*</sup> V. K. Semenchenko, Surface Phenomena in Metals and Alloys, Addison-Wesley, Reading, Mass., 1962.

$$\gamma_{sl} + \gamma_{lg} < \gamma_{sg} \tag{7-23}$$

where s, l, and g denote solid, liquid, and gas. Equation 7-23 neglects the surface energy of the liquid-gas interface before wetting occurred. This quantity is negligible because the surface area of the spherical drop is small compared to the other areas involved; consequently its surface energy is small. The condition for no wetting is

$$\gamma_{sg} + \gamma_{lg} < \gamma_{sl}$$
 (7-24)

For the case of partial wetting, consider the force diagrams of Fig. 7-11(b). The vectors  $\gamma_{2\mu}$ ,  $\gamma_{4\tau}$ , and  $\gamma_{4\mu}$  represent the surface forces exerted on a liquid molecule at the intersection of the three phases. Because the liquid is at rest, the summation of the horizontal forces shown must equal zero:

$$\gamma_{sg} - \gamma_{sl} - \gamma_{lg} \cos \theta = 0 \qquad (7-25)$$

Equation 7-25 can be used as the basis of an experimental arrangement to find one of the surface energy terms if the other two are known. This would be done by measuring the angle \(\theta\). In principle this looks straightforward. In practice it presents several difficulties, one of these having to do with surface clean liness. To have a liquid-solid interface, the solid surface must be clean when the liquid is placed upon it. Generally, solid surfaces tend to adsorb gases when exposed to them; that is, the surface atoms form bonds with the gas atoms. This process helps to satisfy the unfilled surface bonds and lowers the energy of the solid surface. When the liquid is placed upon the solid, the solid surface is usually not clean. Obtaining and maintaining clean surfaces is a major experimental problem. The effect of surface cleanliness on wetting is obvious to anyone who has attempted to solder dirty wires. The solder will not flow over the wires but will form soberical balls.

Surface energy is associated with the interfaces separating two solids or two liquids. For example, consider a tin can. The can consists of sheet steel having tin plated on the steel surface. A surface energy is associated with the steel-tin interface. The same principles can be applied to grain boundaries. A grain boundary separates two crystals which have the same chemical composition but different crystallographic orientations. Each crystal has a different surface energy because each one has different crystallographic planes forming the surface. When they come together, the resulting grain boundary has a surface energy.

## Ouestions

Question 6: Kerosene spreads over water but water does not spread over kerosene. Explain why in terms of surface energy.

Question 7: Consider two specimens of the same material. One is a single

crystal and the other a polycrystal. Both have the same temperature, pressure, and mass. Which has a lower energy? Why?

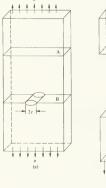
# 7\_7 The effect of cracks in a material

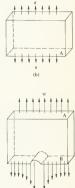
Brittle fracture was defined in Chapter I as fracture which occurred at or below the elastic limit of a material. It was also shown that a solid which fractured in a brittle manner absorbed only a small amount of energy before breaking. The mechanism which causes brittle fracture has been explained by Griffith, \*who postulated that brittle fracture was due to the presence of small cracks in the solid. According to his theory, at sufficiently high stresses these cracks would propagate through the material, resulting in failure. Calculations based upon his model agree well with experimental results, and the Griffith theory of brittle fracture is generally accepted as valid. In this section we shall consider changes in the stress on a material due to the presence of cracks. This information will then be combined with the surface energy concent to explain brittle fracture.

The stresses in a material are influenced by any discontinuities in the material, such as holes or cracks. Figure 7-12(a) shows a solid plate with an elliptic hole passing through it. Plane B passes through an axis of the ellipse, while plane A is parallel to B but is located some distance from it.

\* A. Griffith, Trans. Roy Soc. A221: 163 (1920-1921).

Fig. 7-12. Stress concentration in the region of an elliptic hole. (a) A plate with an elliptic hole is subjected to an utensile stress. (b) A free-body diagram of the upper part of the plate. The stress is the same across the entire cross section of the plate, (c) A free-body diagram with the lower surface passing through the hole. The stress is not transmitted across the hole. This causes stress concentration in the region of the hole.  $\sigma_i$  is the maximum stress.





The plate is subjected to a tensile stress  $\sigma$ . A free-body diagram of the upper portion of the plate is shown in Fig. 7-12(b), using plane A as the lower boundary. The stress is seen to be evenly distributed over the cross section of the plate. If the lower surface of the plate is taken as plane B and a free-body diagram is drawn, a problem arises [Fig. 7-12(c)]. Tensile stress cannot be transmitted across the crack. Because of the discontinuity, the stresses in the region adjacent to the crack edges are considerably higher than those at some distance from the crack. The stress is said to be concentrated in the region of the discontinuity. The ratio of the maximum stress to the applied stress is called the stress concentration factor. For an elliptic hole,

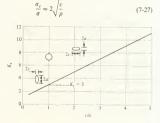
$$K_t = \frac{\sigma_c}{\sigma} = 1 + \frac{2c}{\sigma}$$
(7-26)

where  $K_i$  is the stress concentration factor for an elliptic hole,  $\sigma$  is the stress applied to the plate, and  $\sigma_i$  is the maximum stress that occurs at the tip of the ellipse [see Fig. 7-126]). The quantities 2c and  $2\sigma$  are the major and minor axes of the ellipse. Equation 7-26 assumes that the width of the plate is much larger than the major axis of the ellipse. The stress concentration factor is plotted as a function of  $c_0$  in Fig. 7-13, and the maximum stress is seen to be very sensitive to the shape of the ellipse. The value of the stress concentration factor depends on the shape of the discontinuity. The discussion here will be limited to ellipse.

Stress concentration factors can be very critical in design, and neglecting them can be disastrous. Several years ago a number of Comet jet airliners sustained structural failure in flight and crashed. An intensive investigation was made to determine the cause, and it was found that the failure began at a small rivet hole about an ain, in diameter.

We shall be concerned with cracks in materials, and these cracks can be approximated by long, thin ellipses (large c/a ratio). Figure 7-14 shows a crack formed by a line of atoms missing from a plane. The length of the crack is taken as 2c. The stress concentration factor for a long, thin ellipse can be approximated by an expression that will be more convenient for our use:

Fig. 7-13. Stress concentration factor resulting from an elliptic hole. The shapes of the ellipses for the various regions are shown. K<sub>t</sub> for the circle is 3.



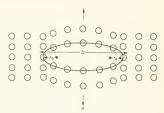


Fig. 7-14. One possible configuration for a Griffith crack. Several atoms from the middle plane are missing, creating a microcrack. The radius of curvature at the crack edge is of the order of research.

where c is half the crack length and p is the radius of curvature at the crack tip. Figure 7-14 shows that the radius of curvature at the crack tip can be approximated by  $r_0$ . Stress concentrations can be quite high for this configuration. For example, if the crack was 100A long and  $r_0$  was 4A, the maximum stress would be 10 times the applied stress. The presence of the crack also affects the manner in which elastic energy is stored in the stressed solid. The material immediately above and below the crack cannot be stressed because tensile forces cannot be transmitted across the crack. Thus this region has no stored elastic energy.

## Questions

Question 8: A large, flat plate, has a small elliptic crack having a c/a ratio of 4. A stress is applied perpendicular to the c axis. The ellipse can be changed to a circle of diameter c by simply running a round drill through the plate. This procedure decreases the maximum stress in the region of the discontinuity. Find the percent decrease in the maximum stress due to drilling the hole.

Question 9: What would happen if the stress at the tip of a crack exceeded the ultimate strength of the material?

# 7-8 Griffith theory of brittle fracture

The equation which governs brittle fracture can be derived from energy considerations, as Griffith originally did, or from force considerations according to Orowan's method. We shall do the latter, but the model used for the energy derivation will be discussed briefly.

Griffith's model for brittle fracture can be described by considering a brittle solid which contains a small crack. The crack could come from a number of sources such as a collection of dislocations, a flaw which occurred during solidification, or a surface scratch. When a solid is stressed in tension, elastic energy is stored when the solid elongates. As the stress on the solid is increased, the elastic energy stored per unit volume increases. At a sufficiently high stress the crack becomes larger and the material fractures. Lengthening the crack causes an increase in the surface area of the crack, and therefore the surface energy of the specimen is increased. There is also a comeensating release of energy. As the crack

becomes longer, the material on both sides of the crack can no longer store elastic energy because tensile stresses cannot be transmitted across the crack. Thus, an increase in the crack length causes the release of elastic energy. Griffith postulated that when the elastic energy released by extending a crack was equal to the surface energy required for crack extension, the crack would grow. This is in accord with our minimum energy criterion because the crack will propagate only when such propagation reduces the total energy of the solid. The derivation of Griffith's theory, based upon this model, has been done very lucidly.\*

Orowan approached brittle fracture from a stress point of view.† He considered a specimen with a crack and postulated that the crack would propagate when the stress at the crack tip was equal to the theoretical tensile strength of the material. The stress at the crack tip is the quantity σ, in equation 7-27 and is shown in Fig. 7-12(c). The theoretical tensile strength is given by equation 7-19:

$$\sigma_{\text{max}} = \sqrt{\frac{\omega E}{r_0}}$$
 (7-19)

$$\frac{\sigma_c}{\sigma} = 2\sqrt{\frac{c}{\rho}}$$
(7-27)

Letting  $\sigma_c = \sigma_{max}$  in accord with Orowan's postulate, substituting this into equation 7-19, combining eqs. 7-19 and 7-27 to eliminate  $\sigma_{max}$ , and rearranging,

$$\sigma = \sqrt{\frac{\omega E \rho}{4cr_0}}$$
(7-28)

The quantity  $\sigma$  in equation 7-28 is the stress applied to the specimen (Fig. 7-12) when  $\sigma_{max} = \sigma_c$ . It is therefore the applied stress at which brittle fracture occurs (or at which the crack propagates) and will be referred to as  $\sigma_{BF}$ . Recall that  $\rho$  is the radius of curvature at the edge of an elliptic crack. From equation 7-28, it is apparent that a small value of  $\rho$  will result in a low fracture stress. The smallest value of  $\rho$  is roughly equal to  $r_0$ , as shown in Fig. 7-14. Letting  $\rho$  equal  $r_0$  in equation 7-28,

$$\sigma_{\rm BF} = \sqrt{\frac{\omega E}{4c}} \tag{7-29}$$

This is the Orowan derivation of Griffith's criterion for brittle fracture. Rearranging.

$$\sigma_{\rm BF}\sqrt{c} = \sqrt{\frac{\omega E}{4}} = {\rm constant}$$
 (7-30)

<sup>\*</sup> A. H. Cottrell, The Mechanical Properties of Matter, Wiley, New York, 1964, p. 344.

<sup>†</sup> E. Orowan, Z. Krist. 89: 327 (1934).

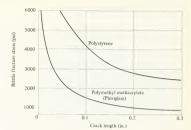


Fig. 7-15. A plot of brittle fracture stress vs. crack length for two polymers. Both curves follow equation 7-30 and fracture according to Griffith's model. [J. P. Berry, J. Polymer Sci. 50:313 (1961).]

Equation 7-30 simply states that the stress level at which brittle fracture occurs in a material diminishes as the crack length increases. The equation has been found to be valid for a variety of materials, both crystalline and amorphous. Griffith's original work was done with glass specimens and these obeyed the equation. A plot of  $\sigma_{\rm BP}$  vs. c for two polymers is shown in Fig. 7-15. Both of these follow equation 7-30. The values of the constant are different for the two curves because the materials have different values for E and  $\omega$ . Brittle fracture caused by crack propagation has been observed at both the macroscopic and atomic levels. At the atomic level, it has been studied with the field emission microscope, which is a device similar to the field ion microscope.\* The theory is valid for both crystalline and amorphous materials.

## Question

Question 10: A specimen of material is stressed and a crack begins to propagate. The stress is maintained at the level which initially caused the crack to grow. Will the crack continue to propagate or will it stop when it reaches some given length which is smaller than the size of the specimen? Recall that  $\sigma_{\rm BF}$  in equation 7-29 is the stress required to initiate crack growth. Does the model used for brittle fracture apply if the load is compressive?

# **7-9** Designing with brittle materials

The derivation in Section 7-8 points out some dangers involved in using brittle materials. The condition for crack propagation was taken to be that the maximum tensile stress in the region of a stress concentration was equal to the theoretical maximum stress of the material. When this condition is met, a crack will propagate until the conditions are changed or the material fractures. Increasing the crack length does not alleviate the condition; it aggravates it. Therefore, once a crack begins to propagate through a brittle material, it will usually continue all the way to fracture. The cracks propagate quickly, and brittle fracture can be catastrophic.

<sup>\*</sup> D. L. Creighton and S. A. Hoenig, Trans. AIME 233:1368 (1965).

No warning is given of impending failure. This is contrary to the behavior of ductile materials.

Equation 7-29 states that the stress at which brittle fracture occurs depends on the length of the longest crack in the material. A piece of material will have some statistical distribution of microcracks within it. The probability that it contains a large crack increases as the size of the material specimen increases. For example, suppose that the probability of finding a crack longer than 1000 Å in a 1-cm3 specimen of some material has been found to be 1 or 20%. The probability of finding such a crack in a 2-cm3 sample would be significantly higher than 20%. This argument indicates that large pieces of brittle material generally fracture at a lower stress (not a lower load) than small pieces of the same material. Consequently, it is risky to test scaled-down models of devices made from brittle materials and extrapolate the results to the full-sized device. This procedure can be catastrophic. The size effect is illustrated in Fig. 7-16. A number of specimens of gray cast iron (a brittle material) were loaded in tension until they fractured. All of the specimens in a given test had the same chemical composition, and only the diameter was varied. After testing the samples, fracture stress was plotted against specimen diameter. Each curve in Fig. 7-16 shows the results of a single set of tests. The procedure was repeated for gray cast irons of different compositions, and each curve in the figure represents the results for a particular chemical composition. The curves show that large specimens fracture at a lower stress than smaller ones, in accord with the above discussion.

One of the fundamental shortcomings of brittle materials is their inability to absorb much energy before fracturing; they are not tough, Toughness was discussed in Section 1-5, and Fig. 1-9 shows the difference in energy absorption between a ductile and a brittle material. Brittle materials do not absorb impact loads very well because crack propagation occurs when the elongation of the material is small and little work has

Fig. 7-16. Size effect in gray cast iron. The tensile strength depends on the cross section of the test specimen. All specimens were the same length; only the diameter was varied. Each of the curves represents a different composition. (J. L. Everhart et al., NBS Circular C447, U.S. Government Printing Office, Washington, D.C., 1943, p. 247.)

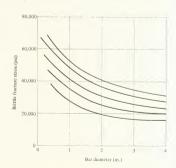




Fig. 7-17. Fracture of a ship caused by a crack propagating around the hull. (Courtesy of E. R. Parker.)

been done by the loading forces. The lack of toughness requires that care be exercised when designing with brittle materials because large impact loads cannot be tolerated.

There is a group of brittle materials which can absorb a large amount of energy during fracture, but not before fracture, and they have some application. These materials shatter when they fail, rather than simply cracking. The shattering results in a large number of small particles; consequently a large surface area is created by the shattering process. Most of the energy absorbed by these materials appears as surface energy. Lightweight ceramics which utilize this principle are used for bulletproof vests. Much of the kinetic energy of an incoming bullet is spent in creating new surfaces in the ceramic. Another violent (but more peaceful) application is automobile safety glass. The glass is observed to shatter during a collision. In most engineering applications, we are not concerned about whether a material cracks or shatters. We are concerned with whether it undergoes brittle fracture or not

It is essential that the engineer be aware of whether a material is ducile or brittle before using it in a design. A result of estimating this the wrong way is shown in Fig. 7-17. A crack has propagated completely around the hull of the ship, leaving it in two pieces. This happened to a number of cargo vessels during World War II and occasionally still occurs with the iron ore ships that operate on the Great Lakes. The problem has been studied in detail, and the results show that the failure is brittle. It was found that the cracks originated at the corners of hatches on the deck of the ship. These are regions of stress concentration. The failures also occurred in cold waters. The embritting effect of temperature will be discussed in Chapter 9, and it will be seen that a material which is ductile at one temperature can show brittle behavior at lower temperatures. The combination of a crack and a brittle material presents a possible failure, particularly if impact loads are applied. Such loads are applied to the hull of a ship in rough waters.

The problems associated with brittle materials do not prohibit their use; cast iron, cement, concrete, and building bricks are examples of commonly

blocks, but the brittle nature of the material must be accounted for in the

design.

The Griffith model assumes that elastic energy cannot be stored in the region of a crack and that loads cannot be transmitted across a crack. This is true of tensile loads but not of compressive ones, and brittle materials show much higher strength in compression than in tension. Normal Portland cement can be stressed to about 3500 psi in compression but fails at about 350 psi in tension. Concrete and brick are used in such a way that the loads which they support are predominantly compressive. If tensile loads are expected, the materials can be reinforced to enhance their tensile capability. In the case of concrete, this is usually done by embedding steel rods in the concrete, as can be observed in construction projects. The reinforcing rods lend tensile strength to the concrete-steel combination but do not greatly affect the compressive properties.

The compressive strength of brittle materials may be utilized in the deep ocean. The outer shell of a deep-diving vehicle (or instrument container) can be designed so that all of the stresses placed upon it are compressive when it is subjected to the hydrostatic pressure of the deep ocean. Some glasses are being considered for this two of service.

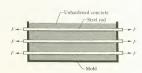
Question

Question 11: One method of improving the tensile capabilities of brittle materials is to prestress them. Suppose that several steel rods were placed in tension (below the elastic limit) and concrete was then poured around them, as shown in Fig. 7-18. The stress was maintained on the rods while the concrete hardened, and the hardened concrete adhered to the steel. The stress was then removed from the steel rods. The resulting product has better tensile properties than it would have if the entire procedure were carried out without stressing the rods. Why?

# 7-10 Summary

The atoms at the surface of a material make fewer bonds than those located within the material; consequently there is an excess energy

Fig. 7-18. Schematic diagram for fabricating a prestressed concrete structural member. The mold and the forces are removed when the concrete has hardened.



associated with each surface atom. This is the surface energy. It was shown that surface energy depended on bonding and structure and could be calculated if these were known. Because we have only treated the ionic bond with rigor, our calculations were limited to that case. The surface energy model did permit us to estimate the surface energy of a nonionic solid by using an experimentally determined quantity related to bonding, that being the heat of sublimation. We were also able to derive an expression for the theoretical tensile strength of a material in terms of surface energy.

The interplay of surface energy and elastic energy can be used to explain the phenomenon of brittle fracture. It can also be explained in terms of stress concentrations at cracks and the theoretical tensile strength, which was the method used in this chapter. Whichever method is used, the quantities which appear in the final equation are dependent on structure and bonding. In this case, the presence of cracks means that we must consider deviations from the ideal structures of Chapter 3.

Brittle materials cover the entire spectrum from the common to the exotic. Normal building materials such as concrete and brick are brittle, as are many of the high-strength whisker materials such as silicon carbide and aluminum oxide. Brittle materials are used in many engineering applications, but care must be exercised when designing with them. The designer must be aware of the size effect, stress concentrations, and toughness of the materials used. In addition, he must recognize the possibility of the behavior changing from ductile to brittle as temperature decreases. Two methods of improving the tensile properties of brittle materials were also discussed. These were reinforcing and prestressing.

## Problems

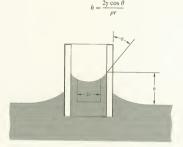
- 1 Two spherical drops of water, having diameters of 0.5 and 0.2 cm, are in contact with each other. They are observed to unite and form a single spherical drop. This occurs in an air environment. The surface tension of the water-air interface is 73 dynes/cm. (a) Find the change in the surface energy of the water due to the two drops joining together. (b) If the joining process takes place at constant temperature, is the energy of the water increased or decreased as a result of the process? (c) Consider 1 lb of a solid material. Is it more stable (lower energy) when it exists as a single solid cube or as a powder? Explain why, considering the results of (a) and (b).
- 2 (a) Estimate the surface energy of an atom of iron if the surface plane is (110). Let the iron be at room temperature, where it has the bcc structure. The energy required to sublimate room-temperature iron is 97 kcal/g-mole. (b) Find the specific surface energy.
- 3 Calculate the surface energy of the (100) plane of NaCl and compare it to the values in Table 7-2.  $E=5.2\times10^{11}~\rm dynes/cm^2$  in the [100] direction.
- 4 Figure 7-4 shows that the iron whisker tested has a maximum strain of about 3.5% when loaded in the [100] direction. If the surface energy of iron is taken as 1900 ergs/cm<sup>2</sup>, what is the maximum elongation that

the whisker could show when loaded in the [100] direction, assuming that no permanent deformation occurs. Figure 7-3(c) should be useful. 5 Calculate the theoretical tensile strength of MgO when it is loaded in the [100] direction.  $E=2.6\times10^{12}$  dynes/cm², and  $\omega$  is given in Table

The temperature dependence of the surface energy of energy is above.

6 The temperature dependence of the surface energy of copper is shown in Fig. 7-8. Give a qualitative explanation of why surface energy decreases with increasing temperature. Note that the energy of all the atoms in a crystal increase as temperature increases.

7 A liquid rising in a capillary tube is shown in the accompanying figure.
(a) Show that the height h to which the liquid will rise is given by



where y is the surface tension of the liquid-air interface and p is the liquid density (mass per unit volume). To derive the equation, consider a free-body diagram of the liquid column. (b) Which term in the equation accounts for the wetting (or nonwetting) of the tube surface by the liquid? Explain your answer.

- 8 A mercury-water interface has a surface tension of 375 dynes/cm, and the mercury-air interface has a value of 380 dynes/cm, while the waterair interface has y equal to 73 dynes/cm. Find the contact angle of a drop of water on a mercury surface.
- 9 The following surface tension values have been measured:

 $\gamma_{\text{water-air}} = 73.05 \text{ dynes/cm}$   $\gamma_{\text{water-benzene}} = 35.0 \text{ dynes/cm}$ 

 $\gamma_{\text{water-benzene}} = 35.0 \text{ dynes/cm}$  $\gamma_{\text{benzene-air}} = 28.85 \text{ dynes/cm}$ 

A drop of benzene is placed on a water-air surface. (a) What type of wetting occurs? (b) If complete wetting occurs, how much energy is released when the benzene spreads over I meter? of water? Assume that the surface area of the benzene drops (before wetting) is negligible.

- 10 The heat of fusion of copper is given as 50 cal/g (or 1.88 × 1010 ergs/cm3) and the surface energy of the solid-liquid interface can be taken as 177 ergs/cm2. Consider what happens when some liquid copper freezes into a spherical solid. Energy is given off because a solid atom has a lower bond energy than a liquid atom, but energy is regulred to form the surface between the liquid and solid. (a) Plot the energy released, due to freezing, as a function of the particle radius. Let this be a negative quantity and call it volume energy. Plot the energy required to form the surface as a function of r. This quantity will be positive. Call it surface energy. On the same graph, plot the sum of the two curves. Use the following values of r for the curves:  $2 \times 10^{-8}$  cm. 4, 5, 6, 8 × 10<sup>-8</sup> cm, and 10<sup>-7</sup> cm. (b) The curve which represents the sum of the volume and surface energies should have a minimum. Find the value of r at the minimum, (c) This value corresponds to a critical radius, as discussed in Section 4-2. Particles having radii larger than the value found in part (b) are nuclei, while smaller particles are embryos. Explain why. (Note: The calculations would have to be done in terms of free energy rather than energy for a rigorous derivation of the critical radius size. The principle is the same.)
- 11 Materials generally become more brittle as their temperature decreases. Can this be attributed to the temperature dependence of the surface energy? Explain your answer.
- 12 Calculate the brittle fracture strength of MgO if it contains cracks that are 1  $\mu$  long.
- 13 If a crack is observed in a brittle specimen before it has propagated, it is possible to inhibit propagation by drilling small holes at the tip and tail of the crack. Consider a piece of brittle cast iron having a surface energy of 2000 ergs/cm². (a) If a specimen of this material has a crack which is  $2 \mu \log_2$  find the stress at which brittle fracture occurs. (b) The entire crack can be eliminated by drilling a hole through the material; therefore a round hole having a diameter of  $\frac{1}{3}$ 2 in. is drilled in the specimen. The stress concentration factor for this hole is 3. Calculate the stress at which brittle fracture occurs.
- 14 Adsorption of gases by surfaces lowers the surface energy. The surface energy of aluminum oxide is 1900 ergs/cm² at room temperature. Hardie and Petch found that the surface energy was reduced by 480 ergs/cm² when an Al<sub>2</sub>O<sub>3</sub> specimen was exposed to air saturated with water vapor. The change was attributed to the adsorption of water by the Al<sub>2</sub>O<sub>3</sub> surface. (a) Find the percent change in the brittle fracture stress of Al<sub>2</sub>O<sub>3</sub> due to the adsorption of water, (b) Does the shape of the crack influence the answer to part (a). (c) If brittle fracture occurred in an Al<sub>2</sub>O<sub>3</sub> specimen by the propagation of an internal crack rather than a surface crack, would the presence of water in the ambient environment influence the brittle fracture stress?

Question 1: 
$$F = 2l\gamma = 2l\omega$$

$$\omega = F/2l = 438/6 = 73 \text{ ergs/cm}^2$$
  
 $\gamma = 73 \text{ dynes/cm}$ 

Question 2: (a) A surface atom on the (100) plane of Cu has 8 nearest neighbors, while an interior atom has 12:

Surface energy per atom = 
$$\frac{(2.63 \times 10^{-12})(4)}{8} = 1.31 \times 10^{-12} \text{ ergs}$$

(b) Number of atoms per cm² on (100) in Cu = 
$$\frac{2}{3.61\times 10^{-8}}$$
 =  $1.55\times 10^{15}$ 

$$\omega = (1.31 \times 10^{-12}) (1.55 \times 10^{15}) = 2030 \text{ ergs/cm}^2$$

- Question 3: The area under the curve represents the bonding energy of an atom in a crystal. When an atom joins a crystal, the amount of energy given off is finite, not infinite; therefore the area under the curve must be finite. This occurs when f approaches zero faster than r approaches oc.
- Question 4: The force per atom is the applied stress divided by the number of atoms per unit area perpendicular to the applied stress. For the (100) plane of iron,

$$\begin{split} &Atoms~per~cm^2 = \frac{1}{(2.86\times10^{-8})^2} = 1.22\times10^{15} \\ &f = \frac{4.14\times10^{10}}{1.22\times10^{15}} = 3.39\times10^{-5}~dynes & when~\epsilon = 0.028 \end{split}$$

- Question 5: It will form a sphere. The sphere has the minimum ratio of area to volume; consequently a volume of material having a spherical surface has the minimum surface energy. Because the energy per unit volume of material is constant, the material has minimum energy when its surface energy is minimized. This explanation neglects gravity forces.
- Question 6: When kerosene wets water, two interfaces are formed (kerosene-air and kerosene-water), while one is eliminated (water-air). The result must be a surface energy decrease because \( \gamma\_{kerosen-air} \) \( \sqrt{\text{pwater-air}} \). For water to wet kerosene, the condition that must be met is

This condition is not satisfied.

Question 7: The single crystal has lower energy because it has no surface energy due to grain boundaries.

Question 8: % decrease = 
$$\frac{\text{initial stress} - \text{final stress}}{\text{initial stress}} \times 100 = \frac{9\sigma - 3\sigma}{9\sigma}$$
  
  $\times 100 = 67\%$ 

where  $\sigma$  is the applied stress and the stress concentration factor for a circle is taken as 3 (see Fig. 7-13).

Question 9: The material at the crack tip would fracture.

- Question 10: Equation 7-29 shows that  $\sigma_{\rm BF}$  decreases as c increases. If a crack begins to propagate and the stress remains constant, it will continue to propagate. The model assumes that elastic energy cannot be stored in the crack region, and that forces are not transmitted across the crack. This is true for tension but not compression, therefore the model is not valid for compressive stress.
- Question 11: Releasing the load on the steel bars causes a compressive stress in the concrete because the steel bars tend to become shorter when the tensile stress is removed. The concrete is prestressed in compression. A tensile stress can be applied to the steel-concrete member, and the concrete will not sustain a tensile stress until the applied stress exceeds the prestress.



CHAPTER 8

# Plastic Behavior of Solids

THE THEORETICAL SHEAR STRENGTH OF A MATERIAL WAS calculated in Section 6-7 and it was found that materials did not exhibit the predicted strength. Consideration of cracks and surfaces enabled us to explain brittle fracture, but it shed no light on the observed behavior of ductile materials beyond the elastic limit (the region of plastic behavior). Structural imperfections called dislocations provide the explanation for crystalline materials. and most of this chapter is concerned with explaining ductile behavior in terms of the dislocation model. The geometry of dislocations was introduced in Chapter 4. Our model will require that the dislocations move through the crystal, and physical properties will be related to the ease with which this motion occurs. It will be seen that dislocation mobility (or the ease of dislocation motion) depends on the number of dislocations present in a piece of crystalline material. This quantity, called the dislocation density, is controllable and gives us a powerful means for controlling the properties of materials. Physical properties are generally temperature dependent. This chapter will deal mostly with room-temperature properties, while thermal effects will be covered in Chapter 9.

Methods of treating metals to obtain certain desired properties were known to the metal workers of antiquity. They were able to form metals into useful shapes by alternately hammering and heating them. Their knowledge was strictly empirical and offered no explanation of why their methods worked. This did not prevent them from fabricating useful devices, but improvements in their methods were the result of either accidents or trial and error procedures. Dislocation theory, which began in the 1930s, provides us with a knowledge of the processes occurring at the atomic level which cause ductile materials to behave as they do. This knowledge provides us with the key for modifying and improving these materials. As is often the case, a particular phenomenon was known to man and used by him, although he did not understand why the phenomenon occurred. Once an explanation was available, he was able to improve his previous product and methods.

The dislocation model is valid for crystalline structures but does not apply to amorphous ones. A short discussion of the plastic deformation of chain polymers is given

### Observation of slip 8-1

A single crystal of a ductile material can be permanently deformed by simply stressing it beyond its elastic limit. Figure 8-1 shows a single crystal of zinc that has been deformed in tension in this manner. The photograph indicates that some parts of the crystal have slipped past other parts and that the slip has taken place in several narrow regions. This is shown schematically in Fig. 8-2. A single crystal subjected to a tensile load is sketched in Fig. 8-2(a). The surface of the crystal is smooth. As the load is increased, the stress exceeds the elastic limit and permanent deformation begins. The onset of permanent deformation is announced by the appearance of slip lines on the surface of the crystal, as seen in Fig. 8-2(b). Entire blocks of the crystal have slipped past each other along a number of parallel planes. The individual blocks are not permanently deformed, and the deformation is the result of slip. If the load is released, the slip lines remain; the deformation is permanent. Under high magnification it is found that slip occurred on a number of planes in a narrow region rather than on a single plane, as shown schematically in Fig. 8-2(c). Each group of closely spaced planes is called a slip band. Typical dimensions for a slip band are given in the figure, and it is seen that only a small fraction of the planes participate in slip.

Polycrystalline materials exhibit similar behavior, as shown in Fig. 8-3. The photomicrograph was taken of a specimen of permanently deformed aluminum. Parallel families of lines appear in each grain. These are called slip lines but are actually slip bands, and the fact that they are parallel indicates that slip has occurred on parallel planes. Some of the grains show two families of slip lines. The slip lines do not extend through the entire specimen but stop at the grain boundaries. This would be expected because each grain has a different crystallographic orientation and the families of slip planes in different grains are not aligned with each other. Each of the

Fig. 8-1. Plastic deformation of a zinc single crystal. The crystal has been stressed in tension beyond the elastic limit. Various pieces of the crystal have slipped past each other, with the slip occurring in narrow bands. (Courtesy of E. R. Parker.)



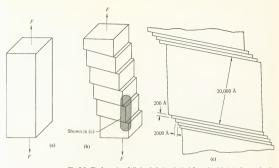


Fig. 8.2. The formation of slip bands during plastic deformation, (a) A single crystal under a tentile load. (b) Slip bands appear when the applied stress exceeds the yield stress. Blocks of the crystal slide past each other. (c) The shaded region of (b) has been magnified. Slip occurs on a large number of closely spaced planes that are parallel. This region is called a slip band. It appears as a line at lower magnification.

observations made from Figs. 8-2 and 8-3 will contribute to the permanent deformation model which will be postulated and refined throughout this chapter and Chapter 9.

The observed deformation mechanism consists of planes slipping past each other. This suggests that a shear force acting parallel to the slip planes is the cause of the deformation. The model which will be used relies upon a shear force such as that shown in Fig. 6-21; however, the concept of one

Fig. 8-3. Plastic deformation in polyery stalline aluminum. The photomicrograph shows that the slip planes are parallel within a grain but are discontinuous across grain boundaries. Some grains show two families of slip planes. Magnification, 60×. (Courtey of G. C. Smith, S. Charter, and S. Childerley.)



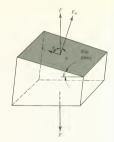


Fig. 8-4. A free-body diagram of the lower block of material in Fig. 8-2(b). The tensile force on the upper face has been resolved into two components, F, and F<sub>n</sub>. The shear force on the slip plane depends on the tensile stress and the angle \$\phi\$.

complete plane of atoms sliding past another (as illustrated in that figure) has already been discarded. Shear stresses are produced in a crystal when it is loaded in tension or compression, as shown in Fig. 8-4. The figure is a free-body diagram of the lowest block of material in Fig. 8-2(b). The downward force F is the applied tensile load, while the equal and opposite force on the upper face represents the force exerted on this face by the atoms in the remainder of the crystal. The upper face is a slip plane, and the force F exerted on it has been resolved into two components,  $F_s$  and  $F_s$ .  $F_s$  lies in the slip plane, while  $F_s$  is perpendicular to it.  $\psi$  is the angle between the slip plane and a horizontal plane. It is seen that  $F_s$  is the shear force on the slip plane, while  $F_s$  is the ensile force normal to it. From the figure,

$$F_s = F\cos\phi \tag{8-1}$$

$$F_n = F \cos \psi$$

$$\phi + \psi = 90^{\circ}$$
(8-2)

Equation 8-1 simply states that when a crystal is subjected to a tensile force, the various planes of the crystal experience both tension and shear. The magnitude of these forces depends on the applied force F and the position of the plane as defined by the angle  $\psi$ .

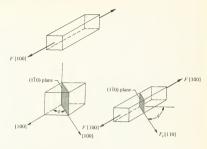
# Example 8-1

A single crystal of aluminum is 6 in. long and has a cross-sectional area of 2 in<sup>2</sup>. The [100] direction is the axial direction, as shown in the sketch. The specimen is subjected to a tensile load of 500 lb in the [100] direction.

(a) Calculate the shear force on the (110) plane in the [100] direction.

(b) Calculate the shear stress on the (110) plane in the [100] direction.

Three sketches are shown here. The first shows the loaded aluminum crystal, the second depicts the fcc unit cell of aluminum and shows the pertinent planes and directions, and the third shows the geometric relationship between the shear force  $F_c$  and the applied load F. The angle  $\psi$  is shown in the second sketch and is seen to be  $45^{\circ}$ 



## (a) From equation 8-1

$$F_s = F \cos \phi = 500 \cos 45^\circ = 353.5 \text{ lb}$$

(b) To find the shear stress on the (110) plane in the [100] direction, the definition of shear stress is used:

$$\tau = \frac{\text{shear force}}{\text{shear area}} = \frac{F_s}{A_{\text{shear}}}$$

 $A_{\rm shear}$  is the shear area of the (1 $\bar{1}$ 0) plane for this problem. The shear area depends on the cross section of the bar and the angle between the normal to the applied force and the slip direction. Letting A equal the cross section of the bar, the second and third sketches show that

$$A_{\text{shear}} = \frac{A}{\cos \psi}$$

Thus.

$$\tau = \frac{F_s}{A/\cos\psi} = \frac{F_s\cos\psi}{A} \tag{8-3}$$

Substituting values,

$$\tau = \frac{(353.5) \ (0.707)}{2} = 125 \ psi$$

At this point it is convenient to substitute equation 8-1 into equation 8-3. This combination yields

$$\tau = \frac{F\cos\phi\cos\psi}{4} = \sigma\cos\phi\cos\psi \tag{8-4}$$

where F is the applied tensile force, A is the cross-sectional area perpen-

dicular to F, and  $\phi$  and  $\psi$  are defined in Fig. 8-4. We shall have occasion to use this equation later in the chapter.

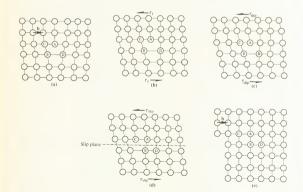
## Question

Question 1: A tensile stress of 1000 psi is applied to a cubic crystal in the [100] direction. What is the shear stress on the (110) plane in the [111] direction?

## Q\_7 The slip mechanism

Slip is observed when a material undergoes permanent deformation. The discussion of observed behavior in Section 8-1 indicated that slip occurred as a consequence of shear stress. We know that the shear mechanism cannot cause whole planes of atoms to slip past each other because materials would then show their theoretical shear strength, as was discussed in Section 6-7. Slip due to shear forces can be explained by considering a specimen having dislocations and investigating what happens to the dislocations when the material is stressed. This section will discuss a slip model based upon motion of dislocations. It is interesting that dislocations or originally postulated in order to explain the slip mechanism;

Fig. 8-5. Slip resulting from disbocation travel. (a) An edge disbocation in a crystal, b is the Burgers vector. (b) The applied stress τ<sub>1</sub> brings atoms A and B closer to each other. (c) Stress is increased. The skeetch shows AB = BC, (d) The disbocation as slipped to the left. Slip continues while the stress is applied, (e) The disbocation emerges at the surface. The crystal now has a deformation tree procreps only to the Burgers vector of (a).



they were not observed until several years afterward. It might help the reader to review the geometry of dislocations in Section 4-8 at this point.

Slip caused by an edge dislocation can be explained with the aid of Fig. 8-5. A single plane of a crystal which has an edge dislocation is shown in Fig. 8-5(a). The crystal is unstressed in this figure, and we shall be particularly concerned with the locations of the atoms marked A. B. C. and D. Applying a shear stress to the crystal [Fig. 8-5(b)] causes a rearrangement of the atomic positions. Atom C has moved to the left relative to atom B, increasing the distance between them and also increasing the energy of the B-C bond. At the same time the distance between atoms A and B is reduced, thereby strengthening the A-B bond. The energy required to increase the B-C distance is somewhat larger than the energy surrendered due to decreasing the A-B distance. The difference is supplied from the work done by the shear stress. Increasing the shear stress causes the configuration shown in Fig. 8-5(c), where the B-C and A-B distances are the same. If the shear stress is increased slightly beyond this value, the configuration shown in Fig. 8-5(d) will be present. In this figure, the A-B distance is smaller than the B-C distance, and atoms A and B are shown as bonded to each other. Atom C is at the bottom of the extra half plane, and the dislocation has slipped by one atomic spacing, The shear stress that was required to initiate slip is shown as  $\tau_{slip}$ . If this shear stress continues to act upon the crystal, the dislocation will continue to slip until it emerges at the crystal surface. The plane on which slip occurs is called the slip plane. Figure 8-5(e) shows the dislocation after it has reached the surface. It has formed a slip step, with the projection of the step being equal to the Burgers vector of the dislocation. This deformation is permanent, and Fig. 8-5(e) shows the crystal with the stress removed. Our slip model requires that the shear stress be high enough so that the crystal acquires the configuration of Fig. 8-5(c). This is just the stress required to sustain dislocation motion and is called the flow stress. It is far lower than the stress required to slide a full plane of atoms past an adjacent plane.

The motions of edge and screw dislocations are illustrated by Fig. 8-6. For the edge dislocation, the figure shows that the Burgers vector and the direction of dislocation motion are aligned and both are perpendicular to the dislocation line. The screw dislocation geometry is somewhat different. The figure indicates that the Burgers vector and the dislocation line are aligned and are perpendicular to the direction of motion. These geometric differences will prove to be significant later in the chapter. The slip of a screw dislocation is due to small atomic rearrangements which are similar to those that occur during edge dislocation slip. Figure 8-6 shows that the slip step due to a screw dislocation emerging at the crystal surface is described by the Burgers vector.

Dislocations are not limited to the edge and screw geometries. It is possible for them to have some edge character and some screw character; these are called mixed dislocations. They can be formed by defining cutting planes and having the crystal slip on the planes. Recall that the screw dislocation was formed in this manner (see Fig. 4-27). Figure 8-7(a) shows a perfect crystal and a cutting plane. Let all of the atoms above the cutting plane be displaced by the Burgers vector shown in the figure. The resulting

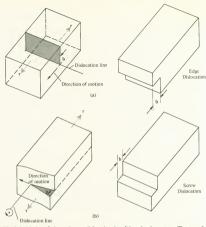
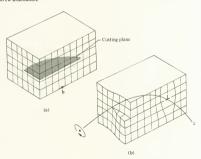


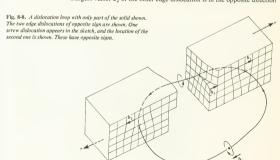
Fig. 8-6. Motion of edge and screw dislocations in solids under shear stress. The steps that appear when the dislocations emerge at a crystal surface are shown. (a) Edge dislocation. (b) Screw dislocation.

Fig. 8-7. Mixed dislocations.
(a) A perfect crystal affect crystal exiting plane is shaded. All atoms above the plane are displaced by the Burger's vector b. (b) The resulting dislocation line is an edge dislocation at one point and a serve dislocation at a second point. It is a mixed dislocation at all other points.



structure [Fig. 8-7(b]] has a screw dislocation on one surface and an edge dislocation on the other. The dislocation line is the boundary of the cutting plane. It is an edge dislocation at only one point (the surface) and a screw dislocation at one point. All other points on the line are part edge and part screw.

In forming the dislocation line of Fig. 8-7(b), one region of the crystal was forced to slip on the slip plane, while the remainder kept its original configuration. The dislocation line forms the boundary between that portion of the crystal whose atoms have slipped and the part whose atoms have not slipped. Because all of the atoms on the slip plane must fall into one category or the other, the boundary between the slipped and unslipped regions must be continuous through the crystal. By continuous it is meant that the dislocation line cannot end within the crystal. To form a boundary it must either terminate at the crystal surfaces or form a closed loop within the crystal. A grain boundary is considered a crystal surface. Mixed dislocations make it possible to have dislocation loops. The configuration of a dislocation loop is illustrated in Fig. 8-8. The figure represents a dislocation loop in a crystal. Half of the crystal is not shown, while the remaining half has been broken into two pieces. The piece on the right contains a quarter of the loop and has the same geometry as the crystal in Fig. 8-7(b). The loop can be extended through the second piece in Fig. 8-8 and an interesting thing occurs. Edge dislocations appear at one point in each piece, but the piece on the left has an extra half plane below the slip plane, while the right-hand piece has the opposite. This necessitates defining the sign of a dislocation. We first select a positive direction for the dislocation line. This is indicated by the arrows in the figure. The Burgers circuits are then taken in the direction of a right-hand screw advancing along the dislocation line. Having defined the manner in which the Burgers circuit is to be taken, we then define the direction of b1 as positive. The Burgers vector b2 of the other edge dislocation is in the opposite direction



and is therefore negative. A screw dislocation having Burgers vector b3 is shown. If the remainder of the crystal were viewed, a screw dislocation would appear opposite the one shown. Its position is indicated in the figure, and its Burgers vector would be in a direction opposite to b. It appears as b.

If the shear stress shown in Fig. 8-8 is applied to the solid, the edge dislocation having Burgers vector b, will move to the right, while the other one will move to the left. This is a consequence of their having opposite signs. Similarly, the screw dislocations will move outward in opposite directions. The same is true of the mixed dislocations, and the applied stress causes the dislocation loop to expand outward until it terminates in steps at the surface. In this manner, expansion of dislocation loops causes permanent deformation. These loops have been observed and Fig. 8-9 shows an electron micrograph of dislocation loops in an aluminum-3.5% magnesium alloy. The dislocation loop mechanism is of great importance and forms the basis for generating dislocations, as will be discussed in Section 8-6.

As previously stated, dislocations either emerge at surfaces or form loops. This enables us to define a quantity called the dislocation density. It is simply the number of dislocations which emerge from the crystal per unit surface area. The symbol  $\rho$  is used to denote it. The surface used to define o can be any surface on the crystal; no crystallographic limitations are placed upon it. The dislocation density will be quite significant to us. It is a measure of the number of dislocations in a volume of material and it can be determined experimentally.

## Ouestion

Ouestion 2: Screw and mixed dislocations were formed by defining a cutting plane and slipping the atoms on this plane. An edge dislocation can be formed in the same way. Let the cutting plane in Fig. 8-7 be extended so that it intersects the left edge of the cube, and let it be rectangular. If the atoms above the cutting plane are displaced by b,

Fig. 8-9. An electron microaraph showing dislocation loops in a specimen of aluminum containing 3.5% magnesium, 25,000 × . [K. H. Westmacott, R. S. Barnes, and R. E. Smallman, Phil, Mag. 8:425 (1962).]



the result is a slip step and an edge dislocation. Sketch the solid showing the slip step, cutting plane, and edge dislocation.

# 8\_3 Critical resolved shear stress

The dislocation slip mechanism described in Section 8-2 occurs at shear stresses significantly lower than the theoretical shear strengths of solids calculated in Chapter 6. The shear stress at which slip begins can be determined experimentally from tension tests. Equation 8-4 is used in conjunction with these experiments:

$$\tau = \sigma \cos \phi \cos \psi \qquad \phi + \psi = 90^{\circ} \qquad (8-4)$$

The equation was derived in Section 8-1 and relates the shear stress in any particular direction to the tensile stress. The quantity  $\tau$  is often called the resolved shear stress because it is found by resolving the tensile stress into two components. If we let  $\tau_{e\tau}$  be the resolved shear stress at which slip first occurs (called the *critical resolved shear stress*) and let  $\sigma_s$  be the tensile stress on the specimen when slip begins, then

$$\tau_{cr} = \sigma_s \cos \phi \cos \psi$$
 (8-5)

This equation has been verified experimentally. The experimental procedure consists of placing a tensile stress on several crystals of the same substance, with the stress on each crystal being in a different crystallographic direction.  $\sigma_e$  is found by observing the tensile stress when slip lines first appear. The angle between the applied stress and the slip direction can also be found from the experiment. Figure 8-10 shows the results obtained using high purity single crystals of 2 zinc stressed at room temperature. Comparison of the data with equation 8-5 gives a value for  $\tau_{er}$  of 26.2 psi. The value of  $\tau_{er}$  is a constant for a given high-purity single crystal at a given temperature. This statement implies that  $\tau_{er}$  depends on purity and

Fig. 8-10. The tensile stress required to initiate slip depends on the slip-plane orientation and the slip direction. The data are for a high-purity single-crystal of its attressed at room temperature. The value of r<sub>ev</sub> for this curve is 26.5 psi. [D. C. Jillson, Trans. AIME 188:1120 (1950).]

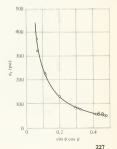


Table 8-1. Critical resolved shear stress for several pure solids at room temperature\*

Solid	Structure	Slip plane	Slip direction	$\tau_{cr}$ $(psi)$
Ag	fcc	((111))	[[1]0]]	54
Al	fcc	((111))	[[1 TO]]	114
Cu	fcc	((111))	[[1 To]]	71
Fe	bcc	((110))	[[T11]]	3,980
Mo	bcc	((110))	[[Ī11]]	10,400
Nb	bcc	((110))	[[I11]]	4,840
Mg	hcp	((0001))	[[1120]]	64
Co	hcp	((0001))	[[1120]]	960
Ti	hcp	((10T0))	[[1120]]	1990
NaC1	NaC1	((110))	[[110]]	285
AgC1	NaCl	((110))	II1 I 011	143

<sup>\*</sup> These values were tabulated from various sources by W. J. M. Tegart, Elements of Mechanical Metallurgy, Macmillan, New York, 1966, p. 106.

temperature in some manner. The nature of this dependence will be discussed later.

The critical resolved shear stress has been determined for a number of solids, and some of these are given in Table 8-1 together with the observed slip plane and slip direction. Inspection of the data reveals several pertinent points. Ter is the shear stress at which slip begins, and plastic deformation is attributed to slip. We would therefore expect that \(\tau\_{-}\) and the yield point are related. For high purity single crystals, the tensile yield stress can be determined from the tabulated values of τ<sub>cr</sub> and equation 8-5. Commercial purity polycrystalline materials generally have yield points from about 10 to 100 times the value of  $\tau_{sr}$ , as determined by experiment. From this, it is apparent that dislocation mobility depends on purity and the presence or absence of grain boundaries, and our dislocation model must account for them. Table 8-1 also shows that to is higher for bcc metals than for metals having closest packing, implying that packing density affects dislocation slip. Inspection of the slip planes and slip directions shows that these are close-packed planes and densely packed directions. This observation is consistent with the slip mechanism shown in Fig. 8-5. According to the model, the specimen had to deform elastically until distance AB was less than BC. The stress required to provide this elastic deformation would depend on the spacing between the atoms of a plane and the shear modulus. Close spacing of the atoms in a plane would mean that the slip condition could be achieved at small deformations. Thus, slip would tend to occur most readily on close-packed planes in close-packed directions.

The dislocation slip problem has been treated analytically,\* but the analysis is beyond the scope of this book. The resulting equation is given below in order to reinforce the qualitative argument of the previous paragraph. The equation is an approximation,

$$\tau_{cr} = 2Ge^{-(2\pi d/b)}$$
(8-6)

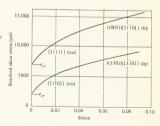
<sup>\*</sup> F. R. N. Nabarro, Proc. Phys. Soc. (London) 59:256 (1947).

where d is the distance between planes and b is the distance between atoms in the slip direction. For the dislocations which we have considered so far, b is equivalent to the magnitude of the Burgers vector. The form of the equation is such that a small Burgers vector corresponds to a low value of  $\tau_c$ . Small Burgers vectors correspond to closely spaced atoms in the slip direction. Large values of d also yield low values for  $\tau_c$ , and large interplanar spacings exist between closely packed planes. Thus, the observed slip on closely packed planes in densely packed directions is predicted by equation 8-6. It is also seen that a large shear modulus increases  $\tau_{c_1}$  as expected from the previous argument.

Table 8-1 does not list any of the high-temperature ceramic materials, such as MgO or Al<sub>2</sub>O<sub>3</sub>. These materials generally exhibit brittle fracture at room temperature; however, the dislocation slip mechanism does operate at higher temperature. Figure 8-11 shows a plot of resolved shear stress vs. strain for high purity single crystals of MgO at 1300°C. The loading and slip directions are indicated. The resolved shear stress is just the component of the applied stress in the slip direction. The critical resolved shear stress is the stress at the point where the curves become nonlinear. It is seen that r<sub>cr</sub> depends on the slip plane and slip direction.

Things are becoming a bit complicated and it might be well to consider what has happened so far. The perfect crystal model proved to be valid within the elastic limit but failed to predict ductile behavior. The model was modified to include the dislocation slip mechanism. For the straight forward case of high purity single crystals, the equation derived from dislocation slip theory (equation 8-6) gives results that correlate reasonably with observed data. If the theory is to be applied to engineering materials, however, it must explain the effects of impurities, grain boundaries, and temperature. In addition, it will be shown that ductile behavior depends on the previously sheformed, previously heated, etc. This is indeed becoming a "can of worms." The next few sections will show that our model is capable of explaining all of these dependencies (except temperature, which is covered in Chapter 9). We shall stay with the single-crystal case a while longer because this eliminates one variable.

Fig. 8-11. Resolved shear stress vs. strain for high-purity MgO single crystals. The tests we made at 1300° to using a compressive stress. The direction of the load and the observed slip systems are shown and indicate the dependence of  $\tau_{id}$  on the slip system. (S. M. Copley and J. A. Pask in Materials Science Research, W. W. Kriegel and H. Palmour III. des. Plenum Press, 1966.)



Question

Question 3: The lower curve in Fig. 8-11 shows that MgO has a critical resolved shear stress of 1900 psi when slip occurs on the (110) plane in the [110] direction. What tensile stress was applied to the specimen when slip first occurred? The tensile stress was applied in the [100] direction.

8-4 Slip systems

A slip system is defined when we specify a slip plane and slip direction. This was done for several materials in Section 8-3, and this section will elaborate on the slip system concept. The number of slip systems that a solid has affects its plastic behavior significantly. The discussion of Section 8-1 showed that the tensile or compressive stress at which slip begins depends on the orientation of the slip plane with respect to the applied load. A crystal having a large number of slip systems will be more likely to have at least one of them favorably oriented for slip than a solid having fewer slip systems. In Section 8-10 we shall discuss methods by which dislocation motion can be hindered. If slip is prevented in a particular slip system (this can be done in several ways), a solid with many slip systems will provide more alternatives for dislocation motion than one with fewer slip systems. In the case of polycrystals (Section 8-14), slip must occur in such a way that the grain boundaries do not separate. This condition can be quite restrictive and is met most readily by solids having numerous slip systems.

The slip systems observed in various crystal structures are shown in Table 8-2. The first slip system shown for each structure is the system on which slip occurs most easily. For example, two slip systems are shown for the NaCl structure. Figure 8-11 shows that the easiest slip is on the system ((110)) [[110]] although slip does occur on the ((001) [[110]] system. The easy slip systems tabulated are the only ones on which slip occurs at low temperatures. As the temperature rises, more slip systems become active. Three systems are shown for hep crystals. All of the hep crystals slip on the ((0001))[[1120]] system. They also slip on only one of the other two systems. Which one it is varies among the different hep solids.

Question

Question 4: Equation 8-6 shows that the critical resolved shear stress decreases as the ratio d/b increases. Find the ratio of d/b for the three slip systems observed in the bcc structure (see Table 8-2). Which system provides easiest slip? Least easy slip?

8-5 Energy of dislocations

The description of dislocations in Chapter 4 showed that there are regions around an edge dislocation in which the material was strained and that both tensile and compressive strains appeared (see Fig. 4-26). In forming a screw dislocation, it was necessary to shear one plane of atoms past another (Fig. 4-27). As a result, material in the vicinity of a screw dislocation has shear strains. Energy was required to produce these strains, and this energy is stored in the region of the dislocation. It is called strain

## 8-5: ENERGY OF DISLOCATIONS

Table 8-2. Slip systems observed in crystal structures

Structure	Slip plane	Slip direction	Number of slip systems	
fcc	((111))	[[1]0]]	4 × 3 = 12	
bcc	((110))	[[[11]]]	6 × 2 = 12	B
	((211))	[[[11]]]	$12\times 1=12$	
	((321))	[[11]]	$24\times 1=24$	
hcp	((0001))	[[1120]]	1 × 3 = 3	<b>B</b>
	((1010))	[[1120]]	$3 \times 1 = 3$	
	((1011))	[[1120]]	6 × 1 = 6	
NaCl	((110))	[[1T0]]	$6\times 1=6$	
	((001))	[[110]]	6 × 1 = 6	
${\rm Al_2O_3}$	((0001))	[[1120]]	1 × 3 = 3	1
	((1010))	[[1120]]	$3 \times 1 = 3$	
CsCl	((110))	[[001]]	6 × 1 = 6	

energy and exists because of crystal distortion near the dislocations. Thus, energy is associated with dislocations. In this section we shall calculate the nergy required to form dislocations. A number of consequences arise as a result of dislocation energy, and the derivation of the dislocation energy equation will be a large help in developing and understanding the dislocation model.

The energy required to form a screw dislocation can be determined with the aid of Fig. 8-12. A screw dislocation of length  $\mathscr L$  is shown in Fig.

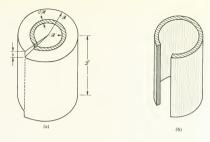
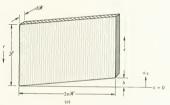


Fig. 8-12. A serve dislocation of length 2<sup>st</sup>. A different A different of width 63<sup>st</sup> is shown. (b) The differential element has been removed from the dislocation and has been parted on the slip plane. (c) The differential element when it has been flattened. The element has been lastically deformed by a distance. b. Deformation is caused by the shear stress.



8-12(a). A differential element of the dislocation having inside radius  $\mathscr{X}'$  and thickness  $d\mathscr{X}'$  is also shown. In Fig. 8-12(b), the differential element has been removed and parted along the plane containing the step. Unrolling this element and flattening it gives it the shape shown in Fig. 8-12(c). This configuration will be used for calculating the strain energy. The shear stress shown in Fig. 8-12(c) is the same as the shear stress originally required to form the dislocation. We shall derive an expression for the elastic energy stored in a differential element due to the shear strain and then integrate this expression over the entire dislocation to find the dislocation energy.

Let  $d\mathscr{E}$  be the elastic energy stored in the differential element and let  $F_s$  be the shear force. The x direction is shown in Fig. 8-12(c). Thus,

$$d\mathcal{E} = \int_{0}^{b} F_{s} dx \qquad (8-7)$$

F must be expressed as a function of x in order to do the integration. This can be done by first letting

$$F_s = \tau \mathcal{L} d\mathcal{R}' = G \gamma \mathcal{L} d\mathcal{R}'$$
 (8-8)

since  $\tau = Gy$ . From the definition of shear strain and Fig. 8-12(c).

$$\gamma = \frac{x}{2\pi \Re'} \tag{8-9}$$

Substituting equation 8-9 into 8-8,

$$F_s = \frac{G \mathcal{L} x}{2\pi \mathcal{R}'} d\mathcal{R}' \qquad (8-10)$$

Substituting 8-10 into 8-7 and integrating over x,

$$d\mathcal{E} = \int_0^b \frac{G\mathcal{L}x \, d\mathcal{R}' \, dx}{2\pi \mathcal{R}'} = \frac{G\mathcal{L}b^2}{4\pi} \frac{d\mathcal{R}'}{\mathcal{R}'} \tag{8-11}$$

The energy of the dislocation can be found by integrating equation 8-11 over the appropriate values of  $\Re$ :

$$\mathscr{E} = \int_{\mathscr{X}'}^{\mathscr{R}} \frac{G\mathscr{L}b^2}{4\pi} \frac{d\mathscr{R}'}{\mathscr{R}'} = \frac{G\mathscr{L}b^2}{4\pi} \ln \frac{\mathscr{R}}{\mathscr{R}''}$$
(8-12)

The upper limit,  $\mathcal{R}$ , is the outer radius of the dislocation, which has a finite value.  $\mathcal{R}'$  is the inner radius. If we take  $\mathcal{R}' = 0$ , the dislocation energy becomes infinite. From a physical point of view, this is nonsense. Large strains exist at the dislocation core (the region near the dislocation line); therefore the assumption of elastic behavior, upon which equation 8-12 is based, does not hold in this region. If  $\mathcal{R}''$  is taken as being equal to the magnitude of the Burgers vector, it can be shown that the strain energy in the region of the core, having a radius of b, is small compared to the energy of the remainder of the dislocation and can be neglected. Thus,

$$\mathscr{E} = \frac{G\mathscr{L}b^2}{4\pi} \ln \frac{\mathscr{R}}{b} \tag{8-13}$$

for a screw dislocation. For an edge dislocation, the energy is expressed as

$$\mathscr{E} = \frac{1}{(1-\mu)} \frac{\mathscr{L}Gb^2}{4\pi} \ln \frac{\mathscr{R}}{b}$$
 (8-14)

In both equations,  $\mathcal{R}$  can be taken as one half the distance between dislocations in the solid.

Dislocation energy increases as the Burgers vector increases, according to equations 8-12 and 8-14. It is therefore easier to form dislocations with small Burgers vectors than with large ones. This is consistent with the discussion of slip systems. Slip occurred on densely packed planes in densely packed directions, implying that the dislocations had small Burgers vectors.

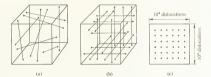
The quantity  $\mathcal{B}$  in equations 8-13 and 8-14 depends on the number of dislocations present in a solid, and the total energy in a solid due to dislocations depends on dislocation length. Both of these quantities can be found from an experimentally determinable quantity, the dislocation density. This was defined in Section 8-2, and  $\rho$  can be found by simply counting dislocations on a photomicrograph or an electron micrograph.

### Example 8-2

A specimen is observed to have a dislocation density of 10<sup>8</sup> dislocations/cm<sup>2</sup>. Find

- (a) The total length of dislocations in 1 cm3 of material.
- (b) The average distance between dislocations.

(a) The dislocations are randomly arranged in the solid, as shown in the 1-cm cube of Fig. (a). Some of the dislocations are longer than 1 cm and some are shorter. It can be shown that the average length is 1 cm if the dislocation arrangement is random. All of the dislocations have a length of 1 cm in Fig. (b), and this figure is the basis for our calculation. According to the observed value of  $\rho$ , there are  $10^9$  dislocations between each pair of parallel faces in the cube, and there are three pairs of such faces. Thus,



Length of dislocations in the cube =  $3 \times 10^8$  cm

(b) The average distance between dislocations can be found by assuming that the  $10^8$  dislocations having the same direction [Fig. (b)] are symmetrically spaced. One face of the cube having such a dislocation arrangement is shown in Fig. (c), and there are  $10^4$  dislocations along each 1-cm edge. Each dot represents a dislocation line intersecting the surface. The distance between dots is thus  $1/10^4 = 10^{-4}$  cm. The value of  $\Re$  is just half this, or  $5 \times 10^{-3}$  cm. This is, of course, an average value, but these average values are commonly used in dislocation calculations.

Dislocations are nonequilibrium entities because their presence increases the energy of a solid. The solid could go into a more stable (lower energy) state if it could rid itself of the dislocations. We shall see that the density of dislocations can be diminished by the proper processing of a material, but they are too tenacious to be completely eliminated.

#### Questions

- Question 5: In going from equation 8-12 to 8-13, it was stated that equation 8-12 assumed elastic behavior. Where in the derivation was this assumption introduced?
- Question 6: Let the dislocations in Example 8-2 have Burgers vectors of 4Å and a shear modulus of 5 × 10° psi (3.45 × 10¹¹ dynes(m²). (a) Calculate the energy of a screw dislocation in the solid. (b) Find the energy associated with a 4-Å length of the dislocation and express the

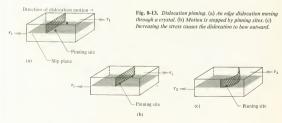
energy in electron volts. *Note:* The energy of a length of dislocation line that is equal to the Burgers vector typically has an energy of several electron volts.

## 8-6 Dislocation sources

Typical metals show dislocation densities varying from about 10<sup>5</sup> to 10<sup>12</sup> dislocations/em<sup>2</sup>; the density in ceramic materials is usually lower. The number of dislocations present in an undeformed ductile solid is not high enough to account for the plastic deformation observed when the solid is stressed beyond the elastic limit (see Problem 8-4). This implies that either dislocations are being created during deformation or the dislocation model is wrong. Visual observations with both optical and electron microscopes show that the density of dislocations increases as a crystalline specimen is plastically deformed; therefore a source of dislocations must be present within the solid. This section will discuss one such source, called the Frank-Read source. It was postulated in order to describe a dislocation-generating mechanism and has been observed in a number of Solids.

The Frank-Read source requires that there be sites within a crystal which a dislocation cannot slip past. These are called pinning sites, implying that a dislocation is pinned, or immobilized, when it comes upon such a site in its slip plane. Pinning sites can be collections of impurity atoms, points at which dislocations intersect, or the presence of a second phase in the solid. Dislocation intersection will be discussed in Section 8-10, but an explanation of second phases must wait until Chapter 11. Because pinning sites reduce dislocation mobility, we would expect that solids containing pinning sites should have a higher flow stress and consequently would exhibit higher yield point values. This is in accord with observation, and controlling the number of pinning sites is a fundamental method of controlling mechanical properties.

Figure 8-13(a) shows the extra half plane of an edge dislocation slipping along through a crystal which has a shear stress 7; applied to it. The dislocation comes upon two pinning sites in its slip plane and cannot continue its motion [Fig. 8-13(b)]. If the shear stress is increased to 7; as in Fig. 8-13(c), the dislocation does not continue to move but increases if



length by bowing outward. In this process, work has been done by the applied shear force to create the additional length of dislocation line. The bowing out of the dislocation as the stress increases is the key to our dislocation generator and will now be considered quantitatively. The bowing out of the dislocation is caused by a force acting on the dislocation, which has its origin in the applied shear stress. The force acting on the dislocation can be expressed as a function of r with the aid of Fig. 8-14. An edge dislocation having length 2° and located a distance s from the edge of the solid is shown in Fig. 8-14(a), In Fig. 8-14(b), the dislocation has emerged from the solid and a step has been formed. The work required to produce the step can be expressed in two different ways. We shall consider both work expressions and combine them to get an equation for the force on the dislocation.

To create the deformation step, that portion of the shear force which was applied to the darkly shaded plane (of area \$2^p\$) has moved through a distance \$b\$; therefore the work done by this force in order to move the dislocation to the surface is \$x\_sD^p\$. Now let \$P\$ be the force exerted on the dislocation by the atoms of the crystal. The work done by this force in moving the dislocation through the crystal is equal to \$P\_s\$. Both of these quantities express the work expended in moving the dislocation to the surface and are therefore equal:

$$\mathscr{F}s = \tau s \mathscr{L}b$$
 (8-15)  
 $\mathscr{F} = \tau \mathscr{L}b$ 

where  $\mathcal{F}$  is the force on the dislocation and  $\tau$  is the applied shear stress.

A diagram of the bowed dislocation is shown in Fig. 8-15(a). Only that part of the dislocation that lies between the pinning sites is shown. The force r\$\mathcal{E}^D\$ acting on the dislocation must be counteracted by an equal and opposite force exerted by the pinning sites because the dislocation is not moving. Note that \$\mathcal{E}\$ is the distance between pinning sites. To find this force, we start with equation 8-14:

$$\frac{\mathscr{E}}{\mathscr{L}} = \frac{Gb^2}{(1-\mu)4\pi} \ln \frac{\mathscr{R}}{b}$$
(8-14)

This equation can be simplified somewhat by considering typical values of  $\Re$  and b for metals. If we take a value for b of 3Å and let  $\Re$  equal 0.0005 cm (corresponding to  $10^9$  dislocations/cm $^3$ ), the term  $\ln$   $\Re$  $/<math>\Re$ 0 equals 9.72. For a dislocation density of  $10^9$ /cm $^4$ , the term comes out to be 5.12. The value of the denominator, taking  $\mu$  as 0.3; 8.79. If we are willing to accept an error of a factor of about 2, we can let the two terms above equal each other. Then

$$\frac{\mathscr{E}}{\mathscr{L}} = Gb^2$$
(8-16)

The energy of a dislocation is proportional to its length, according to equations 8-14 and 8-16. Because of this, we can consider the term  $Gb^2$  as the line tension of the dislocation. This term can be clarified by Fig. 8-15(b). Let the shaded region be a "substance" whose energy is proportional to

Fig. 8-14. Diagrams for determining the force on a dislocation. (a) A shear stress applied to a crystal having an edge dislocation. (b) A step is created when the dislocation reaches the surface. The shear stress has moved a distance b; the dislocation has moved a distance s

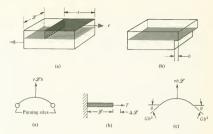


Fig. 8-15. Forces on a dislocation. (a) A pinned dislocation bowing out because of the force τb L. (b) Line tension. (c) Free-body diagram of the forces on a bowed dislocation.

length. For the configuration shown, it has an energy  $\mathscr E$  and is maintained at its length  $\mathscr D$  by the force T, which is the line tension. Line tension is analogous to surface tension, and Fig. 8-15(b) can be compared to Fig. 7-1. To increase the length by 1 unit (call it  $\Delta\mathscr E$ ), the work done by the force is  $T\Delta\mathscr E$ . This work must be equal to the energy per unit length of the "substance," which is  $\mathscr E$ ! $\mathscr E$ . Thus,

$$T\Delta\mathcal{L}=\frac{\mathscr{E}}{\mathscr{L}}=Gb^2$$
 
$$T=Gb^2 \qquad \text{because } \Delta\mathscr{L}=1 \text{ unit}$$

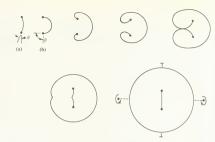
This is analogous to the numerical equality of surface energy and surface tension described in Chapter 7. The line tension can now be used in place of the pinning sites of Fig. 8-15(a). The final free-body diagram is shown in Fig. 8-15(c), and it is seen that

$$2Gb^2 \sin \theta = \tau b \mathcal{L}$$
 (8-17)

We are considering the motion of a particular dislocation in a particular material as shear stress is increased; therefore all of the quantities in equation 8-17 are constant except  $\tau$  and  $\theta$ . Let us consider what happens as  $\tau$  increases and the bowing out becomes more pronounced. The first sketch in Fig. 8-16 shows a slightly bowed dislocation. As  $\tau$  increases,  $\theta$  also increases according to equation 8-17. The second sketch shows  $\theta = 90^\circ$ . According to equation 8-17, this configuration corresponds to the maximum value of  $\tau$ . For this condition equation 8-17 can be written as

$$\tau_{\text{source}} = \frac{2Gb}{\varphi} \tag{8-18}$$

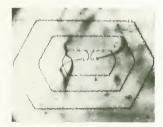
Fig. 8-16. The Frank-Read source, (a) A dislocation is pinned by two pinning sites. It bows out under the influence of an applied shear stress. (b) Increasing the shear stress increases the howing until \theta is 90°. This corresponds to Tsource. If the shear stress is increased slightly, the dislocation will spontaneously pass through the configurations shown and a dislocation loop will be generated.



The quantity  $\mathscr L$  is the length of a dislocation which has not bowed out. Because we are concerned with the part of the dislocation between pinning sites,  $\mathscr L$  is the distance between pinning sites in this equation. If the shear stress is increased beyond  $\tau_{source}$ , the dislocation will spontaneously pass through the configurations shown in Fig. 8-16. The net result of the single cycle illustrated is the production of one dislocation loop, and a dislocation which is again anchored at the pinning sites. The dislocation loop will expand outward because of the applied stress and the source can generate another loop, etc. Thus, the Frank-Read source provides a supply of dislocations, and the stress required for the source to operate is given by  $\tau_{source}$  in equation 8-18. Figure 8-17 shows a source of dislocation loops in silicon. The loops appearing in Fig. 8-9 can also be explained by this mechanism. Note that all of the dislocation loops produced by a Frank-Read source have the same slip plane.

If all of the generated dislocations do not emerge at the surface but some remain in the solid, the dislocation density of the material will increase.

Fig. 8-17. A Frank-Read source operating in a silicon single crystal. (W. C. Dash, Dislocations and Mechanical Properties of Materials, Wiley, New York, 1957. Photograph courtesy of L. V. Azaroff.)



This is observed. If all of the dislocations are pinned, the presence of pinning sites increases the flow stress from that given by equation 8-6 (or Table 8-1) to \( \text{T}\_{source}\) of equation 8-18. Thus, pinning sites decrease dislocation mobility, increase the flow stress, increase the yield point, and strengthen the material. In Section 8-10 we shall see that dislocations interfere with each other at high dislocation densities, and this, too, decreases mobility. Thus, the pinning sites not only directly reduce the mobility but provide dislocations which can hinder the motion of other dislocations.

### Ouestion

Quesiton 7: Suppose that dislocation sources did not exist. You are given a piece of material containing dislocations and you obtain a stress-strain diagram from it. Assume that the slip mechanism operates but the source mechanism does not. (a) Describe the stress-strain diagram. (b) Can you calculate the ultimate tensile strength? How? (c) Is this behavior shown by materials?

# 8-7 Dislocation annihilation and forces

Dislocation density can be decreased as well as increased. The decrease is generally observed at higher temperatures and forms the basis of the amnealing process. The creation of dislocations required energy; their annihilation is exothermic because the energy of a crystal is reduced when dislocations are eliminated. In this section the annihilation of dislocations will be discussed, as well as the forces which exist between dislocations will be shown that the direction of the forces encourages annihilation. This would be expected because annihilation reduces crystal energy. These forces, however, are well below the flow stress in most materials at room temperature and consequently do not strongly influence mechanical properties at room temperature and below.

Annihilation is readily visualized by considering two parallel edge dislocations, as shown in Fig. 8-18. Two edge dislocations having opposite signs but the same slip plane are illustrated in Fig. 8-18(a). When the shear stress shown is applied, the dislocations move toward each other, Their meeting creates a region of perfect crystal, as illustrated. Note that if the direction of the shear stress were reversed, the dislocations would move apart. A slightly different orientation appears in Fig. 8-18(b). In this sketch, the dislocations do not have the same slip plane. When the shear stress is applied, they will move toward each other. The final configuration shows that the two half planes almost meet. The two dislocations have been annihilated and a row of vacancies has been created. A similar situation is depicted in Fig. 8-18(c), but the extra half planes of the dislocations overlap. Dislocation motion here results in annihilation of the dislocations and creation of a row of interstitials. All three of the final configurations have a lower energy than the initial configurations, and the annihilation process moves the crystal toward a lower energy state. Screw dislocations can annihilate each other in an analogous manner.

Each dislocation has a deformed region of crystal associated with it. For edge dislocations, this region is partly in tension and partly in compression (see Fig. 4-26). Regions of shear deformation surround screw

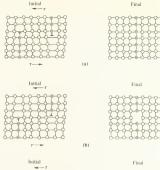
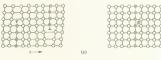


Fig. 8-18. Annihilation of edge dislocations. (a) A positive and a negative dislocation cancel each other to form a region of perfect crystal, (b) A row of vacancies results from two dislocations combining, (c) Dislocation annihilation creates a row of interstitials.



dislocations. These deformed regions affect each other in such a manner that one dislocation will exert a force on a neighboring dislocation, with the force being caused by interaction of the deformed regions. The neighboring dislocation will exert an equal and opposite force on the first one. The direction of these forces is such that if the dislocations moved in the directions of the forces, the energy of the crystal would be reduced. Thus, the dislocations shown in Fig. 8-18 would attract each other with no applied shear force on the crystal.

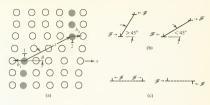
Two parallel edge dislocations having parallel Burgers vectors are shown in Fig. 8-19(a). The force in the x direction, per unit length of dislocation, exerted on dislocation 2 by dislocation 1 is given by the equation

$$\frac{\mathscr{F}_x}{\mathscr{L}} = \frac{G\mathbf{b}_1\mathbf{b}_2}{2\pi(1-\mu)s} \left[\cos\theta \left(\cos^2\theta - \sin^2\theta\right)\right] \tag{8-19}$$

where s is the distance between the dislocations. The derivation of the equation is beyond the scope of this book.\* Equation 8-19 is limited to the case of parallel dislocations. The dislocations in Fig. 8-19 also have

<sup>\*</sup> See J. Weertman and J. A. Weertman, Elementary Dislocation Theory, Macmillan, New York, 1964, p. 66, for the derivation.

Fig. 8-19. (a) Two parallel edge dislocations in a crystal. The dislocations attract each other with small forces, as defined by equation 3-19, (b) and (c) The x component of the force between dislocations. The direction of the force depends on the signs of the dislocations and the analy hetween them.



parallel Burgers vectors, and the quantity  $\mathbf{b}_1 \cdot \mathbf{b}_2$  can have only two values,  $b_1b_2$  or  $-b_1b_2$ . A negative value of  $\mathcal{F}_x$ , of course, indicates that the x component of the force exerted on dislocation 2 by dislocation 1 is to the left. The interaction force for several pairs of parallel edge dislocations is shown in Fig. 8-19(b).

Equation 8-19 can be applied to the dislocations shown in Fig. 8-18(a). The following values, which are typical of metals, can be used. Let  $G = 10 \times 10^6$  psi (or  $6.895 \times 10^{11}$  dynes/cm<sup>2</sup>),  $b_1 = b_2 = 2$ Å,  $\mu = 0.3$ , and  $s = 5 \times 10^{-4}$  cm, which corresponds to a dislocation density of  $10^6$ dislocations/cm2. The attractive force per centimeter of dislocation length turns out to be  $12 \times 10^{-3}$  dynes using these values. If a ceramic were considered, the value of s would be larger because the dislocation density is generally lower than that found in metals. The attractive force is considerably lower than the force required to initiate slip at room temperature (Table 8-1): therefore the attractive forces are too small to cause dislocation motion. As the dislocation density increases, the interaction force increases because s diminishes. At high temperatures the dislocations are more mobile than they are at low temperatures; that is, smaller forces are necessary to initiate slip. The dislocation interaction forces become significant in the high-temperature process of annealing, which is discussed in Chapter 9.

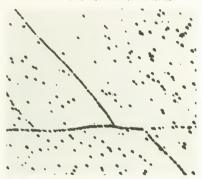
The effect of dislocation interaction explains the observation of lowangle grain boundaries. Consider the interaction between the two edge dislocations shown in Fig. 8-19(b), with  $\theta > 45^\circ$ . The force is such that dislocations having this orientation will tend to align with each other. The result of such an alignment is illustrated schematically in Fig. 8-20. The dislocations are seen to cause a small angular misalignment of adjacent crystal regions; hence the name low-angle grain boundaries in tungsten. To obtain this photograph, the specimen was eiched in a solution which preferentially attacked the regions at which dislocations intersected the surface. Each of the etch pits shown represents a dislocation. The etching technique permits us to observe dislocations with an optical microscope. Low-angle grain boundaries are observed in many materials and are attributed to interaction forces between dislocations.

The parallel edge dislocations used as examples in this section are the simplest geometric case that we can consider. Interactions occur between



Fig. 8-20 (left). Schematic drawing of a low-angle grain boundary. The dislocations have aligned because of the interaction forces. The alignment causes misorientation between two regions of a grain.

Fig. 8-21 (below). Low-angle grain boundaries on the (112) surface of tungsten. Each etch pit represents a dislocation intersecting the surface. The aligned etch pit are caused by dislocations that form low-angle grain boundaries. Magnification, 250×. (H. W. Schadler in Direct Observation of Imperfections in Crystals, J. B. Newkirk and J. H. Wernick, eds. Wilev-Interscience. New York. 1962).



dislocations (edge, screw, and mixed) in all orientations, but they will not be discussed here.\*

## Question

Question 8: Equation 8-19 is applicable to dislocations having parallel dislocation lines. The example in Fig. 8-19 also has parallel Burgers vectors. Sketch a (100) plane of a simple cubic structure and show two edge dislocations whose dislocation lines are parallel but whose Burgers vectors are not.

# **8\_8** Partial dislocations

It often happens that the energy of a dislocation can be reduced if it dissociates into two partial dislocations with each of them having smaller Burgers vectors than the original one. This section will discuss the geometry of partial dislocations. In Section 8-10, it will be shown that these

\* More extensive treatment of dislocation interactions can be found in Weertman and Weertman, op. cit., or J. Fridel, Dislocations, Addison-Wesley, Reading, Mass., 1964

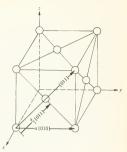


Fig. 8-22. An fcc unit cell illustrating the Burgers vector notation. The two heavily drawn are a[010] and a/2[011],

partial dislocations can interact in such a manner that they immobilize each other.

We have been able to describe Burgers vectors so far by specifying the direction of the vector and letting its length be the distance between atoms in the specified direction. A more straightforward notation has been devised for describing Burgers vectors. The notation can be understood with the aid of the fcc cell shown in Fig. 8-22. The length and direction of a Burgers vector are defined by a number and the direction indices of the vector. As an example, consider a Burgers vector which is parallel to a cube edge, or in the [[100]] direction. To be more specific, let it be the [010] direction shown in the figure. A Burgers vector in this direction, having its length equal to a cube edge, is designated as 1a [010]. The unit of length is  $a\sqrt{u^2+v^2+w^2}$ , where [uvw] are the direction indices and a is the lattice parameter. The 1 which appears in the notation 1a [010] indicates that the length of the Burgers vector is one unit. Suppose we have a Burgers vector along a face diagonal whose length equals the interatomic spacing. The direction of the vector is [011], as shown in Fig. 8-22. The unit of length is now the face diagonal or  $a\sqrt{2}$ , and the Burgers vector length is half this. Thus, the Burgers vector is denoted as a/2 [011] and it has a length of  $a\sqrt{2}/2$ . In the bcc structure, a Burgers vector along a cube diagonal, whose length is equal to the interatomic spacing in this direction, would be called a/2 [111]. The length of this vector is  $a\sqrt{3/2}$ .

A dislocation having a close-packed slip plane is shown in Fig. 8-23(a). The extra half plane, which forms the dislocation, terminates on the lower plane of the figure. The shaded atoms belong to the top plane. The dislocation line is not straight, but zigzags. This configuration applies to both the (I111) planes of a fee pructure or the base planes of a hep crystal. We shall consider the fee case. The Burgers vector b of the dislocation is shown and is denoted by a/2 [110]. Assume that a shear stress is placed on the specimen and the dislocation moves to the left (or the atoms on the left

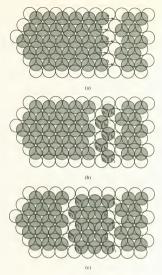


Fig. 8-23. Dissociation of a dislocation into two partial dislocations. (a) An edge dislocation having a close-packed slip plane. The extra half plane of atoms ends on the lower plane of atoms in the figure. (b) Slip can occur in two steps. The row of atoms shown has slipped by b<sub>1</sub>, creating two partial dislocations. (c) Creation of a stacking fault by a dissociated sideocation.

side move to the right). The atoms can move to the right in two ways; they can make a direct move of length b, or they can make the two smaller moves shown by vectors b, and b; in Fig. 8-23(b). In this figure, a row of atoms has already slipped by an amount b, and there are now two dislocations having Burgers vectors b, and b2, respectively. The original dislocation, b, has dissociated into two partial dislocations. The force diagrams in Fig. 8-19 show that the partial dislocations will repel each other, and additional slip will result in the configuration depicted in Fig. 8-23(c). The repulsive force diminishes as the distance between dislocations increases so that the two partial dislocations will both finally move in the same direction, under the impetus of the applied shear force.

Whether or not the dislocation will dissociate into partials can be determined from energy considerations. According to equation 8-16, the dislocation energy is proportional to b<sup>2</sup>. Thus, dissociation will occur if

$$b^2 > b_1^2 + b_2^2$$
 (8-20)

For the case illustrated in Fig. 8-23,  $\mathbf{b_1}$  is a/6 [ $\overline{1}2\overline{1}$ ] and  $\mathbf{b_2}$  is a/6 [ $\overline{2}11$ ]. The dislocation dissociation can be written as

$$\begin{array}{ccc}
\mathbf{b} & \mathbf{b}_1 & \mathbf{b}_2 \\
a/2[\overline{1}10] \to a/6[\overline{1}2\overline{1}] + a/6[\overline{2}11]
\end{array}$$
(8-21)

Equation 8-21 meets the condition specified by equation 8-20; therefore the energy of the crystal will be lowered if the dislocation dissociates. It does.

In Chapter 3 it was shown that the close-packed planes in a fcc crystal had the stacking sequence ABCABC.... This sequence is violated by the atoms in Fig. 8-23(c), which have slipped only by a distance b<sub>1</sub>. For example, let the lower plane in Fig. 8-23 be a B plane and the upper one be a C plane. The A plane lies below the B plane and is not shown. The stacking sequence for the portion of the crystal whose atoms have slipped by b<sub>1</sub> is ABCABABC.... The lack of a C plane in the region of the dislocation is called a stacking fault, and the energy associated with it is called the stacking fault energy. Stacking faults are associated with the base planes of hep crystals as well as the ([111]) planes of fcc solids.

Question

Question 9: Show that the dislocation dissociation reaction of equation 8-21 meets the condition of equation 8-20.

## **Q\_Q** Dislocation mobility

Our model associates plastic deformation with dislocation mobility. At this time it might help to summarize what has been covered and where the chapter is going from the point of view of dislocation mobility. We have found that single crystals of high purity exhibit permanent deformation at low shear stresses and that the deformation occurs as the result of dislocation slip. If deformation occurs at low shear stress, the dislocations in the solid are highly mobile and slip easily. Any process which hinders mobility increases the yield point. It was found that a small Burgers vector enhances mobility. Pinning sites, on the other hand, resist dislocation motion. A pinned dislocation could not move until the applied stress was sufficiently high to cause the operation of a source. This, in turn, resulted in an increase of dislocation density.

Section 8-10 will discuss methods by which one dislocation can reduce the mobility of another. These processes are particularly effective at high dislocation densities; therefore dislocation mobility (and the yield stress of the material) depends on dislocation density, among other things. This topic is followed by an explanation of how the dislocations can change slip planes, thereby leaving a slip plane in which motion is inhibited and entering one of easier slip. The dislocation mechanisms discussed up to this point permit an explanation of the phenomenon of work hardening, which is given. The effect of grain boundaries is then considered, and it will be shown that they reduce dislocation mobility and thereby increase the yield stress in accord with equation 4-3. The effect of intentionally introducing impurity pinning sites is then discussed briefly. This process, of course, also reduces dislocation mobility and increases yield stress. The chapter also reduces dislocation mobility and increases yield stress. The chapter

ends with a discussion of twinning (another deformation mechanism) and ductile fracture and plastic deformation of polymers. It is emphasized that dislocation mobility is controllable to a great extent, as should become clear from the discussion of work hardening. This control is commonly used to modify materials properties according to the needs of the user.

# 8\_10 Dislocation interactions

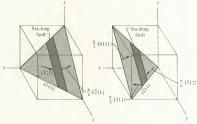
A dislocation moving along its slip plane will encounter other dislocations which intersect the slip plane at various angles. For dislocation motion to continue, the moving dislocation must slip past the others. Some difficulty is involved in this process, and the intersection of two dislocations diminishes the mobility of both. This section will discuss some of the possible interactions which result when dislocations meet.

Let us first consider what happens when two partial dislocations of the type shown in Fig. 8-23 meet. The slip planes are ((111)), and two of these are illustrated in Fig. 8-24. Two adjacent regions of a single crystal have been separated to make the drawing clearer. Partial dislocations are slipping on the (111) and (111) planes. They are shown in front of and behind the stacking fault region (heavily shaded areas). This is in accord with Fig. 8-23. The leading partial dislocations are on a collision course and will meet at the line where the (111) and (111) planes intersect. This line is the [011] direction. When they meet, a dislocation reaction can occur:

$$a/6[\overline{2}11] + a/6[211] \rightarrow a/3[011]$$
 (8-22)

The Burgers vectors involved in this reaction show that the reaction lowers the energy of the crystal. The vector a/3 [011] is shown in the sketch. It lies along a face diagonal of the unit cell. The dislocation formed by the combination of the two partials has its dislocation line along the [011] direction with Burgers vector a/3 [011]; therefore the dislocation line and Burgers vector are perpendicular. The dislocation is thus an edge dislocation and can slip on the (011) plane. This is not an easy slip plane; easy slip occurs on the (1111) in fee crystals. The reaction has produced an immo-

Fig. 8-24. The reaction of two partial dislocations to form a sessile dislocation. Two dissociated dislocations are shown on slip planes in an fec lattice. The Burgers sectors of the partials in front of the stacking faults are a [6[211] and a [6[211]. They come together on the line of intersection of the two slip planes and form a dislocation having a Burgers sector a [3[011] which is not oriented for slip.

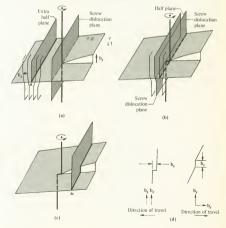


bilized (or sessile) dislocation because it is not favorably oriented for slip. The particular combination shown in Fig. 8-24 is called a Lomer-Cottrell lock. There are other combinations which form sessile dislocations

The two partials which met to form the sessile dislocation are not the only ones whose mobility is impeded by the reaction. Recall that the partial dislocations of Fig. 8-23 exerted repulsive forces upon each other. Because of this, the partial dislocations at the trailing edge of the stacking fault area are also immobilized. The planes shown in the figure are no longer available for slip, and dislocations which were using the plane will pile up behind the Lomer-Cottrell lock. The piled up dislocations will remain immobilized until the shear stress applied to the specimen is high enough to force the leading and trailing partials to recombine.

The intersection of two dislocations usually reduces the mobility of both. An example of intersecting dislocations is shown in Fig. 8-25, which represents a solid having an edge and a screw dislocation. The lightly

Fig. 425. Intersection of an edge and a serve dislocation. (a) 4 solid containing an edge and a serve dislocation. The dislocation lines are the heavy ones in the figure. The applied stress causes slip of both dislocations. (b) Slip has occurred and half the plane containing the serve dislocation is now the extra half plane for the edge dislocation. The screw dislocation when say log. (c) Further motion of the edge dislocation resters a log in its dislocation line. (d) The orientation of the dislocation lines and the Burgers vectors. The jog in the screw dislocation is not criented for slip.



shaded plane in Fig. 8-25 is the slip plane of the edge dislocation. The extra half plane associated with the edge dislocation is also shaded. The darkest shading belongs to a plane which contains the screw dislocation line and is parallel to the edge dislocation. This is labeled "screw dislocation plane." The heavy lines are the dislocation lines. Now let a shear stress be applied to the solid. The horizontal and vertical components of the stress are shown in the figure. The horizontal component causes the edge dislocation to slip, while the vertical component causes screw dislocation slip. Figure 8-25(b) shows the configuration when the edge dislocation is adjacent to the screw dislocation plane. A half plane has joined with the lower portion of the screw dislocation, and the upper part of the screw dislocation plane is now the extra half plane. As a result, the vertical dislocation line (screw dislocation) now has a horizontal jog in it. The length of the jog is equal to the Burgers vector of the edge dislocation, b... The logged dislocation line is one heavy line in Fig. 8-25(b). The vertical part of the line is a screw dislocation, while the jog is an edge dislocation. As slip progresses, the edge dislocation also becomes jogged, as shown in Fig. 8-25(c). The magnitude of this jog is b, and the jog has screw dislocation geometry. Both dislocation lines are shown as heavy lines in the figure. Now consider the effects of the jogs on the dislocation mobility. Figure 8-25(d) shows the jogged dislocations. The Burgers vector of a screw dislocation is parallel to the dislocation line, as shown. For an edge dislocation, the Burgers vector is perpendicular to the dislocation line. These are shown in the figure. For the jogged screw, the Burgers vectors are parallel. The orientation of the Burgers vector, dislocation line, and applied shear stress necessary for slip are shown in Fig. 8-6. Comparison of these conditions with those present in Fig. 8-25(d) shows that the jog in the screw dislocation, which has edge character, will not slip. The entire dislocation is immobilized as a result. Motion can occur if vacancies appear directly in front of the jog, in the direction of slip. The rate at which the dislocation slips will then be determined by the rate at which vacancies arrive in front of the jog. Both the number of vacancies in a crystal and the rate at which they move increase with temperature. We would therefore expect the mobility of jogged screw dislocations to be highly temperature dependent. The Burgers vectors associated with the jogged edge dislocation are also shown. These are oriented for slip, and the edge dislocation will continue to move. The presence of the jog slightly diminishes the ease with which slip occurs.

This section has discussed two typical types of dislocation intersections: there are many others. The examples discussed show that intersections can either immobilize a dislocation or just reduce its mobility, depending on the particular intersection being considered. It is apparent that dislocation mobility decreases as the density of dislocations increases because a density increase causes more intersections. This would imply that the yield stress of a material depends on its dislocation density. The dislocation density can be increased by plastically deforming a crystalline material. During plastic deformation, dislocations are coming out of the crystal at the surface, but they are also being created by dislocation sources. If they are created faster than they surface, the dislocation density increases. This is usually the case.

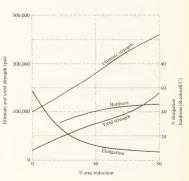
The reduction in the area of a specimen can be used as a measure of plastic deformation. The cross-sectional area of a specimen can be reduced by putting it through rollers under heavy pressure, deforming the specimen in tension, or using other methods. The percent reduction in cross-sectional area is defined as

% reduction = 
$$\frac{\text{initial area} - \text{final area}}{\text{initial area}} \times 100$$
 (8-23)

The effect of deformation on tensile strength, yield point, hardness, and elongation is shown in Fig. 8-26. It is seen that cold working a material (deforming it at a temperature in the neighborhood of room temperature or below) strengthens and hardens it. The amount of elongation which a specimen can sustain before fracture is diminished by cold working; that is, cold working makes it less ductile. All of these phenomena can be qualitatively explained by the reduction in dislocation mobility caused by increasing the dislocation density. Recall that hardness measures the resistance of a material to penetration by a small ball. Because the penetration involves permanent deformation, it depends on dislocation mobility.

The curves in Fig. 8-26 indicate how mechanical properties can be controlled by varying the dislocation density. The strengthening and hardening of materials due to cold working is referred to as work hardening and will be discussed in more detail in Section 8-12. The method is applicable to crystalline solids which are ductile and is therefore generally limited to metals. Ceramics contain dislocations and the slip mechanism is the same; however, the mobility of the dislocations usually is low at room temperature. This will be discussed in Section 8-13.

Fig. 8-26. The effect of cold working on the tensile properties of a stainless steel wire. (J. L. Everhart et al., NBS Circular C447, U.S. Department of Commerce, Washington, D.C., 1943.)



Question

Question 10: Energy is required to form a dislocation jog. Why? Where does the energy come from?

# 8-11 Climb and cross slip

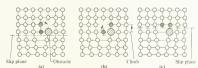
It is possible for dislocations to change their slip planes and thus avoid obstacles in their path. This, of course, increases their mobility. Cross slip and climb are two methods by which this can be done, and they will be discussed in this section. Climb applies to edge dislocations, while cross slip is a policable to serve dislocations.

An edge dislocation has its Burgers vector perpendicular to the dislocation line, and the slip plane contains the dislocation line. Because of the geometry, the slip direction cannot be altered but the slip plane can be changed by the mechanism shown in Fig. 8-27. An edge dislocation meeting an obstacle is shown in Fig. 8-27(a). The dislocation is assumed to be slipping to the right, and the obstacle acts as a pinning site. The slip plane is blocked, and the dislocation can continue its motion only if it changes slip planes. One method of accomplishing this is illustrated in the figure. A vacancy is shown near the extra half plane. In Fig. 8-27(b), one of the atoms in the half plane has moved to the site which contained the vacancy. We can say either that the atom has moved to the right or the vacancy has moved to the left. In reality the atom has moved, but the vacancy is of more interest to us and we therefore consider it to be moving. Figure 8-27(c) shows the configuration when the vacancy has moved to the bottom of the extra half plane. The figure shows only one plane in the crystal. If a similar vacancy migration occurred on every plane in the crystal which is parallel to the one illustrated, the dislocation line would be raised by an amount equal to the lattice spacing and a new slip plane would be established. The new slip plane can be seen in Fig. 8-27(c). Because it is not blocked by the obstacle, slip is unobstructed. The process is called dislocation climb, and it increases mobility.

The entire climb process requires the presence of moving vacancies. The discussion of vacancies in Chapter 4 showed that the number of them existing in a crystal increased with increasing temperature. Chapter 10 will consider vacancy motion as a diffusion process, and it will be shown that vacancies move faster as temperature increases. As a consequence, climb is a temperature-dependent process and is much more prevalent at high temperature shan at low ones. It is one of the important mechanisms that

Fig. 8-27. Climb of an edge dislocation. (a) An edge dislocation. (a) An edge dislocation encounters an obstacle on the slip plane that it cannot slip past. (b) A weacancy mores toward the slip plane. (c) The water of the slip plane collimb. The dislocation is no longer dislocation is no longer blocked by the obstacle.

#### Direction of dislocation motion →



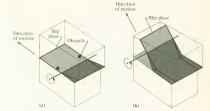


Fig. 8-28. Cross slip of a screw dislocation. (a) A screw dislocation encounters an obstacle on its slip plane. (b) It can avoid the obstacle by changing slip planes. The direction of dislocation motion also changes

takes place in the *annealing* process, which is covered in Chapter 9. It should be noted that we previously encountered a case in which dislocation motion depended on vacancies. This was the jogged screw dislocation of Section 8-10.

A screw dislocation can change its slip orientation more readily than an edge. Recall that a screw dislocation has its Burgers vector parallel to its dislocation line (see Fig. 4-27). Because of this, the possible slip planes of a screw dislocation inee do not be parallel as was required for the edge dislocation. Screw dislocations are capable of avoiding obstacles by a process called cross slip. A screw dislocation moving merrily along its slip plane is shown in Fig. 8-28(a). Obstacles in the slip plane are also shown. The obstacles can be avoided if the dislocation simply changes slip planes, as illustrated in Fig. 8-28(b). A screw dislocation can cross-slip from one easy slip planes on mother, provided that planes of easy slip intersect each other. The resolved shear stress is not the same on all easy slip planes, however. Generally the resolved shear stress on the plane of cross slip is lower than that on the slip plane containing the obstacle. As a result, cross slip occurs at higher stresses than normal slip but is not necessarily a high-temperature process.

The mechanism described implies that cross slip will occur most readily in crystals having a large number of slip systems. A crystal with a large number of slip systems has a greater probability of having one or more slip systems. Which a large resolved shear stress than a crystal with few slip systems. Consider the slip planes shown in Table 8-2. Recall that the first slip system shown for each structure is the easiest one and is often the only one operating at room temperature. The others generally become active at higher temperatures. From the table, it is seen that the fee and bee structures have four and six planes of easy slip, respectively, and these planes intersect. Thus, they meet the geometric requirements for cross slip. This is not true of the hep or Al<sub>2</sub>O<sub>3</sub> structures. The NaCl and CsCl structures also meet the cross-slip conditions. On the basis of structure only, we would not expect hep crystals to cross-slip at room temperature, although bec and fee crystals would. This affects the work-hardening characteristics of hep materials significantly, as described in Section 8-12.

Question

Question 11: A screw dislocation in an fcc crystal has its dislocation line in the [110] direction and is slipping on the (111) plane. If it cross-slips, what is the new slip plane?

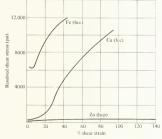
# 8-12 Work hardening of metals

Ductile materials show an increase in strength and hardness when they are plastically deformed. This is called work hardening or strain hardening and can be explained in a general manner. In this section, the stress-strain diagrams of metal single crystals will be considered, and the observed work-hardening behavior will be explained by the dislocation model.

The stress-strain diagrams of three single crystals made of high-purity metals are shown in Fig. 8-29. The elastic region has been omitted. These crystals were oriented such that slip initially occurred on a single family of easy slip planes; that is, the resolved shear stress was considerably larger on one slip system than on the others. The figure shows that the curves depend on crystal structure. In addition, they also depend on orientation. If the crystals are oriented such that slip begins simultaneously on several slip systems, the stress-strain curves will be somewhat different.

A schematic stress-strain curve appears in Fig. 8-30 with the elastic region omitted. The curve has been divided into three parts. Each of the stages shown represents a different behavior of the work-hardening rate. The work-hardening rate can be defined as the increase in stress necessary to produce an incremental increase in strain; it is the slope of the stress-strain curve. The term work hardening implies an increase in straing well as hardness; both result from plastic deformation. The behavior of all three metals shown in Fig. 8-30 can be explained in terms of Fig. 8-30 (however, it will be necessary to delete various portions of Fig. 8-30 for different crystal structures.

Fig. 8-29. Stress-strain diagrams of hish-partly metal single crystals at room temperature. The crystals were oriented so that slip began on a single slip system. [Zn. from W. Fahrenhorst and E. Schmid, Ann. Physis. 64454 (1930); Cu from J. Diehl, Z. Metallk. 47:331 (1956); Fe from B. Edmondson, Proc. Roy. Soc. 4764:176 (1961).]



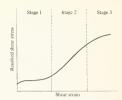


Fig. 8-30. Schematic diagram of the stress-strain curve for a workhardenable metal. Three stages of work hardening are shown.

## Face-centered cubic crystals

The stress-strain diagram for copper in Fig. 8-29 shows all three of the stages outlined in Fig. 8-30. Slip first begins on the favorably oriented slip system. The high purity of the metal assures that impurity pinning sites are fairly widely separated, and therefore the stress required for generating dislocations is initially low. Slip occurs easily under these conditions. This corresponds to stage 1. The work-hardening rate is practically constant, as shown by the linear region of the curve in stage 1. The stress required for increased strain rises very slowly. The slow rise is attributed to a small amount of dislocation interaction and jog formation. These do not occur to a great extent and a low work-hardening rate results. The dislocations on the favorably oriented slip planes thus experience a slowly increasing resistance to their motion.

As the end of stage 1 is approached, the applied stress is high enough so that the critical resolved shear stress is exceeded on a slip system (or systems) other than the one which is most favorably oriented. Table 8-2 shows that the easy slip systems in the fcc structure intersect each other; therefore dislocations moving on these slip systems will intersect. A number of the dislocations will be partial dislocations with stacking faults, and the conditions required for reactions that produce sessile dislocations. such as Lomer-Cottrell locks, are satisfied. These cause dislocation pileups on both slip systems. In addition, the occurrence of slip on intersecting slip systems causes dislocations to intersect and form jogs, which further reduces mobility. The presence of multiple active slip systems corresponds to stage 2 in Fig. 8-30. It is emphasized that all of the operating slip systems correspond to those having easy slip. These are the ((111)) [[110]] systems in the fcc structure, and there are 12 of them. Stage 2 is referred to as the linear work-hardening region because the stress-strain curve is practically linear here. The work-hardening rate is higher than that of stage 1 indicating that dislocation mobility is dropping rapidly as strain (and dislocation density) increases. This is as expected because dislocation interaction is the predominant mechanism in stage 2.

The material continues to work-harden in stage 3, but at a decreasing rate. Stage 3 is often referred to as the region of parabolic work hardening. The high stresses which are present in this region are sufficient to cause cross slip of screw dislocations and recombination of partial dislocations.

## Hexagonal close-packed crystals

The experimental data in Fig. 8-29 show that the zinc crystal remains in stage I throughout its deformation. The easy slip planes for this structure are the base planes, as shown in Table 8-2. Because the base planes do not intersect, slip does not occur on intersecting slip planes. It was precisely such intersections that explained stage 2 work hardening for the fee structure. Because these do not occur in the hcp case, the hcp crystals remain in stage I. As a result of the slip system configurations, hcp metals show very limited work hardening compared to fee metals. This is the first example that we have seen of a significant behavioral difference between the hcp and fee structures.

### Body-centered cubic crystals

The stress-strain curve for an iron single crystal appears in Fig. 8-29. The strain-hardening behavior of bcc crystals differs somewhat from that of fcc crystals. Partial dislocations do not form as readily in bcc materials. As a result, the interaction of partial dislocations to form sessile ones, and thus block slip planes, does not occur to a significant extent. There is an effect which tends to compensate for this, however. Table 8-2 shows that the bcc structure has a large number of slip systems, with some having easier slip than others. If several of the slip systems become active, dislocation intersection and jog formation will become more pronounced than they are in fcc crystals. Keh and Nakada have shown that the rate of stage 1 and stage 2 work hardening depends on the ratio of the number of dislocations utilizing the easiest slip system, ((110)) [[1117], to those on the next slip system, ((211)) [[111]]. The large number of possible slip systems means that the shape of the iron curve in Fig. 8-29 is very dependent on crystallographic orientation. The early appearance of stage 2 work hardening in bcc structures can probably be attributed to dislocation intersection. The large number of slip systems also facilitates cross slip of screw dislocations. Cross slip announces the arrival of stage 3 work hardening and generally occurs at lower strains in bcc crystals than in fcc ones.

#### Ouestion

Question 12: At the beginning of this section it was stated that the shape of the curves in Fig. 8-29 depended on the crystal orientation relative to the applied load. If the copper crystal was oriented so that slip occurred on more than one slip system initially, what changes would occur in the Cu stress-strain diagram?

# 8-13 Dislocation motion in ceramics

The slip mechanism applies to ceramics as well as metals; however, some differences exist due to structure and the requirement of electrical neutrality. An edge dislocation in an ionic crystal having the NaCl structure is

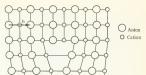


Fig. 8-31. Schematic diagram of an edge dislocation in a solid having the NaCl structure. The (100) plane is shown, and the Burgers vector is a[110].

shown in Fig. 8-31. The plane shown is the (110), while the dislocation line is in the [110] direction. This is an easy slip system according to Table 8-2. To preserve electrical neutrality, the extra half plane must consist of a half plane of cations and a half plane of anions. The Burgers vector is shown as the distance between anions, as can be verified by sketching the Burgers circuit. The magnitude of the vector is larger than that usually found in metals. The shear stress required either for slip or for dislocation generation increases with both G and b. Thus, the flow stress of a crystal having the NaCl structure will be somewhat higher than that of a metal if we take account only of the Burgers vector. Let us also consider the effect of shear modulus on slip. When doing this, we must distinguish between the interesting monovalent jonic compounds (such as the alkali halides) and the compounds of higher valence which have engineering significance (such as metallic oxides). Appendix B shows that the shear moduli of the metallic oxides are higher than those of the metals; consequently the flow stresses for these ceramics are generally higher than those for metals. The higher stresses required for permanent deformation increase the possibility of brittle fracture occurring before the flow stress is reached.

In some cases, a material will begin to deform plastically and then fail by brittle fracture, Consider MgO as an example. If a single crystal of MgO is stressed such that only a single slip system is active, it will deform as shown in Fig. 8-11. It should be noted that the data presented in the figure were taken at 1300°C, and the strain is much greater than would be observed at room temperature. This figure corresponds to stage 1 work hardening. Table 8-2 shows that the NaCl structure has intersecting planes of easy slip; therefore MgO might be expected to exhibit stage 2 and stage 3 work-hardening behavior. When slip begins on intersecting slip planes, however, the dislocations tend to form microcracks, Figure 8-32 shows a crack that has formed at the intersection of two slip bands in a single crystal of MgO. The cracks can propagate, and Fig. 8-33 illustrates this behavior. Several of the cracks in the figure are seen to originate at slip-band intersections. The propagation of microcracks, which is caused by the applied stress, results in brittle fracture. Thus, the plastic deformation of MgO is very limited. MgO crystals show larger deformations when loaded in compression rather than tension because this inhibits crack propagation. The data in Fig. 8-11 were taken for compressive loading. Tensile test data reveal that the amount of plastic deformation shown by a MgO single crystal depends on the treatment which the surface received prior to loading, again indicating a brittle fracture process,

Fig. 8-32. Formation of microcracks at the intersection of slip bands in a MgO single crystal. Magnification, 750×. (E. R. Parker in Mechanical Behavior of Crystalline Solids, NBS Monograph No. 59, U.S. Department of Commerce, Washington, D.C., 1963).



Fig. 8-33. Microcracks formed at slip-band intersections in MgO. Some crack propogation has occurred. Magnification, 187 ×. [R. J. Stokes, T. L. Johnson, and C. H. Li, Phil. Mag. 3:718 (1950)].



Aluminum oxide has a hexagonal structure and is capable of forming stacking faults just as the hexagonal metals do. Once again, however, the combination of large Burgers vectors and ionic forces severely limits dislocation mobility. As a result, brittle fracture is usually observed at room temperature.\*

The competition between brittle fracture and ductile deformation shown by these ceramics applies to crystalline solids in general. Solids with low dislocation mobility require high stresses before slip begins. If the stress required for slip exceeds the brittle fracture stress, brittle fracture will occur. In some cases a small amount of plastic deformation may occur, which is followed by brittle fracture. For MgO single crystals, for example, Figs. 8-32 and 8-33 show that some slip is required to form internal microracks.

#### Ouestion

Question 13: (a) Calculate the energy of 1 cm of a dislocation on an easy slip system in MgO (see Fig. 8-31). For MgO,  $G = 21.5 \times 10^6$  psi. Let the radius of the dislocation be  $5 \times 10^{-4}$  cm. (b) Do the same for copper. (c) Which is easier to form?

<sup>\*</sup> For a more detailed discussion of slip in Al<sub>2</sub>O<sub>3</sub>, see W. O. Kingery, *Introduction to Ceramics*, Wiley, New York, 1967, pp. 565-570.

# **8\_14** The effect of grain boundaries

The dislocation slip model was applied to single crystals in the previous sections. It must be modified somewhat when the effects of grain boundaries are included. Grain boundaries tend to decrease dislocation mobility, and polycrystals generally show higher strength and lower ductility than single crystals of the same substance. The reasons for this behavior will be discussed in this section.

The slip mechanism operates because of the geometric regularity of a crystal. Deviations from perfect crystal structure tend to reduce the mobility of dislocations, as was found in the cases of dislocation intersection and crystal impurities. Because a grain boundary is a surface at which two crystals of different orientation meet, the arrangement of the atoms in the region of a grain boundary deviates considerably from that found in a perfect crystal. We would therefore expect that boundaries are barriers to dislocation motion. Figure 8-34 illustrates the effect of a grain boundary on dislocations coming from a single dislocation source. The first dislocation encounters a barrier which it cannot surmount and is therefore immobilized. This dislocation then exerts a repulsive force on the next dislocation coming down the slip plane, and this one is also immobilized, etc. The grain boundary has caused a dislocation pile up. Such pile ups have often been observed. The electron micrograph in Fig. 5-5 is an example. The pile up of dislocations at the grain boundary is quite evident in the grain on the left side of the figure. Because grain boundaries diminish dislocation mobility, polycrystals are generally stronger and less ductile than single crystals.

The presence of the grain boundaries places a restriction on the manner in which a grain can deform. Consider Fig. 8-35, which shows a specimen having two grains. An applied stress is shown, together with those easy slip systems which first reach their critical resolved shear stress. If slip occurred on the slip systems shown, the two grains would separate. For

Fig. 8-34. Dislocation pile-up at a grain boundary. The grain boundary is an obstacle to slip. As the dislocations pile up, they exert repulsive forces on other dislocations in the slip plane. Figure 5-5 shows this phenomenon in a stainless steel specimen.



Fig. 8-35. Slip in a solid containing two grains. The dashed lines represent the planes on which easy slip would occur if these were single crystals. The presence of the grain boundary places restraints on the slip systems and only multiple slip can occur.



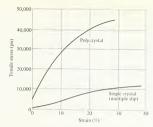


Fig. 8-36. Stress-strain curves of single crystal and polycrystalline copper. The single crystal is oriented for multiple slip. The polycrystal shows higher strength and a higher work-hardening rate. Neither curve shows stage 1 work hardening.

the grains to deform and still maintain the grain boundary, slip must occur on more than one slip system in each grain. As a consequence, slip will not begin when the most favorably oriented slip system reaches its critical resolved shear stress but must wait until multiple slip can begin. In our discussion of work-hardening, multiple slip marked the beginning of stage 2 deformation. Thus, polycrystals do not show stage 1 deformation. The difference in behavior between single crystals and polycrystals is shown in Fig. 8-36. The single crystal in this figure was oriented for multiple slip and does not show stage 1 behavior.

The geometric requirements for slip help explain why polycrystalline MgO is brittle at room temperature. Table 8-2 shows that the NaCl structure has two sets of slip systems, with slip being easiest on the first one listed. For polycrystalline MgO to deform plastically, it has been shown\* that both sets of slip systems must be operating. Only the easy slip systems operate at room temperature, and polycrystalline MgO is therefore brittle. It shows some ductile behavior at higher temperatures, as discussed in Chapter 9.

The above arguments lead us to expect that the yield point of a polycrystal will increase as the grain size decreases because the effect of grain boundaries will be more pronounced in a fine-grained microstructure. This trend is reflected in the Hall-Petch equation, which was introduced in Chapter 4 and is illustrated in Fig. 4-8. The Hall-Petch equation is

$$\sigma_{\text{yield}} = \sigma_{0_{\text{yield}}} + \frac{K}{\sqrt{d}}$$
(4-3)

Recall that  $\sigma_{0_{\text{yield}}}$  and K are constants, while d is the grain size. The form of this equation can be deduced from theory but will not be done here.†

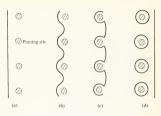
### Question

Question 14: Figure 8-36 shows that the rate of work-hardening during stage 2 deformation is higher for polycrystalline copper than for a single crystal oriented for multiple slip. Explain why.

† The derivation can be found in S. M. Edelglass, Engineering Materials Science, Ronald Press, New York, 1966, p. 387.

<sup>\*</sup> G. W. Groves and A. Kelly, Phil, Mag. 8: 877 (1963).

Fig. 8-37. Movement of a dislocation past a a row of pinning sites, (a) The dislocation approaches the spinning sites, (b) and (c) The pinned dislocation bows out as the resolved shear stress is increased, (d) If the stress becomes sufficiently high, the dislocation can slip through as shown. A dislocation loop remains around each phining site.



# 8-15 Effect of impurity particles

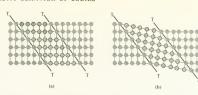
It may have occurred to the reader that dislocation mobility could be decreased by introducing pinning sites into a crystal in the form of impurities. A material having these sites would be stronger and less ductile, and mechanical properties could be controlled by controlling the impurity content. A dislocation encountering a number of such sites is shown schematically in Fig. 8-37(a). The dislocation is pinned at several points. It can pass through the pinning sites only by bowing out in a manner similar to that described in Section 8-6 for a Frank-Read source. According to equation 8-18, the applied shear stress required for dislocation bowing increases as the distance between pinning sites diminishes. This means that physical properties can be controlled by controlling the number and size of the pinning sites. The process of introducing a controlled impurity content into a material and then dispersing the impurities throughout the material is called dispersion hardening.

It is often possible to form a material when it is in a ductile state and then cause it to dispersion-harden through appropriate thermal processes. This provides a material which is easy to fabricate, yet one that has high strength after heat treatment. Aluminum-copper alloys are capable of this type of behavior. A meaningful discussion of dispersion-hardening requires the use of phase diagrams and the diffusion mechanism; therefore the subject will not be pursued here but will be taken up again in Chapter 12.

## 8-16 Twinning

Plastic deformation can occur by means of a process called twinning as well as by slip. The geometry of twinning is illustrated in Fig. 8-38. A region of perfect crystal appears in Fig. 8-38(a). The two diagonal planes labeled T-T are the twinning planes. The shaded atoms which lie outside the planes maintain their positions, relative to each other, during deformation. The cross-hatched atoms, which lie between the planes, will have their positions changed by twinning. Let a stress be applied on the twinning planes. One twin plane will move parallel to the other under the

Fig. 8-38. Deformation twinning. (a) A perfect crystal showing twin planes. (b) The region between the twin planes is distorted, causing deformation. Twinning causes a reorientation of the easy slip systems.



influence of the stress. The region between the twin planes will shear homogeneously, as shown in Fig. 8-38(b). The portion of the crystal outside of the twin planes is undistorted, but it has translated. For example, the sketches in Fig. 8-38 show the shaded atoms to the left of the twin planes at the same vertical positions before and after deformation. The shaded atoms in Fig. 8-38(b) which are to the right of the twin planes, however, are below those in Fig. 8-38(a). The geometry of Fig. 8-38(b) is such that the cross-hatched atoms are the mirror images of either group of shaded atoms, with the twin plane acting as the plane of reflection. This is the origin of the term twin.

Twinning has been observed in bee and fee crystals that were deformed at very low temperatures. It can also be found in bee crystals that have been subjected to very high strain rates at room temperature, such as occur in the process of explosive forming. Generally, it is not a significant deformation mechanism for the cubic metals unless one is concerned with the low-temperature region or fast forming techniques.

Twinning becomes more significant in the case of hep metals and is observed at room temperature. According to Table 8-2, there are only three slip systems available to hep materials at room temperature, and the only allowed slip planes are the base planes. It has been observed that twinning occurs on the (1012) plane in the [1011] direction in hep crystals. Twinning on these systems reorients the crystal region between the twin planes and can thus place the base planes of this region in an orientation that is more favorable for dislocation slip. The actual deformation produced by twinning is small, having a maximum of perhaps several percent for a ductlie hep crystal. The reorientation of the twinned region can significantly affect dislocation slip in hop metals, however.

# 8-17 Fracture of ductile materials

The fracture of ductile materials can be explained in terms of work-hardening coupled with crack nucleation and growth. No general theory is available which covers all cases, and the situation is more complex than for brittle fracture. In this section, the effect of work-hardening will be discussed first. This will be followed by two examples of crack nucleation, and then crack growth will be briefly covered. It is emphasized that the discussion of this section presents only a couple of examples of the ductile fracture mechanism. A number of others exist.

Consider a specimen subjected to a slowly increasing tensile load. When

the elastic limit is exceeded, the material begins to work-harden. Increasing the load increases the permanent elongation and simultaneously decreases the cross-sectional area. The strain is not quite uniform over the entire specimen: that is, some parts of the specimen will elongate more than others because specimens are not completely homogeneous. Let us consider what happens at one of these "weak" regions. The material in this region deforms more than the rest of the specimen; therefore it workhardens more. Its area is simultaneously reduced. If the rate of workhardening  $(d\sigma/d\epsilon)$  is areater than the rate at which the area decreases  $(-dA/d\epsilon)$ , the material can carry a greater load after deformation than it could before deformation took place. It is strengthened. The "weak" region has become a "strong" one and will no longer deform excessively. The entire process will then begin at the next weak region, etc. The net result of this is a specimen having fairly uniform deformation, although each increment of deformation may not have occurred uniformly. Now suppose that the rate of work-hardening is less than the rate at which the area is reduced. This can occur if the work-hardening rate decreases with strain, as in stage 3 of Fig. 8-30. The weak region becomes weaker as a result of the deformation and excessive elongation continues. The associated decrease in area leads to the formation of a neck in the specimen, as illustrated in Fig. 1-6. The necked region has a high dislocation density. and the material is subjected to a complex stress; the stress is no longer simple tension.

Cracks can nucleate in the necked region by several different processes. One of these can be explained by the dislocation pile up shown in Fig. 8-39(a). The dislocations are separated from each other because of the repulsive interaction forces. As the resolved shear stress on the slip plane increases, the dislocations come closer together. If the stress is high enough, a number of dislocations will coalesce to form a crack. This is illustrated in Fig. 8-39(b). Cracks can also form because of the presence of low-angle grain boundaries. Figure 8-40(a) shows the alignment of edge dislocations required to form the boundary. Slip can occur at one of the planes intersecting the boundary. If it does, a crack will be formed because of the misalignment [Fig. 8-40(b)]. These cracks have been observed. Figure

Fig. 8-39. Crack nucleation at a slip-plane obstacle. (a) Dislocation pile up at an obstacle. As the shear stress increases, the dislocations move closer to each other. (b) Adjacent dislocations form a crack. The figure shows a crack caused by three edge dislocations coming together.

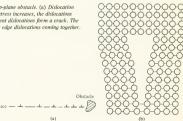


Fig. 8-40. Crack nucleation at a low-angle grain boundary. (a) Lowangle grain boundary. (b) Formation of a crack resulting from an active slip plane intersecting the boundary.





Fig. 8-41. The crack nucleation mechanism of Fig. 8-40 as observed in zinc. Magnification  $10 \times [J. J. Gilman, J. Metals 6:621 (1954) 1$ 

8-41 shows the creation of a crack in a single crystal of zinc by this mechanism.

Once a crack is formed, it can grow by serving as a region which annihilates dislocations. The crack can elongate by having dislocations, which are slipping, meet it. Crack propagation is along the slip plane for this mechanism. These cracks are often capable of penetrating grain boundaries. It is also possible for a number of cracks to coalesce. The necked region of a copper tensile specimen which has been cut open lengthwise is shown in Fig. 8-42. It is seen that internal cracks have developed. These cracks tend to coalesce; consequently one crack grows at the expense of the others. Crack growth finally results in failure.

### Question

Question 15: Ductile specimens that are stressed to failure in tension often fracture on planes that form an angle of about 45° with the applied load. Why?

# **8-18** Permanent deformation of polymers

Dislocation theory explains a great deal about the deformation of crystalline solids that are composed of atoms or small molecules but provides no



Fig. 8-42. Internal cracks in the necked region of a poly-crystalline specimen of high-purity copper. Magnification, 9 × .

[K. E. Puttick, Phil. Mag. 4: 964 (1959).]

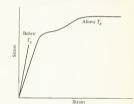
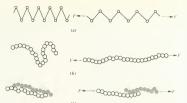


Fig. 8-43. Schematic stress-strain diagrams of two polymers. The polymer which is at a temperature below Γ<sub>g</sub> shows brittle fracture, while the one above Γ<sub>g</sub> exhibits permanent deformation.

help when dealing with amorphous substances or crystalline solids having very large molecules. Alternative mechanisms must be used to explain the behavior of polymers, as will be done briefly in this section.

Two schematic stress-strain diagrams are shown in Fig. 8-43. The first represents a material that is at a temperature above its glass transition temperature, such as polyethylene at room temperature, while the second material is below  $T_\theta$ . Both show elastic behavior at low stresses. The polymer which is above  $T_\theta$  shows permanent elongation, while the one below  $T_\theta$  exhibits brittle fracture. The deformation mechanisms are shown schematically in Fig. 8-44. Elastic behavior is caused primarily by bending carbon bonds in the polymer chains, as shown schematically in Fig. 8-44(a). This occurs for both specimens of Fig. 8-43. An applied tensile force can also cause bent or coiled polymer chains to straighten, as illustrated in Fig. 8-44(b). The deformation associated with chain straightening can cause either elastic or permanent deformation. In the case of

Fig. 8-4. Deformation modes of chain polymers. (a) An applied tensile force changes the bond angles of the chain backbone. Elongation is elastic. (b) The uncolling of chains also results in elongation. This behavior creatls in elongation. This behavior can be either elastic or plastic, depending on whether the chains call up again when the load is released. (c) Slipping between chains causes permanent elongation.



elastomers, the chains return to the coiled shape when the stress is removed; consequently the deformation is elastic. For chain polymers which are not elastomers, the mechanism causes permanent deformation. Figure 8-44(c) shows adjacent chains slipping past each other. The slip is caused by the breaking and reforming of secondary bonds between chains. These processes are highly temperature dependent, as will be discussed in Chapter 9.

The physical properties of a number of polymers at room temperature are given in Appendix C. The tabulated values can be taken as being typical for the given materials, but they are not exact. Polymer properties are very sensitive to parameters such as the amount of cross linking between chains, amount of crystallinity in the solid, density, degree of polymerization, etc. For example, the table in Appendix C lists polyethylene having three different densities. The highest density has the highest strength. This would be expected because high density implies that the chains are packed close together and are therefore held to each other by a larger number of secondary bonds than would be present in the low-density material. The density of polyethylene depends on the process used to make it. Thus, polymer properties depend both on the material being considered and on the manufacturing process used.

Amorphous polymers which are strained at temperatures above T. experience chain uncoiling. As the chains straighten out, they come into contact with other chains that are uncoiling, and the number of secondary bonds between chains increases. A greater number of bonds can be formed between straight chains than between coiled ones. Recall that a crystalline polymer has parallel chains which are bonded to each other. This would indicate that straining a polymer material beyond the elastic limit could increase the fraction of the material which is crystalline and would therefore increase strength and stiffness. This phenomenon has been observed both from stress-strain curves and from X-ray diffraction experiments. For example, the stress vs. elongation curves for rubber in Fig. 3-35 show that the slope of the curve increases as stress increases. Because slope is proportional to stiffness (or elastic modulus), it is seen that the material stiffens as it elongates. The increase in slope is attributed to crystallization, as confirmed by X-ray data. The effect is more pronounced for the unvulcanized rubber. This would be expected because cross-linking a polymer inhibits its ability to crystallize.

The stress vs. elongation curve for a nylon appears in Fig. 8-45 and

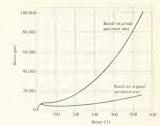


Fig. 8-45. The stress-strain diagram for nylon, made at a strain rate of 610%/min. The increasing stress is caused by crystallization. (F. A. McClintock and A. S. Argon, Mcchanical Behavior of Materials, Addison-Wesley, Reading, Mass, 1966.)

shows the same effect as the rubber curves. Once again, the increasing slope is attributed to crystallization. If Fig. 8-45 represented a metal, we would say that the metal has work-hardened due to dislocation interactions. In the case of a polymer, the cause of the increasing slope is completely different, although the result appears to be the same on the stress vs. strain curve.

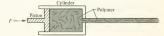
The crystallization phenomena can be used to our advantage by utilizing a drawing process, as illustrated in Fig. 8-46. An amorphous polymer at a temperature above  $T_g$  is in the cylinder. Force exerted on the piston causes the material to be extruded through the hole. The strain which occurs during extrusion causes the chains to align as shown in the figure. This process is useful in producing synthetic fibers and often yields fibers which are highly crystalline. In Chapter 12 we shall encounter an example in which a structural change in a metal is caused by strain.

It is often desirable to reduce the strength of polymers. Processes such as molding or extruding are easier when materials that flow readily are used. For this reason, plasticizers are often added to polymers. Their function is to reduce the bonding between chains and after the structure and properties accordingly. Plasticizers are usually cheaper than polymers; consequently their use reduces the cost of raw materials of a product, as well as making fabrication easier.

#### Question

Question 16: Figure 8-44(c) shows a polymer deformation mechanism in which chains slide past each other. (a) If the force F is large enough to initiate this mechanism, will the chains continue to slide past each other as long as F is applied to the polymer? (b) Would the total strain depend on the length of time that the stress was applied? (c) Explain.

Fig. 8-46. Extrusion of a polymer. The extrusion process tends to align the polymer chains and the extruded polymer is more crystalline than the unextruded.



# 8-19 Comments on ductile materials

Ductile materials are used in a vast number of engineering applications. Volumes have been written on the topic. This section will point out a few examples of how the ductile properties of materials can be utilized to the advantage of the engineer. It is by no means a comprehensive discussion.

There are a large number of applications in which it is desirable to deform a material and have it retain its deformed shape. A very simple example of this is bending an electric conductor (copper wire) to a desired shape and then using it. The wire has been permanently deformed in the process and has retained a useful shape. This also applies to the bending of sheet metal to form all sorts of useful devices. This bending can be done by hand-operated tools in small sheet metal shops, or it may use large presses, such as those which stamp out sections of automobile bodies. The materials are work-hardened by these forming processes. In many cases this has no particular significance, but in others the work-hardening becomes an important consideration.

Work-hardening strengthens a material but reduces its toughness. It is possible to deform a material and then remove the effects of work-hardening (lower the dislocation density) by heating it. This is called annealing and will be covered in Chapter 9. There is a limit to how much deformation a ductile material can withstand before fracturing. The limit can be greatly extended by first deforming the material then annealing it, deforming it more, etc. This procedure enables the fabricator to work with a soft, relatively weak material rather than with a work-hardened one. The forces required to shape soft materials are smaller than those needed for hard ones; consequently smaller equipment can be used. This applies to machining as well as bending. It is often desirable to work with a soft, weak material during fabrication and then strengthen it. Methods of doing this will be described in Chapter 12.

Ductile materials are often used to support loads. In these applications, it is usually necessary to keep the stresses below the yield point. The yield point of many materials can be changed by various processes which will be covered in Chapter 12. Increasing the yield point will generally decrease the toughness (and the ability of the material to withstand impact loads). Thus, the engineer must often decide how much of a decrease he can tolerate in one property in order to obtain an increase in another property. Such decisions are best made with a combination of experience and knowledge of what is physically occurring within the material.

# 8-20 Summary

The estimate of the theoretical shear strength of a crystalline material, which was made in Section 6-7, showed that the results obtained from a perfect crystal model did not agree with observed values. The model was modified to account for structural imperfections, and this chapter considered the effect of dislocations and grain boundaries.

A straightforward dislocation slip model was postulated early in the chapter. From the model, it was seen that plastic deformation depended on dislocation slip, and the relative ease with which a material could be permanently deformed depended on dislocation mobility. It was then found that mobility was a function of a number of factors. Consideration of pinning sites showed that they not only decreased mobility but created dislocation sources, and mobility therefore depended on crystal purity. The sources, in turn, produced dislocations if the applied stress was sufficiently high, thereby increasing the dislocation density. A high density further impeded mobility through dislocation intersections and locking mechanisms. Thus, mobility depended on dislocation density.

Cross slip and the recombination of partial dislocations tended to increase the mobility; however, these processes took place at high stresses. By the time they occurred, the dislocation density was already high and mobility was low. The work-hardening discussion showed that cross slip and recombination decreased the rate of work-hardening, although work-hardening continued. The work-hardening discussion also showed the importance of crystal structure and slip systems in ductile behavior; boc, fec, and hep crystals showed significant differences in behavior which were attributed solely to structure. Also, because of the structural differences, twinning was far more significant for the room-temperature deformation of hep materials than for fec or bee solids.

The effect of the type of bonding became significant when ceramic crystals were considered. These highly ionic crystals require equal numbers of cations and anions, resulting in dislocations which had large Burgers vectors. This, together with the high values of shear moduli that are characteristic of engineering ceramics, caused a low dislocation mobility. Thus, high stresses are required to initiate slip, and brittle fracture often occurs before these stress levels are reached.

The dislocation slip model has been successful in describing ductile behavior. The skeptical reader might still question their existence; however, images obtained with both electron and optical microscopes confirm their existence. A large body of data has been acquired from experiments with ductile materials, and the dislocation model does a fine job of explaining the data in a rational manner.

Dislocation theory is not valid for polymers because they are either amorphous or have very large molecules. The permanent deformation of these materials was shown to depend strongly on the secondary bonds between chains.

#### Problems

- 1 (a) A specimen is loaded in tension. As a result, shear stresses appear on the different planes of the crystal. The magnitude of the shear stress depends on the angle between the applied load and the shear direction being considered. At some value of  $\phi$  (Fig. 8-4) the shear force is a maximum. Find the value of  $\phi$  for which the maximum shear force occurs. (b) Solve part (a) but assume that the load is compressive rather than tensile.
- 2 Sketch the plane in Fig. 8-8 which has the positive and negative edge dislocations. (a) Apply a shear stress in the same direction as that shown in Fig. 8-8. Using sketches similar to Fig. 8-5, show that the two

- edge dislocations move apart when the shear stress is greater than  $\tau_{slip}$ . (b) What happens if the direction of the applied shear is reversed?
- 3 (a) A crystal of Fe contains an edge dislocation which has its dislocation line in the [110] direction. Sketch a (110) plane of the crystal. Include the dislocation in the sketch. (b) Show the magnitude and direction of the Burgers vector.
- 4 Dislocation densities of 10<sup>5</sup>-10<sup>12</sup> dislocations/cm<sup>2</sup> are typically observed in metals. (a) Consider a ductile specimen having 10<sup>8</sup> dislocations/cm<sup>2</sup>. If all of these emerge at the surface of a stressed specimen, what is the strain due to dislocation slip? Assume b = 3Å. (b) Does this explain the observed behavior of ductile materials? Why?
  - 5 Verify that Fig. 8-10 corresponds to a critical resolved shear stress of 26.2 psi.
- 6 The critical resolved shear stress of copper is given as 71 psi in Table 8-1. A tensile force in the [110] direction is applied to a high-purity single crystal of copper, (a) At what tensile stress will slip occur on the (111) [101] slip system? (b) Will slip begin simultaneously on more than one of the systems (111) [101], (111) [011], and (111) [110] for the tensile load direction given?
- 7 Equation 8-6 is an analytical expression for the critical resolved shear stress. Discuss whether or not τ<sub>er</sub> is strongly temperature dependent, according to this equation.
- 8 Table 8-2 shows that a number of slip systems can operate in the bcc structure. Find the ratio of  $\tau_{\rm cr}$  for a ((110)) [[T11]] slip system to  $\tau_{\rm cr}$  for a ((211)) [[T11]] slip system. (*Hint:* Use equation 8-6.)
- 9 A specimen of cold-worked molybdenum has a dislocation density of  $10^{11}$  dislocations/cm<sup>2</sup>. Find the strain energy per cubic centimeter of material.  $G = 19.3 \times 10^6$  psj.  $\Re$  can be taken as half the distance between neighboring dislocations, and  $\mu = 0.3$ . b can be found from Table 8-2. Assume that half the dislocations are edge and half are screw.
- 10 Figure 1-5(b) shows a stress-strain diagram for an aluminum alloy. (a) Consider a 1-in. cube of the alloy. From the curve, estimate the amount of work required to elongate a 1 in. cube by 10%. The load is tensile. (b) Part of this work is done against the elastic forces. The yield point in Fig. 1-5(c) is shown as 72,000 psi. From the curve, find the work necessary for the plastic deformation.
- 11 Consider a piece of copper containing impurities. The impurity atoms are substitutional; that is, an impurity atom replaces a copper atom in the copper crystal structure. (a) Let the copper contain 3 atomic % of impurities and assume that the impurity atoms cluster together in agglomerates of 100 atoms. What is the mean spacing between clusters of impurity atoms? (Hint: Assume the clusters of impurity atoms are symmetrically arranged and find the distance between neighboring clusters of impurity atoms.) (b) Let the clusters of impurity atoms act as pinning sites. If all of the dislocations in the copper are pinned, what is the flow stress of the material?
- 12 Equation 8-16 can be used as an approximation for the energy of a screw dislocation as well as an edge dislocation. Estimate the error

- involved in doing this at dislocation densities of 10<sup>6</sup> and 10<sup>9</sup> dislocations/cm<sup>2</sup>. Assume that the Burgers vector is 3 Å.
- 13 Sketch a block of material having two screw dislocations. Arrange the sketch so that the dislocations will annihilate each other when a shear stress is applied to the material. Show the direction of the shear stress that will cause annihilation.
- 14 An edge dislocation in iron has been immobilized by coming upon an obstacle which it cannot pass. A second edge dislocation having the same slip plane and Burgers vector approaches the first one. Both dislocations have easy slip systems. (a) If the resolved shear stress on the slip plane is 20,000 psi, what will be the equilibrium separation of the two dislocations?  $G = 12 \times 10^6$  psi, and  $\mu = 0.28$ . (b) If a third dislocation approaches the first two, will the distance between the first two increase or decrease? Explain why.
- 15 A low-angle grain boundary is shown in Fig. 8-20. If h is the distance between the dislocations and b is the Burgers vector, show that the misalignment angle between the two grains is  $\theta = b/h$ . (Recall that  $\tan \theta \approx \theta$  for small angles.)
- 16 Using Burgers vector notation, specify the Burgers vector for three of the easy slip systems in the bcc structure.
- 17 Assume that the dissociation reaction of equation 8-21 occurs. The slip plane of the dislocation is the (111) plane of aluminum, (a) What is the energy reduction per centimeter of the original dislocation? (b) Express this as a fraction of the energy per unit length of the original dislocation. (G = 3.9 x 10<sup>o</sup> psi.)
- 18 The jogged screw dislocation in Fig. 8-25 leaves a trail of vacancies when it slips. Explain why.
- 19 Sketch a solid having two perpendicular edge dislocations which do not intersect. Show the two half planes. Now let dislocation 1 slip toward dislocation 2, with dislocation 2 not moving. They will intersect and dislocation 1 will continue to move. (a) Sketch the jog created in dislocation 2 due to the intersection. (b) Is this jog oriented such that it will slip easily if dislocation 2 slips? Explain.
- 20 Dislocation intersections can act as pinning sites. Slip is observed in an aluminum specimen at a stress of 10,000 psi. If all of the dislocations are pinned by other dislocations, the flow stress will be determined by \( \tau\_{source} \). Assuming that every dislocation intersection acts as a pinning site, find the dislocation density in the aluminum specimen. \( G = 3.9 \times 10^6 \text{ psi and } m = 0.32. \)
- 21 (a) Figure 8-29 shows that stage 2 behavior begins in bcc crystals at low strain values. Why? (b) What effect would using polycrystals instead of single crystals have on the bcc and fcc curves in Fig. 8-29?
- 22 Sketch a schematic diagram of true stress vs. true strain for a material which shows *no* work-hardening.
- 23 Figure 8-29 shows a curve of resolved shear stress vs. strain for an iron single crystal. Suppose that slip occurred on slip systems which formed an angle of 45° with the applied tensile stress. (a) If the crystal contained a crack which was 0.00094 cm long, and the crack was perpendicular to the applied tensile stress, at what stress would brittle

fracture occur. (b) How much would the specimen be strained when the crack propagated?

- 24 Edge dislocations can bypass many obstacles by climbing over them. Can a grain boundary be bypassed by the climb mechanism? Explain.
- 25 Two parameters are commonly used to define the ductility of a test specimen. These are percent area reduction and percent elongation, where

% area reduction = 
$$\frac{\text{initial area} - \text{final area}}{\text{initial area}}$$
% elongation = 
$$\frac{\text{initial length} - \text{final length}}{\text{initial leneth}}$$

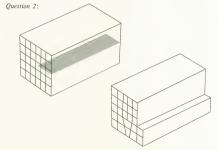
Initial refers to conditions in the unstressed specimen, while final refers to conditions at fracture. The value obtained for percent elongation depends on the length of the specimen tested, while percent area reduction does not, for ductile fracture. Explain why.

26 Three polymer deformation mechanisms are shown in Fig. 8-44, while Fig. 8-43 shows a polymer stress-strain diagram. Identify the deformation mechanism that corresponds to each region of the stress-strain diagram.

Answers

Question 1: From equation 8-4,  $\tau = \sigma \cos \phi \cos \psi = \sigma \sin \phi \cos \phi$ . The given directions yield the following relationships:

$$\cos \phi = \frac{a}{a\sqrt{3}} \qquad \sin \phi = \frac{a\sqrt{2}}{a\sqrt{3}}$$
$$\tau = (1000)\sqrt{\frac{2}{3}}\sqrt{\frac{1}{3}} = 471 \text{ psi}$$



Question 3:  $\tau_{cr} = \sigma_s \cos \psi \cos \phi$ .  $\phi$  is the angle between the [100] and [1 $\overline{10}$ ] direction, which is 45°:

$$\sigma_s = \frac{\tau_{cr}}{\cos \phi \cos \psi} = \frac{1900}{(0.707)^2} = 3800 \text{ psi}$$

Question 4: All three systems slip in the [[111]] directions; therefore  $b = a\sqrt{3/2}$ . To find d, use equation 5-6:

For ((110)) [[T11]],

$$\frac{d}{b} = \frac{a/\sqrt{3}}{a\sqrt{3}/2} = \frac{2}{3}$$

For ((211)) [[111]],

$$\frac{d}{b} = \frac{a/\sqrt{6}}{a\sqrt{3/2}} = \frac{2}{\sqrt{18}}$$

For ((321)) [[111]],

$$\frac{d}{b} = \frac{a/\sqrt{14}}{a\sqrt{3/2}} = \frac{2}{\sqrt{42}}$$

The ((110)) [[T11]] system has easiest slip, while the ((321)) [[T11]] system has least easy slip.

Question 5: Equation 8-8 uses the expression  $\tau = G\gamma$ , which is valid only for elastic behavior.

Question 6: (a)

$$\mathscr{E} = \frac{G\mathscr{L}b^2}{4\pi} \ln \frac{\mathscr{R}}{b}$$

The dislocation length is 1 cm. Therefore,

$$\mathscr{E} = \frac{(3.45 \times 10^{11}) (1) (4 \times 10^{-8})^2}{4\pi} \ln \frac{5 \times 10^{-5}}{4 \times 10^{-8}} = 31.3 \times 10^{-5} \text{ ergs/cm}$$

(b)

$$\mathcal{E} = (31.3 \times 10^{-5}) (6.24 \times 10^{11}) (4 \times 10^{-8}) = 7.8 \text{ eV}/4\text{Å}$$

Question 7: (a) The first part of the curve would be an elastic region. The second part would show permanent deformation and the slope of the σ-ε curve would be lower than in the elastic region. When all of the dislocations have emerged at the surface, the remaining perfect crystal will have a σ-ε diagram like that of a whisker (Fig. 7-4), (b) The ultimate tensile strength would be the same as the theoretical tensile strength and can be calculated from equation 7-19, (c) No.

Ouestion 8:

Question 9:  $b^2 > b_1^2 + b_2^2$ 

$$\left( \frac{a}{2} \sqrt{1^2 + 1^2 + 0^2} \right)^2 > \left( \frac{a}{6} \sqrt{1^2 + 2^2 + 1^2} \right)^2 + \left( \frac{a}{6} \sqrt{1^2 + 2^2 \cdot 1^2} \right)^2$$

$$\frac{4}{7} > \frac{1}{4}$$

and the condition is met.

- Question 10: The energy of a dislocation is proportional to its length. Because a jogged dislocation is longer than a straight one, it has more energy. The energy required to form a jog comes from the work done on the crystal by the applied shear stress.
- Question 11: The direction of the dislocation line remains the same. The (111) plane intersects the (111) plane and the line along which they intersect is the [110] direction. Thus, the new slip plane is (111).
- Question 12: Dislocation intersection would occur at lower values of strain; therefore stage 2 would appear at lower strain values. The rising portion of the stress-strain curve would shift to the left.

Question 13: (a)  $\mathcal{E}/l = Gb^2$  and  $\mathbf{b} = (2)(1.32 + 0.78) = 4.2 \text{ Å}$ :

$$\mathcal{E}/l = (21.5 \times 10^6) (6.89 \times 10^4) (4.2 \times 10^{-8})^2 = 3.1 \times 10^{-3} \text{ ergs/cm}$$

(b) For Cu with a (111) [1][0] slip system.

$$\mathcal{E}/l = (6.7 \times 10^6) (6.89 \times 10^4) (2.56 \times 10^{-8})^2 = 0.302 \times 10^{-3} \text{ ergs/cm}$$

- (c) The dislocation in copper is easier to form. It requires about 10 times as much energy to form a dislocation in MgO.
- Question 14: The rate of work-hardening depends on the rate at which dislocation mobility is decreased (rate with respect to strain). A large number of obstacles causes dislocation density to increase rapidly with strain, and grain boundaries are obstacles. Thus, the polycrystal will work-harden more rapidly.
- Question 15: According to equation 8-4, the resolved shear stress is greatest on planes at 45° to the applied load. Slip will occur most readily on slip systems having this orientation. Because cracks can grow by annihilating dislocations, they can grow on slip planes. If they grow by this mechanism, they should appear at 45° to the applied load.

Question 16: (a) Yes. (b) Yes. (c) If the force is large enough to cause the chains to slip once, it is large enough to make the process continue because chain sliding involves breaking and making secondary bonds. The bonds will break and remake at a rate, and this will determine the rate of deformation. The polymer will deform continuously while it is stressed, just as a liquid does. This region appears as a horizontal line on a stress-strain curve (see Fig. 8-43).



# Temperature on Plastic Behavior

IN CHAPTER 8 the hardness and strength of crystalline materials was shown to depend on dislocation mobility. Any phenomenon which hindered the motion of dislocations increased hardness and strength but decreased ductility, and vice versa. In this chapter we shall consider the effect which temperature has on dislocation motion. It will be shown that mobility increases with temperature and that physical properties change accordingly. The observed mobility increase will be explained by using the concept of a thermally activated process, and consideration of such processes in solids will show that dislocation pinning sites become less effective as temperature rises. Low temperature, on the other hand, reduces mobility and increases strength. This explains the tendency of materials to behave in a brittle manner at low temperature. The transition from ductile to brittle behavior is a significant design consideration, and the effect of both temperature and strain rate on the transition will be considered.

A work-hardened material can be restored to its pre-workhardened condition by annealing it. The annealing process consists of heating the material and holding it at an elevated temperature for a period of time. The dislocation density decreases as a result, and the material becomes more ductile but weaker. Annealing can be considered as roughly the inverse of work hardening. It is a thermally activated process. The three stages of annealing will be discussed. Placing loads on materials at high temperatures causes a competition between the work-hardening and annealing processes; both occur simultaneously. The result is that the material deforms continuously while loaded, and strain becomes dependent on time. This phenomenon is called creep and is a fundamental consideration in the design of devices for hightemperature use. Materials for such devices are usually selected on the basis of their creep resistance. The mechanisms which cause creep will be discussed.

The mechanical properties of polymers are highly temperature sensitive, and the sensitivity often exists in the neighborhood of room temperature. The atomic mechanisms which account for this temperature dependence are not the same as those which occur in metals and ceramics, although the results are very similar. The last part of the chapter deals with temperature sensitive polymer properties and the mechanisms which cause them.

### The observed effect of temperature on strength 9-1

In Chapter 8 it was shown that dislocation mobility depended on both the purity of the material and the dislocation density, at room temperature, We now introduce temperature as a variable, and mobility depends on three parameters. This section will be concerned with the experimentally observed effect of temperature on strength. This behavior will be qualitatively explained by the dislocation model. The explanation will then be refined in later sections. Our first task is to isolate the effects of temperature from those of impurities and dislocation density. We can minimize the effect of impurities by initially limiting the discussion to highpurity materials. Dislocation density can be dealt with by first considering the combined effect of both  $\rho$  and T on the flow stress of a material.

Figure 9-1 shows the results of a series of tests which were performed using high-purity iron polycrystals. The data were obtained by stressing a number of specimens at various temperatures. The dislocation densities of the specimens were measured before the tests began. The figure indicates that the yield point of iron is highly temperature sensitive in the region below room temperature, but this dependence becomes very weak between room temperature and 400°C. The effect of temperature can be separated from the dislocation density effect by considering flow stress as a function of temperature at constant p. The dashed vertical line in Fig. 9-1 represents a constant dislocation density (about 3 × 109/cm2 for the line selected). Points A, B, and C thus give values of yield stress as a

Fig. 9-1. The effect of both temperature and dislocation density on the vield strenath of high-purity polycrystalline iron. The grain size of all the specimens used in obtaining these data was approximately the same. [Adapted from D. J. Dingley and D. McLean, Acta Met. 15:855 (1967).1

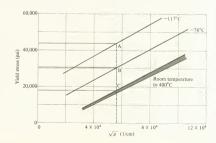
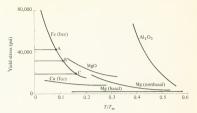


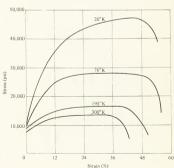
Fig. 9-2. Temperature dependence of the yield stress at constant dislocation density for several materials. The hehavior depends on the solid structure, Points A, B, and C on the Fe curve correspond to the same points in Fig. 9-1. (Data from A. H. Cottrell, The Mechanical Properties of Matter. Wiley, New York, 1964; and S. M. Copley and J. A. Pask in Materials Science Research. W. W. Kriegel and H. Palmour 111, eds., Vol. 3, Plenum Press, New York, 1966.)



function of temperature, at constant  $\rho$ . These points have been plotted in Fig. 9-2, and the Fe curve in this figure passes through them. The abscissa is  $TT_m$  rather than temperature alone. T is the absolute temperature at which the yield stress was measured, while  $T_m$  is the melting temperature. Iron, for example, melts at 1803°K. Room temperature would therefore correspond to a  $TT_m$  of 0.16. If a different dislocation density had been selected in Fig. 9-1, the Fe curve in Fig. 9-2 would shift upward or downward, but the shape of the curve would remain about the same because the data lines in Fig. 9-1 are almost parallel. The iron curve of Fig. 9-2 is typical of many bec metals. Their yield points become highly temperature sensitive at values of  $TT_m$ . Jess than about 0.15 or 0.2.

The fcc metals are represented by copper in Fig. 9-2. It is seen that the yield point is temperature dependent, but not to the extent of the bcc materials. The ultimate strength of fcc solids, however, shows a strong temperature effect, as illustrated in Fig. 9-3. The stress-strain curves are for

Fig 9-3. Stress-strain diagrams of commercial parity aluminum (1100–0) at various temperatures. The ultimate tensile stress is highly temperature sensitive, but the yield stress is not. (K. A. Warren and R. P. Reed, NBS Monograph 63, U.S. Department of Commerce, Washington, D.C., 1963.)



commercial-purity aluminum at various temperatures. The rapid decrease of the ultimate tensile strength with increasing temperature indicates that the work-hardening rate is temperature sensitive. The behavior of the hcp metals depends on whether or not secondary slip systems are active, as shown by the two curves for magnesium in Fig. 9-2. Two metal oxides are also shown, and a strong temperature dependence can be seen for these. The slopes of the metal oxide curves differ, and so does the structure of the solids. Structure is an important parameter when considering thermal effects.

The experimental data discussed so far provide sufficient information to determine which dislocation mechanisms are responsible for thermal effects. These will then be the ones to investigate further. Let us start with the critical resolved shear stress, as expressed by equation 8-6. This equation was considered in Problem 8-7, and the value of \( \tau\_{cr} \) was found to have the same temperature dependence as G. This dependence is not strong enough to explain the behavior shown in Fig. 9-3 and can be eliminated from further consideration. The next things to consider are the structural defects which influence dislocation mobility. Figure 9-2 shows that the behavior of hcp magnesium depends strongly on whether or not secondary slip systems are active. When slip on nonbasal planes occurs. dislocations intersect each other. The data show that the yield stress of hcp crystals is temperature sensitive only if dislocation intersection is permitted. Figure 9-3 shows that the work-hardening rate of fcc solids is temperature sensitive. Because work hardening depends on dislocation interactions and pinning sites, it would be reasonable to say that higher temperatures affect the pinning and interaction mechanisms in a manner that enhances dislocation mobility. The same conclusion can be drawn from the data for Fe in Fig. 9-1. Our explanation of thermal behavior must therefore be based upon pinning and interaction mechanisms. It appears that pinning sites become less effective and that dislocations intersections become easier at higher temperatures. The explanation for this behavior requires that we use the concept of thermal activation.

Question

Question 1: Figure 9-1 shows that the flow stress of high-purity iron is proportional to  $\sqrt{\rho}$ . This can be explained by assuming that dislocation intersections act as pinning sites and that the flow stress is proportional to  $\tau_{\text{towere}}$ . Explain the behavior shown by Fig. 9-1, using the above assumptions. Equation 8-18 and Example 8-2 should help.

# 9-2 Thermally activated processes

There are many thermally activated processes in nature. Perhaps the most familiar are chemical reactions. These will be considered here in order to convey the concepts of activated processes and activation energy. We shall first consider some experimental results and then discuss them from an atomic point of view. The concepts developed in this section will be applied to solids and dislocation pinning mechanisms in Section 9-3.

It is generally observed that the rate of chemical reactions increases with temperature. Consider two monatomic gaseous reactants that combine according to the reaction

$$A + B \rightarrow P$$
 (9-1)

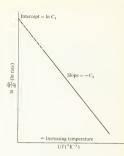


Fig. 9-4. A plot of the logarithm of the reaction rate vs. reciprocal temperature. The straight-line relationship is typical of chemical reactions and applies to many solid-state reactions as well.

The rate at which the reaction occurs is defined as the rate of change of the concentration of the reaction products. If we let p be the mole fraction of products, then rate = dp/dt. Suppose that A and B are mixed together and the reaction rate is measured. It is found that dp/dt depends on the temperature at which the reaction occurs. The relationship between rate and temperature can be found by plotting a curve such as that shown in Fig. 9-4. The natural logarithm of the reaction rate is plotted as a function of reciprocal temperature, 1/T, where T is in absolute temperature units. The linear relationship shown is very often found when reaction rate data are plotted in this manner and will prove to be quite significant. The curve in Fig. 9-4 can be described by the equation

$$\ln \text{ rate} = \ln C_1 - \frac{C_2}{T} \tag{9-2}$$

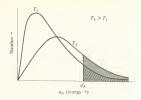
where  $C_1$  and  $C_2$  are constants. Equation 9-2 can be written as

$$rate = C_1 e^{-C_2/T} (9-3)$$

The exponential term in equation 9-3 gives us a good clue as to what is happening at the atomic level during the reaction. Assume that the two gaseous reactants, A and B, were placed in a container and allowed to react. The kinetic energy of the A particles can be represented by a distribution function similar to that discussed in section 4-1. The appropriate function is the Boltzmann distribution, which is shown in Fig. 9-5. It can be derived by the methods of statistical mechanics.\* The quantity q<sub>A</sub> is the kinetic energy of the particles of gas A. The ordinate, which is labeled "number", is related to the number of particles having particular energies. For example, the fraction of A particles having kinetic energies greater than some value, say q<sub>A</sub>, is equal to the area under the curve to the right

<sup>\*</sup> The derivation of the Boltzmann distribution can be found in most statistical metahanics texts. See, for example, E. Knuth, Statistical Thermodynamics, McGraw-Hill, New York. 1966.

Fig. 9-5. The Boltzmann energy distribution which describes the distribution of kinetic energy among the atoms of a monatomic gas. It also describes the distribution of eibrational energy among the atoms of a crystal. The shaded area to atoms of a crystal. The shaded area having energy greater than q.k. when the system is at temperature T<sub>1</sub>. The cross-hatched area is the same quantity for temperature T<sub>1</sub>.



of  $q'_A$ , divided by the total area under the curve. The effect of temperature on the Boltzmann distribution is shown; the curve becomes flatter and wider as the temperature increases. The cross-hatched and shaded areas represent those areas to the right of  $q'_A$  at temperatures  $T_1$  and  $T_2$ . It is seen that the fraction of high-energy atoms increases with temperature. In analytical term

$$\frac{n(q'_A)}{N_A} = e^{-q'_A/kT} \tag{9-4}$$

where

 $n(q_A') =$  number of A particles having kinetic energy greater than  $q_A'$ 

NA = total number of A particles in the container

k = Boltzmann's constant

Equation 9-4 comes from the mathematics of the Boltzmann distribution, which we have not done. The Boltzmann distribution also describes gas B; therefore

$$\frac{n(q'_B)}{N_B} = e^{-q'_B/kT}$$
(9-5)

We can now write an expression which describes the rate at which highenergy A and B particles collide with each other. Let  $C_3$  be the total number of collisions per second that occur between all A and B particles. The number of collisions per second between high-energy A and B particles will then be proportional to  $C_3$  and to the number of high-energy A and B particles in the container, which is  $n(q_3)$  and  $n(q_3)$ :

Collision rate of high-energy A and B particles

$$= C_3[n(q'_A)n(q'_B)] = C_4[e^{-q'_A/kT}e^{-q'_B/kT}] = C_4e^{-q/kT}$$
(9-6)

where  $C_4$  is a constant which includes the total collision rate,  $C_3$ , while  $q = q'_A + q'_B$ .

Comparison of equations 9-3 and 9-6 reveals that they are the same if  $C_2 = q/k$  and  $C_1 = C_4$ . Equation 9-3 came from experimental data, while 9-6 came from considering collisions between reactants having high



Fig. 9-6. Sketch illustrating the activation energy. The reactant must surmount the energy barrier in order to form the reaction products.

kinetic energies. We can therefore conclude that the reaction  $A+B\to P$  occurs only when A and B particles, which have a total kinetic energy greater than q, collide. The energy q is a constant for a particular reaction and can be found from the slope of the curve in Fig. 9-4. Collisions between less energetic particles do not cause reaction. The quantity q is called the activation energy (per particle). Its magnitude depends on the reaction being considered. The activation mechanism is described schematically by Fig. 9-6. The diagram shows that the reactions are not higher energy state than the products, implying that the reaction is exothermic. To react, however, the reactants must surmount an energy barrier whose height is equal to the activation energy. The energy to surmount the barrier comes from the kinetic energy of the reacting particles, and the reaction is therefore called a thermally activated reaction.

As an example of the activation energy concept, consider hydrogen and oxygen coexisting in a container at room temperature. The reaction of these elements to form water is so slow as to be imperceptible. As the temperature increases, however, the kinetic energy of the gases increase and more collisions occur per unit time in which the colliding particles possess the activation energy. The reaction rate increases as a result. At high temperatures, explosion results. This is not a recommended laboratory experiment.

Equation 9-6 was written by Arrhenius, a Swedish chemist, in the latter part of the nineteenth century. The form that he used requires that we multiply both q and k by Avogadro's number. The result is

$$Rate = Ce^{-Q/RT}$$
 (9-7)

where Q is the activation energy per mole and R is the universal gas constant per mole. Equation 9-7 is called the Arrhenius equation and is one of the fundamental equations of chemical kinetics.

### Ouestion

Question 2: In television westerns, the hero is sometimes required to transport a bottle of nitroglycerine across the desert. A great commotion is made about keeping the nitro cool, out of the sun, and not jarring it during the trip. Nitroglycerine decomposes into several products at an explosive rate. What do the above-mentioned preparations tell about the activation energy of the nitroglycerine decomposition reaction?

# **9\_3** Thermally activated processes in solids

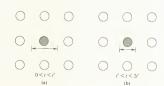
The gas atoms of Section 9-2 moved randomly within the container, and the distribution of kinetic energy among the atoms was governed by the Boltzmann distribution. A solid behaves somewhat similarly. The atoms in the solid are also in motion; however, their motion is vibrational. The atoms oscillate about their equilibrium positions. If energy is added to the solid, the temperature of the solid rises and the amplitudes of the oscillations increase. An energy of oscillation is associated with each atom in the solid just as a kinetic energy was associated with each gas atom. The energies of the lattice atoms are not all the same; the total vibrational energy of the solid is distributed among the atoms in accordance with the Boltzmann distribution. This statement must be modified for very low temperatures because certain quantum effects must then be considered. but we shall be working with temperatures above this range. Thus, Fig. 9-5 describes the distribution of energy among the atoms of the solid. The fraction of atoms in the solid having energies greater than some value, say q, can be written as

$$\frac{n(q)}{N} = e^{-q/kT}$$
(9-8)

where n(q) is the number of atoms whose oscillatory energy is greater than q, and N is the number of atoms in the solid.

It is becoming apparent that q will be an activation energy associated with some rate process in the solid. To make this application, we must consider the energy distribution from a somewhat different point of view. The pertinent question is, "If we could watch a single atom for a period of time, what is the probability that the atom would have an energy greater than q at some instant during the time period?" As the first step towards answering this, suppose that we pick one atom within the crystal to observe. The probability that this atom has an energy greater than q at any given instant is given by equation 9-8, because this probability is exactly equal to n(q)/N. The energies of the individual atoms are constantly changing but in such a way that the distribution of Fig. 9-5 is maintained. The energy of an atom changes with time because it interacts with neighboring atoms in the solid through the vibrational motion. For example, let the shaded atom in Fig. 9-7 be the one that we are observing and let the observation begin at time zero (t = 0). When first observed, it

Fig. 9-7. Schematic diagrams showing the variation of the vibrational amplitude (or vibrational energy) of a single atom in a crystal with time. The amplitude is shown by the arrows. (a) and (b) represent two different energy states. The atom resides in each of these states for a time t'.



is vibrating with the amplitude shown in Fig. 9-7(a). The vibrational energy is a function of the amplitude. The atom will retain the amplitude shown in Fig. 9-7(a) for a period of time, say t', during which it interacts with its neighbors. At the end of one time period the energy of the atom will have changed due to interaction with its neighbors, and its new vibration amplitude is shown in Fig. 9-7(b). Our model for vibrating motion requires that the energy of the atom remain constant for a period t', after which it changes and maintains the second energy for a period t'. etc. According to this model, the number of energy states that an atom passes through in 1 sec is 1/t', where t' is expressed in seconds. The probability that the atom which we are observing has an energy greater than a in a 1-sec time interval is then equal to the probability that the energy is greater than a in any one particular energy state  $(e^{-q/kT})$  times the number of states which it exists in per second (1/t'). The quantity 1/t' is related to the frequency at which the atom vibrates. It is reasonable to assume that the energy state of the atom changes once during a complete oscillation. Making this assumption, 1/t' is just equal to the vibration frequency. Thus,

Probability that an atom has energy greater than q during a 1-sec time

interval = 
$$\frac{1}{t'}e^{-q/kT} = ve^{-q/kT}$$
 (9-9)

where v is the frequency in cycles (or oscillations) per second. The frequency can be calculated for various materials, but the method of doing this is beyond the scope of the book.\*

### Example 9-1

The atoms of a particular lattice vibrate at 10<sup>12</sup> cycles/sec. What is the average length of time that elapses between instants when the atom has a vibrational energy of 1 eV or greater?

- (a) At 300°K
- (b) At 1000°K
  - (a) Probability of an atom having 1 eV or greater in a 1-sec interval

$$= ve^{-q/kT} = 10^{12}e^{-1/(8.6 \times 10^{-5})(300)} = 10^{12}e^{-38.8}$$

$$= 10^{12}10^{-38.8/2.3} = 1.32 \times 10^{-5}$$

The atom has an energy of 1 eV or greater  $1.32 \times 10^{-5}$  times/sec, on the average. Therefore,

Time interval = 
$$\frac{1}{1.32 \times 10^{-5}}$$
 = 7.57 × 10<sup>4</sup> sec = 21 hr

(b) Probability of an atom having 1 eV or greater in a 1-sec interval =  $ve^{-q/kT} = 10^{12}e^{-1/(8.6 \times 10^{-5})(1000)} = 3.16 \times 10^6$ 

Time interval = 
$$\frac{1}{3.16 \times 10^6}$$
 = 3.17 × 10<sup>-7</sup> sec

<sup>\*</sup> The derivation appears in most basic texts on solid-state physics. See, for example, C. Kittel, Introduction to Solid State Physics, 2nd ed., Wiley, New York, 1956, Ch. 6.

Now suppose that an atom in a solid can undergo some process if it has sufficient energy. By sufficient it is meant that the atom has any energy greater than q. The rate at which this process occurs would then depend on the terms on the right-hand side of equation 9-9. In effect, the process has an actitation energy, q, and shows the same sort of temperature dependence as the chemical reaction rates of Section 9-2. The results of Example 9-1 show that the rate at which the process occurs is very dependent on temperature. We shall now discuss the dislocation pinning processes and consider how the inverse process (unpinning) can be considered as thermally activated.

### Jog formation

The formation of jogs by intersecting dislocations was discussed in Chapter 8, and it was found that energy was required for jog formation. The magnitude of this energy can be estimated from equation 8-16. The length of the jog which is created in one dislocation equals the Burgers vector of the dislocation which intersected it, thus determining the value of  $\mathcal{L}$ . The jog is formed in the region of a dislocation core, and the energy to form a unit length of dislocation in this region is less than that required in a region which is undistorted. In metals, it turns out that energies required for jog formation range from a fraction of an electron volt to several electron volts.

The energy required to form jogs can come from the oscillation energy of the atoms. If this happens, jog formation is said to be thermally activated. Formation of thermally activated jogs requires that the atoms at the dislocation intersections have thermal energies large enough to form the jogs. It was shown that the time required for an atom to achieve a 1 eV (or greater) energy state at 300°K was about 1 day (Example 9-1). Thus, the rate of thermally activated jog formation at room temperature would be extremely low for most metals. As temperature increases, the rate of thermally activated jog formation increases. Jog formation does not depend entirely on thermal energy, however. Both the work done by the shear force and the thermal energy make contributions. As the temperature increases, the fraction of the energy coming from the vibrational motion increases; consequently dislocation intersections can occur at lower shear stresses. Thus, the mobility of the dislocations is increased as temperature increases because jog formation can occur at lower stress levels.

### Vacancy motion

Climb enables edge dislocations to bypass obstacles, as discussed in Chapter 8. It was seen that the rate at which climb occurred depended on both the number of vacancies in the crystal and the rate at which they moved. The motion of some jogged dislocations also depends on vacancy motion. The movement of vacancies will now be considered as a thermally activated process.

A plane of atoms having a vacancy is shown in Fig. 9-8(a). Consider what occurs when the shaded atom moves into the vacancy (this is the equivalent of the vacancy moving to the left). As the atom starts to move to the right, the net bonding force on the atom is to the left due to the

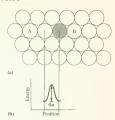


Fig. 9-8. The activation energy required to move an atom into a vacant site. (a) A plane of atoms with a vacancy, (b) The potential energy of the shaded atom as a function of position. The atom can move to the vacant site if it can overcome the energy barrier. The barrier helght is  $g_m$ , which is the activation energy for vacancy motion.

arrangement of the other atoms in its vicinity. The shaded atom has a nearest neighbor to its left but not to its right. Thus, the potential energy (or bond energy) of the shaded atom increases as the atom moves to the right. When the shaded atom moves beyond the midpoint between atoms A and B, the net force on it is to the right. Further movement to the right will decrease its potential energy. This is shown schematically in Fig. 9-8(b), where potential energy is plotted as a function of position. The potential energy of the atom is the same at both lattice positions; however, it must surmount an energy barrier in order to move from one to the other. According to the Boltzmann distribution, the probability that the atom has sufficient energy, during a period t', to overcome the energy barrier is equal to  $e^{-q_m/kT}$ , where  $q_m$  is the activation energy for vacancy motion. There is a second condition that must be fulfilled if motion is to occur; the energetic atom must have a vacancy next to it. According to Section 4-7, the probability of this happening is  $e^{-q_v/kT}$ , where  $q_v$  is the energy required to form a vacancy. The probability of both conditions being met is the product of the probability of each:

Probability of an atom moving into a vacancy during a period t'  $= e^{-(q_m + q_v)/kT} = e^{-q_g/kT}$ (9-10)

where  $q_s$  is called the *activation energy for self-diffusion*. The number of movements made per unit time by the vacancy (rate at which it moves) can be expressed as

Rate of vacancy movement = 
$$ve^{-q_s/kT}$$
 (9-11)

The magnitude of  $q_i$  is generally of the order of  $1 eV_i$  although it varies with different materials. Vacancy motion is a thermally activated process; therefore the rate at which dislocations climb over obstacles increases with rising temperature. Once again, dislocation mobility goes up with temperature. Climb is thermally activated, as is the motion of some jogged dislocations.

Cross slip and recombination of partial dislocations

Cross slip enables screw dislocation to bypass obstacles, as previously dis-

cussed. Screw dislocations dissociate into partials just as edge dislocations do. To cross-slip, the partials must recombine. The energy required for recombination comes both from the work done by the applied stress and from the thermal energy.

Thermal energy alone cannot move a dislocation because the thermal motion is incoherent. By this it is meant that all of the atoms on a dislocation line will not move in the same direction at the same time: the thermal motion is random. In the case of pinning sites or dislocation intersections, synchronized motion of many atoms is not required to unpin a dislocation. It is possible, however, for thermal energy to aid in the recombination of two partial dislocations at a single point. Once this is done, the remainder of the two partials can recombine more easily, with the necessary work being supplied by the shear force. The mechanism by which this occurs will not be discussed here.\*

The effect of temperature on dislocation mobility can be attributed to the thermal energy aiding the applied shear stress in overcoming the barriers which inhibit dislocation motion. The critical resolved shear stress is not highly temperature dependent; however, the processes which cause strain-hardening are strongly influenced by temperature. A material will work-harden at high temperature if the work-hardening processes occur at a faster rate than the unpinning processes just discussed. As a result, high-temperature behavior is the result of two different sets of processes, one of which hardens the material while the other softens it

### Question

Ouestion 3: Equation 4-5 gives the number of vacancies in a crystal when the crystal is at equilibrium. Using the Boltzmann distribution, explain what this equation means and why you would expect it to have this form

# **Q\_4** Effect of strain rate

Thermally activated processes are time dependent, and the behavior of materials consequently depends on whether or not these processes have sufficient time to function. An atom which participates in a thermally activated process must be in a high-energy state before the process will occur, and a finite time will elapse before it acquires the necessary energy. If a specimen is stressed slowly, the atoms participating in thermally activated processes will pass through many energy states while the stress is increased by a small increment. Some of these will be high-energy states. and the effect of thermal activation will be significant. A rapid application of stress, however, will result in rapid strain. If the process is very fast, the thermally activated mechanisms will not have sufficient time to function. Thus, the plastic behavior of materials depends on strain rate as well as temperature.

Figure 9-9 shows several stress-strain curves for mild steel at room temperature. The curves represent different strain rates and show that behavior is strongly influenced by strain rate. The stress-strain curve is

<sup>\*</sup> A discussion of the thermally activated recombination of partial dislocations can be found in R. E. Reed-Hill, Physical Metalluray Principles, Van Nostrand, Princeton, N.J., 1964, p. 587.

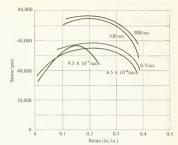


Fig. 9-9. Stress-strain diagrams for mild steel specimens which were tested at different strain rates. The strain rate used for each specimen is shown. All tests were made at room temperature. [A. Manjoine, J. Appl. Mech. 66:215 (1944).]

raised as the strain rate is increased. Comparison of this figure with Fig. 9-3 shows that increasing the strain rate has the same effect as decreasing the temperature. The material shows higher strength characteristics when a load is applied quickly, such as in an impact, than when it is loaded slowly. The advantages of this are obvious; however, certain disadvantages also appear. If the yield strength rises to too high a level, the material becomes subject to brittle fracture; it undergoes a change in the fracture mode.

### Question

Question 4: Would you expect Young's modulus to depend on strain rate?
Why?

# 9-5 The ductile to brittle transition

The increase in the yield stress associated with low temperature or high strain rate can result in a material changing its mode of fracture from ductile to brittle, and this can be very significant when selecting materials to do a particular job. The transition can be qualitatively explained with the aid of Fig. 9-10. Both the brittle fracture stress and the yield stress are plotted as a function of temperature (or strain rate). The brittle fracture stress, as plotted, assumes a particular crack size. The curve rises slightly to the left because surface energy increases as temperature decreases. The yield stress curve shows a strong temperature (or strain rate) dependence, such as that exhibited by bcc metals and metal oxide ceramics in Fig. 9-2. The two curves intersect, and a vertical line has been drawn through the intersection. If a material is stressed at a temperature or strain rate which is to the right of this line, it will reach its yield point before it reaches the brittle fracture stress and will undergo some plastic deformation prior to fracture. Conversely, applying a stress under conditions which lie to the left of the line will result in brittle fracture. The unshaded region in the neighborhood of the line is the region in which a transition from ductile to brittle behavior occurs. If the curves of yield stress and brittle fracture



Fig. 9-10. Schematic diagram showing the brittle fracture and yield stresses of a material. The manner in which a material fractures depends on which of these occurs at a lower stress.



-100

Temperature (°C)

+100

Fig. 9-11. Tensile test results for a number of low-carbon steel specimens at various temperatures. All tests were made at low strain rates. A rapid change in area reduction occurs between —175 and —220°C. This is the ductile to brittle transition region. [A. S. Edlin and S. C. Collins, J. Appl. Phys. 22:1266 (1951).]

stress do not intersect, there is no ductile to brittle transition. The data of Fig. 9-2 show that the yield point of fice materials is not highly temperature sensitive. The yield stress curves for these materials generally lie below the brittle fracture stress curves, and the fcc materials do not usually experience the transition.

The effect of temperature alone on the ductile to brittle transition is shown in Fig. 9-11. A number of specimens of low-carbon steel were loaded in tension at a very low strain rate. Each specimen was tested at a different temperature. The reduction in the cross-sectional area at the time of fracture was recorded, together with the yield stress or fracture stress (whichever came first). Figure 9-11 displays the results. The area reduction falls rapidly over the temperature range between –175 and –220°C; indicating that the fracture mode is changing from ductile to brittle. The temperature range over which the rapid change occurs is called the transition temperature region.

Increasing the strain rate is equivalent to lowering the temperature; therefore we might expect that materials which are ductile when strained slowly at a given temperature will behave in a brittle manner when subjected to high strain rates. This is observed. High strain rates can be achieved in impact-testing machines such as that described in Section 1-5 (see Fig.

40 20 0 20 40 60 Temperature CO

Fig. 9-12. The results of impact tests on notched specimens of low-carbon steel. The ductile to brittle transition region ranges from 0 to 20°C. Impact loads raise the transition temperature. (G. C. Smith in Advances in Materials, P. A. Rottenbury, ed., Pergamon Press, New York, 1964)

1-10). The effect of fast loading can be demonstrated by impact-testing a number of specimens at different temperatures and measuring the energy required to break each specimen. Figure 9-12 shows the results obtained from this procedure, using low-carbon steel specimens. The transition region is somewhat below room temperature. Comparison of Figs. 9-11 and 9-12 shows that impact loading raises the transition temperature. In this set of tests, a standard-sized notch was cut in each specimen prior to testing. The effect of the notch is twofold. First, the stresses in the notched region are not the simple tensile, compressive, or shear stresses we have so far considered. They are more complex, and the notch shape influences the exact nature of these stresses. The data obtained from an impact test depend on the material tested, the specimen size, the shape of the notch, and the type of impact-testing machine used. Specimen sizes, notch shapes, and testing machines have been standardized. The ductile to brittle transition temperature depends on all of the parameters which affect both dislocation mobility and propagation of brittle cracks. These include purity, grain size, notch shape, and strain rate.

160

From a design point of view, the ductile to brittle transition is hazardous. Catastrophic failures have occurred because of it. A dramatic example of one such failure is shown in Fig. 7-17.

### Ouestion

Question 5: Several standard notch shapes are used for impact testing.

What is the effect of notch shape on the ductile to brittle transition temperature of a material?

## 9-6 Annealing

Annealing is a process which softens a material and makes it more ductile but reduces its strength; the effects of annealing are the opposite of work hardening. The process consists of heating a material to a predetermined temperature, maintaining it at that temperature for a period of time, and then cooling it. The change in properties is attributed to a reduction in dislocation density. This section will discuss the experimental observation of annealing and will qualitatively present the mechanisms which are involved.

Work hardening increases the dislocation density of a solid and consequently increases the energy of the solid. When a work-hardened material is heated, it is found that the solid releases energy and simultaneously reduces its dislocation density. In addition, its grain structure may change Experiments have been performed in which cold-worked specimens were heated, and the rate at which energy was released by them was measured as a function of temperature. The results of such an experiment are shown schematically in Fig. 9-13. The exact shape of the curve depends on the material used, the degree to which it has been cold-worked, and the rate at which the specimen is heated. The features of Fig. 9-13 that are of most interest to us are the two humps, which indicate a release of energy in two different temperature ranges. If a specimen is cooled and inspected after it has passed the first hump, it is observed that the dislocation density has diminished somewhat and the material has softened a bit. The grain structure is unchanged. Similar observation after the specimen has passed beyond the second hump shows that the dislocation density is substantially lower and the grain structure has changed. A large change also occurs in the physical properties. The process which causes the first peak is called recovery, while the process associated with the second peak is called recrystallization. At still higher temperatures, arain arouth occurs. These three phenomena are all included in annealing, and each will be discussed separately. The amount of heat given off during annealing is small, and the experiments necessary for acquiring data such as those in Fig. 9-13 are difficult to perform.

The property changes caused by annealing are quite significant, as shown in Fig. 1-12. This data came from aluminum which was coldworked until its area was reduced by 87%. Specimens were then annealed at various temperatures for 1 hr, and the resulting data were plotted. It is seen that some properties change by several hundred percent.

### Recovery

Recovery refers to the modification of the properties of a material which occurs before recrystallization and therefore does not affect the grain structure. The extent to which a property, such as hardness or strength, is modified by recovery is usually small compared to the change caused by recrystallization. Recovery occurs at moderate temperatures; some metals exhibit recovery below room temperature. The process is thought to be the result of dislocations interacting with each other at high dislocation densities, by virtue of attractive and repulsive forces (Section 8-7). These are sometimes aided by applied stresses. The interaction is enhanced by the unpinning of dislocations, and climb appears to be an important unpinning mechanism in the process. Recovery softens a material by reducing the dislocation density. Figure 9-14 illustrates dislocation annihilation in a thin specimen of aluminum held at 200°C. The electron micrographs were taken at 1-min intervals. It is seen that the number of dislocations is reduced rather quickly at 200°C. As the dislocation density diminishes, the interaction forces become smaller and the rate of recovery decreases. The rate is controlled by both the dislocation mobility and the dislocation density.

The climb mechanism also permits dislocations to move so as to form low-angle grain boundaries (see Fig. 8-20). Recall that the edge disloca-

Fig. 9-13. Schematic diagram showing the rate at which heat is released when a work-hardened specimen is heated. Two humps appear in the curve. The one at the lower temperature is due to recovery, while the second is caused by recrystallization. [H. M. Clarebrouch et al., Proc. Rov. Soc. 4232-232 (1955).]

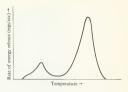


Fig. 9-14. Electron micrographs showing the annihilation of dislocations during recovery. The material is a thin foil of aluminum held at 200°C. The micrographs were taken at 1-min internals with (a) being first. J. Silcox and M. J. Whelan, Phil. Mag. 5:1 (1960).]





Fig. 9-15. Polygonization in polycrystal of MgO at 1800°C. The heavy lines are grain boundaries. The lighter lines are aligned etch pits and represent low-angle grain boundaries. Magnification, 125 × . (R. B. Day and R. J. Stokes in Materials Science Research, W. W. Krigel and H. Palmour III, eds., Vol. 3, Plenum Press, New York, New York, 1966.)

tions of Fig. 8-20 have a lower energy when they are aligned and that the forces between the dislocations encourage this alignment. The formation of low-angle grain boundaries during recovery is called polygonization and contributes to the softening of the material. Polygonization is exhibited by ceramics as well as metals. The formation of low-angle grain boundaries within grains is shown for MgO in Fig. 9-15. The grain boundaries are clearly shown, and the lines within the grains are collections of etch pits. The dislocations associated with the etch pits form the low-angle grain boundaries. The photomicrograph was taken at 1800°C. High temperatures are required for recovery of MgO (polycrystals show brittle behavior below 1600°C). The low-angle grain boundaries often form polygons within the grain-hence the name polygonization.

### Recrystallization

Recrystallization is a process in which new, strain-free grains are nucleated and then grow until they have consumed all of the work-hardened material. New grains having a low dislocation density appear as the result of recrystallization, and the hardness and strength of the material are significantly reduced, while ductility increases. The largest changes in physical properties occur during the recrystallization phase of annealing. The fraction of a material that recrystallizes during annealing depends on both temperature and time. This can be best explained by considering the following example. A number of high-purity copper specimens were cold-worked

Fig. 9-16. Recrystallization of high-purity (99.99%) copper that has been subjected to an area reduction of 98%. The fraction of the material that has recrystallized depends on temperature and time. [B. F. Decker and D. Harker, Trans. AIME 188:887 (1950).]



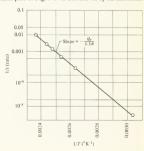
until the area reduction was 98%. They were then heated to different temperatures. At each temperature, the percentage of the solid which had recrystallized was determined as a function of time. The results are shown in Fig. 9-16, and they illustrate the time-temperature dependence of recrystallization.

Part of the data of Fig. 9-16 can be plotted in a manner which indicates that recrystallization is an activated process. To do this, a horizontal line is drawn across Fig. 9-16 at some value of percent recrystallized, say 50%. Each intersection of this line with a data curve gives us a value of time and temperature required for 50%, recrystallization. These data can be plotted as an Arrhenius graph if we use a recrystallization rate instead of time. The rate at which a reaction occurs is inversely proportional to the time which the reaction requires; therefore  $\log(1/t)$  will be used as the ordinate, where t is the time required for 50% recrystallization. Figure 9-17 shows the result of plotting the data in this manner. The straight line shows that the data follow an Arrhenius equation:

$$\log \frac{1}{t} = \log C - Q_r/2.3 \ RT \tag{9-12}$$

The quantity  $Q_r$  is the activation energy per mole for recrystallization. The recrystallization of copper is an activated process, although it is too complicated to allow us to associate  $Q_r$  with any particular atomic mechanism. The Arrhenius plot of Fig. 9-17 is not shown by all materials.

Fig. 9-17. An Arrhenius plot of the data in Fig. 9-16 which corresponds to 50% recrystallization. The straight line implies that the process is an activated one. [B. F. Decker and D. Harker, Trans. AIME 188:887 (1950).]



Recrystallization lowers the energy of a solid by eliminating dislocations; therefore it is the strain energy of the dislocations that causes recrystallization to occur. A crystal which has been severely workhardened has a high dislocation density and therefore releases more energy during recrystallization than one with less work hardening. As a result, heavily cold-worked specimens recrystallize at higher rates. If the recrystallization process follows an equation such as 9-12, the activation energy will diminish as the dislocation density increases. The recrystallization rate is also affected by all of the parameters which influence dislocation mobility, such as impurities and erain size.

### Grain arowth

Heating beyond the recrystallization temperature range causes the size of the recrystallized grains to increase. Some of the grains grow by consuming others. Grain growth lowers the energy of a solid because surface energy is associated with grain boundaries. As in the other annealing processes, high temperature gives the atoms of the crystal sufficient mobility so they can arrange themselves in low-energy configurations. Some softening is associated with grain growth because grain boundaries impede dislocation slip.

### Question

Question 6: In metal-forming operations, it is sometimes necessary to deform materials rather severely. Suppose that an aluminum plate \(\frac{1}{2}\) in. thick must be bent 90°. The material is placed in a bending machine and fractures before the 90° bend is made. Describe a procedure (other than casting) which will produce the desired shape.

# **9-7** Creep

Materials subjected to loads at high temperature will experience both work hardening and annealing simultaneously. This results in strain being dependent on time as well as stress. As an example, consider a solid supporting a load at high temperature. Slip occurs at low stress because of the high temperature. If the dislocation pinning mechanisms were effective, the material would work-harden. At high temperature, however, the thermally activated annealing mechanisms are operating and pinning is not as effective as it would be at lower temperatures. The behavior of the material is determined by two competing rate processes, work hardening and annealing. If dislocations are constantly created by sources and significant work hardening does not occur, the generated dislocations will slip and emerge at the surfaces, thus increasing the strain. Elongation will continue for as long a time as the specimen is loaded, and the total elongation will depend on how long the load was applied. Thus, strain becomes dependent on time as well as stress in the high-temperature region. Timedependent strain is called creep. From a practical point of view, the creep properties of a material usually determine its suitability for hightemperature applications.

The observed creep behavior of a solid is shown schematically in Fig. 9-18. The curve represents the behavior of a material subjected to a constant load and held at constant temperature. When the load is applied,

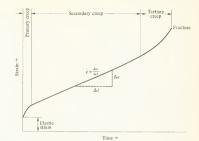


Fig. 9-18 A typical creep curve. The curve represents the time vs. strain behavior of a material having a constant load at constant temperature. The secondary creep region will be of most interest to us.

the specimen first deforms elastically. Following this, it enters the primary creep region where the strain rate (de/dt) decreases with time. This can be seen from the decreasing slope of the curve in the primary creep region. The material is work-hardening; consequently the rate at which work-hardening processes occur is greater than that for annealing processes. The secondary creep region is characterized by a constant value of strain rate. The curve is linear, implying that the flow stress of the material remains constant. Dislocation density is not increasing in this region, and the rate at which dislocations are generated is equal to the rate at which they emerge from the surface plus the rate at which they are annihilated within the solid. The secondary creep region accounts for most of the strain, and we shall mainly be concerned with secondary creep. Strain increases rapidly during tertiary creep. This occurs just prior to fracture and is attributed to necking of the specimen and to the formation of internal voids prior to fracture.

The curve of strain vs. time depends on both stress and temperature. When selecting a material for a particular application, the load which it must support and the temperature at which it must operate are usually known. The designer must be able to predict the time-strain characteristics of the material as a function of stress and temperature. For example, suppose that we were selecting a material for the turbine blades of a turbojet engine. The operating temperature and total load on the turbine blades would be known because these parameters would be fixed by the overall engine design. The maximum allowable strain of the blade would also be known and might be determined by the size of the turbine housing, Materials selection would then depend on the time vs. strain characteristics of the high-temperature materials being considered (neglecting some other factors such as cost). A low creep rate at the operating conditions would mean that the blade could remain in service for a long period of time before it reached the maximum allowable strain and had to be replaced, and vice versa. Materials operating in a creep environment have a finite lifetime and require replacement periodically.

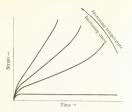


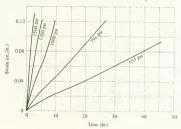
Fig. 9-19. The effect of stress and temperature on creep curves. An increase in either one causes a higher strain rate.

The effect of temperature and stress on creep are shown schematically in Fig. 9-19. Increasing either variable causes the strain rate to increase. The effect of increasing the stress while holding temperature constant is shown in Fig. 9-20. These data were taken from a number of tungsten specimens, all tested at 2400°C but at different values of stress. It is seen that higher stresses cause higher strain rates.

Creep cannot yet be accurately predicted without experimental data, but the dislocation mechanisms which have been discussed supply a good deal of information about how the problem should be approached. The remainder of this section and Section 9-8 will show how both theory and experiment can be combined to aid in the selection of materials for high-temperature environments.

Creep rate depends on both stress and temperature. Let us consider these one at a time, taking temperature first. Because creep rate increases with temperature, we might suspect that it is due to thermally activated processes such as climb, motion of jogged dislocations, or thermally activated cross slip. This speculation can be checked readily with experimental data. Suppose that we take a number of specimens and subject them to creep tests. Every specimen would be tested at the same stress, but each would have a different test temperature. The test results would give a series of curves such as Fig. 9-19. Each of the curves has a single value of

Fig. 9-20. Creep curves for an umber of specimens of arc cast lungsten. Each specimen was tested at 2400°C but at different stresses. The strain rate increases as the stress goes up. (S. B. Conway, Numerical Methods for Creep and Rupture, Gordon & Breach, New York, 1967.)



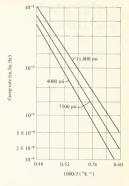
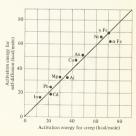


Fig. 9-21. The creep rate of polycrystalline thorium oxide as function of reciprocal temperature. The temperatures are in the neighborhood of 2300° K. The data follow an Arrhenius equation, and the creep has an activation energy. Data were collected at the different values of stress. [L. E. Poteat and C. S. Yust, J. Am. Ceram. Soc. 99-410 (1967).]

creep rate in the secondary creep region, which is the region we shall consider. This creep rate is often called steady-state creep. If the logarithm of this creep rate is plotted against reciprocal temperature (1/T) and the resulting curve is linear, the processes at work during creep are thermally activated because creep can then be described by an Arthenius-type equation. Figure 9-21 shows a plot of log & vs. 1/T for polycrystalline thorium oxide. A set of tests was made for each of the three stress values shown in the figure. Thorium oxide is a high-temperature ceramic, and these tests were made at temperatures in the neighborhood of 2000°K. The curves are indeed linear, and the process is thermally activated.

The activation energy for creep has been determined for a large number of solids. In Fig. 9-22, this quantity is compared with the activation

Fig. 9-22. Comparison of the activation energies for creep and self-diffusion of several metals. The correlation between these quantities indicates that creep depends on vacancy motion. (J. E. Dorn, in Creep and Recovery, American Society for Metals, 1957, p. 255).



energy of self-diffusion for several metals. Recall that self-diffusion refers to the movement of vacancies through a crystal. The excellent correlation shown in the figure suggests that creep depends strongly on processes requiring vacancy motion, such as climb. At this point, we have established that the temperature dependence of creep can be expressed by an exponential term, and we can write an equation for the strain rate in the form

$$\dot{\varepsilon} = C_1 f(\sigma) e^{-Q_c/RT} \qquad (9-13)$$

where

$$\dot{\varepsilon} = \frac{d\varepsilon}{dt} = \text{strain rate}$$

 $C_1 = constant$ 

 $f(\sigma) =$  some function of stress, not yet determined

 $Q_c$  = activation energy for creep

The effect of stress can be determined from test data. To obtain the data, tests would be made with a number of specimens at the same temperature but different stresses, resulting in curves such as those in Fig. 9-20. The steady-state creep rate can be determined for each stress, and a graph such as that shown in Fig. 9-23 can be made. The data for Fig. 9-23 came from tests on aluminum at 647°C. At constant temperature, the exponential term in equation 9-13 is a constant and the equation can be written as

$$\dot{\varepsilon} = C_2 f(\sigma)$$

Thus, Fig. 9-23 is a graph of this equation and provides a means for determining  $f(\sigma)$ . For low stress values, it is found that

$$f(\sigma) = C_3 \sigma^n \tag{9-14}$$

where  $C_3$  and n are constants. Substituting equation 9-14 into 9-13.

$$\dot{\varepsilon} = C \sigma^n e^{-Q_c/RT} \qquad (9-15)$$

Fig. 9-23. The effect of applied tensile stress on the strain rate of aluminum at 647°C, [J. Harper and J. E. Dorn, Acta Mct. 5:654 (1957),]



where C is a constant. The value of n depends on the material and is usually in the neighborhood 5 for metals. The thorium oxide data from which Fig. 9-21 was constructed gives a value of n ranging from 1.04 to 1.50.

Equation 9-15 can be used to determine a reasonable method for plotting creep data. Taking the natural logarithm of the equation,

$$\ln \hat{\epsilon} = \ln C + n \ln \sigma - \frac{Q_c}{RT}$$

$$\log \hat{\epsilon} = C' + n \log \sigma - \frac{Q_c}{2 \cdot 2DT}$$
(9-16)

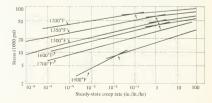
Equation 9-16 shows that a plot of  $\ell$  vs.  $\sigma$  on log-log paper should yield a straight line having a slope of n if n, T, and  $Q_c$  are constants. Data obtained from a high-temperature alloy have been plotted in this manner in Fig. 9-24. The curve for a given temperature is seen to have two different slopes over the stress range considered. The points at which the slopes change are indicated by arrows in the figure. The figure indicates that the value of n depends on stress. The problem is further complicated by the fact that the activation energy is not constant. The three curves in Fig. 9-21, for example, are not quite parallel; therefore each corresponds to a slightly different value of  $Q_c$ . For equation 9-16 to be complete, n and  $Q_c$  must be expressed as functions of n and n. These complications indicate the complexity of the creep phenomena and explain why empirical data are often used in selecting materials. Theoretical knowledge of the creep mechanism, however, is essential for the development of better creep-resistant materials.

Curves such as those in Fig. 9-24 are useful in high-temperature design problems, particularly when the useful life of a device is limited by the rate at which its components creep. The turbine blade problem discussed earlier is an example of this problem type.

# Example 9-2

A tensile load of 20,000 lb is supported by a piece of S-590 alloy. The load must be supported in a 1500°F environment, and the alloy cannot deform by more than 2% over a period of 10,000 hr. Find the required cross-sectional area of the loaded member.





Solution: First find the creep rate which satisfies the problem. Then use Fig. 9-24 to find the allowable stress at 1500°F. From the allowed stress and the load, calculate the cross section:

$$\dot{\varepsilon} = \frac{0.02}{10.000} = 2 \times 10^{-6} \text{ in./in./hr}$$

From Fig. 9-24,  $\sigma = 10,000$  psi at 1500°F and 2 × 10<sup>-6</sup> in./in./hr:

Area = 
$$\frac{F}{\sigma} = \frac{20,000}{10,000} = 2 \text{ in.}^2$$

It was previously stated that creep properties often determine which material will be selected for a high-temperature application. This raises the question of "What is meant by high?" The creep rate is proportional to  $e^{-Q_c/RT}$ , and therefore, strictly speaking, creep occurs at all temperatures. From a practical point of view, however, we are not interested in creep rates that are so low that they defy measurement. A rule of thum b is that creep should be considered if a material is used at a temperature greater than about half its melting point ("K or "R). At temperatures below this, creep can usually be neglected.

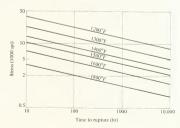
Question

Question 7: Find the activation energy for creep of thorium oxide when it is stressed at 7500 psi (see Fig. 9-21).

# 9-8 Creep rupture

There is another class of design problems which uses creep data in a different form. Situations arise in which we are not overly concerned about how much a single component of a device clongates but in which we are very concerned about it remaining in one piece. An example of this might be a pipe carrying liquid through a boiler or a nuclear reactor. In this case, the pertinent question is, "How long can the pipe be kept in service, at a given stress and temperature, without having it rupture because of creep?" To select a material for this type of application, the time required to

Fig. 9-25. Stress-rupture curves for Timken 35-15 stainless steel (35%, Cr, 15%, N). The curves have been extrapolated from 1000 to 10,000 hr. (F-J. Clauss in Deformation and Fracture at Elevated Temperature, N. J. Grant and A. W. Mullendore, M. M.I.T. Press, Cambridge, Mass., 1965.)



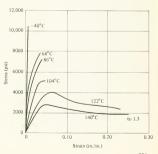
rupture the material must be known as a function of temperature and stress. Rupture occurs as the result of a material changing its dimensions during creep. The cross-sectional area is reduced until it can no longer support the applied load. The time required to rupture a piece of material in creep (t<sub>1</sub>) should be inversely proportional to the creep rate. We would therefore expect that a plot of stress vs. t<sub>1</sub>, on log-log paper will yield a straight line at a given temperature. Figure 9-25 shows such a plot for a stainless steel containing 35% Cr and 15% Ni. Test data were obtained for values of t<sub>1</sub>, up to 1000 hr (about 42 days) and have been extrapolated to 10,000 hr (about 14 months). The linearity of the curves makes the extrapolation fairly easy. Recall that theoretical considerations suggested plotting the data in this manner.

# **Q\_Q** Thermal effects in polymers

Polymers exhibit elastic behavior at low temperature and creep at high temperature, just as metals and ceramics do. In addition, they often show rubbery behavior at intermediate temperatures. The structure and bonding of polymers differ significantly from that of metals and ceramics, and therefore we would expect the atomic mechanisms which are responsible for polymer behavior to be different from those which explain metal and ceramic behavior. The dislocation model does not apply, and polymer behavior depends strongly on the secondary bonds which hold the chains together.

The effect of temperature on the stress-strain curves of polymethyl methacrylate is shown in Fig. 9-26. Some interesting characteristics appear, First, no yield point is shown by the curves taken at -40, 68, and 86°C. At 104°C, a maximum does appear, but large elongations are shown only at higher temperatures. Behavior is brittle for the three low-temperature curves, as might be expected because  $T_{\nu}$  (glass transition temperature) is about 100°C for polymethyl methacrylate (Fig. 4-19). Another interesting

Fig. 9-26. Tensile stress vs. strain for polymethyl methacrylate at various temperatures. A ductile to britle transition occurs between 86 and 104°C. (T. Alfrey, Mechanical Behavior of High Polymers, Wiley-Interscience, New York, 1967).



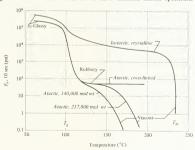
observation is the absence of work hardening at high strain. The figure also shows that this polymer undergoes a ductile to brittle transition and that the transition occurs in the neighborhood of T<sub>o</sub> if the stress is applied slowly. Fast loading (impact) raises the ductile to brittle transition temperature, just as it did in the case of metals and ceramics.

The temperature dependence of the elastic modulus of polystyrene is shown in Fig. 9-27, and these data provide the basis for the explanation of the processes that are occurring at the atomic level. E., which is called the relaxation modulus, is plotted as the ordinate. This quantity is somewhat different from Young's modulus. At temperatures above  $T_a$ , polymers will creep, and strain becomes dependent on both stress and time. To determine E., the specimen is first strained to a predetermined value, and the corresponding stress is observed after a predetermined period of time. Stressstrain curves can be constructed from these data, and  $E_r$  can be found from the stress-strain curves. Figure 9-27 is constructed from stress measurements which were taken 10 sec after the material was strained-hence the notation E. (10 sec).

The material is in a glassy state when it is below the glass transition temperature. In this region, deformation occurs primarily by bending the carbon bonds in the polymer chains as discussed in Section 8-18. The behavior is elastic and occurs for both the atactic and isotactic specimens. The isotactic material used for Fig. 9-27 was crystalline, while the atactic was amorphous. At temperatures slightly above Ta, some local slipping occurs between polymer chains, particularly between short ones. This is accomplished by the breaking and reforming of secondary bonds. In Fig. 9-27, this phenomenon corresponds to the sharp drop in E, which appears at about 100°C for the atactic specimens. The effect of temperature on the relaxation modulus of the crystalline polymer is not very great in the neighborhood of  $T_a$ . Recall that the properties of crystalline polymers do not change significantly at the glass transition temperature (see Fig. 4-18).

Figure 9-27 shows the behavior of three different atactic specimens

Fig. 9-27. The relaxation modulus of polystyrene as a function of temperature. Data are shown for four specimens that have structural differences. The cross links are formed by 0.25 mole % of divinyl benzene. (A. V. Tobolsky, Properties and Structure of Polymers. Wiley, New York, 1960.)



above Ta. One of these contains cross links, while the other two differ in degree of polymerization. Following the local slippage at  $T_a$ , the crosslinked polymer maintains a value of E, that is almost constant over an interval of 130°C. This is the rubbery region, and elongation occurs by the uncoiling of polymer chains [see Fig. 8-44(b)]. Cross linking inhibits uncoiling, and E, remains practically constant as a result. The specimens that are not cross-linked experience sliding between chains [Fig. 8-44(c)] after a small amount of rubbery behavior. The ease with which this slipping occurs depends on the degree of polymerization. Figure 9-27 shows two atactic polystyrene specimens having different chain lengths (or chains having different average molecular weights). The longer chain shows a greater resistance to sliding past its neighbors. The crystalline material does now show a rubbery behavior region. Some sliding between chains occurs at temperatures above Ta, but the effect is not as pronounced as for the atactic specimens. The crystalline polymer begins to flow readily at the melting point, which is 230°C for polystyrene. Note that the property differences between the four materials shown in Fig. 9-27 are due to structural variations which cause differences in the bonding between chains,

The polystyrene curves can be divided into three regions. Below the glass transition temperature, the behavior is elastic, and this is the elastic region. At high temperatures, the chains slide past each other easily, and the polymer behaves as a viscous fluid. This is called the viscous region. Between these, the behavior is partly elastic and partly viscous. Deformation in this middle region is due to bonds bending, chains uncoiling, and chains slipping past each other. Deformation due to chains slipping is permanent, while chain uncoiling may be plastic or elastic. The middle region is called the viscoelastic region, implying that both viscous and elastic deformations are active. These three regions are generally shown by thermoplastic polymers.

According to the models given, the glass transition temperature corresponds to the temperature at which chain sliding and uncoiling occur. Sliding is inhibited if the chains have bulky side groups because the groups on adjacent chains would tend to interfere with each other. This is verified by the data in Table 4-2, Polyethylene, which has only hydrogen atoms on the carbon backbone, has a glass transition temperature of  $-110^\circ\mathrm{C}$  and is in the viscoelastic region at room temperature. Polywinglehloride has a bulky chlorine atom and has a  $T_g$  equal to  $80^\circ\mathrm{C}$ . Polystyrene and polymethyl methacrylate have large side groups, and both show a glass transition temperature of  $100^\circ\mathrm{C}$ 

In the first part of this section it was noted that the stress-strain curves for polymethyl methacrylate did not show an increase in stiffness as strain increased (Fig. 9-26). Compare this to the stress-strain curve of nylon (Fig. 8-45). The difference in the shapes of the curves is due to the nylon crystalliza as it is strained, while the polymethyl methacrylate does not. Its crystallization is prevented by bulky side groups. In the case of polystyrene, the side groups in the isotactic structure have a very regular geometric arrangement and can be crystallized. The atactic structure, however, resists crystallization because of the less regular arrangement of the bulky side groups.

Question

Question 8: The discussion of creep in crystalline materials showed that the strain rate (or creep rate) increased as the applied stress increased. If a load is applied to a chain polymer which is not cross-linked but is above T<sub>g</sub>, would you expect the same behavior?

# 9-10 Summary

The change in the plastic behavior of crystalline solids due to temperature is attributed to thermally activated processes. The reduction in yield and ultimate stress as temperature increases indicates that dislocation mobility has increased as the result of thermally activated unpinning mechanisms. These include climb of edge dislocations, motion of jogged screw dislocations, and recombination of partial dislocations. The reduced mobility of dislocations at low temperatures provided an explanation of the transition from ducile to brittle behavior shown by many materials.

The increase of dislocation mobility with temperature explains the important process of annealing. During the first stage of annealing, dislocations tend to either align themselves as low grain boundaries or annihilate each other. These processes can occur at relatively low temperatures. The first stage of annealing is called recovery. Heating beyond the recovery temperature range results in the growth of new grains. The new grains have a lower dislocation density than those grains which they replace; consequently recrystallization causes significant property changes. It removes the effects of work hardening and leaves the solid more ductile while reducing the strength characteristics. Heating to still higher temperatures causes the grains to grow. The annealing process is a complicated one, and the rate at which it occurs depends on all of the parameters which affect dislocation mobility. If a material is loaded at high temperature, both the work-hardening and annealing mechanisms function simultaneously. This results in strain increasing with time and is called creep. Creep is thermally activated and depends largely (but not solely) on the migration of vacancies. It is a complex process and is usually treated by methods which include both theoretical and experimental considerations. Creep properties are very important when selecting materials which must function in high-temperature environments.

The properties of polymers are very temperature sensitive. Below the glass transition temperature they are elastic. In the viscoelastic region they show both elastic and creep behavior. The behavior is somewhat similar to that shown by metals and ceramics, but the atomic mechanisms associated with the behavior are quite different. Generally, plastics exhibit creep at temperatures which are low compared to the creep temperatures of metals and alloys, although exceptions do exist.

Problems

- 1 A mixture of gasoline and air is compressed in a gasoline engine. The mixture does not ignite until a spark plug fires, producing a spark in the mixture. Discuss the purpose of the spark, in terms of activation energy.
- 2 The rate of a chemical reaction  $A + B \rightarrow P$  has been measured at four

temperatures. The results are shown in the accompanying table. (a) Make a graph of  $\ln(dp/dt)$  vs. 1/T. (b) Find the activation energy of the reaction. (c) Express dp/dt in units of mole fraction per minute instead of mole fraction per second. Does this change the answer to part (b)?

$\frac{dp}{dt} \left( \frac{\text{mole fraction}}{\text{sec}} \right)$	0.5	0.14	0.037	0.0
Temperature (°K)	625	556	500	45

- 3 Consider a solid containing 1 g-mole of atoms. The atoms have a vibrational frequency of  $10^{13}$  cycles/sec, and the temperature of the solid is 800°K. The energy barrier to vacancy motion  $(q_m)$  is 2 eV. (a) How many times per minute, on the average, does an atom have an energy of 2 eV or greater? (b) The energy required to form a vacancy is 1 eV. How many vacancies does the solid have? (c) How many vacancy movements occur per minute in the entire solid?
- 4 (a) Figure 9-3 shows that the work-hardening rate increases as the temperature decreases. Explain why. (b) The work-hardening rate increases as the strain rate increases. Explain why. (c) A specimen can sustain a small amount of ductile elongation and then fracture in a brittle manner. How does the work-hardening rate of the specimen affect the amount of elongation that occurs before brittle fracture?
- 5 Figure 9-10 illustrates the interplay of yield stress and brittle fracture stress in the ductile to brittle transition. Sketch a similar diagram for a fcc metal that does not have a ductile to brittle transition.
- 6 The activation energy for self-diffusion of a number of metals is given in Fig. 9-22. The melting point of these materials is given in Appendix A. (a) Plot melting point vs. activation energy for self-diffusion. (b) Melting point can be used as a rough measure of bond energy. Explain the trend shown in the curve of part (a). [Hint: Figure 9-8(b) should help.]
- 7 (a) Find the activation energy for recrystallization of high-purity copper (Fig. 9-17). (b) If impurity pinning sites were present in the copper, would the activation energy increase or decrease?
- 8 If a bar of lead 1 ft long is hung on a string, it will continuously elongate at room temperature. Explain why.
- 9 A structural member is to be made of alloy S-590 (Fig. 9-24). It must hold a tensile load of 50,000 bin a 1350°F environment, and the creep strain is limited to 5.5%. If the structural member must operate for 5 years, what is the smallest cross-sectional area that can be used?
- 10 The terms thermoplastic and thermosetting are used for describing polymers, as discussed in Section 3-10. Are the terms accurate and descriptive? Why?
- 11 A stress-strain diagram is made using polyethylene at room temperature. Should this curve most closely resemble that of polymethyl methacrylate at 86°C or at 122°C (see Fig. 9-26) or of nylon as shown in Fig. 8-45. Why? Table 2-9 may help.

Answers

- Question 1: Equation 8-18 states that  $\tau_{\text{warree}} = 2Gb/\mathcal{L}$ , where  $\mathcal{L}$  is the distance between pinning sites. If we assume that dislocation intersections act as pinning sites, then  $\mathcal{L}$  is the distance between dislocations. From Example 8-2, the dislocation spacing is  $1/\sqrt{\rho}$  and  $\tau_{\text{towaree}} \propto \sqrt{\rho}$ . Because yield point is proportional to  $\tau_{\text{towaree}}$ , yield point  $\propto \sqrt{\rho}$ , as shown.
- Question 2: The activation energy is low. Equation 9-6 or 9-7 shows that a low value of activation energy corresponds to a high rate. In an explosion, the reaction rate is very high. Keeping the nitroglycerine at low temperature decreases the energy of the reactants, which also lowers the reaction rate. Jarring the nitro results in a fast transfer of mechanical energy to it, which increases the number of high-energy particles.
- Question 3: From the Boltzmann distribution, the fraction of atoms having energies greater than  $q_v$  is  $e^{-q_v/4T}$ . Because equation 4-5 was written for equilibrium, we can say that every atom which has enough energy to form a vacancy will form one. The fraction of vacancies at equilibrium is then  $e^{-q_v/kT}$ .
- Question 4: No. Elastic behavior is the result of stretching or compressing interatomic bonds. The forces and energies involved in stretching or compressing bonds have no time dependence; therefore Young's modulus should not depend on strain rate.
- Question 5: The notch shape determines the value of the stress concentration factor. A sharp notch (V-shaped notch) has a higher stress concentration factor than a smoother (or more circular) notch. A large stress concentration causes brittle fracture at a small applied stress. In terms of Fig. 9-10, a sharp notch will lower the curve for brittle fracture stress. The intersection of this curve and the yield stress curve will occur at higher temperature (or lower strain rate). Thus, a specimen with a sharp notch will have a higher ductile to brittle transition temperature than one with a smoother notch.
  - Question 6: The material should be alternately deformed and annealed.

    A small bend (less than 90°) can be made, after which the material is annealed. The annealed material can then be bent further, etc.
- Question 7:  $\ln \dot{\varepsilon} = -\frac{Q}{RT} + \ln C$

Figure 9-21 uses common logarithms rather than natural logarithms. Therefore,

$$\log \dot{\varepsilon} = -\frac{Q}{2.3RT} + \log C.$$

The slope of the line is -Q/2.3R. The slope can also be found from any two points on the curve. Selecting points at  $\dot{\varepsilon}=10^{-2}$  (1/T=0.000527) and  $\dot{\varepsilon}=10^{-3}$  (1/T=0.000567).

$$-\frac{Q_c}{2.3R} = \text{slope} = \frac{\Delta(\log \delta)}{\Delta(1/T)} = \frac{-2 - (-3)}{0.00527 - 0.00567} = -24,400$$

 $Q_c = (24,400) (1.987) (2.3) = 111,600 \text{ cal/g-mole}$ 

Question 8: Yes. The rate at which chains slide is governed by the rate at which the bonds between chains can be broken. They will be broken more rapidly at higher values of applied stress. This can also be explained in terms of viscous fluids. The deformation rate of a viscous substance is proportional to the stress causing deformation.



# Diffusion

THE ATOMS IN A SOLID are in constant motion. In Chapters 8 and 9, we discussed atoms vibrating about their equilibrium lattice positions and how this vibration caused vacancy motion and contributed to dislocation motion. In this chapter, it will be shown that atomic vibrations and vacancies allow atoms to move through a solid. The motion of matter through other matter is called diffusion. We have already encountered one example of diffusion in the motion of a vacancy. The discussion of Fig. 9-8 showed that the shaded atom in the figure could move to the right (or the vacancy to the left) if the atom possessed the required activation energy. Such motion is diffusion because matter (the shaded atom) moves through other matter (the remaining atoms of the solid).

The diffusion process is a commonly observed one. As an example, the smell of food cooking in the kitchen often permeates several rooms of a house. Gaseous molecules from the food have diffused (or moved) through the air from the cooking pot to the observer's nose. Another common example is a lump of sugar placed at the bottom of a cup of coffee. The sugar will eventually be dissolved by the coffee and will diffuse through it. The coffee will be sweetened uniformly throughout its entire volume if a long enough period of time elapses. It is not necessary to stir the coffee in order to distribute the sugar unless you are either impatient or like your coffee hot. These are everyday examples of diffusion. We shall be concerned with diffusion in solids, which is not usually within the realm of our experience.

Physical models which describe solid-state diffusion will be postulated in the first part of this chapter. The models will then be used to explain the mathematical expressions which govern the diffusion process. It will be seen that the rate at which diffusion occurs is highly temperature dependent. Two applications of diffusion will be given in this chapter and the concepts will also be applied in Chapters 11 and 12. Chapter 12 considers methods by which materials can be strengthened. The strengthening mechanisms depend on diffusion, among other things.

We have seen one application of diffusion in Chapter 1. The joining of materials by diffusion bonding was discussed briefly, and an example was given in Fig. 1-15. This technique is very useful

when more conventional methods, such as welding or brazing, cannot be used.\* Another example of an important diffusion process is the doping of semiconductors which are used as electronic components. Doping consists of adding a well controlled number of impurities to a very high purity semiconductor. This is often accomplished by diffusing the impurities into the semiconductor.

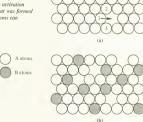
# 10\_1 Diffusion mechanisms

Several atomic mechanisms have been proposed to explain diffusion. All of them rely on the vibrational energy of the atoms in the solid. This section will discuss the two diffusion mechanisms that are most prevalent: the vacancy mechanism and the interstitial mechanism.

## The vacancy mechanism

Diffusion can occur by atoms moving into adjacent sites that are vacant. This mechanism was used to explain the motion of vacancies in Section 9-3 (see Fig. 9-8). Diffusion by the vacancy mechanism is illustrated in Fig. 10-1(a), which shows a close-packed plane of atoms in a pure solid. For atom 1 in the figure to move into the adjacent vacant site, it must squeeze past atoms 2 and 3. Energy is required to move these atoms apart, and this is just the activation energy for vacancy motion, q<sub>m</sub>, discussed in Section 9-3. If the solid is composed of a single element (pure copper, for example), the movement of the atom is called self-diffusion because the moving atom and the solid are the same chemical element. Note that any of the atoms which are adjacent to the vacancy can move into it; such motion

Fig. 10-1. The vacancy mechanism for atomic diffusion.
(a) Diffusion of atoms in a pure sollid. Any of the atoms adjacent to a acaancy can move into the vacancy if it possesses the activation energy for motion. (b) A substitutional solid solution that was formed by substituting B atoms for A atoms. Either A or B atoms can move into the society sites.



<sup>\*</sup> For a practical discussion of diffusion bonding, see F. V. Alm, Machine Design, January 4, 1968.

is not limited to atom 1. Let the plane in Fig. 10-1(a) be part of an fcc lattice. Because each atom has 12 nearest neighbors, the vacancy will have 12 adjacent atoms. Any one of these can move into the vacancy provided it possesses the activation energy.

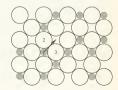
The discussion so far has been limited to pure substances, but we also want to talk about solids composed of more than one element. One simple way of forming such a solid is merely to substitute atoms of one element for atoms of another. For example, let the atoms in Fig. 10-1(a) be designated as A atoms. To form a solid which contains two elements, we can simply replace some of the A atoms by atoms of element B, while maintaining the same lattice. The result of this substitution is shown in Fig. 10-1(b), where the shaded atoms are B atoms. Each vacancy has both A and B atoms around it; consequently either type of atom can move into the vacancy. Which one moves depends on which first acquires the necessary activation energy. Because both A and B atoms can move, we shall be concerned with the diffusion of two kinds of atoms within the same solid.

The solid in Fig. 10-1(b) is called a substitutional solid solution because B atoms were simply substituted for A atoms. If the solid is a metal, it is called a substitutional alloy. Often there are limits to the number of B atoms which can be substituted into an A lattice; these are called solubility limits and wilb be covered in Chapter II. For purposes of this chapter it is assumed that A and B are mutually soluble in all proportions; that is, A and B may be mixed in any proportions and the structure will remain the same. This is the case for a number of real solids. Copper and nickel, for example, are mutually soluble in all proportions in the solid state. The atomic radii of the atoms in a substitutional solid solution must be approximately the same; otherwise the solid structure will become distorted.

#### The interstitial mechanism

Interstitial solutions (or alloys) may occur when a solid is composed of two or more elements whose atomic radii differ significantly. The large atoms occupy lattice sites, while the smaller ones fit into the voids created by the large atoms. The voids are called interstices. The diffusion mechanism in this case is similar to vacancy diffusion except that interstitial atoms stay on interstitial sites. This is illustrated in Fig. 10-2, which shows the (100) plane of an fcc solid. A number of interstitial sites are occupied. Atom I in the figure can move into an adjacent interstitial site, which is vacant, if

Fig. 10-2. An interstitial solid solution. The small atoms occupy interstitial sites and can move to adjacent interstitial sites that are vacant. An activation energy is associated with interstitial diffusion.



it can squeeze past atoms 2 and 3. The figure shows that atoms 2 and 3 touch; however, if this was viewed in three dimensions, it would be seen that atom 1 could follow an easier path. It would come slightly out of the plane of the paper and would follow a "channel" in the crystal structure to arrive at the vacant site. To move through the channel, it must still squeeze past neighboring atoms. The energy required to push these atoms aside comes from the vibrational energy of the moving atom; consequently interstitial diffusion is a thermally activated process. The rate at which atoms move in both interstitial and substitutional alloys is given by equation 9-11:

Rate at which atoms (or vacancies) move =  $ve^{-(q_m+q_u)kT} = ve^{-q_d/kT}$ (9-11)

where  $q_d$  is called the activation energy for diffusion.

The basic difference between the two mechanisms has to do with structure. In a substitutional solution, the two kinds of atoms share a set of atomic sites in a lattice. For interstitial solutions, each kind of atom has its own set of sites. The two mechanisms discussed are the ones most prevalent in solid-state diffusion. Other mechanisms have been proposed and may be present in special situations. They will not be discussed here.\*

Question

Question 1: Figure 10-1 shows a close-packed plane; let it be the (111) plane of an fic crystal. Consider the vacancy that has atom 1 adjacent to it. Any of the atoms adjacent to the vacancy can move into the vacancy site if the atom acquires the activation energy. What is the probability that the atom which moves into the vacancy site is atom 1?

# 10-2 Fick's first law

Solid-state diffusion can be mathematically described by two differential equations which are called Fick's first and second laws. Fick's first law describes the rate at which diffusion occurs and will be discussed in this section. The second law will be covered in Section 16-3.

Figure 10-3 shows the model which will be used for the discussion. As block of material is a substitutional alloy composed of elements A and B. The concentration of B atoms is defined as the number of B atoms per unit volume of the solid and is given the symbol C<sub>B</sub>. Similarly, C<sub>A</sub> denotes the concentration of A atoms. The B atoms are not uniformly distributed throughout the solid; the concentration of B atoms is greater on the left side of the solid. The shaded plane in Fig. 10-3(a) has been redrawn in Fig. 10-3(b) and the atomic structure is emphasized. For simplicity, let this be the (100) plane of a simple cubic structure. The interatomic distance is d. The B atoms are shaded in the figure. Their concentration decreases as we go from left to right across the solid. To put this on a more quantitative basis, the positive x direction is shown in the figure and we shall let x equal zero at the left edge of the solid. The concentration of B atoms can be plotted as a

<sup>\*</sup> These mechanisms are discussed in P. Shewmon, Diffusion in Solids, McGraw-Hill, New York, 1963, Ch. 2.

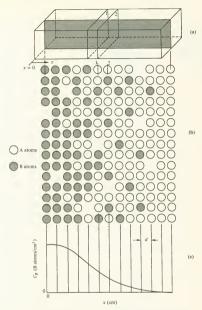


Fig. 19.3. Model for Illustrating diffusion. (a) A solid block of a substitutional alloy. The x direction is shown, and the origin is at the left edge of the block. (b) The arrangement of the atoms on the shaded plane of (a). The concentration of B atoms decreases in the x direction. The distance between atoms is d, and the lattice to simple cubic. (c) The concentration of B atoms plotted as a function of x. The planes labeled 1 and 2 are referred to in the text.

function of x, as shown in Fig. 10-3(c). The curve of concentration vs. position will be called the *concentration profile*. Experiment shows that if a substitutional solid solution has the concentration profile shown in Fig. 10-3(c), B atoms will diffuse to the right and A atoms to the left.

## Example 10-1

Find the concentration of B atoms on plane 1 in Fig. 10-3. Let the lattice parameter of the crystal be 5Å.

Plane 1 is shown in Fig. 10-3(a). The calculation will be based upon a 1-cm<sup>2</sup> area of this plane. The quantity that we want is number of B atoms per cubic centimeter of plane 1. Thus, we first find the number of B atoms on 1 cm<sup>2</sup> of the plane and then find the "volume" that the 1-cm<sup>2</sup> "plane" occupies:

Total number of atoms/cm<sup>2</sup> of plane 
$$1 = \frac{1}{(5 \times 10^{-8})^2} = 4 \times 10^{14}$$

The fraction of these that are B atoms can be found from Fig. 10-3(b). The figure shows that of 14 atoms on plane 1, 5 are B atoms (the vacancy does not count either way). Thus, five-fourteenths of the atoms are B atoms:

Number of B atoms/cm<sup>2</sup> of plane 
$$1 = \left(\frac{5}{14}\right)(4 \times 10^{14}) = 1.43 \times 10^{14}$$

The volume occupied by 1 cm<sup>2</sup> of plane 1 is just the area times the distance between the planes that are parallel to plane 1. This distance is d (or  $5\text{\AA}$  in this problem):

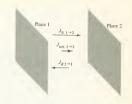
$$C_{\rm B} = \frac{1.43 \times 10^{14}}{1 \times (5 \times 10^{-8})} = 2.86 \times 10^{21} \text{ B atoms/cm}^3$$

B atoms in Fig. 10-3 will diffuse to the right, and the rate at which they diffuse is governed by Fick's first law. This law can be derived by considering the flow of B atoms, in the x direction, between two planes in the solid. We shall consider the flow between planes 1 and 2. Let J be the number of B atoms moving from a unit area of one plane to a unit area of another plane per unit time. This quantity is called the flux and has dimensions of atoms per square centimeter per second. According to the vacancy model, B atoms can move from plane 1 to plane 2 and can also move from plane 2 to plane 1. Flow in both directions is illustrated schematically in Fig. 10-4.  $J_{B_1-2}$  is the flux of B atoms from plane 1 to plane 2, while  $J_{B_2-1}$  represents the flux from plane 2 to plane 1. The net flux of B atoms from plane 1 to plane 2 is given by

$$J_{\text{net }1 \rightarrow 2} = J_{\text{B }1 \rightarrow 2} - J_{\text{B }2 \rightarrow 1}$$
 (10-1)

We want an expression for the net flux in terms of concentration. It will be seen that a net flux exists because the concentration of B atoms is greater on plane 1 than on plane 2.

Fig. 10-4. The flux of atoms between two planes  $J_{B,1-2}$  is the flux of B atoms from plane 1 to plane 2.  $J_{B,2-1}$  is the flux from plane 2 to plane 1. The net flux of B atoms between the planes is the difference of these quantities.



Consider all of the quantities which will determine  $J_{B1-2}$ . The rate at which a single atom moves is given by equation 9-11 and depends on the quantities v,  $q_s$ , and T. This equation gives the number of moves per second that the atom makes in all directions. When an atom in plane I (Fig. 10-3) makes a move, there are six directions that it can move in (the atom has six nearest neighbors because the structure is simple cubic, and any of these may be a vacancy). We introduce the quantity  $\beta$  to account for the direction of the imms. Thus.

Rate at which an atom moves from plane 1 to plane 2
$$= \beta v e^{-q_d/kT} = D' \text{ atoms/sec}$$
(10-2)

The rate at which B atoms move from 1 cm<sup>2</sup> of plane 1 to 1 cm<sup>2</sup> of plane 2 is just equal to D' multiplied by the number of B atoms per square centimeter on plane 1:

$$J_{\text{B1}\to 2} = D' \text{ (number of B atoms/cm}^2 \text{ on plane 1)}$$
 (10-3)

The number of B atoms per square centimeter of plane 1 can be expressed in terms of the concentration of B atoms on plane 1, which will be called  $C_{\rm B1}$ . From Example 10-1,

Number of B atoms/cm<sup>2</sup> of plane  $1 = C_{B_1}$  (volume of 1 cm<sup>2</sup> of plane 1) =  $C_{B_1}d$  (10-4)

Substituting equation 10-4 into 10-3,

$$J_{B1\to 2} = D'dC_{B1}$$
 (10-5)

Similarly,

$$J_{B2\to 1} = D'dC_{B2} (10-6)$$

Equations 10-5 and 10-6 can now be substituted into equation 10-1 to find the net flux:

$$J_{\text{net }1\to2} = D'dC_{B1} - D'dC_{B2} = D'd(C_{B1} - C_{B2})$$
 (10-7)

Equation 10-7 shows that diffusion occurs because of a concentration difference between adjacent planes.

Fick's first law can be obtained from equation 10-7 by writing the

concentration difference,  $C_{\rm B1}-C_{\rm B2}$ , in terms of the concentration profile of Fig. 10-3(c):

$$C_{B1} - C_{B2} = -d \frac{\delta C_B}{\delta x} \qquad (10-8)$$

where  $\delta C_B/\delta x$  is the slope of the concentration profile between planes 1 and 2. The negative sign in equation 10-8 is sometimes confusing. Physically, it tells us that diffusion occurs in the direction of decreasing concentration. This means that  $\delta C_B/\delta x$  is a negative quantity in the diffusion direction. For the arrangement shown in Fig. 10-3, the left-hand side of equation 10-8 is positive and the right-hand side must also be positive. Because  $\delta C_B/\delta x$  is a negative quantity, the minus sign causes the right-hand side of the equation to be positive, as required. Substituting equation 10-8 into 10-7.

$$J_{\text{net } 1 \to 2} = -D'd^2 \frac{dC_B}{dx} = -D \frac{dC_B}{dx}$$
 (10-9)

where  $D = D'd^2$  and the  $\delta$ 's have been replaced by derivatives. Equation 10-9 can be written so that it describes diffusion for the general case:

$$J_{\text{net}} = -D \frac{dC}{dx} \tag{10-10}$$

This is Fick's first law. The quantity D can be measured experimentally. It is called the diffusivity (or coefficient of diffusion), and its significance will be unrawled in Section 10-4. The quantity dC/dx is often called the concentration gradient. Equation 10-10 is applicable to diffusion in interstitial solutions as well as in substitutional ones.

Questions

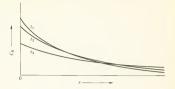
Question 2: In Chapter 9, the motion of vacancies was shown to depend on temperature and activation energy. Diffusion by the vacancy mechanism should therefore depend on T and  $q_d$ . Where does this dependence appear in equation 10-10?

Question 3: Show that the units of D are square centimeters per second.

# 10-3 Fick's second law—time dependence

Equation 10-9 shows that the rate at which diffusion occurs depends on  $dC_{\rm B}/dx$ . The model used for the derivation does not have a constant value for this quantity; Fig. 10-3(b) shows that the concentration gradient varies with x. A large negative slope corresponds to a high diffusion rate (or a large flux). The B atoms will diffuse from the left side of the solid toward the right side in accordance with Fick's first law. The net migration of B atoms to the right means that  $C_{\rm B}$  will decrease on the left side of the solid and will increase on the right side as diffusion progresses. This is shown schematically in Fig. 10-5. The curve labeled  $t_{\rm L}$  corresponds to the concentration profile at a given instant of time. At a later time,  $t_{\rm S}$ , the concentration profile has changed, as indicated in the figure. The change is due

Fig. 10-5. Schematic illustration of the time dependence of diffusion. The concentration of B atoms at time t<sub>1</sub> is such that B atoms flow from left to right, causing the concentration vs. position curves to change. The curves labeled t<sub>3</sub> and 1 sepresent the concentration profiles at different times.



to the diffusion of B atoms that has occurred in the time interval  $I_2 - I_4$ . The  $I_2$  curve represents the concentration profile at a still later time. The diffusion process is trying to distribute the B atoms uniformly throughout the solid solution. It is emphasized that we are dealing with solutions in which the components are mutually soluble in all proportions. The tendency for uniform distribution of the components must be modified if solubility limits occur, as will be done in Chapter 11. Figure 10-5 shows that the concentration gradient becomes less negative as time increases. This means that the diffusion rate becomes slower as the diffusion process progresses.

Fick's first law allows us to calculate the instantaneous mass flow rate (or flux) past any plane in a solid but gives no information about the time dependence of the concentration. The time dependence is contained in Fick's second law, which can be derived by using Fick's first law and the conservation of mass. The derivation is beyond the scope of this book.\* Fick's second law is

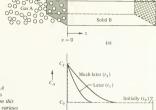
$$\left(\frac{dC}{dt}\right)_{x} = \frac{d}{dx} \left[ D\left(\frac{dC}{dx}\right)_{t} \right]$$
 (10-11)

The notation  $(dC/dt)_x$  means that dC/dt is the derivative of C with respect to t while x is held constant, and similarly for  $(dC/dx)_t$ . Equation 10-11 provides a relationship between C, x, t, and D. Recall that D depends on temperature and structure. The differential equation has been solved for a number of cases which are of engineering interest, and two of these will be discussed.

# Diffusion with constant surface concentration—case hardening

Case hardening is a process in which one element (usually in gaseous form) is diffused into another (a solid) and the diffusion is limited to a small region near the surface. The properties of the region near the surface are changed as a result. Generally the surface region becomes harder and more brittle. A piece of material which has been case-hardened has a ductile interior and a hard surface. This combination is often desirable. For example, some of the surfaces of a camshaft in an automobile engine are constantly sliding past cam followers. These surfaces are subjected to wear as a result. The effects of wear can be reduced if the cam surfaces are hard,

<sup>\*</sup> See P. Shewmon, op. cit., p. 148.



(b)

Fig. 10-6. Diffusion of a gas into a solid. (a) Gas A impinges upon the shaded plane of solid B. The gas maintains a concentration of A atoms, called C<sub>1</sub>, on this surface. (b) Concentration profiles of element A at various times. The solid contained a uniform concentration of A, called C<sub>0</sub>, before diffusion started.

but a hard and brittle camshaft is undesirable. It is possible to fabricate a ductile camshaft with a hard surface by case hardening. It is an important industrial process.

Case hardening is governed by Fick's second law, and we shall consider the solution of equation 10-11 for this process. A typical case-hardening setup is shown in Fig. 10-6(a). Gas A is in direct contact with the shaded surface of solid B. Let B be an alloy (or solid solution) which contains some of element A even before the gas and solid are placed in contact. The initial concentration of element A in alloy B is denoted by  $C_0$ . When the gas and solid are placed in contact, gas atoms adhere to the solid surface; that is, the surface adsorbs the gas. The adsorbed A atoms will diffuse into the solid by one of the mechanisms discussed in Section 10-1. Case hardening usually involves interstitial alloys. As A atoms diffuse from the surface and form an interstitial alloy with B, they are replaced by other A atoms, which leave the gas and adhere to the surface. The rate at which A atoms leave the surface and diffuse into the solid is just equal to the rate at which gaseous A atoms are adsorbed onto the surface, provided that the pressure of gas A remains fairly constant. Because the two rates are equal, the concentration of A atoms on the surface remains constant with time. The surface concentration is shown as  $C_s$  in Fig. 10-6(b). The concentration profile of element A, immediately after the gas and solid have been placed in contact, is shown by the dashed line in Fig. 10-6(b). At time to, gas has been adsorbed by the solid surface, but no diffusion has occurred. The concentration of A atoms on the surface is shown as C, and this quantity remains constant throughout the process. The curves labeled t1 and t2 in Fig. 10-6(b) represent the concentration profiles at two later times. It is seen that the depth to which the A atoms penetrate increases with time. Thus, the depth of the interstitial alloy increases as diffusion progresses.

The solution of equation 10-11 for this physical situation gives the equation of the concentration profile. The solution given here assumes that the value of D remains constant and that the solid extends to infinity in the +x direction. In a practical sense, the requirement that the solid

Table 10-1. Tabulated values of the error function

Z erf $Z$		Z	$\operatorname{erf} Z$	
0	0	1.00	0,843	
0.025	0.028	1.10	0.880	
0.05	0.056	1.20	0.910	
0.10	0.113	1.30	0.934	
0.15	0.168	1.40	0.952	
0.20	0.223	1.50	0.966	
0.30	0.329	1.60	0.976	
0.40	0.428	1.80	0,989	
0.50	0.521	2.00	0.995	
0.60	0.604	2.20	0.998	
0.70	0.678	2.40	0.999	
0.80	0.742	00	1.0	
0.90	0.797			

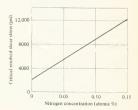
extend to infinity can be relaxed somewhat. It is necessary only that the concentration of A at the right edge of the solid [cross-hatched plane in Fig. 10-6(b)] not rise significantly above  $C_0$  during the diffusion. The solution of Fick's second law for this arrangement is

$$\frac{C_s - C}{C_s - C_0} = \operatorname{erf}\left(\frac{x}{2\sqrt{Dt}}\right) \tag{10-12}$$

where C is the concentration of A atoms at any given value of x and t. The symbol erf represents the error function, which is a mathematical function whose values are given in Table 10-1. The values of the error function are tabulated in most handbooks which include mathematical tables, just as the trigonometric functions are tabulated.

Case hardening can best be discussed by considering an example. Nitrogen can be dissolved in the interstitial sites of an iron crystal, and the resulting Fe-N alloy is stronger, harder, and more brittle than the original iron. The effect of nitrogen concentration on the critical resolved shear stress of an Fe-N alloy is shown in Fig. 10-7. The interstitial atoms inhibit dislocation motion. Suppose that we want an Fe-N alloy which has a hard, strong surface but a more ductile interior. This could be achieved by

Fig. 10-7. The effect of nitrogen concentration on the critical resolved shear stress of iron. The nitrogen occupies interstitial sites in the iron lattice. Data are for room temperature. [Y. Nakada and A. S. Keh, Acta Met. 16:903 (1968).]



diffusing nitrogen into the iron. An arrangement such as that shown in Fig. 10-6 would be used, and the nitrogen concentration would be highest near the surface, in accordance with the concentration profiles of Fig. 10-6(b). The material would be case-hardened. Case hardening of iron or steel by nitrogen diffusion is called nitriding. Iron and steel can also be case-hardened by carbon, in which case the process is called carburizing.

Figure 10-6 shows that the concentration of A at any particular position depends on how long the diffusion has been going on. It also depends on temperature because the diffusivity, D, appears in equation 10-12. The depth to which the gas atoms diffuse in the solid is controllable and can be predicted by equation 10-12.

# Example 10-2

A piece of pure iron is to be nitrided until the concentration of N is 0.10 atomic % on a plane which is 0.05 cm below the surface. The process to be used is that shown in Fig. 10-6, and the surface concentration will remain fixed at 0.5 atomic % N throughout the process. The apparatus will be kept at 800°C, How long should diffusion be allowed to occur?

The solution consists of substituting appropriate quantities into equation 10-12:

$$C_s$$
 = surface concentration = 0.5 atomic %

C = concentration at the point of interest (i.e., x = 0.05 cm) = 0.1atomic %

$$C_0$$
 = initial concentration of N in Fe = 0 atomic %

$$D = 3.48 \times 10^{-6} \text{ cm}^2/\text{sec}$$
 at  $800^{\circ}\text{C}$  (handbook value)

$$x = 0.05 \text{ cm}$$

Substituting values,

$$\frac{0.5 - 0.1}{0.5 - 0} = \operatorname{erf}\left(\frac{0.05}{2\sqrt{3.48 \times 10^{-8}t}}\right)$$
$$0.80 = \operatorname{erf}\left(\frac{134}{\sqrt{t}}\right)$$

From Table 10-1, if erf Z = 0.80, then Z = 0.90:

$$\frac{134}{\sqrt{t}} = 0.90$$

$$t = \left(\frac{134}{0.90}\right)^2 \text{ sec} = 22,000 \text{ sec} = 6.11 \text{ hr}$$

Concentration was expressed in units of atomic percent for Example 10-2, while units of atoms per cubic centimeter were used in deriving Fick's first law. The change in units was permissible because equation 10-12 involves a ratio of concentrations. Because atoms/cc = atomic %x constant, the constant will cancel in the ratio. Concentration is often

expressed as either atomic percent or percent by weight rather than as atoms per cubic centimeter.

# Diffusion couple

In Example 10-2 we had to consider only the diffusion of A atoms into solid B because the surface concentration remained constant with time. Fick's second law has also been solved for the diffusion couple, which is a more complicated case. A diffusion couple consists of two solids, having different compositions, in contact with each other. An example is shown in Fig. 10-8(a), with the shaded plane representing the surface of contact. Let the two blocks both be pure substances, which we shall call A and B. When the blocks are placed in contact, A diffuses into B and B diffuses into A; this is called interdiffusion. Interdiffusion is responsible for diffusion welding. The rate of diffusion of A into B and B into A at any given value of x is described by Fick's first law and can be written as

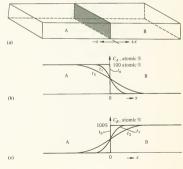
$$J_{\text{net A}} = -D_A \frac{dC_A}{dx}$$

$$J_{\text{net B}} = -D_B \frac{dC_B}{dx}$$

The values of the diffusivities  $D_A$  and  $D_B$  are not necessarily equal.

The concentration profiles of both A and B are shown in Fig. 10-8(b) and (c). The profiles are drawn for different times. Time  $t_0$  is the instant at which diffusion begins, and the concentration profiles show a step change at the contact surface. A and B diffuse into each other, and the concentration profiles change with time (curves  $t_1$  and  $t_2$ ). The concentration of either A or B, as a function of x and  $t_1$  can be found from the solution of

Fig. 10-8. (a) A diffusion couple composed of elements A and B. The surface at which the two blocks of material meet is shaded. (b) The concentration profile of A at three different times,  $t_0 < t_1 < t_3$ . A atoms diffuse into B. (c) The concentration profile of B showing that B atoms have diffused into A.



Fick's second law as applied to the diffusion couple. For element A, the solution is

$$\frac{C_{mA} - C_A}{C_{mA}} = \operatorname{erf}\left(\frac{x}{2\sqrt{D_A t}}\right) \tag{10-13}$$

where  $D_{\rm A}$  is the diffusivity of A diffusing into B.  $C_{\rm mA}$  is the mean concentration of A in the entire diffusion couple and can be evaluated from the expression

$$C_{mA} = \left(\frac{C_A \text{ in solid A} + C_A \text{ in solid B}}{2}\right)_{\text{evaluated at t = 0}}$$
(10-14)

From Fig. 10-8, it is seen that  $C_{mA}$  is 50 atomic % for the problem being considered. The origin of x is taken at the interface; therefore x can be positive or negative. Negative values can be handled readily because

$$\operatorname{erf}(-Z) = -\operatorname{erf} Z \tag{10-15}$$

Time is measured from the instant of contact. The concentration profile of B is governed by a similar expression:

$$\frac{C_{mB} - C_{B}}{C_{mB}} = \operatorname{erf}\left(\frac{x}{2\sqrt{D_{B}t}}\right) \tag{10-16}$$

The diffusion couple provides one method of experimentally determining the coefficient of diffusion. For example, suppose that a diffusion couple were made and diffusion occurred for a given period of time. The concentration profile could then be determined experimentally by using one of several available methods. Small samples could be machined from the diffusion couple at various values of x, and the concentrations of A and B in these samples could be determined by "wet" chemical analysis. Concentrations could also be found by using X-ray diffraction or the electron microprobe. Once  $C_A$  and  $C_B$  are known as functions of x, and the time of diffusion is known, these quantities can be substituted into equations 10-13 and 10-16. The only unknowns in these equations would be  $D_A$  and  $D_B$ ; therefore a diffusion couple experiment and Fick's second law permits us to experimentally determine diffusion coefficients.

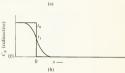
#### Self-diffusion

Self-diffusion was discussed in Chapter 9 in connection with vacancy motion. It was found that self-diffusion was important in both annealing and creep and that the activation energy for creep correlated very well with the activation energy for self-diffusion (see Fig. 9-22). Thus, the coefficient of self-diffusion, D\*, is an important quantity and must be measured. The question is, how does one measure the rate of diffusion of atoms when the diffusing atoms are the same chemical species as the lattice atoms? None of the methods given in the previous section will work.

Radioactive tracers have proved to be very useful in determining self-diffusion coefficients. Figure 10-9(a) shows a block of element A in contact



Fig. 10-9. Method for determining self-diffusion coefficients. (a) A diffusion couple made of element A and a radioactive isotope of A. (b) The concentration profile of radioactive A, which can be found by radioactivity measurement.



with a second block of the same substance; however, the second block contains a radioactive isotope of A. A diffusion couple is formed by the blocks, and interdiffusion occurs. The radioactive isotopes diffuse into the block of nonradioactive A, and the concentration of radioactive particles can be measured by determining the radioactivity of the material. This measurement can be made by using a suitable radiation detector. The concentration of the radioactive isotope can then be plotted as a function x [Fig. 10-9(b)], and  $D^*$  can be found by combining the experimental data with an appropriate solution of Fick's second law.

## Example 10-3

A diffusion couple is made of a block of pure copper and a block of copper containing 5 atomic % radioactive copper isotope. Diffusion proceeds for 35 hr at a temperature of 1200 ff. At the end of this period, it is found that the concentration of radioactive copper is 0.645 atomic % at a plane located 0.013 cm to the right of the interface [the arrangement of the blocks is the same as shown in Fig. 10-9(a)]. Find D\*\*.

The solution consists of substituting appropriate values into equation 10-13, considering the radioactive atoms as A atoms:

$$\begin{split} \frac{C_{mA} - C_A}{C_{mA}} &= \text{erf}\left(\frac{x}{2\sqrt{D^*t}}\right) \\ C_{mA} &= \frac{5+0}{2} = 2.5 \, \text{atomic} \, \% \\ C_A &= 0.645 \, \, \text{atomic} \, \% \\ x &= 0.013 \, \, \text{cm} \\ t &= (35) \, (3600) = 1.26 \times 10^5 \, \, \text{sec} \\ \text{erf}\left(\frac{x}{2\sqrt{D^*t}}\right) &= \frac{2.5-0.645}{2.5} = 0.742 \end{split}$$

From Table 10-1.

$$\frac{x}{2\sqrt{D^*t}} = 0.80$$

$$D^* = \frac{x^2}{4t(0.8)^2} = \frac{(0.013)^2}{(4)(1.26 \times 10^5)(0.64)} = 5.3 \times 10^{-10} \text{ cm}^2/\text{sec at } 1200^\circ \text{K}$$

Ouestion

Question 4: Useful shapes can be fabricated from powdered metals by a process called sintering. Metal powder is placed in a mold and subjected to high pressure. The mold is then heated to a high temperature (but below the melting point) and is kept there for a period of time. When the mold is opened, it is found that the powdered particles have joined together to form a solid. (a) Why do the particles join together to form a solid? (b) Is the energy of the metal raised or lowered by the sintering process?

# 10-4 Quantities affecting the diffusion coefficient

The diffusion coefficient emerged during the derivation of Fick's first law in Section 10-2. We shall now consider this quantity in more detail and consider which physical quantities affect its value.

The diffusion coefficient is defined by equations 10-2 and 10-9:

$$D = d^2\beta v e^{-q_d/kT} \qquad (10-17)$$

The quantity d is the distance between planes in the crystal; this distance is measured in the direction of diffusion,  $\beta$  is a geometric factor discussed in Section 10-1. The terms  $d^2$ ,  $\beta$ , and  $\nu$  are usually grouped together in a single term, and D can then be written as

$$D = D_0 e^{-q_d/kT} (10-18)$$

The quantity  $D_0$  depends on the structure and the vibrational frequency of the atoms, while the exponential term shows the effect of temperature and activation energy. Equation 10-18 shows that a plot of  $\log D$  vs. 1/T should yield a straight line, as is characteristic of an activated process. These plots are shown for a number of materials in Fig. 10-10, and the exponential temperature dependence is clearly indicated by the straight lines. The activation energy, for any of the diffusion combinations shown, can be found from the slope of the line, while  $D_0$  can be determined from the intercept. The activation energy and  $D_0$  for many diffusing materials are tabulated in a number of reference books, and several of these values are given in Table 10-2. The tabulated values of the activation energies are given in kilocalories per gram-mole, while  $q_0$  is the activation energy per atom for diffusion. The conversion between the two is easily made because

$$\frac{q_d}{kT} = \frac{Q_d}{RT}$$

Activation energy is often expressed on a molar basis.

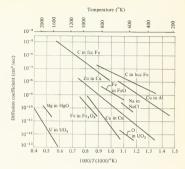


Fig. 10-10. Diffusion coefficients for a number of substances, plotted as a function of temperature. The straight lines indicate that these diffusion coefficients obey equation 10-18.

The diffusion coefficient is affected by concentration, but this effect is usually small when compared to the effect of temperature. The diffusion mechanisms discussed in Section 10-1 assumed that atoms jumped from one site to another. The rate at which the atoms jumped depended on wibrational frequency, crystal structure, activation energy, and temperature. The activation energy depends on the energies of the bonds which are formed between the jumping atom and its neighbors. The bond energies,

Table 10-2. Approximate values of  $D_0$  and  $Q_d$  for several systems

Aaterial diffused into	Diffusing material	Do (cm <sup>2</sup> /sec)	Q# (kcal/g-mole	
Aluminum	Copper	2.0	33.9	
Aluminum	Magnesium	0.12	28.6	
Copper	Copper	0.20	47.1	
Copper	Nickel	0.000065	29.8	
Copper	Zinc	0.00058	42.0	
Germanium	Germanium	7.8	69.0	
Germanium	Arsenic	6.0	57.5	
Gold	Silver	0.000534	29.8	
Iron (bcc)	Iron (bcc)	0.01	69.0	
Iron (bcc)	Carbon	0.0079	18.1	
Iron (bcc)	Nitrogen	0.014	17.7	
Iron (fcc)	Carbon	0.21	33.8	
Iron (fcc)	Nickel	0.5	66.0	
Niobium	Niobium	4.13	95.0	
Silicon	Lithium	0.0023	15.0	
Silver	Gold	0.029	38.0	
Silver	Silver	0.895	45,95	
Tantalum	Tantalum	2.0	110.0	
Zinc	Copper	0.34	45.6	

<sup>\*</sup> To find q, divide Q by Avogadro's number.

#### Ouestions

Question 5: Is Do an isotropic quantity? Why?

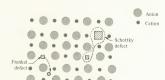
Question 6: Table 10-2 shows that the activation energy for silver diffusing into gold is 29.8 keal/mole for low concentrations of silver. Self-diffusion of silver requires 45.95 keal/mole. For the diffusion couple shown in Fig. 10-8, let A be silver and B be gold. Consider the silver atoms diffusing on the right side of the interface. Will the activation energy for these atoms increase, decrease, or stay the same as diffusion progresses? Why?

# 10-5 Diffusion in oxides and ionic crystals

Diffusion in oxides and other crystalline compounds that have ionic or partial ionic bonds can occur by the mechanisms previously discussed. The process is somewhat complicated by the requirement of electrical neutrality. Vacancies must be formed in such a way that the crystal does not acquire an electric charge. Two possible vacancy formation mechanisms are illustrated in Fig. 10-11, which represents a plane of an ionic crystal. Electrical neutrality can be maintained if the vacancies form in pairs, with each pair consisting of one cation and one anion vacancy. This combination

\* See, for example, W. Jost, Diffusion in Solids, Liquids and Gases, Academic Press, New York, 1952.

Fig. 10-11. Vacancy formation in ionic crystals. If the crystal maintains electrical neutrality, a single ion cannot be removed. The squares represent vacancies.



is called a Schottky defect and is shown in the figure. The formation of a Frenkel defect is also shown, and it is caused by one of the small ions (usually the cation) creating a new site for itself. This leaves a cation vacancy and maintains charge neutrality. The presence of these defects permits both cations and anions to diffuse by a vacancy mechanism; however, they do not diffuse at the same rate. The cations diffuse through cation vacancies and the anions through anion vacancies. Activation energies are not the same for both processes.

Diffusion in ionic crystals and oxides is very sensitive to the concentration of impurities because these strongly affect the number of vacancies.

For example, suppose that an NaCl crystal contained cadmium as an
impurity. The valence of Na is +1, while that of Cd is +2. The Cd enters
the lattice as a Cd<sup>2+</sup> ion; therefore a single cadmium ion would have to
replace two sodium ions in the crystal in order to maintain electrical
neutrality. If the cadmium atom occupied a single sodium site, one empty
sodium site (cation vacancy) would have to be created. This site would
then be available for cation diffusion, and the rate at which sodium
diffused through NaCl would increase. This has been observed.\* The
impurity effect also occurs in metallic oxides, and the rate of oxygen
diffusion through an oxide is often increased by the presence of impurities
which occury vanion sites.

The diffusion process is quite useful in fabricating parts from high-temperature ceramics. The high melting point of these materials often makes it impractical to melt and east them. In many cases, useful parts can be made by sintering powdered ceramic materials. The sintering process was discussed in Question 4, and it was seen that powdered particles would bond together by diffusion. Because diffusion occurs below the melting point, parts can be sintered at temperatures below the melting point.

Question

Question 7: Ionic crystals do not have free electrons as metals do, but nevertheless they conduct electricity. They do not conduct nearly as well as metals. The conductivity of ionic crystals increases almost exponentially with temperature. How do the ionic crystals conduct?

10-6 Grain boundary and surface diffusion

Diffusion occurs along the surfaces of a solid and in the grain boundaries of a polycrystal as well as through the volume of a material. Surface atoms form fewer bonds than atoms in the interior of a solid. The energy barrier that an atom must overcome in order to move (see Fig. 9-8) depends on bond energy; therefore we would expect surface diffusion to have a lower activation energy than volume diffusion. This is generally observed. The data in Table 10-3 show that the activation energy for thorium diffusion on a tungsten surface is lower than the activation energy for volume diffusion. We have encountered surface diffusion before. Our discussion of solidification involved atoms migrating on a surface (see Section 4-1). This migration is surface diffusion. Atoms in the region of grain boundaries are not bonded as tightly as interior atoms; consequently they diffuse more

<sup>\*</sup> See P. Shewmon, op. cit., p. 148.

Table 10-3. Volume, grain boundary, and surface-diffusion coefficients for the silver-silver and tungsten-thorium systems

Type of diffusion	Solvent material	Diffusing material	D <sub>0</sub> (cm <sup>2</sup> /sec)	Q <sub>d</sub> (kcal/g-mole)
Volume	Silver	Silver	0.9	40.0
Grain boundary	Silver	Silver	0.03	20.2
Surface	Silver	Silver		
Volume	Tungsten	Thorium	1.0	120.0
Grain boundary	Tungsten	Thorium	0.47	90.0
Surface	Tungsten	Thorium	0.47	66.4

readily. Values of  $D_0$  and Q are given for the grain boundary diffusion of two systems in Table 10-3. By comparing the values of D for surface, grain boundary, and volume diffusion given in the table, it is seen that

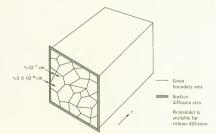
$$D_{
m surface} > D_{
m grain\ boundary} > D_{
m volume}$$

Diffusion coefficients for surface and grain boundary diffusion can be used in Fick's first law to find the rate at which atoms move by these mechanisms. Equation 10-10 is written in terms of flux. The rate at which atoms move through a solid is just the flux times the area; therefore

Diffusion rate = 
$$JA = -DA \frac{dC}{dx}$$
 atoms/sec (10-19)

The area term in equation 10-19 becomes quite significant if we want to compare grain boundary and surface diffusion with volume diffusion. The 'width' of a grain boundary can be taken as equal to several atomic distances (approximately  $10^{-7}\,\mathrm{cm}$ ). The area available for grain boundary diffusion is generally small, but varies with grain size. This is illustrated in Fig. 10-12. If the diffusion is in the x direction, the area available for grain boundary diffusion is shown as the darkened areas. The area available for surface diffusion is still smaller and is shown as the shaded area. For most solids, we have a situation in which  $D_{uurface} > D_{grain} \, boundary > D_{cylume} \, but$ 

Fig. 10-12. Schematic drawing of a polycrystal showing the areas available for volume, grain boundary, and surface diffusion in the x direction.



#### PROBLEMS

 $A_{\text{surface}} < A_{\text{grain boundary}} < A_{\text{volume}}$ . Which of these will predominate depends on grain size and the dimensions of the specimen (see Problem 10-11)

#### Ouestion

Question 8: Would you expect surface diffusion to be important in a sintering process? Why?

# 10-7 Summary

The diffusion process has been described as the movement of atoms through a solid by an activated mechanism which depends on vacancies. The rate at which diffusion occurs is described by Fick's laws and depends on the diffusion coefficient and the concentration gradient, dCldx. The diffusion coefficient, in turn, is highly temperature sensitive and depends on concentration and crystal structure as well as on temperature. Diffusion is thus a function of temperature, bonding, and structure.

Three applications of diffusion were discussed: diffusion bonding, sintering, and case hardening. The temperature dependence of the diffusion process is used in all of these. For example, a material can be case-hardened at high temperature and a concentration gradient will be formed near the surface when case hardening is completed. The solid can then be cooled to room temperature, and the concentration gradient will remain. According to Fick's first law, diffusion should continue because a concentration gradient exists; however, the rate may be so small at room temperature that the diffusion is negligible. This is similar to the situation encountered with annealing, which was another thermally activated process. The usefulness of diffusion is by no means limited to the processes discussed. We shall have need for the diffusion concept in Chapters 11 and 12. It plays an important role in several of the mechanisms used to strengthen materials.

#### Problems

- 1 The (100) plane of an fcc crystal is shown in Fig. 10-2. The location of the interstitial sites is also shown. Let \$\mathscr{H}\$ be the radius of the large atoms and \$\mathscr{H}\$\_1 the radius of the interstitials. Find the ratio of \$\mathscr{H}\_1/\mathscr{H}\$ for which the interstitial atoms just touch their neighbors.
- 2 The number of jumps that an atom makes per second is given by equation 9 + 11, (a) A substitutional alloy contains A and B atoms. One percent of the lattice sites are occupied by B atoms. The activation energy for movement  $(q_n)$  is  $2 \in V$  for a B atom, and  $q_n$  is  $1 \in V$ . How many jumps will a B atom make in  $1 \sec a t 1000^n \text{K} \cdot V = 10^{12} \text{Jec.}$  (b) Solve part (a) considering that the B atoms are interstitials. Use the same values as in part (a) and let  $1^{1/2}$  of the interstitial sites be occupied. (Hint: Recall that the jump rate equation includes the probability of vacancies. This probability is different for parts (a) and (b) even if  $q_n$  is the same.
- 3 Figure 10-3 shows the concentration profile of B atoms in an AB solid solution. (a) Sketch the concentration profile of A atoms in this solu-

- tion. (b) What is the direction of the flux of A atoms? (c) Is the slope of the concentration profile negative in this direction?
- 4 Planes 1 and 2 of Fig. 10-3 were used to derive Fick's first law. The concentration of B atoms on plane 1 was found in Example 10-1. (a) Find the concentration of B atoms on plane 2, again letting d = 5Å. (b) Find the slope of the concentration profile between planes 1 and 2. (This quantity is exactly  $\Delta C_B/\Delta x$ , and  $\Delta x = d$ .)
- 5 Fick's first law is given by equation 10-10, and concentration is expressed as atoms per cubic centimeter. Concentration is often expressed as atomic percent rather than atoms per cubic centimeter. If this is done, an additional constant must be introduced. Find the value of this constant in terms of the lattice parameter if the structure is fcc.
- 6 Figure 10-5 shows the concentration profiles of B at three different times. These concentrations exist in the block shown in Fig. 10-3(a). (a) Imagine that a plane, which is parallel to planes 1 and 2, is placed at some position x. Does the flux of B atoms past this plane increase or decrease as time increases? Why? This can be answered by inspection of Fig. 10-5. (b) How much time will elapse before the B atoms are uniformly distributed throughout the block?
- 7 Nitrogen has been diffused into pure iron, with the diffusion taking place at 800°C for 4 hr. The surface concentration of nitrogen was maintained at 0.6 atomic % during the diffusion. Plot the resulting concentration profile of nitrogen in iron from x = 0 to x = 0.5 cm. Do the calculation for each 0.1-cm increment in order to construct the curve. Express concentration in atomic percent.  $D = 3.65 \times 10^{-6}$ cm2/sec.
- 8 Find Do and Q for the diffusion of uranium, in UO2, using the data in Fig. 10-10.
- 9 A diffusion couple is shown in Fig. 10-8. Let element A be silver and element B be gold. Suppose that the concentration of silver on the right side of the interface (the region that was initially pure gold) has a concentration profile that is described by

Atomic % silver = 
$$\frac{5.0}{(0.1 + r)}$$

at some time t. The equation is valid for positive values of x (see Fig. 10-8). (a) Calculate the flux of silver atoms past a plane located 0.3 cm to the right of the interface. The plane is perpendicular to the x direction. Diffusion occurs at 600°C. The data in Table 10-2 can be used to find D for silver diffusing into gold. (b) Calculate the flux of gold atoms past this plane. Use the value of D for gold diffusing into silver. (c) In which direction do more atoms move?

- 10 (a) Find the coefficient of diffusion of nitrogen into iron at 800°C and at room temperature. (b) If a piece of iron is case-hardened with nitrogen at 800°C and then cooled to room temperature, would you expect the concentration profile of nitrogen to remain about the same for a period of several years? Explain.
- 11 Assume that a piece of polycrystalline tungsten has cubic grains and that thorium diffuses through the tungsten. The width of the grain boundaries is 5 × 10<sup>-8</sup> cm. If diffusion occurs at 1200°K, what must the grain size be in order for equal diffusion to occur through the grain

- boundaries and the volume? (Note: The assumption of cubic grains is unrealistic).
- 12 To form a diffusion bond, the two pieces to be bonded are pressed together, and the temperature of the pieces is raised. The pieces are not smooth, on an atomic scale, at the interface (the plane at which they meet). Discuss the role of surface diffusion in the early stages of diffusion bonding.

Answers

- Question 1: Each atom in the fcc structure has 12 nearest neighbors; therefore the vacancy has 12 atoms adjacent to it. Each of these has the same probability of acquiring the activation energy. Thus, the probability that atom 1 will acquire the activation energy first is ⅓.
- Question 2: In going from equation 10-2 to 10-3, we let  $D' = \beta v e^{-sahT}$ ; therefore D' included the dependence of flux on  $q_a$  and T. In equation 10-9, we let  $D = d^2D'$ ; thus D depends on  $q_a$  and T. In equation 10-10, the dependence of flux on temperature and activation energy is included in the diffusivity, D.

Question 3: 
$$J_{\text{net}} = -D \left( \frac{-\operatorname{atoms/cm}^3}{\operatorname{cm}} \right)$$
$$D = \frac{\operatorname{atoms/cm}^2 \sec}{\operatorname{atoms/cm}^4} = \frac{\operatorname{cm}^2}{\sec}$$

- Question 4: (a) The powdered particles join each other because of diffusion.

  Atoms of one particle diffuse into another at points where they touch and bonds are formed. The pressure insures intimate contact between adjacent particles. (b) The energy of the metal is reduced by sintering because the surface area is greatly diminished. Powder particles have a large area per unit mass.
- Question 5:  $D_0$  is not isotropic. Both d and  $\beta$  depend on the crystallographic direction of diffusion. This effect is generally very small compared to other effects, such as temperature, impurities, etc., and is usually neglected.
- Question 6: Increases. At the start of diffusion, the concentration of silver in the gold is very low, and the activation energy of 29.8 Kealfg-mole is vallid. As the concentration of silver in the gold increases, the activation energy changes. The direction of the change is toward the activation energy for self-diffusion of silver; therefore the activation energy increases as silver concentration increases. The relationship between activation energy and concentration is not linear.
- Question 7: Electric charge is transported by the diffusion of ions. Negative ions are attracted toward the side of the crystal having a positive applied voltage and vice versa. Motion of these ions constitutes an electric current. In some cases cation diffusion predominates; in others anion diffusion is greater.
- Question 8: Yes. Powdered particles have a large surface to volume ratio; consequently a great deal of diffusion can occur on the surface in the early stages of sintering. As sintering progresses, surfaces are eliminated and surface diffusion becomes less important.



# Phase Diagrams, and Phase Transformations

SOLUBILITY refers to the ability of one substance to dissolve in another. In Chapter 10 we discussed diffusion of solids which were soluble in each other (or mutually soluble). These substances formed solid solutions. There are many combinations of substances in nature that are mutually soluble in all proportions; that is, they form solutions regardless of the relative amounts of solute and solvent. Other combinations are completely insoluble. Partial solubility is also observed in many cases. Alcohol and water provide an example of complete solubility between two liquids. while copper and nickel are mutually soluble in all proportions in the solid state. There are also combinations of substances that are insoluble, as in the case of petroleum and water. In Section 8-6 we considered an example of insolubility in the solid state. There we postulated that dislocation pinning sites could be caused by collections of impurity particles. The impurities had to be insoluble in the parent material if they agglomerated to form pinning sites because soluble impurities would disperse throughout the solid. Many substances are partially soluble in each other; there is a limit as to how much solute a particular solvent can dissolve. A common example of this is salt water. Salt will be dissolved by water until the water is saturated. Further addition of salt merely results in solid salt falling to the bottom of the container.

The solubility characteristics of substances are often represented by phase diagrams. This chapter will explain phase diagrams and will discuss the information which they contain. Gibbs phase rule and its application to phase diagrams will also be covered. The solidification of materials is strongly affected by solubility characteristics, as will be explained. In addition, many solids can undergo a change of phase as temperature changes. This is analogous to melting or freezing except that the material is a solid both before and after the change. Such changes are called

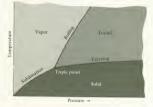
solid-state phase transformations and can be predicted from phase diagrams. The occurrence of solid-state transformations affects the properties and microstructure of solids. Microstructure changes will be covered in this chapter. Methods of manipulating microstructure and phase transformations in order to impart a desired set of physical properties to a material will be covered in Chapter 12; however, the explanation of why these methods are successful rests largely with phase diagrams. The last topic covered is the effect of solubility on diffusion.

#### 11.1 Equilibrium phase diagram of a pure substance

Consider a pure substance (an element or a compound) which can exist as a solid, liquid, or vapor. Which of these states the substance will assume depends on the temperature and pressure. As an example, H<sub>2</sub>O at a pressure of 1 atm is liquid at temperatures between 0°C and 100°C. solid below 0°C, and vapor above 100°C. Vapor and liquid can coexist in equilibrium at the boiling point, while solid and liquid can coexist in equilibrium at the freezing point. If the pressure applied to the H2O is decreased, the boiling temperature decreases and vice versa. This is commonly observed when cooking at high altitude, as in the mountains. Water boils at a lower temperature there than at sea level; consequently it takes longer for food to cook. The boiling and freezing temperatures of a pure substance can be measured at various pressures and the measured values can be plotted on a curve of temperature vs. pressure. The result of doing this is shown schematically in Fig. 11-1. The figure also shows a line labeled "sublimation" which gives the pressures and temperatures at which the solid and vapor coexist in equilibrium. The sublimation curve can be determined in the same manner as the boiling and freezing curves.

The data for Fig. 11-1 can be obtained by observing a system which contains the substance of interest. We shall use the word system to mean the volume occupied by the substance that we are interested in (or are observing). The figure is divided into three parts. Each part contains a single phase of the substance. A phase is defined as a homogeneous region of a system. A homogeneous region is a region (or volume) in which the

Fig. 11-1. Equilibrium phase diagram of a pure substance showing the solid, liquid, and vapor phases. The curves labeled freezing, boiling, and sublimation are the phase boundaries. Phases coexist along the phase boundaries.



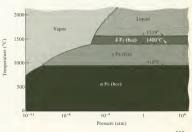
properties of the system are uniform. The boiling, freezing, and sublimation curves in Fig. 11-1 form the boundaries between phases; two phases can coexist in equilibrium at the temperatures and pressures defined by the lines. There is also one point at which all three phases coexist; this is called the triple point. Figure 11-1 can be considered as a map of the regions in which the different phases exist when the system is in equilibrium. It is called a phase diagram.

Figure 11-1 represents a simple case. Many materials are capable of forming more than one solid phase. According to the definition given, a phase is homogeneous. If a material is solidified into two or more crystal structures, each structure would occupy a homogeneous region and the solid would have more than one phase. Pure iron behaves in this way. It can have either an fec or a bec structure, depending on temperature and pressure. The equilibrium phase diagram of pure iron is shown in Fig. 11-2. Three different solid phases are shown  $(\alpha, \gamma, \delta)$ . The boundaries have the same physical meaning as melting, boiling, and sublimation curves. For example,  $\alpha$  and  $\gamma$  iron can coexist at a temperature of  $910^{\circ}\mathrm{C}$  and a pressure of 1 atm. At temperatures slightly above this, the iron is  $\gamma$ , while at lower temperatures it is  $\alpha$ .

It should be noted that the melting temperature and the temperature at which the solid-phase transitions occur in iron are not very sensitive to pressure. The boiling temperature is pressure dependent; however, we shall be concerned with melting and solid-state phase transitions, not boiling. For many materials, the melting and phase transition temperatures are not very pressure sensitive, and we shall make use of this observation later on.

The question that often arises at this point is, "Why do solids sometimes show more than one structure?" The answer lies in the condition required for equilibrium, which is that the system be in that state which has the minimum value for the free energy. We encountered this condition previously in Section 4-7. According to Fig. 11-2, the free energy of cei ron is lower than that of bec iron between 910 and 1400°C. In principle, equilibrium phase diagrams can be constructed from the minimum free-energy criterion. This is seldom done in practice; phase diagrams are usually con-

Fig. 11-2. The equilibrium phase diagram of pure iron. Iron forms three different solid phases, as shown. The temperatures shown on the phase boundaries are the phase transition temperatures at a pressure of 1 atm.



structed from experimental data. This is the course that will be followed in the present chapter.

Questions

Question 1: Can y iron melt, or will it undergo a solid-state phase change before melting? Can it sublimate?

Question 2: How many triple points appear in Fig. 11-2? What phases coexist at these points?

# 11-2. Binary diagrams and solubility

The phase diagrams of Section 11-1 used pressure and temperature as the coordinates, and the regions in which the different phases appeared were mapped. Because these diagrams were for pure substances, the systems considered had only one component. In this section, composition is introduced as a variable, and we shall consider a system which is within the realm of our experience, salt and water. This is called a binary (or two-component) system. The discussion in this chapter will be limited to binary systems.

It is commonly observed that salt dissolves in water and that there is a limit to the amount of salt that a quantity of water will dissolve. If a small amount of salt is added to a glass of water at room temperature, it dissolves. Salt can be added until it no longer dissolves; the water is saturated. If still more salt is added, it merely falls to the bottom of the glass. If the temperature of the saturated solution is lowered, salt precipitates from the solution. The solubility of salt in water is temperature dependent. These simple observations show that a system composed of salt and water can contain more than one phase. The system having an excess of salt contained two phases, salt water and salt. Salt water is a solution of NaCl and H<sub>2</sub>O (called brine) and conforms to the definition of a single phase. Which phase or phases appear in the system depends on temperature, NaCl concentration, and pressure.

The phase diagrams of binary systems generally use temperature and concentration as the coordinate axes of the diagram. The experiments which provide the data for constructing the diagrams are performed at constant pressure, usually 1 atm. Maintaining constant pressure eliminates pressure as a variable but also means that the diagram is valid only at a single pressure. For many systems this is not a significant limitation because they are not very pressure sensitive, as discussed in Section 11-1. All binary phase diagrams in this book were made at a pressure of 1 atm.

One procedure for determining the NaCl- $H_2$ O phase diagram will now be described. NaCl and  $H_2$ O are held in the container shown in Fig. 11-3 at a pressure of 1 atm. The container is surrounded by a bath at a given temperature, say 10°C. Let the solution be 25% salt by weight. If the temperature of the solution is lowered slowly, salt is observed to precipitate from the solution at -6°C. Thus, at -6°C, salt is in equilibrium with brine that contains 25%, NaCl by weight. This point is on a phase boundary and is plotted as point a in Fig. 11-4. The requirement that the temperature be lowered slowly is quite critical. Because we are constructing an equilibrium, the system must be given sufficient time to attain equilibrium, tet the temperature of the system be reduced to -10°C and



Fig. 11-3. A temperature-controlled system containing NaCl and H<sub>2</sub>O at a pressure of 1 atm. This apparatus can be used for constructing a phase diagram.



Fig. 11-4. The NaCl-H<sub>2</sub>O equilibrium phase diagram at a pressure of 1 atm.

held there long enough to attain equilibrium. More salt will precipitate due to the cooling. A very small sample of brine is then removed and analyzed. It is found to contain 24.5% NaCl (point b in Fig. 11-4). The salt content of the brine has been diminished because some salt has precipitated from the solution. The system still has 25% salt, and its overall state is depicted by b' in Fig. 11-4; the system is a mixture of salt and brine. Repeating the above procedure at -15°C yields point c; the overall system is at c'. At  $-21^{\circ}$ C, the brine contains 23.3 wt. % NaCl. If heat is removed from the system, ice begins to form and more salt precipitates because salt is not soluble in ice. The freezing can continue at constant temperature until all of the brine is converted to ice and salt. The line containing points a, b, and c forms the boundary between a single-phase region (brine) and a two-phase region (salt + brine). This same line would be found if we had started with a solution containing more than 25% salt; the 25% figure was arbitrary. The portion of the phase diagram which we have determined so far gives quite a bit of information. It tells us the the temperature at which the system enters the two-phase (salt + brine) region, the composition of each phase in this region as a function of temperature, and the temperature at which the reaction

Brine 
$$\rightarrow$$
 ice  $+$  salt (11-1)

begins.

The same procedure can be used to determine the left side of the phase diagram. Let us start with a solution containing 5% salt at 10°C and cool it slowly. Ice begins to form at  $-3^{\circ}$ C (point d in Fig. 11-4). Note that solutions having low NaCl concentrations precipitate ice; those with high NaCl concentrations precipitate salt. Further cooling increases the amount of ice. The ice does not contain salt; therefore the NaCl concentration in the brine has increased. If the temperature of the system is held at -10°C long enough for equilibrium to occur, the brine is found to contain 14% NaCl (point e in the figure). This procedure can be used to find point f, etc. At -21°C, the brine remaining in the system freezes as ice and salt. The state of the entire system is shown by the vertical line at 5% NaCl. Between -3 and -21°C, the container of Fig. 11-3 had a mixture of ice and brine; it contained two phases. The concentration of salt in the brine is given by the line containing points d. e. and f.

The phase diagram gives complete information about the composition of the phases when the system is in a two-phase region. Suppose the system was at point f'. The compositions of the two phases could be found by following line f''f'f to the phase boundaries closest to f'. The composition of the ice phase is given by f" and that of the brine phase by point f. The line f"f'f is called a tie line. No information is given about how much of each phase is present. This information can be obtained from the phase diagram, as will be shown in Section 11-5.

# Example 11-1

A system containing 10 wt. % NaCl and 90% H2O is at -10°C (point e" in Fig. 11-4). What phases are present? What is the concentration of salt in the brine? In the ice?

The point at -10°C and 10% salt is in the ice + brine region; therefore these two phases are present. The concentration of salt in the brine is given by point e, which is 14%. Following the tie line to the left edge of the diagram, the salt concentration in the ice is zero.

The phase diagram indicates a method for desalinating seawater. The concentration of salt in seawater is on the left side of the phase diagram in Fig. 11-4; therefore desalination can be accomplished by cooling seawater to a temperature slightly below -21°C, separating the ice from the brine, and melting the ice to obtain fresh water. Several years ago, the Office of Saline Water (a U.S. government agency) set up several desalination pilot plants. One of these utilized the freezing principle indicated by Fig. 11-4. The method worked well, but it was found that other methods were cheaper.

# Questions

Question 3: How many phases appear in Fig. 11-4? How many can coexist at -21°C and 23.3% NaCl?

Question 4: It was found that a system containing 10% NaCl and 90%  $H_2O$  at  $-10^{\circ}C$  (point  $e^{\prime\prime}$ ) had ice in equilibrium with brine and that the brine contained 14% salt. The same thing was true of a system containing 5% salt (point e'). The systems contain different concentrations of salt, yet the concentration of salt in the brine is the same for both. Explain how this can happen.

# 11-3 Gibbs phase rule

Two types of phase diagrams have been considered so far. For pure substances, the various phases were mapped using pressure and temperature as coordinates (Figs. 11-1 and 11-2). Two component diagrams used temperature and composition as coordinates while keeping the pressure constant. Thus, the three pertinent variables that we are dealing with are T, P, and composition. It is of interest to determine how many of these variables can be changed without having the system change its phase. This information is given by Gibbs phase rule.

Gibbs phase rule can be derived by using the science of thermodynamics. We shall not derive it but shall simply state that it is a consequence of the system being in its minimum free-energy state at equilibrium. The phase rule is

$$P' + F' = C' + 2 (11-2)$$

P' is the number of phases which coexist in a system. Inspection of Fig. 114-4 shows that the number of phases which coexist depends on which part of the diagram we are considering. C' is the number of components in the system. A component can be an element, a compound, or a solution. F' is the number of variables (pressure, temperature, and composition) which can be changed independently without changing the phase or phases of the system. F' is called the number of decrees of freedom.

# Single-component systems

The information given by equation 11-2 can best be understood by considering an example. The single-component system of Fig. 11-1 will be considered because it is a relatively simple system. Letting C' equal 1 in equation 11-2.

$$F' = 3 - P' (11-3)$$

for a system having one component. Consider a point completely within a single-phase region in Fig. 11-1. The system contains one phase (P' = 1). Using this in equation 11-3,

$$F' = 2$$

This tells us that two quantities (temperature and pressure) can be varied independently and the system will remain in a single phase. The extent to which either of these variables can be changed, without causing a phase change, is limited by the phase boundaries. If we select a point which lies on the boundary between phases (say on the freezing line), the system will contain two phases, solid and liquid (P'=2). Substituting into equation 11-3,

$$F' = 1$$

Because there is one degree of freedom, only one quantity (T or P) can be

changed independently and still have the system contain two phases. If, for example, the pressure is changed, there is only one temperature at which solid-liquid equilibrium will exist. The temperature is dependent on the pressure in the region of two-phase equilibrium. At the triple point, three phases are in equilibrium (P' = 3); consequently

$$F' = 0$$

The triple point is called an invariant point because none of the variables can be changed and still maintain the coexistence of three phases.

# Binary systems

Application of the phase rule to a binary system can be illustrated by considering the phase diagram in Fig. 11-4. This diagram was made under the condition of constant pressure, and equation 11-2 must be changed to

$$P' + F' = C' + 1 \tag{11-4}$$

because one degree of freedom (pressure) has been removed. The number of components is two (NaCl and H<sub>2</sub>O): therefore

$$P' + F' = 3 (11-5)$$

for a binary system at constant pressure. The quantities which can be varied are temperature and composition. Consider the ice + brine region (P'=2). For the region where these two phases coexist.

$$P' = 1$$

The one degree of freedom means that if we vary the temperature, the composition of the two phases will change in a predetermined manner. For example, a system at -10°C in the ice + brine region contains pure solid H2O (ice) and brine which has an NaCl concentration corresponding to point e in Fig. 11-4. The temperature can be arbitrarily changed; suppose it is reduced to -15°C. The two phases which coexist are pure ice and brine whose NaCl concentration corresponds to point f. The composition of the phases depends on the temperature in the two-phase region.

The point at -21°C and 23.3% NaCl represents three-phase equilibrium (salt, ice, and brine). Substituting P' = 3 into equation 11-5 yields F' = 0. A point with zero degrees of freedom is an invariant point. If the temperature is changed, three phases will no longer coexist. Later in the changer we shall be concerned with phase changes that occur at invariant points. Suppose that the system in Fig. 11-4 was at the invariant point and contained ice, salt, and brine. If a small amount of thermal energy were removed from the system, some of the brine would be converted to ice and salt. The temperature of the system would remain at -21°C. The phase change experienced by the brine is called an invariant reaction and is described by equation 11-1. The term simply denotes a reaction (phase change) that occurs at an invariant point (F' = 0) on the phase diagram.

Questions

Question 5: Locate the invariant points on the iron phase diagram (Fig. 11-2).

Question 6: How many degrees of freedom exist in the brine region of Fig. 11-4? In the salt + brine region?

# 11\_4 Systems with complete solid solubility

The discussion of diffusion in Chapter 10 considered two elements which were completely soluble in each other. There are a number of systems which exhibit complete solubility, and the phase diagrams of these systems will be discussed in this section.

The conditions under which two elements are soluble in each other in all proportions, in the solid state, have been formulated by Hume-Rothery and are known as the Hume-Rothery rules. These conditions are

- The crystal structure of each element of the solution must be the same.
   The size of the atoms of the two elements must not differ by more than 15%.
- 3. The elements should not form chemical compounds with each other because the resultant solid would be a compound and not a solution. An equivalent statement is that there be no appreciable difference between the
  - 4. The components must have the same valence.

electronegativities of the two components.

The Hume-Rothery rules are not inflexible, but rather they provide guidelines for predicting elements which will be completely miscible in each other. Complete solubility is not limited to elements. There are also compounds which are completely soluble in all proportions.

The phase diagram for a binary system can be found using the method described for the NaCl-H2O system. Consider two components, A and B. which are mutually soluble in all proportions. The melting points of pure A and pure B can readily be determined and plotted on a temperaturecomposition diagram, as shown in Fig. 11-5. Points f and a correspond to these melting points. Next, a 50:50 mixture (by weight) of A and B is placed in a container such as the one in Fig. 11-3. The mixture is heated until it melts and then it is cooled very slowly. At temperature T2 a very small amount of solid is formed. Analysis of the solid shows that it contains 92% B (point b" in the figure). Thus, at T2 we have a solid containing 92% B in equilibrium with a liquid containing 50% B (represented by point b'). The temperature of the system is then reduced to  $T_3$  and held there until equilibrium exists. The composition of the liquid is found to be 28% B (point c') and that of the solid is 85% B (point c''). Point c'' corresponds to the composition of the entire solid phase, which is homogeneous. Solidification began at T2, and the first solid which emerged contained 92% B. At T3, the solid has only 85% B. For this to occur, the solid which was formed at T2 had to change its composition by surrendering some B atoms. This is accomplished by the diffusion of B atoms from the solid that formed at  $T_2$ . Thus, the entire system was held at  $T_3$  long enough to allow this diffusion to occur. Similar measurements are made at T4, and points d' and d" are determined. The last liquid freezes at T5 and has a composition corresponding to e'. The composition of the solid is 50% A-50% B at  $T_5$ . This would be expected because the composition of the system does not depend on temperature. The system composition is given by points b', c, d, and e" at the various temperatures. The phase diagram for the AB

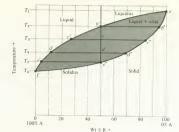
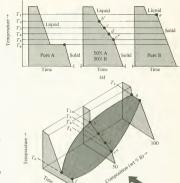


Fig. 11-5. The equilibrium phase diagram of a system containing components A and B. The components are mutually soluble in all proportions in both the liquid and solid states. Liquid and solid coexist in the shaded region.

system can be found by joining the experimentally determined points, as shown in Fig. 11-5. The upper curve, called the *liquidus*, forms the boundary between the single-phase liquid region and the two-phase region. The lower curve, called the *solidus*, separates the solid from the two-phase region. The same experiment can be made using a different initial concentration of B, and additional points on the liquidus and solidus curves would be found. The horizontal lines joining points b' and b'', c' and c'', etc., are called the lines.

The experiment outlined above is difficult to perform if we are dealing with materials having high melting points. It is often easier to determine the phase diagram by using cooling curves. These are obtained by heating the material to a temperature in the liquid region, cooling it slowly, and recording temperature as a function of time. Three cooling curves for the AB system are shown schematically in Fig. 11-6(a). The first one is for pure A and is characteristic of the freezing of a pure substance. Starting at high temperature, heat is removed slowly from the liquid, and the temperature decreases smoothly with time. At T6, the A freezes. Heat is removed, but the temperature stays constant as the phase change occurs. The heat removed is the latent heat, and the temperature-time curve shows a horizontal line at the freezing point. The curve for pure B shows the same characteristic, with freezing occurring at T1. The freezing temperatures correspond to points f and a in Fig. 11-5. The freezing behavior of a substance composed of 50% A and 50% B is different, as shown by the second curve in Fig. 11-6(a). The first solid begins to freeze at  $T_2$ . The solid has a composition corresponding to point b" of the phase diagram (Fig. 11-5) and is rich in component B. As a result of this solid forming, the concentration of B in the liquid is reduced. The composition of the remaining liquid corresponds to a point slightly to the left of b' in Fig. 11-5, and further freezing will not occur unless the temperature is again decreased. As a result, the latent heat of freezing is not released at a single temperature, but freezing occurs over the entire temperature range between T2 and T5. The slope of the cooling curve decreases in this region, as shown in the 50:50 curve of Fig. 10-6(a). The decreased slope is the result of both



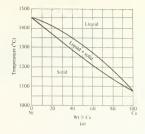
(b)

Fig. 11-6. The relationship between cooling curves and phase diagrams. (a) Cooling curves for the AB system. The three curves for the AB system. The three curves represent pure, pure B, and a 50:50 mixture, (b) The cooling curves con he used to draw it time-temperature-composition diagram. The three parallel planes are the cooling curves of (a). A plane view of this diagram, viewed in the direction of the arrow, gives the phase diagram.

sensible and latent heat being removed. Thus, the temperatures at which freezing begins and ends correspond to changes in the slope of the cooling curve. The points b', c, d, and e' in Fig. 11-6(a) correspond to the same points in Fig. 11-5. Cooling curves can be made for a number of different compositions and can be combined to form the time-temperature-composition plot shown in Fig. 11-6(b). The points at which freezing began and ended have been joined by two lines. If we now view the three-dimensional diagram from the direction indicated by the arrow (along the time axis) and draw a front view of this, the result is Fig. 11-5. The upper curved line in Fig. 11-6(b) represents the liquidus because it joins all points at which freezing commences. Similarly, the lower curve is the solidus. A front view of the heavily shaded plane in Fig. 11-6(b) corresponds to the liquid + solid region of Fig. 11-5.

The phase diagram of Fig. 11-5 is typical of binary systems whose components are mutually soluble in all proportions. Two such systems are shown in Fig. 11-7. The first is for copper-nickel alloys, while the second is for the ceramic system, MgO-NiO. The Cu-Ni system is composed of elements and follows the Hume-Rothery rules. The NiO-MgO system, however, is made up of two compounds. Both of these oxides form the NaCl structure (see Fig. 3-21). The structure can be considered as an foc lattice with oxygen ions at the lattice sites. The Mg and Ni ions occupy interstitial sites within this lattice. The interstices are large enough to accommodate either Mg or Ni. If we consider the MgO-NiO system as





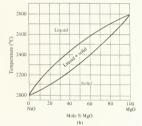


Fig. 11-7. Equilibrium phase diagrams of two systems having components that are mutually soluble in all proportions, both in the liquid and solid states, (a) The nickel-copper system, (b) The NiO-MgO system.

a special case of the Hume-Rothery rules, it is seen that the Mg and Ni cations follow rules 1, 2, and 4. The concentration in Fig. 11-7(b) is given in terms of mole percent, while Fig. 11-7(a) uses weight percent. Both are commonly used, although weight percent appears more often.

## Questions

Question 7: How many degrees of freedom does the Cu-Ni system have in each of its three regions?

Question 8: What are the compositions of the phases in equilibrium when a binary system containing 40% MgO and 60% NiO is at 2300°C? If the system contained 20% MgO at 2300%C? If it contained 80% MgO at 2300°C?

# 11-5 The lever rule

The number and composition of the phases in a system can be found from the phase diagram. In a two-phase region, we can determine the composi-

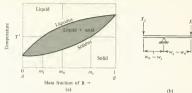


Fig. 11-8. (a) Phase diagram used for deriving the lever rule. The system is at temperature T'. The mass fraction of component B for the entire system is mo; the mass fractions of B in the solid and liquid are m, and m; respectively. (b) The lever analogy, according to equation 11-13. The fulrram of the seesaw is located at w. The mass fractions of the liquid and solid (X, and X) are the "loads" on the seesaw.

tion of each phase but so far have neglected how much of each phase is present. This can be found from the phase diagram by using a relationship called the *lever rule*, which is derived in this section.

Figure 11-8(a) shows the phase diagram of a system containing A and B. Let the total mass of the system be 1 lb,, and let the mass of B in the system be  $m_0$ . Thus,  $m_0$  is also the mass fraction of B. The figure shows the system at temperature T' and shows the tie line at this temperature. The mass fraction of the system which is liquid and that which is solid will be denoted by  $X_1$  and  $X_2$ , respectively. We can write

$$X_t + X_s = 1 \tag{11-6}$$

Now consider B. The mass fraction of component B in the solid is shown as  $m_s$ ; therefore the mass of B in the solid portion of the system is  $m_t X_t$ . Similarly, the mass of B in the liquid part of the system is  $m_t X_t$ . Applying the conservation of mass to component B,

$$m_0 = m_s X_s + m_l X_l$$
 (11-7)

Substituting equation 11-6 into 11-7 to eliminate  $X_{i,j}$ 

$$m_0 = m_s X_s + m_l (1 - X_s) ag{11-8}$$

Solving 11-8 for  $X_s$ ,

$$X_s = \frac{m_0 - m_l}{m_s - m_l} \tag{11-9}$$

Equation 11-9 expresses the mass fraction of the system which is in the solid state in terms of the mass fractions of component B, which can be found from the phase diagram. Phase diagrams usually use either weight percent or mole percent rather than mass fraction as the abscissa (see Fig. 11-7). While mass and weight are different quantities, the mass fraction of one component of a system is the same as its weight fraction, and weight

percent is, of course, the weight fraction expressed as a percentage. Equation 11-9 can be rewritten as

$$X_s = \frac{w_0 - w_l}{w_s - w_l} \tag{11-10}$$

where w is either weight fraction or weight percent. An expression for  $X_l$  can be derived similarly:

$$X_{l} = \frac{w_{s} - w_{0}}{w_{s} - w_{l}} \tag{11-11}$$

The ratio of equations 11-10 and 11-11 is sometimes useful. This ratio is

$$\frac{X_s}{X_l} = \frac{w_0 - w_l}{w_s - w_0}$$
(11-12)

or

$$X_t(w_t - w_0) = X_t(w_0 - w_t)$$
 (11-13)

Equations 11-10, 11-11, 11-12, and 11-13 are different forms of the lever rule. The reason for this name can readily be seen from equation 11-13, which expresses the weight fractions in terms of "lever arms," A seesaw analogy of this equation is shown in Fig. 11-8(b). The fulcrum is located at  $m_0$ , and the lengths of the lever arms on each side of the fulcrum correspond to lengths on the tie line of Fig. 11-8(a). The left arm has a length corresponding to the distance from  $m_0$  to the liquidus, and similarly for the other side. The applied "loads" are X, and X, are X.

# Example 11-2

A Cu-Ni alloy contains 60% Cu by weight and is at a temperature of 1250°C. How much of the alloy is solid and how much liquid?

From Fig. 11-7(a),

$$w_s = 50\%$$
  $w_l = 66\%$   $w_0 = 60\%$ 

Substituting into equation 11-9,

$$X_s = \frac{60 - 66}{50 - 66} = \frac{-6}{-16} = 0.375 = 37.5\%$$

$$X_t = 1 - X_s = 0.625 = 62.5\%$$

The fractions are by weight.

The lever rule can also be used when the abscissa of the phase diagram is given in units of mole fraction or mole percent [see Fig. 11-7(b)]. The entire derivation can be done in terms of moles (see Problem 11-7) and equations analogous to 11-10, 11-11, and 11-12 can be derived. The equations are the same as those given above except that mole fraction is

substituted for weight fraction and  $X_s$  and  $X_t$  are then the mole fractions of solid and liquid.

Ouestions

Question 9: Derive equation 11-11.

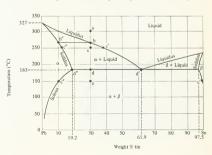
Question 10: A Cu-Ni alloy contains 70% Cu by weight. It is at a temperature of 1200°C. If the system contains 5 lb<sub>m</sub> of alloy, how many lb<sub>m</sub> of liquid are in the system?

# 11-6 The binary eutectic system

Most binary systems do not show complete mutual solubility in both the liquid and solid states. This section will discuss the eutectic diagram, which is a common type of phase diagram. Eutectic systems have components which are completely miscible in the liquid state but have limited solid solubility.

A typical eutectic system is lead and tin. The phase diagram of the system can be found by either of the methods discussed in Section 11-4. and the results are shown in Fig. 11-9. This is a eutectic diagram. It bears a close resemblance to the NaCl-H2O system (Fig. 11-4) except for the two phases labeled  $\alpha$  and  $\beta$ . Let us consider this difference in some detail. In the NaCl-H<sub>2</sub>O system, salt was completely insoluble in ice. When salt water solidified, the result was a mixture of two phases, pure ice and pure salt. For the lead-tin system, however, each component is capable of dissolving a limited amount of the other; they have limited solubility. The solubility limit of tin in lead is shown by the solvus line on the left side of the diagram. For example, the solvus passes through a point at 10% tin and 150°C (point e"). This tells us that lead and tin can exist as a solid solution (at 150°C) as long as the tin concentration does not exceed 10% by weight. The α region of the diagram thus represents a solid solution of lead and tin which is rich in lead. It is a single-phase region, Similarly, the solvus line on the right side of the diagram represents the solubility limit

Fig. 11-9. The equilibrium phase diagram of the lead-tin system. It is a typical eutectic diagram.



of lead in tin,  $\beta$  is a solid solution which is rich in tin. The diagram shows that most solid compositions fall outside of the single-phase regions. For example, a solid lead-tin alloy having 40% tin at 100°C falls in the region labeled  $\alpha + \beta$ . This region contains a mixture of  $\alpha$  phase and  $\beta$  phase, just as the NaCl-H<sub>2</sub>O diagram showed a mixture of ice and salt in the solid state. The important distinction between these systems is that a and B are both solid solutions; they are not pure substances. It is essential to consider the  $\alpha + \beta$  region as containing a mixture of two solutions. It should not be considered as a region containing a mixture of pure lead and pure tin. The proportions of  $\alpha$  and  $\beta$  in a solid can be found by the lever rule. For an alloy containing 40% tin at 100°C,

wt. 
$$\%$$
  $\alpha = \frac{100 - 40}{100 - 6} = 62.5\%$   
wt.  $\%$   $\beta = 100 - 62.5 = 37.5\%$ 

The calculation assumed that the solubility of lead in tin is negligible at 100°C, as indicated by the phase diagram.

Consider what happens when an alloy containing 30% tin is slowly cooled from 300°C (point a in the figure). The first solid appears when the temperature has fallen to 267°C (point b) and is a solid solution (\alpha phase) which contains 10% tin (point b"). Further cooling causes more solidification. At 250°C, the liquid has a tin concentration corresponding to point c', while the concentration of tin in the solid is shown by c''. The tin concentration in the liquid follows the liquidus line and that in the solid follows the solidus line. The amounts of liquid and solid at any particular temperature can be determined by the lever rule. The concentration of tin in the solid increases as freezing progresses. To maintain equilibrium, the tin content of the solid which was formed at higher temperatures (low tin concentration) must increase. This occurs by diffusion, and the freezing rate must be slow enough to allow this diffusion if equilibrium is to be maintained. In some cases it is not desirable to maintain equilibrium, and the alloy is cooled quickly, as will be discussed in Chapter 12.

The composition of the liquid follows the liquidus line and that of the solid follows the solidus line as freezing progresses. At 183°C, all of the liquid remaining in the system freezes. It is of interest to consider this freezing in some detail. The composition of the liquid at 183°C is given by point d' in Fig. 11-9. This is an invariant point and is called the eutectic point. The temperature and composition which correspond to it are called the eutectic temperature  $(T_e)$  and eutectic composition. At a temperature slightly above  $T_e$ , the system contains  $\alpha$  having 19.2% tin (point d'' in Fig. 11-9) and liquid having 61.9% tin. The α which formed at temperatures above  $T_e$  is called primary  $\alpha$ . When the system is cooled through the eutectic point, liquid freezes into both  $\alpha$  and  $\beta$  phases. The  $\beta$  phase has 97.5% tin at this temperature. The freezing which occurs at the eutectic point is called the eutectic reaction and is written as

$$Liquid \rightarrow \alpha + \beta \tag{11-14}$$

This is called an invariant reaction because it occurs at an invariant point

#### 11-6: THE BINARY EUTECTIC SYSTEM

(the eutectic point). Cooling the alloy below  $T_e$  results in changing the composition and relative amounts of  $\alpha$  and  $\beta$ , because the solubilities of lead in tin and tin in lead diminish with decreasing temperature in the solid state.

## Example 11-3

One pound of an alloy containing 55% tin and 45% lead is slowly cooled. Find the weight of  $\alpha$  and  $\beta$  formed in the eutectic reaction.

The solution requires that we determine how much of each phase exists both before and after the invariant eutectic reaction. This is done with the lever rule.

Before: 
$$X_s = \frac{w_0 - w_1}{w_s - w_1} = \frac{55 - 61.9}{19.2 - 61.9} = \frac{6.9}{47.2} = 0.105$$

$$X_1 = 1 - 0.105 = 0.895$$
After:  $X_s = \frac{w_0 - w_\beta}{w_s - w_\beta} = \frac{55 - 97.5}{19.2 - 97.5} = \frac{42.5}{78.3} = 0.543$ 

Liquid consumed = 0.895 lb

$$\beta$$
 created = 0.457 lb

 $X_n = 1 - 0.543 = 0.457$ 

$$\alpha \text{ created} = X_{\alpha}(\text{after}) - X_{\alpha}(\text{before}) = 0.543 - 0.105 = 0.438 \text{ lb}$$

In terms of equation 11-14,

Liquid 
$$\rightarrow \alpha + \beta$$
  
 $0.895 \rightarrow 0.438 + 0.457$ 

The phase diagram in Fig. 11-9 can be used to predict the microstructure that a lead-tin alloy will have. First consider an alloy having the eutectic composition. This alloy solidifies only at the eutectic temperature and forms a mixture of  $\alpha$  and  $\beta$ . The structure of the eutectic solid is shown in Fig. 11-10(a). The dark regions are  $\alpha$  (lead rich), while the light regions are  $\beta$  (tin rich). The eutectic forms a lamellar structure, with alternating regions of  $\alpha$  and  $\beta$ . Suppose we had started with a liquid containing more than 61.9% (in, say 80%. During freezing, the system would pass through

Fig. 11-10. Microstructure of two lead-tin alloys. (a) The alloy has the eutectic composition. The structure is composed of alternating layers of a solid solution (dark) and B solid solution (light). Magnification, 500 ×. (b) The alloy has a high tin content. The light islands are primary B. They are surrounded by eutectic. Magnification, 100 ×. (W. G. Moffat, G. W. Pacrall, and J. Wall, The Structure and Properties of Materials, Wiley, New York, 1964.)



a two-phase region ( $\beta$  + liquid), and primary  $\beta$  would be formed. At  $T_e$ , the remaining liquid would freeze and form the characteristic eutectic structure. The final structure of the solid will have islands of primary  $\beta$ surrounded by a matrix of the eutectic structure. This is shown in Fig. 11-10(b). The light areas (both the islands and the light areas of the eutectic) are β phase, while the dark areas are α. It should be noted that not all eutectics form the lamellar structure shown in Fig. 11-10. In some cases, the two phases segregate from each other more completely.

Questions

Ouestion 11: Describe the sequence of events that occur when a lead-tin alloy containing 10% tin is cooled from 200 to 100°C.

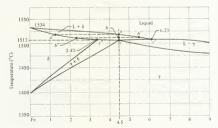
Ouestion 12: Lead-tin alloys are commonly used as solder. What composition would you use for a low-melting-point solder?

#### The binary peritectic system 11-7

The eutectic diagram resulted from a binary system in which the components were completely miscible in the liquid state but had only partial solubility in the solid state. This same set of conditions can also yield the peritectic diagram, which is discussed in this section.

Figure 11-11 shows a typical peritectic diagram; it is a portion of the binary phase diagram for the Fe-Ni system. The diagram has two solid phases (\delta and \gamma) and one liquid phase. Comparison of Figs. 11-11 and 11-2 shows that  $\delta$  is a solid solution of Ni in bcc iron, while  $\gamma$  is a solid solution of Ni in fcc iron. The point which is located at 1512°C and 4.5 wt. % Ni is called the peritectic point (point c in the figure). The point is invariant, and its temperature and composition are referred to as the peritectic temperature  $(T_n)$  and the peritectic composition. The peritectic reaction occurs when the system passes through the peritectic point. This can be understood by considering the cooling of an alloy of iron and nickel having the peritectic composition. At temperatures above point a in Fig. 11-11, the alloy is liquid. At a temperature corresponding to a, the

Fig. 11-11. A portion of the iron-nickel diagram illustrating the peritectic phase diagram. Point c is the peritectic point.



Wt % nickel

first solid forms and has the composition indicated by point a''. This solid is the  $\delta$  phase. Further cooling results in more solidification so long as the system is in the liquid  $+\delta$  region (or above 1512°C). At a temperature corresponding to point b, the compositions of liquid and solid in equilibrium are given by points b' and b'', respectively. Just above the perietetic emperature, we have  $\delta$  phase containing 3.4%. Ni in equilibrium with liquid having 6.2% Ni. Below  $T_p$ , the entire alloy is  $\gamma$  phase containing 4.5% Ni. The peritectic reaction occurred when the alloy was cooled through  $T_c$ . The reaction can be written as

Liquid 
$$+ \delta \rightarrow \gamma$$
 (11-15)

Figure 11-11 illustrates an interesting point about the effect which alloying has on phase changes. In pure iron, the y to  $\delta$  phase change occurs at 1400°C. Addition of Ni raises the temperature at which  $\delta$  iron appears. If the Ni concentration is above 6.2%, the alloy can be melted without the  $\delta$  phase ever appearing. Apparently the presence of nickel inhibits the formation of  $\delta$  iron. In Chapter 12, we shall again refer to the role of alloying elements in inhibiting phase changes.

#### Questions

Ouestion 13: Show that the peritectic point is invariant.

Question 14: Explain the sequence of events that occurs when an alloy containing 4% Ni and 96% Fe is cooled from 1550 to 1475°C.

## 11\_8 Invariant reactions

Two invariant reactions have been discussed so far, the eutectic and peritectic. Both of these involved freezing of a liquid. Other invariant reactions exist, some of which involve only solid phases. This section will classify these reactions, and examples of them will be given in Section 11-9. Several of the strengthening mechanisms discussed in Chapter 12 will depend on what occurs during these phase transitions.

The invariant reactions can be classified in two categories.

 A single phase produces two phases when a system is cooled through an invariant point.

Two phases produce a single phase when a system is cooled through an invariant point.

The invariant reactions are summarized in Table 11-1. The first three belong to category 1, while the next three fall into category 2. In the table,  $\alpha$ ,  $\beta$ , and  $\gamma$  all represent solid phases, while  $L_1$  and  $L_2$  represent different liquid phases. The monotectic and synectic reactions occur in systems

Table 11-1. Invariant reactions

Reaction name	Reaction		
Monotectic	$L_1 \rightarrow \alpha + L_2$		
Eutetic	$L \rightarrow \alpha + \beta$		
Eutectoid	$\gamma \rightarrow \alpha + \beta$		
Synectic	$L_1 + L_2 \rightarrow \beta$		
Peritectic	$L + \alpha \rightarrow \beta$		
Peritectoid	$\alpha + \gamma \rightarrow \beta$		

whose components are not completely miscible in the liquid phase; we shall not be particularly concerned with these, although one example appears in Section 11-9. The eutectoid reaction is analogous to the eutectic reaction except that all three phases involved are solid phases. The same applies to the peritectic and peritectoid reactions.

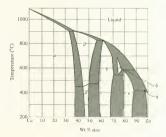
11-9 Phase diagrams with intermediate phases and intermediate compounds The phase diagrams which we have considered so far have been relatively simple. They have contained a small number of phases and have had only one invariant point. This section presents three examples of more complicated systems. Before studying them, it is convenient to classify solid solutions as terminal phases or intermediate phases. The  $\alpha$  and  $\beta$  solid solutions of the eutectic diagram (Fig. 11-9) are at the two ends of the diagram. The range of concentrations for which the a phase exists includes 100% lead, while the β concentration range includes 100% tin. A phase which includes the pure form of one of the components is called a terminal phase: α and β in Fig. 11-9 are both terminal phases, Solid solutions can also occur over composition ranges that do not include 100% of either

component; these are called intermediate phases.

The phase diagram for the copper-zinc system (Fig. 11-12) provides an example of both intermediate and terminal phases. This system shows eight single-phase regions. The  $\alpha$  and  $\eta$  phases are terminal phases, while the others are intermediate phases. The shaded regions contain two phases. The diagram contains a number of invariant points; there are five peritectic points and one eutectoid point on it. Two of the peritectic points are shown by the dark dots in the figure. The eutectoid point is at the bottom of the  $\delta$ -phase region.

The left side of Fig. 11-12 is the region which includes the brasses. Most commercial brass is either 70 wt. % Cu-30% Zn or 60% Cu-40% Zn. The phase diagram shows that the 70:30 alloy is a single phase. α brass has the fcc structure that is typical of copper. The 60:40 alloy, however, is a mixture of  $\alpha$  and  $\beta'$  at room temperature. The  $\beta'$  has the bcc structure. Both  $\beta$  and

Fig. 11-12. The copper-zinc diagram. The diagram is complicated by eight single-phase regions.



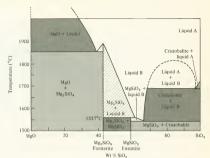


Fig. 11-13. The MgO-SiO<sub>2</sub> system. This system forms two intermediate compounds, forsterite and enstatite. These compounds appear in several of the two-phase regions.

 $\beta'$  are bcc; the difference between them is the manner in which the Cu and Zn atoms are arranged. In the  $\beta$  phase, they are arranged randomly on the lattice sites, while an ordered arrangement exists in the  $\beta'$  phase.

The components of the phase diagrams considered so far have formed solutions with each other but have not formed chemical compounds. Phase diagrams can be made for compound-forming systems. MgO and SiO<sub>2</sub>, for example, form two stable compounds called forsterite (MgSiO<sub>2</sub>). The and enstatite (MgSiO<sub>3</sub>) are effect of these intermediate compounds on the phase diagram is shown in Fig. 11-13. The solid region to the right of MgSiO<sub>3</sub> is a solid mixture of this compound and cristobalite. Recall that cristobalite is one of the crystalline forms of SiO<sub>2</sub>, as was discussed in Section 3-6. The solid region between the two compounds as a mixture of MgSiO<sub>3</sub> those intermediate compounds can be thought of as intermediate phases which exist only at a single concentration rather than over a concentration range. The fraction of a compound in the solid at any point in a two-phase region can be found by the lever rule. For example, the weight percentage of forsterite in a solid material containing 20% SiO<sub>2</sub> and 80% MgO is

Wt. 
$$\%$$
 Mg<sub>2</sub>SiO<sub>4</sub> =  $\frac{41 - 20}{41} \times 100 = 46.2\%$ 

In the liquid phase, MgO and SiO<sub>2</sub> are not soluble at all temperatures. There is a two-phase liquid region, labeled "liquid A + liquid B." For a given system composition, the amount of each in the two-phase liquid region can be found by the lever rule. The immiscibility of the liquids causes a monotectic invariant point, which is shown by the dark dot in the figure.

Figure 11-14 is the phase diagram of zirconium and carbon. It contains a single intermediate phase, which has a high melting point. From the

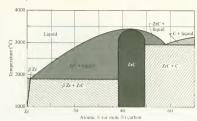


Fig. 11-14. The zirconiumcarbon system. ZrC is formed as an intermediate phase.

temperature scale, it can be seen that zirconium-carbon alloys can be used at high temperatures. The single intermediate phase is also shown by several refractory metal-carbon systems including Ti-C, Cb-C, and Ta-C.

#### Ouestions

Question 15: Write the equation describing the reaction which occurs when an alloy in the  $\delta$  phase (Fig. 11-12) is cooled through the eutectoid point.

Question 16: Write the equation for the reaction that occurs at the monotectic point in Fig. 11-13.

# 11-10 The iron-carbon system

The iron-carbon system forms part of the basic foundation of our society, as these are the primary components of steel. Man has been investigating and improving steels since his prehistoric ancestors accidentally discovered that adding carbon to iron made a strong and versatile material. The properties of steels can be varied greatly by heating and cooling them at appropriate rates. The heating and cooling processes are called heat treatments and provide the basis for the versatility of steels. This section will discuss the iron-iron carbide phase diagram. The diagram will then be used in Chapter 12 to explain why and how heat treatment can alter the properties of steel.

The word steel covers many different alloys. It is common to alloy various elements with iron and carbon in order to impart particular physical properties to steels. Impurities usually appear in steel because they are difficult and expensive to remove. The composition of some typical commercial steels are shown in Table 11-2. This discussion will be limited to the plain carbon steels because these contain the fewest components. Table 11-2 shows that steels are identified by a numbering system. The plain carbon steels are identified by a first two digits of a four-digit number. The last two digits give the carbon concentration. For example, 1040 steel is a plain carbon steel are considered and the containing 0.40% carbon, 1060 steel has 0.60% carbon, etc.

## 11-10: THE IRON-CARBON SYSTEM

Table 11-2. Composition of several commercial

		W C C I D							
A1SI number*	%C	%Mn	%P	%S	%Si	%Ni	%Cr	%Mo	%Cu
Plain carbon steel									
1019	0.17	0.92	0.014	0.033	0.07	0.04	0.01	0.01	0.03
1050	0.50	0.91	0.046	0.041	0.13				
1080	0.79	0.76	0.026	0.030	0.21				
Manganese steel									
1321	0.20	1.88	0.018	0.022	0.30	0.03	0.04	0.02	0.04
1340	0.43	1.58	0.020	0.019	0.31	0.01	0.05	0.01	0.02
Vickel steel									
2340	0.37	0.68	0.014	0,021	0.21	3.41	0.05	0.00	0.07
2512	0.10	0.52	0.007	0.016	0.28	5.00	0.07	0.03	
Silicon steel									
9260	0.62	0.82	0.029	0.030	2.01	0.04	0.07	0.00	0.00

<sup>\*</sup> AISI is an abbreviation for American Iron and Steel Institute.

The phase diagram for the iron—iron carbide system is shown in Fig. 11-15(a) and contains four solid phases and one liquid phase. A description of each solid phase is given below.

#### Ferrite

The  $\alpha$  phase is called ferrite and has the bcc structure. If this phase contains no carbon, it corresponds to the  $\alpha$  iron in Fig. 11-2. The diagram shows that carbon is not very soluble in  $\alpha$  iron, the maximum solubility being 0.025% C at 723°C and falling to 0.008% C at 0°C. The dissolved carbon is held at interstitual sites in the bcc lattice.

## Austenite

The y phase has been named austenite. It is a solid solution of fee iron and carbon. The solubility of carbon in austenite is much greater than in ferrite. The diagram shows that austenite can dissolve 1.98% C at 1130°C and that the solubility diminishes to 0.8% at the eutectoid temperature (723°C). The difference in carbon solubility between the ferrite and austenite phases is attributed to the difference in structure (bcc and fee, respectively). This solubility difference will be quite significant in our discussion of changing the properties of steel. Dissolved carbon is held at interstitial sites in the fee lattice.

## δ ferrite

The  $\delta$  phase is called  $\delta$  ferrite and is bcc. We shall not be particularly concerned with it.

#### Cementite

The components which are used for the phase diagram are iron and iron carbide (Fe<sub>2</sub>C). The iron carbide is called cementite and has an orthorhombic unit cell containing 12 iron atoms and 4 carbon atoms. It is a hard and brittle substance

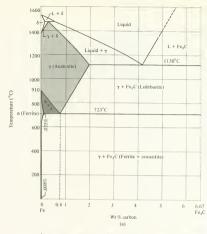
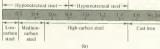


Fig. 11-15. (a) The Fe-Fe<sub>3</sub>C phase diagram. (b) Classification of steels based upon carbon content.



The question that naturally arises is, "Why are iron and cementite used as the components in the phase diagram rather than iron and carbon?" Cementite forms naturally during the solidification of iron-carbon alloys containing less than about 2 or 2.5% C. It is a relatively stable phase but does not actually represent equilibrium of the iron-carbon alloy. The equilibrium (lowest free-energy) state of the system is iron and carbon (graphite): therefore the reaction

$$Fe_3C \rightarrow 3Fe + C$$
 (11-16)

must occur if the equilibrium state is to be reached. This reaction does occur, but usually so slowly at room temperature that it is imperceptible. The carbide would exist for several thousand years before the reaction had occurred to a significant extent, and Fe<sub>2</sub>C is called a metastable phase.

There are a number of terms that are used to classify iron-carbon alloys.

Some of these have evolved as a result of common usage, while others are directly related to Fig. 11-15(a). These terms are shown in Fig. 11-15(b). The carbon in cast irons appears either as cementite or carbon (graphite) depending on the earbon content, the rate at which the cast iron was cooled after solidifying, impurities which are present, and other factors. We shall not be concerned with cast irons in this book.\* The Fe-Fe<sub>3</sub>C phase diagram is used for describing steel; however, the Fe-C diagram is often more useful when working with cast irons. Figure 11-15(a) shows that the system has a peritectic point at high temperature, a eutectic point in the cast-iron region, and a eutectoid point at 0.8% C and 723°C. The eutectoid reaction will be of primary interest; we shall not be concerned with the other two invariant points. It is seen that the classifications "hypoeutectoid" and "hypereutectoid" in Fig. 11-15(b) are based upon the eutectioid composition.

Let us consider the events which occur when iron containing 0.8% C (eutectid composition) is alowly cooled from the austenite region, through the eutectoid point, and into the ferrite + cementite region. At temperatures above 723°C, the material is austenite, and its microstructure is simply that of a single phase with grain boundaries. The eutectoid reaction

$$\gamma \rightarrow \alpha + Fe_3C$$

occurs at 723°C provided that the material is cooled slowly enough to permit the reaction to occur. The reaction produces significant changes in the steel microstructure. The amounts of ferrite and cementite which form at the eutectoid temperature can be calculated by the lever rule:

Wt. % ferrite = 
$$\frac{6.67 - 0.8}{6.67 - 0.025} \times 100 = 91\%$$
  
Wt. % cementite =  $(1.0 - 0.91) \times 100 = 9\%$  (11-17)

The microstructure of the steel below the eutectoid temperature is shown in Fig. 11-16. Figure 11-16(a) was taken at high magnification and clearly shows layers of ferrite and cementite. The light area is the ferrite, as would be expected from equation 11-17. This lamellar structure is called pearlite, and it is the structure formed by the eutectoid reaction. Figure 11-16(b) shows pearlite at a lower magnification. This figure illustrates that each grain of steel contains a large number of layers of ferrite and cementite. Note the similarity between the structure of pearlite and the eutectic solid of the lead-tin system (Fig. 11-10).

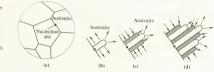
The pearlite structure can be explained by considering the phase change mechanism. Figure 11-17(a) schematically shows several grains of austenite. As the austenite is cooled through the eutectoid temperature, the phase transition occurs by the nucleation and growth of ferrite and cementite. The growth of these phases consumes the austenite. In this respect, the solid-state phase change is similar to freezing. A single nucleation site is shown on a grain boundary in Fig. 11-17(a). Grain boundaries usually provide many good nucleation sites. Figure 11-17(b) shows a ferrite

<sup>\*</sup> A good discussion of cast iron is given by A. G. Guy, Elements of Physical Metallurgy, 2nd ed., Addison-Wesley, Reading, Mass., 1969, pp. 211-226.

Fig. 11-16. The microstructure of a 0.8% C steel. The structure is called pearlite, (a) The layers of ferrite and pearlite are clearly shown at a magnification of 2500 × . The light area is ferrite. (Courtesy of H. E. Knechtel, U.S. Steel Corp.) (b) The grain structure is seen at lower magnification. Each grain contains a large number of layers of ferrite and cementite. Magnification 200 × . (A, R, Bailey, The Role of Microstructure in Metals. Metallurgical Services, Betchworth, Surrey, England, 1966.)



Fig. 11-17. Schematic diagram of the formation of pearlite, (a) Several austenite grains, One nucleation site is shown on a grain boundary. (b) Ferrite forms at the nucleation site and grows. Carbon diffuses out of the ferrite region. (c) The austenite surrounding the ferrite transforms to cementite, absorbing the carbon rejected by the ferrite. Additional carbon comes from the surrounding austenite. (d) The process continues.



region starting to grow from the nucleation site. The ferrite contains only 0.025% C, while the austenite has 0.8%. For the ferrite to form, carbon must be removed from the ferrite region. This is accomplished by carbon diffusion in the directions indicated by the arrows. The diffusion process causes regions of high carbon concentration to appear around the ferrite lamellae. High carbon content is a necessary condition for the formation of cementite, and cementite appears. The cementite took carbon from the surrounding region as shown by the arrows in Fig. 11-7(c). The adjacent carbon-poor region then solidifies as ferrite, etc. Figure 11-17(d) schematically shows the microstructure after several lamella have formed. It should be noted that pearlite formation requires carbon diffusion and that

diffusion requires time. This will be a significant consideration in the heat treating of steel.

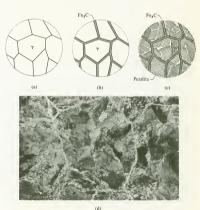
The microstructure of steels can also be explained by the phase diagram; consider the slow cooling of a plain carbon steel having 1.0% C. The steel is in the austenite region until the temperature falls to 790°C [see Fig. 11-15(a)]. The austenite structure appears in Fig. 11-18(a). As the steel is cooled below 790°C, cementite begins to form. Cementite which is formed above the eutectoid temperature is called proeutectoid cementite. Once again, nucleation sites are provided by the grain boundaries; consequently this is where the cementite grows. The microstructure of the steel when it is just above the eutectoid temperature is shown in Fig. 11-18(b). The percentage of cementite in this structure can be found by the lever rule:

Wt. % cementite = 
$$\frac{1.0 - 0.8}{6.67 - 0.8} \times 100 = 3.4\%$$

The austenite in Fig. 11-18(b) has the eutectoid composition just above 723°C. As the steel is cooled through the eutectoid point, the austenite transforms to pearlite, as described in the previous paragraph. The resulting structure is shown in Fig. 11-18(c) and consists of pearlite and cementite. This structure can be also seen in Fig. 11-18(d), which is a photomicrograph of steel containing 1.2% C. This structure is typical of hypereutectoid steels. In the case of hypoeutectoid steels, proeutectoid ferrite is formed. The final structure is then a mixture of refrite and pearlite.

Fig. 11-18. Phase changes in a hypereutectoid steel during slow cooling. (a) Austenite. (b) Cementite forms at the austenite grain boundaries. The steel is in the y-Fe3C region of the phase diagram. (c) The eutectoid reaction transforms the eutectoid austenite to pearlite. (d) Photomicrograph of a hypereutectoid steel containing 1.2%, C. The light areas are cementite. Magnification, 500 x. (Photomicrograph courtesy of H. E. Knechtel, U.S. Steel

Corp.)



The microstructure consists of either ferrite in a pearlite matrix or vice versa, depending on the quantities of pearlite and ferrite in the steel. We shall return to the iron-carbon system and steel microstructures in Chapter 12.

### Questions

Question 17: Figure 11-15(a) covers carbon concentrations from 0 to 6.67 wt. %. Show that 6.67 wt. % C corresponds to 100 mole % of Fe<sub>3</sub>C. Note: 100 mole % of Fe<sub>3</sub>C has 25 atomic % carbon because every fourth atom in Fe. C is carbon.

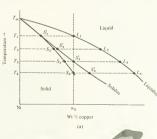
Question 18: Explain the changes which occur in a steel containing 0.58% C as it is cooled from the austenite region to the ferrite + cementite region.

# 11-11 Nonequilibrium solidification of alloys

The phase diagrams considered so far have been for systems at equilibrium. It has been assumed that temperature changes occurred slowly and that there was sufficient time for diffusion and the growth of new phases. In this section, we shall consider what happens when a binary alloy is solidified quickly and there is insufficient time for diffusion.

The copper-nickel system provides a good example of nonequilibrium solidification. The equilibrium phase diagram for the system is shown in Fig. 11-7 and a portion of it is reproduced in Fig. 11-19(a). Consider a Cu-Ni solution in the liquid state. The solution contains w<sub>0</sub>% copper. Let it be cooled until the melt temperature is T<sub>1</sub> and solidification begins, as shown in the figure. The first bit of solid that freezes has the composition corresponding to point S<sub>1</sub>. Figure 11-19(b) is a sketch of the solid, and the

Fig. 11-19. Nonequilibrium solidification of a Ni-Cu alloy, (a) A portion of the phase diagram showing the nonequilibrium' solidus, (b) Structure at T<sub>2</sub>. A concentration gradient exists. (c) Structure at T<sub>3</sub>. The composition at the center of the solid is S<sub>1</sub>', the outermost portion has concentration s<sub>3</sub>'. The overall concentration is S<sub>2</sub>.







small part having composition  $S'_i$  is darkly shaded. Let the temperature fall to  $T_2$ . The composition of the alloy that solidifies here is  $S_2$ , according to the phase diagram. The solid having composition S's surrounds that having composition  $S'_1$ , as shown in Fig. 11-19(b).  $S'_1$  corresponds to a higher nickel concentration that S'2. If the cooling were slow, nickel would diffuse from the S' volume, through the S' volume, to the liquid. This diffusion would continue until the composition of the entire solid was  $S'_2$ , and the solid would then be in equilibrium with liquid at  $L_2$  according to the phase diagram. We are postulating high cooling rates, however, and sufficient time is not available for the diffusion process. The solid will remain as shown in Fig. 11-19(b). The average Ni concentration of this solid lies between  $S'_1$  and  $S'_2$ . It is shown as  $S_2$  on the phase diagram. The situation in the liquid is different. Diffusion is rapid there, and it is reasonable to say that it maintains its equilibrium concentration. Thus, the composition of the liquid is accurately given by the liquidus line, but the solidus line no longer predicts the composition of the solid. Further cooling to T3 results in solidification of more solid, which has the composition  $S_3'$  [Fig. 11-19(c)]. The overall composition of the solid at this point is  $S_3$ . Figure 11-19(a) has a line joining points  $S'_1$ ,  $S_2$ , and  $S_3$ . This can be called the nonequilibrium solidus; it corresponds to the actual average composition of the solid. Solidification continues until T4 is reached. At this point, the nonequilibrium solidus has a copper concentration of we and solidification is complete.

The explanation just given implied that solidification took place in finite steps because this simplified the discussion. Actually, solidification occurs at all temperatures between  $T_1$  and  $T_4$ , and the corresponding compositions of the solid vary continuously. Thus, the solid is not actually the layered structure shown in Fig. 11-19(b) and (c), but rather it has a continuous concentration gradient. A photomicrograph of a specimen of  $\alpha$  brass (70:30 Cu–Zn) is shown in Fig. 11-20. The material was frozen

Fig. 11-20. The microstructure of a brass (70% Cu, 30% Zn) after non-equilibrium cooling. The structure is cored and concentration gradients exist in the solid. Monaphication, 200×.(A. R. Balley, The Role of Microstructure in Metalls, Metallurgical Services, Betchworth, Surrey, England, 1965.)



rapidly and equilibrium was not maintained. The light dendrite-like pieces froze first. These pieces are not homogeneous but contain concentration gradients. This structure is called a cored structure.

Most processes used for casting alloys produce cored structures. The coring can be eliminated by allowing diffusion to occur. Diffusion can be aided by heating the material to a high temperature (but below the nonequilibrium solidus) where the value of the diffusion coefficient is high and maintaining this temperature long enough so that the concentration gradients are practically eliminated. This process is called homogenization because it results in a homogeneous structure. The microstructure of the alloy after homogenization is the same as any single-phase polycrystalline material. It should be noted that the room-temperature diffusion rate is low enough in most solids so that a cored structure will remain cored unless the material is heated.

Question

Question 19: The amount of liquid and solid which coexist during nonequilibrium solidification can be found by applying the lever rule between the liquidus and nonequilibrium solidus. Referring to Fig. 11-19(a). at temperature  $T_2$ , is more liquid present during equilibrium or nonequilibrium? Does this agree with what you would intuitively expect?

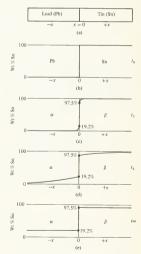
#### 11-12 Phase diagrams and diffusion

Chapter 10 treated the diffusion of one substance into another but was limited to the case of complete mutual solubility of the components. With this restriction, we found that diffusion would occur in the presence of a concentration gradient. Substances with limited solubility do not behave in quite this way. For example, consider Fig. 11-10. The α phase of the lead-tin system contains 19.2% tin (at the eutectic temperature), while the β phase has 97.5% tin. The two phases are adjacent to each other in the solid; consequently there is a very high concentration gradient at the boundary between the phases. Despite the gradient, diffusion does not occur if the phases have the compositions indicated by the equilibrium phase diagram. Another example of this is pearlife, shown in Fig. 11-16. The ferrite and cementite lamella are in contact with each other. Concentration gradients exist across the phase boundary, yet diffusion between phases does not occur.

This can be explained in two ways, one based upon equilibrium and the other upon solubility. The systems which we are dealing with are in their equilibrium states when their free energy is a minimum, as was briefly discussed in Section 4-7. Recall that a system at equilibrium does not change its state. In this chapter, we have covered phase diagrams from an experimental point of view. It is also possible, in principle, to construct phase diagrams by considering the state of a system when the free energy is a minimum. This is seldom done for a number of reasons. Nevertheless. the equilibrium criteria from which phase diagrams can be constructed predict that equilibrium exists when various phases are in contact with each other. Because systems in equilibrium do not change their states (by the definition of equilibrium), the phases coexist without diffusion. From this point of view, we can say that when diffusion does occur, the system is moving toward its equilibrium state and diffusion therefore lowers the free energy of the system.

The solubility explanation will probably be clearer to the reader because the equilibrium explanation is based upon thermodynamic arguments with which he may not be familiar. The solubility explanation can best be done with an example; therefore consider a diffusion couple made of lead and in which is maintained at a temperature just below the eutectic point (the Pb-Sn diagram is shown in Fig. 11-9). The diffusion couple is shown in Fig. 11-21(a) with the origin of the position coordinate (x) located at the interface. The concentration profile of tin immediately after the lead and tin are placed in contact (time  $t_0$ ) appears in Fig. 11-21(b). This begins to diffuse into the lead and vice versa. At time  $t_1$ , the maximum concentration of Sn in the Pb is 19.2% [Fig. 11-21(c)]. This corresponds to the maximum amount of tin that the  $\alpha$  phase can dissolve, and it will accept no more. At the same time, the maximum concentration of lead in the  $\beta$  phase is 2.5%. Thus,  $\beta$  has a minimum tin concentration of 97.5%. The concentration profile in Fig. 11-21(c) is such that tin will diffuse to the left in the

Fig. 11-21. (a) A lead-tin diffusion couple. (b) The concentration profile at the start of diffusion. (c) and (d) Concentration profiles at later times, t<sub>1</sub> and t<sub>2</sub>. (e) Concentration profile of tin when diffusion has ceased.

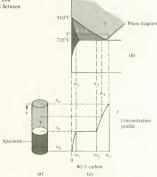


 $\alpha$  phase and lead will duffuse to the right in the  $\beta$  phase. When this diffusion occurs, the Sn concentration in \( \alpha \), at the interface, will fall below 19.2%. It can now accept more tin from the  $\beta$  phase. Tin can be transferred from  $\beta$ to a only if the Sn concentration of the a phase, at the interface, is less than the solubility limit (19.2%). A second condition must also be met if tin is to be transferred from  $\beta$  to  $\alpha$ . The tin content of the  $\beta$  phase, at the interface. must be greater than 97.5% or its solubility limits will be violated when tin diffuses. When these conditions are met, mass is transferred between phases. The concentration profile at a later time, to, is shown in Fig. 11-21(d). The tin content in the a phase has increased; however, the maximum concentration of 19.2% is maintained at the interface. Diffusion ceases when the solubility limits of  $\alpha$  and  $\beta$  have been reached. This is shown in Fig. 11-21(e) and corresponds to a very long diffusion time. t... This figure represents the equilibrium condition and shows that  $\alpha$  and  $\beta$  are in contact and that diffusion has ceased. The situation can be summarized by stating that the diffusion process, as described by Fick's laws, is valid for single-phase regions. When discussing the transfer of mass between phases, the equilibrium diagram must be considered.

### Ouestion

Question 20: The cylindrical iron specimen shown in Fig. 11-22(a) has been case-hardened by diffusing carbon into the iron. Diffusion occurred through the end of the rod located at x<sub>s</sub>, where s denotes "surface." During case hardening, the temperature was maintained at T', as shown in Fig. 11-22(b). The concentration profile after case hardening was completed appears in Fig. 11-22(c). Note that concentration has units of weight percent in this problem. The surface concentration has units of weight percent in this problem. The surface concentration has units of weight percent in this problem. The surface concentration has units of weight percent in this problem. The surface concentration has units of weight percent in this problem. The surface concentration has units of weight percent in this problem. The surface concentration has units of weight percent in this problem.

Fig. 11-22. The concentration profile of carbon in iron which results from case hardening at temperatures between 723 and 910°C.



tration remained at  $w_i$  throughout the entire process. The portion of the rod between position coordinates  $x_i$  and  $x_i$  is in the  $\gamma$  phase, while the portion between  $x_i$  and  $x_i$  is in the  $\alpha$  phase. A step change in carbon content occurs at  $x_a$ . Explain why the concentration profile has the shape shown, and particularly why the step change in concentration occurs.

# 11-13 Summary

Many useful engineering materials are combinations of two or more elements or compounds. The manner in which these components join together to form a solid depends on solubility limits, among other things. The concepts of phase diagrams and phase regions were introduced, and it was found that multicomponent solids behave somewhat differently than pure elements. In the simple case of two components having complete mutual solubility, freezing (or melting) occurs over a temperature range rather than at a single melting point.

The more complicated phase diagrams often show invariant points, and invariant reactions are associated with these points. An invariant reaction is one which occurs at a given temperature, pressure, and composition. The phase changes caused by the invariant reactions greatly affect the microstructure of the material. In Chapter 12, the effect of microstructure and invariant reactions on the physical properties of materials will be described.

The iron-carbon system was considered, and several interesting features appeared which are not limited to this system alone. First, we encountered the metastable phase, Fe<sub>2</sub>C or cementite. Other metastable phases occur, as will be seen in Chapter 12. The formation of pearlite was discussed, and it was seen that pearlite formation depended on nucleation and growth. In this respect, the invariant reaction was similar to freezing. In addition, the rate at which pearlite grew was diffusion controlled. The requirement for diffusion in phase transformations will be used quite extensively in Chapter 12 because it is an essential part of several practical strengthening mechanisms.

The effect of nonequilibrium solidification was considered, and it was seen that the equilibrium phase diagram is not capable of predicting the results of fast cooling. In Chapter 12 we shall have occasion to cool materials through invariant points quickly, with some dramatic results. Metastable phases will result, and the manipulation of these phases will provide a method for varying physical properties. Phase diagrams affect diffusion, and the laws of diffusion developed in Chapter 10 apply to a single-phase region. Mass transfer between phases depends on solubility limits (or equilibrium criteria).

#### Problems

1 A latent heat is associated with the freezing of iron and is also associated with each of the solid-state phase transitions. The latent heats of the solid-state phase transition are smaller than that of freezing. A quantity of iron is slowly cooled from 2000°C to room temperature.

The iron is at a pressure of 1 atm during the cooling. Assume that heat is removed from the iron at a constant rate. Sketch a curve (schematically) of iron temperature vs. time during cooling. Identify the various phases of iron on your sketch.

- 2 The properties of materials change when they undergo phase transitions. Consider iron at a pressure of 1 atm. γ iron is fee and has a lattice parameter of 3.464 Å just above 910°C. α iron is bee and has a lattice parameter of 2.896 Å just below 910°C. Calculate the change in density due to the transition of iron from the γ to the α phase.
- 3 Ice can be removed from sidewalks by spreading NaCl on the ice. If salt is spread on ice on a -10°C day, the ice will slowly melt and form brine. (a) Using Fig. 11-4, explain why this occurs. (b) Would this method be effective at -25°C? Wh?
- 4 A number of elements are listed in the accompanying table. Their atomic radii and crystal structure are also tabulated. List those pairs of elements that should should show complete solid solubility.

Element	Crystal structure	Atomic radius (Å
Gold (Au)	fcc	1.44
Potassium (K)	bcc	2.31
Molybdenum (Mo)	bcc	1.36
Sodium (Na)	bcc	1.85
Silver (Ag)	fcc	1,44
Magnesium (Mg)	hcp	1.59
Tungsten (W)	bec	1.36
Rubidium (Rb)	bcc	2.43

5 Portions of phase diagrams can be constructed by slowly cooling the molten material and observing the temperatures at which the first solid appears and the last liquid disappears. Al<sub>2</sub>O<sub>3</sub> and Cr<sub>2</sub>O<sub>3</sub> are mutually soluble in all proportions. The accompanying table gives the temperatures at which freezing begins and ends for various Al<sub>2</sub>O<sub>3</sub>-Cr<sub>2</sub>O<sub>3</sub> compositions. Construct the phase diagram.

(wt. %) Cr <sub>2</sub> O <sub>3</sub>	Temperature at which freezing begins (°C)	Temperature at which freezing ends (°C)
0	2048	2048
20	2094	2070
40	2141	2098
60	2192	2136
80	2240	2187
100	2277	2277

6 The lattice parameters and structures of  $\alpha$  and  $\gamma$  iron are given in Problem 2. Nickel forms solid solutions with both phases, but Ni and Fe are mutually soluble in all proportions for only one of these iron

phases. Which one? *Note:* The valence of each metal is indicated by the oxide that it forms. Nickel forms NiC. Iron forms FeO, Fe<sub>2</sub>O<sub>3</sub>, and Fe<sub>3</sub>O<sub>4</sub> and consequently shows several valences. If any of these safisfy rule 4 of the Hume-Rothery rules, the rule can be considered as satisfied.

7 Derive the lever rule (equation 11-10) in terms of mole fractions.

8 A system containing 50 mole % MgO and 50 mole % NiO is cooled from 2600°C. Plot the mole percent of the system which is liquid as a function of temperature for a temperature range of 2600-2200°C. Calculations performed at increments of 100°C are sufficiently accurate for plotting the curve.

9 Sketch the cooling curves which result when lead-tin alloys having the following compositions are cooled from the liquid region to 150°C:

(a) 10% tin, (b) 19.2% tin, (c) 50% tin, (d) 61.9% tin, and (e) 90% tin.

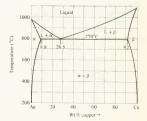
10 A lead-tin alloy containing 10% tin is cooled from 200 to 100°C. How much β (weight percent) precipitates from the alloy as a result of the cooling?

11 The phase diagram of the silver-copper system is shown in Fig. 11-23. It has a single eutectic point at which the reaction

Liquid 
$$\rightarrow \alpha + \beta$$

occurs. Answer the following questions approximately. (a) What are the compositions of the three phases involved in the eutectic reaction? (b) A system contains 70% Cu and 30% Ag b weight. What fraction (by weight) of the system is liquid at 900°C? (c) What fraction is liquid just above the eutectic temperature? If the system contains 5 lb of the alloy, how many pounds of liquid are in the system at a temperature just above  $T_*$ . (d) The system is cooled to a temperature just below  $T_*$ . How many pounds of  $\alpha$  are created by the eutectic reaction? How many pounds of  $\beta$ ? (e) What is the total weight of  $\beta$  in the solid at a temperature just below  $T_*$ , that is, the weight of both primary  $\beta$  and  $\beta$  which exists in the lameliar eutectic structure? The total weight of  $\alpha$ ? (f) What is the weight fraction of the solid which exists as the layered eutectic structure at a temperature just below  $T_*$ ? (g) Sketch the microstructure of the alloy just above  $T_*$ , and just below  $T_*$ .

Fig. 11-23. The copper-silver equilibrium phase diagram.



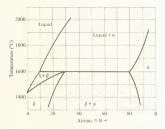
- 12 Figure 11-11 shows the peritectic portion of the Fe-Ni equilibrium phase diagram. Describe the sequence of events that occur when alloys having the following compositions (by weight) are cooled from 1550 to 1475°C: (a) 95% Fe-5% Ni and (b) 93% Fe-7% Ni. (c) Which of these alloys go through the peritectic reaction during cooling?
- 13 Figure 11-24 shows a peritectic phase diagram for a system composed of elements A and B. For elements, atomic percent is the same as mole percent. The diagram has a peritectic point at 1600°C and 30 atomic % B. At this point, the reaction

Liquid 
$$+ \alpha \rightarrow \beta$$

occurs. Consider a system containing 50 atomic % B. (a) What atomic fraction of the system is liquid at 1800°C? (b) What atomic fraction is liquid just above T\_? (c) What are the compositions of the three phases involved in the peritectic reaction? (d) How much  $\beta$  (atomic fraction) is formed when the system is cooled through  $T_n$ ? How much  $\alpha$ ? (e) What is the atomic fraction of a that exists in the system at a temperature slightly below T.?

- 14 Identify the phases which occupy each of the shaded regions of the Cu-Zn diagram (Fig. 11-12).
- 15 Figure 11-13 shows the MgO-SiO<sub>2</sub> system. (a) Describe the sequence of events that occur as a system containing 50 wt. % MgO and 50 wt. % SiO2 is slowly cooled from 1600 to 1500°C. (b) What weight fraction of the system is forsterite just above 1557°C and (c) just below 1557°C.
- 16 The solubility of C is much greater in austenite than in ferrite. Carbon fits in the interstitial sites in both  $\alpha$  and  $\gamma$  iron. Show that the interstitial sites in fcc iron are better suited (bigger) for carbon than the bcc interstitial sites. Could this explain the difference in carbon solubility? Note: The lattice parameters for fcc and bcc iron are given in Problem 2.
- 17 Steel containing 0.5% C is cooled slowly from the austenite region. (a) What phases are present just above the eutectoid temperature? (b) What weight fraction of each is present? (c) What is the weight fraction of pearlite just below 723°C? (d) What is the weight fraction of proeutectoid ferrite just below 723°C?

Fig. 11-24. The equilibrium phase diagram of elements A and B.



- 18 Figure 11-22 shows the carbon concentration in a specimen which was case-hardened at a temperature between 723 and 910°C. Suppose this case hardening had taken place above 910°C, say 1000°C, in the austenite region. The surface concentration of carbon was 1½ by weight during the process, (a) Schematically draw the concentration profile of the carbon at 1000°C when case hardening has been completed. (b) The specimen is then cooled to room temperature. The cooling is slow enough so that all of the phase transitions occur but is rapid enough so that no significant diffusion occurs. Thus, the concentration profile at room temperature is essentially the same as it was at 1000°C. Sketch the microstructure of the specimen. (c) Do you think it is more advisable to case-harden above or below 910°C? Why?
- 19 Diffusion couples can be used to find the solubility limits of various substances. (a) Explain how a copper-silver diffusion couple could be used to find the solubility of copper in silver and silver in copper at 600%C. (b) How could such data be used to construct the solvus lines in Fig. 11-23?

#### Answers

- Question 1: The y phase in Fig. 11-2 does not have a phase boundary with the liquid phase; therefore it cannot transform from y to liquid. It does have a phase boundary with vapor in the low-pressure region; therefore it can sublimate.
- Question 2: Three. The coexisting phases are  $\alpha$ ,  $\gamma$ , vapor;  $\gamma$ ,  $\delta$ , vapor; and  $\delta$ , liquid, vapor.
- Question 3: Three phases. These are ice, salt, and brine. Note that pure water is considered as brine with 0% salt. At -21°C and 23.3% NaCl, all three phases coexist.
- Question 4: From conservation of mass, both systems can have the same NaCl concentration in the brine; however, the system with the higher overall NaCl concentration must contain more brine. Thus, the mass fraction of brine (mass of brine/mass of system) will be greater for the system having 10% NaCl than for the system having 5% NaCl. Methods for calculating mass fraction will be covered in Section 11-5.
- Question 5: For a one-component system, F' = 3 P'; therefore invariant points correspond to P' = 3. There are three points in Fig. 11-2 at which three phases coexist; therefore there are three invariant points. Question 6: For a two-component system at constant pressure,

$$P' + F' = 3$$

- In the brine region, P' = 1; therefore F' = 2. In the salt + brine region, P' = 2; therefore F' = 1.
- Question 7: For a binary system at constant pressure, use equation 11-5, P' + F' = 3. In the liquid region, P' = 1 and there are two degrees of freedom (temperature and composition). The same is true of the solid region. The liquid + solid region has P' = 2; therefore F' = 1.
- Question 8: For 40% MgO at 2300°C, liquid having 25% MgO is in equilibrium with solid containing 49% MgO. The system with 20%

MgO is a single phase (liquid) at 2300°C, while the system with 80% MgO is all solid at 2300°C.

Question 9: 
$$m_0 = m_s X_s + m_t X_t$$
 (11-7)  
 $X_s = 1 - X_s$  (11-6)

(11-6)

Substituting 11-6 into 11-7.

$$m_0 = m_s(1 - X_t) + m_t X_t$$

Solve for  $X_i$ :

$$X_{l} = \frac{m_{0} - m_{s}}{m_{l} - m_{s}} = \frac{w_{0} - w_{s}}{w_{l} - w_{s}}$$

Question 10:

$$X_{l} = \frac{w_{0} - w_{s}}{w_{l} - w_{s}} = \frac{0.70 - 0.60}{0.77 - 0.60} = \frac{0.10}{0.16} = 0.625$$

from Fig. 11-7(a)

Mass of liquid = (mass of system)  $X_t = (5)(0.625) = 3.125 \text{ lb}_m$ 

Ouestion 11: The alloy is in a single-phase region from 200°C to 150°C, and no changes occur over this temperature range. At 150°C, β begins to form. It precipitates from the α phase, and diffusion is required for β formation. As the temperature is decreased from 150 to 100°C, the fraction of  $\beta$  increases. Precipitation of one phase from another will be used in Chapter 12.

Ouestion 12: The eutectic composition has the lowest melting point.

Ouestion 13: From equation 11-5, P' + F' = 3. Liquid,  $\delta$ , and  $\gamma$  coexist at the peritectic point; therefore P' = 3 and F' = 0.

Question 14: Solid begins to form at a temperature corresponding to the intersection of the liquidus line and the 4% Ni line. The solid is γ containing about 0.5% Ni. As freezing progresses, the composition of the liquid follows the liquidus line and the composition of the solid follows the solidus line. Just above  $T_p$ ,  $\delta$  solid (3.4% Ni) coexists with liquid (6.2% Ni). The peritectic reaction occurs, consuming all of the liquid and some of the  $\delta$ . The product of the reaction is  $\gamma$ , which exists below 1512°C, From 1512°C to 1495°C, γ and δ solid coexist. Cooling from 1512°C to 1495°C causes an increase in the amount of γ present. Below 1500°C, the system contains a single phase, γ.

Question 15:  $\delta \rightarrow \gamma + \epsilon$ 

Ouestion 16: Liquid A → cristobalite + liquid B

Question 17: For 100% Fe<sub>3</sub>C,

Wt. % C = 
$$\frac{\text{atomic wt. C}}{\text{atomic wt. Fe}_{3}\text{C}} = \frac{12}{(3)(55.85) + 12} = 6.67\%$$

Question 18: Start with the material in the austenite region. When the temperature falls below about 790°C, the material enters the  $\alpha + \gamma$ region. Ferrite forms as the temperature drops. When the temperature is just above 723°C, ferrite having 0.025% C is in equilibrium with austenite of the eutectoid composition. Further cooling converts the austenite to pearlite. The final structure is a mixture of ferrite and pearlite. Note the similarity with Fig. 11-10(b).

Question 19: The mass fraction of liquid for equilibrium cooling is

$$X_{l} = \frac{w_{0} - S_{2}'}{L_{2} - S_{2}'}$$

For nonequilibrium cooling, this quantity is

$$X_{l} = \frac{w_{0} - S_{2}}{L_{2} - S_{2}}$$

and  $X_l$  is larger for the nonequilibrium case,

Question 20: The surface concentration  $w_s$  is high enough so that the  $\alpha$  iron at the surface transforms to  $\gamma$  at the start of case hardening (or diffusion). We now have a diffusion couple consisting of  $\gamma$  and  $\alpha$ , and the couple has an interface. Carbon is continually added to the  $\gamma$  phase because of the case-hardening arrangement. Carbon diffuses across the interface into the  $\alpha$  phase until the solubility limit of  $\alpha$  is reached. At this point,  $\gamma$  has concentration  $w_1$ , More carbon then reaches the interface from the  $\gamma$  side, and the concentration rises above  $w_2$ . The concentration requirements for equilibrium between  $\gamma$  and  $\alpha$  are no longer met at the interface, and some of the  $\alpha$  transforms to  $\gamma$ . The interfaces slowly moves down the rod as this occurs. The step change in concentration is due to the existence of two phases. It would not appear if case hardening was done above 910°C (in the single-phase  $\gamma$  region).



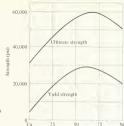
CHAPTER 12

# Strengthening Mechanisms

THE DISLOCATION MODEL was formulated and used to explain plastic deformation in Chapter 8. It was found that any phenomenon which inhibited dislocation slip also caused materials to become harder and more brittle. Work hardening was discussed, and we called it a strengthening mechanism because it increased the yield point and the ultimate stress. Several other methods of increasing the yield strength will be discussed in this chapter. All of them will be based upon reducing dislocation mobility, and the methods of this chapter are mainly applicable to metals. Generally, increasing the yield point also increases the ultimate strength but diminishes the strain sustained by the material at fracture. Thus, strengthening a material usually makes it more brittle.

The chapter starts by considering the strengthening effect caused by combining two materials that are mutually soluble. Following this, solids containing two phases are considered. The methods for strengthening these depend on arranging the phases of the material in particular ways. This is generally accomplished by subjecting the material to various thermal processes. The rate at which the material is heated and cooled significantly affects the geometry of the phases, and this, in turn, affects the strength and other properties. The changes in geometry due to the thermal processes can be seen in the microstructure of the materials. The only thermal treatment (or heat treatment) encountered so far has been annealing, which was a softening process. It will be seen that certain heat treatments can have the opposite effect on some alloys.

Phase changes can also be caused by stress in some cases. This phenomenon has seldom been utilized in a practical way; however, methods are available for increasing the toughness of steel by a stress-induced phase transition. This will also be discussed. The last topic in the chapter concerns solids which are made of wires or whiskers of one material embedded in a matrix of a second material. These combinations show very high strength and often have excellent creep properties.



Wt % nickel

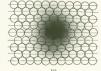
Fig. 12-1. The effect of composition on the yield and ultimate strengths of copper-nickel alloys. The alloy is a single phase over the entire composition range. The data are for room temperature. (L. H. Van Vlack, Elements of Materials Science, Addison-Wesley, Reading, Mass., 1964.)

# 12-1 Solution hardening

Single-phase materials are less complex to deal with than multiphase ones; therefore our discussion of strengthening mechanisms will begin with solid solutions. The concepts of solid solutions and diffusion in these solutions were introduced in Section 10-1 and will be used here. It is generally found that the strength of a crystalline material is increased if a second material, which forms a solid solution with the first one, is added. "Increasing the strength" means that both the yield point and ultimate strength are increased. This is accompanied by an increase in hardness; consequently strengthening mechanisms are also referred to as hardening mechanisms.

The Cu-Ni system illustrates the effect of alloying two soluble metals. Figure 12-1 shows that both the yield and the ultimate tensile strength of Cu-Ni alloys depend on composition. The maximum strength is shown by an alloy containing about 65%, Ni, and this alloy is stronger than either pure copper or pure nickel. The same strengthening effect is observed in systems which have limited solubility, provided that the solubility limits are not exceeded. The increase in strength can be explained in terms of two mechanisms. Both can operate simultaneously, First, the solute atoms do do not fit into the solvent lattice perfectly. This is illustrated schematically for a substitutional solution in Fig. 12-2. A close-packed bane containing

Fig. 12-2. Schematic drawings of crystal distortion caused by solute atoms. Both planes are close-packed, (a) The substitutional atom is larger than the solvent atoms. This causes the lattice to expand. Distortion occurs in the shaded region. (b) A small solute atom causes the crystal to contract locally. The shaded area is distorted as a result of this contraction.





(b)

a substitutional atom is shown in Fig. 12-2(a). The substitutional atom is larger than the solvent atoms; therefore the lattice must expand in the region of this atom. This expansion disrupts the crystal symmetry, and strained regions appear as a result. The shaded area in Fig. 12-2(a) is strained. If the solute atoms were smaller than the solvent atoms, the crystal would contract in neighborhoods of the solute atoms and the crystal would again have strained regions. This is illustrated in Fig. 12-2(b). Interstitial atoms can have a similar effect. Consider an interstitial site which is too small to accommodate an atom. The site can be enlarged by expanding the crystal in the neighborhood of the site, and the atom can then occupy it. This results in a disruption of the crystal symmetry similar to that shown in Fig. 12-2(a). Imperfections in the symmetry of a crystal tend to hinder dislocation motion; consequently the presence of substitutional or interstitial atoms tends to strengthen metals.

The presence of dislocations also disrupts the crystal symmetry and provides the basis for our second solution-hardening mechanism. An edge dislocation is shown in Fig. 12-3(a). The geometry of an edge dislocation is such that a space appears at the bottom of the extra half plane. This space is too small to accommodate a solvent atom. Figure 4-26 shows that this region is in tension and that strain energy is associated with it. If the crystal contains small solute atoms, either interstitial or substitutional. some of these atoms will take up positions at the bottom of the extra half plane. The shaded atom in Fig. 12-3(a) represents a small solute atom. If the small atom occupied a site which was not near a dislocation it would cause a strained region [see Fig. 12-2(b)] and strain energy would be associated with this region. The crystal distortion caused by the solute atom is reduced if it occupies the site shown in Fig. 12-3(a). In addition, the distortion in the region of the dislocation is diminished if the atom occupies the site shown. This reduces the strain energy in the neighborhood of the dislocation. Thus, the total energy of the crystal is reduced if the atom migrates to a dislocation. The same sort of thing occurs with large solute atoms, as illustrated in Fig. 12-3(b). In this case, two large substitutional atoms are accommodated just below the dislocation line. Once again, the strain energy of the crystal is lower if the atoms are in the region of the dislocation than if they are in a region of perfect crystal. Consider what happens when either of the dislocations in Fig. 12-3 slips. The strain energy of the crystal will increase when slip occurs because the solute atoms do not move with the dislocation. Slip will create strained regions. The energy required to form the strained regions must come from the forces acting on the dislocation. Thus, these forces must not only overcome

Fig. 12-3. Solute atoms in the neighborhood of a dislocation. (a) The energy of the crystal is lowered when the small solute atom occupies the position shown rather than a site that is distant from the dislocation. (b) An energetically favorable position for two large substitutional atoms.





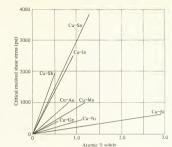


Fig. 12-4. The effect of various alloying elements on the critical resolved shear stress of copper. The increase in strength depends on both the alloying element and its concentration. (After Linde, Lindell, and Stade, Arkiv Fysik 2:88 [1950].)

the normal resistance to slip but must also provide sufficient energy to create the strained regions which the dislocation would leave behind. As a result, the stress required for slip is raised, and the solute atoms have a dislocation pinning effect. The sketches in Fig. 12-3 are simplified. Actually, a number of solute atoms tend to take up positions in the neighborhood of edge and screw dislocations. These collections of atoms are called Cottrell atmospheres and reduce the strain energy of the crystal.

The strengthening effect of solute atoms has been determined for many systems. Figure 12-4 shows the effect of alloying small quantities of various elements with copper. The critical resolved shear stress increases linearly with atomic percent solute, provided the solute concentration is small. At higher concentrations, the linear relationship no longer holds. The data in Fig. 12-4 are typical of many systems, both interstitial and substitutional. The iron-nitrogen system, for example, shows similar characteristics (see Fig. 10-7).

#### Question

Question 1: Figure 4-26 shows the strain fields associated with an edge dislocation. The region above the dislocation line is in compression. Draw a sketch showing that the strain in this region would be reduced if several of the atoms were replaced by smaller solute atoms. Would this kind of substitution reduce the strain energy of the crystal? Would the substitution tend to pin the dislocation? Why?

# 12-2 Dispersion hardening

The effect of impurity pinning sites on dislocation mobility was briefly discussed in Section 8-15. The possibility of purposely introducing pinning sites into a crystal was mentioned then and will now be covered in some detail. In this section we shall deal with two-phase materials in which one phase provides pinning sites while the second forms the matrix which surrounds the sites. The material is strengthened by dispersing the pinning sites throughout the matrix; consequently, this type of strengthening is called dispersion hardening. In some cases the formation and/or dispersion of the second phase depends on diffusion. The theory of dislocations interacting with pinning sites was worked out in Chapter 8, and it might help the reader to review this with particular emphasis on Sections 8-5, 8-6, 8-12, and 8-15

The effect of a number of pinning sites on dislocation motion was a dislocation held by two pinning sites bowed out between sites just as a dislocation held by two pinning sites bowed out. The two-site problem resulted in the Frank-Read source, and the shear stress required to operate the source was found to be

$$\tau_{\text{source}} = \frac{2Gb}{\mathcal{L}}$$
(8-18)

where b is the Burgers vector and  $\mathscr L$  is the distance between pinning sites. Equation 8-18 can also be applied to the problem of a dislocation pinned by several pinning sites (Fig. 8-37). The quantity  $\mathscr L$  is then the distance between adjacent pinning sites. The stress required to move a pinned dislocation can be written as

$$\tau_{\text{flow}} = \tau_0 + \tau_{\text{source}} = \tau_0 + \frac{2Gb}{\mathscr{L}}$$
 (12-1)

where  $\tau_{nim}$  is the shear stress at which flow (or permanent deformation) begins and  $\tau_0$  is the shear stress required for slip in the absence of pinning sites. Equation 12-1 provides the key to the dispersion-strengthening mechanism. If we can introduce dislocation pinning sites into a crystal, we can diminish dislocation mobility. This, in turn, will increase the stress required to initiate slip, and the yield point of the material will rise as a consequence. The equation shows that a small value of  $\mathscr L$  corresponds to a large value of the shear stress required for flow. In addition to increasing the yield strength of a material, the presence of pinning sites generally increases the ultimate strength and the work-hardening rate.

A number of methods are available for dispersing pinning sites throughout a crystal. Which one is chosen depends on the materials that make up the particular system of interest. We shall discuss several dispersionhardened systems and shall start with steel. Steel is a two-phase solid containing ferrite and cementite. The photomicrographs in Figs. 11-16 and 11-18(d) show the two-phase microstructures. The pearlite in both of these structures is lamellar, consisting of alternate layers of ferrite and cementite. Because of the lamellar structure, the ferrite and cementite are in contact with each other over an extensive area. There is a surface energy associated with this area, but the area would be reduced (and the energy of the steel would be lowered) if the cementite balled up into spheres. Recall that a sphere has the lowest ratio of surface area to volume of all geometric shapes. To change the shape of the cementite phase, the atoms of the solid must be mobile enough to rearrange themselves. The atoms are made mobile by heating the steel to a temperature just below the eutectoid point [see Fig. 11-15(a)]. This temperature is maintained for a fairly long period of time, generally greater than 10 hr. Diffusion occurs at the elevated



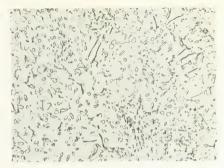
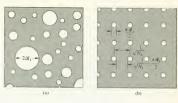


Fig. 12-5. Photomicrograph of spheroidized steel containing 0.8% C. The structure was all pearlite before the spheroidizing heat treatment. The small particles in the figure are cementite, and the matrix is ferrite. Magnification, 1000 x. (A. R. Bailey, The Role of Microstructure in Metals, Metallurgical Services, Betchworth, Surrey, England, 1966.)

temperature, and the cementite forms spheres. The exact time required for diffusion depends on the composition and microstructure of the steel. A photomicrograph of spheroidized steel is shown in Fig. 12-5. The structure consists of cementite spheres in a ferrite matrix and is called spheroidite. The size and spacing of the cementite spheres depends on the carbon content of the steel and the width of the pearlite lamella before the spheroidizing process began.

The cementite particles are much harder and stronger than the ferrite and therefore act as pinning sites because they resist slip more strongly than the ferrite. The quantity & in equation 12-1 can be determined from photomicrographs such as Fig. 12-5. To find  $\mathcal L$  consider a cube of material containing dispersed spheres, all having the same radius Rs. A plane through the cube is shown in Fig. 12-6(a). The intersection of a sphere and a plane is a circle, and each circle in the figure represents a spherical pinning site. The circle radii in the figure are not the same, although our model assumes that the sphere radii are the same. This is due to the fact that the plane intersects the spheres at different positions. The largest circle in Fig. 12-6(a) represents a sphere cut at its equator, and it has a radius of R.. The problem now is to determine an average spacing between particles, L, for the geometry of Fig. 12-6(a). The average radius of the circles can be found by considering the intersection of a plane with randomly spaced spheres, with each sphere having radius R. The problem has been solved and will not be done here. It has been found that the average radius of the circles in the plane is  $\pi \mathcal{R}_s/4$ . The number of circles per unit

Fig. 12-6. Geometry used for finding the average distance between spheres. (a) A plane cutting through spheres of equal radius, which are randomly spaced in three dimensions. (b) The model used for finding SE.



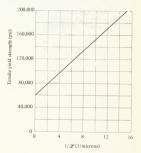
area can be counted on a photomicrograph; let this quantity be  $N_s$ . Figure 12-6(b) shows  $N_s$  particles distributed uniformly over an area of 1 unit. The distance between the centers of the circles is  $1/\sqrt{N_s}$ , and the circle diameters are  $\pi \theta_s/2$ , as illustrated in the figure. The shortest distance between particles is seen to 4.

$$\mathcal{L} = \frac{1}{\sqrt{N_s}} - \frac{\pi \mathcal{R}_s}{2} \tag{12-2}$$

Finding the sphere radius for equation 12-2 is a bit more difficult than finding N<sub>s</sub>. It can be determined from the volume fraction of the solid which forms pinning sites and the number of spheres per unit volume. This is left for the reader (see Problem 12-2).

The figure shows the yield stress of spheroidized steel at room temperature as a function of 1/2. The figure shows the yield stress of spheroidized steel at room temperature as a function of 1/2. The linear relationship predicted by the equation is clearly obeyed, and the value of  $\tau_0$  is seen to be 60,000 psi. The specimens used were polycrystalline, and  $\tau_0$ , therefore, depends on grain size as well as purity. The theory has been further verified by electron microscopy. The

Fig. 12-7. Tensile yield stress plotted as a function of 1/2. for steel, where 2½ is the awareap particle spacing. The data are in accord with equation 12-1. (Apr. C. S. Roberts et al., Trans. Am. Soc. Metals 44:1150 [1952]; and A. Turkalo and J. R. Low, Jr., Trans. AIME 212:750 [1958].



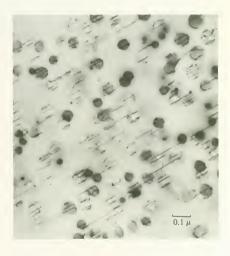


Fig. 12-8. An electron micrograph of a stainless steel specimen containing phaning sites. The pinning sites are Ni<sub>3</sub>Ti particles. Dislocation loops appear around each pinning site in accordance with the model shown in Fig. 8-37. Magnification, 90,000  $\times$ . (L. K. Singhal and J. W. Martin, Acta Met. 16:950 [1968].)

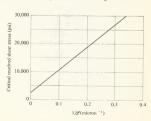
pinning mechanism postulated in Fig. 8-37 shows that the pinning sites have dislocation loops around them after a dislocation has passed. Figure 12-8 is an electron micrograph of a stainless steel in which Ni<sub>2</sub>Ti particles act as pinning sites. Dislocation loops are seen around a number of the particles.

The Orowan theory, which produced equation 12-1, is basically valid. Refinements have been made, such as basing  $\tau_{\text{topute}}$  on the actual distance between randomly spaced particles rather than on the average spacing, but these refinements are more accurate ways of performing calculations that are still based upon the Orowan model. The value of  $\mathscr L$  depends on the shape of the pinning sites or second phase. We considered only spheres; however, second phases can form as either rods or platelets also.

The pinning sites in spheroidized steel were formed by the controlled heating of an iron-carbon alloy. There are many systems which cannot be dispersion-hardened so simply, but other methods are available for some of these. Some materials can be dispersion-hardened by internal oxidation, Silver is a typical material that will harden in this manner. Silver is capable of dissolving small quantities of oxygen; consequently oxygen can diffuse through silver. Small quantities of oxide-forming elements can be dispersed in the silver matrix during fabrication of the silver. Aluminum is typically used. When oxygen is diffused into silver having dispersed aluminum, it reacts with the aluminum to form Al<sub>2</sub>O<sub>3</sub>. The hard oxide particles serve as pinning sites. Silver which has been dispersion-hardened by internal oxidation is often used for contact points in electrical equipment. Internal oxidation is not limited to silver. Figure 12-9 shows the critical resolved shear stress of dispersion-hardened copper. The oxide particles, which are SiO2, BeO, or Al2O3, were formed by internal oxidation. The figure is in accord with equation 12-1.

It is possible to introduce dispersed pinning sites into a matrix by still other methods. One of these involves the sintering process. Sintering was discussed briefly in Question 4 of Chapter 10 and consists of agglomerating powdered particles, by means of diffusion, under high temperature and pressure. Dislocation pinning sites can be introduced during the sintering process by controlling the composition of the powder. An example of this is a commercially available material composed of an aluminim matrix with dispersed  $\Delta l_2 O_3$  particles. The process for forming this material

Fig. 12-9. The effect of internal oxidation on the critical resolved shear stress of copper. The pinning sites are A1<sub>2</sub>O<sub>3</sub>, SiO<sub>2</sub>, or BeO. (After M. H. Lewis and J. W. Martin, Acta Met. 11: 1207 [19631.)



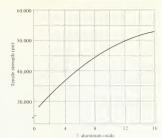


Fig. 12-10. The effect of aluminum oxide content on the ultimate tensile strength of SAP. The size of the dispersed particles depends on the fabrication process. (After A. S. Bufferd in Modern Composite Materials, L. J. Broutman and R. H. Krock, eds., Addison-Wesley, Reading, Mass., 1967.)

begins with powdered aluminum. The powdered aluminum particles are ground in a controlled oxygen environment. Aluminum oxide forms on the particle surface, and some of it separates from the particles during grinding. When the powder is sintered, both Al and Al<sub>2</sub>O<sub>3</sub> appear in the product. Al<sub>2</sub>O<sub>3</sub> has a very low solubility in Al; consequently it forms as a separate phase. The dispersed Al<sub>2</sub>O<sub>3</sub> particles act as pinning sites. This material is called SAP (sintered aluminum powder). The strength of SAP depends on the number of dispersed pinning sites. This, in turn, depends on the total oxide content, as shown in Fig. 12-10.

The opportunities which sintering provides for dispersion hardening have led to some rather involved methods of preparing sintering powders. An example of this is the powder used for fabricating nickel that contains dispersed particles of thorium oxide. To form the powder, a chemical reaction is caused to occur which precipitates a nickel salt and thorium oxide. The salt is then decomposed to NiO. By properly treating the NiO-ThO, mixture with hydrogen, the NiO is reduced to Ni (powdered) while the ThO2 is unchanged. The powder is then sintered, and the resulting material is nickel with dispersed ThO, (thoria) pinning sites. This is called TD nickel (TD for "thoria dispersed") and has very good creep properties. It is interesting that thoria performs quite a different function when used in tungsten. Tungsten is normally a brittle material; however, the addition of 2 or 3% thoria enhances its ductility. This may be due to the thoria particles acting as obstacles to crack propagation. The different effect of thoria in these two systems indicates that while a general theory has been developed for dispersion hardening, each materials system must be considered separately. The same dispersed phase will not always have the same effect in different systems.

#### Ouestion

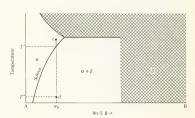
Question 2: The microstructure of pearlite is shown in Fig. 11-16. The width of the alternate layers of ferrite and cementite can be varied by controlling the rate at which steel is cooled from the austenite region. Fine pearlite has a higher yield point than coarse pearlite. Explain why.

# 12-3 Precipitation hardening

The dispersion-hardened materials discussed in Section 12-2 can be divided into two general categories. The first category includes those materials in which it was necessary to "artificially" introduce pinning sites. These materials could not be dispersion-hardened by simply heattreating them. Internally oxidized materials, SAP and TD nickel, fit this category. The cost of these materials is high because of the processing that is required. It is possible to harden some materials by subjecting them to a proper heat treatment; this is the case with steel. Heat treatment is generally cheaper than sintering or internal oxidation. In this section, we shall discuss a group of alloys that can be dispersion-hardened by heat treatment. The hardening process depends on the precipitation of one solid phase from another as the material is cooled; it depends on a phase transition like the one described in Section 11-6. Particles of the precipitated phase then diffuse and join each other to form dispersed pinning sites. The process of forming these sites is called precipitation hardening and is a special case of dispersion hardening.

Precipitation hardening can be explained in a general way with the aid of the binary phase diagram of Fig. 12-11. We shall not be concerned with the cross-hatched region of the diagram. The slope of the solvus line shows that the solubility of B in A diminishes with decreasing temperature. This is a necessary condition for precipitation hardening, as will be seen. The  $\beta$ phase which appears in the  $\alpha + \beta$  region can be an intermediate phase, a terminal phase, or a compound. We shall not be concerned with which of these it is. To demonstrate the precipitation-hardening process, consider a solid system containing  $w_0$ % B by weight. Let the system be in the singlephase region, as shown by point c in Fig. 12-11. If the system is cooled slowly.  $\beta$  will be formed at temperatures below T'. The rate of  $\beta$  formation is controlled by the diffusion rate of B atoms in the a solid solution. If the material is cooled very quickly to a low temperature, shown as T" in the figure, there will not be sufficient time for diffusion to occur and the system will remain in the \alpha phase. Point d on the equilibrium diagram of Fig. 12-11 shows that the system would be an  $\alpha + \beta$  mixture if equilibrium existed. For the system to reach equilibrium after a fast cooling, diffusion

Fig. 12-11. Phase diagram of a system that can be precipitation-hardened. The cross-hatched region is not of interest. The solubility of B in A diminishes as the temperature is reduced. This is required for precipitation hardenina.



must occur. The diffusion rate is extremely slow at low temperature and can be neglected for practical purposes. Thus, quick cooling of the system from the \( \alpha \) results in a supersaturated \( \alpha \) phase. The temperature and overall composition of the system are represented by point \( d \), but the system is \( not \) in the two-phase region and is not in equilibrium. The process of heating the system and maintaining it in the single-phase region is called \( solution \) into the first process.

Pinning sites are created by precipitating a finely dispersed  $\beta$  phase from the supersaturated  $\alpha$  solution. The precipitation is accomplished by heating the system to a temperature below T' and maintaining this temperature for a period of time. This process is called aging. The aging temperature is high enough to promote diffusion, and  $\beta$  particles precipitate during aging. The size and number of  $\beta$  particles depends on the time and temperature of the aging process, and the strength of the material therefore depends on the aging process. If aging proceeds too long, the precipitate particles can coalesce, resulting in larger but fewer pinning sites. This is called overaging. Systems which must be heated in order for precipitation to occur are said to a require artificial aging; those which precipitate at room temperature are said to a gen atturally.

The iron-molybdenum system provides a straightforward example of precipitation hardening (or age hardening). The solvus line on the ironrich side of the diagram has the same shape as that in Fig. 12-11. The B phase for this case is Fe2Mo. The Fe-Mo system has been investigated to a limited extent, and data are available for age-hardened Fe containing 6 atomic % Mo.\* A number of specimens of this alloy were solutionized and quenched. Quenching is a fast-cooling process and consists of plunging a hot specimen into a cool liquid. Following the quench, each specimen was subjected to a different aging process. The effect of aging conditions on the stress-strain curves is shown in Fig. 12-12. Two different aging temperatures were used, and specimens were aged for various periods of time before being tested. The data show that short aging times lower the stressstrain curve, while long aging times raise them. The lowering of the curves is probably due to an annealing effect. Quenching a specimen from the solutionizing temperature can increase the dislocation density. Because the outside of the specimen cools more slowly than the inside, strains due to thermal contraction are induced in the material during quenching. The initial heating acts as an annealing process. For short aging times, the softening due to annealing is greater than the hardening due to precipitation. At longer aging times, precipitation hardening becomes quite significant. The curves show that the aging process occurs quicker at 650°C than at 550°C. This would be expected because the process depends on diffusion. The aging at 550°C has a greater effect on yield point than 650°C aging, implying that the distance between precipitate particles is smaller for the specimens aged at 550°C. This was verified by electron microscopy. The spacing between Fe2Mo particles was found to be 2600 Å after aging at 650°C for 100 hr and 1800 Å after aging at 550°C for 1219 hr. In this work the Fe2 Mo particles did not tend to agglomerate and

<sup>\*</sup> A. Urakami, H. L. Marcus, M. Meshii, and M. E. Fin, Trans. Am. Soc. Metals 60:344 (1967).

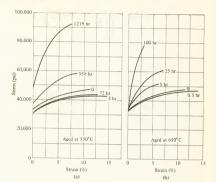


Fig. 12-12. The effect of aging on an Fe-6% Mo alloy. The stress-strain characteristics depend on the aging process used. Lower aging temperature generally results in higher strength, but a longer aging time is required. (After A. Urakami et al., Trans. Am. Soc. Metals 60, 344 [1967].

form large particles, perhaps because the aging time was not long enough. Thus, softening at long aging times (overaging) is not observed.

#### Question

Question 3: The Cu–Zn diagram is shown in Fig. 11-12.  $\alpha$  brass contains 70% Cu–30% Zn, which  $\beta$  brass is 60% Cu–40% Zn. Which of these can precipitate a second phase? Describe a heat treatment that will result in particles of one phase being dispersed in a matrix of the other phase.

# 12-4 Guinier-Preston zones

The Fe-6%, Mo alloy considered in Section 12-3 is a straightforward example of precipitation hardening because the only precipitate is Fe<sub>2</sub>Mo. In many cases, the precipitate can form a metastable phase which will change to a stable one under particular aging conditions. This type of precipitation hardening is typical of aluminum alloys and is largely responsible for the commercial importance of these alloys. Pure aluminum is not a particularly strong material and is used more for its corrosion resistance and electrical conductivity than for its strength. A large part of the world's aluminum production is used for high-strength alloys. Most of these derive their strength characteristics from precipitation hardening. In this section we shall consider the precipitation hardening of aluminum-copper alloys, whose behavior is typical of the more complicated aluminum alloys.

Figure 12-13 shows the Al-rich part of the Al-Cu equilibrium phase diagram. This portion of the diagram is a typical cutectic with  $\alpha$  as a terminal phase. The second phase, called  $\theta_1$  is an intermediate one which has the approximate composition CuAl<sub>2</sub>. An alloy containing less than

Wt % copper

Fig. 12-13. The copper-aluminum equilibrium phase diagram. The solvus line has the shape required for age hardening.

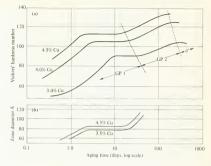
5.65 wt. % copper can be heated into the  $\alpha$  region, quenched, and aged. The equilibrium diagram shows that we would expect  $\theta$  particles in an  $\alpha$  matrix after aging. Actually, three metastable precipitate phases form before  $\theta$  appears. Because they are metastable, they do not appear on the equilibrium phase diagram. The regions of the alloy which contain the first two metastable phases are called Guinier-Preston zones, after the men who first studied and described them. The zones were originally found by means of X-ray diffraction experiments. The third metastable phase is called  $\theta'$  and is similar to the equilibrium phase  $(\theta$  or CuAl<sub>3</sub>).

The first structure which is observed when a supersaturated solution of Cu in Al is aged appears in Fig. 12-14. Copper atoms have clustered together. The copper region is called a GP I zone (GP for Guinier-Preston). The copper atoms are coherent with the aluminum matrix; that is, they occupy sites on the aluminum lattice. Because the copper atoms are smaller than the aluminum ones, the crystal is strained in the region of the GP I zone. This is shown schematically in Fig. 12-14. The zones have been found to be circular disks about 100 Å in diameter and perhaps two or three atoms thick. The coherence (or alignment) of the copper atoms with the aluminum matrix permits dislocations to slip through the GP I zones; however, the strains caused by the small copper atoms make slip more difficult than if the copper atoms were absent. Recall that the reduction of dislocation mobility caused by a strained lattice was the mechanism for

Fig. 12-14. Schematic drawing of a cluster of atoms that form coherently within a matrix. The size difference between the atoms in the cluster and those in the matrix causes strains within the crystal.



Fig. 12-15. The effect of aging at 110°C on the handness of cognet at 110°C on the handness of cognet adminim alloys. Zone aluminim alloys. Zone the first it is shown on the lower curve and increases as precipitation proceedings to middle the proceedings of the first of the fir



solution hardening (Section 12-1). The hardening effect of GP 1 zones is shown in Fig. 12-15 for three different copper concentrations. The figure has Vickers hardness number as the ordinate. The Vickers hardness test is one of several standard hardness tests used, as described in Section 1-6. Hardness is seen to increase with increasing time, as does the size of the zone. The amount of copper precipitated increases with time during the formation of GP 1 zones. The maximum zone diameter is in the neighborhood of 100A and cannot be found with an optical microscope.

Increased aging results in the formation of GP 2 zones, Figure 12-15 shows that the strength of the alloy begins to increase again as these zones make their appearance. The GP 2 zones have about the same composition as the  $\theta$  phase, indicating that the precipitate is moving toward the equilibrium state. The zones are disc-shaped, with each having a diameter of about 1500 Å and a thickness of perhaps 150 Å. The GP 2 zones have the tetragonal crystal structure and the zones are not coherent with the lattice in the thickness direction. The transformation of the precipitate from GP 1 to GP 2 involves changes in both the composition and the structure of the precipitate phase. Figure 12-15 shows that maximum hardness (and maximum strength) corresponds to fully developed GP 2 zones. Further aging causes the formation of the  $\theta'$  precipitate. This is similar to the GP 2 but is incoherent with the matrix in the radial as well as thickness directions. The hardness begins to fall when  $\theta'$  is formed, and this marks the beginning of overaging. The  $\theta'$  particles have about the same size as GP 2 zones. If the aging is continued, the equilibrium phase will form with a further reduction in hardness.

The aluminum-copper system overages by phase transitions of the precipitate particles. If a specimen of this alloy is severely overaged, the  $\theta$  particles will agglomerate. Figure 12-16 shows a photomicrograph of a severely overaged specimen. The agglomeration of  $\theta$  particles, caused by



Fig. 12-16. Photomicrograph of a severely overaged specimen of Al-4% Cu. The dark regions are the A phase Magnification, 2000 × . (A. R. Bailey, The Role of Microstructure in Metals, Metallurgical Services, Betchworth, Surrey, England, 1966.)

overaging, permits us to see the precipitate with an optical microscope. Electron microscopy is required to observe GP 1, GP 2, and  $\theta'$ . The small precipitate size is typical of many precipitation-hardening systems. For example, the Ni<sub>3</sub>Ti particles in Fig. 12-8 were precipitated and cannot be found with an optical microscope.

#### Ouestion

Question 4: Does equation 12-1 apply to aluminum-copper alloys which have been heat-treated such that they contain GP 1 zones? Explain vour answer.

# 12-5 Grain size

The effect of grain size on strength is given by the Petch equation (equation 4-3), and the mechanisms which cause higher strength in fine-grained materials were covered in Chapter 8. Strength properties can be controlled to some extent by varying grain size, but this is usually less effective than dispersion or precipitation hardening. Grain size can be controlled by introducing particles which serve as nuclei in the recrystallization process; consequently small-grained solids can be formed either by freezing or by recrystallization. Materials using dispersed particles for control of grain size are sometimes called dispersion strengthened, although the strengthening mechanism is quite different from that discussed previously.

We shall consider a case in which the grain size of Al2O3 was controlled by means of molybdenum particles.\* Mo powder was mixed with Al<sub>2</sub>O<sub>3</sub> powder, and the combination was sintered. The grain size of the resulting solid was found to decrease as the molybdenum content increased.

<sup>\*</sup> C. O. McHugh, J. T. Whelan, and M. Humenik, Jr., J. Am. Ceram. Soc. 49:486 (1966).

#### 12-6: MARTENSITE-DIFFUSIONLESS TRANSFORMATIONS

Table 12-1. The effect of molybdenum particles on the strength of Al<sub>2</sub>O<sub>3</sub> at room temperature\*

Mo (vol. %)	Strength (thousand psi)	
0	36.5	
4.3	80.0	
5.0	83.9	
5.5	84.5	

\* C. O. McHugh, J. T. Whelan, and M. Humenik, J. Am. Ceram. Soc. 49: 486 (1966).

The sintered specimens were tested, and it was found that the smallergrained specimens (higher molybdenum content) had higher strength, as shown by the data in Table 12-1. It should be noted that experiments of this type are difficult because the specimens often fail by brittle fracture rather than by ductile fracture, and the mechanism being investigated does not significantly affect the brittle fracture process. Particular attention must be paid to surface condition, and efforts must be made to minimize the voids which form in the interior of the ceramic during sintering.<sup>4</sup>

This is the first example that we have considered in which a ceramic was strengthened, although our previous dispersion-hardening discussion utilized ceramic particles to strengthen metals in some cases. Dispersed particles will act as dislocation pinning sites in ceramic crystals, and the bowing of pinned dislocations has been observed in ceramics. If the ceramic is to be used at low temperatures and is to be loaded in tension or bending, there is no advantage to dispersion hardening or hardening by grain refinement if the material fails by brittle fracture. In the high-temperature region, however, an increase in yield strength may be desirable and useful.

#### Ouestion

Question 5: Explain how a strengthening mechanism can cause a material, which was ductile before strengthening, to fail in a brittle manner after strengthening. Figure 9-10 may be helpful.

# 12-6 Martensite—diffusionless transformations

Precipitation hardening involved quenching an alloy in order to get a supersaturated solution, and then precipitating a second phase by aging. This sequence of events does not always occur. In some systems, a new phase appears at the end of a quench, and the supersaturated solution never occurs. Quenching implies a very rapid temperature change; therefore any phase transitions which occur during quenching cannot depend on diffusion. This section will cover a diffusionless transformation. This transformation will be used in Sections 12-7 and 12-8 to help explain the heat treatment of steel.

† Voids that are formed during sintering have a significant effect on physical properties. This topic will not be pursued here. The interested reader can find pertinent information in R. L. Coble and W. D. Kingery, J. Am. Ceram. Soc., 39:377 (1956).

‡ The bowing of a dislocation between pinning sites in MgO appears in G. Thomas, Transmission Electron Microscopy of Metals, Wiley, New York, 1962, p. 225. The diffusionless phase change that we are interested in occurs with solids whose crystal structure depends on temperature. Iron is an example of this. A structural change (or phase transformation) occurs when iron is cooled from a temperature above 910°C to some temperature below it (see Fig. 11-2). The phase change can be written.

$$\gamma(fcc) \rightarrow \alpha(bcc)$$
 (12-3)

The mechanism by which the structure changes can be understood with the aid of Fig. 12-17. The dashed lines in the figure represent two fcc cells which are adjacent to each other. The large circles, both shaded and unshaded, are atoms that belong to these cells. Several of the atoms at the face-centered positions have been omitted for clarity. The nine large shaded atoms form a body-centered tetragonal unit cell as defined by the solid lines. The unit cell of the structure can be considered as either fcc or body-centered tetragonal. The body-centered tetragonal is more convenient for explaining the structure and lange. These are shown as a and c, respectively, in the figure. For this cell to go through the transition of equation 12-3, it is necessary only for the a dimensions to increase and the c dimension to decrease until c = a. This will transform the fcc structure to a become without diffusion.

Now consider a eutectoid steel in the austenite region [see Fig. 11-15(a)]. The carbon is held at interstitial sites in the fcc austenite. If this steel is quenched, there is insufficient time for pearlite to form because pearlite formation requires diffusion (see Fig. 11-17). The steel can transform from the fcc structure to a body-centered structure during quenching because the transition does not require diffusion. The carbon does not have time to diffuse. It takes up interstitial sites in the transformed body-centered structure cannot accommodate all of the carbon atoms, but the tetragonal body-centered structure cannot accommodate all of the carbon atoms, but the tetragonal body-centered structure cannot accommodate all of the carbon atoms, but the tetragonal bructure is shown in Fig. 12-17. The two small atoms in the figure are carbon atoms, and the other interstitial sites are shown as x's. The Fe-C tetragonal structure is called martensite and is a metastable phase. It should be noted that the martensite unit cell does not quite

Fig. 12-17. The broken lines define two fcc cells. Several face-centered atoms are not shown. The lattice can also be considered as having the body-centered tetragonal structure defined by the solid lines. The small atoms and the sites marked × are available for small intersitials.

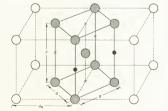




Fig. 12-18.
Photomicrograph of 1080 steel quenched from the austenite region. The platelet structure of the martensite appears.
Magnification, 2000 ×. (Courtesy of H. E. Knechtel, U.S. Steel Copp.)

correspond to that shown in Fig. 12-17. During the transformation, the a dimension does increase and the c dimension decreases. The size of the cell depends on the carbon content of the steel. Martensite appears as platelets in a quenched steel microstructure, and its formation is accompanied by lattice strain. The platelet structure can be seen in the photomicrograph of Fig. 12-18. The amount of martensite which forms during the quenching of a particular specimen depends on the cooling rate and carbon content. If sufficient time is available, some ferrite can form. Fe-C martensite is very hard but very brittle and is not particularly useful in its hardest form.

A number of systems are capable of forming martensite, such as Fe-Ni, Tion, Au-Cd, and In-TI. These all undergo a solid-state phase transition just as the Fe-C system does, and martensite formation occurs as a diffusionless transformation. The geometric changes which occur during the martensite transformation have been studied in detail but will not be presented here.\*

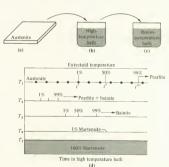
## 12-7 Heat treatment of steel

The structure and properties of steel depend on both the composition of the steel and its thermal history. The rate at which steel is cooled from the austenite region greatly affects its properties. The properties of quenched steels can be altered by again subjecting the material to a heat treatment. In this section, we shall discuss both of these aspects of the heat treating of steel.

\* The interested reader can find this in R. Reed-Hill, *Physical Metallurgy Principles*, Van Nostrand, Princeton, N.J., 1964, Ch. 15.

It is apparent that there are many ways in which a specimen of austenite can be cooled. The cooling rate is very significant in determining the final structure and properties. The effect of many different cooling processes on a single type of steel can be summarized on a graph called the isothermal transformation diagram (abbreviated as I-T diagram). The information contained in I-T diagrams can best be understood by discussing the procedure used in making them because the procedure involves a number of phase transformation mechanisms. The apparatus required for making an I-T diagram is shown in Fig. 12-19. Suppose that we want a diagram for 1080 steel. We begin with a number of thin sheets of the steel, all at a temperature in the austenite region. One of these is shown in Fig. 12-19(a). The specimen is quenched in the high-temperature bath as shown in Fig. 12-19(b). The bath is kept at a predetermined temperature. Let this temperature be T<sub>1</sub>. It is held in the high-temperature bath for a predetermined length of time and then quenched to room temperature. Following this, it is polished. etched, and examined for pearlite. The amount of pearlite (if any) in the structure is recorded. The same procedure is followed for a number of specimens; however, the time which the specimen spends at T1 is varied. The results can be recorded as in Fig. 12-19(d). A horizontal line appears at T1 in this figure, and a number of dots are on the line. Each dot represents the length of time that a particular specimen was held at T. The specimen which was held at this temperature for time t' had 1% pearlite; specimens held at T1 for shorter times showed less than 1% pearlite. Time t" represents a structure having 50% pearlite, while the austenite → pearlite transformation is 99% completed at time t". This completes the data taken at temperature  $T_1$ . The high-temperature bath is then cooled to  $T_2$ and the process is repeated. If T2 is low enough (below about 550°C), it is observed that all of the cementite and ferrite do not form the lamellar pearlite structure. Instead, some of the cementite forms in a needle-like

Fig. 12-19. Apparatus and method used for determining an isothermal transformation diagram. (a) A large number of thin sheets, heated to the austenite region, are used. (b) The sheets are quenched in a hightemperature bath and kept in the bath for varying periods of time. (c) They are then quenched in a room-temperature bath, (d) The microstructure is examined and the data from the microstructure are plotted as shown.

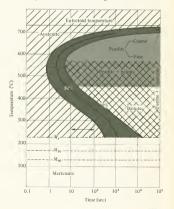


structure which is surrounded by a ferrite matrix. This structure is called bainite. It is emphasized that both pearlite and bainite are mixtures of cementite and ferrite; the difference between them is in the way that the two phases are arranged. The appearance of bainite does not complicate the experiment; we merely record the amount of bainite + pearlite present in the microstructure. Once again the time required for 1, 50, and 99% transformation are recorded and are shown in Fig. 12-19(d) at temperature  $T_2$ , The dots indicating the points at which data were acquired have been omitted. The same procedure is then followed for a number of temperatures. When the high-temperature bath is maintained at TA, martensite begins to appear in the microstructure. The amount of martensite that forms depends on the temperature of the high-temperature bath (T, in this case) but is independent of the length of time that the specimen spends in the bath. As the temperature of the bath is decreased, the amount of martensite formed by quenching increases. All of the steel transforms to martensite when the high-temperature bath is maintained at T<sub>5</sub> or lower.

The data gathered from the above experiment can be presented in an orderly, concise manner. The result is the I-T diagram shown in Fig. 12-20. All that has been done is join all of the points in Fig. 12-19(d) for which the transformation

is 1% complete. The line formed by joining these is labeled "1%" in Fig. 12-20. Similarly, the points representing 50% transformation and 99% transformation have been joined and the resulting lines labeled. The

Fig. 12-20. The isothermal transformation diagram of 1080 steel. It is constructed from data such as those shown in Fig. 12-19. (Adapted from Atlas of Stothermal Transformation Diagrams, U.S. Steel Corp., Pittsburgh, 1951.)



darkly shaded region between the 1% and 99% lines represents the region in which the transformation of equation 12-4 occurs. To the left of this region the material is austenite, while to the right it is ferrite + cementite The ferrite + cementite can form as either pearlite or bainite. Which one appears depends on the transformation temperature, as shown in Fig. 12-20. The line labeled M, represents the temperature at which martensite starts to form. At the temperature corresponding to M50, 50% of the microstructure is martensite, etc.

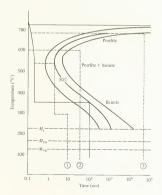
Consider a specimen that is quenched to the  $M_{eq}$  temperature. Half of the steel is transformed to martensite while the remaining half is austenite. If the  $M_{50}$  temperature is maintained long enough, the austenite will transform to bainite. If the temperature is reduced before the bainite forms, more martensite will form. Thus, in performing the experiments from which the I-T curve is constructed, it is necessary to hold the specimen at temperatures in the martensite range for fairly long times.

## Example 12-1

A thin specimen of 1080 steel is quenched from the austenite region to 350°C, held at 350°C for 100 sec, and then quenched to room temperature. What is the microstructure? The time vs. temperature curve for this quench is shown as the solid line in Fig. 12-21.

The path of the time-temperature line shows that the specimen remains in the austenite region until it reaches 350°C, and it is held at this temperature until half of it has transformed to bainite. It is then quenched to room temperature, and the remaining austenite transforms to martensite. The final structure thus contains 50% bainite and 50% martensite.

Fig. 12-21. The I-T diagram for 1080 steel showing several cooling curves. The cooling curves shown by the broken lines will be used in Problem 12-10.



The cooling path used for Example 12-1 has vertical lines. This implies that the temperature has changed by a finite amount in zero time or that cooling has occurred instantaneously. This is not physically realistic because time is required for heat flow. Thin specimens can be cooled more quickly than thick ones, and they approximate instantaneous cooling better. This is why thin specimens are used for constructing 1-T diagrams. If we consider a bar of finite dimensions that is quenched, it is apparent that the material near the surface of the bar will cool more quickly than that in the interior. As a result, the microstructure and physical properties of the bar will vary from point to point. This will be pursued in Section 12-8.

### Tempering

The heat treatments discussed so far have all resulted in hardening. Steel can also be made softer and more ductile by appropriate heat treatment. These softening processes will now be considered.

Tempering is a heat treatment in which hardened steels containing a significant fraction of martensite are softened. Steel which has been quenched directly into the martensite region is too brittle for most purposes and must be softened. The tempering process provides a method for transforming martensite into ferrite and cementite. How much of the martensite is transformed depends on the temperature and time of the tempering process. Tempering is thought to occur in four stages. Heating a hardened steel to temperatures up to 200°C causes the martensite to reject some of the interstitial carbon. In doing this, the tetragonal martensite structure comes closer to the equilibrium bcc structure of ferrite. The rejected carbon combines with some martensite to form a carbide whose composition ranges from Fe<sub>2</sub>C to Fe<sub>3</sub>C. This precipitate is called epsilon carbide. Its presence distorts the martensite matrix and results in a slight hardening of the steel. Further heating, to about 300°C, causes any austenite that was retained by the steel after quenching to decompose into ferrite and cementite. Some softening accompanies this transformation. Further heating, to about 350°C, causes the epsilon carbide to transform to cementite and ferrite. Most of it forms cementite because the composition of epsilon carbide is close to that of cementite. This portion of the tempering process causes significant softening. If the transformation is allowed to progress long enough, the final structure will consist of cementite and ferrite. Often the tempering process is stopped at a point where the steel contains cementite, ferrite, and martensite. If tempering is done at temperatures just below the eutectic point, the cementite forms spheres. Spheroidized steel was discussed in Section 12-2. The difference in hardness between hardened and spheroidized plain carbon steels is illustrated in Fig. 12-22. The hardness of plain carbon steels is seen to depend on both composition and heat treatment, or, to phrase it differently, on bonding and structure.

## Annealing

The annealing of pure metals was discussed in Chapter 9, and the annealing process caused dislocation annihilation. The annealing of steel depends largely on a microstructure change rather than on dislocations. The process

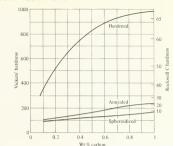


Fig. 12-22. The effect of carbon content and heat treatment on the hardness of steel. The data are approximate since hardness also depends on the spacing of the lamella in pearlite and the grain size. (After E. C. Bain, Functions of Alloying Elements in Steel, American Society of Metals, Cleveland, 1939.)

consists of heating the steel to the austenite region and allowing it to furnace-cool. Furnace cooling means that the heat supply to the furnace containing the steel is shut off, and the furnace and steel slowly cool together as heat is transferred through the furnace walls. The definition of furnace cooling does not seem very scientific to some people, but it serves its purpose. The structure of furnace-cooled steels is very close to the equilibrium structure described in Section 11-10. According to Fig. 12-22, annealed steel is harder (and stronger) than spheroidized steel. Cementite inhibits dislocation motion more effectively when it is dispersed as layers in pearlite than when it is dispersed as spheres. The values given in Fig. 12-22 can be taken only as approximate. The strength of steel containing pearlite depends on the spacing between cementite lamella, while the strength of spheroidized steel depends on the sphere size and sphere dispersion.

#### Normalizina

The normalizing process is similar to the annealing process except that the cooling rate is somewhat faster. Normalizing is done by first austenizing the steel, removing it from the furnace, and allowing it to cool in the air. The cooling rate will differ from point to point in a piece of steel because the cooling rate depends on geometry, thermal properties of the steel, and the rate at which heat is transferred to the air from the steel surface. Thick specimens will have somewhat different overall properties than thin ones because the cooling rates are different. Steel is often normalized rather than annealed because the process is cheaper. It is not necessary to tie up an oven during the cooling.

At this point, the reader may be a bit confused both by the numerous new terms which apply to steel and the variety of properties and heat treatments. It is this variety that makes steel versatile. The general trends

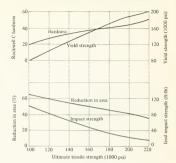


Fig. 12-23. Approximate properties of medium carbon steels that have been hardened and tempered. The properties depend on the carbon content and the specific heat treatment used; consequently the values shown are indicative only of the properties and are not exact.

of the physical properties of medium carbon steels are shown in Fig. 12-23. Strength increases with hardness, while ductility diminishes. The curve is presented in a general manner because of the number of variables that affect the properties. For plain carbon steels, the most important variables are carbon content and heat treatment. These determine which phases are present in the microstructure as well as how the phases are distributed. Distribution includes such things as whether pearlite or bainite represent the eutectic structure, the grain size, the distance between spheres in spheroidized steel, distance between lamella in pearlite, etc.

### Questions

Question 6: Figure 11-17 shows that cementite begins to form at sites on the austenite grain boundaries. The I-T curve in Fig. 12-20 was made for a particular austenite grain size. The curve will shift slightly to the right or left if the grain size differs from that used for constructing the diagram. If you are quenching an austenite specimen having a grain size smaller than that used for Fig. 12-20, will the curves shift to the left or right? Explain. Note: A shift to the left implies that the rate of the austenite — pearlite transformation has increased and vice versa.

Question 7: When martensite is heated to the spheroidizing range (about 700°C), cementite precipitates and forms spheres. The steel is softened in the process. Precipitation causes hardening in the Al-Cu system. Explain why one alloy softens and the other hardens as the result of precipitating a phase.

12-8 The effect of alloying elements on steel transformation—hardenability

Commercial steels contain alloying elements in addition to carbon. Table

11-2 shows the compositions of just a few of the standard steels that are

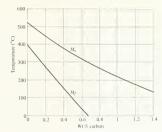


Fig. 12-24. The effect of carbon concentration on the temperature at which martensite starts to form (M.) and the temperature at which the martensite transformation is finished (M1), (After A. R. Trojano and A. B. Greninger, Metal Progr. 50: 303 [1946].)

available. In the previous section, an experimental method for obtaining the I-T diagram of a steel was described, and the heat treatment of a eutectoid steel was discussed in terms of the diagram. The I-T diagram changes as the steel composition changes; therefore the extent to which the properties of a steel can be changed by heat treatment depends on which alloving elements and how much of each are present. A simple example of this is the effect of carbon content on the temperatures at which the martensite transformation begins and ends. Figure 12-24 shows that the transformation temperature diminishes as the carbon content increases. The various commonly used alloying elements can also cause the eutectoid temperature to vary. According to Fig. 12-25, this temperature can be either raised or lowered by the various elements. Often, several of these elements will be combined with iron and carbon to form a steel having particular properties. It is becoming apparent that the alloying of various elements with steel can be quite complicated. Volumes have been written on the topic, and it is fairly well understood. A great deal of empirical information is also available. For example, the I-T diagrams for many

Fig. 12-25. The eutectoid temperature depends on which elements (in addition to C and Fe) are included in the steel. Alloying elements can cause either an increase or decrease in the eutectoid temperature. (After E. C. Bain and H. W. Paxton, Alloving Elements in Steel, American Society of Metals, Pittshurah, 1961.)

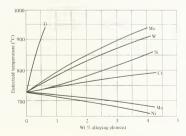


Table 12-2.
Distribution of alloying elements between ferrite and a carbide phase\*

Element	Dissolved in	ferrite	Combi	ned in carbide
Nickel	Ni			
Silicon	Si			
Aluminum	Al			
Copper	Cu			
Manganese	Mn	-	-	Mn
Chromium	Cr	-	-	Cr
Tungsten	W	-	_	W
Molybdenum	Mo	-		Mo
Vanadium	V	_	-	V
Titanium	Ti		-	Ti

<sup>\*</sup> After E. C. Bain and H. W. Paxton, Alloying Elements in Steel, 2nd ed., American Society for Metals, Metals Park, Ohio, 1961.

alloy steels have been determined.\* It is not the intent of this book to delve deeply into alloy steels; however, the mechanisms which cause the properties will be discussed briefly.

The alloying elements can affect either the ferrite or the cementic. Table 12-2 lists the elements commonly used in steels and shows which phase the element affects. Several of the elements can either dissolve in the ferrite or form carbides. Which of these is predominant is shown by the arrows in the table. For example, titanium is a strong carbide former, while manganese is a weak one. All of the elements which dissolve in ferrite tend to strengthen it by solution hardening; however, these elements do not affect the strength of steel as much as the carbide-forming elements. The carbides formed by the elements at the bottom of Table 12-2 are hard and brittle. In this respect they are similar to cementic and inhibit dislocation motion. The details of the effect of each of these on steel behavior will not be covered here.<sup>4</sup>

The concept of hardenability is an important one for steel. Hardenability is a measure of the ease with which steel can be hardened by heat treatment and is strongly affected by alloying elements. Let us consider what happens when a round bar of steel is quenched. The I-T diagram of Fig. 12-20 utilized thin specimens which underwent transformation at constant temperature. The normal quenching process is not isothermal, and the effects of both temperature and time must be considered. This is done by using the continuous cooling diagram instead of the isothermal transformation diagram. The continuous cooling diagram maps the region in which phase transformations occur when steel is cooled at a constant rate. For this type of cooling, temperature varies continuously with time. The continuous cooling diagram for 1080 steel is shown in Fig. 12-26. Transformation occurs in the shaded regions, and the dashed lines labeled A, B, C, and D represent typical cooling curves. The position

<sup>\*</sup> I-T diagrams can be found in Atlas of Isothermal Transformation Diagrams, United States Steel Corp., Pittsburgh, Pa., 1951.

<sup>†</sup> The interested reader can find a discussion of steels which should be understandable to him in S. H. Avner, Introduction to Physical Metallurgy, McGraw-Hill, New York, 1964, pp. 172-343.



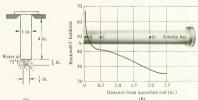
Eutectoid temperature 700 600 500 Femperature (°C) 400 200 100 Martensite Martensite + nearlite pearlite pearlite 100 102 Time (sec)

Fig. 12-26. The continuous cooling diagram for 1080 steel. The transformation regions are shaded. The solid curves show the location of the I-T diagram: the dashed lines represent cooling curves at different points in a material. (After Atlas of Isothermal Transformation Diagrams, U.S. Steel Corp., Pittsburgh, 1951.)

of the I-T diagram is shown by the two solid lines, and it is seen that the austenite to pearlite transition takes place a little bit later for continuous cooling than for the isothermal process. Let curve A represent the timetemperature curve of the surface of a round bar. The figure shows that the surface will transform completely to martensite. Cooling will take place more slowly at the center of the bar. If curve C represents the cooling curve at the center, the center will be all pearlite. Because the cooling rate at any point in the bar depends on the distance from the point to the surface, the microstructure and hardness of the bar will vary from the surface to the center. A large amount of martensite in the final structure corresponds to a high hardenability. Note that the actual shape of the cooling curves depends on the quenching medium because this affects the heattransfer rate from the bar.

One of the standard hardenability tests used is the Jominy test. The apparatus used for this test is shown in Fig. 12-27(a). The specimen to be tested is a cylindrical bar 1 in. in diameter and 4 in. long. The bar is

Fig. 12-27, (a) The standard arrangement used for hardening a Jominy bar, (b) The hardness of a Jominy bar made of 1080 steel after being avenched as shown in (a) The naints labeled A, B, C, and D correspond to the four cooling curves in Fig. 12-26. (After Atlas of Isothermal Transformation Diagrams, U.S. Steel Corp., Pittsburgh, 1951.)



austenized, removed from the furnace, and placed in the apparatus. One end of the specimen is then quenched by water having a temperature of  $75^{\circ}\mathrm{F}$  and a specified flow rate. When the entire bar has cooled to room temperature, hardness readings are taken every  $\gamma_0^1$  in. from the quenched end. Figure 12-27 shows hardness as a function of distance from the end of the bar for 1080 steel. The points labeled A, B, C, and D correspond to the four cooling curves in Fig. 12-26 that are labeled similarly. It is seen that the hardness falls rather quickly with distance for this material. For steels having a higher hardenability, the curve will not fall as fast. Hardenability can be quantitatively defined in terms of "idealized" quenching liquids and bar diameters. but we shall not pursue this: "

The hardenability of steel can be increased by supressing the austenite—pearlite transition. In terms of Fig. 12-26 or 12-20, this would correspond to moving the transition regions (shaded regions) to the right. If this were done, martensite could form at lower cooling rates, and a piece of steel could be hardened to a greater depth when quenched. The alloying elements commonly used with steel (Table 11-2) generally increase the hardenability by increasing the time required for the austenite—pearlite transformation. Alloying elements also increase the temperature required for tempering martensite. Particular alloying elements are used for enhancing particular properties. Nickel, for example, generally increases toughness, while chromium aids the wear properties by forming very hard chromium carbides. It is common to use several alloying elements in a single steel in order to get a desired combination of properties.

Questions

- Question 8: The curve in Fig. 12-27 changes its slope rather abruptly at about 0.4 in. Explain why. (Consider cooling curves B and C in Fig. 12-27.) Why does hardness continue to diminish as distance increases beyond this point?
- Question 9: Two pieces of plain carbon steel are hardened, tempered, and then welded together. During welding, the metal in the region of the weld joint is melted and additional material is added (this is the welding rod). Assume that the composition of the rod is the same as that of the two pieces of steel. The welded joint is air-cooled. (a) Will the physical properties of the steel in the neighborhood of the weld be the same as the properties at some distance from the weld? (b) If the steel is highly hardenable, will the weld joint tend to be more or less brittle than the original material?

# 12-9 Strain-induced transformations

The phase changes and transformations that have been discussed so far were caused by temperature changes. In some systems it is possible for transformations to occur as the result of strain, although they are not nearly as common as those caused by temperature. This section will discuss strain-induced transformations in two types of steels. In both cases, a metastable system transforms to a more stable one as the result of strain. The temperature at which martensite begins to form can be changed by

\* The procedures for defining hardenability are given by A. G. Guy, Elements of Physical Metallurgy, Addison-Wesley, Reading, Mass., 1959, pp. 481-486.

adding various alloying elements to steel. For example, the effect of carbon content on the  $M_s$  and  $M_f$  temperatures of plain carbon steels is shown in Fig. 12-24. Some of the elements commonly used in steelmaking tend to reduce the temperature at which martensite begins to form. It is possible to add appropriate alloving elements to steel and reduce the M temperature to a value below room temperature. If such an alloy steel is cooled from the austenite region to room temperature, it will retain the austenite structure. This occurs with a class of stainless steels that contain about 18% chromium and 8% nickel; they are austenitic at room temperature. The fact that the fcc structure is maintained at room temperature can be attributed to the high nickel content. Other stainless steels which have about the same chromium concentration but less nickel will go through a martensitic transformation during quenching. The room-temperature austenite is metastable because the equilibrium state of these steels would be a mixture of ferrite (with other elements dissolved in it) and carbides. The rate at which the austenite transforms to ferrite and carbides at room temperature is very slow; therefore the austenite remains. When these steels are deformed at room temperature, it is found that the work-hardening rate is much higher than would be expected from a dislocation interaction mechanism. Table 12-3 shows the effect of cold working on two commercially available austenitic stainless steels. The very large increase in strength that occurs when the material is cold-worked has been attributed to the transformation of austenite to martensite during straining. The phenomenon has been observed. The dislocation entanglement mechanism discussed in Chapter 8 is present in this work-hardening process; however, most of the hardening is due to the inability of the dislocations to slip in the newly formed martensite.

Stress-induced transformations can be used to increase the ductility of steel by inhibiting necking. The mechanism for this has been demonstrated in the laboratory.† The discussion of ductile fracture in Chapter 8 explained that the necking of a specimen began when the work-hardening rate of the material in the neighborhood of the neck was too low to counteract the effect of the decreasing neck area. As a material was

† See E. R. Parker and V. F. Zackay, Sci. Am. 219:36 (Nov. 1968), for a more detailed discussion.

Table 12-3, Effect of cold working on two austenitic stainless steels\*

Type of stainless steel	Alloying elements (wt. %)	Condition	Yield strength (psi)	Ultimate tensile strength (psi)
301	[0.15% C, 2.0% Mn] 16-18% Cr 6-8% Ni	Annealed	33,000	117,000
	16-18% Cr	25% cold-rolled	127,000	165,000
[6-8% Ni	45% cold-rolled	200,000	225,000	
302	[0.15% C, 2.0% Mn]	Annealed	36,000	94,000
	[0.15% C, 2.0% Mn] 17-19% Cr 8-10% Ni	20% cold-rolled	121,000	139,000
	8-10% Ni	50% cold-rolled	151,000	177,000

<sup>\*</sup> Data from R. M. Brick, R. B. Gordon, and A. Phillips, Structure and Properties of Alloys, McGraw-Hill, New York, 1965.

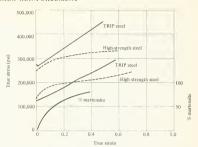


Fig. 12-28. Stress-strain curves of TRIP steels and highstrength seeds that have comparable yield points. The TRIP steels have a higher work hardening rate at large strain. TRIP steels form matteristic as deformation progresses. The percent matternite is shown as a function of strain in the lower curve. (E. R. Parker and V. F. Zackay, Sci. Am. 219: 36

strained, more slip took place in some regions than in others. The highly slipped regions were likely candidates for neck formation. In TRIP steels, heavy deformation causes an austenite to martensite transformation and thereby strengthens the most heavily deformed region of the solid. TRIP stands for transition-induced plasticity. The martensite transformation has been observed to take place at the slip planes; consequently it is very effective in preventing further slip. This, of course, inhibits the formation of a neck. Because necking is inhibited, more of the specimen has a chance to deform prior to fracture and the elongation is increased. Special processing of the steel is required in order to have the transformation occur at the slip planes.

The strain-hardening rate of two TRIP steels are compared to two commercial high-strength steels in the true stress-true strain diagrams of Fig. 12-28. Each pair of materials has about the same yield stress; however, the work-hardening rate of the conventional steels diminishes with strain. The work-hardening rate of the TRIP steels remains practically constant until fracture. The lower curve shows that the percentage of martensite in TRIP steel increases as the strain increases, in accordance with the hardening mechanism.

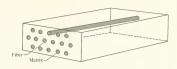
## Question

Question 10: The data for type 301 stainless steel (Table 12-3) show that the difference between the yield stress and the ultimate stress is greatest if the steel is in the annealed condition at the start of a tensile test. This implies that the annealed steel work-hardens more than the coldrolled stainless steel. Explain why.

## 12-10 Fiber and whisker reinforcement

The strengthening mechanisms discussed so far have depended on dispersed particles, phase changes, or both. The desired changes in the materials were brought about by heat treating and diffusion. It is also possible to increase strength by embedding fibers or whiskers of one

Fig. 12-29. Schematic drawing of a fiber composite material. The fibers are alianed with an axis of the material, and all are parallel to the single fiber shown fully in the figure.



material in the matrix of another. The properties of these fiber- or whiskerreinforced composites can often be tailored for a specific application. The major disadvantage of the method is cost. This section will cover some of the principles of fiber and whisker reinforcement. The entire topic is currently receiving a lot of attention, and the discussion in this section is by no means comprehensive.\*

A simple case of fiber reinforcement is shown in Fig. 12-29. The fibers are aligned with one axis of the solid block. If a stress is applied parallel to the fibers, it is carried by both the fibers and the matrix. The fibers are bonded to the matrix at the fiber-matrix interface, and the bonding is quite critical. If the bond is strong enough to transmit loads between fiber and matrix, then the composite will deform as a single piece of material; that is, the fibers and the matrix will elongate the same amount when the composite is loaded. The fibers generally have a higher elastic modulus than the matrix. Because both elongate equally, the fibers will be more severely stressed than the matrix. The fibers, however, are usually stronger than the matrix and can withstand the higher stress. Thus, they strengthen and stiffen the matrix. Note that this discussion is based upon strong bonds between the matrix and fiber materials. To form these bonds, the matrix material must be capable of wetting the fiber. The requirement of strong interface bonds often results in special processing of the material with an accompanying rise in cost,

The properties of some fibers and whiskers which are used for making composites are shown in Table 12-4. The ceramics and metals in the table

\* For a more extensive discussion, see L. J. Broutman and R. H. Krock, Modern Composite Materials, Addison-Wesley, Reading, Mass., 1967.

Table 12-4. Properties of some fibers and whiskers that are used for composite materials†

Tensile strength (million psi)	Elastic modulus (million psi)	Melting temperature (°C)		
3.0	70-125	>2200		
6.2	70-330	2000		
3.0	145	>3000		
0.3	66	2200		
0.7	12.4	760 (softens)		
0.22	42	1285		
	3.0 6.2 3.0 0.3 0.7	(million psi) (million psi)  3.0 70-125 6.2 70-330 3.0 145  0.3 66 0.7 12.4		

<sup>†</sup> Data tabulated from various sources by P. T. B. Shaffer in Modern Composite Materials, L. J. Broutman and R. H. Krock, eds., Addison-Wesley, Reading, Mass., 1967, p. 216.

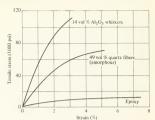


Fig. 12-30. Stress-strain diagrams of an epoxy polymer showing the effect of using quarte fibers and Al<sub>2</sub>O<sub>3</sub> whiskers as reinforcement. The specimens were elongated slowly, (O.O.3 in-min.) during the test. (After W. H. Sutton, B. W. Rosen, and D. G. Flom, SPE J. 20: 1203 [1964]).

all show high values for strength, modulus, and melting point. The S-glass which is listed has a composition of 65% SiO<sub>2</sub>, 25% Al<sub>2</sub>O<sub>3</sub>, and 10% MgO. It can be processed into thin fibers suitable for reinforcement and shows high strength.

Fiber reinforcement and whisker reinforcement have been used successfully for both metals and plastics. Probably the best known composite is fiberglass, which consists of glass-reinforcing fibers in a matrix of either an epoxy polymer or a polyester. In many applications, such as boat hulls and automobile bodies, the fibers are not arranged like those in Fig. 12-29. In these cases, the glass is woven into cloth and the cloth provides reinforcement. For other applications, the glass can be chopped into short lengths, which then assume random positions within the matrix. If whiskers are used as reinforcement, they can either be aligned or random, depending on the process used for making the material. The effect of quartz fibers and Al<sub>2</sub>O<sub>3</sub> whiskers on the stress-strain characteristics of an epoxy polymer is shown in Fig. 12-30. The strength increase is significant (and so is the cost increase).

Fiber and whisker reinforcement are very effective strengthening processes at high temperature. The cylindrical shape of the fibers and needle-like shape of the whiskers are more effective barriers to dislocation climb and cross slip than dispersed particles; consequently reinforced composites generally have better creep and high-temperature properties than dispersion- or precipitation-hardened materials. This is illustrated for silver in Fig. 12-31. The dispersion-strengthened curve represents silver containing Al<sub>2</sub>O<sub>3</sub> particles. The oxide was formed by the internal oxidation of Al particles in the Ag matrix. It is seen that whisker reinforcement is more effective for high-temperature strengthening than is dispersion hardening, although the strength difference at room temperature is not significant. Reinforced aluminum shows similar characteristics; fiber- or whisker-reinforced aluminum has high-temperature properties which are superior to dispersion-hardened SAP.

#### Question

Question 11: Fig. 12-32 shows that the ultimate tensile strength of agehardened aluminum falls rapidly with temperature but that that of SAP falls more slowly. Why?

Fig. 12-31. The effect of Al.O. whiskers and particles on the ultimate tensile strenath of silver. Both dispersion strengthening and whisker reinforcement are effective at low temperatures, but the whiskerreinforced material is superior at high temperatures, (After W. H. Sutton and J. Chorne, Fiber Composite Materials, American Society of Metals, Metals Park, Ohio, 1965: A Gatti and R. I. Fullman Trans. AIME 215: 762 [1959].)

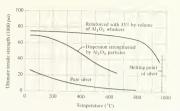
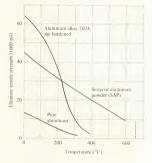


Fig. 12-32. The effect of temperature on the ultimate tensile strength of an age-hardened Al alloy and SAP. The main alloving element in 2024 Al is copper. The age-hardened material is affected more strongly by temperature than is the SAP. (After L. H. Van Vlack, Elements of Materials Science, 2nd ed., Addison-Wesley, Reading, Mass., 1964.)



#### Designing with strengthened materials 12-11

The strengthening mechanisms discussed in this chapter provide methods for manipulating the properties of many materials. It is often possible to process materials so that they have optimum combinations of properties for a particular task. When considering materials for design applications, the term optimum includes more than just strength, ductility, and the other physical properties discussed in the book. It also includes cost and other parameters which will vary with different applications. These parameters might include factors such as weight, reliability, ease of fabrication, corrosion resistance, maintenance, etc. The selection of a material for a specific application is usually based upon a combination of knowledge of fundamental principles, as presented in this book, and experience. It is quite apparent that this section will not provide design experience, but it is worthwhile to consider a few cases in which various parameters become significant.

Let us start with automobile bodies; materials selection is very strongly cost dependent. By coat dependent we mean the total cost of the automobile body, not just the cost of materials. Most bodies are made of low-carbon steel. The fabrication consists generally of pressing sheet steel into the desired shapes by means of large presses and dies. The cost of the tooling is high, while the steel cost is low. Thus, the procedure is suitable for production of a large number of units. If a requirement for a small number of a particular automobile body arises, the cost of making dies for large presses makes steel fabrication economically impractical. In this case, it is cheaper to fabricate the bodies from fiberglass. The cost of fiberglass is significantly higher than that of low-carbon steel; however, the cost of fabricating a small number of units is much lower for the fiberglass because of tooling. Both materials have physical properties which are adequate for automobile bodies; cost of fabrication is the determining factor.

Materials selection for aircraft and space vehicles is often based upon weight considerations. The size and engine requirements for these vehicles usually depend on the weight of the system; therefore it is advantageous to make the components of the system as light as possible. Expensive materials are often used if they result in a lightweight component. The cost saving of the system due to the decrease in weight of a component can be much greater than the higher cost of material. Many of the newer materials, such as whisker-reinforced composites, will probably find their first uses in the aerospace industry. Aircraft provide a good example of the effect of temperature on materials selection. Aluminum alloys have been used for airframe construction for many years. As aircraft speeds have increased, the operating temperatures of the aircraft structures have increased because of aerodynamic heating. The strength of aluminum alloys diminishes rather rapidly with temperature, as shown in Fig. 12-32. For high-speed aircraft whose structure is subjected to fairly high temperatures, stainless steels are better materials than aluminum. Despite the fact that stainless steels have higher densities than aluminum, their high-temperature strength is so much greater than that of aluminum that a weight saving is realized by using stainless. At higher speeds (about Mach 2) the operating temperature is still higher, and titanium alloys are used in place of stainless steels.

Maintenance requirements often are very strong considerations in materials selection. Consider a tube containing cooling fluid in a nuclear reactor. Replacement of this part would be a more difficult and expensive operation than replacing a tube in a steam boiler. As a consequence, using more expensive materials in a reactor could be justified on the basis of reduced maintenance costs. A less exotic example is found in building maintenance. Vinyl tile has become a very popular floor material. It requires periodic washing and waxing. Rugs are more expensive but require less maintenance; periodic vacuum cleaning is usually sufficient. Economic analyses show that it is cheaper to use rugs in some cases, although the initial cost of vinyl flooring is quite a bit less.

Ease of fabrication also plays a role in materials selection, and it is here that the versatility of steel proves useful. Annealed or spheroidized steels can be machined into useful shapes readily, but hardened steels are difficult to machine. If we wish to fabricate a component and the com-

fabrication

ponent must be hard and strong (and somewhat brittle), the fabrication can be done when the steel is in the annealed state. Following fabrication, the steel can be hardened by appropriate heat treating. The differences in the case of fabrication can be demonstrated by the following simple experiment. Anneal a block of 1040 or 1045 steel, and drill a hole through it on a drill press. Take the same block, heat it to the austenizing range, and quench it in water. Then try to drill the same sized hole that you previously drilled. The screeches of anguish that come from a normal drill as it attempts to penetrate the hardened steel should convince the reader that annealed steels are far more machinable than hardened ones. The same argument can be applied to age-hardenable alloys. These are often fabricated when they are in the solutionized state and are ase-hardened after

These are just a few examples of factors which must be considered when selecting materials. The engineer is required to exercise judgment. The judgment is based upon knowledge and experience. If this book has imparted some detailed knowledge of why materials act as they do and how the behavior can be altered, then it has fulfilled its functions.

#### Problems

- 1 The strength of solution-hardened solids can be increased by work-hardening them. Solution-hardened copper has a higher work-hardening rate than pure copper. (a) Explain why. (b) On the basis of your explanation, would you expect that a solution-hardened material will generally have a higher work-hardening rate than the pure material? Explain.
- 2. A sample of TD nickel contains 85% Ni and 15% ThO<sub>2</sub> by volume. The ThO<sub>2</sub> is dispersed as spheres throughout the nickel. A surface of the material was polished and etched, and it was found that  $4 \times 10^6$  ThO<sub>2</sub> spheres intersected 1 cm<sup>2</sup> of the plane. (a) Determine the radius of the spheres. Note: This can be done with the aid of Fig. 12-6(b). Consider that the area shown in the figure is 1 cm<sup>2</sup>. Consider a volume of material having a cross section of 1 cm<sup>2</sup> and a thickness of  $\pi \mathcal{B}_s | 2$ . This volume contains  $N_s$  spheres. (b) Find the average distance between ThO<sub>2</sub> spheres. This is the quantity  $\mathcal{L}'$  in equation 12-1.
- 3 The examples of dispersion hardening used in Section 1.2-2 all had dispersed phases which were much harder than the matrix, and their behavior was predicted reasonably well by equation 12-1. This equation is not valid if the dispersed phase is soft, that is, if dislocations slip easily through them. Explain why.
- 4 Figure 12-12 shows that the yield stress of an iron-6% molybdenum alloy, which has been age-hardened at 550°C for 1219 hr., is 50,000 psi. The distance between Fe<sub>2</sub>Mo particles was observed to be 1800Å. Is this in agreement with equation 12-1? *Note*: The yield stress of the solutionized alloy can be found from the lowest curve in the figure. G = 12 x 10° psi.
- 5 Quenching of certain materials causes the high-temperature structure of the material to be maintained at lower temperatures. Suppose a

- piece of pure copper was quenched from 1000 to 300°K. What fraction of the lattice sites would contain vacancies? The energy required to form a vacancy is about 1 eV.
- 6 The rate at which an alloy precipitation hardens depends on the diffusion rate. An Al-Cualloy containing 4% Cu reaches maximum hardness in 200 hr at a temperature of 420°K. (a) Estimate how long the material should be aged at 460°K in order to attain maximum hardness. (Hint: Assume that the time to maximum hardness is inversely proportional to the diffusion coefficient and solve the problem by using a ratio of diffusion coefficients.) The activation energy for diffusion is 36,900 cal/mole. (b) How long can this alloy be kept at room temperature before it reaches maximum hardness?
- 7 A specimen of steel having the eutectoid composition has been quenched from the austenite region. If all of the austenite transforms to martensite, what fraction of the interstitial sites in the martensite structure will contain carbon atoms?
- 8 The rate at which the transformation austenite → ferrite + cementite occurs depends on the temperature at which it occurs. The rate is inversely proportional to the time required for the reaction. The time required for this transformation, at a given temperature, can be found from Fig. 12-20 for 1080 steel. (a) Plot a curve (schematically) of the transformation rate vs. temperature. (b) In Problem 1 in Chapter 4, the freezing rate of copper was plotted as a function of temperature. The curve obtained for part (a) of this problem should have the same general shape as the curve in Problem I in Chapter 4. This might indicate that the freezing process and phase transformation process have similarities. Discuss the similarities.
- 9 The cementite lamella are thinner in fine pearlite than they are in coarse pearlite, and the distance between neighboring cementite regions is therefore smaller in the fine structure. Fine pearlite has a higher yield strength than coarse pearlite. Explain why.
- 10 Three cooling paths are described by the broken lines in Fig. 12-21. These paths are labeled 1, 2, and 3. Three specimens of steel are cooled from the austenite region, one along each path. (a) What is the room-temperature microstructure of each piece? (b) Which is strongest? (c) Which is most duetile?
- 11 Figure 12-22 shows that annealed steel is harder than spheroidized steel. The difference between the two is due to the difference in the distribution of cementite; in one the cementite forms lamella, while in the other it forms spheres. (a) Which of these would make cross slip and climbof dislocations more difficult? (b) Why? (c) Does this help to explain the data in Fig. 12-22?
- 12 The rate at which a specimen cools during quenching depends on the geometry and composition of the specimen and the liquid that is used as the quenching medium. Three common quenching liquids are used for steel: brine, water, and quenching oil. Brine is the most effective in removing heat from the surface of a specimen, while quenching oil is least effective. Identical specimens of austenite are quenched in each of these liquids. Which liquid yields (a) the strongest steel after the quench and (b) the most ductile? (c) If the liquid is stirred during

quenching, will the steel be harder than if the liquid was not stirred? Why?

- 13 A number of strengthening mechanisms have been discussed. These are strengthening due to strain, solid solution, particle dispersion, grain size, diffusionless phase transformation, and redistribution of a phase in a matrix. Which of the mechanisms contributes most to the strengthening when materials are processed in the following manner: (a) Nucleation sites in the form of impurities are added to molten magnesium, after which a casting is made. (b) Aluminum sheet which is ½; in. thick is rolled into aluminum foil. (c) Coarse pearlite is austenized and then cooled in a manner that yields fine pearlite. (d) Zinc and copper are mixed, melted, and slowly cooled to form 70% Cu-30% Zn brass. (e) Aluminum containing 4% copper is quenched from a single-phase region, after which it is heated to 200°C for 2 hr. (f) Spheroidized 1080 steel is austenized and quenched to room temperature.
  - 14 Sketch the microstructure of the Jominy bar (Fig. 12-27) at points B, C, and D.
  - 15 Steel reinforcing rods are commonly used in building construction. They are welded at the building site and are not heat-treated. Should these rods have high or low hardenability? Why?
  - 16 Figure 12-29 shows a composite material having fibers in one direction. Let the fibers be boron, and let the fibers occupy 30% of the volume. The matrix is copper. (a) Find the elastic modulus of the composite material in the direction of the fibers. (b) Is the composite material anisotropic? Why?
  - 17 Figure 12-31 shows that Al<sub>2</sub>O<sub>3</sub> is more effective at high temperature in whisker form than in particle form. Does the argument used in answering Problem 11 help to explain this? Why?

Answers

Question 1: The solid lines in the accompanying sketch represent the dislocation when all of the atoms have the same size. The dashed lines



show the configuration when some of the solvent atoms on the extra half plane are replaced by smaller solute atoms. The distortion of the crystal is reduced by the substitution; therefore the strain energy is reduced. Slip is inhibited because the dislocation would leave a strained region if it slipped. Energy to create this region would have to come from work done by the applied force.

- Question 2: The more dispersed the cementite particles are, the more effective they are in inhibiting dislocation motion. The cementite in fine pearlite is more dispersed than that in coarse pearlite. This can also be considered from another point of view. Slip occurs in the ferrite more readily than in cementite. The smaller the ferrite regions, the stronger the material because reducing the size of the ferrite regions in pearlite is somewhat analogous to reducing the grain size in a polycrystal.
- Question 3: The 60:40 brass is in a two-phase region at room temperature. To disperse \( \tilde{P} \) throughout the matrix, heat the brass into the singlephase (\( \tilde{P} \)) region. A temperature of about 800°C is required. Quench and age. An aging temperature below about 750°C can be used. This process results in a \( \tilde{P} \) has dispersed in an \( \tilde{m} \) that been found that maximum hardness requires an aging temperature of about 250°C.
- Question 4: No. Equation 12-1 is based upon a Frank-Read source. For the equation to apply, a dislocation must not be able to slip through pinning sites but must generate new dislocations. GP 1 zones hinder dislocation motion by disrupting the crystal symmetry. They do not necessarily pin a dislocation strongly enough to have it act as a source.
- Question 5: Figure 9-10 shows that the ductile-to-brittle transition occurs at the intersection of the two curves. Strengthening a material raises the yield stress curve, thereby raising the ductile-to-brittle transition temperature. If the strengthening process raises the transition temperature above the temperature at which the material will be used, then the strengthening process has produced a brittle material.
- Question 6: The curves shift to the left. The transformation requires nucleation and growth of new phases. If either nucleation or growth is speeded up, the transformation occurs more quickly. The presence of more nuclei decreases the nucleation time and provides more sites at which the phase change can occur. A larger number of grain boundaries increases the number of nucleation sites.
- Question 7: Martensite is brittle and therefore has very limited dislocation mobility. The dislocation mobility is *Increased* by the phase change. The opposite is true of the Al-Cu system. In the martensite case, we had a hard material before the transformation. The Al-Cu alloy was soft in the single-phase state.
- Question 8: The slope is falling rapidly at point B. Figure 12-26 shows that both martensite and pearlite are present. As we go from B toward C, the amount of martensite decreases, and hardness falls rapidly. The rather sharp change in the slope indicates that martensite is not being formed at about 0.4 in, from the end of the bar. At C, the structure is fine pearlite. In going from C to D, this changes to coarse pearlite. The downward slope of the hardness curve in this region indicates that fine pearlite is harder than coarse pearlite.
- Question 9: (a) No. The material near the weld has been subjected to a different heat treatment than the remainder of the steel. The weld material is austentitie shortly after it solidifies. The rate at which it cools from the austenite region will determine its final properties. Heat is removed from the weld joint both by being conducted down the steel rod and by being transferred to ambient air. Cooling will be somewhat

- faster than the cooling rate during normalizing (especially on a cold, windy day). (b) A highly hardenable steel will tend to form martensite as it cools and will be more brittle than the original material.
- Question 10: Work hardening is largely attributed to martensite formation. A material that contains no martensite before deformation can form more of it during straining than a material which initially has some martensite in it. As a result, the steel initially having no martensite will strain-harden more. Cold-rolling (or cold-working) the steel causes some martensite formation.
- Question 11: Maintaining age-hardened aluminum at high temperature causes overaging. The effectiveness of the pinning sites is thereby diminished. This does not happen with SAP.

# Appendixes

- A Properties of the elements 414
- B Properties of selected ceramics 418
- C Properties of selected polymers at room temperature 420
- D Planes and directions in hexagonal crystals 422
- E Taylor's expansion 424
- F Answers to selected problems 426
- G Physical constants 429
- H Conversion factors 429
- I Systems of units 429
- J Symbols 429

APPENDIX A: Properties of the elements
(rare earths and actinons are not included)

Element	Symbol	Atomic number	Atomic weight*	Approximate atomic radius† (Å)	Approximate ionic radius* (Å)
Aluminum	Al	13	26.98	1.43	0.51
Antimony	Sb	51	121.75	1.45	0.62
Argon	Ar	18	39.95	1.92	1.54
Arsenic	As	33	74.92	1.25	0.58
Astatine	At	85			0.62
Barium	Ba	56	137.34	2.17	1.34
Beryllium	Be	4	9.01	1.11	0.35
Bismuth	Bi	83	208,98	1.55	0.96
Boron	В	5	10.811	0.97	0.23
Bromine	Br	35	79.91	1.19	1.96
Cadmium	Cd	48	112,40	1.48	0.97
Calcium	Ca	20	40.08	1.99	0.99
Carbon	C	6	12,011	0.77	0.16
Cesium	Cs	55	132.91	2,62	1,67
Chlorine	CI	17	35,45	1.07	1.81
Chromium	Cr	24	52.00	1.24	0.63
Cobalt	Co	27	58,93	1.25	0.72
Copper	Cu	29	63.54	1.28	0.96
Fluorine	F	9	19.00		1.33
Francium	Fr	87			1.80
Gallium	Ga	31	69.72	1.22	0.62
Germanium	Ge	32	72.59	1.22	0,53
Gold	Au	79	196.97	1.44	1.37
Hafnium	Hf	72	178.49	1.59	0.78
Helium	He	2	4.003	1.00	0.70
Hydrogen	H	1	1.008		
Indium	In	49	114.82	1.62	0.81
Iodine	I.	53	126.90	1.35	2.20
Iridium	Îr	77	192.2	1.36	0.68
Iron	Fe	26	55.85	1.24	0.74
Krypton	Kr	36	83.80	1.97	0.64
Lead	Pb	82	207.19	1.75	1.20
Lithium	Li	3	6.94	1,51	0.78
Magnesium	Mg	12	24.31	1.60	0.78
Manganese	Mn	25	54.94	1.12	0.80
Mercury	Hg	80	200,59	1.50	1.10
Molybdenum	Mo	42	95.94	1.36	0.70

<sup>\*</sup> R. C. Weast, ed., Handbook of Chemistry and Physics, 47th ed., Chemical Rubber Co., Cleveland, Ohio, 1967.

<sup>†</sup> C. J. Smithels, *Metals Reference Book*, Vol. II, 2nd ed., Wiley-Interscience, New York, 1955.

Valence at given ionic radius*	Young's modulus at room Temperature† (polycrystalline) (psi × 10 <sup>-6</sup> )	Melting point* (°C at 1 atm)	Boiling point* (°C at 1 atm)	Density* (g/cm³ for solids at 20°C, 1 atm)
+3	9.9	660.2	2467	2.699
+5		630.5	1380	6.691
+1		-189.2	-185.7	Gas
+3 +7				5.73
+2		725	1140	3.5
+2	43	1278	2970	1.848
+3		271.3	1560	9.747
+3		2300		2.34
-1		-7.2	58.78	Liquid
$\pm 2$		320.9	765	8.65
+2	3.0	846	1487	1.55
+4		3550		3.51
+1		28.5	690	1.873
-1		-101	- 34.6	Gas
+3	36	1890	2482	7.19
+2	30	1495	2900	8.9
+1	18	1083	2595	8.96
$-1 \\ +1$		-219.6	-188.1	Gas
+3		29.8	2403	5.907
+4		937.4	2830	5.323
+1	11.4	1063	2966	19.32
+4	20	2150	5400	13.29
			-268.6	Gas
		-259.1	-252.5	Gas
+3	1.6	156.6	2005	7.31
-1		113.5	184.35	4.93
+4	75	2410	4527	22.42
+2	28.5	1535	3000	7.874
+3		-156.6	-152.3	Gas
+2	2.3	327.5	1744	11.35
+1		179	1317	0.534
+2	6.5	651	1107	1.738
+2		1244	2097	7.3
+2		- 38.9	356.6	Liquid
+4	42	2610	5560	10.22

Element	Symbol	Atomic number	Atomic weight*	Approximate atomic radius† (Å)	Approximate ionic radius† (Å)
Neon	Ne	10	20.18	1.60	1.12
Nickel	Ni	28	58.71	1.25	0.69
Niobium	Nb	41	92.91	1.42	0.69
Nitrogen	N	7	14.007	0.71	1.71
Osmium	Os	76	190.2	1.34	0.88
Oxygen	O	8	15.9994	0.60	1.32
Palladium	Pd	46	106.4	1.37	0.65
Phosphorous	P	15	30.97	1.09	2.12
Platinum	Pt	78	195.09	1.38	0.80
Polonium	Po	84	210	1.40	0.67
Potassium	K	19	39.10	2.31	1.33
Radium	Ra	88	226		1.43
Radon	Rn	86	222		
Rhenium	Re	75	186.2	1.37	0.72
Rhodium	Rh	45	102.91	1.34	0.68
Rubidium	Rb	37	85.47	2.43	1.47
Ruthenium	Ru	44	101.07	1.32	0.67
Scandium	Sc	21	44.96	1.60	0.73
Selenium	Se	34	78.96	1.16	1.91
Silicon	Si	14	28.09	1.18	0.42
Silver	Ag	47	107.87	1.44	1.26
Sodium	Na	11	22.99	1.85	0.97
Strontium	Sr	38	87.62	2.15	1.12
Sulfur	S	16	32.06	1.06	1.84
Tantalum	Ta	73	180.95	1.43	0.68
Techtenium	Tc	43	99		0.98
Tellurium	Te	52	127.60	1.43	2.11
Thallium	TI	81	204.37	1.70	0.95
Tin	Sn	50	118.69	1.40	0.71
Titanium	Ti	22	47.90	1.45	0.68
Tungsten	W	74	183.85	1.37	0.70
Vanadium	V	23	50.94	1.31	0.74
Xenon	Xe	54	131.30	2.18	
Yttrium	Y	39	88.91	1.79	0.89
Zinc	Zn	30	65.37	1.33	0.74

<sup>\*</sup> R. C. Weast, ed., Handbook of Chemistry and Physics, 47th ed., Chemical Rubber Co., Cleveland, Ohio, 1967.

<sup>†</sup> C. J. Smithels, Metals Reference Book, Vol. II, 2nd ed., Wiley-Interscience, New York, 1955.

Valence at given ionic radius*	Young's modulus at room Temperature† (polycrystalline) (psi × 10 <sup>-6</sup> )	Melting point* (°C at 1 atm)	Boiling point* (°C at 1 atm)	Density* (g/cm³ for solids at 20°C, 1 atm
+1		-248.7	-245.9	Gas
+2	30	1453	2732	8.902
+5	15	2468	4927	8.57
-3		- 209.9	- 195.8	Gas
+4		3000	5000	22.57
-2		-218.4	-183	Gas
+4	17	1552	2927	12.02
-3		44.1	280	1.82
+2	22	1769	3827	21.45
+6		254	962	9.32
+1		63.7	774	0.862
+2		700		5(?)
		-71	-61.8	Gas
+4		3180	5627	21.02
+3	41	1966	3727	12.41
+1		38.9	688	1.532
+4		2250	3900	12.41
+3		1539	2727	2.992
-2		217	684.9	4.79
+4		1410	2355	2.33
+1	11.0	960.8	2212	10.50
+1		97.8	892	0.971
+2		796	1384	2.54
-2		112.8	444.6	2.07
+5	27	2996	5425	16.6
+7		2200		11.5
-2		449.5	989.8	6.24
+3		303.5	1457	11.85
+4	6.8	231.9	2270	7.31
+4	16	1675	3260	4.54
+4	52	3410	5927	19.3
+3	20	1890	3000	611
		-111.9	- 107.1	Gas
+3		1495	2927	4.45
+2	14	419.4	907	6.53

Appendix B: Properties of selected ceramics\*

Material and temperature at which properties were measured (°F)		Density (g/cm³ at room temperature)	Melting °C	point °F	Modulus of elasticity (polycrystalline) (psi $\times$ 10 <sup>-6</sup> )
Al <sub>2</sub> O <sub>3</sub>	70 1000 2000	3.98	2037	3700	50 47 42
BeO	70 1000 2000	3.01	2452	4445	40-55 38-50 20-44
HfB <sub>2</sub>	70	11,20	3250	5880	32-64
MgAl <sub>2</sub> O <sub>4</sub>	70 1000 2000	3.59	2135	3875	38 36 30
MgO	70 1000 2000	3.57	2947	5340	40 38 34
SiC	70 1000 2000	3.21	2700	4940	50-70 50-70 45-60
SiN <sub>4</sub>	70	3.43	1900	3450	8-13
ThO:	70 1000 2000	10,00	3267	5910	35–45 32 30
TiC	70 1000 2000	4.92	3140	5700	45-60 40 —
WC	70	15.77	2775	5025	75–100
UO <sub>2</sub>	70	10.96	2877	5210	27

<sup>\*</sup> From E. R. Parker, Materials Data Book, McGraw-Hill, New York, 1967.

Poisson's ratio	Coefficient of thermal expansion (in./in./°F × 10 <sup>6</sup> )	Ultimate tensile strength (psi $\times$ 10 <sup>-3</sup> )	Ultimate compressive strength (psi × 10 <sup>-3</sup>
0.2-0.3	3.0	25-35	400
0.3	3.1	20-35	200
0.3	3.3	15-30	100
0.2	3.0	12-18	110-250
0.2	4.0	10-16	30-80
0.2	4.5	3-10	20-50
0.15	2.8	-	220
0.3	3.0	18	270
_	3.0	13	190
_	3.0	7	90
0.3	5,0	15	200
_	5,5	15	_
-	6.0	10	_
0.2	2.7	20	200
-	3.0	_	_
_	3.3	_	_
_	1.4	16	90
0.3	6,0	14	220-400
_	6.0	_	80
	7.0	_	40
	3.5	30	190-550
_	4.0	38	_
	4.5	40	-
	3.0	50 74	
0.3	4.0	_	80-140

APPENDIX C: Properties of selected polymers at room temperature\*

Material	Type of Polymer	Density (gm/cm <sup>3</sup> )
Epoxy, cast Aluminum filler Glass fiber filler	Thermosetting	1.1-1.4 1.4-1.8 1.6-2.0
Melamine-formaldehyde Cellulose filler Asbestos filler Glass fiber filler	Thermosetting	1.48 1.50 1.7-2.0 1.8-2.0
Nylon 6	Thermoplastic	1.13
Polyethylene Low density Medium density High density	Thermoplastic	0.91-0.93 0.93-0.94 0.94-0.96
Polymethyl methacrylate	Thermoplastic	1.17-1.20
Polypropylene	Thermoplastic	0.90-0.91
Polystyrene Impact resistant	Thermoplastic	1.04-1.06 0.98-1.10
Polytetrafluoroethylene	Thermoplastic	2.1-2.2
Polyvinyl chloride Flexible	Thermoplastic	1.35-1.45 1.16-1.35
Urethanes, cast molded	Thermosetting	1.2–2.5 1.2

<sup>\*</sup> From E. R. Parker, *Materials Data Book*, McGraw-Hill, New York, 1967.

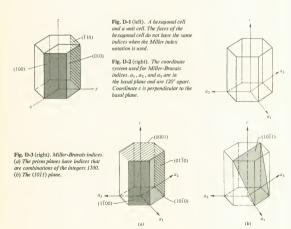
Modulus of elasticity (psi × 10 <sup>-5</sup> )	Tensile strength $(psi \times 10^{-3})$	Compressive strength (psi × 10 <sup>-3</sup> )	Tensile elongation (%)	Coefficient of thermal expansion (in./in./°F × 10 <sup>-5</sup>
3.5	4-13	15-25	3.6	2,5-3,5
_	7-12	15-33	0.5-3	3.0
30.0	10-30	25-40	4	0.6-2.0
_	_	40-45	_	
11	5-13	25-45	0.6	2.0
19	5-7	30	0.4	1.0-2.5
24	5-10	20-35	_	1.0
1.5-4	7–12	7–13	25-300	4.0
0.2-0.4	1-2	_	90-800	9.0
0.3-0.6	1-3	_	50-600	_
0.6-1.5	3-5	_	15-100	6.0
3.5-5	8-11	11-19	2-7	2.7-5.0
1.5-2	4-5.5	6-8	200-700	3.0-5.0
4-5	5-9	11-16	1-2	3.0-4.0
2-4	3-7	4-9	5-80	2.0-11.0
0.6	2-4.5	1.7	200-400	5.0
36	5-9	8-13	2-40	3.0-10.0
_	1.5-3	1-2	200-400	4.0-13.0
	1-10	20	100-1000	6
	4-8	20	300-600	6

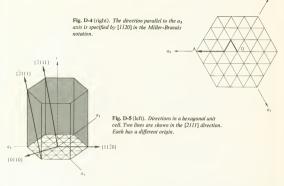
### APPENDIX D: Planes and directions in hexagonal crystals

Miller indices are very convenient when dealing with unit cells that have six sides. In these cases equivalent planes have similar indices, and the same is true of equivalent directions. In describing materials having the hexagonal structure, however, it is often desirable to use a hexagonal unit cell [Fig. 3-15(a)] rather than the unit cell shown in Fig. 3-15(b). Each vertical face of the hexagonal solid is an equivalent plane and should have similar indices. The Miller index notation does not provide this, as shown in Fig. D-1.

A notation system has been devised for hexagonal unit cells which meets the requirement that equivalent planes and directions in the cell have similar indices. The system requires four indices rather than three, and these are called the Miller-Bravais indices. The four axes of the coordinate system are shown in Fig. D-2. A plane is described by the notation ( $\hbar k l l$ ). The indices are the reciprocals of the intersection of the plane being described with the axes  $a_1$ ,  $a_2$ ,  $a_3$ , and c. They are defined the same way as the Miller indices for six-sided unit cells. A plane in space is defined by its intersection with three axes not in the same plane; therefore one of the Miller-Bravais indices is not independent. The l index is considered as the dependent one, and it must satisfy the condition that

$$h + k = -i (D-1)$$





The indices of several of the planes which form the unit cell are shown in Fig. D-3(a). It is seen that the vertical planes (or prism planes) all have similar indices and are combinations of I100. The basal planes are (0001). In this notation, the close-packed planes of an hcp structure would be the (0002) family. Figure D-3(b) illustrates the (10T1) plane. Note that the indices of all these planes obey equation D-1.

Directions in a hexagonal crystal are specified using the four axes defined by Fig. D-2. The notation for a direction is [hkil], and equation D-1 is still applicable. The procedure for finding direction indices is similar to that used for six-sided unit cells. A vector is drawn in a direction from the origin, and the components of the vector are resolved along each of the coordinate axes. They are then reduced to the smallest integers, and these are the indices [hkil]. Equation D-1 introduces a small complication. To see this, consider Fig. D-4. The base plane has been divided into a net of equilateral triangles, and the unit of length is taken as an edge of one of the small triangles. Consider the vector OA, which is in the a direction. At first thought, it might seem reasonable to describe this as the [0010] direction, but this notation does not obey equation D-1 and is therefore unacceptable. We can go from the origin to point A by many routes. Suppose we go one unit in the  $-a_1$  direction, one unit in the  $-a_2$ direction, and two units in the a3 direction. This takes us from the origin to A, and results in the notation [TI20], which obeys equation D-1. This is the proper notation for direction OA. Several directions in the unit cell are shown in Fig. D-5. The [2111] direction is shown by two different lines, corresponding to two different locations for the origin of coordinates. Any lattice point can be selected as the origin.

### APPENDIX E: Taylor's expansion

Taylor's expansion provides a method for expressing a mathematical function as a power series. We shall first consider McLauren's expansion, which is a special case of Taylor's expansion.

Figure E-1 shows a plot of f(x) vs. x. We wish to express this function as a power series, which has the form

$$f(x) = a_0 + a_1 x + a_2 x^2 + a_3 x^3 + \dots + a_n x^n + \dots$$
 (E-1)

where the a's are constants that must be determined. Not all functions can be expanded in this manner; there are necessary and sufficient conditions which the function must meet. We shall not derive these but shall simply state that the force vs. r and potential energy vs. r functions that are used in Chapter 6 meet the requirements. The problem is to evaluate the constants in equation E-1. The equation holds for all values of x; therefore it must be valid for x = 0. Letting x = 0, the first constant,  $a_n$  is seen to be

$$f(0) = a_0$$

This quantity is simply the intersection of the curve in Fig. E-1 with the f(x) axis, as shown. The remaining constants can be evaluated by first taking successive derivatives of equation E-1:

$$f'(x) = a_1 + 2a_2x + 3a_3x^2 + \dots + na_nx^{n-1}$$
 (E-2)

$$f''(x) = 2a_2 + (3)(2)a_3x + \dots + n(n-1)a_nx^{n-2}$$
 (E-3)

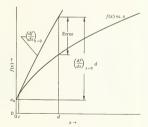
$$f'''(x) = (3)(2)a_3 + \dots + n(n-1)(n-2)a_n x^{n-3}$$
 (E-4)

Each of these equations permits the evaluation of one constant. Let x = 0 in equation E-2, Then

$$\left(\frac{df}{dx}\right)_{x=0} = a_1$$

The subscript with the derivative means that df/dx must be evaluated at

Fig. E-1. A plot of f(x) vs. x, showing various quantities that are pertinent to the use of equation E-6.



x = 0 because this was the condition chosen. Following the same procedure for equation E-3, E-4, etc,

$$\frac{1}{2} \left( \frac{d^2 f}{dx^2} \right)_{x=0} = \frac{1}{2!} \left( \frac{d^2 f}{dx^2} \right)_{x=0} = a_2$$

$$\frac{1}{3 \times 2} \left( \frac{d^3 f}{dx^3} \right)_{x=0} = \frac{1}{3!} \left( \frac{d^3 f}{dx^3} \right)_{x=0} = a_3$$

or generally,

$$\frac{1}{n!} \left( \frac{d^n f}{dx^n} \right)_{x=0} = a_n$$

Substituting these values of the constants into equation E-1 gives f(x) expressed as a McLauren's series:

$$f(x) = a_0 + \left(\frac{df}{dx}\right)_{x=0} x + \left(\frac{d^2f}{dx^2}\right)_{x=0} \frac{x^2}{2!} + \dots + \left(\frac{d^nf}{dx^n}\right)_{x=0} \frac{x^n}{n!} + \dots$$
 (E-5)

Equation E-5 permits f(x) to be found for any value of x if the various derivatives can be evaluated at x = 0.

Now consider the conditions under which the various terms in equation E-5 may be neglected. For small magnitudes of x (x| x|, terms such as  $x^2$ /21,  $x^3$ /31, etc., are small compared to x and may be neglected. For a small region about x = 0, equation E-5 can be approximated by

$$f(x) = a_0 + \left(\frac{df}{dx}\right)_{x=0} \quad |x| \leqslant 1 \tag{E-6}$$

In Fig. E-1, this approximation is shown for x = c and x = d. At x = d, the magnitude of the second term is shown graphically, and the error due to using equation E-6 is also shown. The error is significant, and the approximation cannot be used. At x = c, equation E-6 is a reasonably valid equation.

We are interested in an expression like equation E-6 which is valid in a small region in the neighborhood of x = d (this is analogous to a small region about  $r = r_0$ , as used in Chapter 6). To obtain such an expression, we expand f(x) in a power series about x = d rather than about x = 0. This expansion is Taylor's expansion. The series is written d.

$$f(x) = b_0 + b_1(x-d) + b_2(x-d)^2 + b_3(x-d)^3 + \dots + b_n(x-d)^n + \dots$$
(E-7)

Once again, the constants must be evaluated. Letting x = d, equation E-7 becomes

$$f(d) = b_0$$

The procedure for evaluating  $b_1, b_2, \ldots, b_n, \ldots$  is the same as that used

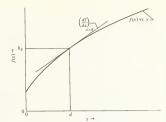


Fig. E-2. A plot of f(x) vs. x used for the Taylor's expansion about x = d. Equation E-10 is valid in the region about x = d, which is shown as a darkened line.

for the McLauren's expansion, except that the expressions are evaluated at x=d. The general result is

$$b_n = \left(\frac{d^n f}{dx^n}\right)_{x=d} \frac{(x-d)^n}{n!}$$
(E-8)

Substituting values of b into equation E-7,

$$f(x) = f(d) + \left(\frac{df}{dx}\right)_{x=d}(x-d) + \left(\frac{d^2f}{dx^2}\right)_{x=d}\frac{(x-d)^2}{2!} + \cdots + \left(\frac{d^3f}{dx^6}\right)_{x=d}\frac{(x-d)^6}{dx^6} + \cdots$$
 (E-9)

For small values of x - d the function f(x) can be approximated by

$$f(x) = f(d) + \left(\frac{df}{dx}\right)_{x=d}(x-d) \quad |x-d| \le 1$$
 (E-10)

The argument for doing this is the same as the argument used for the McLauren series. The result is shown graphically in Fig. E-2 and represents the approximation used in deriving equation 6-24.

APPENDIX F: Answers to selected problems
Chapter 1

- 1 (a) 25,500 psi; (b)  $8.5 \times 10^{-4}$  in./in.; (c) 0.0204 in.; (d) 78,500 lb
- 3 (b) 10 × 10<sup>6</sup> psi; (c) 38,000 psi; (d) 60,000 psi
- 3 (b) 10 × 10° psi; (c) 38,000 psi; (d) 60,000 ps 5 116,000 lb

### Chapter 2

- 1 (a) -13.59 eV, -3.397 eV, -1.51 eV; (b) -12.08 eV; (c) emitted
- 3 (a) -27.18 eV
- $5.1.36 \times 10^{-8}$  cm
- 8 (a) 4; (b) 4; (c) 8; (d) 9

#### APPENDIX F

- 10 (a)  $3.23 \times 10^{-8}$  cm; (b)  $-3.1 \times 10^{-11}$  ergs
- 12 (a)  $2.88 \times 10^{-8}$  cm; (b)  $2.14 \times 10^{-4}$  dynes
- 17 (a) 3.12 Å; (b) 0.0703 kcal/mole

### Chapter 3

- 2 (a) 4: (b) 8
- 7 (a)  $1.7 \times 10^{15}$  atom/cm<sup>2</sup>; (b)  $6.95 \times 10^{14}$ ; (c)  $5.7 \times 10^{14}$ ;
  - (d) 1.845 × 10<sup>15</sup>
- 9 (a)  $6.61 \times 10^{22}$ ; (b) 3.92 Å; (c) 1.385 Å
- 11 (a) -9.5%; (b) +3.5%; (c) bcc,  $1.251\text{\AA}$ ; fcc,  $1.29\text{\AA}$
- 13 (a) 4.20 Å; (b) 3.64 g/cm<sup>3</sup>
- 15 14,000
- 17 5.45 Å

### Chapter 4

- 2  $K = 14,500 \text{ psi} \sqrt{mm}$ ;  $\sigma_{0 \text{ yield}} = 56,750 \text{ psi}$
- 4 1.48%
- 8 (a)  $2.9 \times 10^{15}$  vacancies: (b)  $2.2 \times 10^{-5}$
- 9 (b) [[100]]

### Chapter 5

- 1 (a)  $10 \pm 0.25 \,\mu$ ; (b)  $1.052 \times 10^6 \,\mathrm{psi}$ ,  $0.949 \times 10^6 \,\mathrm{psi}$ ; (c) 5.1%
- 4 1.54 Å
- 5 (a) 18.7°
- 7 0.054 Å
- 8 Nickel 10 (a)  $\Delta d/d = \operatorname{ctn}(\theta \Delta \theta)$

### Chapter 6

- 1 (a) 0.000476 in./in.; (b) 0.001428 in.; (c) 0.00273°
- 3 3.52576 Å × 3.52344 Å × 3.52344 Å
- 5 0.5

$$\begin{split} 6 & f_{(c-1)} = \frac{3e^2a}{(a|2)^{3/2}\sqrt{8}} \\ & f_{(c-2)} = \frac{3e^2a}{\left[(a^2/8) + (2a^2/3)\right]^{3/2}\sqrt{8}} \end{split}$$

$$f_{(c-3)} = -\frac{3e^2a}{[(a^2/3) + (a^2/6)]^{3/2}}$$

- 8 (a)  $\log G = \log c 6.35 \log r_0$ ; (b)  $3.82 \times 10^9 \text{ psi Å}^{6.5}$
- 12 Steel
- 14 (a) 3.00018 in.; (b) Mg; (c) 448°F; (d) yes

### Chapter 7

- 1 (a) -6.98 ergs; (b) decreased; (c) single solid
- 3 340 ergs/cm<sup>2</sup> 5 5.61 × 10<sup>6</sup> psi

- 8 0°
- 9 (a) Complete wetting: (b) 9.20 × 104 ergs
- 12 58,300 psi
- 14 (a) 13.5%; (b) no; (c) no

#### Chapter 8

- 1 (a) 45°: (b) 45°
- 4 (a) 3%; (b) no
- 6 (a) 164 psi; (b) yes
- 8 0.0192
- 10 (a) 7305 in.-lb; (b) 261 in.-lb
- 11 (a) 33.4Å; (b) 1.01 × 106 psi
- 14 (a) 330Å; (b) decrease
- 17 (a)  $-7.31 \times 10^{-5}$  ergs/cm; (b) -33.2%
- 20  $2.02 \times 10^9$  dislocation/cm<sup>2</sup>
- 23 (a) 18,400 psi; (b) 20%

### Chapter 9

- 2 (b) 12,930 cal/mole; (c) no
- 3 (a) 2.39; (b)  $28.8 \times 10^{16}$ ; (c)  $1.73 \times 10^{13}$
- 7 (a) 22,500 cal/mole
- 9 2.5 in.2

### Chapter 10

- 2 (a)  $6.3 \times 10^{-4}$ ; (b) 78.5
- 4 (a)  $2.29 \times 10^{21}$  atoms/cm<sup>3</sup>; (b)  $-1.14 \times 10^{28}$  atoms/cm<sup>3</sup>
- 5 4/100a3
- 8 4.8 × 10<sup>-4</sup> cm<sup>2</sup>/sec, 76,200 cal/mole
- 9 (a)  $13.14 \times 10^{10}$  atoms/cm<sup>2</sup>/sec; (b)  $6.49 \times 10^{10}$  atoms/cm<sup>2</sup>/sec
- 11 0.0284 cm

### Chapter 11

- $2 1.26 \text{ g/cm}^3$
- 4 Au-Ag, K-Rb, W-Mo
- 4 Au-Ag
- (a) Liquid with 28.5% Cu, α with 8.8% Cu, β with 92% Cu; (b) 70.7%;
   (c) 34.6%, 1.83 lb; (d) 1.32 lb of α, 0.51 lb of β; (e) 1.32 lb of α, 3.68 lb of β; (f) 66.5%
- 17 (a)  $\alpha + \gamma$ ; (b) 38.7%  $\alpha$ , 61.3%  $\gamma$ ; (c) 61.3%; (d) 38.7%

### Chapter 12

- 2 (a)  $3.76 \times 10^{-4}$  cm; (b) 0.0158 cm
- 4  $\tau_{flow} = 65,000 \text{ psi}$
- 6 (a) 6.45 hr; (b)  $2.15 \times 10^6$  years
- 10 (a) Path 1: 50% martensite, 50% pearlite; path 2: fine pearlite and bainite; path 3: coarse pearlite
- 13 (a) Grain size; (b) strain; (c) redistribution of a solid phase in a matrix; (d) solid solution; (e) particle dispersion; (f) diffusionless phase transformation
- $16 32.4 \times 10^6 \text{ psi}$

### APPENDIX G: Physical constants

Avogadro's number  $N_* = 6.023 \times 10^{23}$  molecules/g-mole Boltzmann's constant  $k = 1.381 \times 10^{-16} \text{ ergs/}^{\circ} \text{K}$  $= 8.611 \times 10^{-5} \text{ eV/}^{\circ}\text{K}$  $e = -4.803 \times 10^{-10} \text{ esu}$ Electron charge  $= -1.602 \times 10^{-19}$  coulombs Gas constant  $R = 8.314 \times 10^7 \text{ ergs/g-mole }^{\circ}\text{K}$ = 1.987 cal/g-mole °K

 $= 6.6256 \times 10^{-27}$  erg-sec Planck's constant Speed of light in vacuum  $c = 2.998 \times 10^{10}$  cm/sec

# APPENDIX H: Conversion factors

1 cm = 0.3937 inLength:  $1 \text{ Å} = 10^{-8} \text{ cm}$ 

1 micron = 1  $\mu = 10^{-4}$  cm

Force:  $1 \text{ dyne} = 2.248 \times 10^{-6} \text{ lb}_c$ 

Mass: 1 gm = 0.002205 lb<sub>m</sub> Energy: 1 eV =  $1.6021 \times 10^{-12}$  ergs =  $3.829 \times 10^{-20}$  cal  $1 \text{ erg} = 6.2419 \times 10^{11} \text{ eV} = 2.3901 \times 10^{-8} \text{ cal}$ 1 eV/particle = 9.6494 × 1011 ergs/g-mole

 $= 23.0621 \times 10^{3} \text{ cal/g-mole}$  $1 \text{ cal/g-mole} = 4.34 \times 10^{-5} \text{ eV/particle}$ 

 $= 6.944 \times 10^{-17}$  ergs/particle  $1 \text{ in.-lb} = 1.1298 \times 10^6 \text{ ergs}$ 

Pressure or 1 psi = 68947.6 dynes/cm<sup>2</sup> stress:  $1 \text{ dyne/cm}^2 = 1.4504 \times 10^{-5} \text{ psi}$ 

APPENDIX I: Systems of units

Quantity	mks system	cgs system	English system
Time	Second	Second	Second
Mass	Kilogram	Gram	Pound <sub>m</sub> , slug
Force	Newton	Dyne	poundal, pound
Energy	Joule	Erg	Foot-pound <sub>f</sub>
Length	Meter	Centimeter	Foot
Charge	Coulomb	Statcoulomb (e	su)

# APPENDIX J: Symbols

A	Area	b	Constant in the bonding
a	Constant in the bonding		equations
	equations	b	Burgers vector
	Lattice parameter	C	Concentration
a, b, c	Unit vectors for a space	C'	Number of components
	lattice		in a system
B	Bulk modulus	С	Half the crack length
D	Magnetic field ventor		Smood of light

D	Coefficient of diffusion	$m_s$	Spin quantum number
$D^*$	Coefficient of self-	N	Number of particles in
	diffusion		a system
d	Diameter	$N_A$	Avogadro's number
	Distance between planes		Number of A particles
	of a family		in a system
	Grain size	$N_{\mathcal{E}}$	Number of particles in
E	Modulus of elasticity		a system that have
$E_{\bullet}$	Relaxation modulus		energy &
8	Energy	$N_s$	Number of spheres
8	Mean energy in an		intersected by a unit
	energy distribution		area of a plane
е	Magnitude of the	$N_v$	Equilibrium number of
	electron charge		vacancies in a system
F	Force or load	N	Number of atoms per
F'	Number of degrees of		unit area of a plane
	freedom of a system	n	Constant in the bonding
$F_*$	Normal force		equations
$F_s$	Shear force		An integer
Ť	Force on a dislocation		Principal quantum
f	Force between atoms or		number
,	ions	n(q)	Number of particles in
f <sub>r</sub>	Force exerted on an	(4)	a system that have
^	atom or ion, in the x		energy greater than q
	direction, by the other	P	Pressure
	atoms or ions in a	P'	Number of phases in
	crystal		a system
G	Shear modulus	P	Angular momentum
H	Free energy	0	Activation energy per
$H_{\star}$	Heat of sublimation	~	gram-mole
h	Planck's constant	$Q_c$	Activation energy for
(hkl)	Miller indices of a plane	200	creep
((hkl))	Miller indices of planes	$Q_r$	Activation energy for
	of a form	~	recrystallization
J	Flux of atoms	$\Delta Q$	Heat added to a system
Κ,	Stress concentration	q ~	Activation energy per
	factor in tension		particle
k	Boltzmann's constant		Electric charge of a
$\mathscr{L}$	Dislocation length		particle
	Distance between pinning	$q_A$	Energy of an A particle
	sites	$q_A$	Activation energy for
l	Length		diffusion
	Orbital angular	$q_m$	Activation energy for
	momentum quantum		vacancy motion
	number	$q_s$	Activation energy for
m	Exponent in the bonding		self-diffusion
	equations	$q_v$	Energy required to form
	Mass		a vacancy
$m_l$	Orientation quantum	R	Universal gas constant
	number	R	Radius of a dislocation

$\mathcal{R}_A$	Anion radius	x	Position coordinate
$\mathcal{R}_a$	Radius of an atom	Z	Charge of an ion,
$\mathcal{R}_{\mathcal{C}}$	Cation radius		expressed in units of the
$\mathcal{R}_s$	Radius of a sphere		electron charge
r	Distance between atoms or ions		g-
r <sub>n</sub>	Orbit radius of a hydrogen electron		
r <sub>0</sub>	Equilibrium distance between atoms or ions (bond length)		
S	Entropy	α	Shear angle
S	Distance	u	Thermal expansion
	Distance between		coefficient
	dislocations	0	
Δs	Shear deformation	α, β, γ	Direction angles of a line
T T	Line tension	β	Factor accounting for
1			the effect of crystal
$T_{\bullet}$	Temperature		structure in diffusion
	Eutectic temperature	γ	Shear strain
$T_g$	Glass transition		Surface tension
	temperature	δ	Tensile or compressive
$T_I$	Liquid temperature		deformation
$T_m$	Melting temperature	3	Tensile or compressive
$T_p$	Peritectic temperature		strain
$\Delta T$	Number of degrees of	Ė	Strain rate or creep rate
	supercooling	ε'	Strain due to hydrostatic
	Time		tension
	Period of oscillation of	θ	Diffraction angle
	an atom	λ	wavelength
t <sub>r</sub>	Time to rupture	μ	Electric dipole moment
[uvw]	Direction indices in a		Poisson's ratio
	crystal		Microns
[[uvw]]	Indices describing	ν	Frequency
	directions of a form	ρ	Dislocation density
V	Potential energy		Radius of curvature
	Volume	σ	Tensile or compressive
V'	Voltage		stress
v	Velocity	$\sigma_{\mathrm{BF}}$	Tensile stress at which
$w_i$	Weight fraction of a		brittle fracture occurs
	system component in the	$\sigma_c$	Maximum stress at a
	liquid phase	- c	stress concentration
$W_{\pi}$	Weight fraction of a	σ	ticHydrostatic stress
	system component in the	σ <sub>max</sub>	Theoretical maximum
	solid phase	max	tensile stress
$X_I$	Mass (or weight)		
1	fraction of a system in	$\sigma_s$	Tensile or compressive
	the liquid state		stress at which slip is
$X_s$			observed
A 8	Mass (or weight)	τ	Shear stress
	fraction of a system in the solid state	$\tau_{cr}$	Critical resolved shear
	the solid state		stress

τ<sub>source</sub> Shear stress required to operate a dislocation source

φ Angle between an applied stress and a slip direction Angle between an applied stress and a normal to the slip direction Specific surface energy

ω

# Index



	Boltzmann energy distribution, 97,
A	279
	temperature dependence of, 280
Activation energy, 281	Bond bending, 263
for creep, 297	Bond energy
for diffusion, 315, 325	of carbon, 47t
for recrystallization, 293	covalent, 47
	diagram, 38
for self-diffusion, 285	ionic, 39, 40
for vacancy formation, 116	metallic, 44
for vacancy motion, 285	secondary, 50
Addition polymerization, 50	Bond length
Age hardening, see Precipitation	of carbon, 47t
hardening	equilibrium, 39
Alternating copolymer, 55	* '
Angular momentum, orbital, 30	of NaCl, 41
spin, 31	Bonding forces, ionic
Anisotropic, 61	attractive, 37
behavior for iron, 196	in a crystal, 160
behavior for MgO, 174	diagram, 38
Annealing, 17, 266, 275, 289	equation for repulsive, 39
effect on cold-rolled Al, 16	exponent for repulsive force, 41t
mechanisms of, 290	repulsive, 38
of steel, 395	Bonds, chemical
Arrhenius equation, 281	covalent, 45
Atactic structure, 87, 302	effect on modulus of elasticity, 16
Atomic radius, 75	effect on surface energy, 191
tables, 78t, 414t	hydrogen, 48
Atomic weight of the elements, 414	ionic, 37
Attractive bonding forces, see	metallic, 43
	mixed, 90
Bonding forces and	nondirectional, equal sized atoms,
Coulomb's Law	71
Austenite, 355	nondirectional, unequal sized
	atoms, 77
	secondary, 48
	silicate, 81
В	see also Bond energy, ionic;
_	Bonding forces, ionic; Carbo
Bainite, 393	
Billiard ball model, see Hard-ball	bonds; Free electron theory of metals
model	
Binary phase diagram, see Phase	Bragg's Law, 140
diagram, see Phase	Bravais lattices, 64
	Brittle fracture, 9, 13
Block copolymer, 55	due to impact, 14
Body-centered cubic structure, 76	effect of compressive loads, 208
Bohr theory, 26	Griffith theory, 203, 205
Boiling point of the elements, 414	size effect in, 208

Brittle fracture stress equation for, 206 strain rate dependence of, 289	effect of temperature, 173 of selected ceramics, 418 <i>t</i> of selected polymers, 420 <i>t</i>
temperature dependence of, 288	Cold working, see Work hardening
Bulk modulus, 156	Columnar zone, 107
Burgers vector	Composite materials, 403
direction of, 225	Concentration, 312
edge dislocation, 117	calculation of, 314
effect on slip, 228	gradient, 316
in an ionic solid, 255	profile, 314
notation, 243	Condensation polymers, 56
screw dislocation, 118	Continuous cooling curve, 400
	Conversion factors, 429
	Cooling curves, 342, 343
C	Coordination number, 77, 80t, 81t
C	Coordination polyhedra, 80, 81t
	Copolymers, 55
Carbon bonds, 45	Cored structure, 362
diamond, 45	Cottrell atmosphere, 376
energy, 47t	Coulomb's Law, 25
graphite, 46	applied to a crystal, 162
length, 47t	Covalent bond, see Bonds, chemical
orbitals, 45	Cracks, 203
saturated, 47	formed by slip, 256
unsaturated, 47	internal, in copper, 263
Carburizing, 320, 364 Case hardening, 317	nucleation of, 261
Cast iron, 357	Creep, 294
Casting, 107	activation energy, 297
control of microstructure in, 109	of chain polymers, 302 rate, 296
Cementite, 355	stress dependence, 296
proeutectoid, 359	temperature dependence, 296
Ceramics, properties of, 418t	Creep rupture, 300
Chain polymerization, 50	Cristobalite, 83fig
Chain sliding, 265	Critical radius, 100
Chain straightening, 263	of copper, 101
Chemical bonds, see Bonds, chemical	Critical radius ratio, 78, 80t, 81t
Chemical reaction rates, 279	Critical resolved shear stress, 227
Chill zone, 107	for copper solid solutions, 376
Cleaving, 199	for internally oxidized copper, 381
Climb, 250	for iron, effect of nitrogen, 319
thermally activated, 285	for MgO, 229
Closest packed planes, 72	for several solids, 228t
in fcc, 74fig	for zinc, 227
in hcp, 73fig	Cross-linking, 85
Coefficient of diffusion, 316, 324,	effect on relaxation modulus, 302
325t	in rubber, 89
measurement of, 324	Cross-slip, 251
Coefficient of thermal expansion, 172	Crystal directions, 66

Crystal growth

atomic model, 96

couple, 321, 363

effect of solubility limits, 362

grain boundary, 327, 328t

interstitial mechanism, 311

in pearlite formation, 358

in ionic crystals, 326

model for, 313fig

effect of screw dislocation on, 119	time dependence, 317
single crystals, 106	vacancy mechanism, 310
Crystal structure	welding, 18
body-centered cubic, 76fig	see also Coefficient of diffusion
cesium chloride, 80	Diffusivity, see Coefficient of
diamond, 45	diffusion
effect on critical resolved shear	Dipole, electric, 48
stress, 228	fluctuating, 49
effect on elastic modulus, 168,	permanent, 48
196	Direction vector, 66, 422
effect on surface energy, 192, 195	Directions of a form, 67
effect on work hardening, 252	Dislocation density, 226
face-centered cubic, 73, 74	effect on dislocation mobility, 248
graphite, 46	increase due to sources, 238
hexagonal close packed, 73	Dislocations
polyethylene, 85	annihilation, 239
sodium chloride, 79, 160	during recovery, 290
see also Bravais lattices and	dissociation, 244
Silicate	formation of mixed, 223
Crystal systems, 64	intersection, 247
Crystallographic equivalence	jogs, 248
directions, 67	thermally activated, 284
planes, 69	loops, 225
	expansion of, 226
	formation of, 238
TD.	mobility, 245
D	motion in ceramics, 254
	partial, 244
Degree of polymerization, 86	pile up, 247
Degrees of freedom, 339	at a grain boundary, 130, 257
Delta ferrite, 355	reactions, 246
Dendrites, 104	see also Frank-Read source and
Density	Pinning sites
of elements, 414	Dislocations, edge, 116, 117fig
of selected ceramics, 418	climb of, 250
of selected polymers, 420	energy of, 233
Diamond cubic structure, 45	force on, 236
Diffraction angle, 137	forces between, 240
Diffusion, 17	geometry, 117
activation energy, 315, 325t	motion of, 224

rate, 315

surface, 96, 327, 328t

radius of, calculation, 234

slip mechanism of, 222

strain field of, 117

Dislocations, screw

energy of, 231

cross-slip of, 251

forces between, 240

Dislocations, screw (cont.) Elongation, 4 geometry of, 118 of selected polymers, 420t motion of 224 Embryo, 100 radius of, calculation, 234 Energy Dispersion hardening, 377 bond, see bond energy by internal oxidation, 381 of an edge dislocation, 233 by spheroidizing, 378 elastic, 171, 205 Distance between planes of a family, of a screw dislocation, 231 see also Activation energy effect on slip, 228 Epsilon carbide, 395 Ductile to brittle transition, 287 Equilibrium phase diagram, see for polymers, 301 Phase diagram strain rate dependence of, 289 Error function, table, 319 temperature dependence of, 288 Etch pits, 241 Ductile fracture, 8, 260 Etching, 126 crack formation in 262 Entectic effect of work hardening rate, 261 diagram, 347fig, 367fig Dynamic equilibrium, 98 point, 348 reaction, 348 structure of Pb-Sn, 349 temperature, 349  $\mathbf{E}$ Eutectoid reaction, 357 Edge dislocation, see Dislocations Elastic behavior, 4  $\mathbf{F}$ force curves and, 165 Elastic energy, 171 in brittle fracture, 205 Face-centered cubic structure, 73, 74 Elastic solid, model, 170figs Families of planes, 70 Elastomers, 87 distance between 141 dienes, 54 effect on slip, 228 polyisoprene, 87 Ferrite, 355 Electron proeutectoid, 359 configuration, 31 Fick's first law, 312 energy levels, 33 Fick's second law, 316 gas, 43 for constant surface concentration. orbit radius, 26, 31 scattering, 129, 131 for diffusion couple, 321 shells, 34 Field ion microscope, 131 Electron affinity, 36t Flow stress, 377, see also Critical Electron cloud, 28 resolved shear stress and in carbon, 45 Vield stress in ionic bonding, 37 Flux of atoms, 314 in metallic bonding, 43 Forces, bonding, see Bonding forces Electron microprobe, 147 Forces on a dislocation, 236 Electron microscope Forces between dislocations, 239 scanning, 130 Formaldehyde bridge, 57 transmission, 128 Fracture, see Brittle fracture and Elements, properties, 414t Ductile fracture

Frank-Read source, 237	annealing, 395
in dispersion hardening, 377	furnace cooling, 396
mechanism, 238	hardenability, 397
shear stress for operating, 237	martensite, 389
in silicon, 238	normalizing, 396
Free electron theory of metals, 43	quenching, 384, 389
Free energy, 114, 362	spheroidizing, 378
Freezing rate, 98	of steel, 391
Frenkel defect, 327	see also Solutionizing
Functionality, 55	Heterogeneous nucleation, 101, 358
Furnace cooling, 396	Hexagonal close-packed structure, 73
	Homogeneous nucleation, 99
	Hooke's law, derivation
6	from experiments, 5
G	for ionic solid, 164
	Hume-Rothary rules, 341
Gibbs phase rule, 339	Hydrogen atom, 24
Glass transition temperature, 111,	Bohr theory of, 26
113t	energy of, 26
in ductile to brittle transition, 301	orbit radius, 26, 31
Graft copolymer, 55	Hydrogen bond, 48
Grain boundaries, 102	Hydrostatic stress, 157, 165
as barriers to dislocation motion, 257	
field ion micrograph of, 133	*
Grain boundary diffusion, 327	1
coefficient of, 328t	
Grain growth, 294	Impact test, 14
Grain size, 102	in ductile to brittle transition, 289
effect on yield strength, 103, 388	Intermediate phase, 352, 354
Graphite structure, 46	Internal oxidation, 381
Griffith theory, see Brittle fracture	Interstitial mechanism of diffusion,
Guinier-Preston zones, 385	311
effect of aging, 387	Interstitial solutions, 311, 319
	C in Fe, 356fig
	effect of misfit, 375
TT	N in Fe, 319
H	Invariant point, 340, 349, 350, 351,
	351t
Hard-ball model, 47fig, 71fig	Invariant reaction, 340, 348, 351,
Hardenability of steel, 397	357
effect of alloying elements, 399	Ionic bond, see Bonds, chemical
Hardness, 15	Ionic radius, 77, 78t, 414t
Brinell, Knoop, Rockwell,	Ionization energy, 35
Vickers, 16	in metallic bonding, 36t, 43
testing, 15	Isotactic structure, 87fig, 302
see also Work hardening	Isothermal transformation diagram,
Heat treatment	392
of Al-Cu alloys, 387	Isotropic properties, 61

# J

Jominy test, 400

of the elements, 414t as a function of  $r_0$ , 168 of MgO, calculated, 167 of selected ceramics, 418t of selected polymers, 420t Monomer, 54

## L

Lattice, see Bravais lattices and Space lattices Space lattices Lattice parameter, 73 Lever rule, 345, 361 Line tension, 237 Liquidus curve, 342 Logic, deductive and inductive, 3 Lomer-Cottrell lock, 247 Low-angle grain boundaries, 241 in MgO, 292 in tungsten, 242

# N

Necking, 10, 261, 402 Network polymers, 57 Noble gases boiling and melting points, 49t in periodic table, 34t Nondirectional bonds, see Bonds. chemical Nonequilibrium solidification, 360 of brass, 361 of Cu-Ni alloys, 360 Nonequilibrium solidus, 361 Normalizing, 396 Notation for electrons in an atom, 33 Nucleation heterogeneous, 101, 358 homogeneous, 99 Nucleus, 100, 101

## M

Martensite, 389 effect of carbon on formation, 398 Mass fraction, 345 Melting point ceramics, 418t elements, 414t ionic solids, 42t metals, 100t noble gases, 49t polymers, 113, 420t Melting rate, 98 Metallic bond, see Bonds, chemical Metastable state, 356 Miller-Bravais indices for hcp structure, 422 Miller indices, 68 Mixed bonds, 90 Mixed dislocations, see Dislocations Models of nature, concept, 2 Modulus of elasticity derivation of, 164 effect of stress direction, 196 effect of temperature, 174

# 0

Offset yield strength, 9
Optical microscope, 126
Orbital angular momentum, 30
Orbitals, 45
Orowan's derivation, 206

# P

Packing factor, 75
Partial dislocation, 244
recombination of, 286
Pauli exclusion principle, 31
Pearlite, 357
nucleation, 358

structure, 358	spheroidized cementite, 378
Period of vibration, 282	in stainless steel, 380
Periodic table, 31t	Planes of a form, 69
derivation of, 33	Plastic deformation, see Permanent
Peritectic	deformation
diagram, 350fig, 368fig	Plasticizers, 265
point, 350	Point defects, 114
reaction, 350	Poisson's ratio, 157
temperature, 350	for selected ceramics, 418t
Permanent deformation 7, 219	Polycrystals, origin, 102
effect on dislocation density, 248	Polyethylene chain, 51
effect on mechanical properties,	crystal, 85
249	Polygonization, 291
mechanism in polymers, 262	of MgO, 292
slip mechanism for, 222	Polymer structures
see also Dislocations and Slip	amorphous, 84, 111
Phase, 334	chain, 51
intermediate, 352	copolymers, 55
terminal, 352	cross-linked, 85
Phase boundary, 335, 336	crystalline, 85, 111
Phase diagram, 334fig	diene, 54
binary 337fig	effect on relaxation modulus, 302
for complete solubility, 341	due to extrusion, 265
eutectic, 347fig	network, 57
with intermediate compounds,	stereoisomers, 86
353fig	vinyl, 52
with intermediate phases, 352fig	vinylidene, 53
peritectic, 350fig	Polymerization
for pure substance, 334fig	addition, 50
Phase diagrams	chain, 50
Cu-Ag, 367fig	condensation, 56
Cu-Zn, 352fig	copolymers, 55
Fe-Fe <sub>3</sub> C, 356fig	Polymers, properties, 420t
Fe-Ni, 350fig	Polymethyl methacrylate
iron, 335fig	elastic modulus, 112
MgO-SiO <sub>2</sub> , 353fig	structure, 53
NaCl-H <sub>2</sub> O, 336, 337fig	temperature dependence of stress-
Ni-Cu, 344fig	strain curve, 301
NiO-MgO, 344fig	Powder camera, 145
Pb-Sn, 347fig	Precipitation hardening, 383
Zr-C, 354fig	of Al-Cu, 387fig
Physical constants, 429	of Fe-Mo, 384
Pinning sites	Prestressed concrete, 210
due to dislocation intersections,	Primitive cell, 63
247	Primitive vectors, 63
for Frank-Read sources, 235	Properties
due to grain boundaries, 130, 257	of the elements, 414t
due to multiple impurities, 259	of selected ceramics, 418t
in solid solutions 375	of selected polymers 420r

# Q

Quantum numbers, 29 allowed values, 31 Quartz, 83 Quenching, 384, 389

## R

Random copolymer, 55
Recovery, 290
Recrystallization, 292
activation energy, 293
of copper, 293
Reduction in area, 12, 261, 402
Relaxation modulus, 302
Repulsive bonding forces, see
Bonding forces
Resolved shear stress, 221
Resolving power or resolution, 127, 129, 131, 149r

# S

SAP, 382fig
Saturated bonds, 47
Schottky defect, 326–327
Screw dislocation, see Dislocation
Self-diffusion, 285, 310, 323
activation energy, 285
coefficient of, 322
measurement of, 322
Self-interstitial, 114, 115fig
Sessile dislocation, 246
Shear modulus, 155
effect on slip, 228
as a function of bond leneth, 168

as a function of bond length, 108
Shear strength, theoretical, see
Theoretical shear strength
Shielding model of atoms, 28, 29fig
Silicate
chain, 82fig

chain, 82fig cristobalite, 83fig sheet, 83 tetrahedral structure, 81fig Single crystal growth, 106 Sintering, 324, 329, 381, 388

quartz, 83fig

Size effect in brittle fracture, 209 Slip in Al polycrystal, 219 bands, 218

lines, 218
mechanism of an edge dislocation,

observation of, 218 observation in polycrystals, 257 planes, 223, 225 of polymer chains, 265

systems, 230
in zinc single crystal, 218
Sodium chloride structure, 79, 161

Solid-liquid interface, 98, 105 Solid phases, multiple, 335 Solid solutions, 311, 319, 341, 347,

Solid solutions, 311, 319, 356
Solidification, 97
Solidus curve, 342
Solubility, 17, 333, 336
limit, 336, 347

Solution hardening, 374 in Cu–Ni system, 374 Solutionizing, 385 Solvus curve, 347

Space lattices ihree-dimensional, 63 two-dimensional, 62

Specific surface energy, 188, 190t, 195t

derivation of equation for, 192 effect on brittle fracture, 205 effect on wetting, 201 estimate of for copper, 190 of MgO, calculation, 194

Spheroidizing, 378 Spherulites, 112 Spin angular momentum, 30 Stacking faults, 245

Steel, 354
composition of, 355t
equilibrium microstructure, 358,

359

hypereutectoid, 357	measurement of, 200
hypoeutectoid, 357	Symbols, used in this book, 429t
low, medium, and high carbon,	Syndiotactic structure, 87fig, 302
356	Systems of units, 429
see also Heat treatment and	
Hardenability of steel	T
Stereoisomers, 86	•
Strain, 5	Taylor's series, 164, 424
engineering, 11	TD nickel, 383
shear, 155	Temperature gradients, 104
true, 11	for dendrite growth, 105
Strain hardening, see Work	for single crystal growth, 106
hardening	Tempering, 395
Strain-induced transformations	Terminal phases, 352
in austenitic stainless steels, 402t	Testing machines
in TRIP steel, 403fig	impact, 14
Strain rate, 286	universal, 7
Strength, see Ultimate tensile	Theoretical shear strength, 175
strength and Yield stress	calculated values, 179t
Stress, 5	Theoretical tensile strength, see
engineering, 11 hydrostatic, 156	Ultimate tensile strength
shear, 155	Thermal energy of a crystal, 96, 280
true, 11	distribution of, 97
see also Critical resolved shear	effect of temperature on, 96
stress	effect on thermal expansion, 172
Stress concentration, 203	also see Vibration energy
factor of, 204	Thermal expansion, 171
Stress-strain diagram	coefficient of, see Coefficient of
engineering, 12fig	thermal expansion
experimental method, 9	of MgO and Al <sub>2</sub> O <sub>3</sub> , 173fig
true, 12fig	of selected ceramics, 418t
Structure, see Crystal structure and	of selected polymers, 420t Thermally activated process, 278
Polymer structures	in solids, 282
Substitutional solid solution, 311,	Thermionic emission, 43
341, 347	Thermoplastic polymers, 90
effect of misfit, 375	Thermosetting polymers, 90
Supercooling, of metals, 100t	Toughness, 13
of polymers, 111fig	Triple point, 334
Surface atom migration, 98, 327	Twinning, 259
Surface diffusion, 327	5, = -
coefficient of, 328t	U
Surface energy, 187	C
measurement of, 197	VIII.
origin of, 189	Ultimate compressive strength of selected ceramics, 418t
in spheroidizing, 377	of selected polymers, 420t
see also Specific surface energy	Ultimate short strangth 175

Surface replicas, 129 Surface tension, 187 Ultimate shear strength, 175

of polycrystals, 179t

Ultimate shear strength (cont.) of whiskers, 1791
Ultimate tensile strength, 9 effect on brittle fracture, 206 of iron, calculated, 196 of selected ceramics, 418t of selected polymers, 4201 temperature dependence of, 277 theoretical, 195
Unit cell, 63 body-centered cubic, 76 face-centered cubic, 74 hexagonal close-packed, 73
Littly tectors, 67

Unsaturated bonds, 47

observed shear strength, 179¢ stress-strain diagram for, 12fig, 197 Work hardening, 17 in bee crystals, 254 effect in ductile fracture, 261 effect on properties of stainless steel, 249 in fee crystals, 253, 258 in hep crystals, 254 of nylon by crystallization, 265 in polycrystals, 258 of a polymer by crystallization, 265 stages 1, 2, and 3, definition, 252 temperature dependence, 286 of Zn. Cu. and Fe. 252

### V

Vacancies, 114, 116 activation energy, 285 effect on jogged dislocations, 248 energy of formation, 116 rate of movement, 285 role in climb, 250 Vacancy mechanism of diffusion, 310 Van der Waal's bonds, see Bonds, chemical, secondary Vibration energy distribution of, 280 of a solid, 97, 172, 282 see also Thermal energy of a crystal Vibration frequency of an atom, 283, 315 Viscoelastic region, 303 Viscous region, 303 Vitrification, 111

# w

Wetting of surfaces, 201 Whiskers, 121, 404

Vulcanizing, 88

# X

X-ray diffraction, 136 from bee crystals, 143 conditions for, 137, 143*t* data interpretation, 144 from fee crystals, 143 order of, 139 X-ray source, 133 scattering, 136 spectrum, 135

## **%**7

Yield stress, 9, 223
effect of grain size on, 103
effect of temperature and
dislocation density on, 276
as a function of particle
dispersion, 379
temperature dependence of, 277,
288

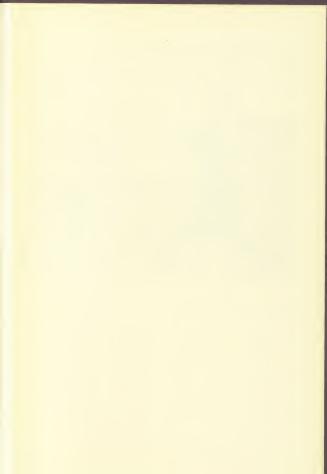
Young's modulus, see Modulus of elasticity



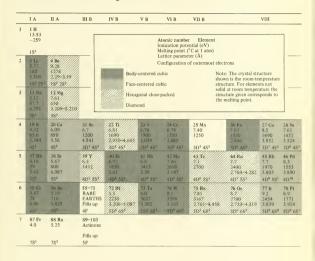








# Periodic Table of the Elements



IB	II B	III A	IV A	V A	VI A	VII A	0
							2 bb 24 47 - 270 2 54-5 64 55-5 64
		5 B 8.25 2300 2S <sup>2</sup> 2P <sup>1</sup>	6 C 11.20 3.568 2S <sup>2</sup> 2P <sup>2</sup>	7 N 14.47 -210 2S <sup>2</sup> 2P <sup>3</sup>	8 O 13.55 -218 2S <sup>2</sup> 2P <sup>4</sup>	9 F 18.6 -223 2S <sup>2</sup> 2P <sup>5</sup>	10 Ne 21.47 -249 4.52 2S <sup>2</sup> 2P <sup>6</sup>
		13 AI 5.96 660 4.049 3S <sup>2</sup> 3P <sup>1</sup>	14 Si 8.08 1420 5.428 3S <sup>2</sup> 3P <sup>2</sup>	15 P 11.11 44 3S <sup>2</sup> 3P <sup>3</sup>	I6 S 10.31 113-119 3S <sup>2</sup> 3P <sup>4</sup>	17 Cl 12.96 -103 3S <sup>2</sup> 3P <sup>5</sup>	18 Ar 15.69 -189 5.43 38 <sup>2</sup> 3P <sup>6</sup>
29 Cu 7.68 1083 3.615 3D <sup>10</sup> 4S <sup>1</sup>	30 Za 9 36 419 7,564-4,945 3019 454	31 Ga 5.97 30 3.62-8.75 48 <sup>2</sup> 4P <sup>3</sup>	32 Ge 8,09 958 5,658 4S <sup>2</sup> 4P <sup>2</sup>	33 As 10.5 817 4S <sup>2</sup> 4P <sup>3</sup>	34 Se 9.70 217 4S <sup>2</sup> 4P <sup>4</sup>	35 Br 11.30 -7 4S <sup>2</sup> 4P <sup>5</sup>	36 Kr 13.94 -157 5.69 4S <sup>2</sup> 4P <sup>6</sup>
47 Ag 7.54 960 4.086 4D <sup>10</sup> 5S <sup>1</sup>	48-E4 8-96 328 2-979-5-617 4D <sup>(4)</sup> -55 <sup>2</sup>	49 In 5.76 155 5S <sup>2</sup> 5P <sup>1</sup>	50 Sn 7.30 232 6.46 5S <sup>2</sup> 5P <sup>2</sup>	51 Sb 8.35 630 5S <sup>2</sup> 5P <sup>3</sup>	52 Te 8.96 453 5S <sup>2</sup> 5P <sup>4</sup>	53 I 10.44 113 5S <sup>2</sup> 5P <sup>5</sup>	54 Xe 12.08 -112 6.24 \$\$^2 \$p^6
79 Au 9.20 1063 4.078 5D <sup>10</sup> 6S <sup>1</sup>	80 Hg 10.38 -40 5D <sup>10</sup> 6S <sup>2</sup>	81 TI 6.07 303 6S <sup>2</sup> 6P <sup>1</sup>	82 Pb 7.38 327 4.949 6S <sup>2</sup> 6P <sup>2</sup>	83 Bi 8.0 271 6S <sup>2</sup> 6P <sup>3</sup>	84 Po 7.25	85 At 9.4	86 Rn 10.96

